PACIFIC EARTHQUAKE ENGINEERING
RESEARCH CENTER

Rehabilitation of Nonductile RC Frame Building Using Encasement Plates and Energy-Dissipating Devices

Mehrdad Sasani
University of California, Berkeley

Vitelmo V. Bertero
University of California, Berkeley

James C. Anderson
University of Southern California

PEER 1999/12
DEC. 1999

Rehabilitation of Nonductile RC Frame Building Using Encasement Plates and Energy-Dissipating Devices

Mehrdad Sasani
Department of Civil and Environmental Engineering
University of California, Berkeley

Vitelmo V. Bertero
Department of Civil and Environmental Engineering
University of California, Berkeley

James C. Anderson
Department of Civil and Environmental Engineering
University of Southern California, Los Angeles

PEER Report 1999/12
Pacific Earthquake Engineering Research Center
College of Engineering
University of California, Berkeley
December 1999

ABSTRACT

The main objective of the study reported herein has been to develop a general seismic rehabilitation and upgrade approach for existing nonductile **reinforced concrete (RC)** moment frame buildings. A review of the design and as-built drawings of such existing buildings reveal that one of the main weaknesses is the lack of transverse (shear) reinforcement in the beam-column joints. Thus it was decided to attempt an upgrade approach centered on the use of a steel jacket placed around each of these joints. Furthermore, it was considered desirable that the study be conducted on an existing instrumented building that had already been subjected to at least moderate **earthquake ground motions (EQGMs)** so it would be possible to calibrate the analytical models and computations involved in the analyses of its response and degree of damage.

The studies conducted to achieve the main objective stated above are presented and discussed in this 12-chapter report. In the first chapter, after discussing the main objective and the scope of the studies, a brief description of the selected building and its performance during past earthquakes (EQs) are presented. The building selected is a 15-story (13 stories above ground and a 2-story basement) RC building that was designed in 1964 and constructed in 1965. While the 13 stories above grade consist of a RC moment frame structural system, the 2 levels below ground are enclosed by structural walls. The foundation consists of 34-foot concrete piles. After the 1971 San Fernando EQ, this building was instrumented with 15 accelerometers. Since construction, the building has been subjected to several moderate EQGMs, the main ones being the 1971 San Fernando and the 1994 Northridge EQs. During the San Fernando EQ, the four corner columns suffered some structural damage at the first and second stories. Also a short structural wall below the grade experienced some minor diagonal cracking. Drywall partitions shifted and buckled on the second floor.

During the 1994 Northridge EQ, cracking of the RC walls, columns, beams, and slabs were observed at the basement. Moderate damage to the beam-column joints was also reported. In general, the structural and nonstructural damage was slight. The contents of the building suffered moderate damage. From the recorded response of the building, it was found that the periods in the transverse and the longitudinal directions were about 3.2 and 3.0 sec, respectively. Although the **peak ground velocity (PGV),** the **peak ground displacement (PGD),** and the

peak ground acceleration (PGA) were all larger in the N-S (transverse) direction, the maximum displacement at the roof level in the E-W (longitudinal) direction was 1.85 times higher than the maximum displacement in the N-S direction. Using the available recorded motions at the instrumented floors and using judgment in interpolating the displacements at other noninstrumented floors, it was estimated that the maximum **interstory drift index (IDI)** was about 1.1% at the first story and occurred in the E-W direction. The estimated values of the IDI justified the observed moderate damage.

From the analyses of the building design, the as-built drawings, the characteristics of the site, and the observed and recorded performances during the past EQGMs to which it has been subjected, it was concluded that this building has a very flexible structure with several weaknesses, the effects of which need to be studied. The building is located at a site where the soil is recent alluvial deposit that is generally moderately firm with soft layers at varying depths. The predominant period of the EQGMs on this type of soil is about the same as the fundamental period of the structure, which could lead to high dynamic amplification of the building response.

The second chapter summarizes the studies that have been conducted to analyze in detail the weaknesses of the building and to assess its global, story, and local vulnerability. To achieve this, a **three-dimensional (3D)** linear elastic model was developed, and its behavior analyzed using the SAP2000 (1998) computer program. By comparing the predicted **periods (T)** and the values of the response parameters obtained using the recorded time history of the Northridge EQGMs with those obtained directly from the recorded accelerations, it was possible to calibrate the developed model. Attempts were made to improve the estimation of the T from the recorded acceleration at the roof level, the Fourier transformation technique (using 3 windows each of 20 sec duration, and 6 windows each of 10 sec duration), and judgment. Analysis of the results obtained using Fourier transformation together with comparison of the computed top displacement of the model with that obtained from the recorded response of the real building when subjected to the recorded time history of the EQGMs indicate that the values 3.2 sec and 3.0 sec for the fundamental periods T in the N-S and the E-W direction, respectively, are better estimations of these periods. The vulnerability was assessed by computing the response of the developed model to the 1997 UBC spectrum and then determining the demand/capacity ratios for the main global, story, and local response parameters. Analysis of the values obtained for these ratios permitted identifying story weaknesses and softnesses. The corner columns at the first

story have a strength demand up to five times the strength capacity. At the second floor the beams have flexural strength demand over strength capacity ratios that vary from 1.38 to 2.36 for negative bending moments and from 1.26 to 4.28 for positive bending moments. The upper limit of 4.28 is due to the inadequate anchorage of the beam bottom reinforcement bars at the columns. Considering the possibility of the 1997 UBC severe near-field EQGMs, the IDI can reach values up to 3.7% that are unacceptable.

Chapter three presents and discusses the results obtained in a detailed analysis of the local vulnerability of the different elements of the structure. The analysis of the local vulnerability has been conducted through the use of a limit analysis and capacity procedure. The demands and capacity of the critical regions of beams, columns, and joints have been estimated. The results obtained indicate that the building has several weaknesses, the main ones being (1) weak corner columns; (2) excessive IDI; (3) excessive shear stress in the exterior joints; (4) inadequate spacing of the transverse reinforcement along the columns and at the joints; (5) inadequate anchorage of the beam bottom reinforcement; (6) inadequate splicing of the main reinforcement; and (7) inadequate amount and detailing of the main longitudinal reinforcement of the beams.

In order to study the probable effects that the structural weaknesses (identified in the studies reported in the previous chapter) might have on the global, story, and local response under severe EQGMs, it was considered necessary to develop and study the response of an inelastic model of the building. Chapter four presents and discusses the development of a simple nonlinear one-interior frame model and one-exterior frame model for the frames in the transverse (N-S) direction and then how these models were used to model the building for the study of its response when subjected to severe EQGMs in the transverse direction. Two inelastic models were developed, one based on the assumption that the columns above grade were fixed at the ground level and the other based on two sources of flexibility: the first is the rotation flexibility of the beams and columns in the two-level basement; and the second source is the deformation of the foundation due to the vertical deformation and movement of the piles. It was planned to conduct two types of nonlinear analysis, a static nonlinear pushover and a dynamic nonlinear time-history analyses. The pushover analysis using increasing lateral loads of inverted triangular shape shows that for a roof ID of 1.0 % the corner columns are submitted to axial tension forces that led to the development of **plastic regions** [or so called **plastic hinges (PHs)**] at the bottom of the first story and that for a global **displacement ductility** (μ_δ) = 1.45, all the beams in the

lower 6 stories developed PHs at their end, the maximum IDI being about 1.5 (occurring at the third story). The rotation ductility (μ_θ) of the beam at this floor under negative bending moment is about 2.9, twice as large as the global μ_δ. The μ_θ at the ends under positive bending moments, particularly where the poorly anchored reinforcing bars pulled out, were even higher. Using the results obtained in the pushover analysis, it was estimated that the maximum lateral load [or maximum **base shear** (V_B)] that the developed model could resist was 0.16W and that under this load the maximum global DI and IDI would be 1.35% and 2.10% respectively. Because the developed inelastic models led to some numerical instability under higher loads, it was decided to revise the models before proceeding with the time history nonlinear dynamic analyses.

Chapter five discusses the modifications introduced to the simplified inelastic models that have been discussed in chapter four. In these new models, the bond slip of beam reinforcement in the joints is modeled explicitly using a zero length bilinear rotational element. In addition to the end rigid zones, each beam is modeled by 5 segments. To avoid the lack of convergency created by modeling the columns as just one element, in the revised models all the columns have middle nodes. The revised refined two models, one assuming a fixed base and the other including basement and foundation flexibility, were used to conduct the analyses of the behavior of the building as built as well as for the different seismic upgrading approaches that have been attempted. While the model with the fixed base has a fundamental period T = 2.5 sec, the model including basement flexibility increases the T to 2.6 sec. By adjusting the axial stiffness of the added elements to consider the possible effects of the foundation rotation, the period was further increased to 3.2 sec, which is the one that was considered to be the most reliable. Two different types of nonlinear analyses were conducted on these refined models: static pushover and time-history dynamic analyses using severe pulse-type EQGMs (idealized as well as recorded).

Chapter six presents and discusses the main results obtained on the behavior of the as-built building. The results of the pushover analysis show that at a roof displacement of 53 in., a convergency problem developed when an increase in load was attempted. Under this displacement, corresponding to a global μ_δ of about 2.9 and to an average DI of about 2.7%, the maximum IDI of 4.3% occurs at the second and third stories. This results in a maximum beam μ_θ of 13.9 that occurs under positive bending moment (tension of the bottom). This indicates that this local μ_θ is about 4.8 times the global μ_δ, contradicting the assumption that is usually made: that these two ductilities may be considered as equal. Comparison of plastic rotation demands

and capacities of the beams as well as at the bottom of the first-story columns shows that the building as built cannot develop a roof displacement of 53 in. Regarding the response of the as-built building to severe pulse-type EQGMs, an analysis of the available recorded EQGMs of this type shows that for a value of T near 3.0 sec, the two most demanding records were those obtained at the Los Gatos station during the 1989 Loma Prieta EQ and at the Takatori station during the 1995 Kobe EQ. The maximum IDI under Los Gatos EQGM was about 5.4%, which is unacceptable. The plastic rotation demands at the first-story column and at the beams were far beyond the available capacities. Thus it was concluded that if this existing building can be subjected to this type of EQGMs, its structure needs to be upgraded. For this purpose, both traditional and innovative methods of upgrading the existing structure were studied to control its response against severe pulse-type EQGMs.

Chapter seven summarizes and discusses the results obtained in the studies conducted to control structural response by using the innovative strategy of increasing the energy dissipation through the addition of supplementary damping. Despite claims in the current literature that the use of damping is not effective for structures subjected to pulse-type excitations, the high intensity and long duration of the ground velocity pulses in this type of EQGMs are worthy of detailed study to determine the degree of effectiveness of increasing the **damping coefficient (ξ)**. To do this, recorded pulse-type EQGMs were idealized and the response of **single-degree-of-freedom systems (SDOFSs)** to idealized EQGMs were then studied by computing the **displacement (S_d)** and the **yielding strength coefficient (C_y)** spectra and normalizing them with respect to the **peak ground velocity (PGV)** and **the duration of the displacement pulse (t_d)**. These normalizing parameters have been demonstrated (through wave propagation analysis) to be very important parameters affecting the response of structures to severe pulse-type EQGMs. From analysis of these normalized response spectra corresponding to fault normal EQGMs, it is concluded that if the period of the structure is close to the duration of the severe ground displacement pulse (say in the range of $0.5 \leq T/t_d \leq 1.2$), increasing ξ could considerably reduce the response of the SDOFSs and therefore of the real structure. For shorter and longer T, the effectiveness in increasing ξ to decrease the response is reduced. The normalized response spectra could be used to find the most critical EQGM for any given structure. Generally speaking, the larger the PGV and the t_d, the larger the lateral displacement will be. However, it is necessary to pay attention to the value of T/t_d and the fact that not always would a larger value of

t_d result in a larger lateral displacement. Another important observation made from the analysis of the normalized C_y spectra is that structures with μ_δ up to 3 and periods up to values that give $T/t_d \leq 0.75$ shall be designed with a yielding strength coefficient C_y equal or higher than the PGA/g. This fact is not properly addressed by present 1997 UBC requirements.

The response of the as-built building, with added damping (i.e., ξ_{eff} = 30%) and considering the foundation and basement flexibility, when it is subjected to the recorded EQGMs at Los Gatos and Takatori stations are presented and discussed in chapter eight. Although the increase in damping from ξ_{eff} = 5% to ξ_{eff} = 30% resulted in a significant decrease in the lateral displacement of the building (about 40%) under the Los Gatos EQGMs, the maximum IDI at the 4th and 5th stories was about 3.2%, still significantly larger than the usually acceptable value of 2%. Even if the drift caused by the rocking of the foundation is excluded, i.e., considering what can be called the maximum IDI_{tang} , this will be about 2.7%. It is also shown in this chapter that the increase in ξ_{eff} led to an increase in the maximum base shear of about 15%, which can be significant.

Chapter nine summarizes and discusses the results obtained in the analyses conducted on the behavior of the as-built building assuming a fixed base and carried out using a static nonlinear pushover analysis under inverted triangular distributed lateral load and then nonlinear dynamic time-history analysis under severe pulse-type EQGMs (Los Gatos and Takatori records). These results are then compared in Table 9.1 with those obtained in chapter eight, assuming flexible foundation and flexible basement, as well as those that have been obtained using the response spectra of the recorded EQGMs. From analysis of the results reported and compared, it can be observed that (1) The lateral displacements obtained from the response spectra at a height equal to 2/3 of **total height (H)** are larger than those obtained from the time-history dynamic analyses, and in some cases the overestimation was on the order of 50%; (2) The response obtained with the fixed-base model results in somewhat higher IDI_{max} (under Los Gatos 6.1% vs. 5.4% for ξ_{eff} = 5% and 3.1% vs. 3.2% for ξ_{eff} = 30%; (3) The values of the IDI_{max} and even those of the IDI_{tang} exceeded the usually acceptable value of 2.0% and even the value of 2.5%; (4) The ratios between the IDI_{max} /IDI_{ave} were larger than 1.5 and reached values up to 1.8; (5) The increase in ξ from 5% to 30% contributes significantly to smooth the distribution of the values of the IDI_{max} along the height of the building, and for the case of the response to the Takatori EQGM, the location of the story at which the IDI_{max} occurs is changed from the 10th story to the

5th story; and (6) In spite of the fact that for ξ_{eff} = 30%, there is significant reduction in response demands that still exceed the capacities available at the critical regions (weaknesses) of the as-built structure.

In view of the last observation made above, it becomes clear that even if the innovative strategy of increasing ξ_{eff} up to 30% is used, it will be necessary to increase somewhat the stiffness and strength of the members, and particularly the toughness of the critical regions of the as-built structure. Thus it was decided to conduct studies to answer the following two questions: (1) Can the as-built structure be seismically upgraded in an efficient way just by using the traditional strategy of increasing the stiffness, strength, and ductility (i.e., the toughness) by steel jacketing the beam-column joints and columns and encasing the girders and part of the slabs with steel plates? and (2) Would it be technically and economically better to use a proper combination of the innovative strategy of increasing ξ_{eff} and of the conventional strategy of using steel jacketing and encasement? Chapter ten presents and discusses the results obtained in the analyses conducted to answer the first question and throws light on answering the second question. After several preliminary attempts, it was decided to use ½-in. thick enhancement steel plates for all the columns. The same plate thickness (½-in.) was used for the second-floor beams, then the thickness was gradually decreased down to 3/16 in. at the 14th floor (roof). Two analytical models, one with a fixed base and the other including foundation and basement flexibilities, were developed and subjected to static nonlinear pushover and dynamic (spectral response and time history) analyses. These analyses show that using ½-in.-thick steel plates and ξ_{eff} = 5% led to a soft first-story mechanism that for the Los Gatos fault normal EQGM demanded an IDI_{max} of about 3.4%, which is unacceptable. Thus the ½-in. steel plate at the first-story column was replaced by a 1.0-in. plate. From analysis of the results obtained and summarized in Table 10.1, the following observations can be made: (1) The fundamental T of the as-built building has been reduced from about 3.2 sec to 2.3 sec, if the flexibility of basements and foundations are included, and from 2.6 sec to 1.3 sec for the fixed-base model; (2) Under Los Gatos EQGM and for ξ_{eff} = 5%, the IDI_{max} varies from an unacceptable 3.8% when a flexible base is assumed, to an acceptable 1.7% for a fixed base; (3) Under the Takatori EQGM for a fixed-base model and ξ_{eff} = 5%, the IDI_{max} is 2.8% (unacceptable); and (4) The $(V_B)_{max}$ for ξ_{eff} = 5% is 58%W for a flexible-base model and 66%W for a fixed-base model.

In view of the above unacceptable demanded values, particularly the very high V_{Bmax} (58% to 66%W) that would lead not only to an uneconomical superstructure, but would also require upgrading the basements and foundation, it was decided to study whether using ξ_{eff} = 30% instead of ξ_{eff} = 5% would lead to a better response and a significant reduction of the demanded V_{Bmax} . The steel jacketed and encased models wre analyzed again using ξ_{eff} = 30%. The results obtained show that: (1) The IDI_{max} were reduced to acceptable values (1.8% for the flexible-base model and 1.5% for fixed-base); and (2) While the V_{Bmax} was reduced to 35%W for the flexible-base model, which might be acceptable, for the fixed-base model the V_{Bmax} was increased from 66% to 71%W. Since this value is unacceptable, it was decided to try the following new combination of the conventional and innovative strategies: To use the thinnest practical steel plates to remove the weaknesses of the as-built RC frame that were due to the poor amount and detailing of the reinforcement, and then to add supplementary damping to increase the ξ_{eff} from 5% to 30%.

Chapter 11 presents and discusses the results of the analyses conducted on the models of the building that have been obtained by using 1/8-in.-thick steel plates and ξ_{eff} = 5% and ξ_{eff} = 30%. The results show that a soft first story is developed that lead to unacceptable IDI at this story. To avoid the weak-column strong-beam mechanism at this first story, the first-story column steel plate was increased from 1/8 in. to ¼ in. Introducing this change in the models, their behaviors were analyzed and the results summarized in Table 11.1 that indicates the following: (1) The fundamental T for the model that includes the flexibility at the base is 2.6 sec, i.e., an increase of 13% of the T for the heavily jacketed model; (2) The IDI_{max} under Los Gatos for ξ_{eff} = 30% was 2.1% and the corresponding IDI_{tang} was 1.4%, both acceptable values; (3) The V_{Bmax} was 34%W, also an acceptable value; and (4) If supplemental ξ_{eff} is not provided, i.e., for ξ_{eff} = 5%, the demanded IDI_{max} by Los Gatos EQGM would be 4% and its corresponding IDI_{tang} of 3.3% could result in damage too severe (unacceptable) to the nonstructural components and contents of the building.

In chapter 12, after a brief summary of the weaknesses of the existing building and of the strategies to seismically upgrade it, the following main conclusions are offered: (1) The conventional strategy of increasing the stiffness, strength, and ductility (toughness) of the as-built structure will not lead to an efficient economical solution because it leads to a significant increase in the stiffness and strength demands; (2) Because of the observed weaknesses of the

existing as-built structure, it was clear that no matter what upgrading strategy was used, it was necessary first to use the traditional strategy of increasing the toughness of the critical regions of the structure using what appeared to be one of the most promising techniques — the use of steel jacketing and/or encasement of the members (at least in their critical regions) by using the minimum practical steel plate thickness; (3) Once this increase in toughness was achieved, it was necessary to control the demands by using an efficient innovative approach that for this particular structure appeared to be the use of energy-dissipation devices that increased its effective damping ξ_{eff} up to about 30% in order to control the response to the probable severe near-field EQGMs that could occur at the site of the building; (4) From the analysis of idealized and recorded severe pulse-type near-field EQGMs and of their effects on the response of the nonlinear models of the building structure, it became clear that an increase of the ξ_{eff} from 5% to 30% could decrease the demanded IDI_{max}, the IDI_{tang}, and the nonlinear (inelastic) deformations by at least 40%; and (5) Although the increase in ξ_{eff} could lead to an increase in the V_{Bmax} , this does not seem to be significant. However, the reliability of the classical procedure used in estimating the shear forces due to ξ is questionable.

Recommendations for further research are also formulated in chapter 12, the main ones being the following: (1) To investigate how the increase in ξ_{eff} from 5% to 30% can be attained efficiently in the field, i.e., how many dampers are needed and where they should be located in the total structural system; (2) To study how these needed dampers will be supported, i.e., to design what can be called the secondary structure; (3) To investigate how the dampers can be interconnected with the main existing structural system (primary structure) and the secondary structure; (4) To study how the dynamic characteristics of the primary structure are modified by the addition of the secondary structure and the dampers; and (5) To study what would be the response of the new upgraded structural system to the critical EQGMs that could be expected in the future, with particular emphasis on the effects on the total story shear as well as on the effects on the shear and axial forces of the primary structure columns, i.e., the existing columns.

ACKNOWLEDGMENTS

This report is based on the studies conducted on a PEER research project which was conducted at the PEER Center.

Most of these studies were conducted by Mr. Mehrdad Sasani, a graduate student of Structural Engineering, Mechanics and Materials of the Department of Civil and Environmental Engineering, University of California, Berkeley. The project was supervised by Professors Vitelmo V. Bertero and James C. Anderson who wish to acknowledge the valuable typing assistance and editing and provided by Barbara Mauk and Janine Hannel.

This work was supported in part by the Pacific Earthquake Engineering Research Center through the Earthquake Engineering Research Centers Program of the National Science Foundation under Award number EEC-9701568. This research project would not have been possible without the financial assistance of PEER and this support is gratefully acknowledged.

CONTENTS

1 Introduction

1.1 OBJECTIVES AND SCOPE

The main objective of the project reported herein has been to develop a general seismic rehabilitation and upgrading approach centered on the use of a steel jacket placed around the joints of existing nonductile reinforced concrete (RC) moment frame buildings. The jacket can include a bracket steel plate to allow the attachment of diagonal steel bracing and/or supplementary energy-dissipation devices. Also beam enhancement plates and column enhancement steel plates or fiber wrapping can be used.

After reviewing the drawings and information available on several existing RC buildings having nonductile RC moment-resisting frames (M-RF), a 15-story instrumented building was selected for carrying out the assessment of its seismic behavior in order to identify its main weaknesses. In chapter one the performance of the building during past earthquakes is studied. A calibrated linear model of the building is developed in chapter two, and the global and story vulnerability of the building is studied by finding the strength and deformation demand-capacity ratios under UBC-97 spectra. The local vulnerability of the bottom stories is studied in chapter three, incorporating limit analysis and the capacity procedure. Both the strength and deformation demands and capacities of beams, columns and joints are examined. In chapter four, the development of two inelastic models of the structure in the transverse direction for conducting nonlinear static pushover analysis and also nonlinear dynamic analysis under severe pulse-type of **earthquake ground motions (EQGMs)** are discussed in detail. Utilizing the results from the pushover analysis of the inelastic model, the limiting factors on the performance of the building could be found. Chapter five describes the modifications that were introduced in the inelastic models, discussed in chapter four, to eliminate some numerical instabilities that resulted using

such models. The revised and refined two models, one assuming a fixed base and the oth considering the flexibility of the foundation and the two levels of the basement, are used conduct the analyses of the behavior (response) of the as-built building structure. Chapter s presents and discusses the main results obtained in the as-built structure.

Chapter seven summarizes and discusses the main results obtained in the studi conducted regarding the possibility of controlling the response of the structure through the use the innovative strategy of dissipating large amounts of the seismic energy input by the additi of supplementary damping. Chapter eight presents and discusses the results obtained on tl response of the flexible-base model with supplementary damping that increases the ξ_{eff} from 5 to 30% when this model is subjected to the near-field EQGMs recorded at Los Gatos ar Takatori stations. Chapter nine summarizes and discusses the results obtained in the studi conducted on the nonlinear seismic behavior of the inelastic as-built structure model with a fix base using a static nonlinear pushover method and then nonlinear dynamic time-history analys as well as the response spectra methods of recorded EQGMs at near-field stations.

Chapter ten describes the studies conducted to answer the following question: Can the a built structure be seismically upgraded in an efficient way by using only the traditional strate of increasing its stiffness, strength, and ductility (toughness) through the technique of jacketir and/or encasing its members with steel plates? Chapter 11 summarizes and discusses the resul obtained in the analyses conducted by upgrading the as-built model with a flexible base using combination of a traditional strategy (based on jacketing and encasing its members with tl thinnest practical steel plates) and an innovative strategy (based on controlling the seism response demands by supplementary damping). Finally, chapter 12 presents a summary of tl studies, results, and conclusions, followed by recommendations for future work needed f seismically upgrading existing nonductile RC frame buildings.

1.2 DESCRIPTION OF BUILDING

The building selected for conducting the studies described herein is a 15-story reinforc concrete (RC) building designed in 1964 under the requirements of the Los Angeles Ci Building Code. The building was constructed in 1965. As described and illustrated by Blun (1973), the lateral resisting system for the 13 stories above the first floor at grade is a fran structure with beams spanning 27 ft longitudinally and 32 ft transversely. The building has typical story height of 11 ft 9 in., except for the first story, which is 23 ft 6 in.. Two stories belo

the ground level are enclosed by structural walls. The foundation of the building consists of concrete 34-ft-deep piles. The soil is recent alluvial deposit and is generally only moderately firm with soft layers at varying depth. The columns are made of normal weight concrete while lightweight concrete is used in the beams above the ground floor. The foundation plan, a typical plan, and the roof framing system at the 2nd and 14th floors are given in Figures 1.1 and 1.2, respectively. Figure 1.3 shows the east elevation of the building and a typical transverse section is given in Figure 1.4. After the 1971 San Fernando earthquake, the building was instrumented with 15 accelerometers.

1.3 SUMMARY OF OBSERVED AND RECORDED PERFORMANCE OF BUILDING DURING PAST EARTHQUAKES

1.3.1 1971 San Fernando Earthquake

As discussed by Blume (1973), the building was located approximately 17 miles south of the epicenter of the 1971San Fernando earthquake. The four corner columns suffered some damage at the first and second stories, see Figures 1.5 to 1.8. Some spandrel beams also experienced cracking at the second floor. At the second floor level, the top and bottom spandrel beam reinforcement did not extend as far into the corner columns as indicated on the design drawings, Figure 1.9a (Blume, 1973). This situation is reported to have been corrected above the second floor. The situation at the corner joints at the second floor level were corrected by a scheme that consisted of drilling a longitudinal hole down the axis of the spandrel and threading post-tensioning tendons into the hole, Figure 1.9b. A short structural wall below the grade also experienced some minor diagonal cracks. Drywall partitions shifted and buckled on the second floor.

1.3.2 1994 Northridge Earthquake

Observed Damage. As reported by Naeim (1997), the building was located at an epicentral distance of about 6 miles during the January 17, 1994, earthquake. Some cracking to the RC walls and also beams, columns and slabs was observed at the basements. Also moderate damage to beam-column connections was reported. Based on ATC 13 (1985), the damage to nonstructural elements was slight (0% to 1%), the structural damage was light (1% to 10%), and the damage to the content of the building was moderate (10% to 30%). No damage to mechanical systems was reported.

Recorded Damage. The 15 installed accelerometers are mounted at different locations, Figure 1.10. Figure 1.11 shows the ground motion recorded at the second basement in the N-S direction (transverse direction) and Figure 1.12 shows the corresponding spectra. Also Figures 1.13 and 1.14 show the ground motion and the corresponding spectra recorded at the second basement in the E-W direction (longitudinal direction). The time history of the motion at the roof level and at the ground level in the N-S direction are given in Figures 1.15 and 1.16, respectively. Similar plots for the motion in the E-W direction are given in Figures 1.17 and 1.18. Comparing Figure 1.11 with Figure 1.16 and also Figure 1.13 with Figure 1.18, the velocity and displacement time histories are almost the same at the second basement and at the ground level. However, the acceleration time histories are not so similar.

Although the Peak Ground Displacement (PGD), Peak Ground Velocity (PGV), and Peak Ground Acceleration (PGA) in the N-S direction are all larger than those in E-W direction, the maximum displacement at the roof level in the E-W direction is equal to 13.5 in., which is almost twice as much as that in the N-S direction with a top displacement of 7.3 in. (Figures 1.15 to 1.18). This has been attributed to stronger long-period harmonic motion recorded at the second basement and also at the ground level in the E-W direction around 35 sec with a period close to the period of the building, discussed in more detail below.

In modal analysis, if the mode shapes are all normalized to one at the top, the modal participation factor (MPF) of the first mode of vibration is larger than that of higher modes. For this building, based on the model developed in chapter 2, the ratio between MPF in the first mode and that in the second mode is about 2.7 in the transverse direction and 3.0 in the longitudinal direction. Also the displacement spectrum ordinate for the first mode is usually larger than that of the higher modes. In calculating the top displacement using the SRSS (Square Root of Sum of Squares) method, the squared value of the multiplications of the modal participation factors and the spectral displacement corresponding to different modes show the relative contribution of different modes in the top displacement. Thus, the displacement at the top of a structure is mainly controlled by the response of the first mode of vibration (Sasani, 1997).

Figures 1.15 and 1.17 imply "apparent" periods of about 3.2 sec and 3.0 sec in the transverse and longitudinal directions, respectively, during the Northridge earthquake. Figures 1.19 and 1.20 show the displacement response spectra of the ground motion in the N-S and E-W directions, respectively. The ordinate of the displacement response spectra corresponding to the

apparent first periods of the structure in the N-S and E-W directions are 5.6 and 9.7 in. (Figures 1.19 and 1.20). In other words, the ratio of the spectral displacement at the first mode in the E-W direction to that of the N-S direction is about 1.73. This ratio is comparable to the ratio of the recorded top displacement in two directions, which is about 1.85.

Utilizing the recorded motions at the ground floor, second and eighth floors and also at the roof, cubical interpolations are used to calculate the profiles of the displacement, story drifts, story forces and shears (Naeim, 1997). The lateral displacement at the time of the maximum top displacement in the N-S and also the E-W directions are given in Figures 1.21 and 1.22, respectively. Note that for some reason the maximum roof displacement in the N-S direction given in Figures 1.15 and 1.21 are not the same. Figures 1.23 and 1.24 show the story drift ratio at the time of maximum displacement in the N-S and the E-W directions, respectively. As shown, the maximum drift in the N-S direction is about 0.55% and occurs at the sixth story, while the maximum drift in the E-W direction is about 1.1% and occurs at the first story. The story shears at the time of maximum base shear in the N-S and E-W directions are given in Figures 1.25 and 1.26, respectively. The maximum base shear in the N-S direction is about 18.5% of the total weight of the building, while this value in the E-W direction is only about 7.5% of the total weight of the building. In other words, the maximum base shear in the N-S direction is about 2.5 times that in the E-W direction, while the maximum top displacement in the N-S direction is only about 0.54 times that in the E-W direction. A discussion on the comparison between the response of the building in two directions is given in section 2.1.

1.3.3 Discussion

As discussed above, the period of the building in two directions is about 3 sec. Also, as shown in Figure 1.11, 1.13, 1.16, and 1.18, because of having moderately firm soil with soft layers, the ground motion has a large period of about the period of the building. Therefore, had the building undergone a stronger long-period harmonic type of ground motion, or experienced a severe-pulse-type of ground motion of long duration, particularly with a short rising time, the lateral displacement could have been much larger. In other words, this flexible structure at a site with long-period dynamic characteristics calls for increasing the stiffness of the structure to prevent possible damage not only to the nonstructural elements and the content of the building but also to the structure itself.

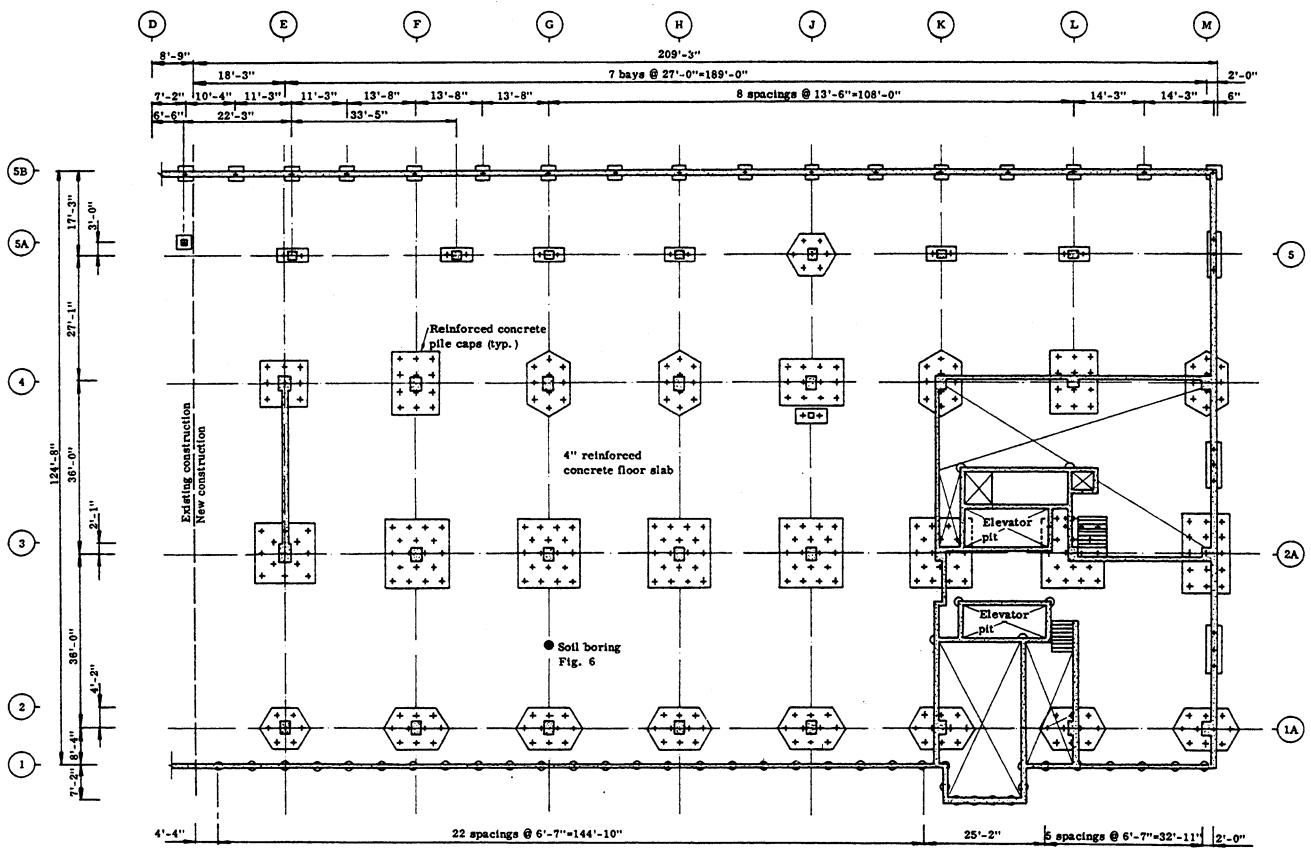

Figure 1.1(a) Foundation plan (After Blume, 1973).

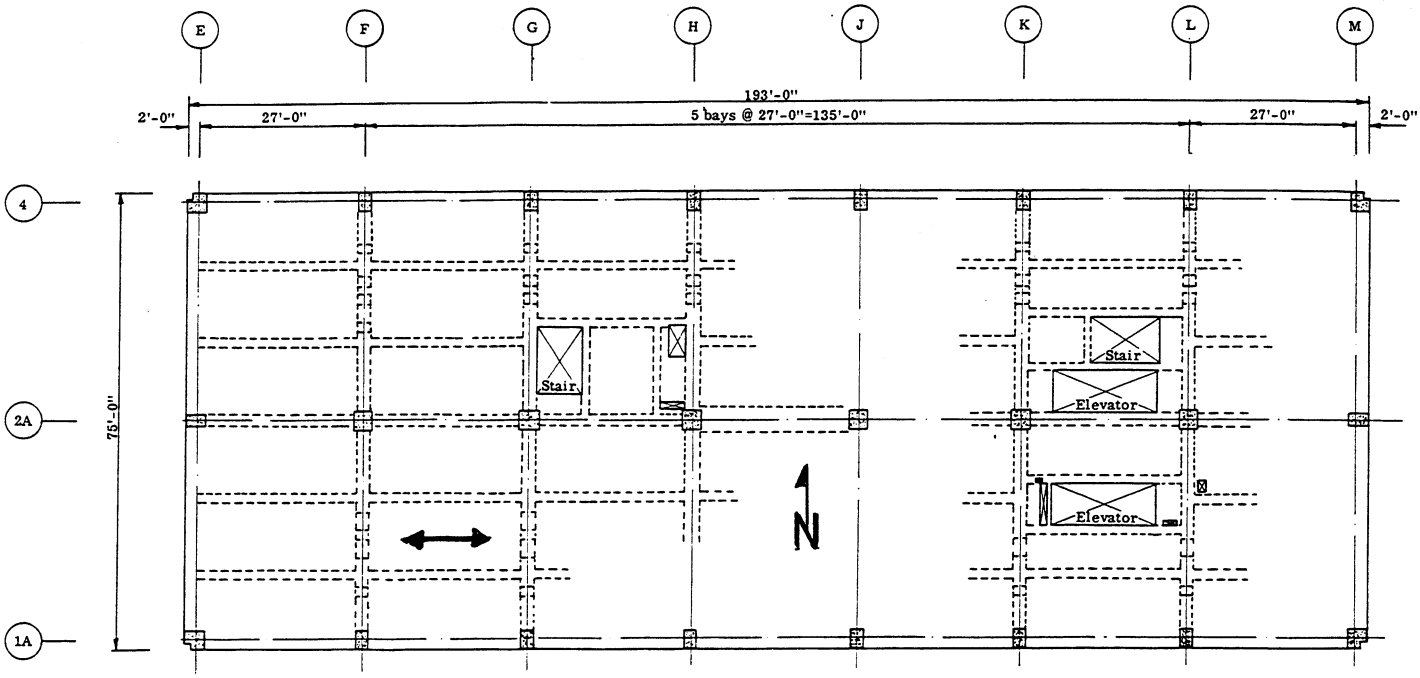

Figure 1.1(b) Typical floor-framing plan (After Blume, 1973).

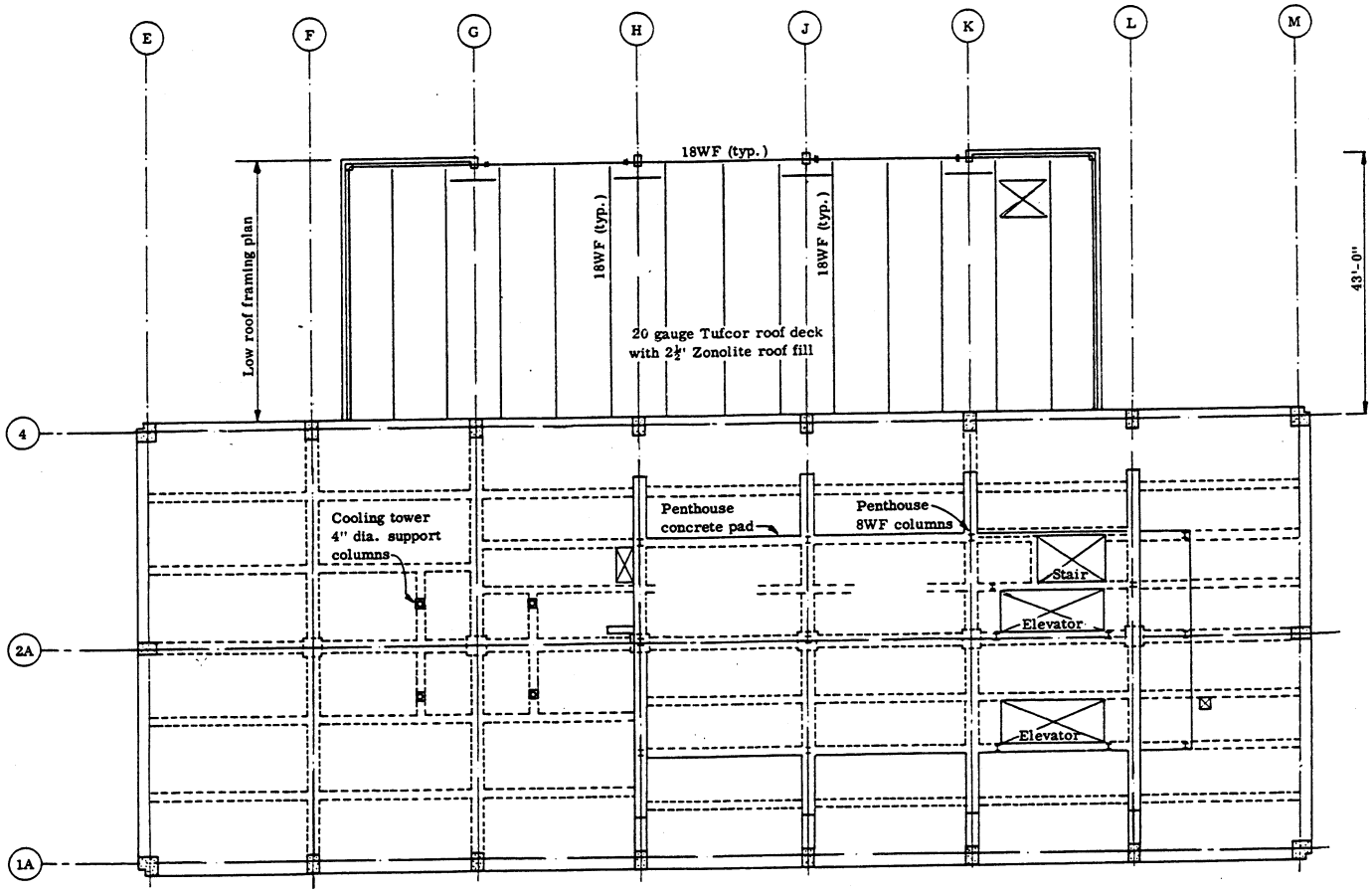

Figure 1.2 Roof framing plan at the 2nd and 14th floors (After Blume, 1973).

Figure 1.3 East elevation (After Blume, 1973).

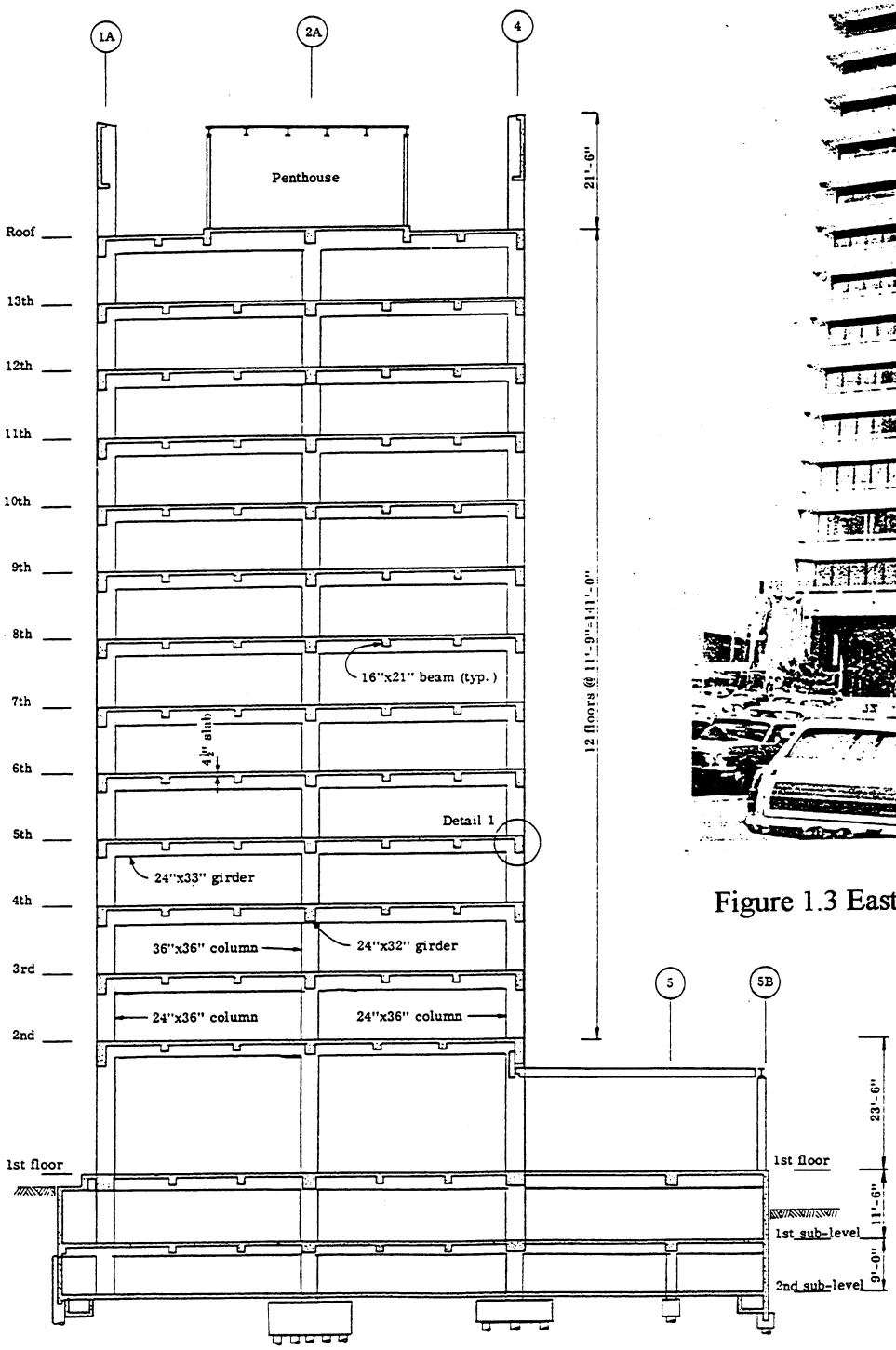

Figure 1.4 Typical transverse section (After Blume, 1973).

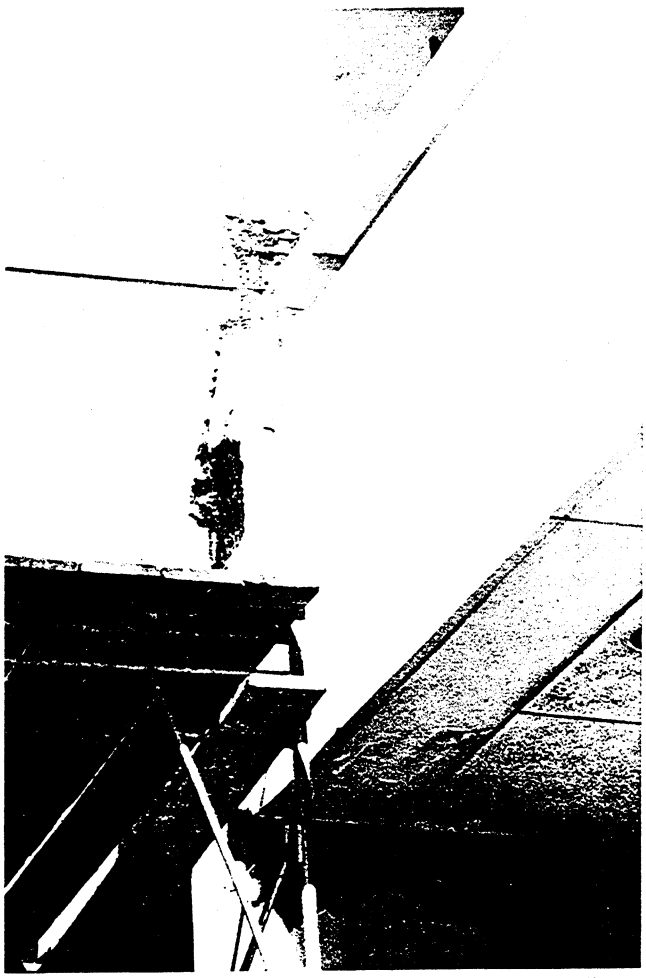

Figure 1.5 Southwest corner column at second floor (After Blume, 1973).

Figure 1.6 Southeast corner column at second floor (After Blume, 1973).

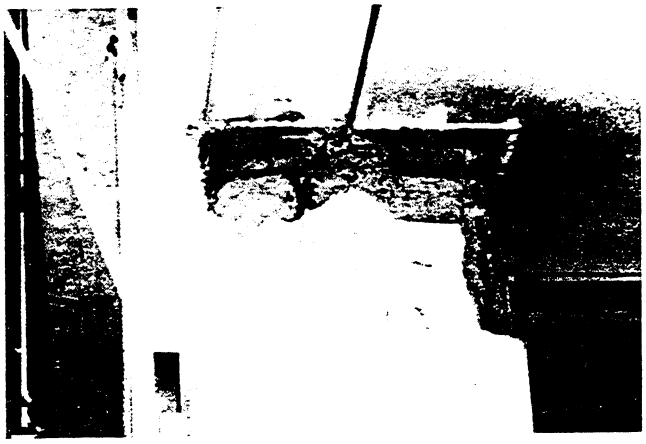

Figure 1.7 East face of southwest corner column at second floor (After Blume, 1973).

Figure 1.8 Southwest corner column at second story (After Blume, 1973).

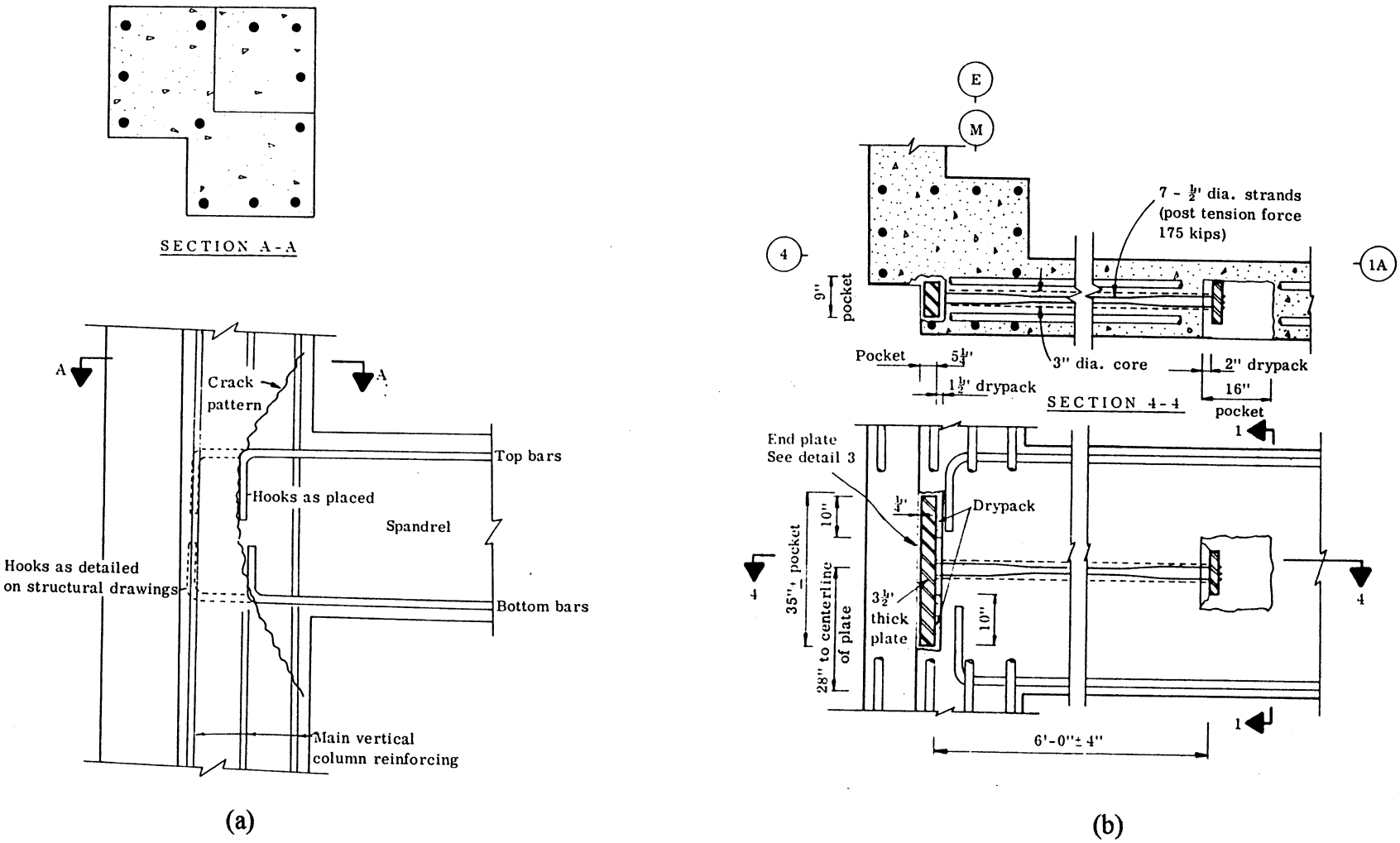

Figure 1.9 Second-floor corner column spandrel connection: (a) before repair and (b) after repair (After Blume, 1973).

SHERMAN OAKS - 13 STORY COMMERCIAL BLDG.

(CSMIP STATION NO. 24322)

SENSOR LOCATIONS

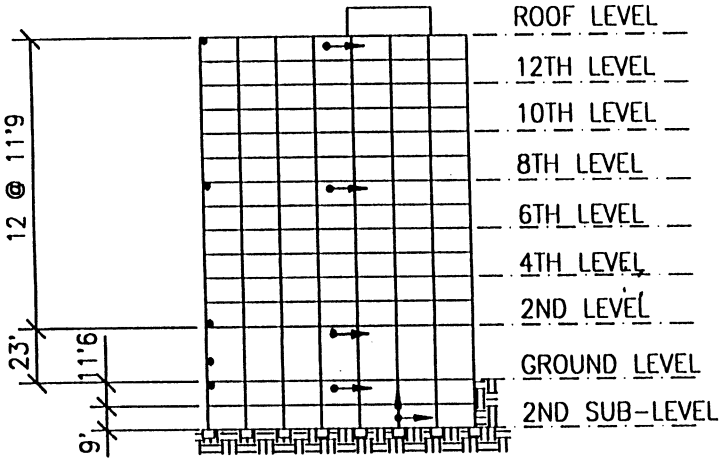

W/E ELEVATION

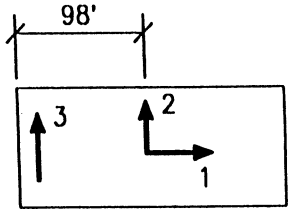

ROOF PLAN

N REF

STRUCTURE REFERENCE
ORIENTATION: N=15°

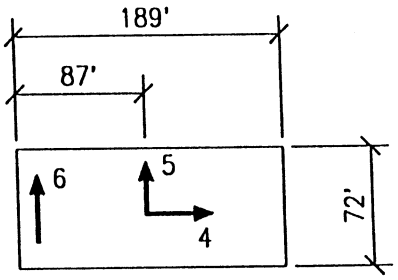

8TH FLOOR PLAN

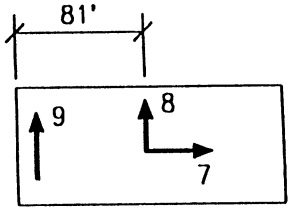

2ND FLOOR PLAN

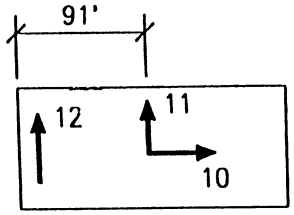

GROUND LEVEL

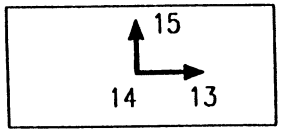

2ND SUB-LEVEL PLAN

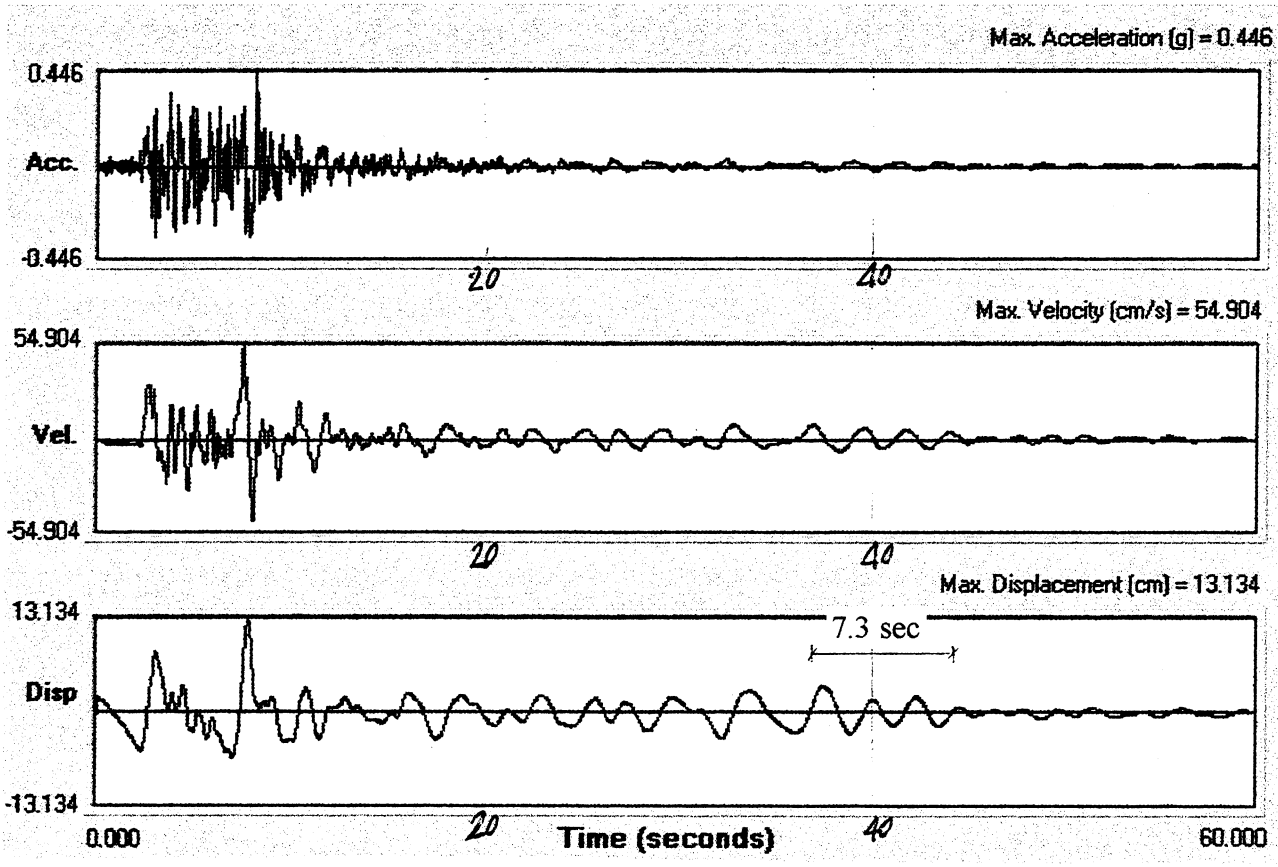

Figure 1.11 Ground motion at the second basement in the N-S direction.

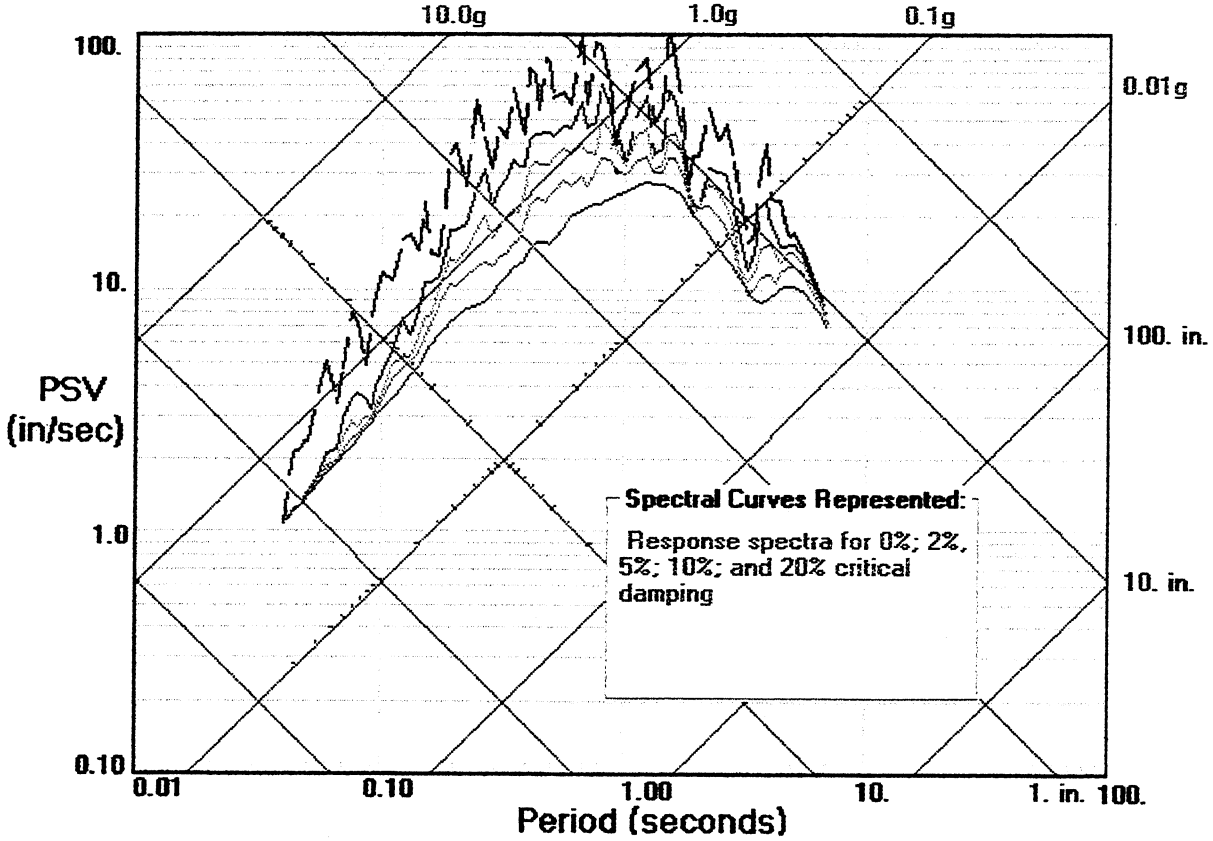

Figure 1.12 Response spectra of the record at the second basement in the N-S direction.

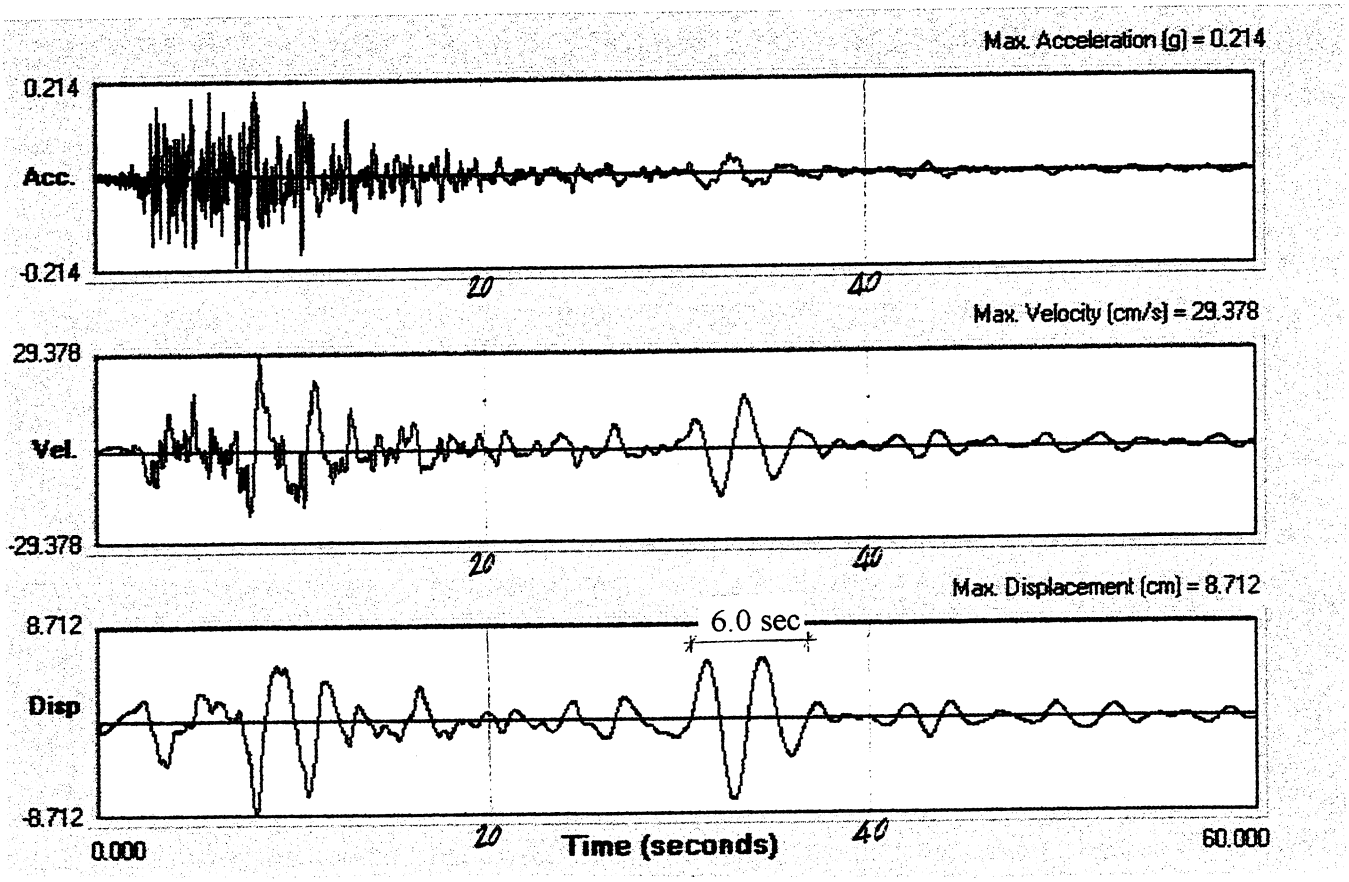

Figure 1.13 Ground motion at the second basement in the E-W direction.

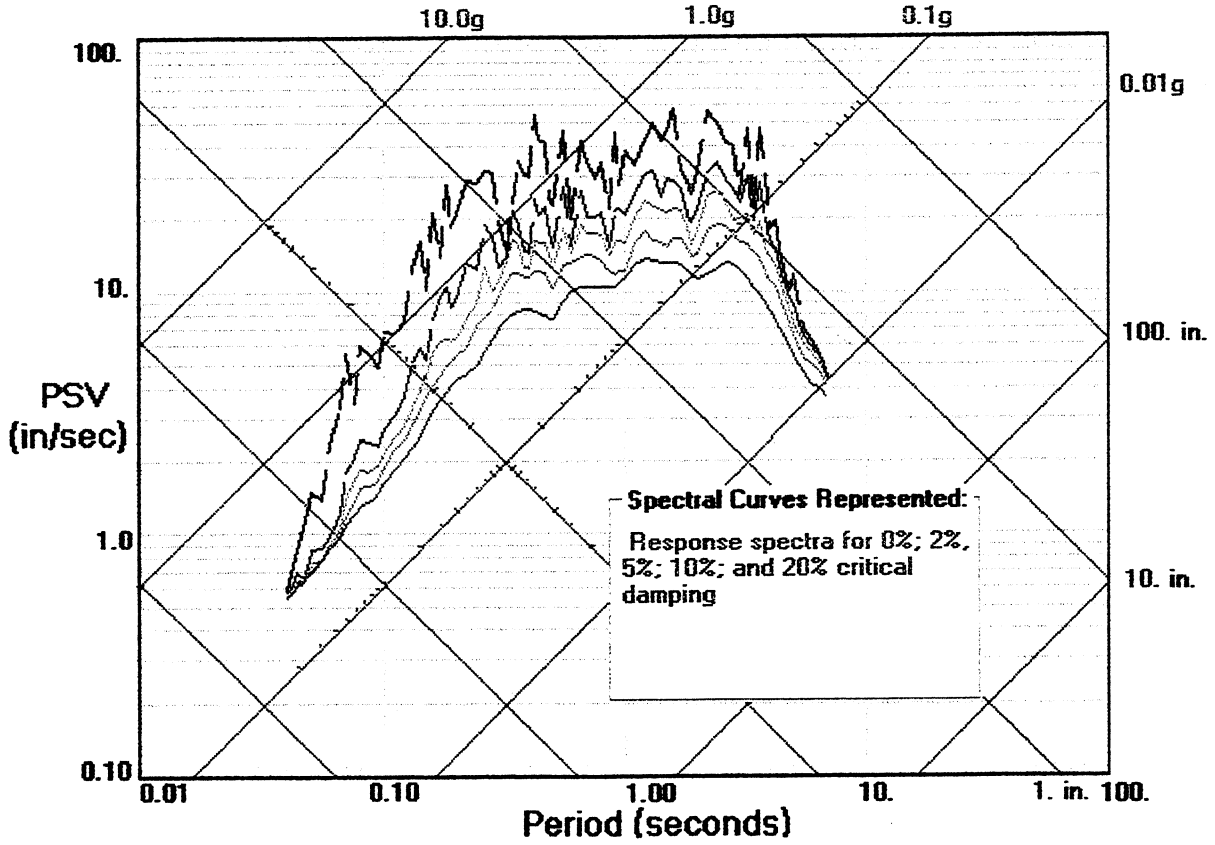

Figure 1.14 Response spectra of the record at the second basement in the E-W direction.

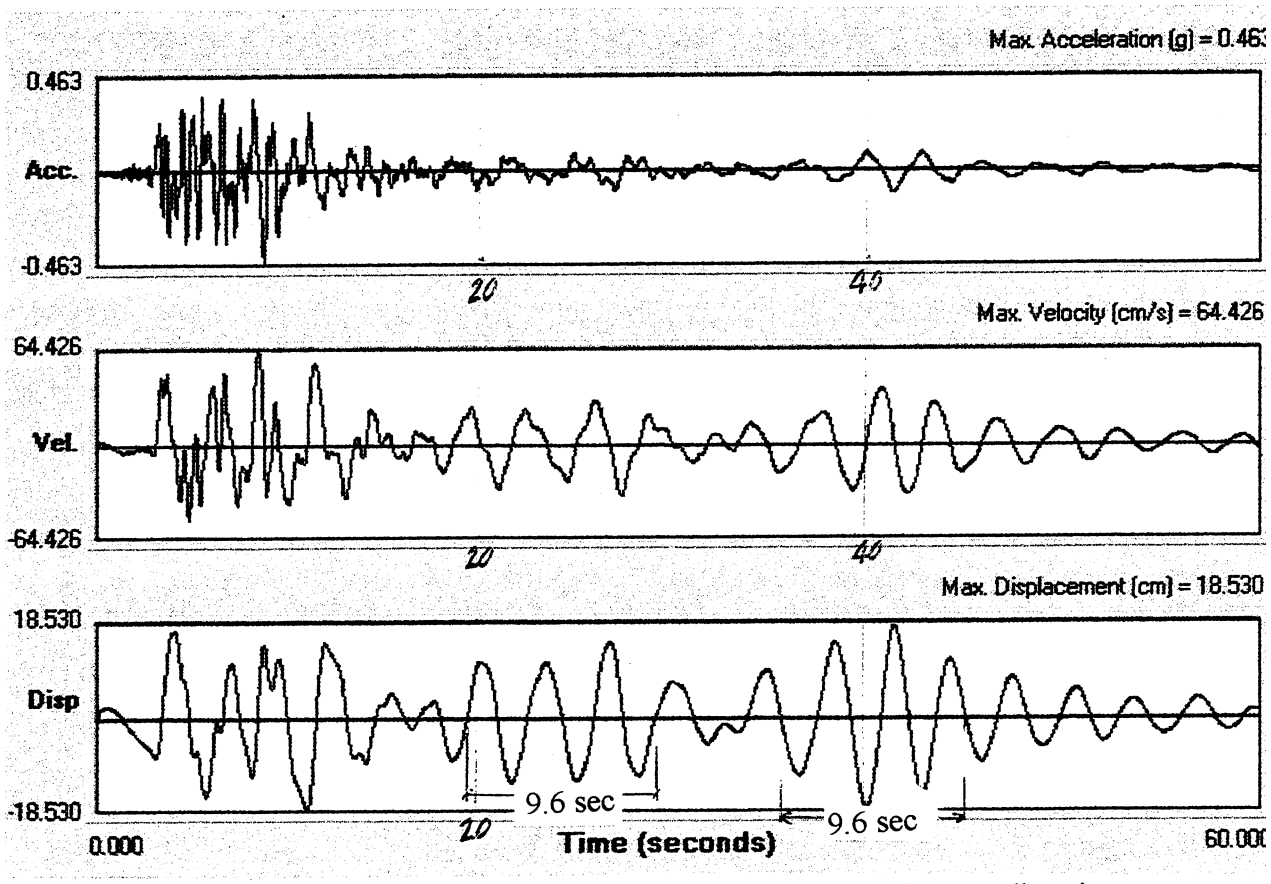

Figure 1.15 Time history of the motion at the roof level in the N-S direction.

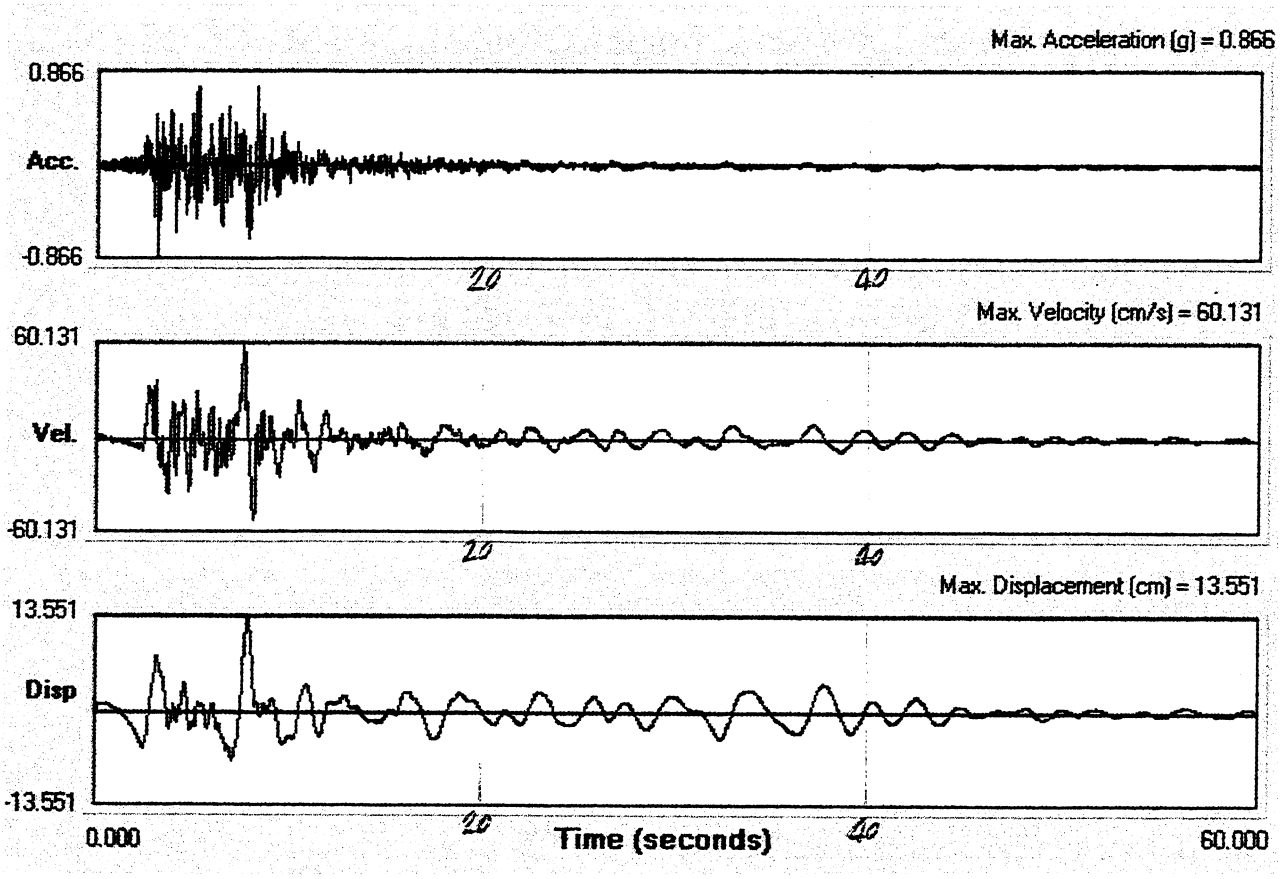

Figure 1.16 Ground motion at the ground level in the N-S direction.

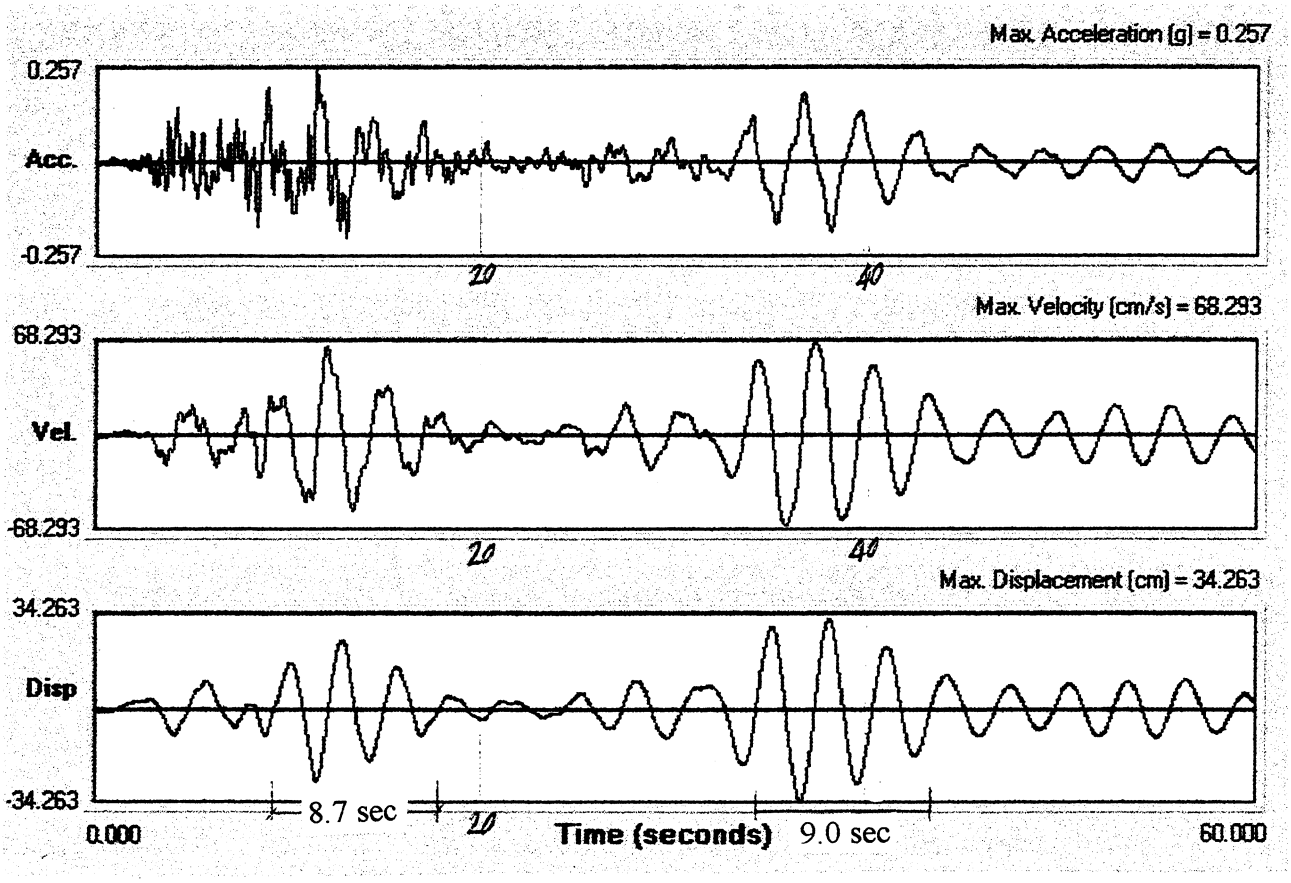

Figure 1.17 Time history of the motion at the roof level in the E-W direction.

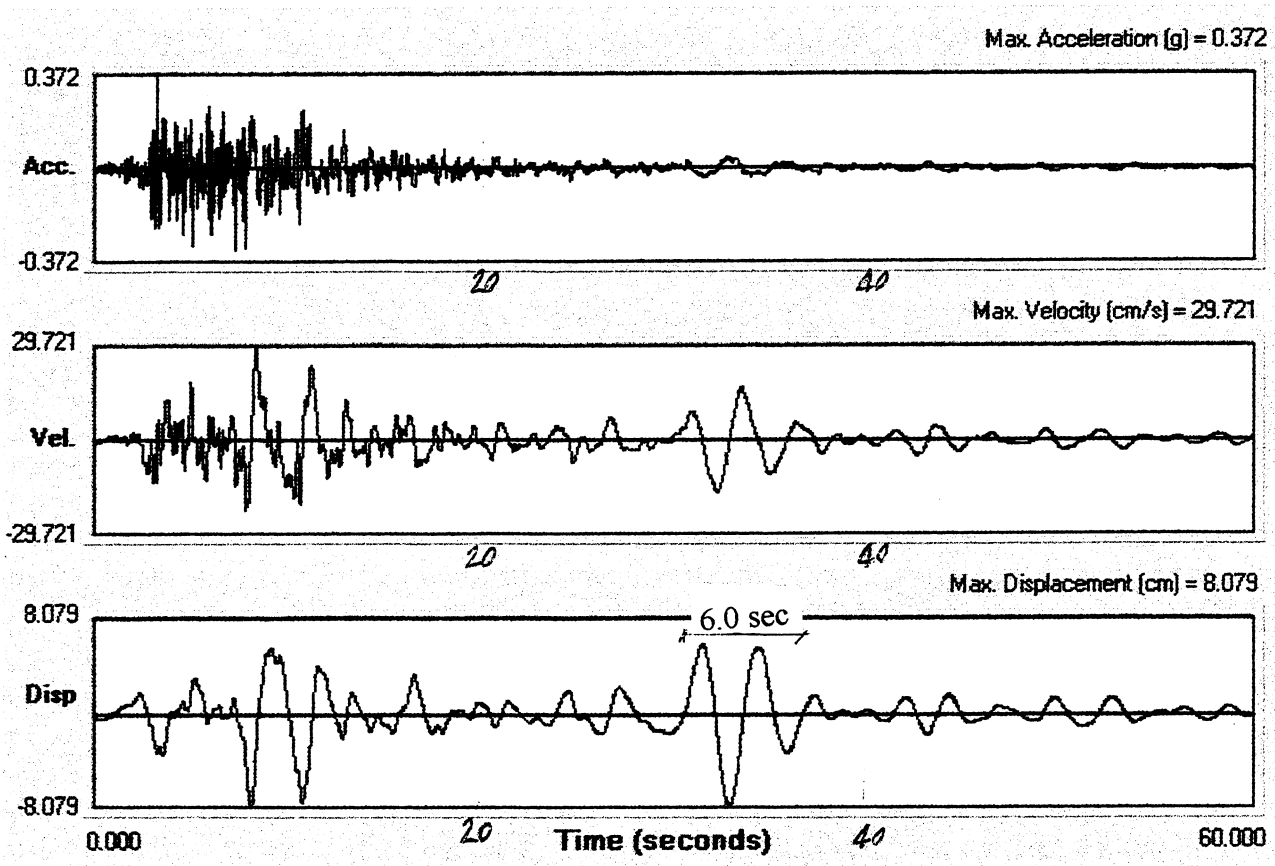

Figure 1.18 Ground motion at the ground level in the E-W direction.

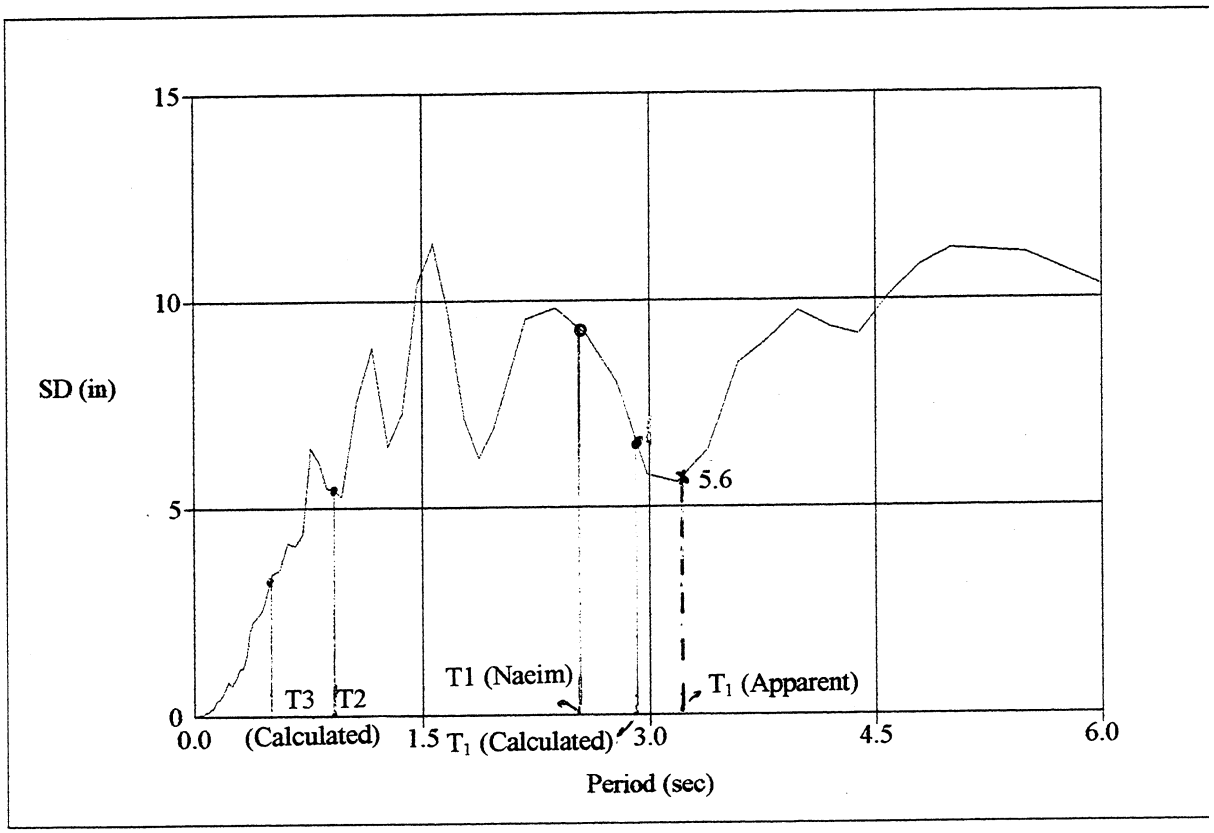

Figure 1.19 The displacement response spectra in N-S direction (5% damping).

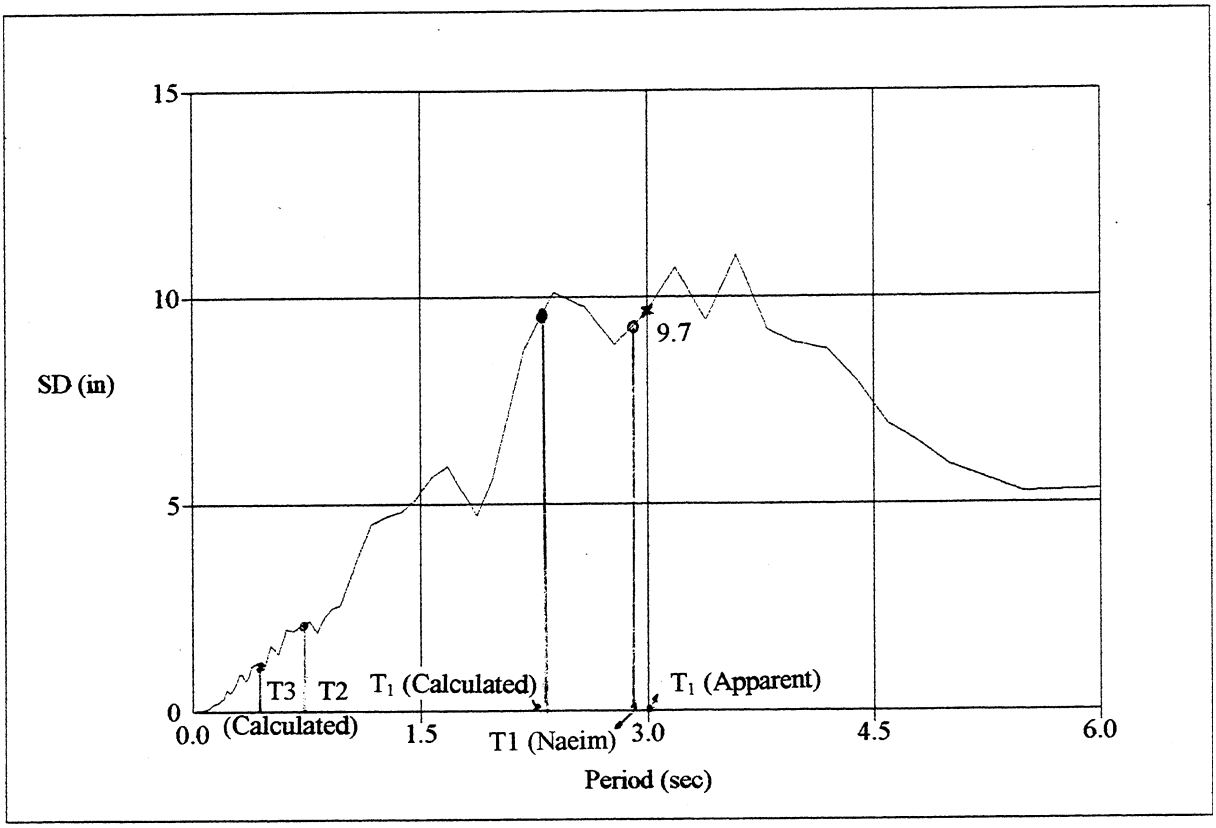

Figure 1.20 The displacement response spectra in E-W direction (5% damping).

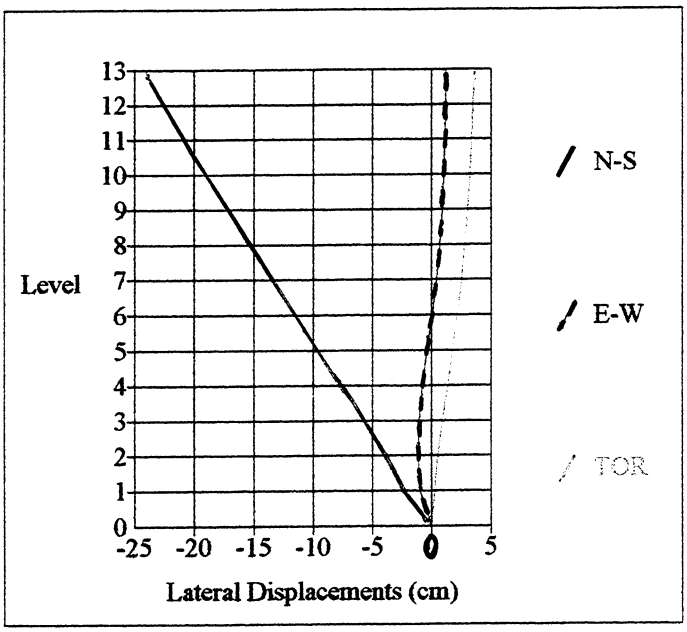

Figure 1.21 Lateral displacement at time of maximum displacement in N-S direction (t=10.86 sec.)

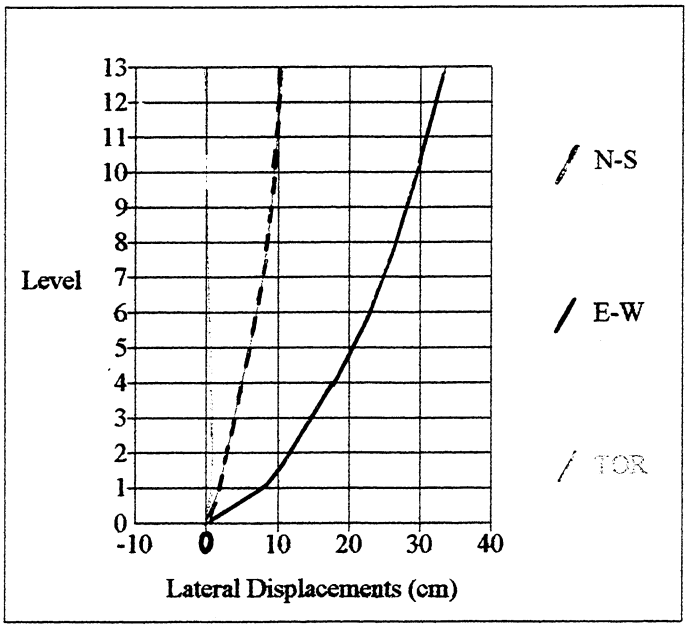

Figure 1.22 Lateral displacement at time of maximum displacement in E-W direction (t=37.98 sec.)

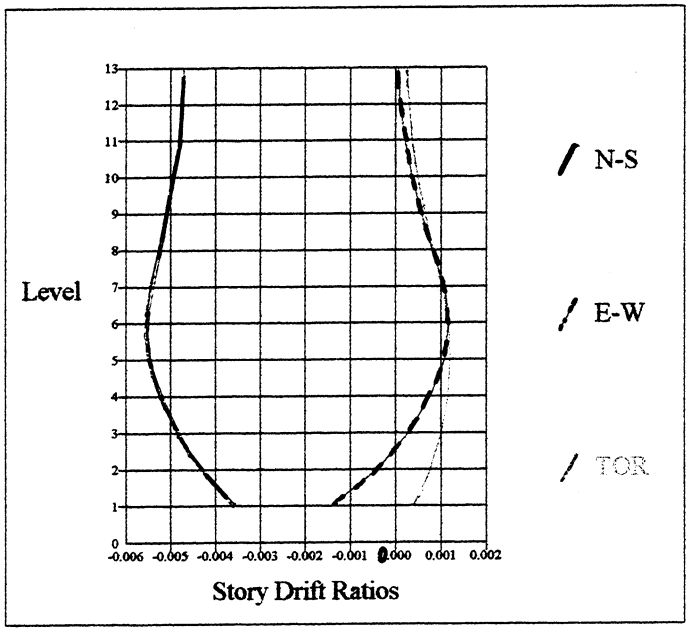

Figure 1.23 Story drift ratio at time of maximum displacement in N-S direction (t=10.86 sec.)

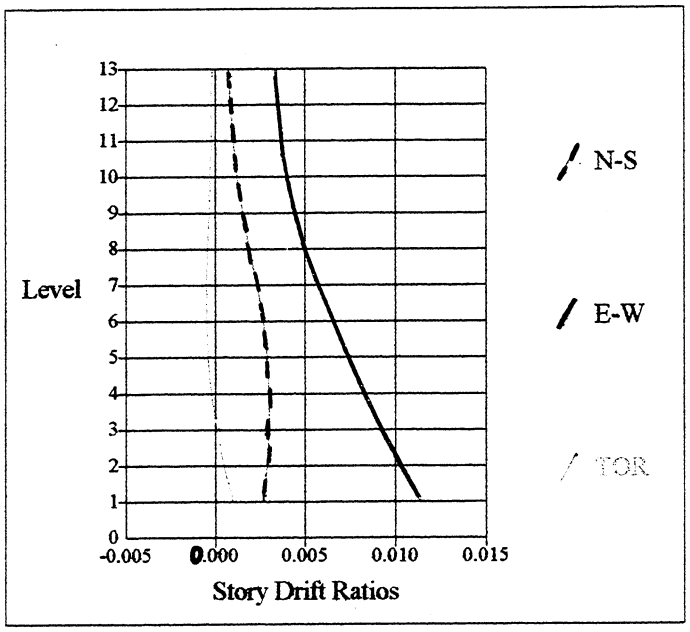

Figure 1.24 Story drift ratio at time of maximum displacement in E-W direction (t=37.98 sec.)

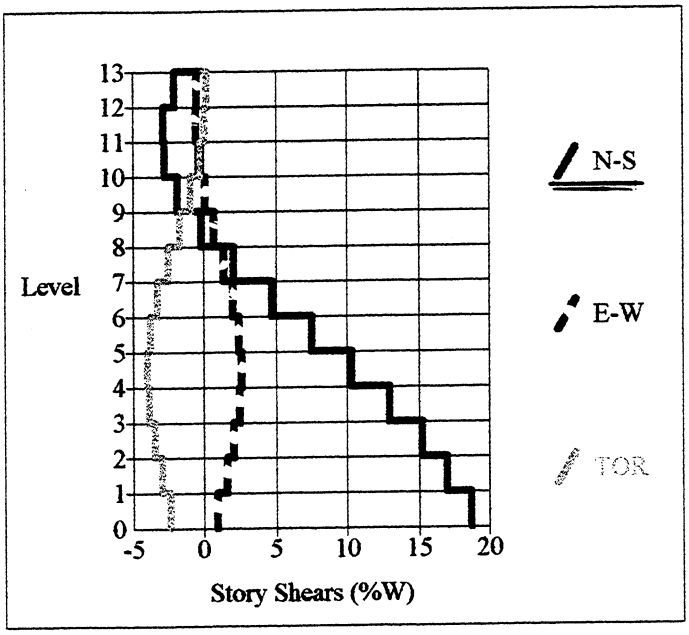

Figure 1.25 Story shear at time of maximum base shear in N-S direction (t=5.14 sec.)

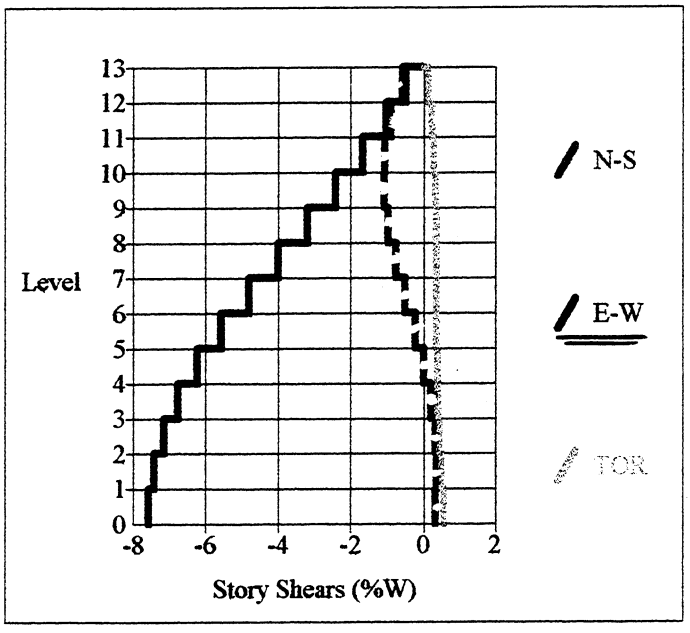

Figure 1.26 Story shear at time of maximum base shear in E-W direction (t=12.72 sec.)

2 Linear Dynamic Analyses (Global and Story Vulnerability)

2.1 THREE-DIMENSIONAL MODEL OF STRUCTURE

Using the computer program SAP2000 (1998) a three-dimensional linear model of the structure is developed. Because the basements are enclosed by RC walls, only the model of the structure above the ground level is studied as representative of RC frame structures. An isometric view of the SAP model is given in Figure 2.1. The accidental torsion is included. In each direction first four modes of vibration are considered. The percentage of the effective modal mass included is more than 98% in each direction. Note that the mass of the penthouse and the perimeter walls above the roof are added to the mass of the roof . Also the mass of the attached one-story building, which does not have a lateral force resisting system, is added to the mass of the second floor. Based on the ACI 318-95 (1995) recommendations, the flexural stiffness of different sections are calculated. For estimating the flexural stiffness of the columns, 70%, and for beams 35%, of their gross moment of inertia is used. Also a uniform dead load and live load of 120 and 50 lb/ft^2/floor, respectively, are used in this model. The load combinations are based on FEMA-273 (1997). With fixed-base supports, the first periods of the structural model in the transverse (N-S) and longitudinal (E-W) directions are 2.9 sec and 2.3 sec, respectively. As discussed in section 1.2.2, the apparent periods of the structure found from the time history of the roof displacement during the Northridge earthquake are about 3.2 sec and 3.0 sec in the transverse and longitudinal directions, respectively (Figures 1.15 and 1.17).

Using the recorded motions at the roof level and also at the basement, one can find different periods of the building, using Fourier transformation. By dividing the Fourier amplitudes of the recorded motion at the roof level by those of the corresponding records at the

basement, the frequency response functions of the building in two directions could be found. Figure 2.2 shows the frequency response function of the building in the E-W direction from 10 to 30 sec, during the Northridge earthquake. Using three windows of each 20 sec long, the first period of the building in the E-W direction is about 2.6 sec during the first 20 sec of the earthquake, and about 2.9 sec from 20 to 40 sec and also from 40 to 60 sec (Figure 2.3). If instead of three intervals of 20 sec long, one uses six intervals of 10 sec long, a relatively different variation of the period in the E-W direction is found (Figure 2.4). Note that each dot in Figures 2.3 and 2.4 at different times shows the first period of the building during the corresponding interval prior to that time. The above figures probably suggest that defining one period for a building from recorded motions is open to engineering judgments. It should be noted that the period of the structure obtained from the earthquake records could have been longer if there were no stiffening effects of the partitions.

One measure to see if the structural model reasonably represents the real building is to compare the top displacement of the model with that of the real building under a given ground motion. Newmark and Hall (1982) suggest a 3-5% damping ratio for RC structures with considerable cracking and a 7-10% damping ratio at the yield point. Since the damping ratio for higher modes are usually assumed to be higher, 5% damping in the first and second modes and 7% damping in the third and fourth modes of vibrations in each direction are used. Using the recorded input ground motion in the transverse (N-S) direction during the Northridge earthquake, the time history of the top displacement is calculated and compared with the top displacement found from the recorded roof acceleration (see Figure 2.5). As shown, there is relatively good agreement between the two. The maximum roof displacement of 9.2 in. is calculated. The maximum roof recorded displacement is about 7.3 in. At the swing that the maximum recorded displacement of about 7.3 in. occurs, the peak calculated displacement is about 8 in. A similar comparison is made for the transverse displacement at the 8^{th} floor, see Figure 2.6. Again, there is relatively good agreement between the recorded and calculated displacements. Figure 2.7 compares the top displacement found from the recorded roof acceleration with the calculated one when the period of the structural model is increased from 2.9 sec to be almost equal to the apparent period of about 3.2 sec (this can be obtained by considering that the moments of inertia of the beams are about 0.29 times their gross moments of inertia). As shown, the agreement in Figure 2.7 is better than that in Figure 2.5.

Figure 2.8 compares the top displacement found from the recorded roof acceleration with the calculated top displacement under the ground motion in the longitudinal (E-W) direction during the Northridge earthquake. The lack of agreement between the recorded and calculated displacements is particularly pronounced at about 35 to 40 sec, where the ground motion has a harmonic type of motion with a period of about 3 sec (see Figure 1.13). In other words, when the motion is of harmonic type, having a structure with a period closer to the period of the ground motion results in larger displacement. Figure 2.9 compares the top displacement found from the recorded roof acceleration with the calculated one, when the period of the structural model is increased from 2.3 sec to be almost equal to the apparent period of about 3.0 sec (the moment of inertia of the beams are about 0.21 times the gross moment of inertia of beams). As shown, the agreement in Figure 2.9 is much better than that in Figure 2.8. It should be emphasized that the long period of the structure could be in part due to the foundation rotational flexibility and not only due to cracked concrete sections.

Figure 2.10 compares the calculated displacement in the transverse direction at the center of the roof under ground motion only in the transverse direction with the response under ground motions in both directions. As expected, for such a symmetric structure, the two responses are practically identical.

The first period of the structure, for the developed model, in the N-S and E-W directions are 2.9 and 2.3 sec, respectively. The shorter period in the E-W direction is attributed to the fact that the flexural stiffness of the beams in this E-W direction is larger than that in the N-S direction. The maximum base shear of the model computed in this study under the acceleration spectra of the recorded motion in the N-S and E-W directions are 10% and 16% of the total weight of the building, respectively. Figures 2.11 and 2.12 illustrate the acceleration spectra values for the first three modes. A summary of the results is given in Table 2.1. Dynamic analyses using the time histories of the ground motion in two directions, recorded during the Northridge earthquake, result in similar maximum base shear forces.

Naeim (1997) estimates that the first period of the structure in the N-S direction is 2.6 sec and is shorter than that in the E-W direction, with a first period of about 2.9 sec. If the second and third period of the model, used in the current study, in each direction are proportionally adjusted, i.e., if these periods are multiplied by the ratio of the first period estimated by Naeim (1997) to the first period of the model used in this study, the second and third periods of the structure are 0.82 and 0.45 sec in the N-S direction and 0.93 and 0.53 in the E-W direction,

respectively. Using these periods and the corresponding spectral accelerations (Figures 2.13 and 2.14) and also the **Effective Modal Mass (EMM)** of the model in each mode, the base shear in the N-S and E-W directions are equal to 16% and 10% of the total weight of the structure, respectively, which are in relative agreement with 18.5% in the N-S direction and 7.5% in the E-W direction given by Naeim (1997). A summary of the results is given in Table 2.1.

Comparing Figure 2.11 with Figure 2.13 and Figure 2.12 with Figure 2.14, one can explain a larger base shear in the N-S direction than in the E-W direction. By decreasing the first and proportionally higher periods of the structure in the N-S direction from the calculated ones used in the current study, acceleration spectra, S_a, for the first and second modes are significantly increased (see Figures 2.11 and 2.13). This is mainly due to the sharp variations of the acceleration spectra around the first and second modes of vibration of the structure in the N-S direction. By increasing the first and proportionally the higher periods of the structure in the E-W direction, S_a for the first, second, and also the third modes are significantly decreased (see Figures 2.12 and 2.14). These new values of S_a result in smaller base shear in the E-W direction than in the N-S direction.

As discussed above, the base shear forces reported by Naeim (1997) are based on a cubical interpolation of the recorded motion at three floors. Although strictly speaking, this procedure is questionable, since in calculating those base shears, the periods and the mode shapes of the structure are not directly used, the above agreements suggest that the result given by Naeim (1997) might be considered reliable. However, if one uses the first periods of vibration in two directions estimated by Naeim (1997) i.e., 2.6 sec and 2.9 sec in the N-S and E-W directions, respectively, the larger top displacement in the E-W direction can not be achieved, see Figures 1.19 and 1.20. In spite of the above discrepancy, some modification of the model used in this study could be justifiable, such as including some flexibility at the base, not only because of the existence of the basements, but also because of the soil-structure interaction, and also by modifying the effective flexural stiffness of elements as suggested by ACI 318-95.

2.2 ASSESSMENT OF RESPONSE OF STRUCTURE UNDER UBC-97 SPECTRUM

Modal analyses of the structure under the UBC-97 (1997) elastic spectrum for soil type S_c and without any near-field amplification factors are also carried out. The maximum base shear in the N-S and E-W directions are 18% and 23% of the total weight of the building, respectively. The maximum interstory drift index (IDI) is about 1.6% and occurs at the fourth story in the

transverse direction. The variation of the IDI along the height of the building in the transverse direction for the first interior frame is shown in Figure 2.15. Based on UBC-97, the maximum inelastic interstory drift, Δ_m, is equal to 70% of the elastic IDI. It should be noted that because of the limitations of SAP2000, the IDI corresponds to the values at maximum floor displacement. To find the IDI correctly, one has to find the IDI for each story at different modes and combine them using the CQC method.

The results of the analysis show an unusual shear force distribution between different columns in the first few bottom stories. For instance, the shear forces in the columns of the perimeter frames, except for corner columns, in the transverse direction are 172 and 362 kips in the first and second story, respectively. In the longitudinal direction, the ratio of the shear force carried by a perimeter frame and that carried by the interior frame is equal to 0.65, 4.0, 1.0, and 1.4 at the first, second, third, and fourth stories. These kinds of behavior are attributed to the large height of the first story and the larger flexural stiffness of the corner columns in comparison with other perimeter columns in the plane of the perimeter frames. It should be noted that the flexural stiffness of the perimeter beams are about 1.4 times that of interior beams above the second floor, therefore exterior frames are stiffer than interior ones in each direction, in spite of the fact that interior columns of the interior frames are about three times stiffer than the corresponding columns of perimeter frames. As noted above, as we move further up in the building, the shear force carried by the exterior frames is larger than that of the interior frame in the longitudinal direction.

2.3 IDENTIFICATION OF POSSIBLE STORY FLEXURAL WEAKNESS AND SOFTNESS

2.3.1 Columns

The results of the analysis of the structure under the UBC-97 elastic spectrum (with no reduction factors) for soil type S_c and with no near-field effect show that the corner columns have a strength demand up to about five times the strength capacity at the first floor. The values for the second and third floor corner columns is about 1.65 and 1.55, respectively. Note that if the bi-directional earthquake was considered, these values become even larger.

At the first story, the strength demand over the strength capacity of the columns along the north and south sides of the structure (except for the corner columns) is about 1.09 in the

transverse direction (N-S) and about 1.07 in the longitudinal direction. Note that these values are at the bottom of the first-story columns with the assumption that the base connections are fixed.

At the second story, the strength demand over the strength capacity of the columns of the longitudinal and transverse perimeter frames, except for the corner columns, are about 1.26 and 1.06, respectively (at the bottom of columns). Note that as discussed above, the shear force of these columns is unusually high. Except for the corner columns, all the columns at the third story remain elastic, with a maximum strength demand over the strength capacity of about 0.75.

Each column has the same dimensions over the entire height of the building, and only the amount of reinforcement decreases as we move further up. Columns above the first story have the same length; as an example of the behavior over the height, the strength demand over the strength capacity of the exterior columns of the interior transverse frames is equal to 0.7 at the second story and equal to 0.73 at the eighth story (the maximum over the entire height).

2.3.2 Beams

At the second floor, the flexural strength demands over that of the capacity for beams vary from 1.38 to 2.36 for negative bending moments (tension at the top) and from 1.26 to 4.8 for positive bending moments (see Figure 2.16). The upper limit for the positive bending moments is at the faces of the interior columns in the transverse direction, when the bottom reinforcement bars with inadequate development length (anchor length of only 6 in.) are pulled out. This ratio at the third floor varies from 1.07 to 2.62 for negative bending moments and from 1.51 to 4.0 for positive bending moments (see Figure 2.17). The upper limit is for the case when the bottom reinforcement bars with inadequate development length are pulled out.

Since the ratio of strength demand and strength capacity for the exterior beams at the second floor (see Figure 2.16) are much larger than the ratio for the columns of longitudinal and transverse perimeter frames (except for corner columns) which are 1.26 and 1.06, respectively, it is concluded that it is unlikely for these columns to form plastic hinges. Therefore, except for the corner columns and at the base of the columns at the first story, all other columns remain elastic. The flexural strength demand over that of capacity for an interior transverse frame is shown in Figure 2.18.

It should be noted that (1) the period of the structure is much larger than the values obtained using the equation recommended by UBC seismic codes; (2) a load factor of one has been used in the linear dynamic analysis: the strength reduction factor of one is used to calculate

the strength capacities, while in the original design of the building probably a working stress design method was used and thus the allowable stresses used could be significantly smaller than the yield stress of the reinforcements. Therefore, even under UBC elastic spectrum, the strength demands over that of the capacities are not as high as one could expect.

Based on the above discussions, it is concluded that from the point of view of flexural behavior (i.e., assuming that there is no brittle mode of failure) the inelastic seismic behavior of the structure is controlled by a beam mechanism, and the development of a soft or weak story is not a major concern.

2.4 BEHAVIOR UNDER SEVERE NEAR-FIELD EARTHQUAKE GROUND MOTIONS

So far, it has been assumed that the soil type is S_c (see UBC-97) and that there are no near-field effects. The soil type is a deep moderately firm alluvium, therefore it could be easily assumed as type S_d or even S_e. Assuming soil type S_d and also assuming the near-field factors of N_v=2.0 and N_a=1.5 (see UBC-97), this results in a maximum IDI of about 3.7%, which in turn could result in severe nonstructural damage and large ductility demand on the beams. Again it should be noted that based on UBC-97, the maximum inelastic interstory drift, Δ_m, should be computed as 70% of the $R\Delta_s$ being $R\Delta_s$, the linear elastic IDI.

Table 2.1 Base shear calculation using modal analysis for the model used in the current study and the model based on the first periods of vibration in two directions given by Naeim (1997). The acceleration spectra of the recorded motion during Northridge earthquake with 5% damping is used. W and M are the total weight and total mass of the building and EMM is the Effective Modal Mass.

A. Transverse Direction (N-S)

Mode Number	Effective Modal Mass	Model used in current study			Model based on T_1 (Naeim,1997)		
		T (sec)	Sa (g)	EMM*Sa	T (sec)	Sa (g)	EMM*Sa
1	0.811M	2.9	0.077	0.0624W	2.6	0.14	0.1140W
2	0.110M	0.91	0.61	0.0671W	0.82	0.88	0.0968W
3	0.044M	0.50	1.13	0.0487W	0.45	1.13	0.0497W
BASE SHEAR			**0.103W**			**0.157W**	

B. Longitudinal Direction (E-W)

Mode Number	Effective Modal Mass	Model used in current study			Model based on T_1 (Naeim,1997)		
		T (sec)	Sa (g)	EMM*Sa	T (sec)	Sa (g)	EMM*Sa
1	0.858M	2.3	0.18	0.1540W	2.9	0.115	0.0987W
2	0.094M	0.74	0.38	0.0357W	0.93	0.285	0.0268W
3	0.028M	0.42	0.58	0.0162W	0.53	0.46	0.0137W
BASE SHEAR			**0.160W**			**0.103W**	

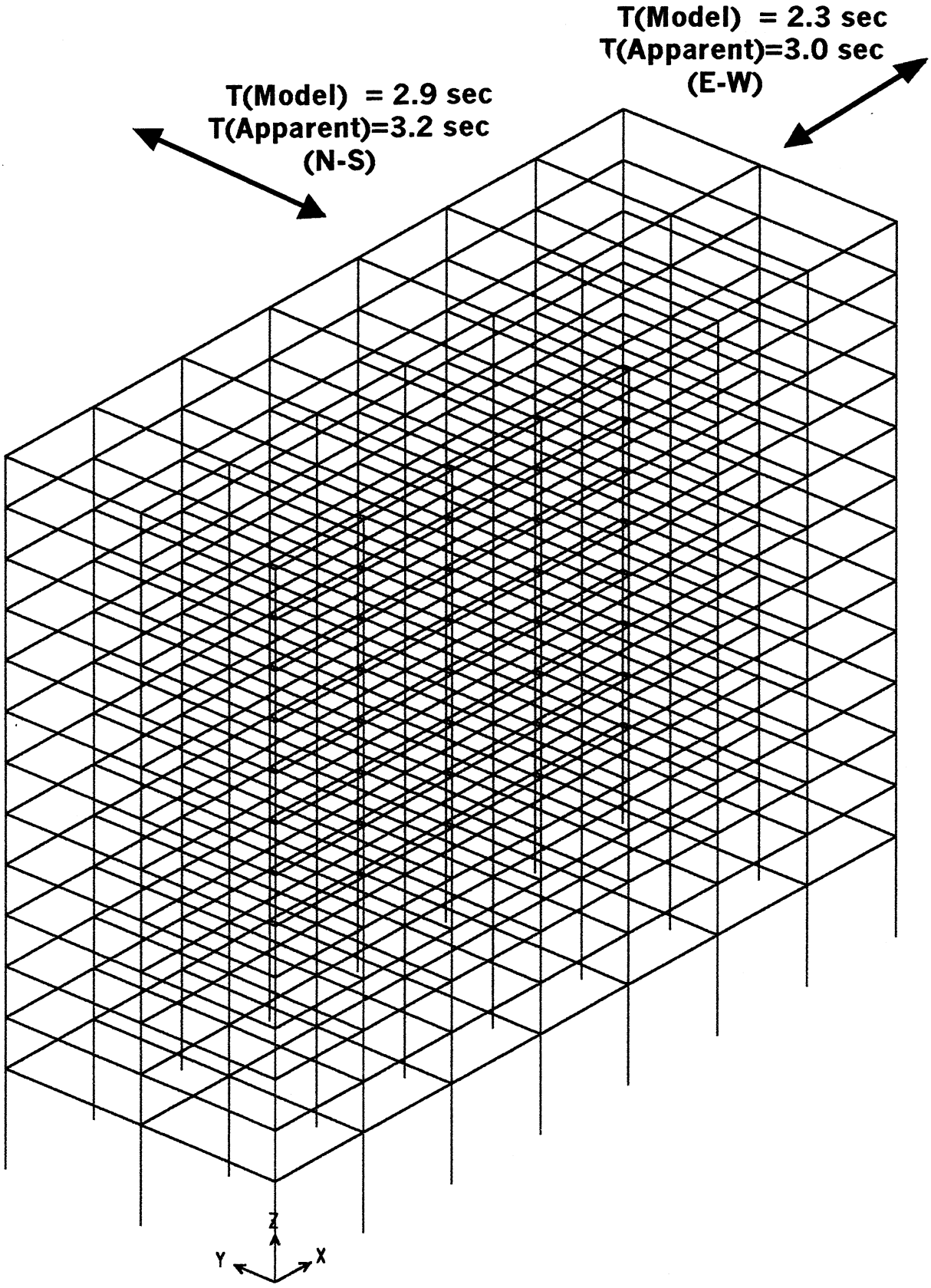

Figure 2.1 The isometric view of the model used in this study.

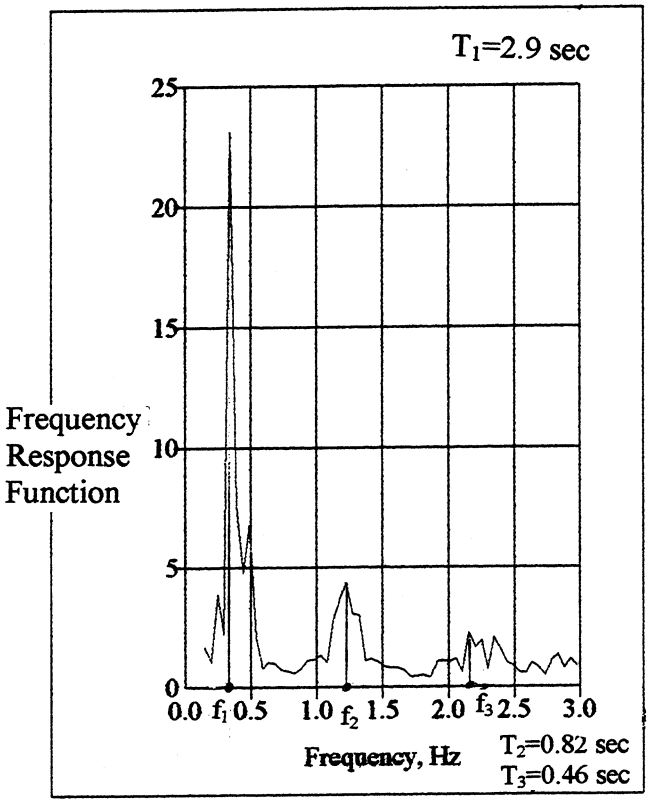

Figure 2.2 Frequency response spectrum in E-W direction from 10 to 30 sec.

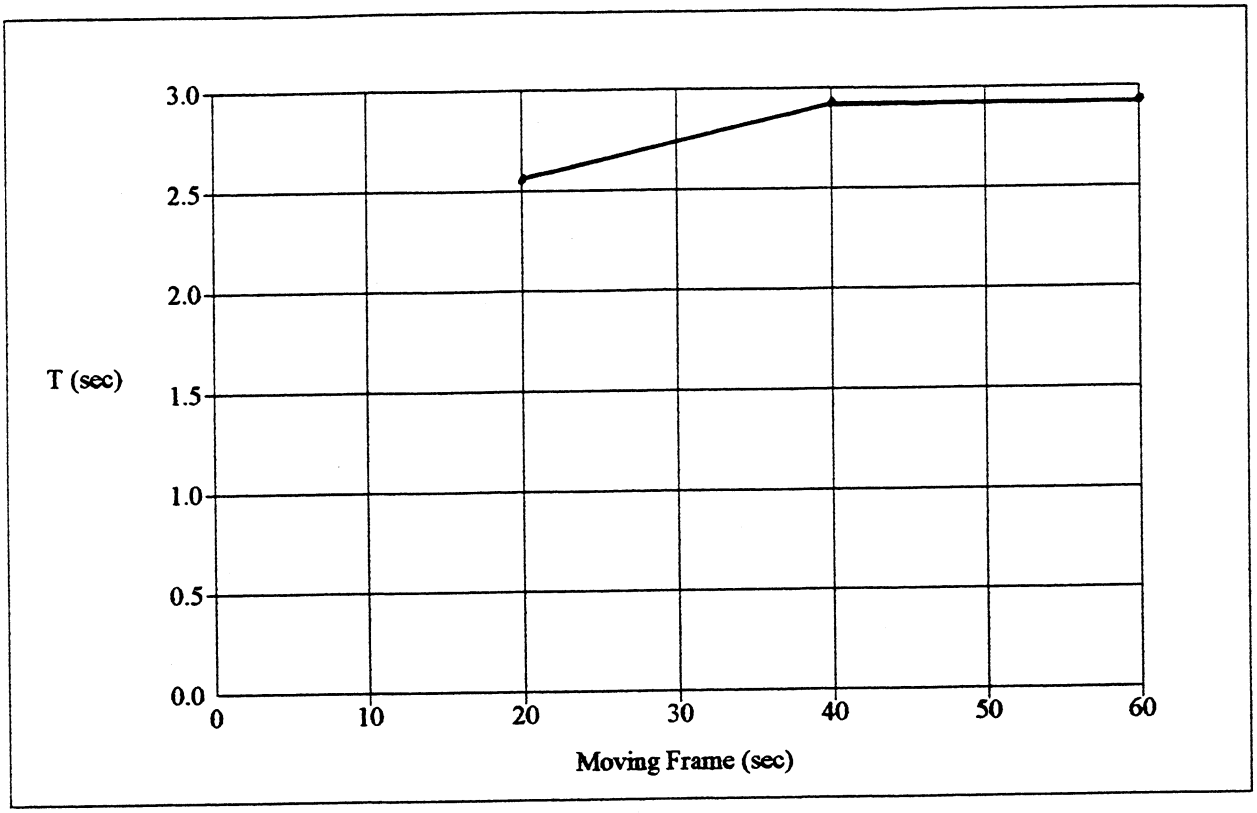

Figure 2.3 The period of the structure in E-W direction sampled at 20 sec windows.

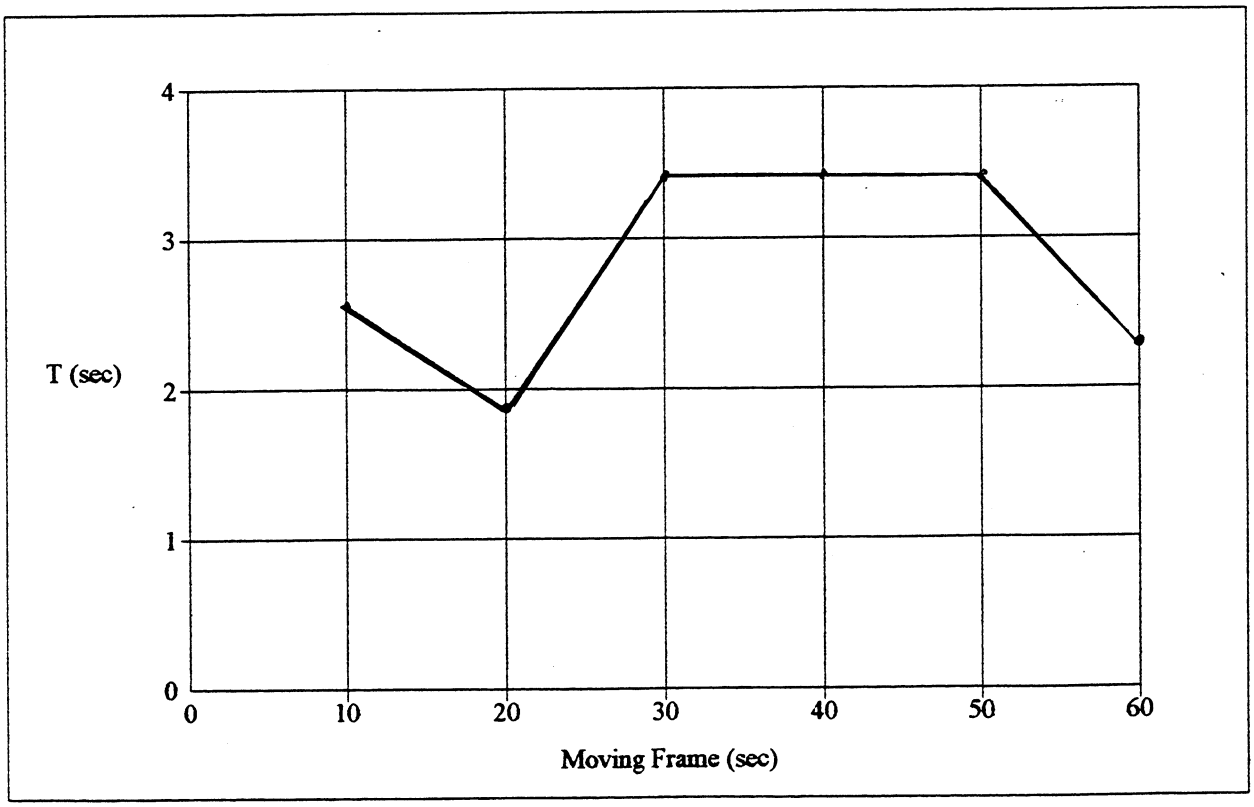

Figure 2.4 The period of the structure in E-W direction sampled at 10 sec windows.

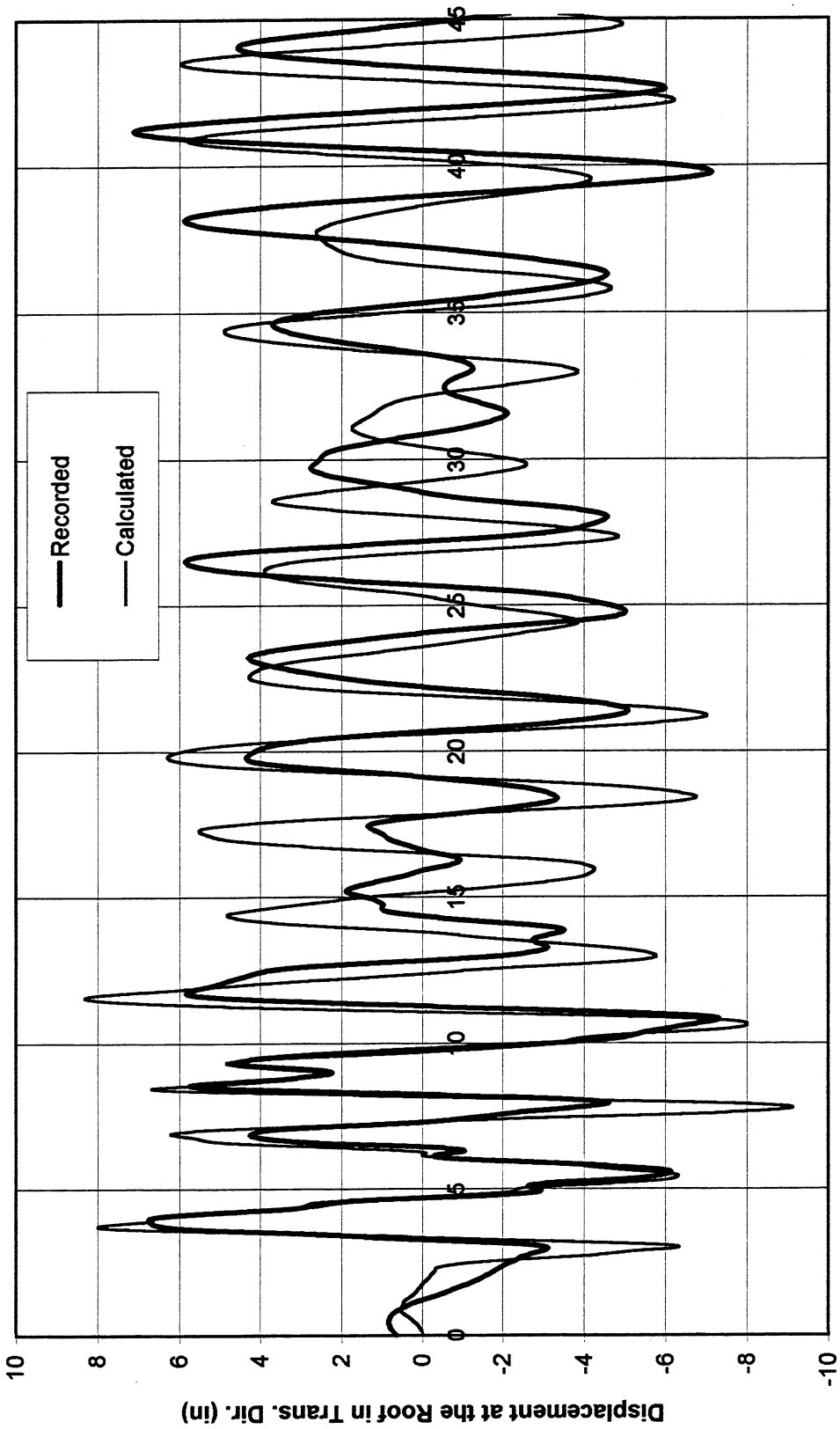

Figure 2.5 Comparison between roof recorded and calculated displacement in transverse (N-S) direction.

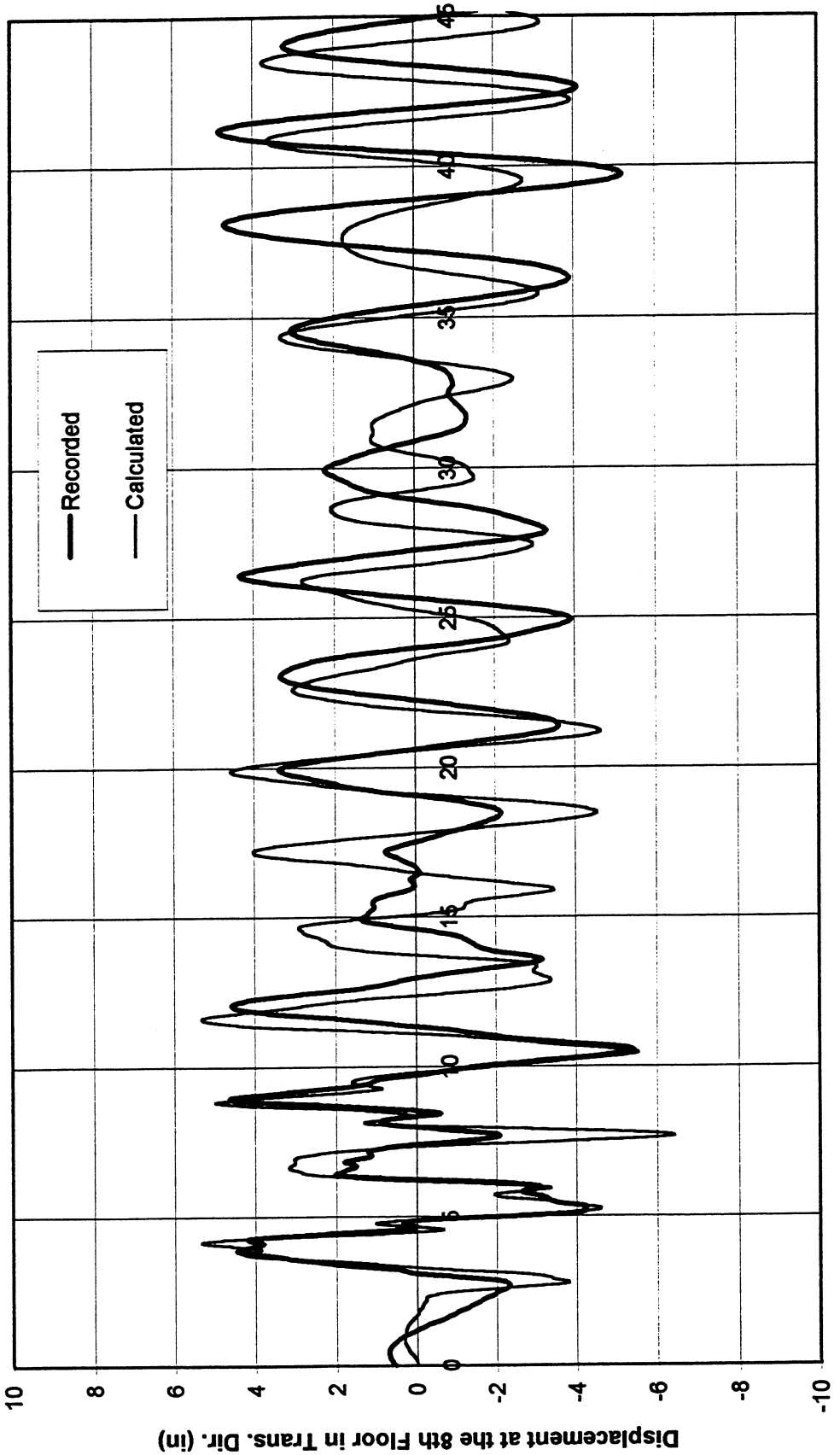

Figure 2.6 Comparison between 8th floor recorded and calculated displacement in transverse (N-S) direction.

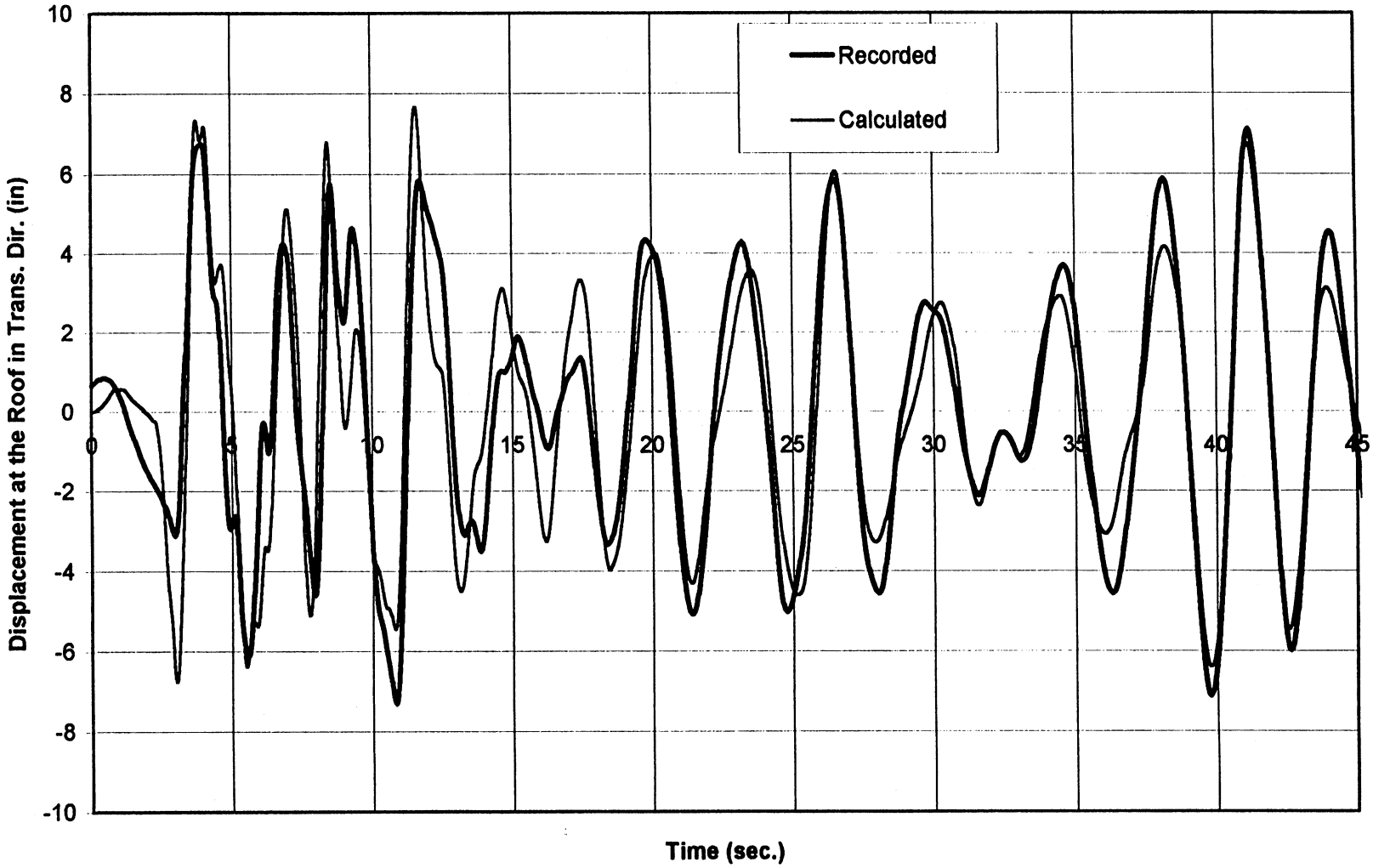

Figure 2.7 Comparison between roof recorded and calculated displacement in transverse (N-S) direction (period of model is increased to be equal to the apparent period in N-S direction).

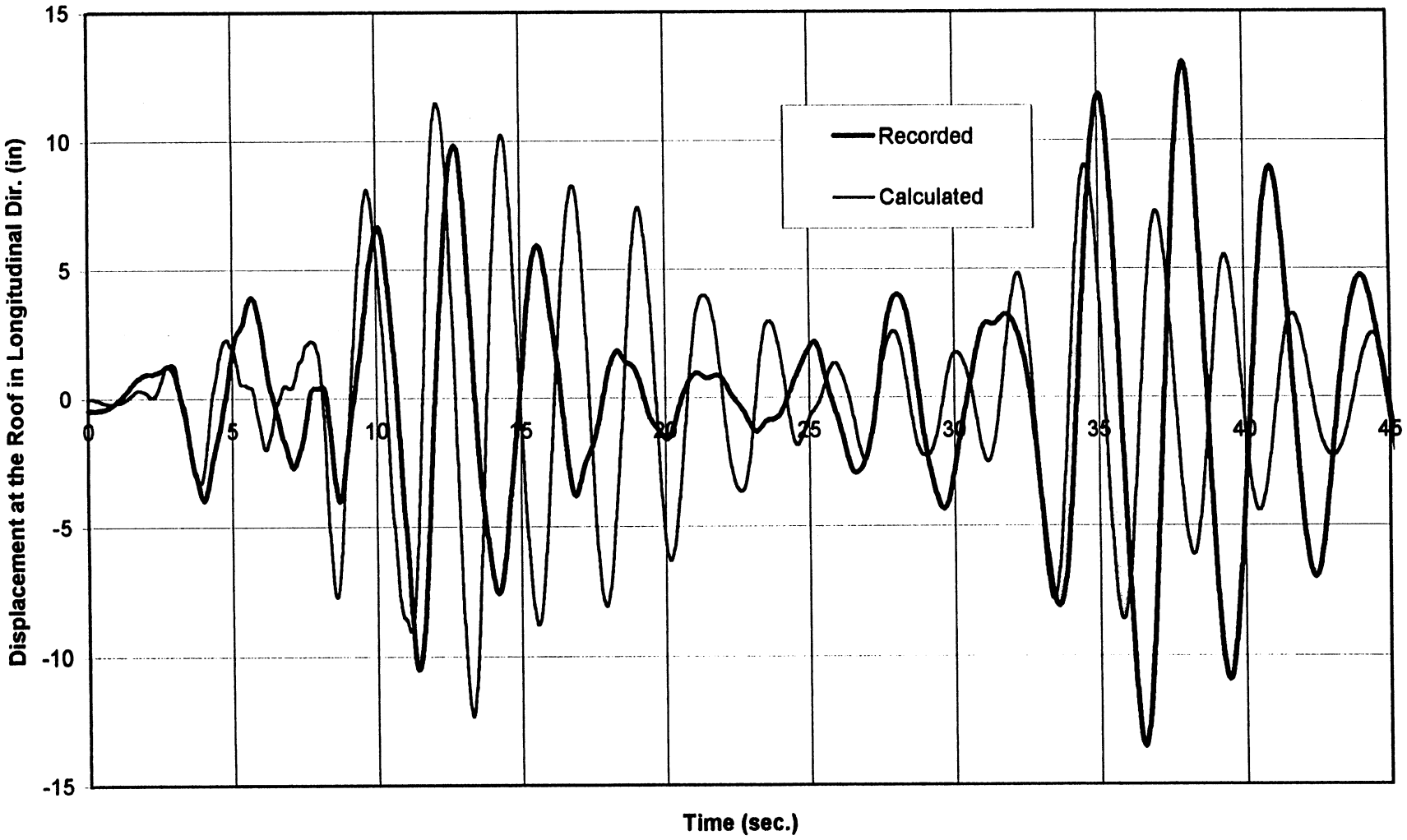

Figure 2.8 Comparison between roof recorded and calculated displacement in longitudinal (E-W) direction.

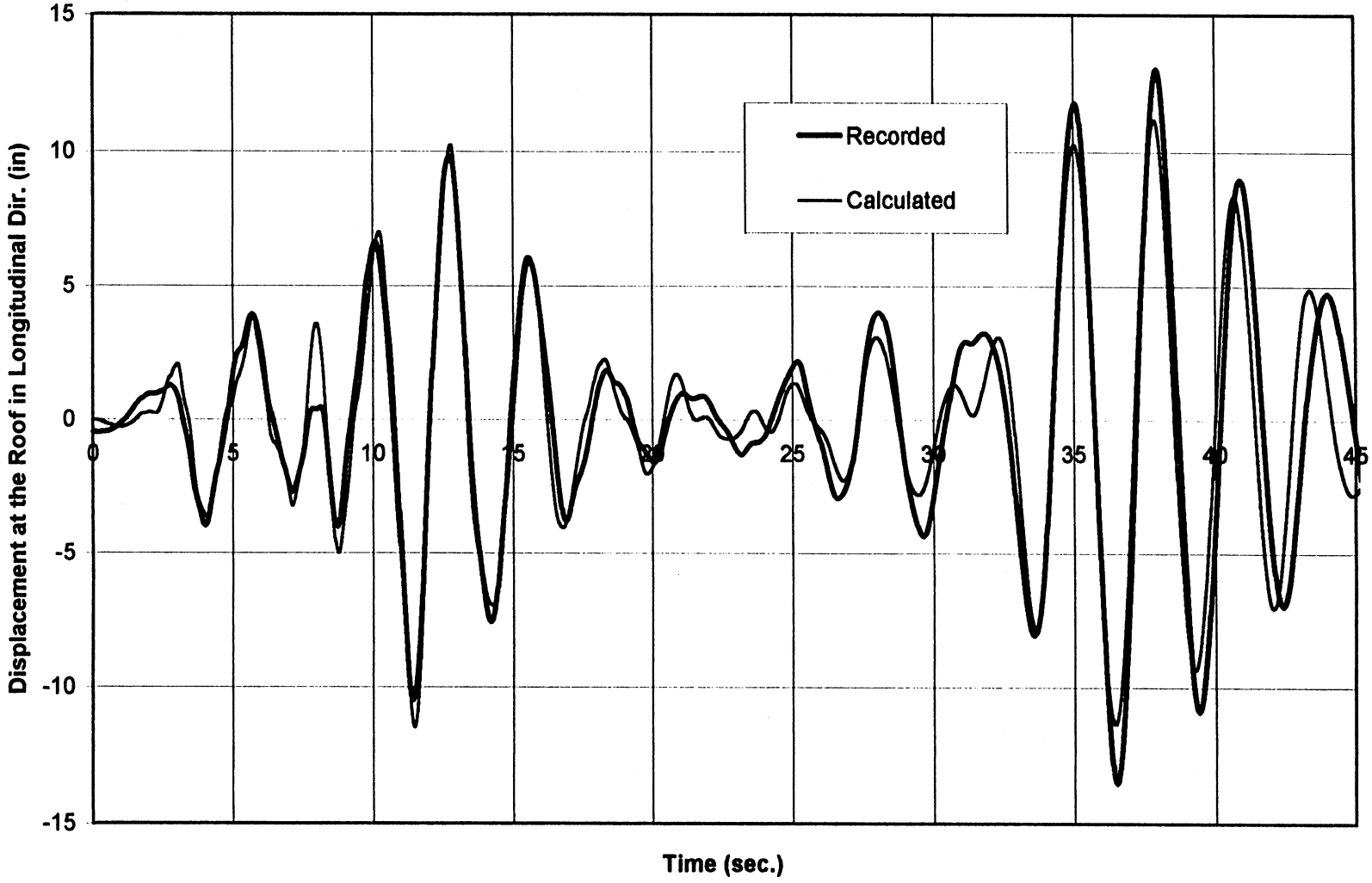

Figure 2.9 Comparison between roof recorded and calculated displacement in longitudinal (E-W) direction (period of model is increased to be equal to the apparent period in E-W direction).

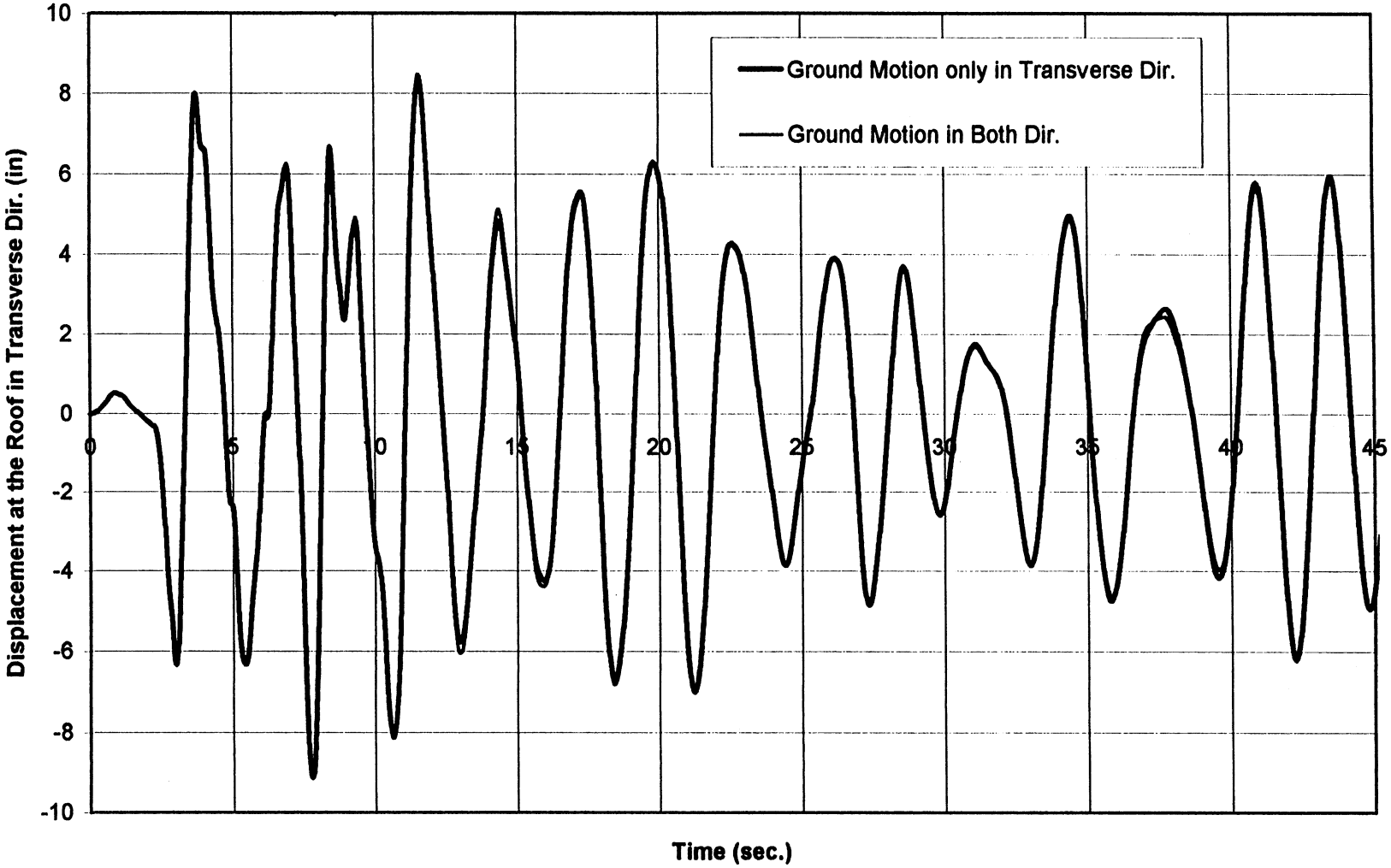

Figure 2.10 Calculated displacement in transverse direction at the center of roof.

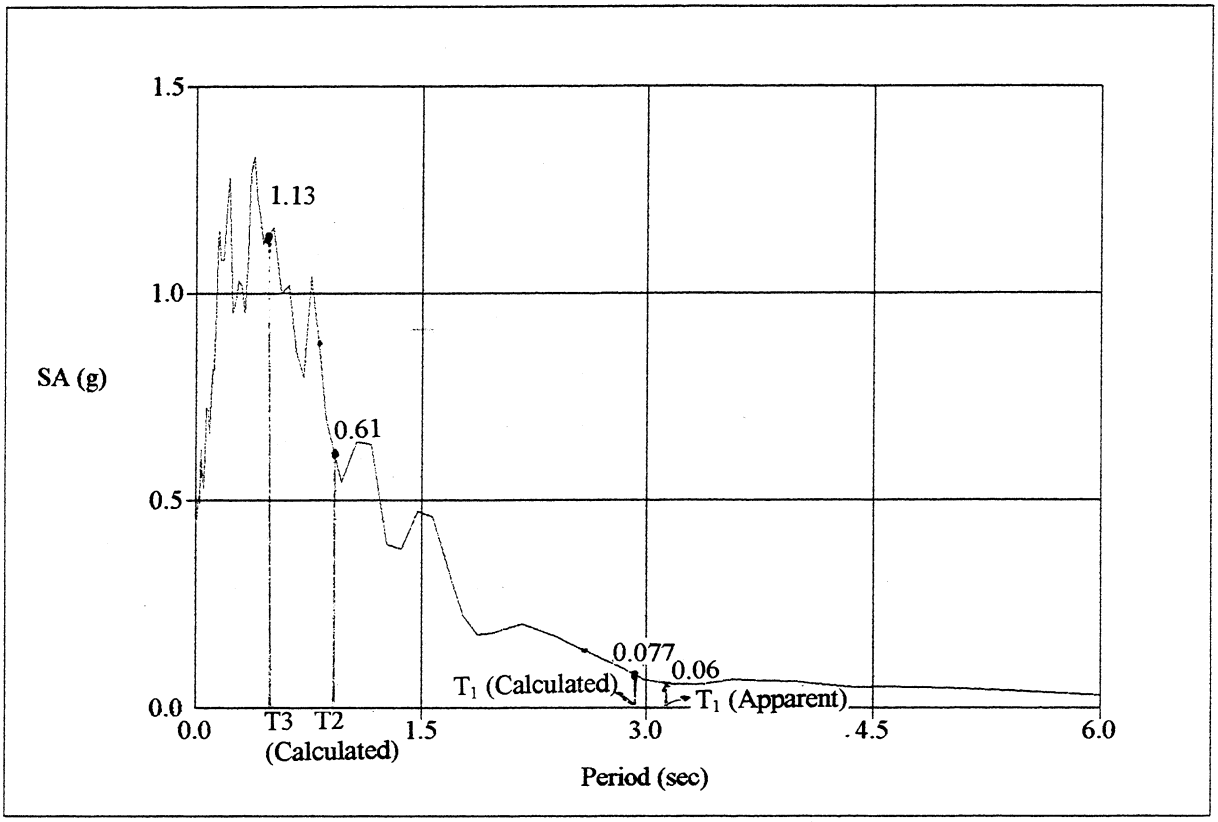

Figure 2.11 The acceleration response spectrum in N-S direction (5% damping).

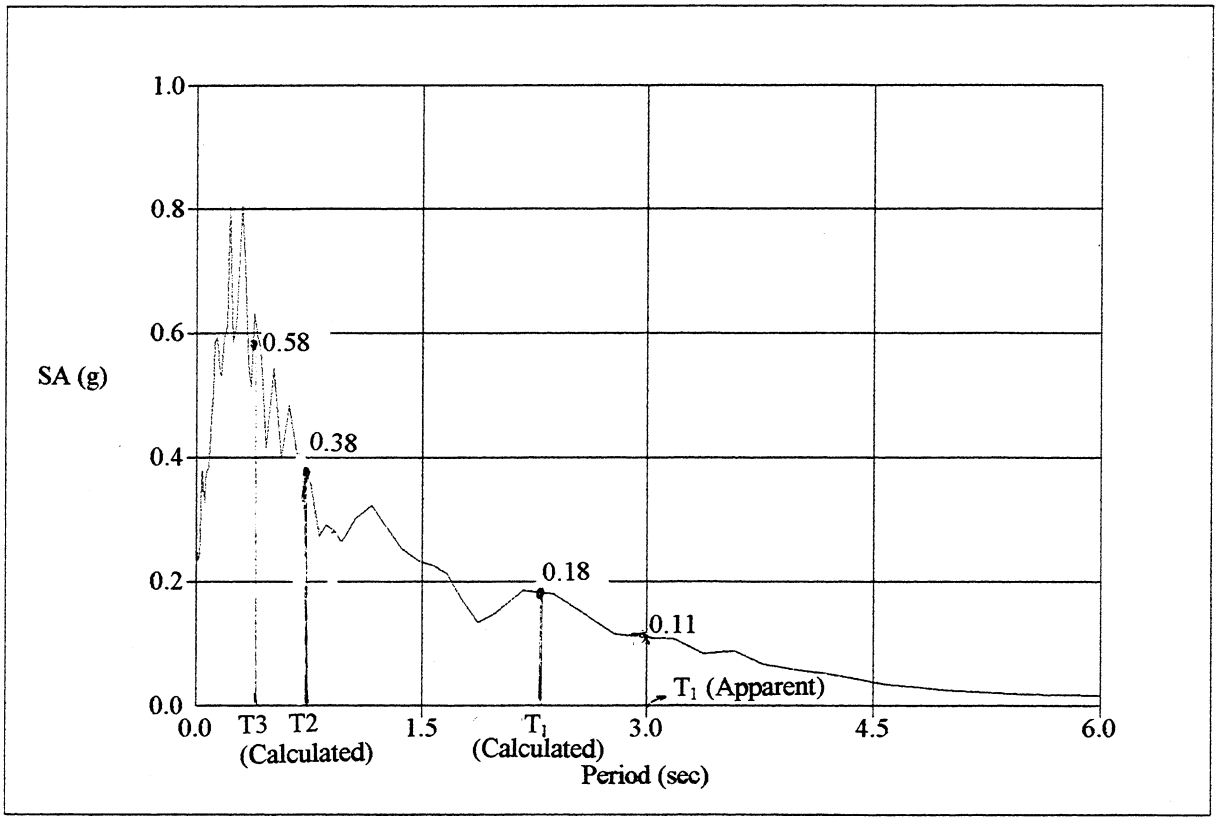

Figure 2.12 The acceleration response spectrum in E-W direction (5% damping).

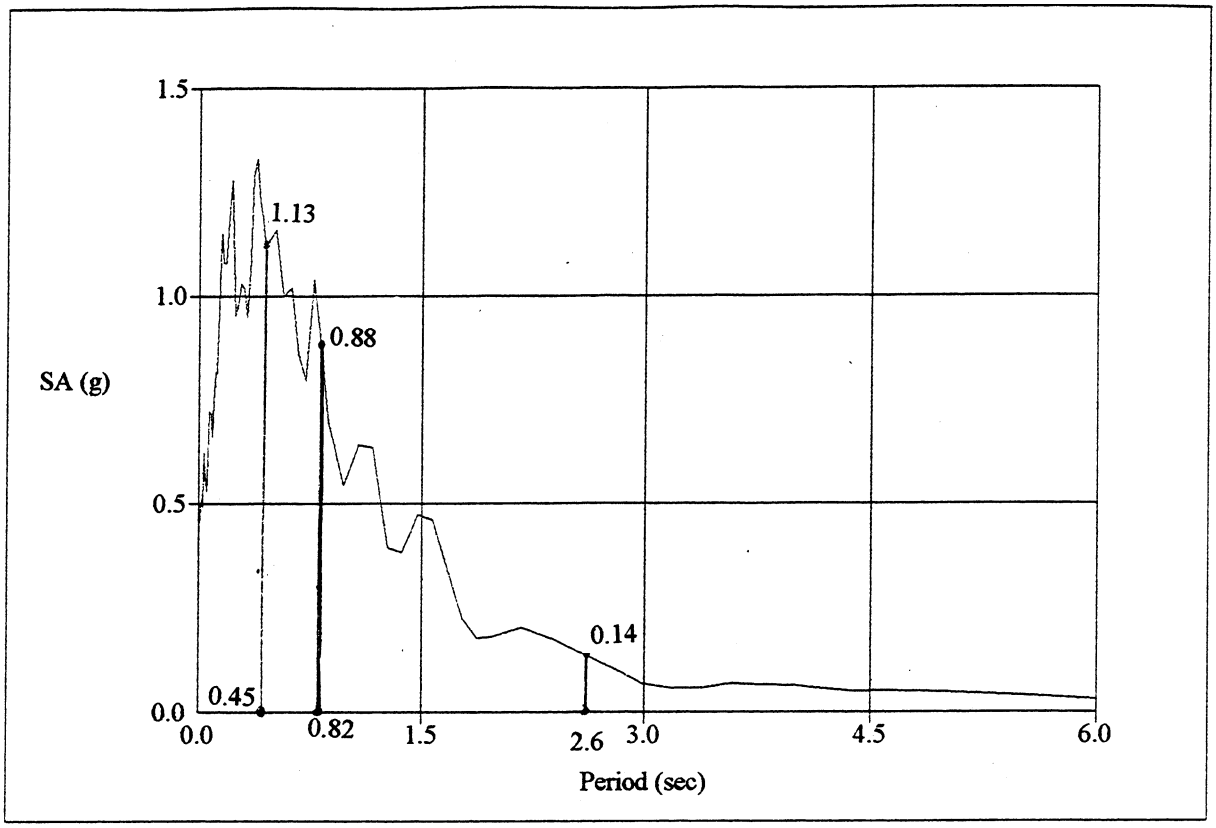

Figure 2.13 The acceleration response spectrum in N-S direction (5% damping).

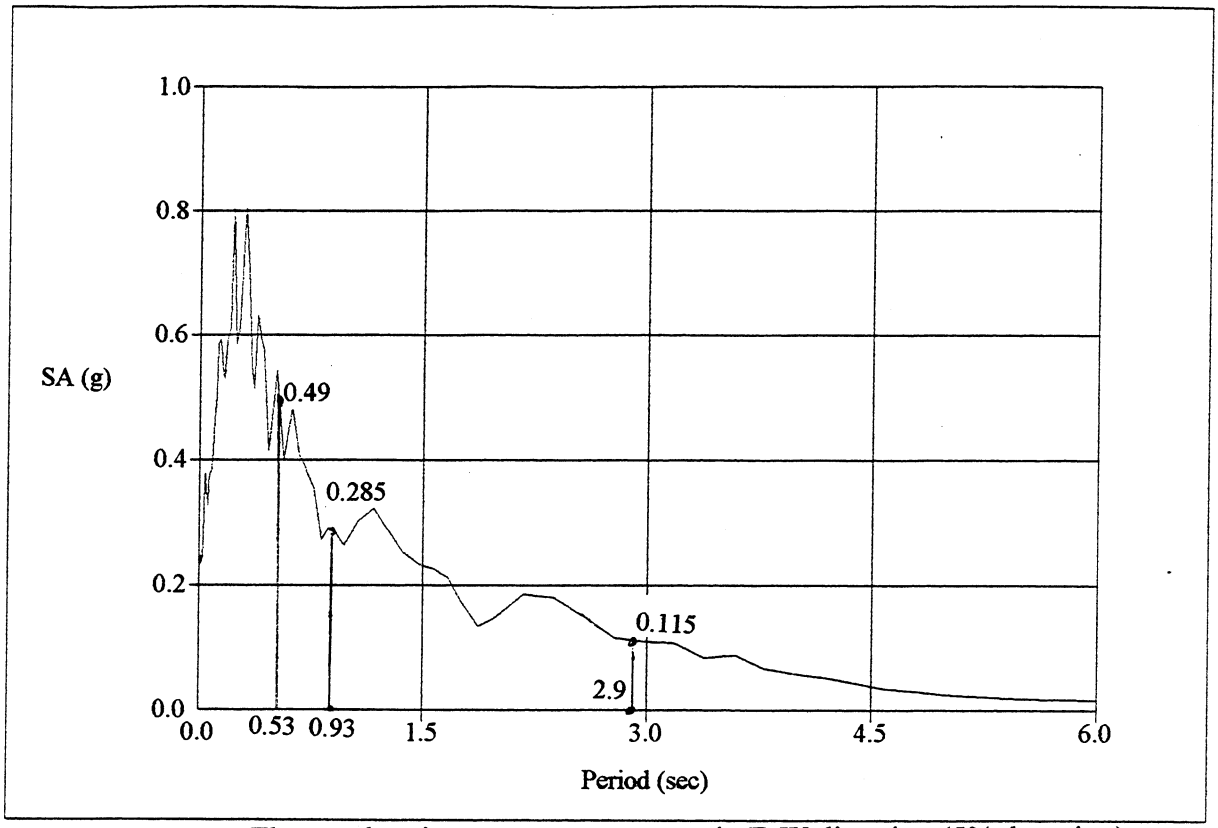

Figure 2.14 The acceleration response spectrum in E-W direction (5% damping).

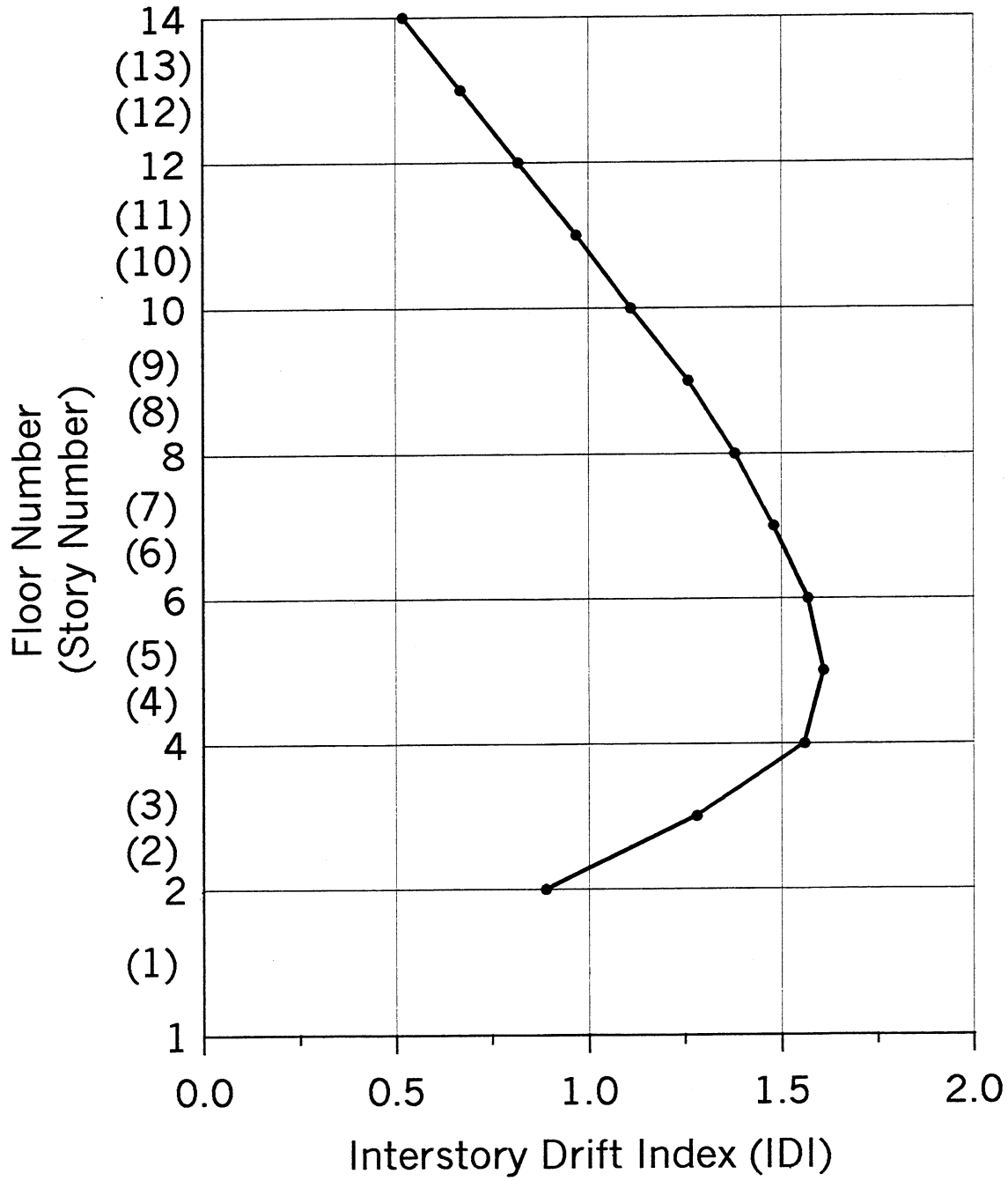

Figure 2.15 Interstory drift index for the first interior transverse frame under UBC-97 spectrum for soil type S_c with no near source amplification factor. (Plotted at the top floor of each story)

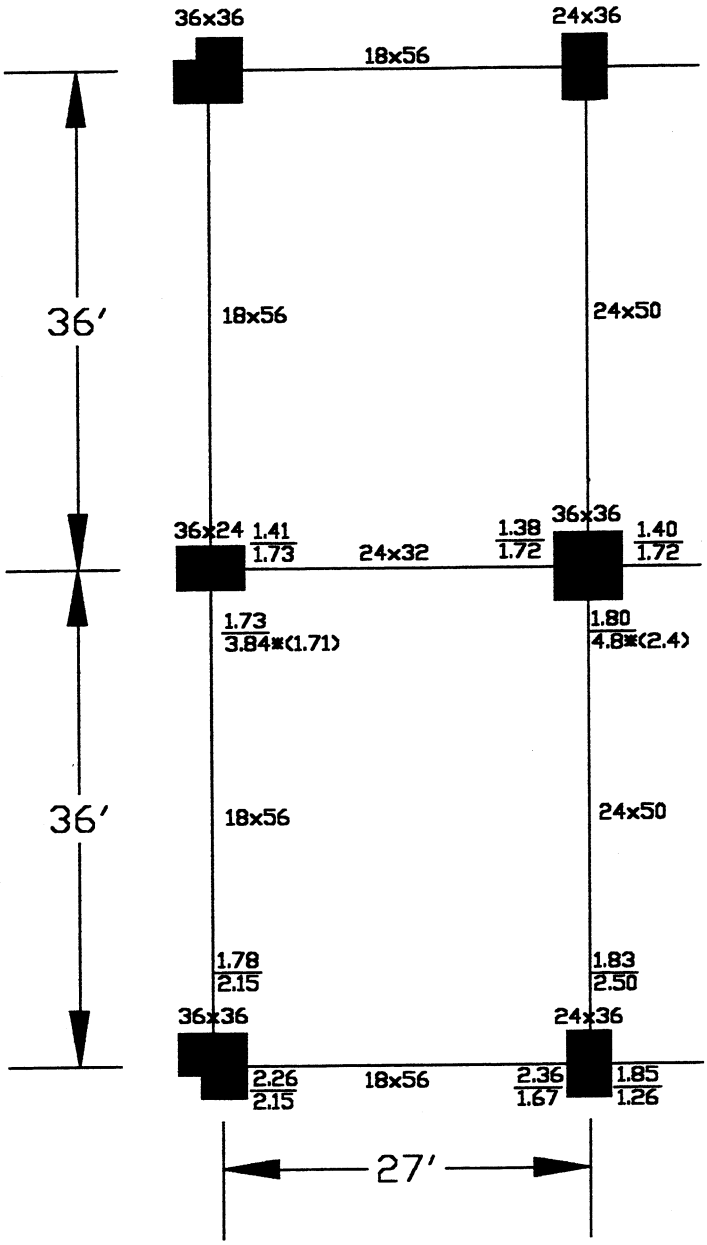

Note 1: The top numbers at beam-ends correspond to top reinforcement in tension. The bottom numbers are when bottom reinforcement is in tension.

Note 2: The numbers with * are when reinforcement bars with inadequate development length are pulled out and the numbers in parentheses are for the case that no pullouts occurred

Figure 2.16 The ratio of the elastic flexural strength demand to strength capacity at the 2nd floor.

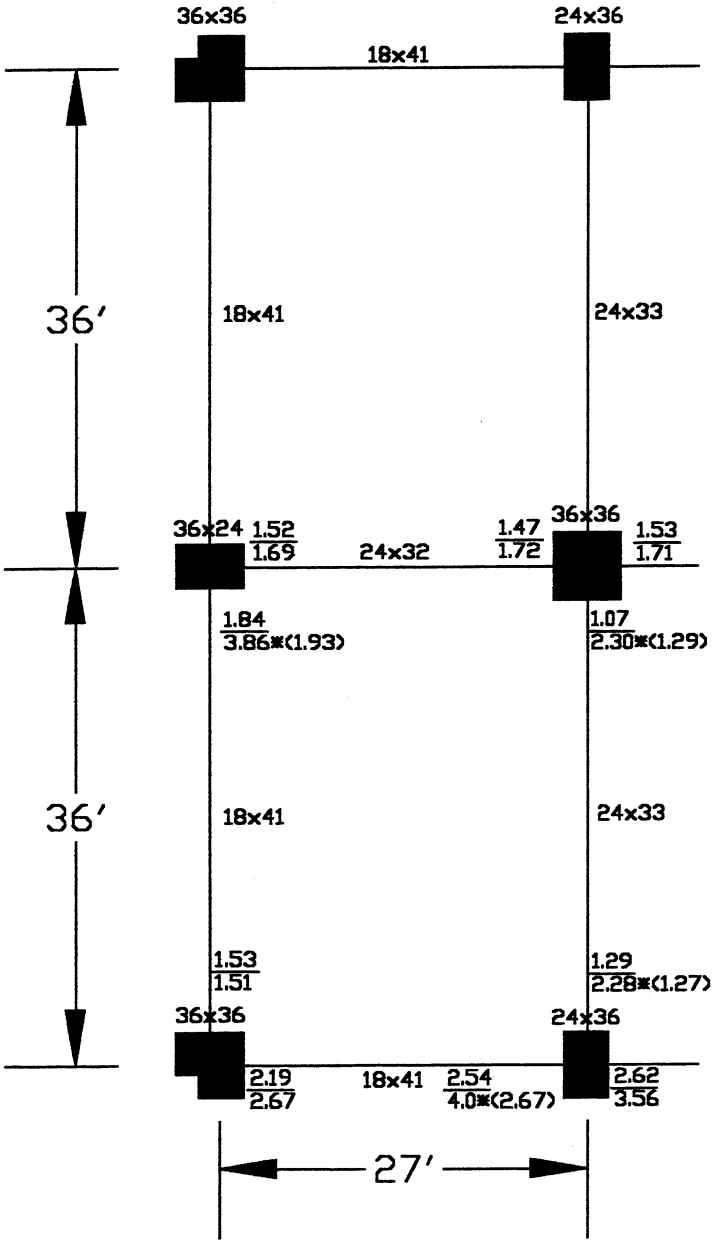

Note 1: The top numbers at beam-ends correspond to top reinforcement in tension. The bottom numbers are when bottom reinforcement is in tension.

Note 2: The numbers with * are when reinforcement bars with inadequate development length are pulled out and the numbers in parentheses are for the case that no pullouts occurred

Figure 2.17 The ratio of the elastic flexural strength demand to strength capacity at the 3rd floor.

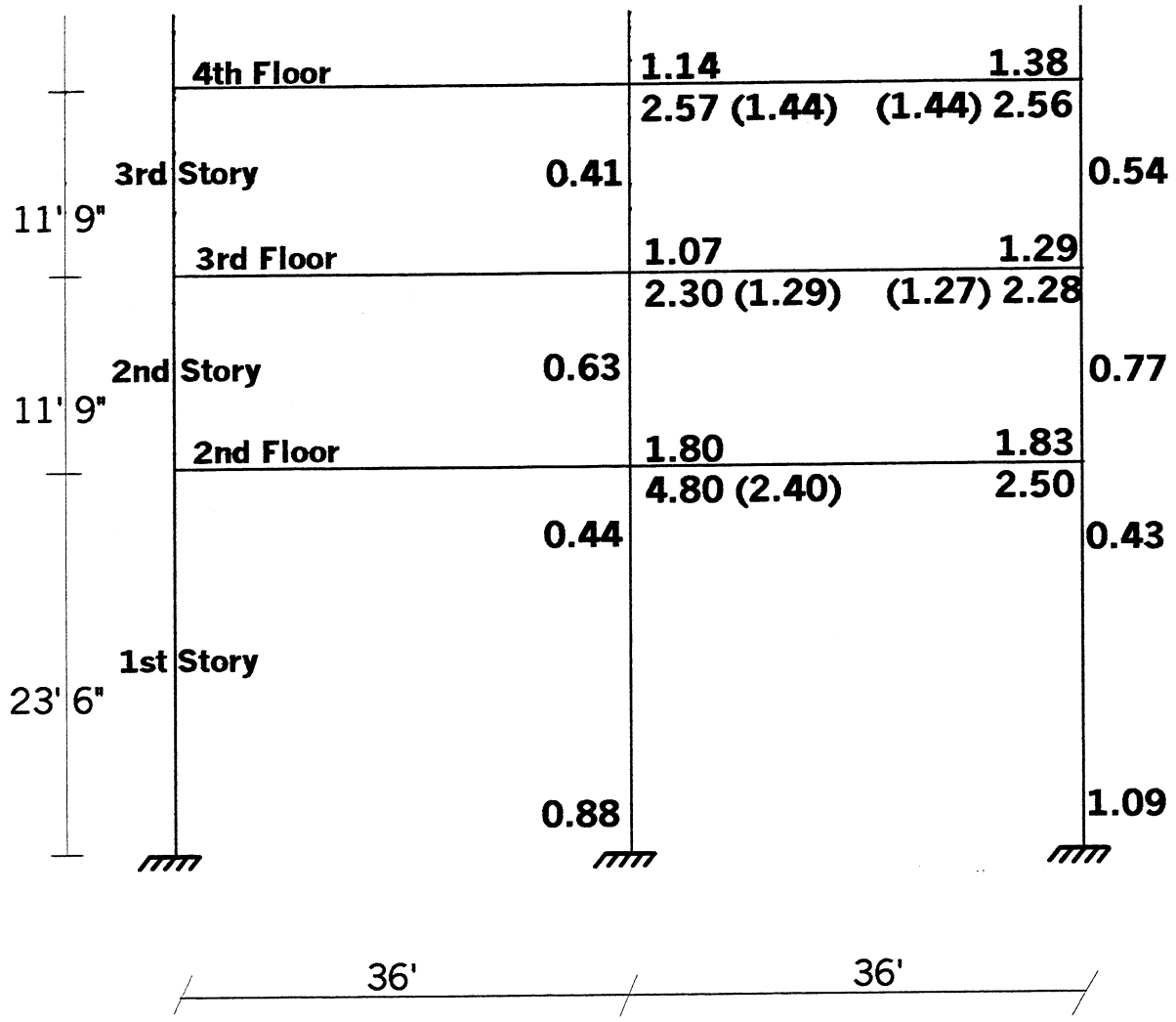

Figure 2.18 Ratio of the elastic flexural strength demand to the strength capacity for interior frames.

Note 1: The numbers at the top of the beams correspond to negative bending moment (tension at the top).

Note 2: The number in the parentheses is for the case that the bottom reinforcing bars with 6" embedded length are NOT pulled out.

3 Limit Analysis and Capacity Procedure (Local Vulnerability)

Each column has a constant cross section over the height of the building. Also, the transverse reinforcement of the columns are the same over the first few stories. Except for the second floor, the cross section of each beam is constant over the height of the building. The transverse reinforcement of each beam is also fairly constant at different floors. Therefore, to check the possibility of brittle failure due to the combined effects of bending with axial loads, shear, and/or bond, only the first three stories of the structure are studied. Figure 3.1 shows the reinforcement details for the 3rd floor beam of interior transverse frames.

3.1 BEAMS

3.1.1 Bending Moment Capacity

- The possibility of pullout of the positive reinforcement at exterior and interior joints of the transverse frames. Except for the exterior joints at the second floor, all the interior transverse frame beams in the second to fifth floors have two #9 bottom bars that have only a 6-inch embedment length into the interior and exterior columns. In addition to these two bars, there are 2#9 or 2#10 bottom bars that can barely be considered to have enough embedment length to develop adequate anchorage for these bars. The exterior frames in the transverse direction have some bottom bars with 6-inch embedment length only at the interior joints in all floors. Also at the third floor, at some interior joints of the perimeter frames in longitudinal direction, some of the bottom reinforcing bars have the same 6-inch embedment length. These bars could pull out during severe earthquake ground motion and not only increase the ductility demands of the beams but also lead to brittle failure of the bars that remain anchored.

- The ratio of positive to negative moment capacity. The ratio of positive to negative beam reinforcement at the faces of columns, for the locations where pullout can occur, varies between 0.27 to 0.81, which results in positive to negative bending moment ratio of about 0.3 to 0.82. The lower limit is not acceptable according to present seismic code regulations and requires a minimum ratio of positive to negative reinforcement of 0.5. Note that the lower limit occurs at the faces of the interior transverse beams with the interior columns of interior frames at the second to fifth floors.

3.1.2 Shear Force Demand and Capacity

To calculate the shear force demands of the beams, in addition to the factored gravity loads, probable bending moment capacities corresponding to 1.25 times the nominal steel yield stress are considered at the ends of the beams. It should be mentioned that because the real yield stress might be larger than the nominal one and because the A432 Billet steel bars (used in this building) have a relatively higher post-yielding modulus of elasticity than currently used reinforcing bars, a coefficient larger than 1.25 could be more realistic (reliable). In the worst-case scenario, it is assumed that pullout of the bottom reinforcing bars does not occur. If based on current seismic design codes, the contribution of the concrete in the shear force capacities of beams is neglected (which can be questioned), the ratio of the shear force demands to that of capacities varies from 1.09 to 1.45 at the second floor and from 0.93 to 1.29 at the third floor. Figures 3.2 and 3.3 give the details of these ratios along with the details of the transverse reinforcement in the beams.

In this structure, since the beams are relatively long, from a capacity-design point of view, the shear forces associated with the gravity loads are considerable in comparison with those of lateral loads. It is also obvious that these two shear forces add up at the end of a beam at which the bending moment from the seismic loads is negative. In other words, the higher shear force occurs at the end where the seismic bending moment is negative. In the locations where the seismic bending moments are negative, the bending moment demands over the bending moment capacities are less than 2.6 (Figures 2.16 and 2.17), i.e., a relatively small curvature ductility ratio is required. Therefore, it is concluded that having zero contribution from the concrete in carrying the shear forces is too conservative. In all the cases considered, the difference between the shear force demands and capacities is less than one half of the concrete shear strength. Therefore, it is concluded that the shear force demands in the beams are close to the acceptable

values. Note that the maximum value of average shear stress demand in the beams is equal to $2.5\sqrt{f'_c}$.

3.1.3 Rotational Ductility Demand and Capacity

For the negative bending moments, the maximum value of $(\rho-\rho')/\rho_b$ is equal to 0.35 occurring at the interior transverse beams at the third floor: ρ and ρ', are the reinforcement ratios of the tensile and compressive reinforcement, respectively, and ρ_b is the balanced reinforcement ratio. Based on FEMA-273 (1997), for the available level of confinement at d/4 and relatively low level of shear stress demand in the beams (less than $2.5\sqrt{f'_c}$), a rotational ductility of about four could be achieved and be acceptable at the life-safety level of behavior.

Assuming that shear failure is prevented, the result of a section analysis under a negative bending moment of the interior transverse beams at the faces of interior columns at the third floor gives a curvature ductility of about 9.6. Note that the available transverse reinforcement is #5 at 7 in. and the maximum useable concrete compressive strain is calculated based on the equation suggested by Scott et al. (1982) which is found to be equal to 0.01. Also note that these sections are the critical sections, as far as the curvature ductility of beams under negative bending moments is concerned. For a half-span beam under a concentrated load at the tip, assuming a plastic hinge length equal to one half of the depth of the section, with the length of the beam divided by the depth of the section (aspect ratio) of 12, a rotational ductility of about 3.8 is achievable, which is close to the value given by FEMA-273 (1997). However, as mentioned above, the maximum useable concrete strain is assumed to be a function of the amount of confining steel, and if instead of #5 at 7 in. the confining steel was #3 at 7 in. (i.e. a drop of about three times in the amount of confining steel), the available rotational ductility based on FEMA-273 (1997) was still equal to four. It should be mentioned that for this structure with considerable effects of gravity load on the internal forces, the bending moment distribution of the beams are different from that under seismic loads alone and the relation between the curvature and rotational ductility used above is just an approximation. A more detailed study on this topic is given in chapter four.

Having a beam mechanism under lateral loads since the plastic hinges are mainly developed at the beams of the lower floors, the rotational ductility demands on the beams at the

floors are larger than the global displacement ductility demand of the entire structure. Assuming that the equal displacement rule holds for this long-period structure and the rotational ductility demand of the beams at the lower floors is about 1.5 times global the displacement ductility demand of the structure, and also assuming that there are no sections under large concentrated plastic curvature, since the maximum ratio of the flexural strength demands over that of capacity for the negative bending moments in the beams is about 2.6, which is also equal to (3.9/1.5), it is concluded that the beams have a large enough rotational capacity under the negative bending moments at the life-safety level.

The maximum ratio of the flexural strength demand to that of the capacity for positive bending moments, after pullouts, is about 4.8. For the positive bending moments, the amount of tensile reinforcement is smaller than that of compressive reinforcement and as a result, with the available level of confinement at d/4 and a relatively low level of shear stress in the beams (less than $2.5\sqrt{f'_c}$), a relatively large level of rotational ductility could be achieved. Also, since under positive bending moment the variation of bending moment is slow, the length of the plastic hinge is larger than that under a negative bending moment. In spite of this available large ductility, since under lateral loads plastic rotations can concentrate at the sections where pullout occurs, a nonlinear analysis is required to find the rotational ductility demands of the beams with these kinds of sections.

3.2 COLUMNS

3.2.1 Bending Moment Capacity in Comparison with Those of Beams (Check on strong-column weak-beam mechanism under worst-level axial loads)

At all the joints, the sum of the plastic bending moments of the beams (considering 1.25 times steel yield stress) are smaller than the sum of the ultimate bending moments of the columns, under the worst possible axial loads. Also, the result of the elastic analysis conducted suggests that except for the corner columns, all the other columns are strong enough to prevent development of plastic hinges in the columns. Therefore it is concluded that if the corner columns were not weak, the strong-column weak-beam mechanism could develop in this building.

3.2.2 Shear Demand and Capacity

Developing plastic hinges at the ends of the beams, the shear demands on the columns are calculated. The beam bending moments are distributed between the top and bottom columns based on their flexural stiffness. To have the worst possible condition for the shear demand, it is assumed that no pullout occurs. To include the effect of axial loads on the exterior columns it is assumed that plastic hinges are developed at the ends of all beams over the entire height of the structure. It is also assumed that the stress in the beam reinforcement bars could go up to 1.25 times the yield stress. To increase the possible tensile force in the columns, only 90% of the dead load is considered.

It should be noted that when an exterior column is under tensile force from lateral loads, the bending moments at the end of the beams framed to the columns under consideration are positive, i.e., the bottom reinforcement is under tension. On the other hand, when the beams at the face of the exterior columns are under negative bending moments, the moments transferred to the columns are usually larger, though the column is under compression not only from the gravity loads, but also from the lateral loads. In other words, when the shear (bending moment) demand in an exterior column corresponds to the negative bending moments in the beams which are relatively large, the column is experiencing a compression force from the lateral loads that increases its shear capacity, and when the column is under tension from lateral loads, the shear force are smaller because it corresponds to the positive bending moments in the beams.

To calculate the shear force capacity, the following equation [Equation (6-3) in FEMA-273 (1997)] is used.

$$V_c = 3.5\lambda\left(k + \frac{N_u}{2000A_g}\right)\sqrt{f'_c}\,b_w d \qquad (3\text{-}1)$$

where: V_c is the shear force capacity of the concrete section; λ is one for normal weight concrete; N_u is the axial force; A_g is the area of the cross section in inch^2; f_c' is the strength of concrete in psi; and b_w and d are the width and the effective depth of the section. Excluding the corner columns, the worst columns in the structure are the columns located at the north or south sides of the building at the second story. Assuming that all the beams have developed plastic hinges at the ends, these columns in the transverse direction could experience a tension force of up to 50 kips. Under this tension force, the maximum shear force demand in the columns is only 99 kips,

while the shear force capacity is about 202 kips. When the columns are under compression force, the maximum shear force demand could go up to 207 kips. Based on Equation 3-1, the larger the axial compression force in the column, the larger the shear strength capacity. Therefore, neglecting the axial compression force due to seismic loads results in more conservative shear strength capacity of the columns. The shear strength capacity of the columns under only 90% of the dead load (axial stress of about 0.19 f_c') is about 261 kips. Therefore it is concluded that the shear strength capacities of the columns in the transverse direction are acceptable.

In the longitudinal direction, the columns located at the north and south sides of the building at the second story can undergo a shear force demand of 314 kips, which is larger than the 239 kips available capacity. Note that for interior columns, the axial load from the seismic effects is negligible. The ratio of the shear force demand to that of capacity is about 1.31.

Considering the above discussions, except for the interior columns of the perimeter frames in the longitudinal direction (particularly at the second story) the shear demand is less than the shear capacity in the columns. However, the transverse reinforcement in the columns is #3 spaced at 18 in. According to ACI-95 the spacing close to the joint is limited to 4 in. and the maximum spacing over the remaining part of columns is 6". Obviously none of these requirements are satisfied.

3.2.3 Main Reinforcement Splices

Based on the available drawings, a 24-bar diameter is used for the splices, which is not enough, particularly in tension, see UBC-97. This code also requires that not more than four bars can be spliced at any sections which, according to the drawings, has not been complied with.

3.3 JOINTS

Current seismic codes require that joints must have some minimum amount of transverse reinforcement. The joints in this building have no transverse reinforcement and therefore do not satisfy this requirement. Based on ACI-95, the nominal shear force demand in a joint can be calculated using the following equation:

$$V_{jh}=T_{lb}+C_{rb}-V_{tc} \qquad (3\text{-}2)$$

where V_{jh} is the horizontal shear force in the joint. T_{lb} and C_{rb} are the tension force in the left beam top reinforcement and compression force at the top of right beam (or vise versa) respectively, and V_{tc} is the shear force in the top column. To estimate the critical shear force demand in a joint, the ultimate bending moments of the beams assuming a steel stress equal to 1.25 times nominal yield stress are used. As the shear force in the top column reduces the shear force in the joint, it is assumed that half of the beam bending moments is transferred to the top column, and the other end of the top column is under zero bending moment. The maximum nominal horizontal shear stress in the exterior joints of the interior transverse frames at the second and third floor is about $9\sqrt{f'_c}$. It should be mentioned, however, that when this large level of shear stress takes place, the compressive axial load is larger than that of the gravity loads alone. Except for the case where the compressive axial load is so large that it could lead to compressive shear failure of the joint, the larger the compressive axial load, the larger the shear capacity of the joint. If only 90% of the dead load is considered, the axial stress at the joint is about 0.19 f'_c, and increasing the compressive axial load because of the seismic loads increases the shear capacity of the joint. The nominal horizontal shear stress in the exterior joints under maximum axial tension force of about 50 kips (maximum tensile stress of about 0.06 f'_c) is about $4.5\sqrt{f'_c}$. For these joints, the perimeter beams cover only half of the side faces of the joints, which according to ACI-95 the joints should be considered as if they are not confined by the transverse beams. FEMA-273 (1997) assumes a shear stress capacity of $6\sqrt{f'_c}$ for the exterior joints without transverse beams, regardless of the amount of axial load, if there is little or no transverse reinforcement in the joints. Therefore, being that the demands ($9\sqrt{f'_c}$) are significantly higher than the capacity accepted by FEMA ($6\sqrt{f'_c}$), the exterior joints are vulnerable and need to be upgraded.

The demands of shear stress for the interior joints of the exterior and interior transverse frames, at the second floor could go up to $10\sqrt{f'_c}$. Based on the 1997 FEMA-273, the maximum shear stress capacity of interior joints without and with transverse beams are $10\sqrt{f'_c}$ and $12\sqrt{f'_c}$, respectively.

3.4 VULNERABILITY OF EXISTING BUILDING

The problems that this building faces, aside from the corner columns, are listed below. There could be excessive story drift, which can lead to severe nonstructural damage. The shear stress in exterior joints is excessive. The splicing of main reinforcements is inadequate. Also the transverse reinforcement in the columns are spaced at 18 in., which is not desirable even if the columns are much stronger than beams. The pullout of some bottom reinforcement bars that have an embedment length of only 6 in. is another weakness of this building.

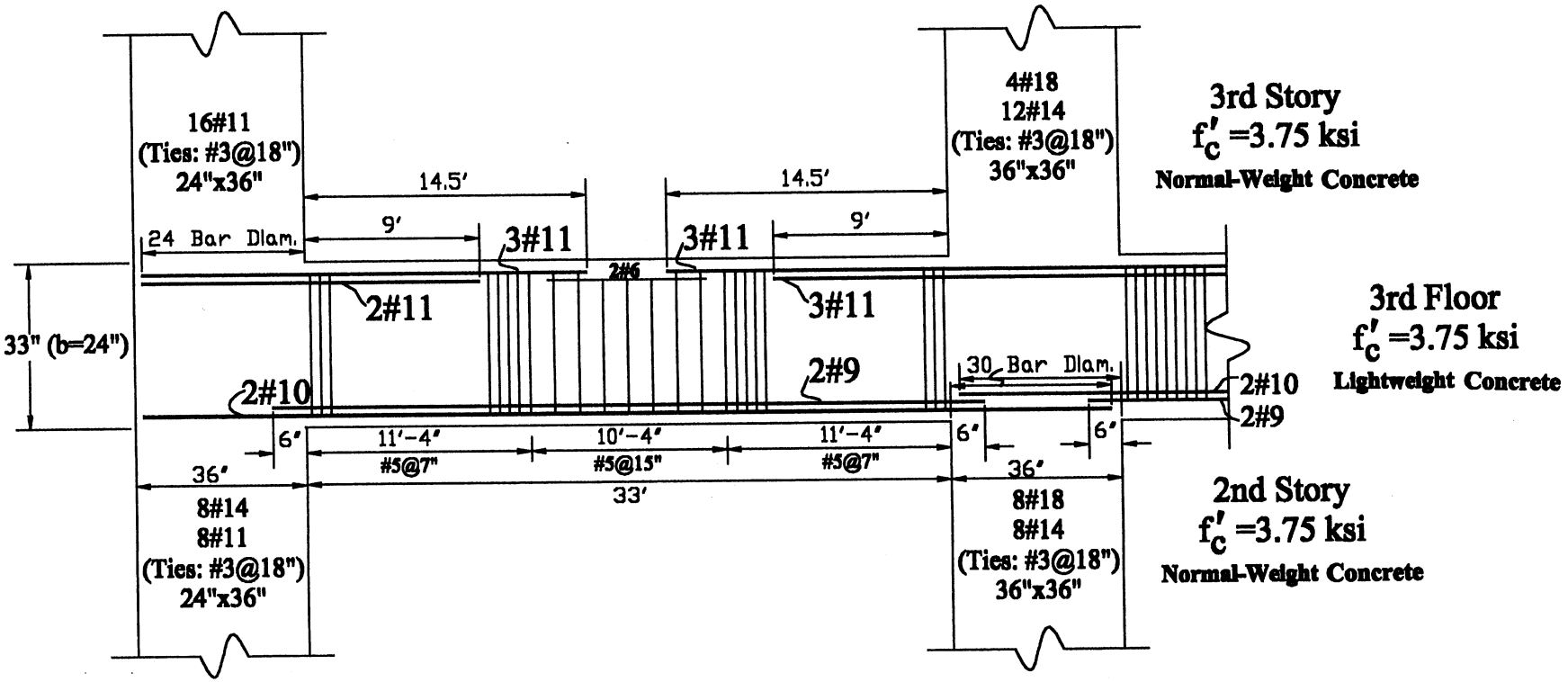

Figure 3.1 Reinforcement details for the 3rd floor beams of interior transverse frames.
(Similar beam reinforcement is used at the 4th and 5th floors.)

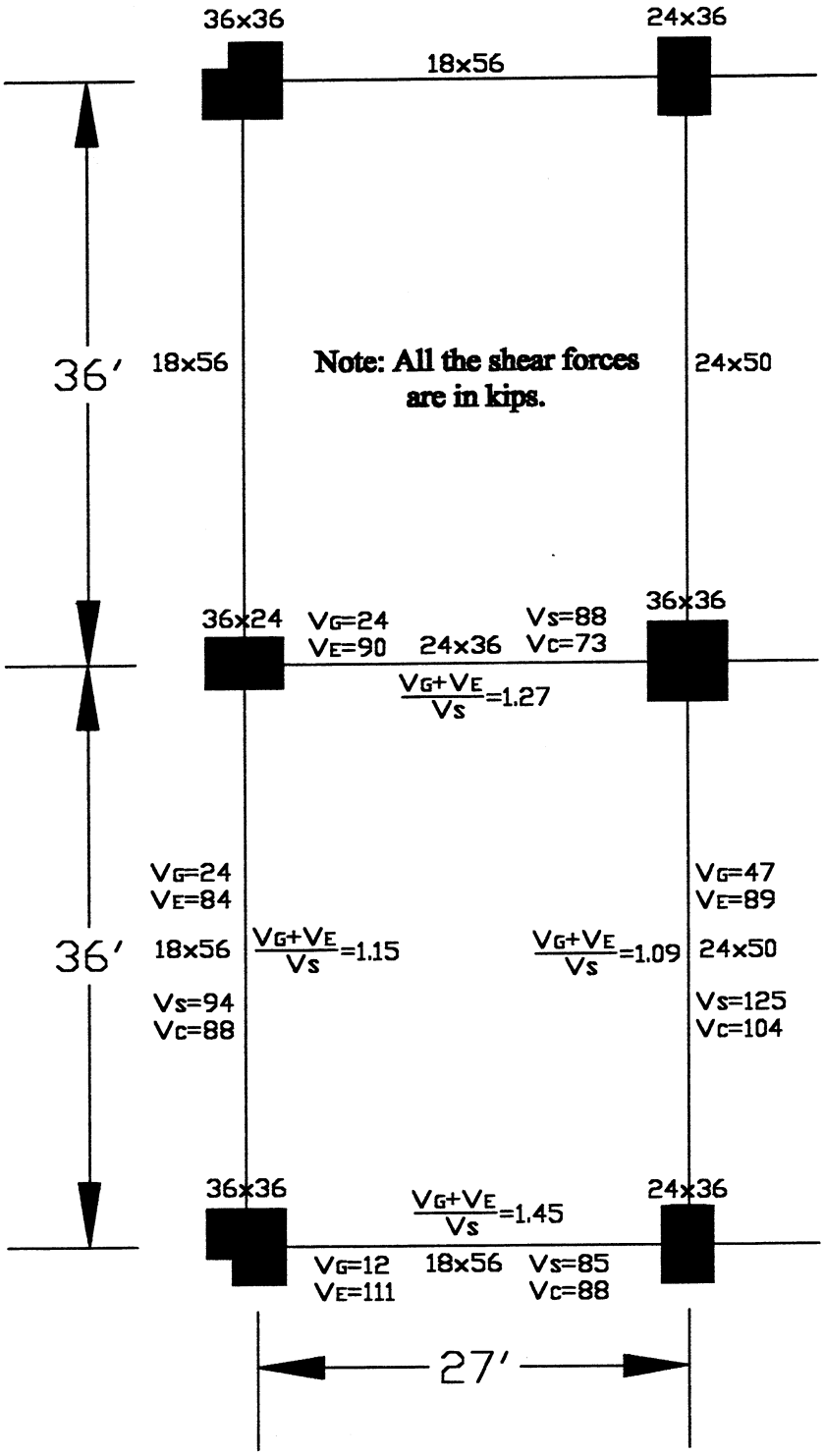

Figure 3.2 The ratio of shear strength demand to strength capacity at the second floor.

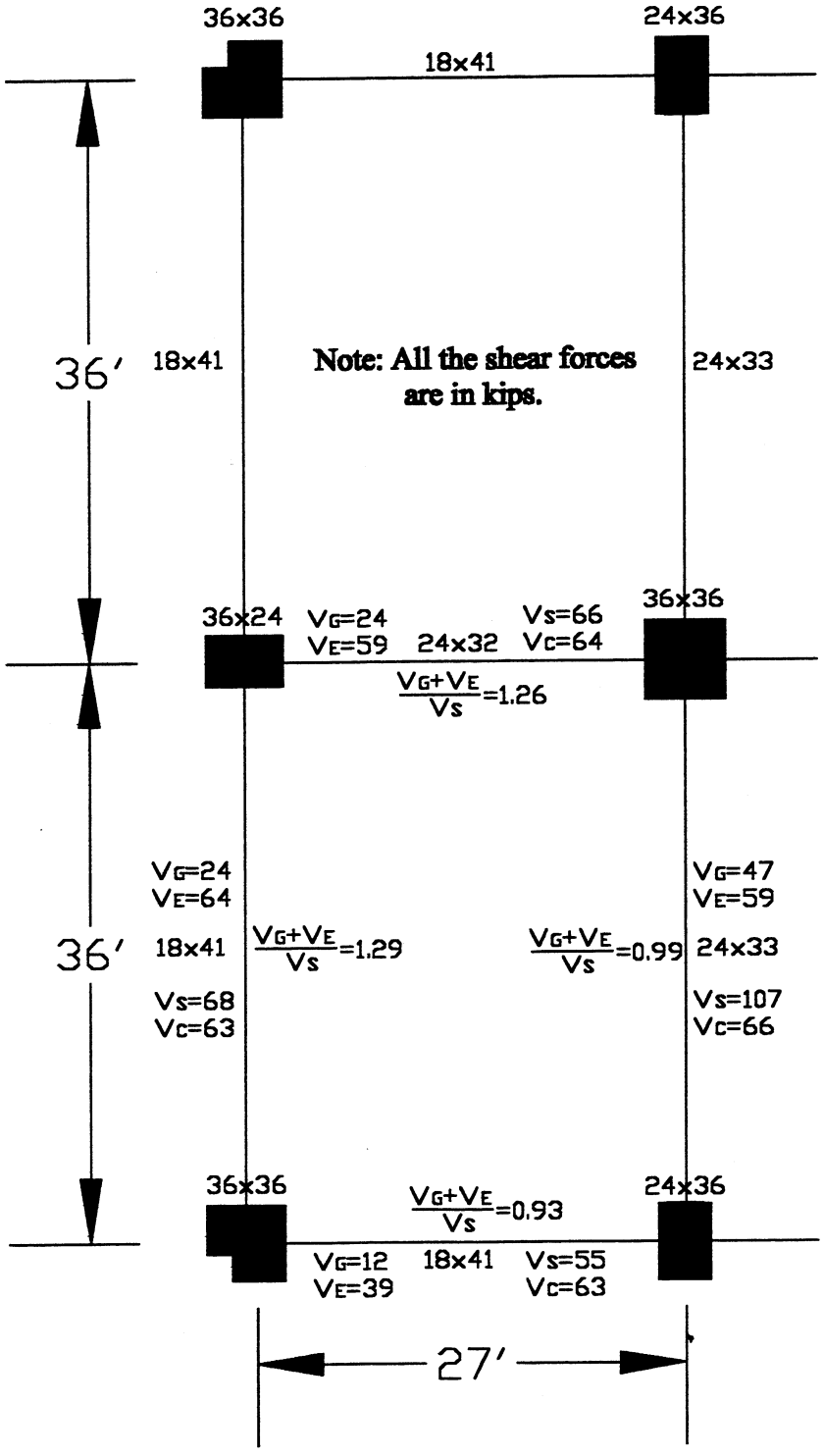

Figure 3.3 The ratio of shear strength demand to strength capacity at the third floor.

4 Inelastic Model of Structure in Transverse Direction (Pushover Analysis or Response to Severe Pulse-Type Ground Motions)

4.1 SIMPLE NONLINEAR ONE-INTERIOR-FRAME MODEL

To start with a relatively simple model of the structure, one interior transverse frame of the structure is modeled. Having rigid floors and assuming that torsion could be neglected, if the lateral stiffness of frames at different stories varies gradually and proportionally with height, in the elastic domain, the lateral inertia forces developed by each frame in the direction under consideration are proportional to its lateral stiffness. As soon as plastic hinges start to form, the distribution of the lateral forces between different frames deviates from the distribution valid in the elastic region. However, if the strength and stiffness of different elements, and particularly those of the beams for this structure, are fairly proportional, formation of plastic hinges will not significantly alter the distribution of lateral loads between different frames. Since in the elastic domain, the two end frames in the transverse direction are almost 30% stiffer than the six equal interior transverse frames, it can be assumed that a good estimation of the seismic response of a single interior frame to EQGMs can be obtained by conducting a dynamic analysis of the frame considering as a reactive mass at each floor, 1/(6+2*1.3)=0.116 times the total mass at this floor. Note that the gravity load carried by each interior frame comes from the vertical tributary (27-ft-wide) area of the frame. Using the flexural stiffness of beams and columns equal to 0.35 and 0.70 times the flexural stiffness corresponding to the gross moment of inertia, as was used in the three dimensional model of the building, the first period of the model is found equal to 2.85 sec, which is close to the first period of the three-dimensional model which was 2.9 sec.

In order to have a more realistic estimation of the flexural stiffness of the elements, the following section analyses are carried out. Assuming linear behavior of concrete in compression before the yielding of the reinforcement in tension, the flexural stiffness of the transformed cracked sections of lightweight RC beams is calculated. The calculation also assumes that all the six-inch embedded reinforcing bars at the bottom of the beams which are only at the first four floors are pulled out. At the third floor, the flexural stiffness of the beam sections under negative bending moments (tension at the top) and positive bending moments (tension at the bottom) at the face of the columns are approximately 0.75 E_cI_g and 0.35 E_cI_g, respectively, where I_g is the gross moment of inertia of the rectangular section, neglecting the reinforcement and E_c is the modulus of elasticity of concrete defined by ACI 318-95. It should be noted that under positive bending moments the contribution of the slab acting as a flange of a T-beam with a certain effective flange length has been considered and will be discussed later. Note that the calculated flexural stiffness of the sections at the third floor holds for almost all the beam end sections of the interior frames in the transverse direction (except for the second floor) along the height of the structure.

Using the average flexural stiffness of the beam cracked sections under the positive and negative bending moments, a value of 0.55 E_cI_g can be used for all the beams. This new value makes the structure stiffer and results in a period of about 2.3 sec. It should be noted that if Equation (9-7) of ACI 318-95 were used, the stiffness of the beams would have been even further increased as a result of tension stiffening, and the period of the structures would have become shorter. On the other hand, including the effect of slippage of the bars in the joints would decrease the stiffness of the beams. For simplicity, the effects of the tension stiffening and slippage of the bars in the joints are neglected.

Since the period of the structure in the transverse direction under the Northridge earthquake was about 3.0 sec, one can increase the period of the structure by including some flexibility at the bottom of the first-story columns. There are two main sources for the base flexibility. One is the fact that although the shear walls in the basements could limit the lateral displacement of the ground floor to a negligible value, there is some rotational flexibility at the base of the first-story columns that comes from the flexibility of beams and columns in the basement. The second source that contributes to the flexibility of the structure is the pile foundation that can result in some vertical flexibility of the base supports.

To include these two sources of the base flexibility, three elements as shown in Figure 4.1 are added to the model. The flexural stiffness of each added element is set equal to the summation of the flexural stiffness of beams and columns in the plane of the transverse frames that are connected to the bottom of the first-story columns. It should be noted that the main portion of this flexural stiffness comes from the basement columns. Adding some rotational flexibility by including the flexural stiffness of these elements below the first-story columns increases the period of the model to 2.4 sec (at this stage, the axial stiffness of the added elements is set equal to a large number). Then the axial stiffness of these elements are adjusted such that the period of the model is increased to 2.9 sec, which is equal to the period of the previous three-dimensional model in the transverse direction. Also, to avoid any effect on the distribution of the forces under gravity loads, the axial stiffness of the element at the center of the transverse frame is adjusted further to have equal vertical displacement at the bottom of first-story columns, under the gravity loads.

Using the flexural stiffness of beams and columns equal to 0.55 and 0.70 times the flexural stiffness corresponding to the gross moment of inertia and also limiting the flexural strength of the beams to their ultimate strength, the response of the model under the recorded motion at the building during the Northridge earthquake is studied. Using the first two periods of the structure, in the damping matrix, $C=\alpha M+\beta K$, α and β are found such that 5% damping in the first two modes of vibration is achieved; M and K are the mass and stiffness matrices, respectively. Note that the resultant modal damping in the third and fourth modes of vibration are 7.8% and 8.4%, respectively. It should be noted that the structure did not experience too much inelastic behavior; the maximum plastic rotation occurred at the exterior end of the second floor beam and was equal to 0.0031 radian. The roof displacement of the structure due to the recorded motion during the Northridge earthquake is compared in Figure 4.2.

4.2 DETAILED MODEL OF STRUCTURE IN TRANSVERSE DIRECTION

4.2.1 Interior Frames

The details of the beam reinforcement at the 2^{nd}, 3^{rd} to 5^{th}, 6^{th} to 8^{th}, 9^{th} to 11^{th}, and 12^{th} to 13^{th} floors, and at the roof of the interior frames, are given in Figures 4.3 to 4.8, respectively. Also the details of all column reinforcement are given in these figures.

Under the gravity loads, beams undergo negative bending moments at the ends and positive moments at the middle parts. Under added monotonically increasing lateral loads the

distribution of the bending moment changes. By increasing the lateral loads, when the beam end moments have different signs, at one ends of the beams the top reinforcement and at the other ends the bottom reinforcement are in tension. Assuming the most possible bending moment distribution under the combined action of the gravity loads and seismic loads, the flexural stiffness of different segments of the beam (before and after yielding) and also the flexural strength of the segments are calculated.

4.2.1.1 Moment-curvature analysis for beam sections

- Beams at the third to fifth floors. Figures 4.9 shows the stress-strain relationship for Billet steel (Large and Chen, 1968) and Figures 4.10 shows the stress-strain relationship for lightweight concrete used in the building. Figure 4.11 shows the moment-curvature relationship for the beams at the interior ends at the third floor, under a negative bending moment. The maximum curvature is controlled by the maximum concrete strain in the confined concrete. The maximum useable concrete strain, ε_{cu}, is calculated based on the following Equation recommended by Scott et al. (1982) for the case of columns of normal weight concrete.

$$\varepsilon_{cu} = 0.004 + 0.02\, \rho_H\, f_y \qquad (4\text{-}1)$$

where ρ_H and f_y are volumetric confining reinforcement and the corresponding yield stress, respectively. It should be noted that the maximum useable concrete strain, in the above equation, is the value at the first hoop fracture. Also the above equation is suggested for normal weight RC columns under concentric loads. Under eccentric loads, since only a portion of the section is under compression, larger values for ε_{cu} are reported (Scott et al., 1982). Depending on the relative strength of the cement and the aggregate, ε_{cu} for lightweight concrete sections could be larger or smaller than that of normal weight concrete. In this study it is assumed that ε_{cu} for lightweight concrete beams could be calculated from Equation (4-1). For ρ_H = 0.0073 (#5 at 7 in. available in the interior transverse beams at the third floor and up) and f_y =40 ksi, ε_{cu} =0.01 is found. It is assumed that buckling of the reinforcing bars can not occur at this level of compressive strain.

To have an equivalent bilinear moment-curvature relationship, the following procedure is used. Since the steel could have higher yield and ultimate stresses, the ultimate curvature based on ε_{cu} as given by Equation (4-1) of the section is calculated assuming 10% higher steel yield

and ultimate stresses. Figure 4.12 shows the moment-curvature relationship of the section having stronger reinforcement.

To linearize the post-yielding behavior, a line segment is drawn such that the maximum strength and the total area under the bilinear and nonlinear models are the same. It should be noted that the two compressive #9 bars with 6-inch embedded length are conservatively neglected: their inclusion would result in larger ultimate curvature and a little larger moment.

Figure 4.13 shows the moment-curvature relationship for the T-section beam at the exterior ends of the third floor under a positive bending moment. The slab is 4 in. thick and the effective flange on each side of the beam is considered 32 in. wide. It is assumed that the two 6-inch embedded #9 bars are pulled out. The same procedure as described above for negative bending moments is used to linearize the post-yielding behavior. As a first try, the linearization is done up to a curvature value of 0.0025 1/in. If the results of the nonlinear analysis show that the curvature of the section under consideration exceeds the assumed maximum curvature of 0.0025 1/in., the post-yielding portion will be modified. Note that the ultimate curvature of the section (about 0.0042 1/in.) is now controlled by the fracture of the steel and not by the maximum concrete strain. The maximum concrete strain at the ultimate curvature is only about 0.005 1/in.

Figure 4.14 shows the moment-curvature relationship for the beams at the exterior ends at the third floor, under a negative bending moment. The moment-curvature relationship for the T-section beam at the interior ends of the third floor, under a positive bending moment, is similar to that of Figure 4.13, and having six or five #11 bars in the compression region of a T section has a minor effect on the moment-curvature relationship.

In the portion of the beam, which is under negative bending moment, a relatively large slope of the bending moment diagram is expected. As a result, it is assumed that the second end nodes which are 4.5 ft away from the face of the column (see Figure 4.1) and have the same strength as the section at the face of the columns, do not undergo plastic deformation. This assumption will be checked after the nonlinear analysis is carried out. In the portion of the beam which is under positive bending moment, the slope of the bending moment diagram is rather small, however, the second end nodes which are 4.5 ft away from the face of the column are stronger than the section at the face of the columns, because pullout is not expected at the second end node. Therefore it is assumed that the second nodes do not undergo plastic deformation. This

assumption will be checked after the nonlinear analysis is carried out. Therefore the post-yielding behavior of the interior nodes of the beams is not studied at this stage.

- Beams at the second floor. Figure 4.15 shows the moment-curvature relationship for the beams at the interior ends of the second floor under a negative bending moment. For ρ_H = 0.0047 (ties are #4 at 6 in.) and f_y =40 ksi, ε_{cu} =0.0078 is found. Although the two #9 bars with 6 inch embedment are in compression under negative moments, it was considered that they could not resist these compression forces because they could have been pulled out by a positive moment acting previous to the negative moment. Figure 4.16 shows the moment-curvature relationship for the beams at the exterior ends of the second floor under a negative bending moment. Since there is no pullout of the #9 bars at the exterior ends, the ultimate strength and curvature are larger than those shown in Figure 4.15.

Figure 4.17 shows the moment-curvature relationship for the T-beam sections at the interior ends of the second floor, under a positive bending moment. Note that the ultimate curvature of the section (about 0.0026 1/in.) is now controlled by the fracture of the steel and not by the maximum concrete strain. Comparing Figures 4.13 and 4.17, since the depth of the beam at the second floor is larger than that at the third floor, a smaller ultimate curvature value is obtained.

Figure 4.18 shows the moment-curvature relationship for the T-beam sections at the exterior ends of the second floor under a positive bending moment. Since there is no pullout, the ultimate strength is larger than that shown in Figure 4.17; however, since the distance of the tensile reinforcement bars to the neutral axis in two cases is almost equal (the depth of neutral axis is very small for these T-sections) and since the maximum curvature is controlled by the fracture of tensile reinforcement, the ultimate curvature in two cases is almost the same.

- Beams at the sixth floor and up. The concrete cross sections and the amount of ties (except on the roof) are all the same as those at the third floor. The results of the beam section analyses of these floors are summarized below.

4.2.1.2 Beam bending moment distribution

Considering the gravity loads (dead load plus 20% live load; FEMA-273), the beam bending moment is found such that the end moments are equal to M^-_y and M^+_y which are negative and

positive yield bending moments at the ends of the beam (Figure 4.19). These values are found from bilinear models of the moment-curvature relationships of the beam end sections.

Using the above moment diagram of a beam, an estimation of the bending moment sign over different portions of the beam is made.

4.2.1.3 Beam flexural stiffness

As discussed above, assuming linear behavior of concrete in compression before the yielding of the reinforcement in tension and considering the sign of the bending moment, the moment of inertia of the transformed cracked sections before yield is calculated. If the moment of inertia at two ends of a beam segment (i.e., between adjacent nodes) are not close (more than 20% difference) the stiffness matrix of a linearly varied cross section is calculated and used in the analysis. The flexibility method of analysis is used to find the flexibility matrix of a simply supported beam with the rotation with respect to the cord (a line that connects two ends of the beam) as the variables, Figures 4.20 and 4.21. Then the stiffness matrix is found by calculating the inverse of the flexibility matrix and the result is used as input data to the computer program Drain-2DX.

- Beam moment-rotation relationship. Since the input data to the Drain-2DX program should be in terms of moment-rotation, the bilinear moment-rotation relationship for each beam segment that is expected to undergo plastic rotation is calculated. Based on the assumed ratio of the bending moment at two ends of each segment as discussed above, the post-yielding flexural stiffness is calculated (as shown on pages 4-8). It is assumed that except for the second floor beam, all other beams have almost the same ratio of bending moment values at two ends of each segment as given in Figure 4.19.

Yield and Plastic Rotations for Beams with Linear Bending Moment Distribution[1]

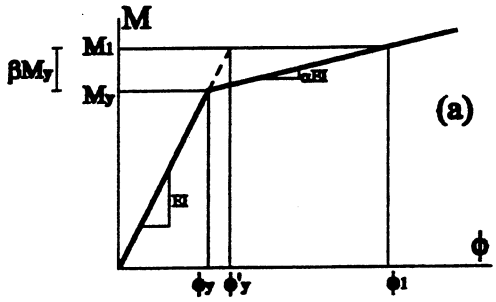

Moment-Curvature Relationship

$\alpha = EI_{p1}/EI_{e1}$

$\beta M_y = M_1 - M_y$

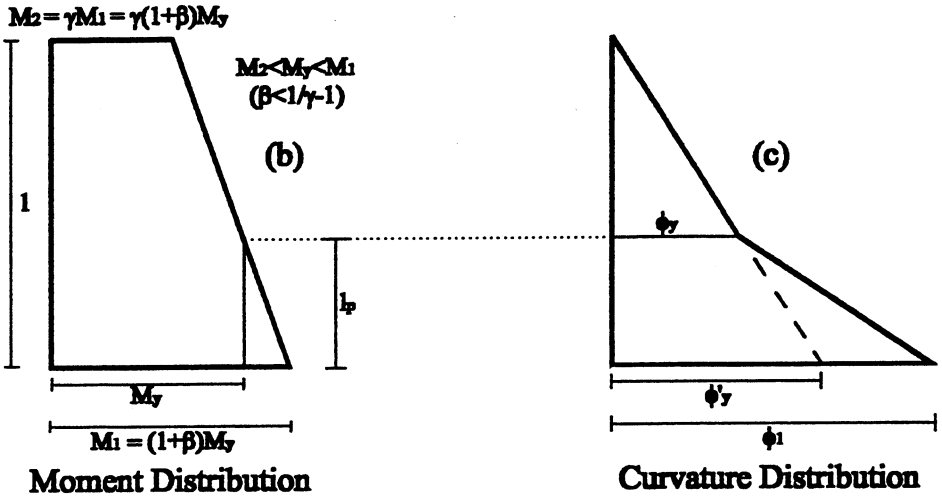

Moment Distribution

Curvature Distribution

From Figure (a): $\dfrac{\beta M_y}{\phi_1 - \phi_y} = \alpha EI \Rightarrow \phi_1 = \left(1+\dfrac{\beta}{\alpha}\right)\dfrac{M_y}{EI} = \left(1+\dfrac{\beta}{\alpha}\right)\phi_y$

In Figures (a) and (b): $\phi'_y = (1+\beta)\phi_y$

From Figure (b): $\dfrac{M_1 - M_y}{M_1 - M_2} = \dfrac{l_p}{l} \Rightarrow l_p = \dfrac{\beta}{(1+\beta)(1-\gamma)} l$

Therefore: $\theta_p = (\phi_1 - \phi'_y)\dfrac{l_p}{2} \Rightarrow \theta_p = \dfrac{\beta^2(1/\alpha - 1)}{2(1+\beta)(1-\gamma)}\phi_y l$

For β=0, from Figure (b): $\theta_y = \dfrac{1+\gamma/2}{3}\phi_y l$

[1] Because of the concentrated gravity loads, the moment distribution of the beams is linear.

As shown in Figures 4.3 to 4.8, under positive bending moments the amount of the flexural reinforcement of the ends of the beams are smaller than that of the sections somewhat far from the ends. This end flexural weakness results in a shorter plastic region. The effect of this phenomena on the moment-curvature relationship is studied in the following page. Using the equations given in the previous and next pages, the moment-rotation for all the end segments of the beams are calculated. Figures 4.22 to 4.28 show the results for the second and third floors. A similar procedure is carried out for other floors.

4.2.1.4 Slippage of reinforcing bars within joints

The slippage of reinforcing bars within the joints can contribute to increase the flexibility of the structure. Although there is some slipping even before the reinforcing bars yield, since it is a local effect, the slippage is considered only after the bars at the ends of the beam yield. Assuming a length equal to about 1.5 d_b as the free length of the bars at the face of the columns (Oesterle, 1986) and assuming a linear variation of stress over the remaining portion of the bars, the elongation of the bar is calculated. Then dividing this value by the distance from the bar to the neutral axis, the additional rotation corresponding to the steel strain at maximum curvature is calculated; see Figures 4.22 to 4.28. It should be noted that under a positive bending moment, since the maximum curvature is controlled by the steel fracture, the additional rotation is larger than that under the negative bending moment where the maximum curvature is controlled by the concrete strain.

Although including the slippage before yielding results in a larger period of vibration, including tension-stiffening results in stiffer elements and a shorter period of vibration. For simplicity both effects are neglected. The results of all the above analyses are summarized in Figures 4.29 to 4.31.

4.2.1.5 Flexural properties of columns

Moment-curvature and moment-rotation relationships for the columns in the first story are given in Figures 4.32 to 4.35.

Plastic Rotations for Beams with Pullout Problem (Weak End Flexural Strength)

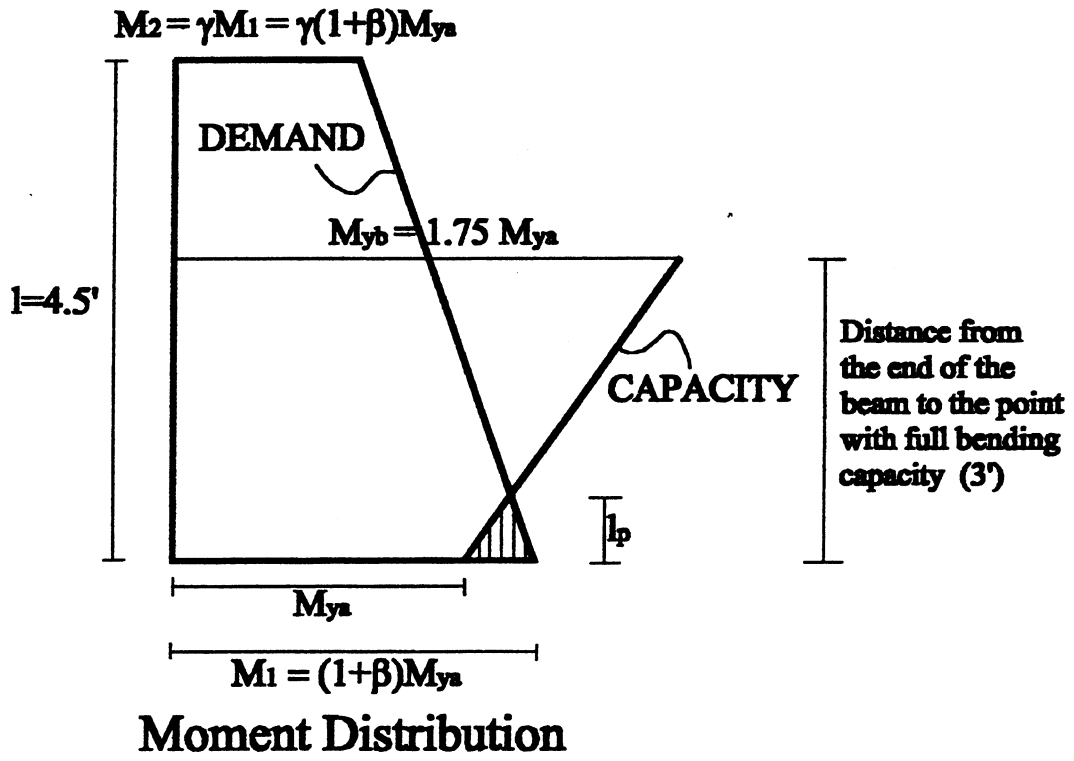

Moment Distribution

$$l_p = \frac{\beta}{1.125 + (1+\beta)(1-\gamma)}\, l$$

$$\phi_1 = \left(1 + \frac{\beta}{\alpha}\right)\phi_y \Rightarrow \theta_p = \frac{\beta\, l_p}{2\alpha}\phi_y$$

Note: Yield strength of 2#9 and 2#10 bars is almost 1.75 times that of 2#10 bars.

4.2.2 Exterior Frames

The details of the beam reinforcement at the 2nd, 3rd to 5th, 6th to 8th, 9th to 11th, and 12th to 14th floors of the exterior frames are given in Figures 4.36 to 4.40, respectively. Also the details of all column reinforcement are given in the above figures.

Since the corner columns of the building are under relatively light axial gravity loads and since the exterior frames are stiffer than the interior frames, it is expected that under lateral loads, corner columns undergo tensile axial loads. Figure 4.41 shows the moment-curvature relationship of the corner column under a tensile axial force of 250 kips which is expected to be carried under combined gravity and lateral loads. Figure 4.42 shows the corresponding moment-rotation relationship. Figures 4.43 and 4.44 show the moment-curvature and moment-rotation relationship of the corner column under a compressive axial force of 1200 kips, respectively. Properties of other members are developed in the same way as were those for interior frames.

4.2.3 Model of Building and Some Results

The model of the building in the transverse direction is given in Figure 4.45. All six similar interior frames are modeled as one frame with strength and stiffness set equal to six times those for one interior frame. Similarly, the two end frames are modeled as another frame that is linked to the previous frame by axially rigid pinned-end truss elements. The first period of this model is also 2.9 sec, as it was for the simple model. A pushover analysis of the complete two-dimensional model of the structure in the transverse direction under increasing inverted triangular lateral load is carried out. Figure 4.46 shows the force-displacement relationships of the model up to a total drift of 1%. The corresponding displacement ductility is about 1.45. Figure 4.47 shows the profile of displacement along the height of the building. This profile is close to being linear, suggesting that the inverted triangularly distributed lateral load might be a reasonable shape for the lateral load on this building. From analysis of Figure 4.47, it is clear that the maximum IDI takes place at the third story and that its value is about 1.5 the average or total Drift Index.

Figures 4.48 and 4.49 show the plastic rotations and some of the internal forces for one interior and one exterior frame, respectively. The column shear forces are below their capacities. Note that the corner columns that experience tensile force from lateral loads have developed plastic hinges at the bottom of the first story. All the plastic rotations of the beams are within acceptable limits. As an example, the maximum plastic hinge rotation under negative bending

moment at the third floor of the interior frame is about 0.0055 radian. Figure 4.23 shows that this plastic hinge rotation corresponds to a rotation ductility of about 2.9 which is twice as large as the ductility of the whole structure, which could be explained by the fact that the beam plastic hinges are developed only in the bottom floors of the structure, so the demand is localized. The rotation ductility under positive bending moments, particularly where the pullout occurs, is even higher.

4.2.3.1 Probable maximum base shear

Assuming that the shear capacity of the columns is larger than the shear demand (this assumption will be checked later) the maximum base shear is controlled by the end bending moments of the first-story columns. By increasing the lateral loads, at a total lateral load of 0.150 W, where W is the total weight of the building, the exterior columns of interior frames that are under tensile axial force from the lateral loads and the corner columns (exterior columns of exterior frames) that are under compressive axial force from the lateral loads, reach their maximum plastic rotation at the bottom of the first story. At a total lateral load of 0.155 W and 0.163 W, the other exterior columns of interior frames and the interior columns of interior frames reach their maximum plastic rotation at the bottom of the first story, respectively. Note that after reaching the maximum plastic rotation, the bending moment carrying capacity at the base will drop which is not modeled in the Drain-2DX model. At this level, none of the beam ends have reached maximum rotation capacity. Knowing that there are six interior frames and only two exterior frames and knowing that at a total lateral load of 0.164 W, all the bottoms of the columns of the interior frames and also the bottoms of the two corner columns have reached their maximum plastic rotation (maximum bending moment), and considering the fact that at this level the bending moment at the top of the first-story columns of the interior frames is at most about 1/4 of the bottom bending moments and cannot increase the shear force of the columns considerably, while the bending moments at the bottom are decreasing, one can conclude that the probable maximum base shear in the transverse direction is between 0.150 W and 0.163 W. It should be noted that at this level, the shear force demands of the columns are less than those of capacities. Also it should be mentioned that the real drop in the bending moment carrying capacity at the bottom of the columns could be found by examining the moment-curvature relationships and the drop occurs before reaching the maximum rotation capacity.

4.2.3.2 Maximum interstory drift index and maximum global drift

Under a total lateral load of 0.163 W, the maximum interstory drift equal to 2.1% at the third and fourth stories occurs. At this level, the maximum global drift is about 1.35%. Since a story drift of about 2% is usually the maximum drift that the nonstructural elements could undergo without excessive damage, and since beyond this level of the lateral loads the load should drop and the demand on the flexural strength and consequently the demand on the shear strength of 20 columns (out of 24) at the bottom of the first story should decrease (which is not possible to compute with the available model of the building), the above-mentioned values can be assumed to be reasonable maximum values for the as-built structure.

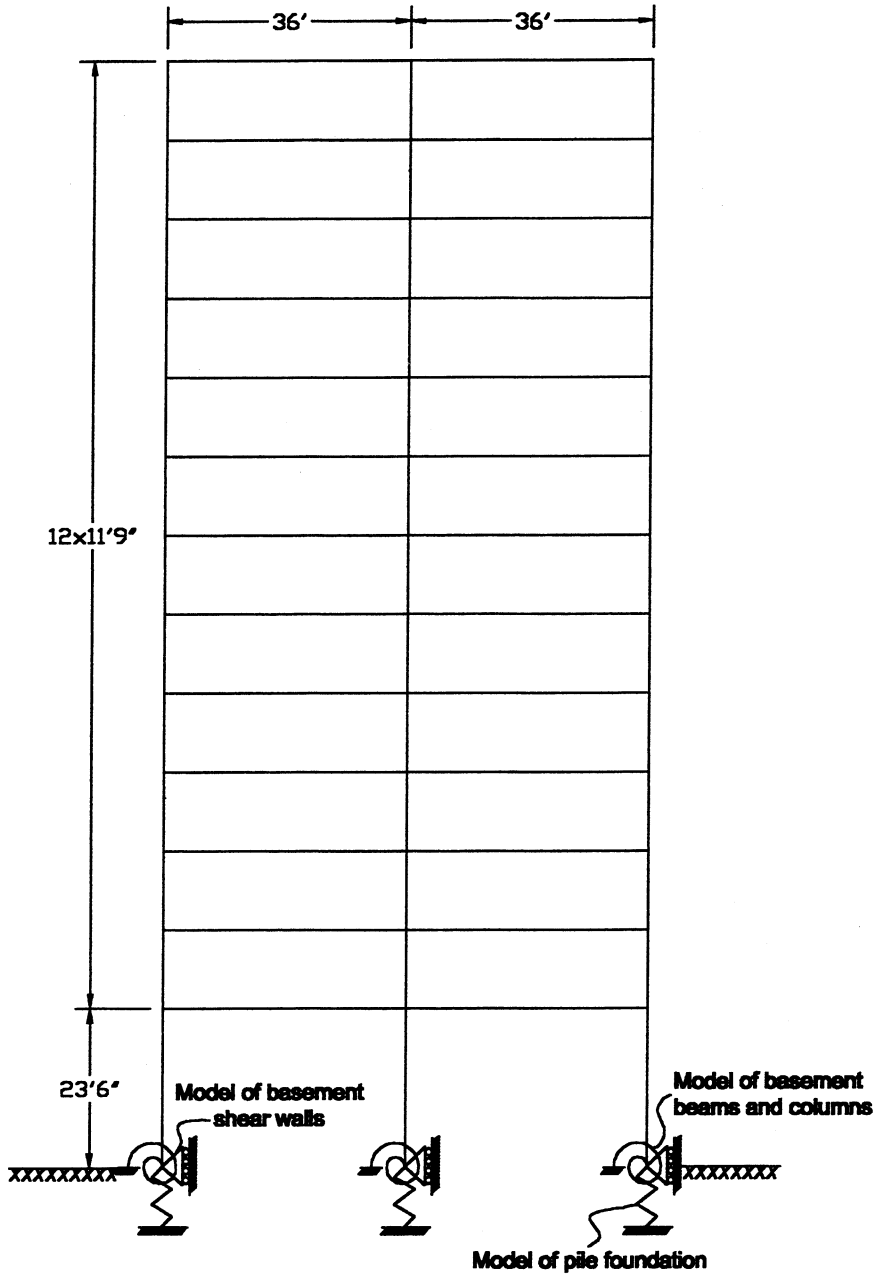

Figure 4.1 The model of an interior frame.

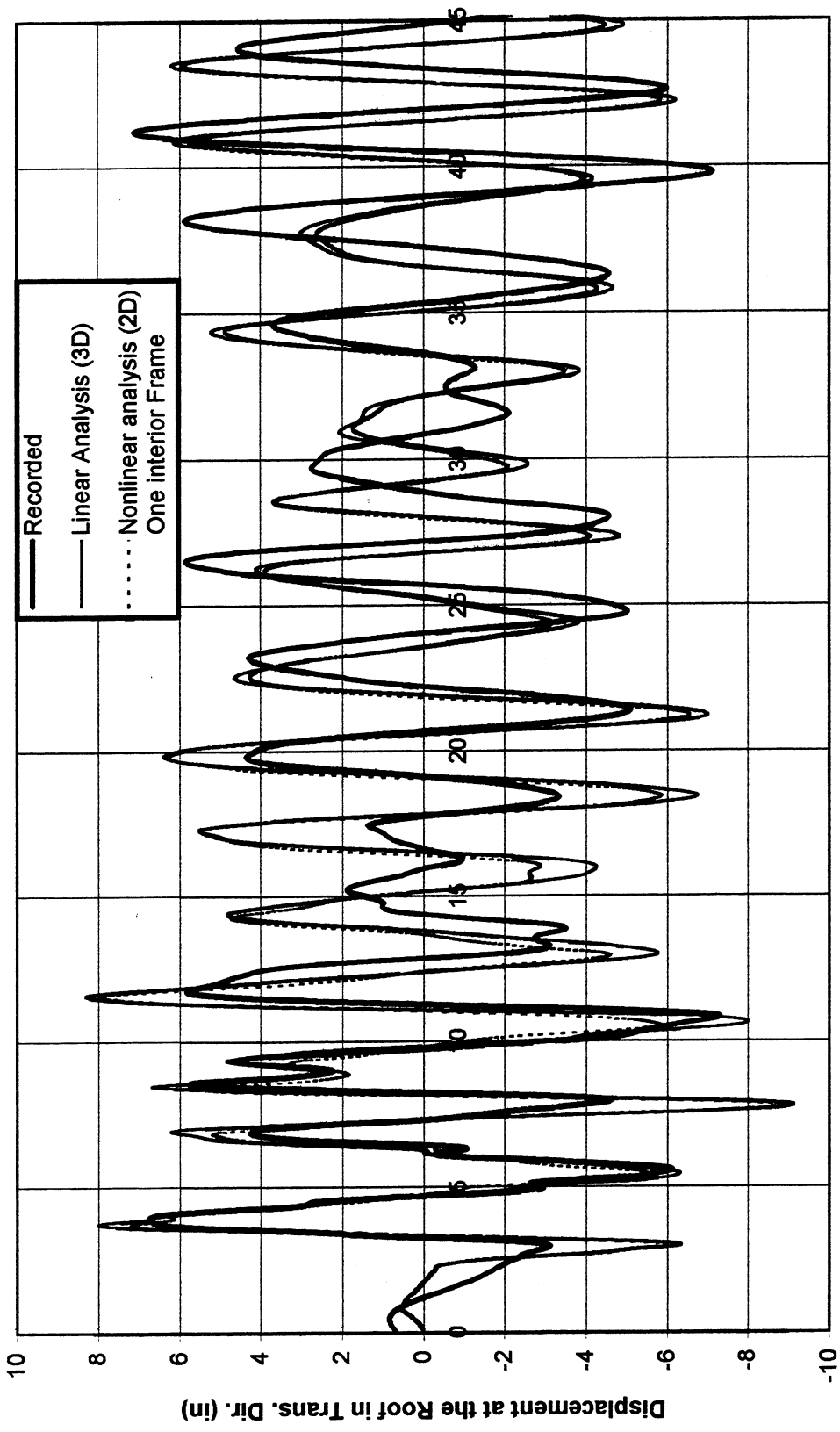

Figure 4.2 Comparison between roof recorded and calculated displacement in transverse (N-S) direction.

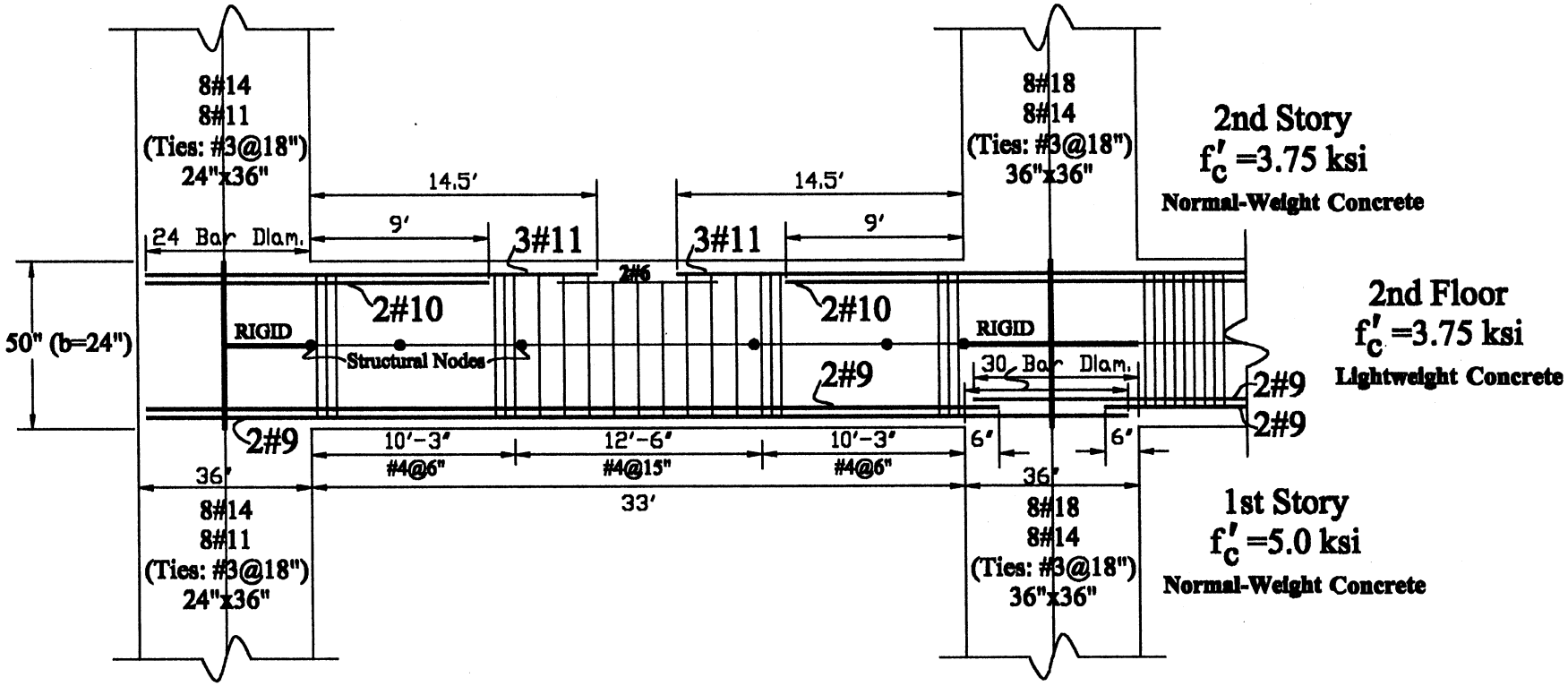

Figure 4.3 Reinforcement details for the 2nd floor beams of interior transverse frames.

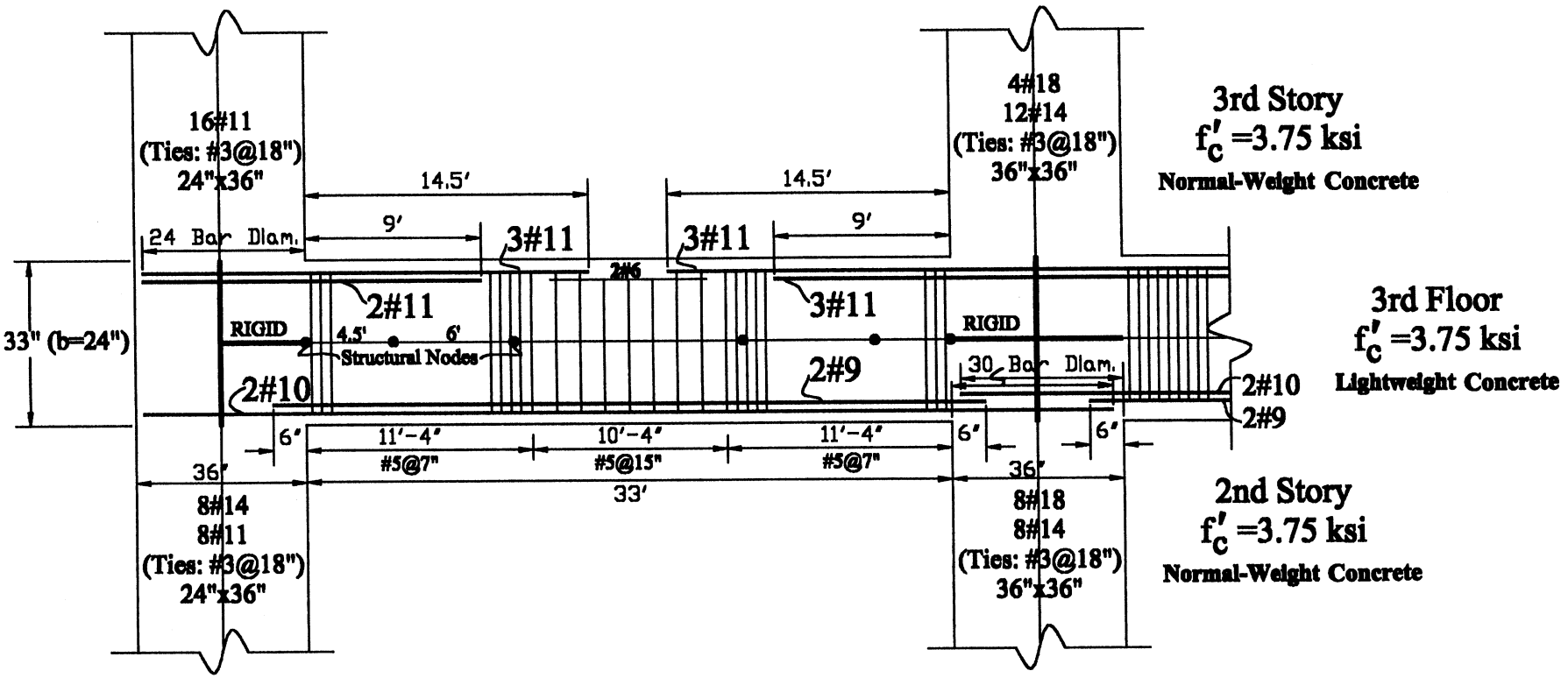

Figure 4.4 Reinforcement details for the 3rd floor beams of interior transverse frames.
(Similar beam reinforcement is used at the 4th and 5th floors.)

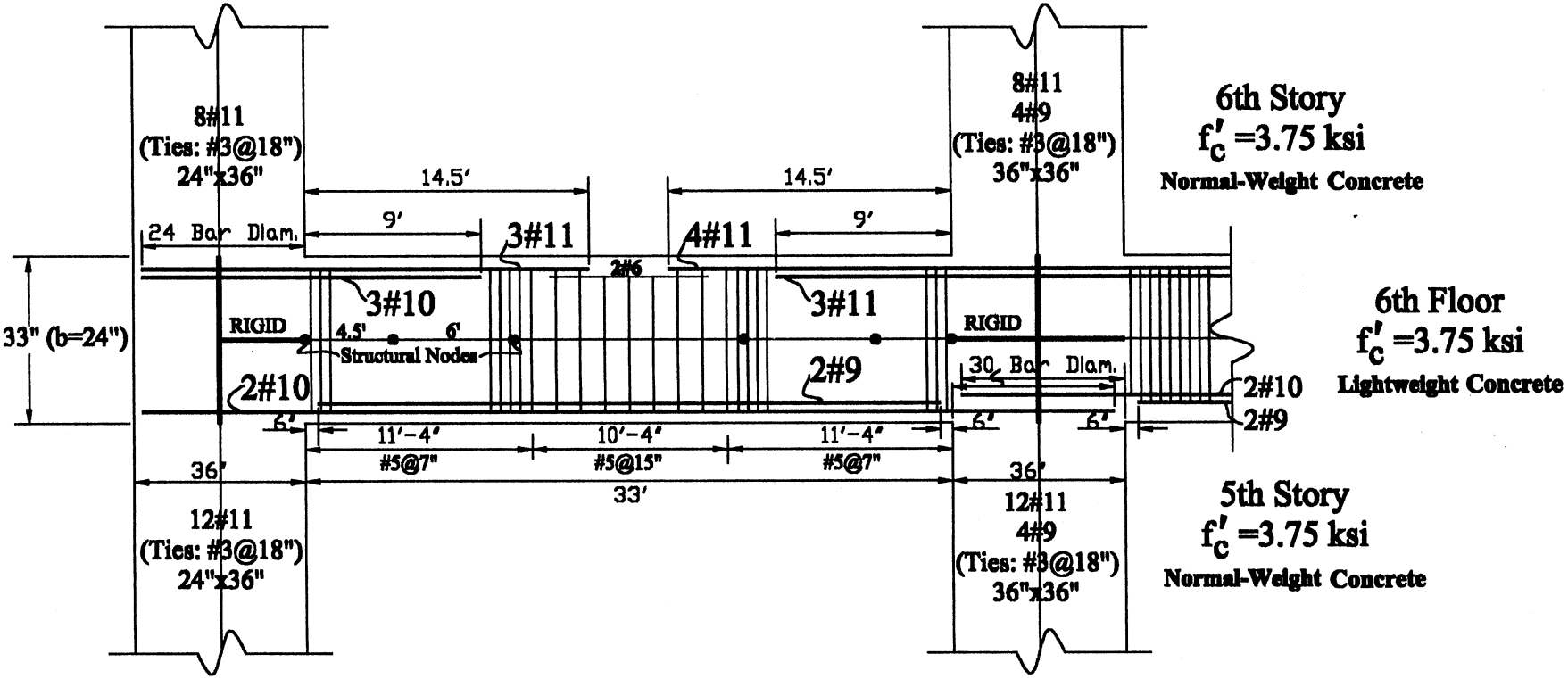

Figure 4.5 Reinforcement details for the 6th floor beams of interior transverse frames.
(Similar beam reinforcement is used at the 7th and 8th floors.)

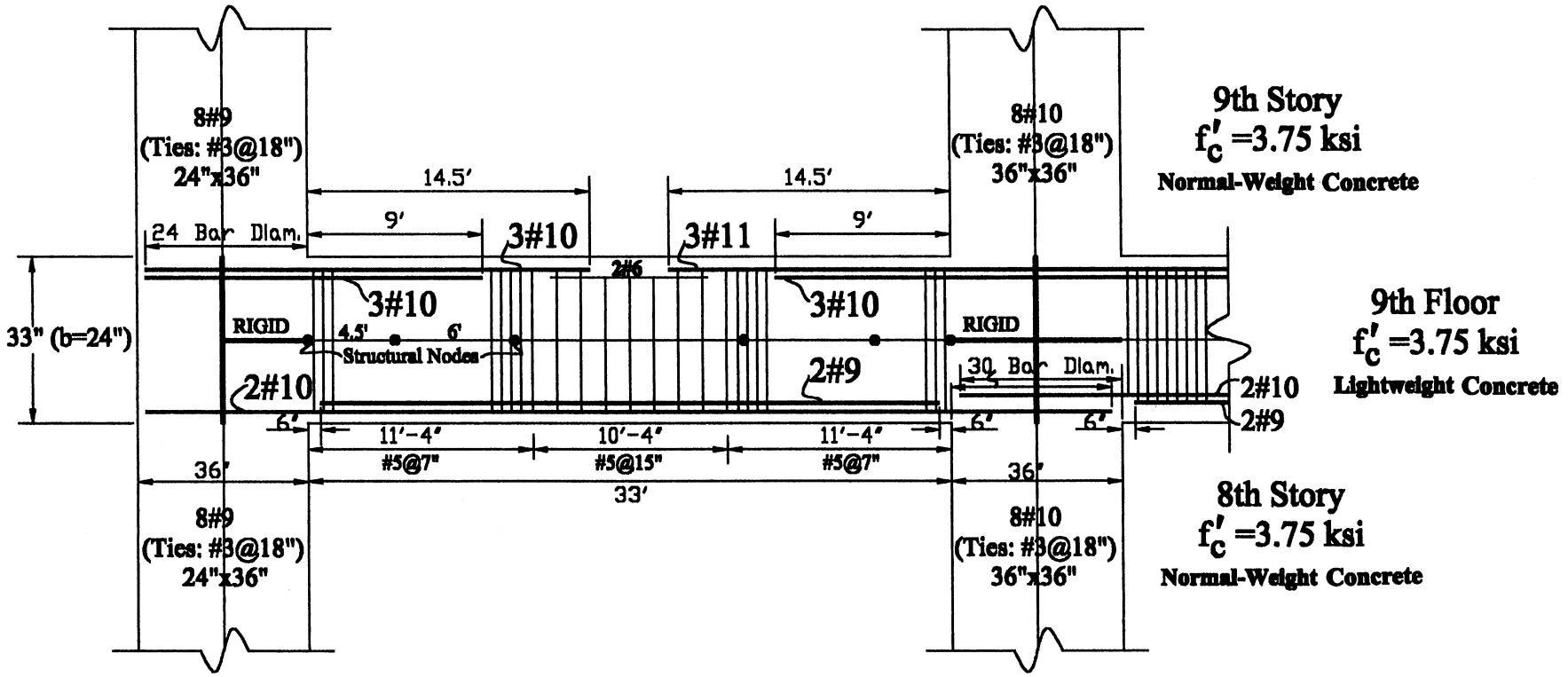

Figure 4.6 Reinforcement details for the 9th floor beams of interior transverse frames.
(Similar beam reinforcement is used at the 10th and 11th floors.)

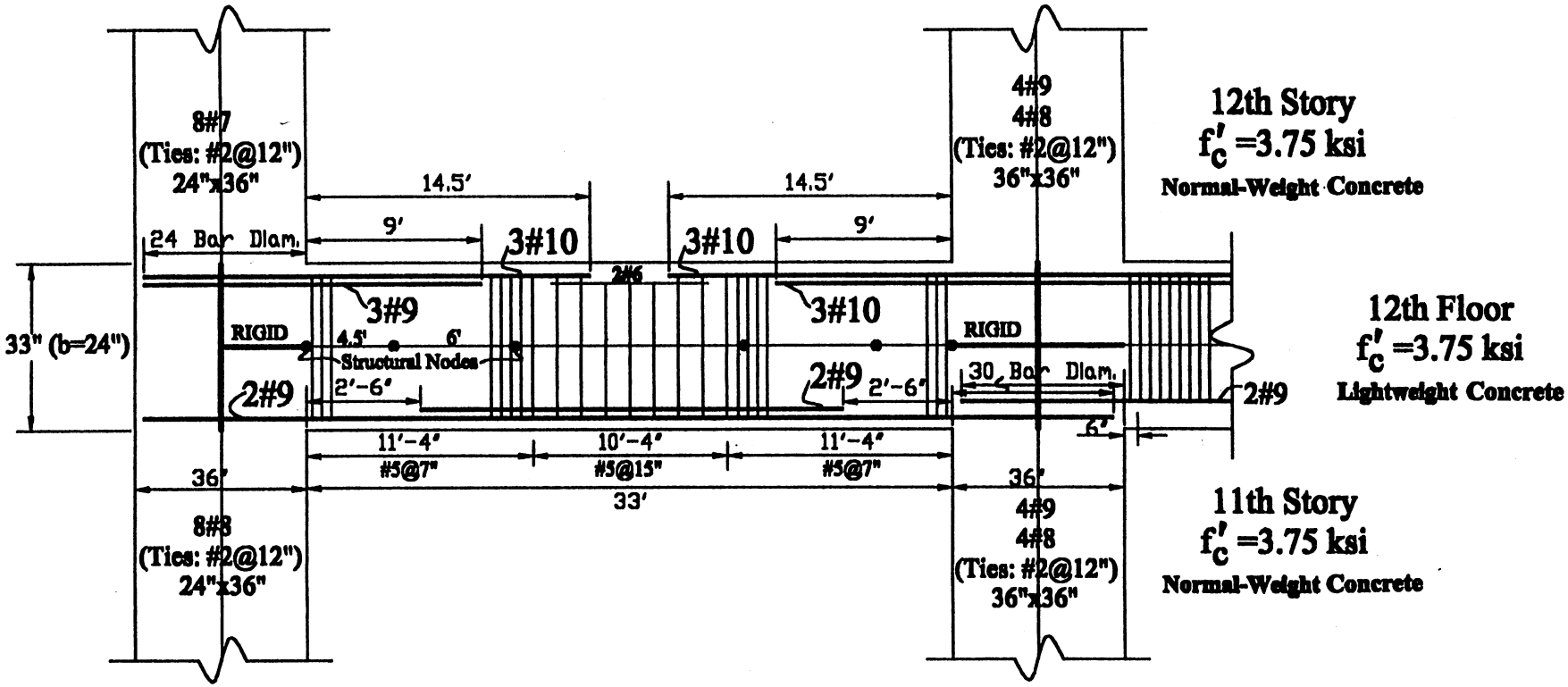

Figure 4.7 Reinforcement details for the 12th floor beams of interior transverse frames.
(Similar beam reinforcement is used at the 13th floor.)

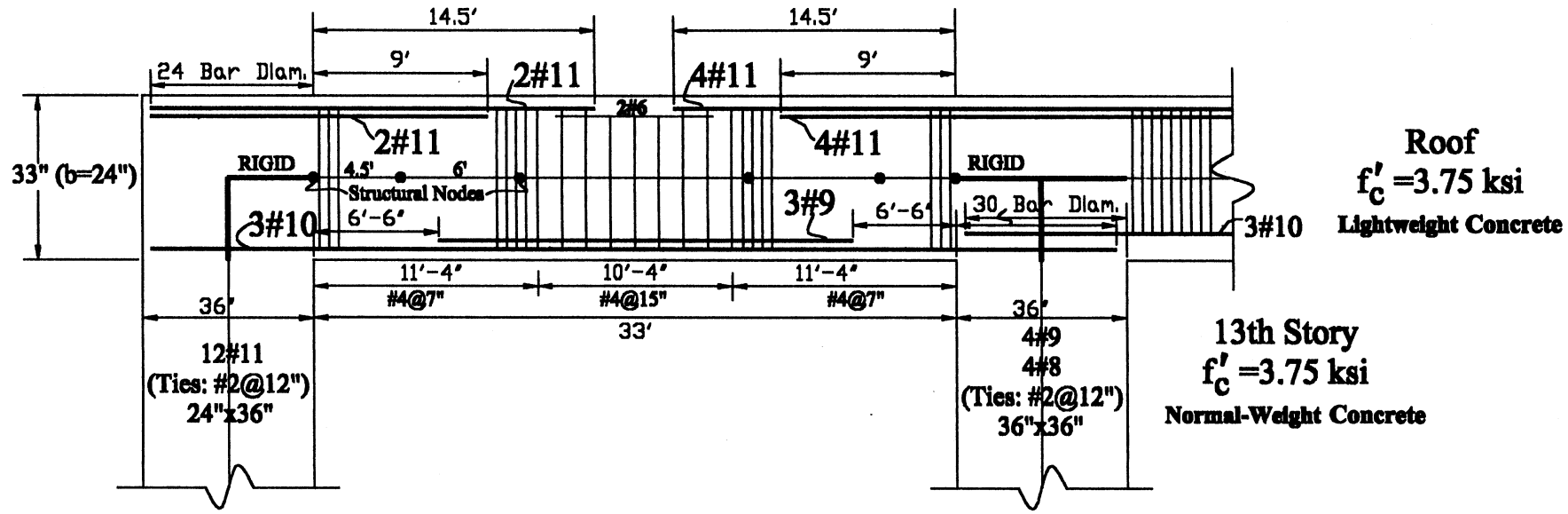

Figure 4.8 Reinforcement details for the 14th floor beams (roof) of interior transverse frames.

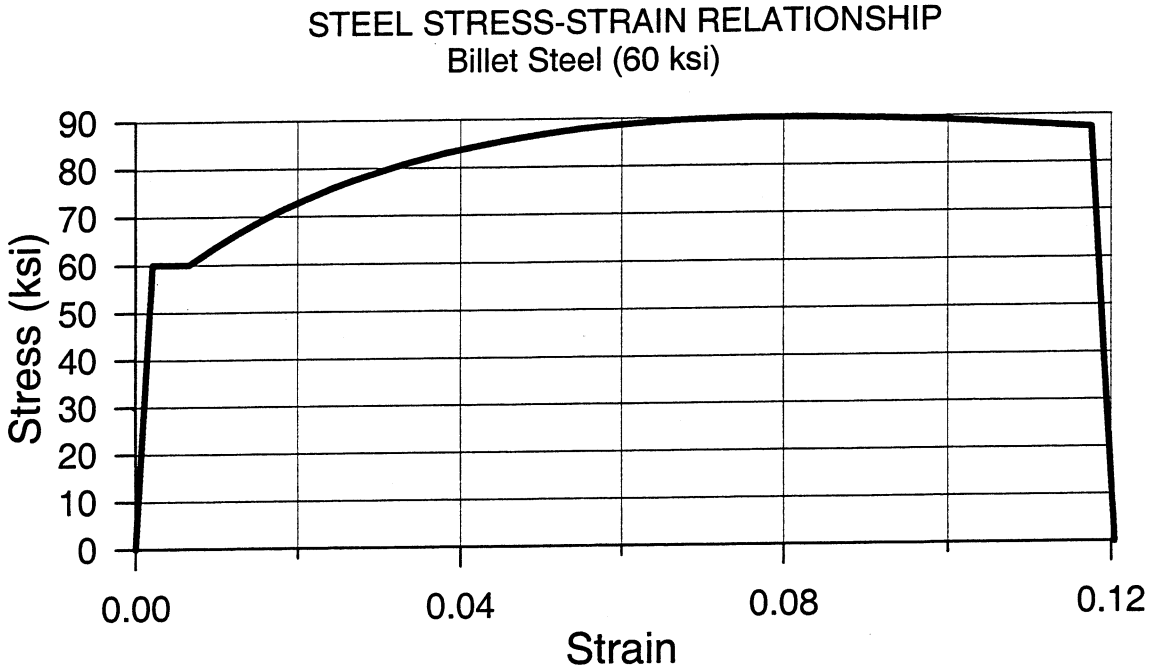

Figure 4.9 Stress-strain relationship for Billet steel (After Large and Chen, 1968).

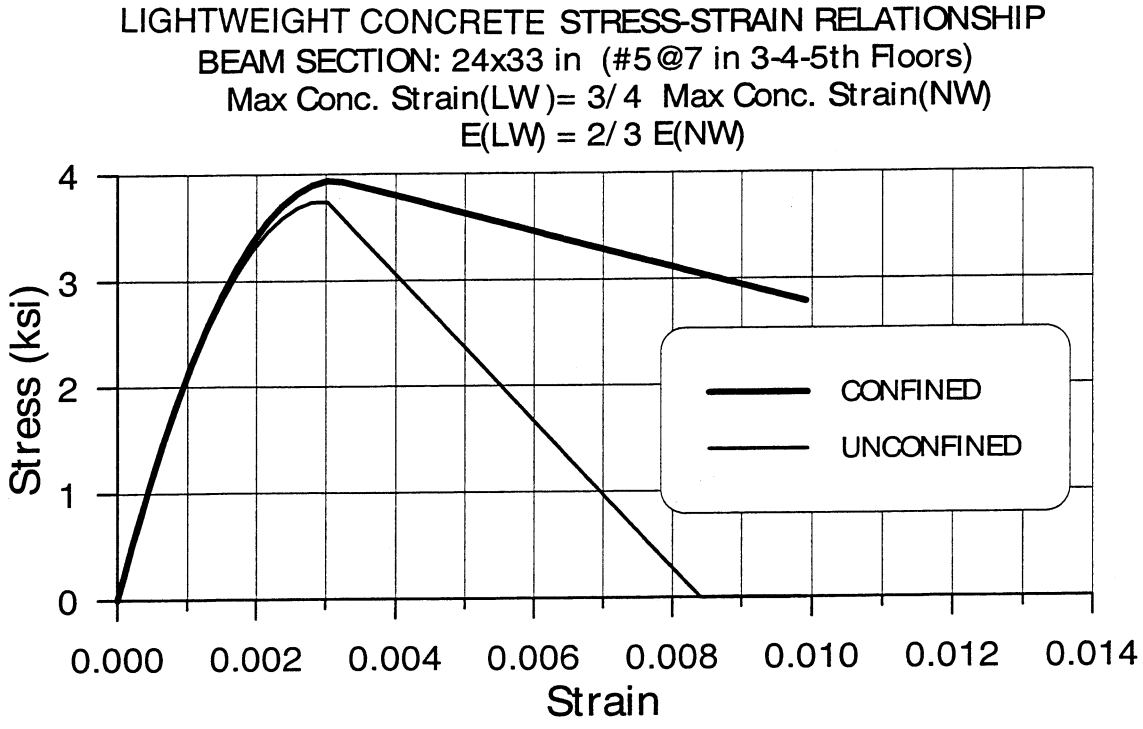

Figure 4.10 Stress-strain relationship for concrete.

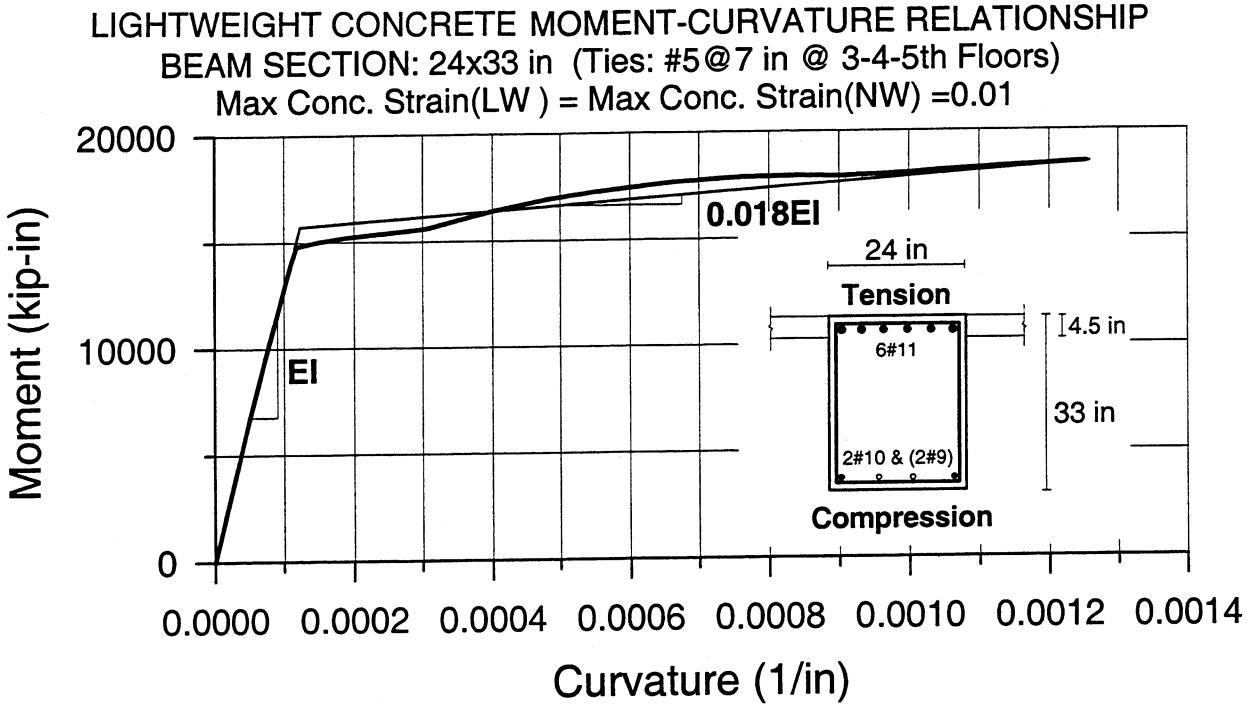

Figure 4.11 Moment-curvature relationship for interior beam ends (3rd floor) under negative moment.

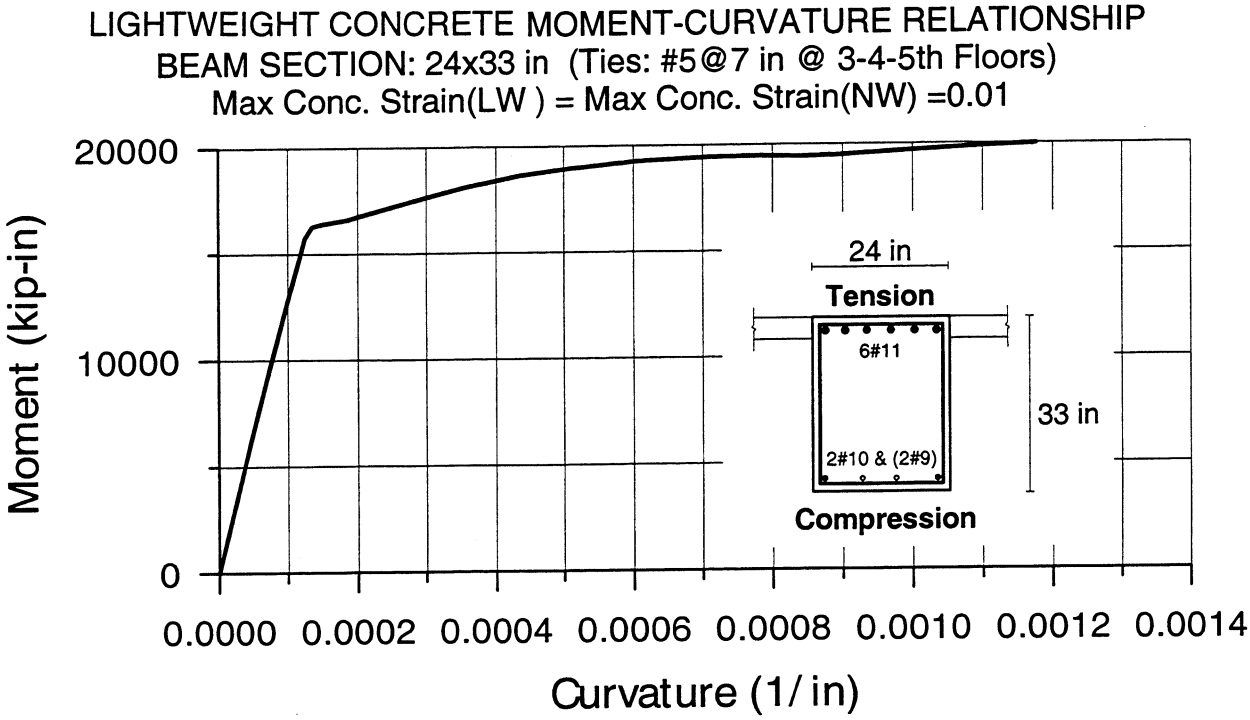

Figure 4.12 Moment-curvature relationship for interior beam ends (3rd floor) under negative moment (Steel has 10% higher yield and ultimate strength).

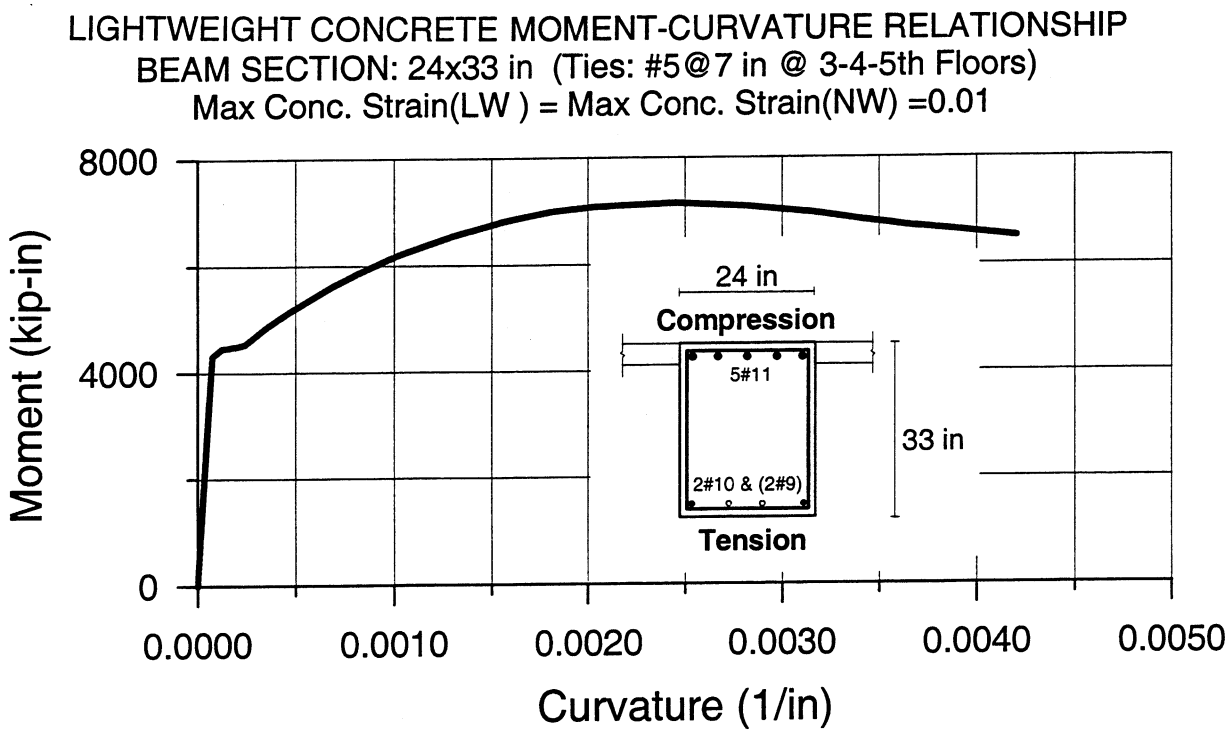

Figure 4.13 Moment-curvature relationship for exterior beam ends (3rd floor) under positive moment.

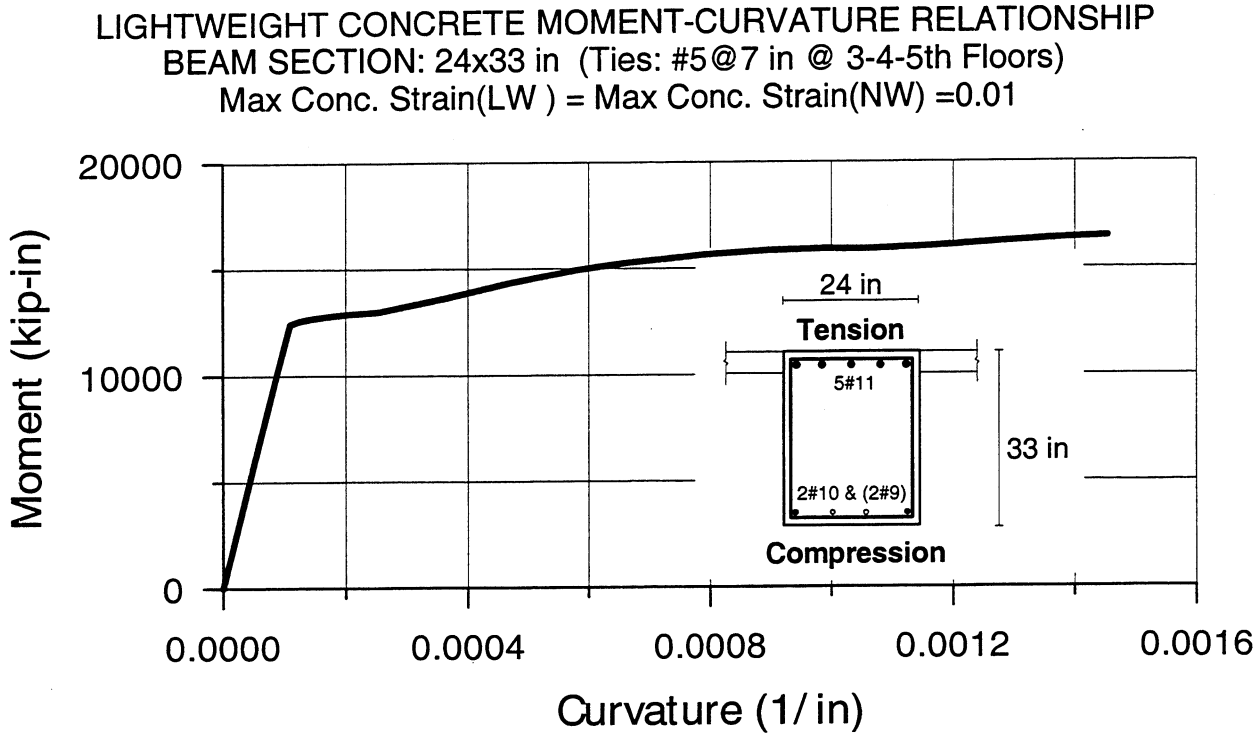

Figure 4.14 Moment-curvature relationship for exterior beam ends (3rd floor) under negative moment.

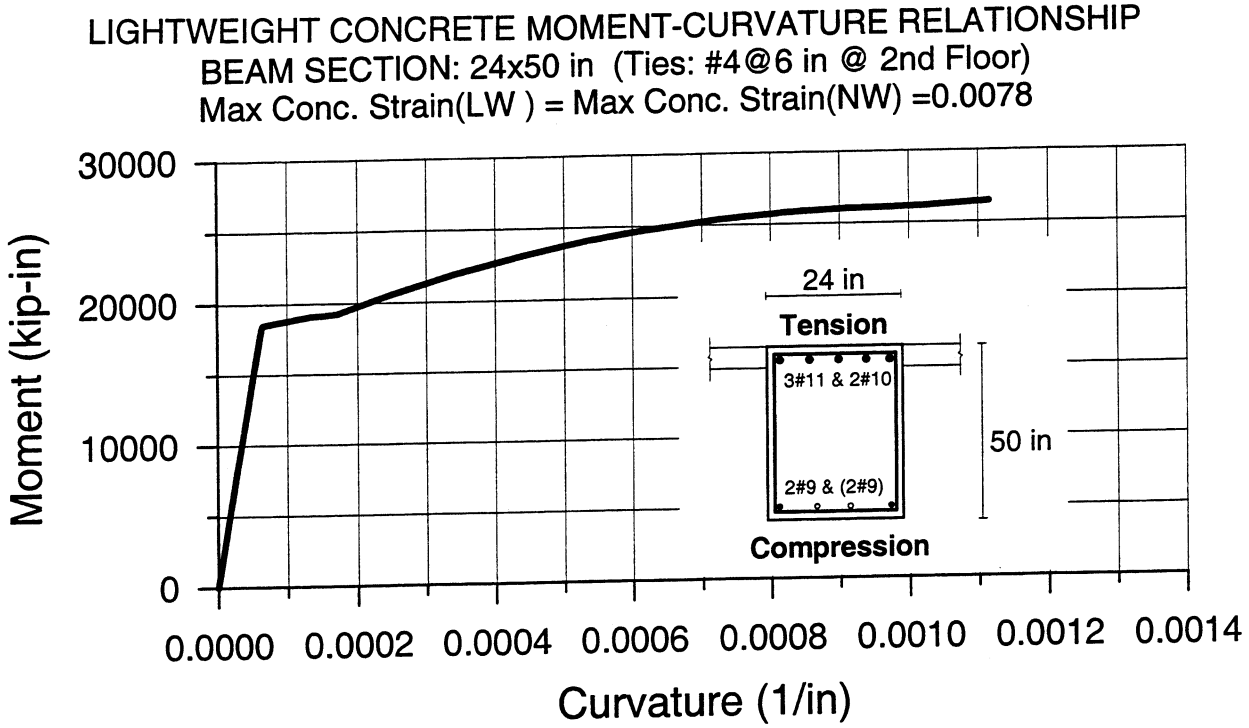

Figure 4.15 Moment-curvature relationship for interior beam ends (2nd floor) under negative moment.

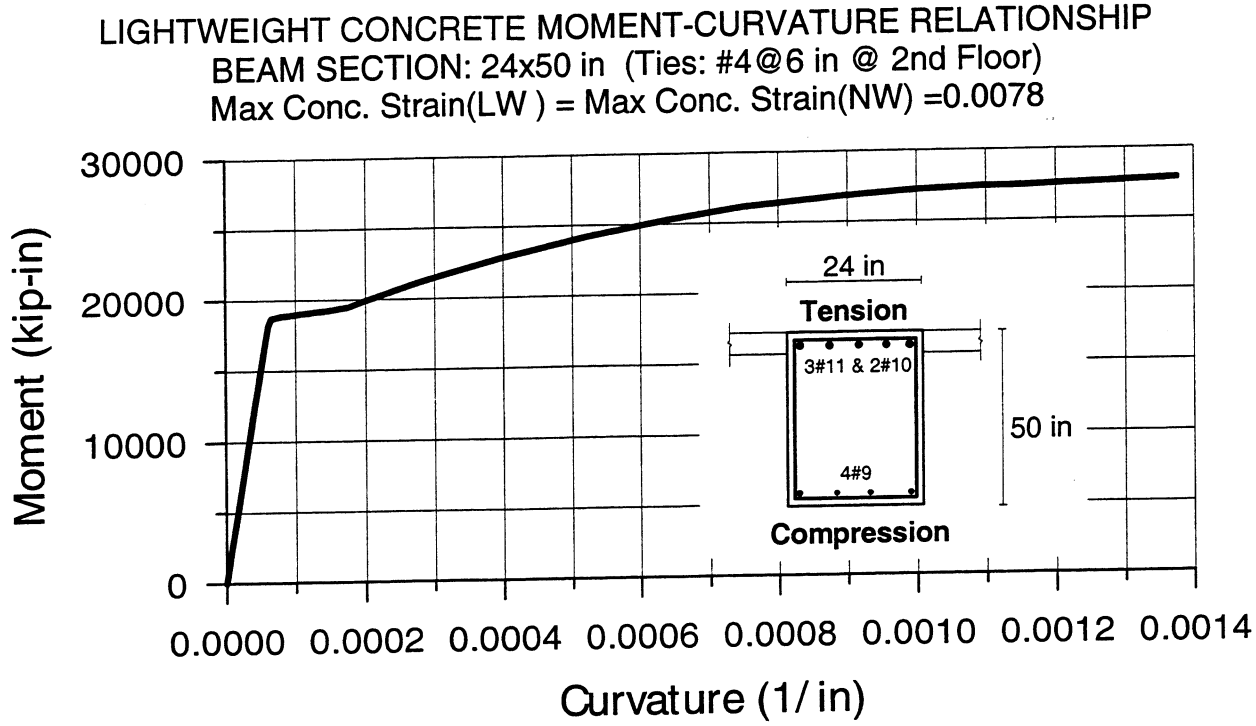

Figure 4.16 Moment-curvature relationship for exterior beam ends (2nd floor) under negative moment.

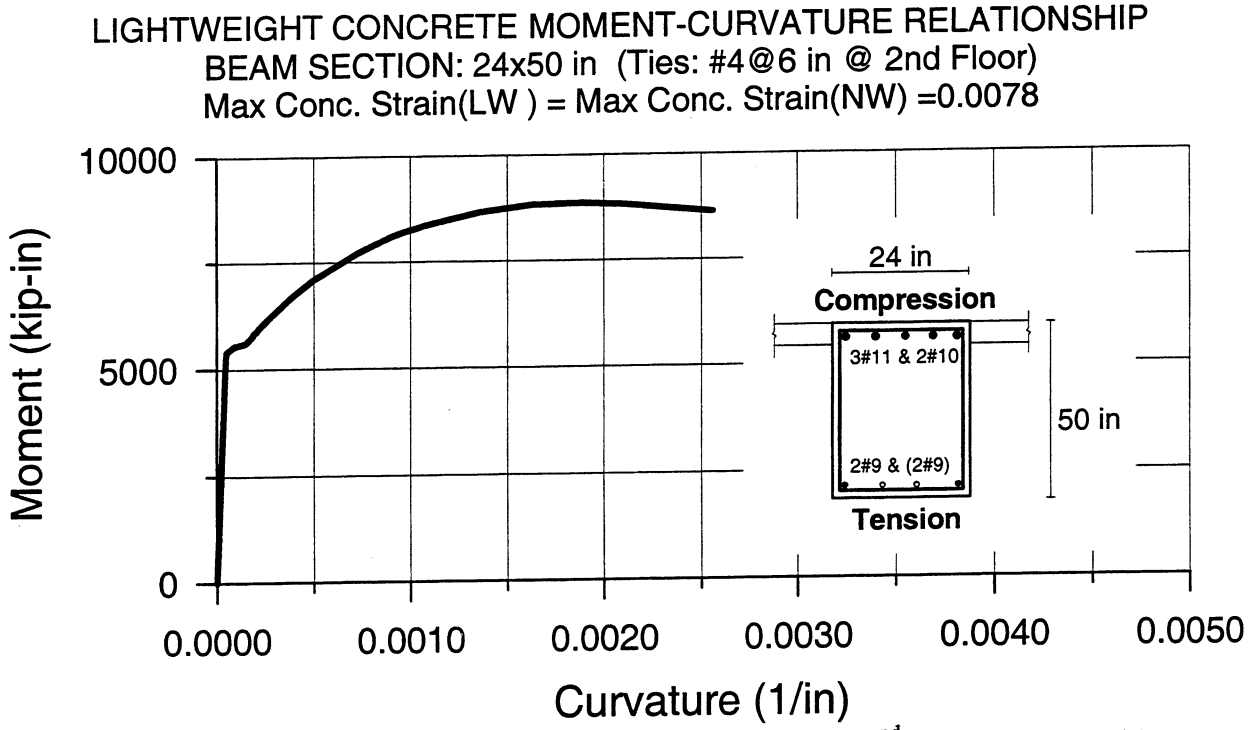

Figure 4.17 Moment-curvature relationship for interior beam ends (2nd floor) under positive moment.

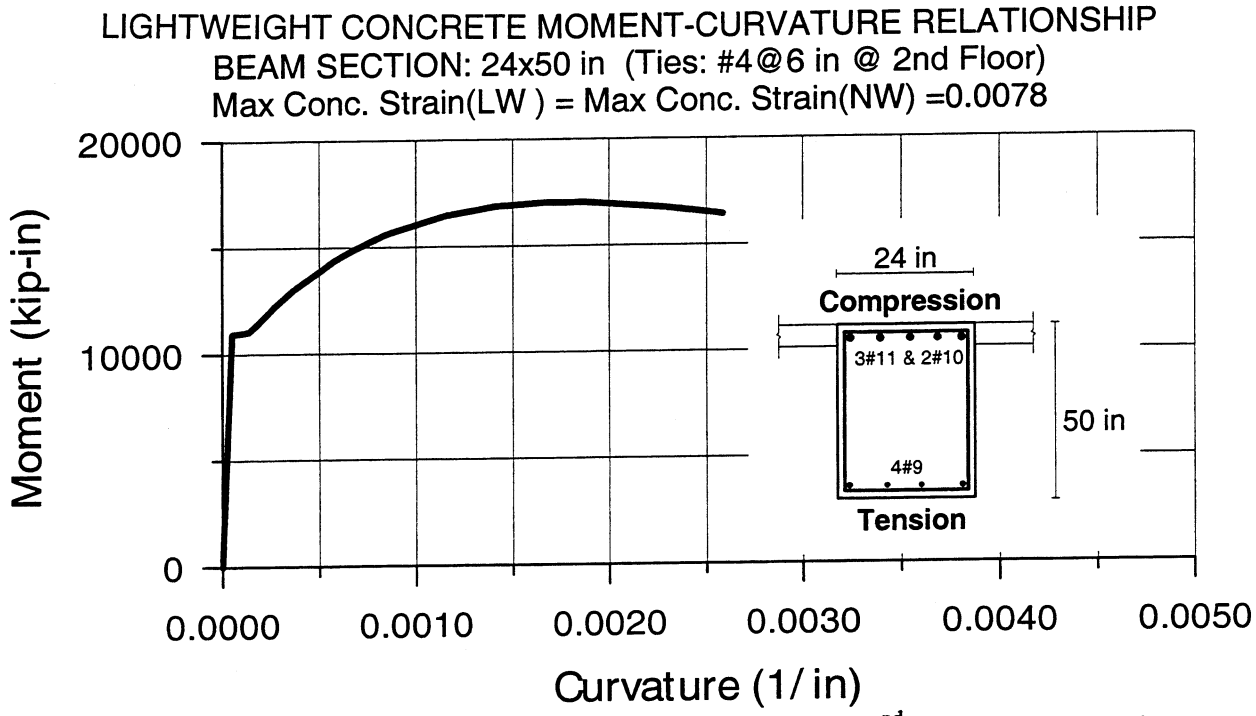

Figure 4.18 Moment-curvature relationship for exterior beam ends (2nd floor) under positive moment.

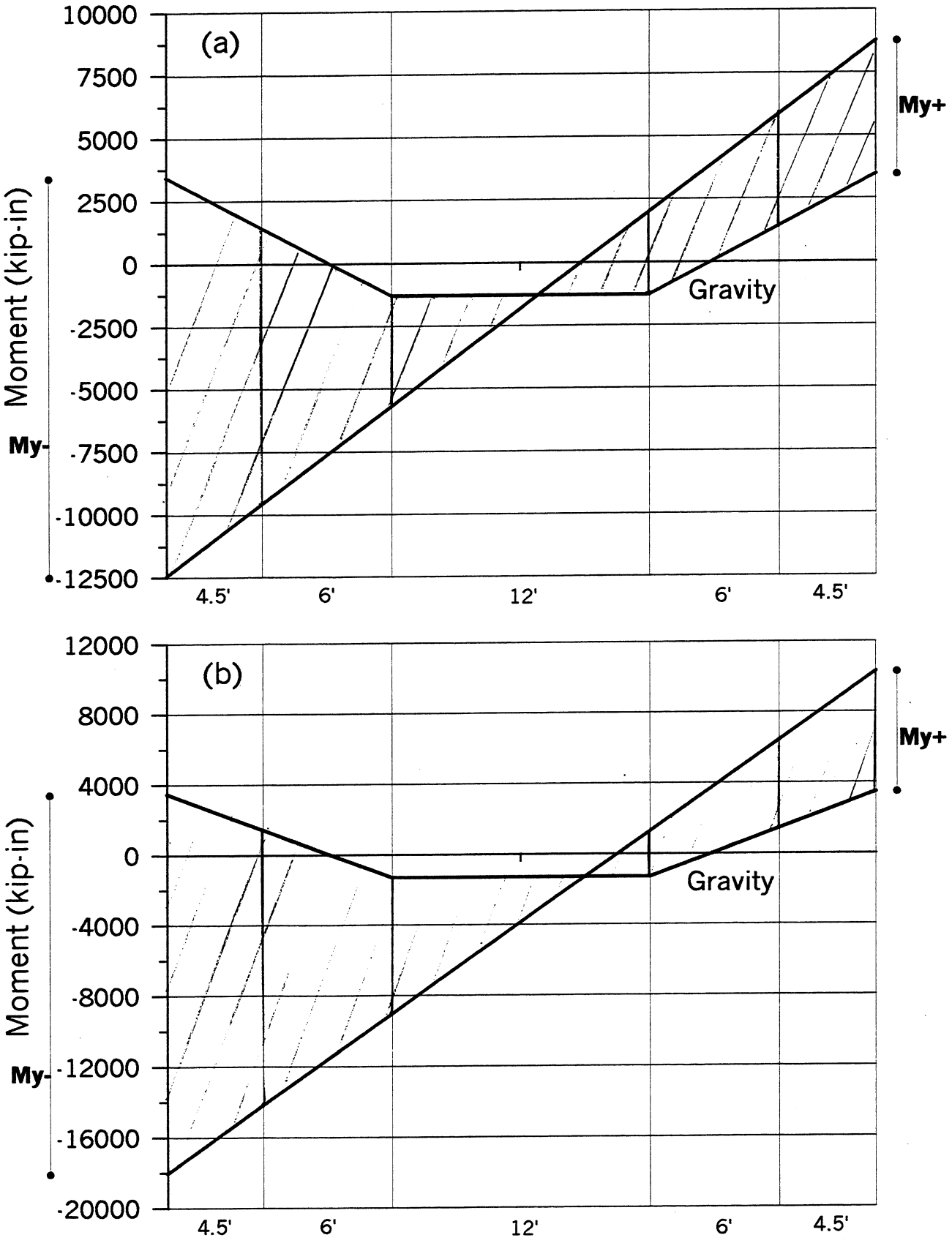

Figure 4.19 Assumed bending moment diagram of interior frames at (a) 3rd floor (b) 2nd floor.

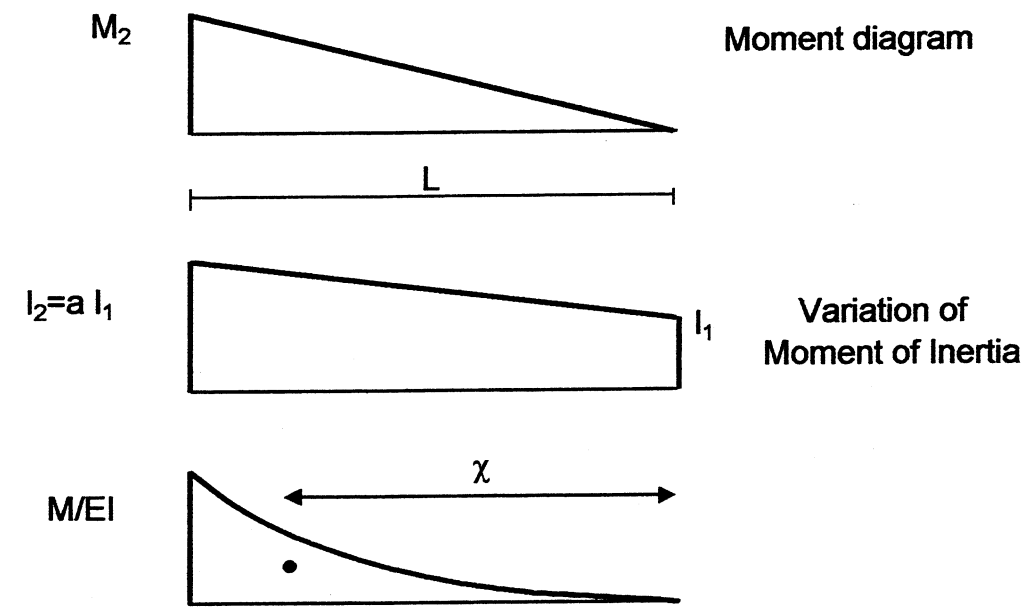

a= 1.54688

Area(M/EI)= $[a-1-\ln(a)]/(a-1)^2$ M_2L/EI_1= 0.3699 M_2L/EI_1

χ=L $[a^2-4a+3+2\ln(a)]/[(a-1)(a-1-\ln(a))]/2$= 0.6429 L

θ(left)= 0.2378 M_2L/EI_1

θ(right)= 0.1321 M_2L/EI_1

$$\begin{bmatrix}\theta_{right}\\ \theta_{left}\end{bmatrix}=\begin{bmatrix}0.2784 & -0.1182\\ -0.1182 & 0.2036\end{bmatrix}\begin{bmatrix}M_{right}\\ M_{left}\end{bmatrix}$$

Note: $\theta_{y\ right}=f_{11}M_y+f_{12}M_2=(f_{11}+f_{12}\gamma)M_y$

$\gamma=M_2/M_1$

Figure 4.20 Flexibility coefficients for a beam with linearly varying moment of inertia.

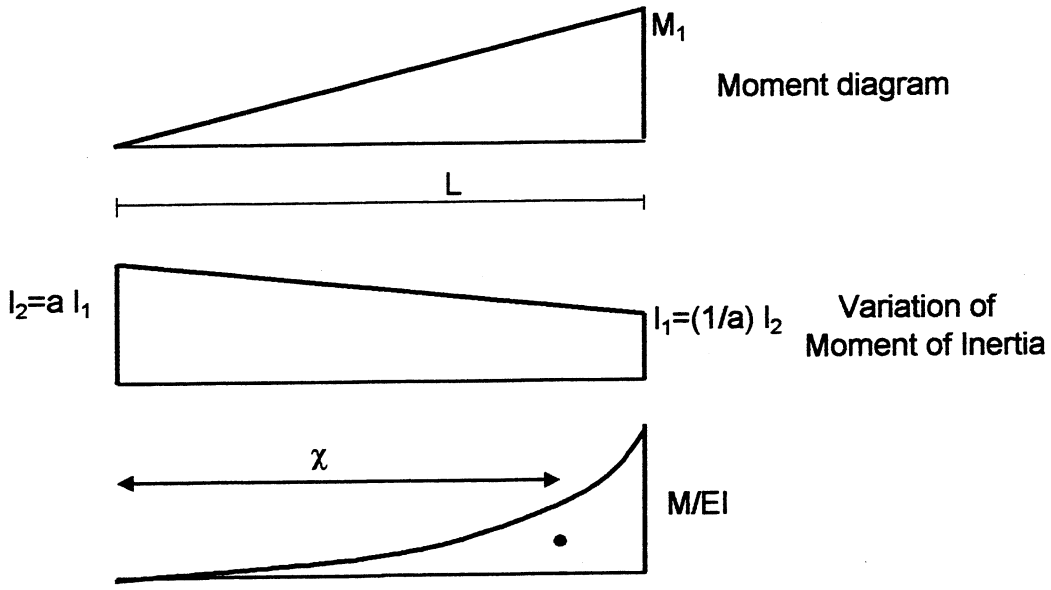

$b=1/a=$ 0.533

$\text{Area}(M/EI)= b*[b-1-\ln(b)]/(b-1)^2 * M_1L/EI_1 =$ 0.39659 $* M_2L/EI_1$

$\chi =$ L* $[b^2-4b+3+2\ln(b)]/[(b-1)*(b-1-\ln(b))]/2 =$ 0.702 *L

$\theta(\text{left}) =$ 0.1182 $* M_2L/EI_1$

$\theta(\text{right}) =$ 0.2784 $* M_2L/EI_1$

Figure 4.21 Flexibility coefficients for a beam with linearly varying moment of inertia.

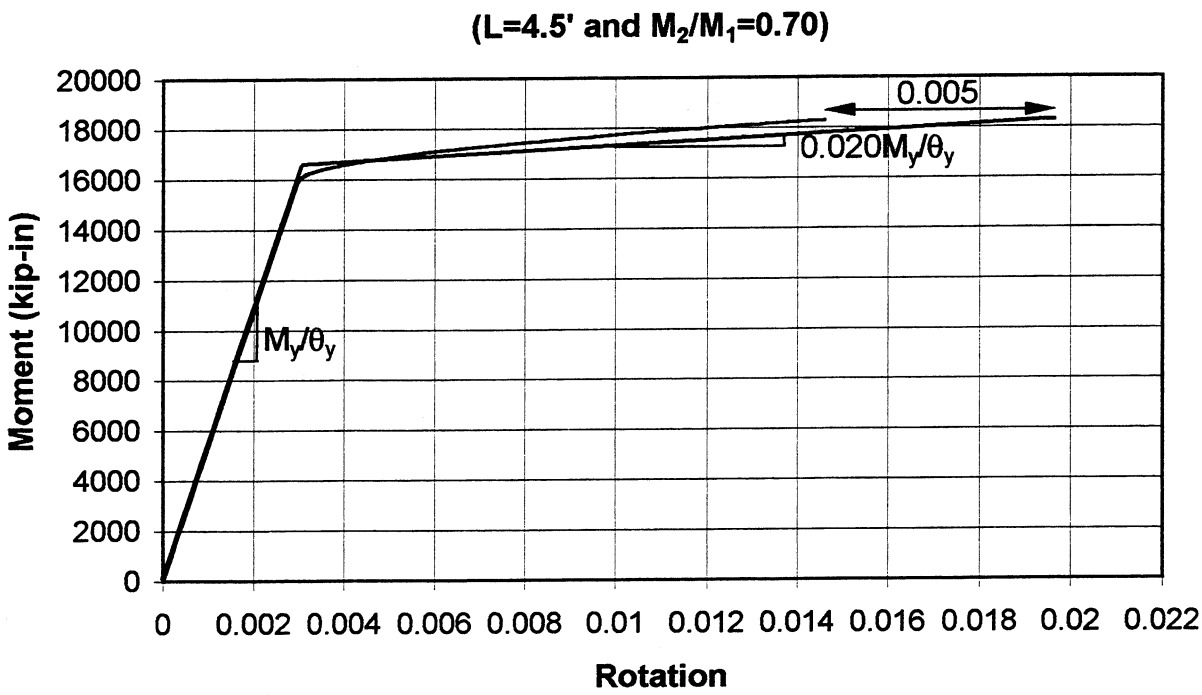

Figure 4.22 Moment-rotation relationship for interior beam ends (3rd floor) under negative moment; effect of slippage is included.

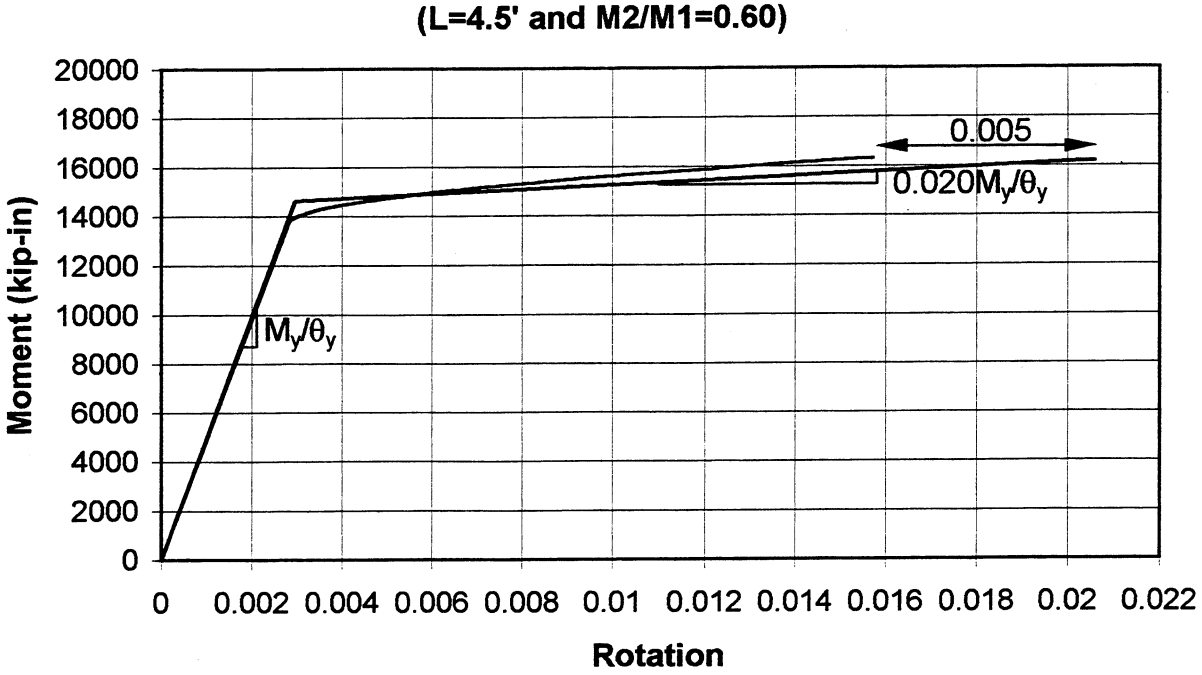

Figure 4.23 Moment-rotation relationship for exterior beam ends (3rd floor) under negative moment; effect of slippage is included.

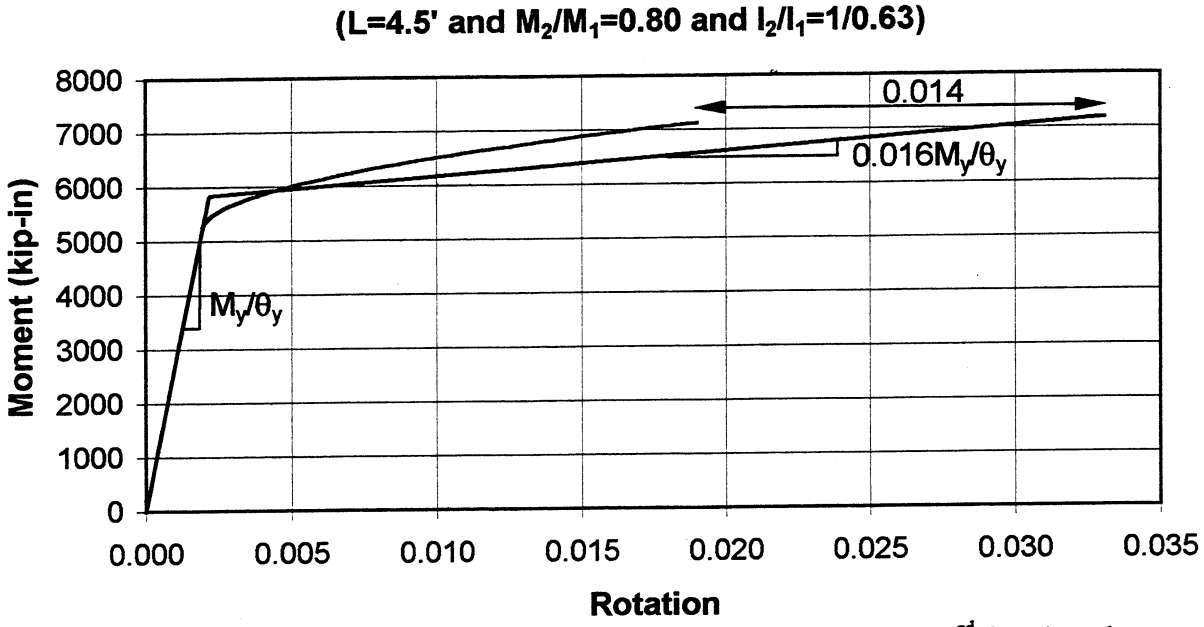

Figure 4.24 Moment-rotation relationship for exterior beam ends (3rd floor) under positive moment; effect of slippage is included.

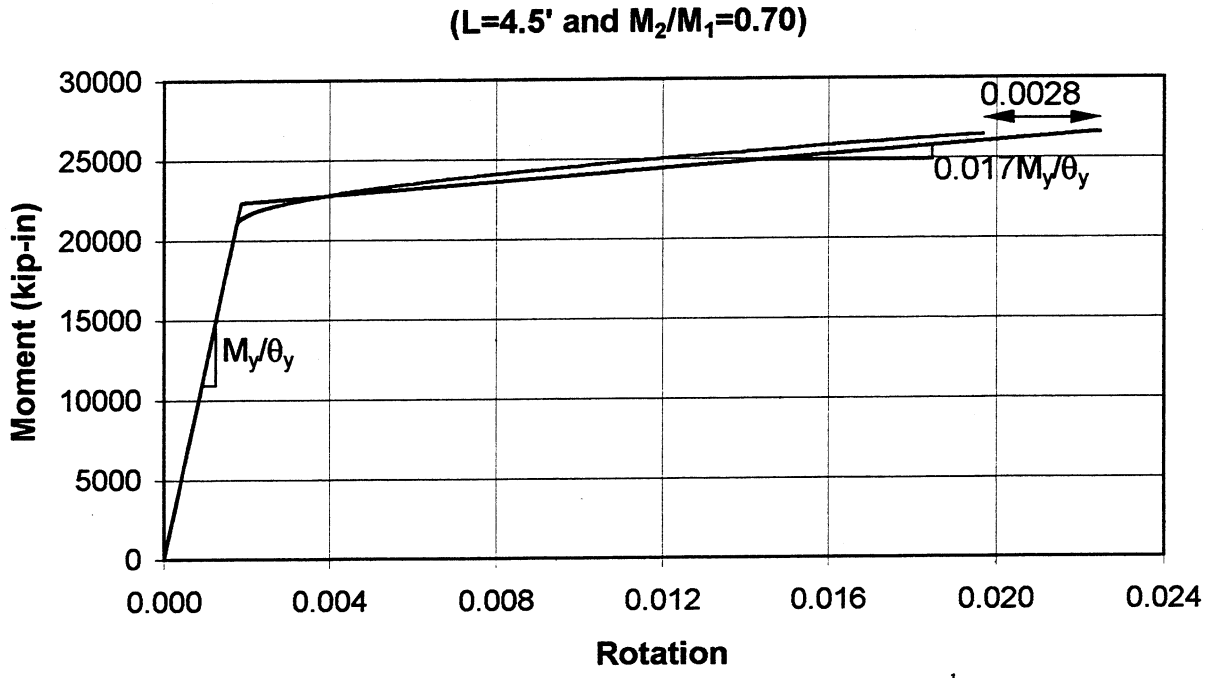

Figure 4.25 Moment-rotation relationship for interior beam ends (2nd floor) under negative moment; effect of slippage is included.

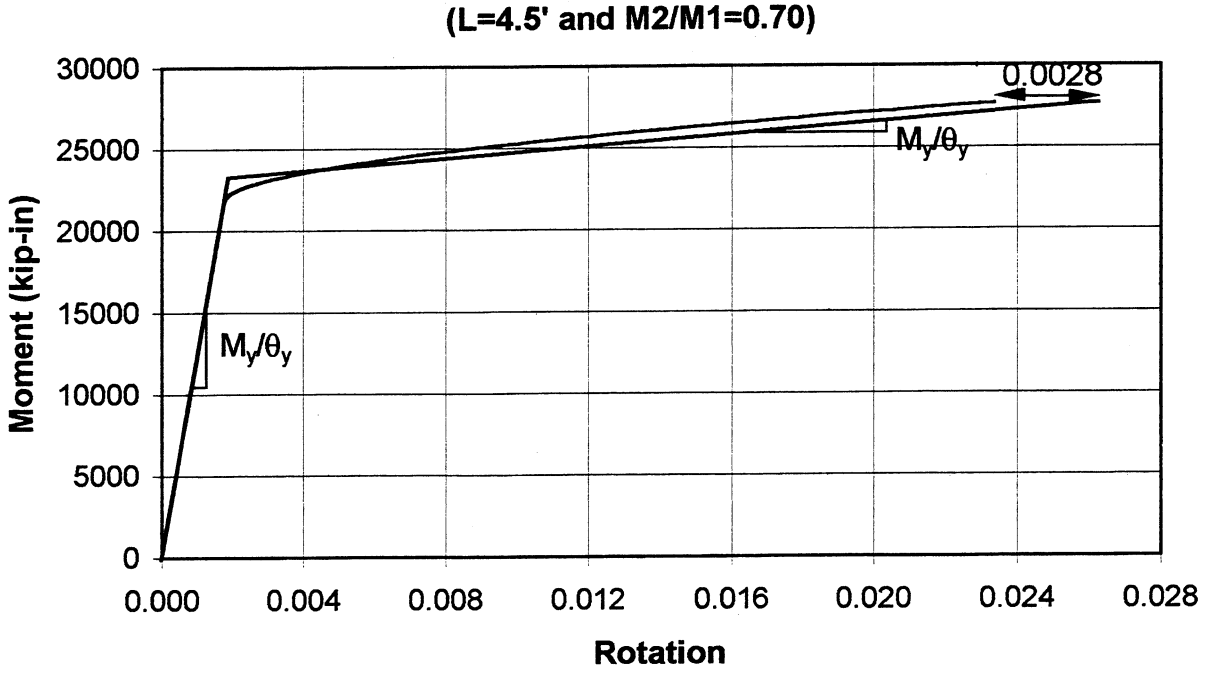

Figure 4.26 Moment-rotation relationship for exterior beam ends (2nd floor) under negative moment; effect of slippage is included.

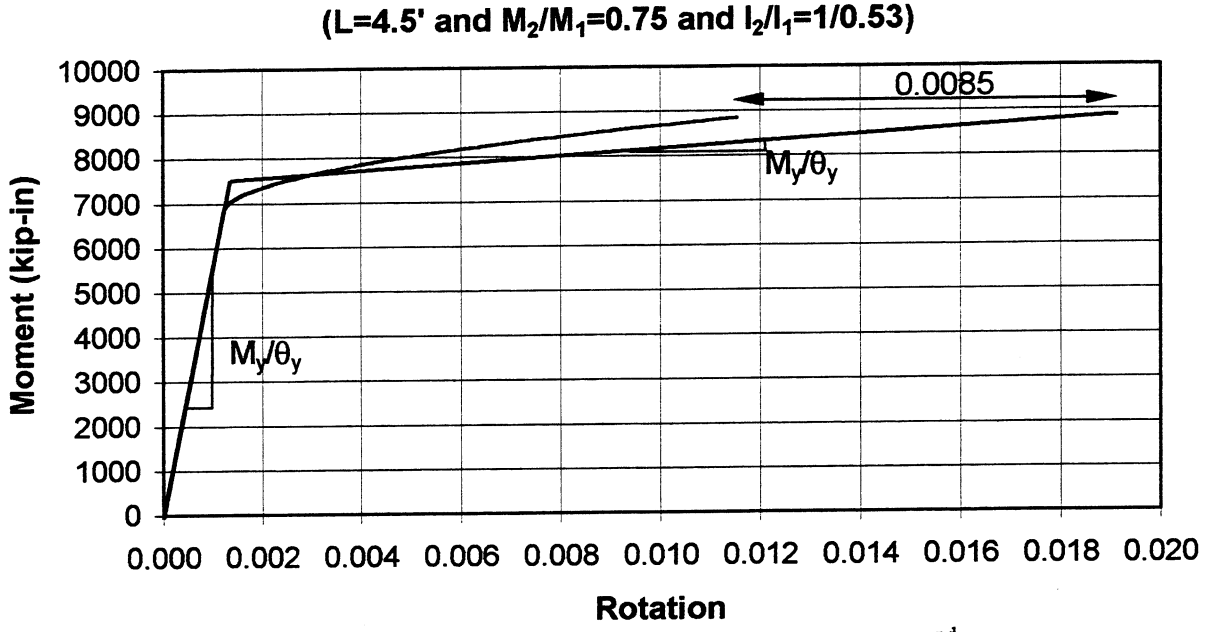

Figure 4.27 Moment-rotation relationship for interior beam ends (2nd floor) under positive moment; effect of slippage is included.

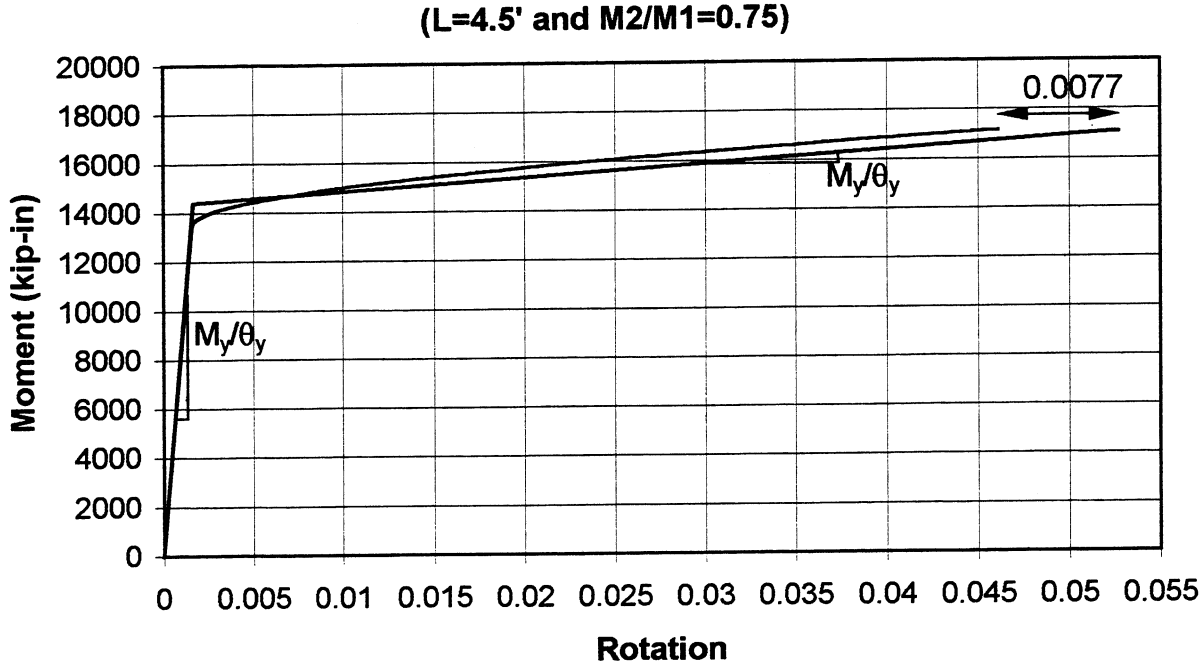

Figure 4.28 Moment-rotation relationship for exterior beam ends (2nd floor) under positive moment; effect of slippage is included.

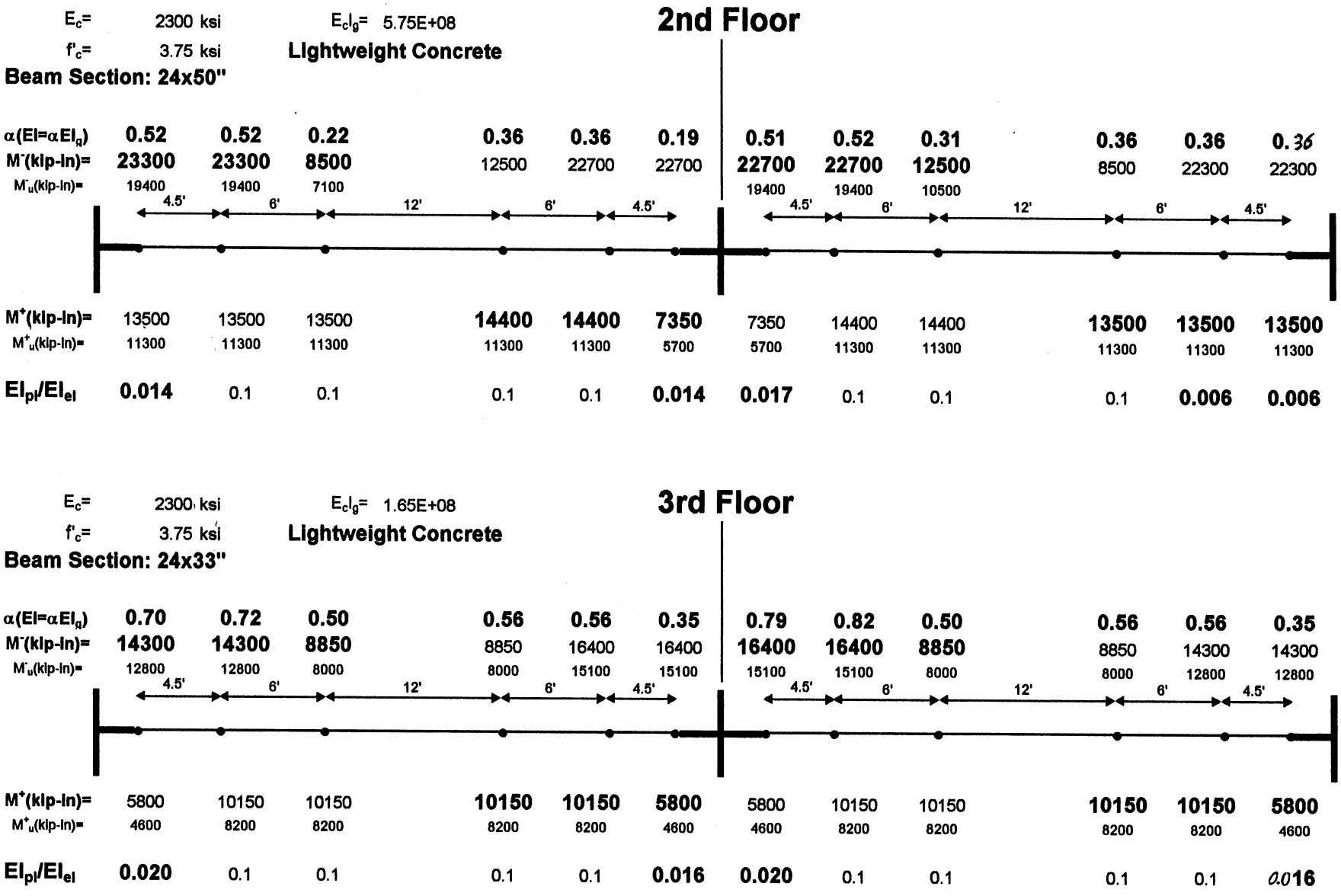

Figure 4.29 Section properties at the locations of the nodes in the Drain-2DX model (The lateral load is applied from right to left).

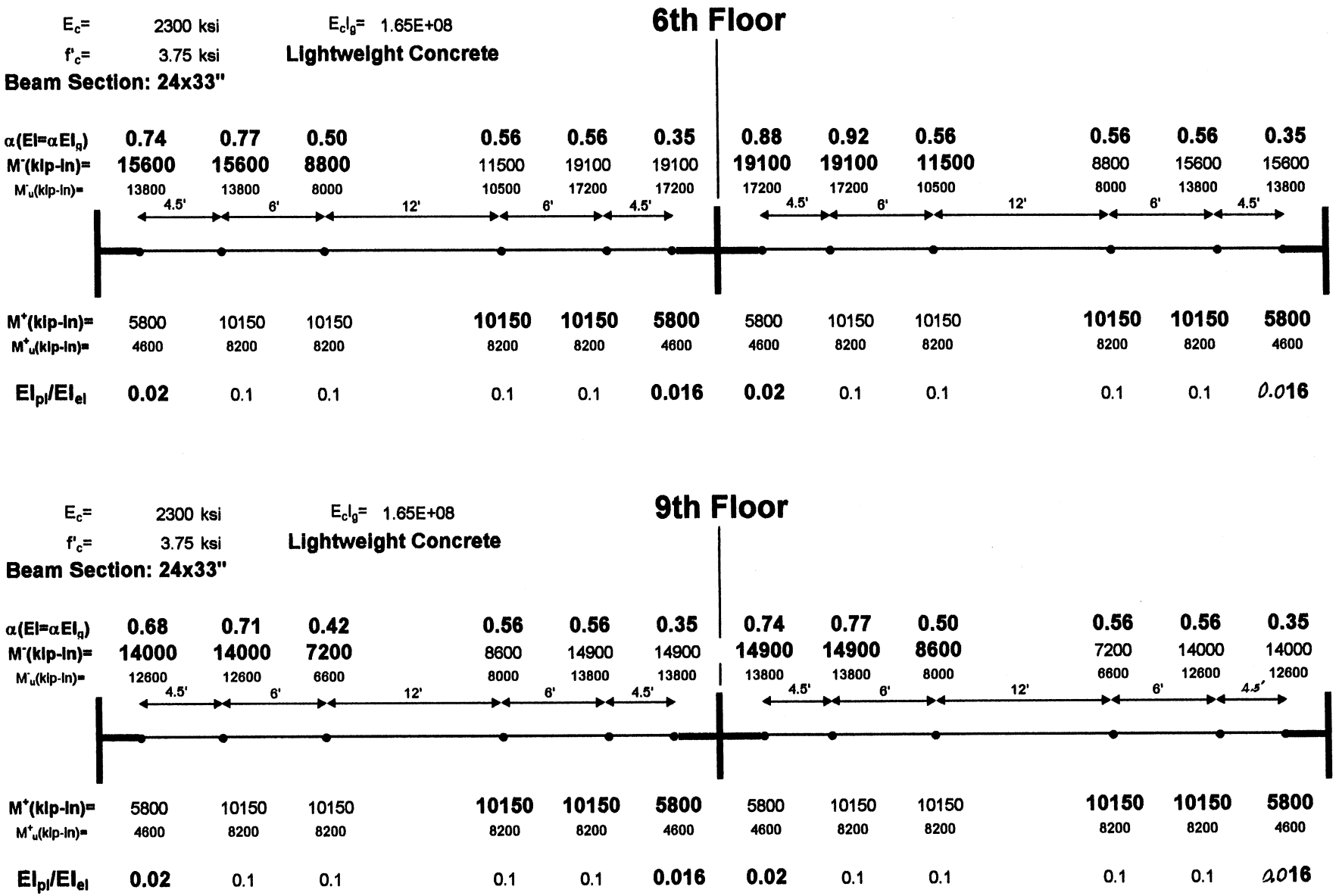

Figure 4.30 Section properties at the locations of the nodes in the Drain-2DX model (The lateral load is applied from right to left).

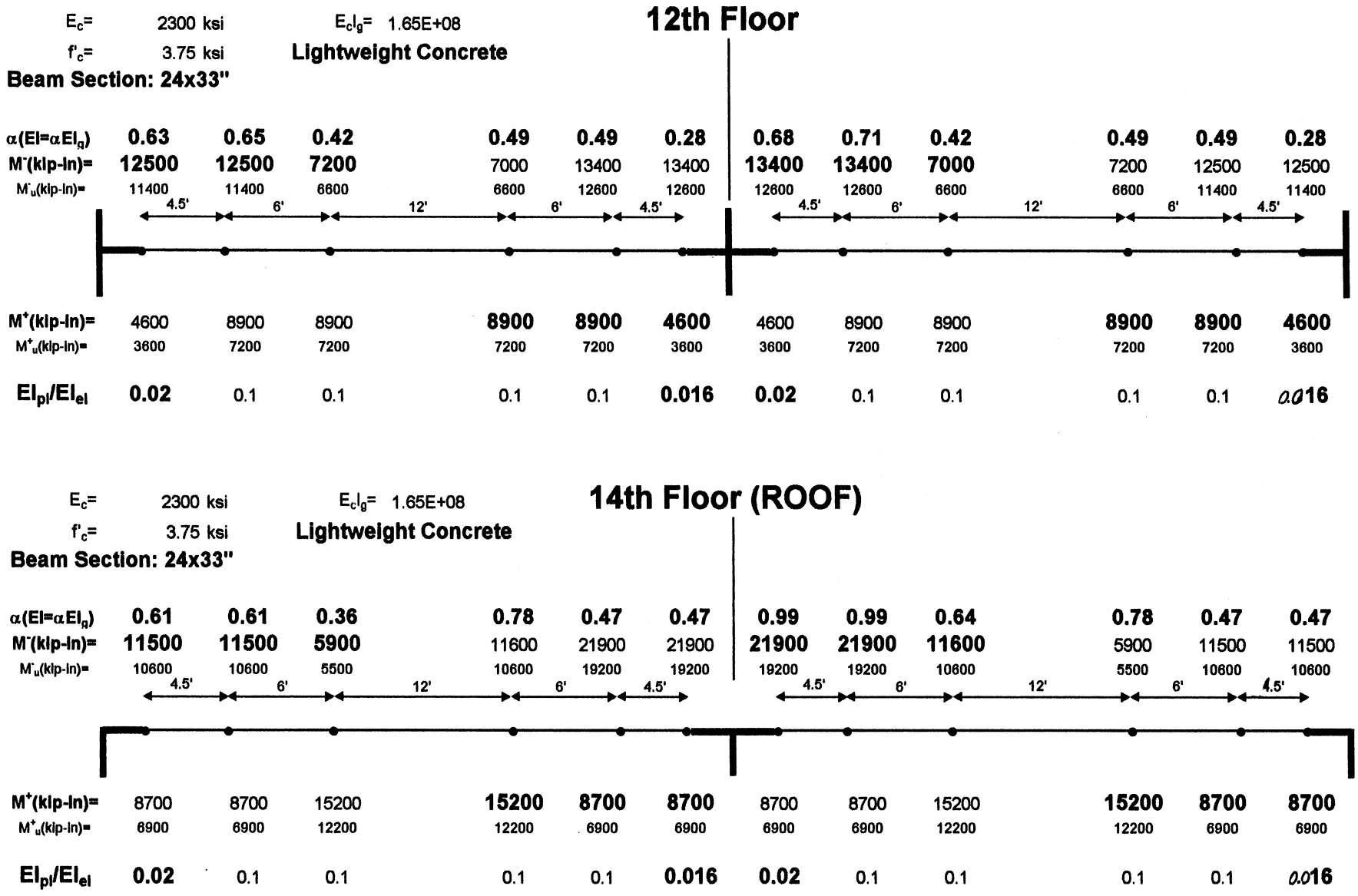

Figure 4.31 Section properties at the locations of the nodes in the Drain-2DX model (The lateral load is applied from right to left).

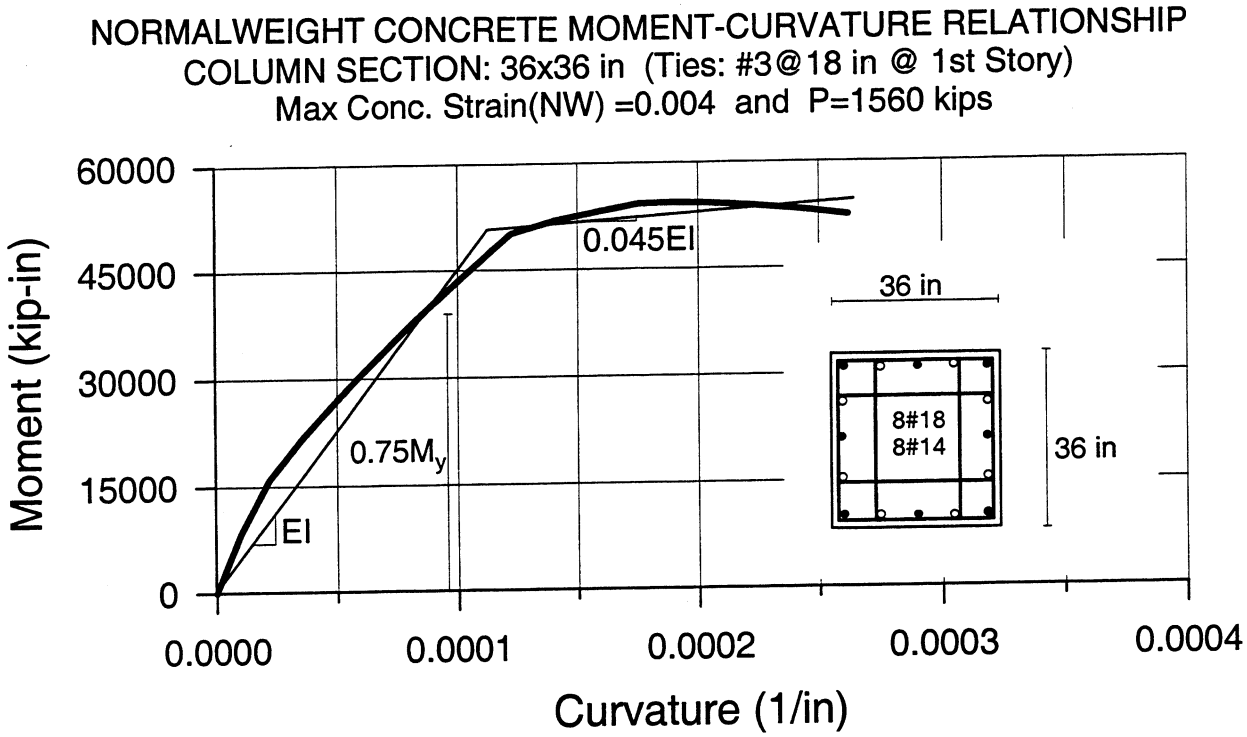

Figure 4.32 Moment-curvature relationship for interior columns of interior frames at 1st story.

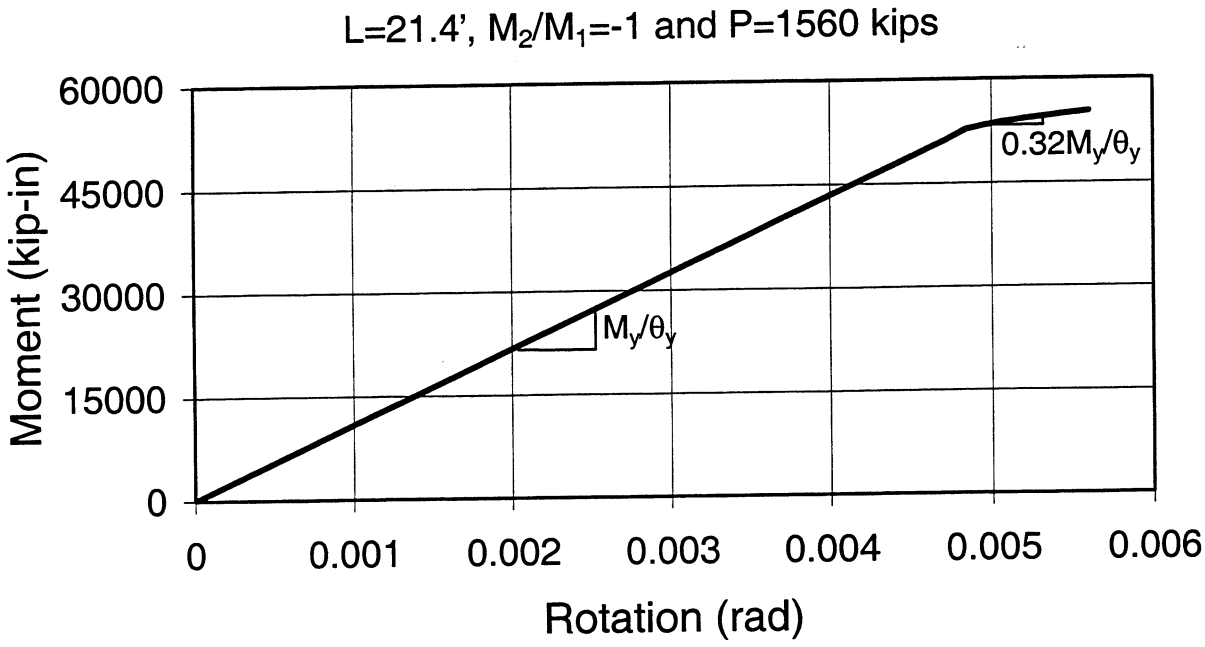

Figure 4.33 Moment-rotation relationship for interior columns of interior frames at 1st story.

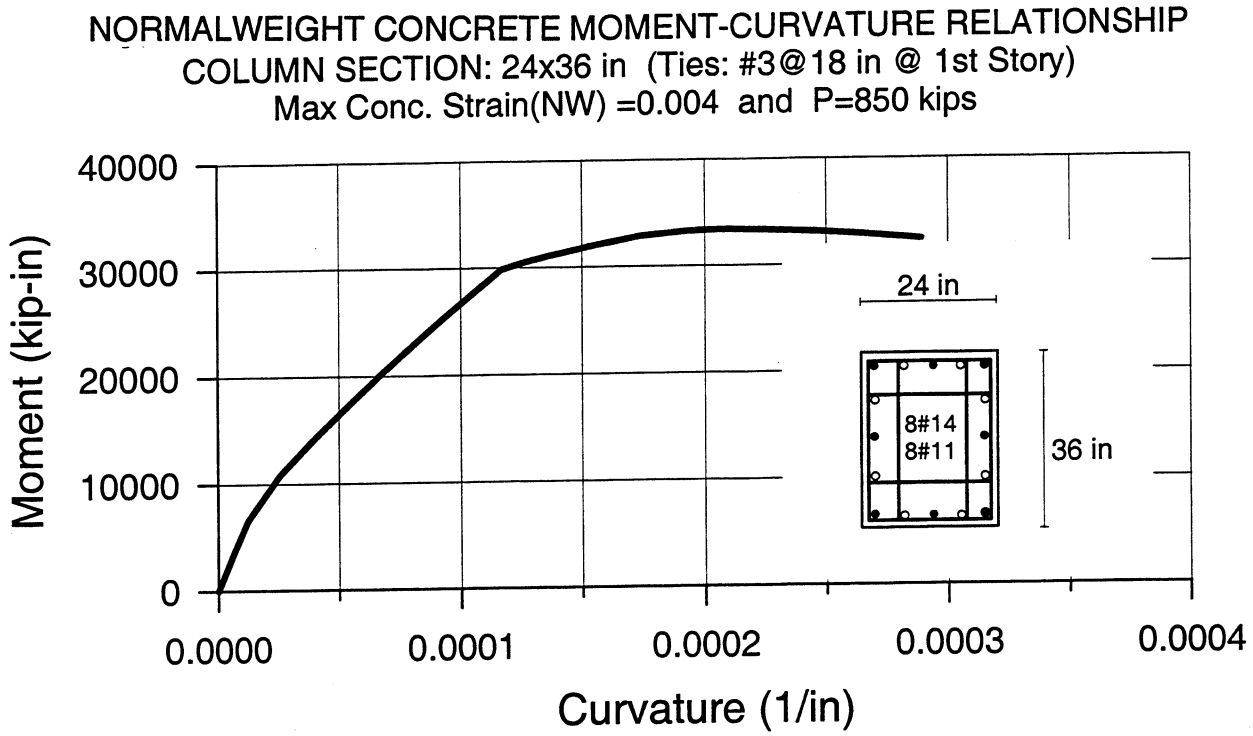

Figure 4.34 Moment-curvature relationship for exterior columns of interior frames at 1st story (about main axis).

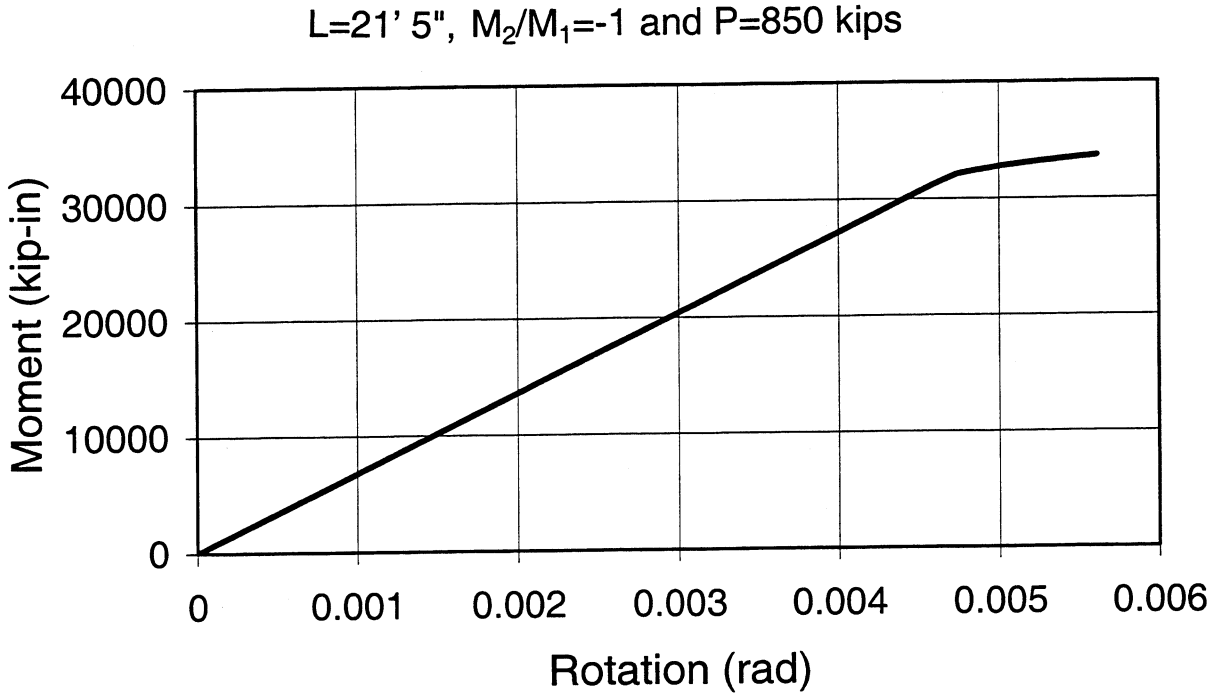

Figure 4.35 Moment-rotation relationship for exterior columns of interior frames at 1st story (about main axis).

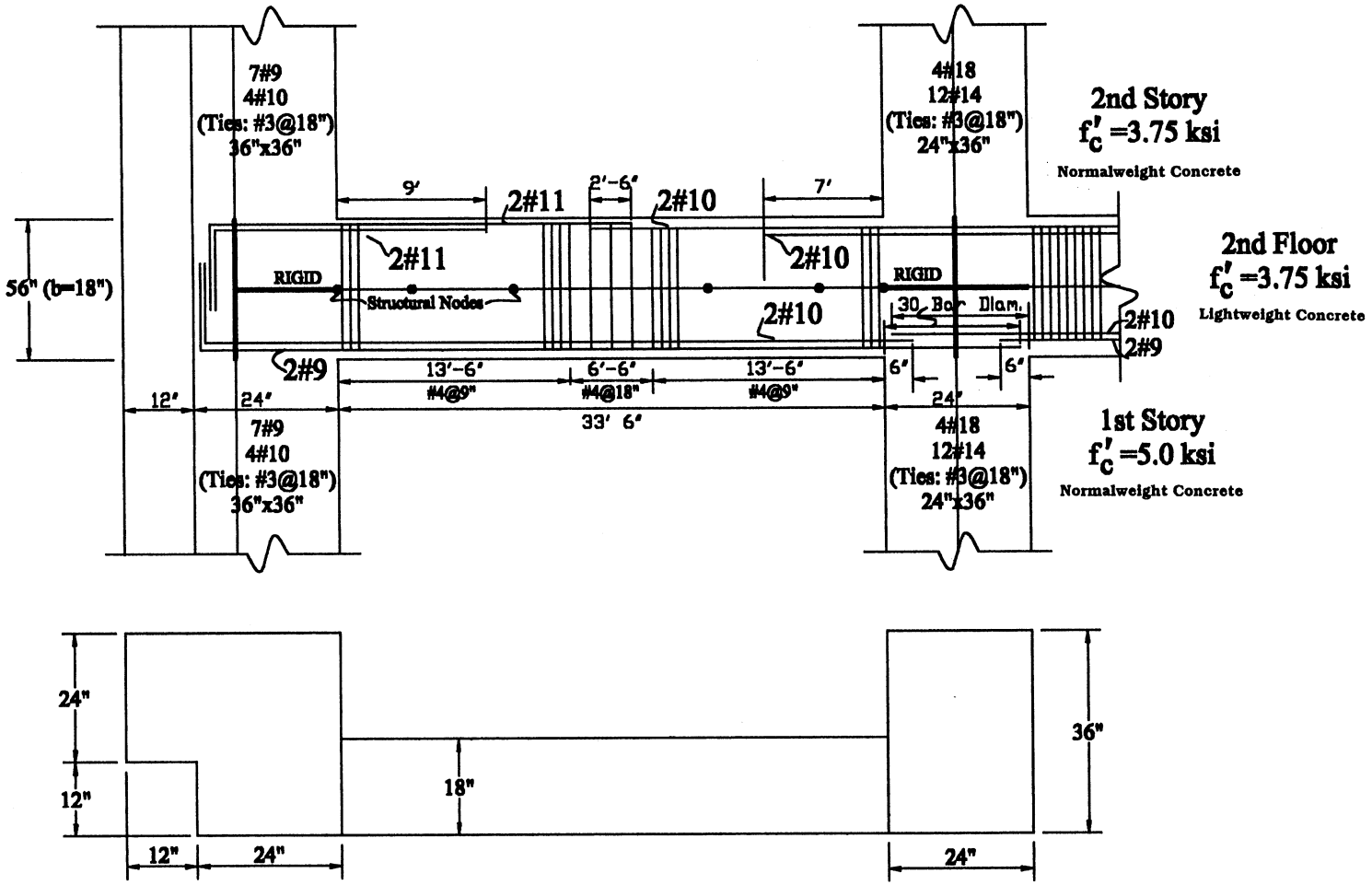

Figure 4.36 Reinforcement details for the 2nd floor beams of exterior transverse frames.

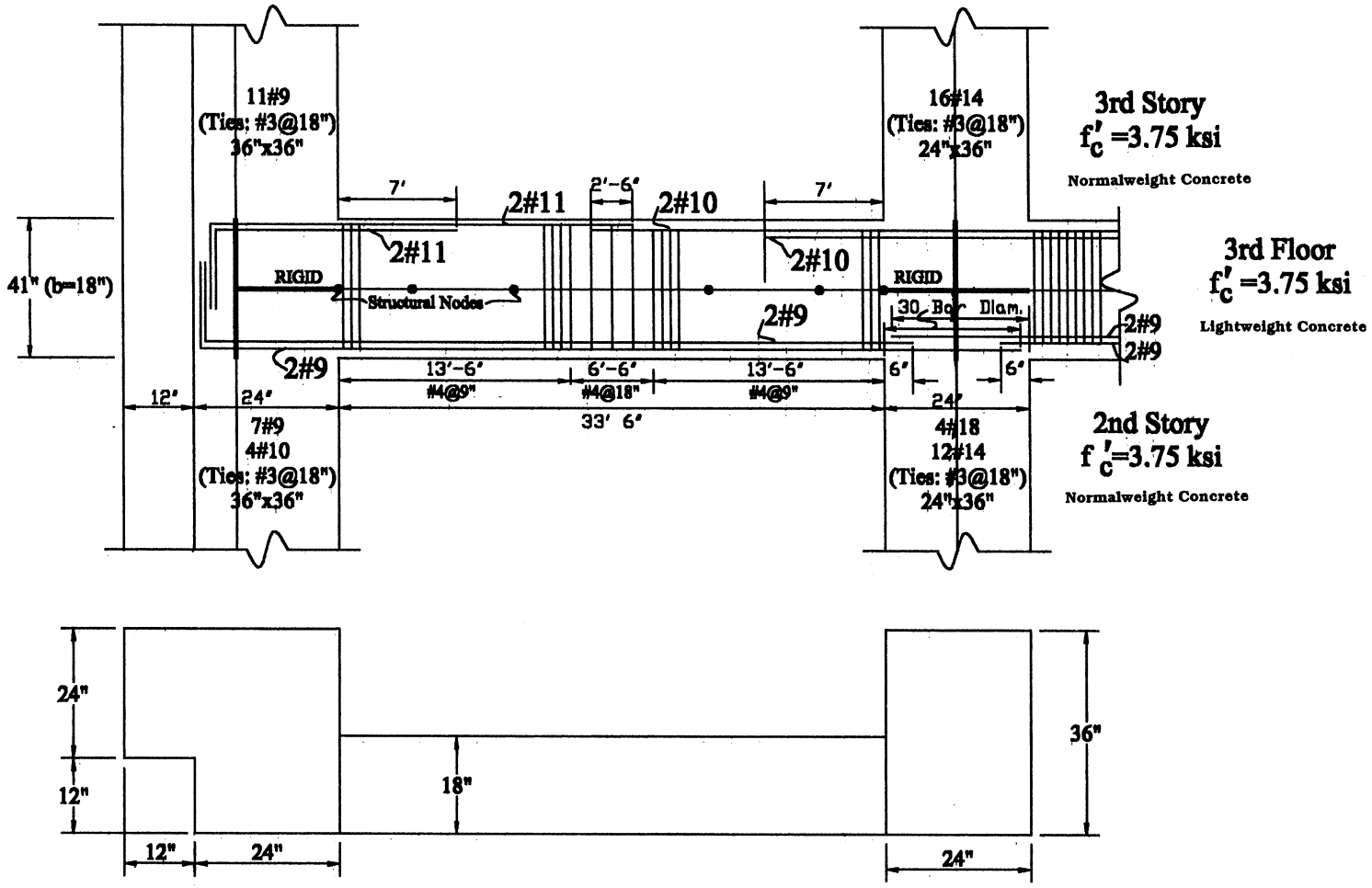

Figure 4.37 Reinforcement details for the 3rd to 5th floor beams of exterior transverse frames.

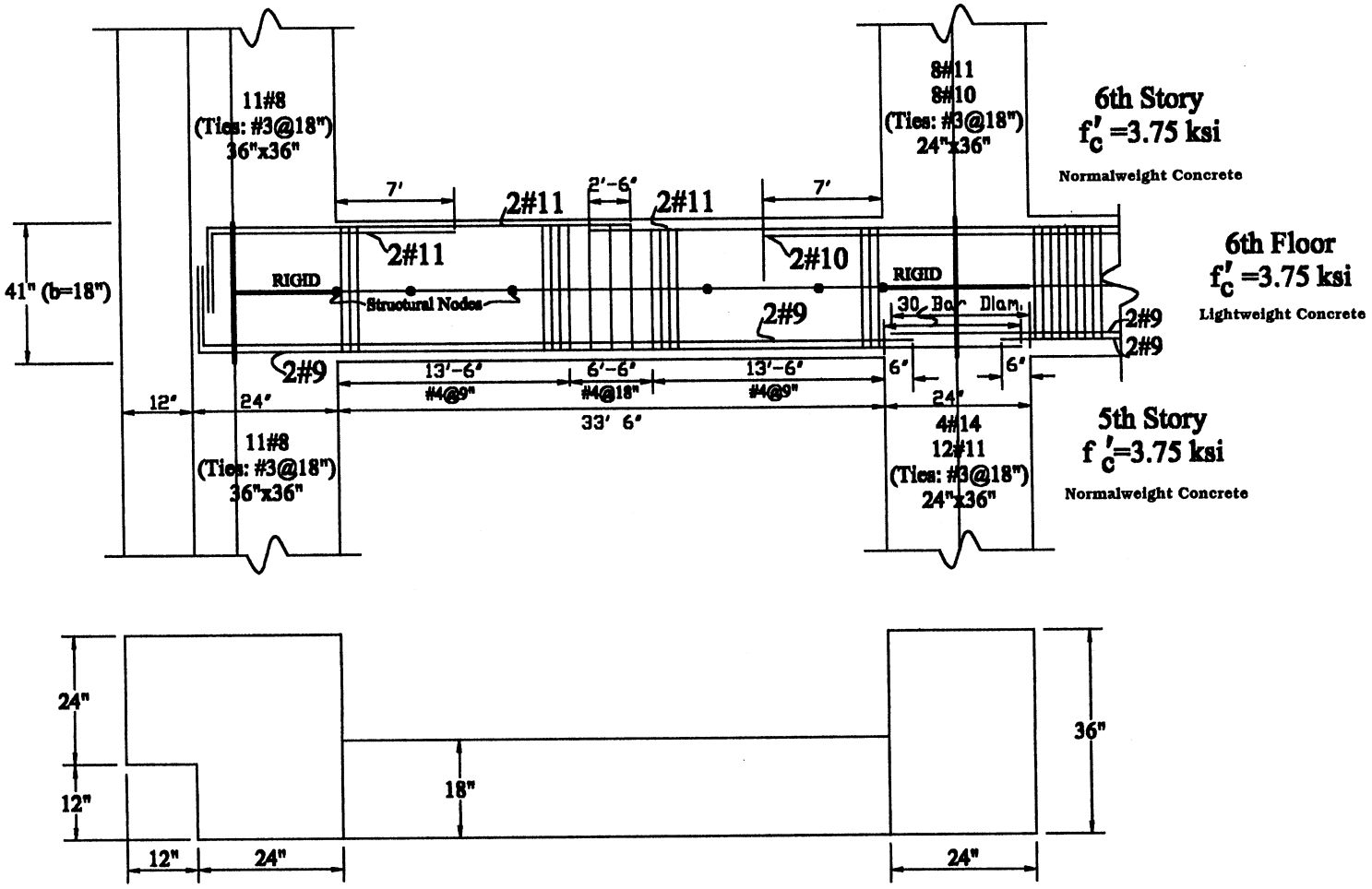

Figure 4.38 Reinforcement details for the 6th to 8th floor beams of exterior transverse frames.

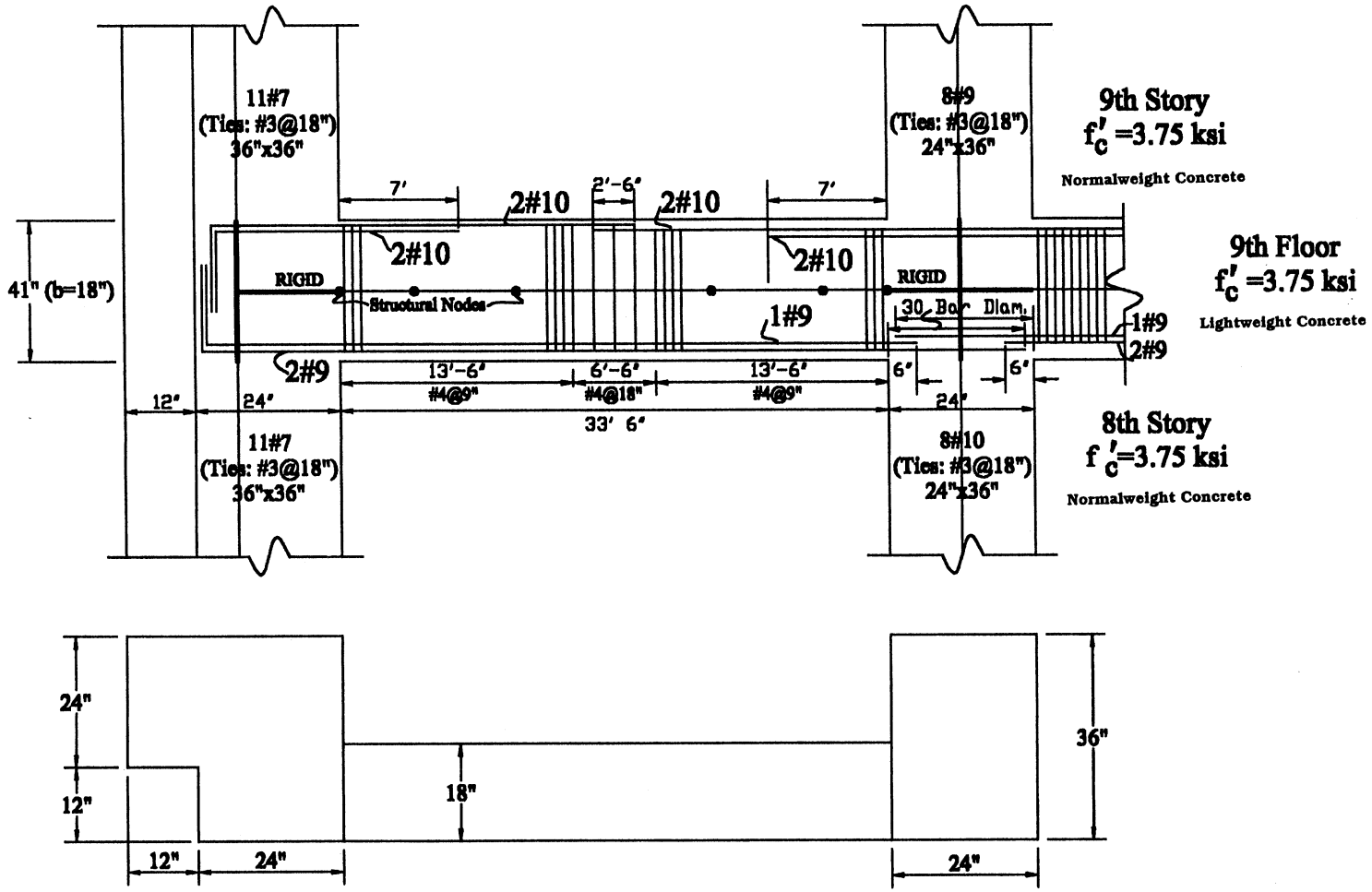

Figure 4.39 Reinforcement details for the 9th to 11th floor beams of exterior transverse frames.

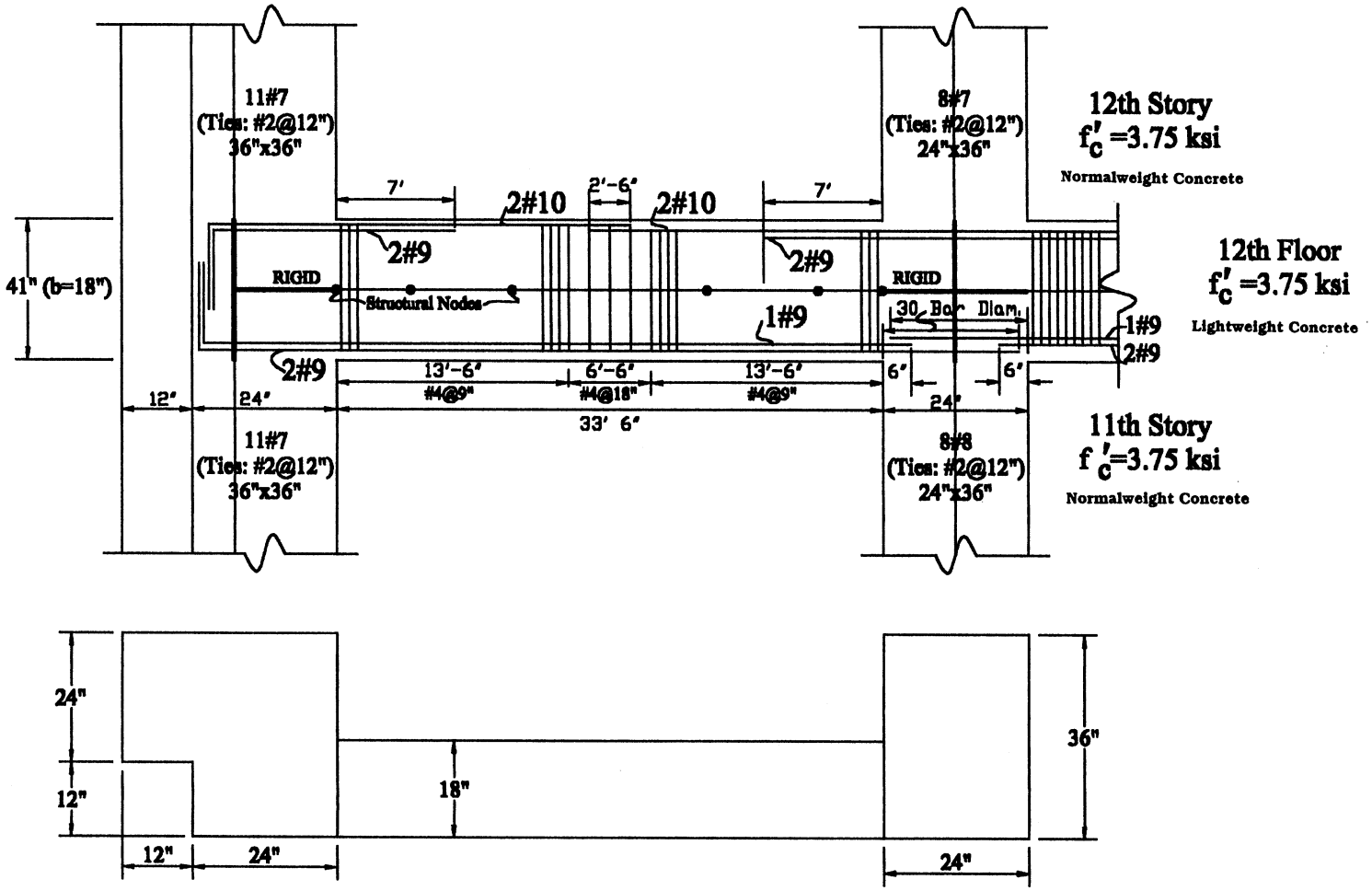

Figure 4.40 Reinforcement details for the 12th to 14th floor beams of exterior transverse frames.

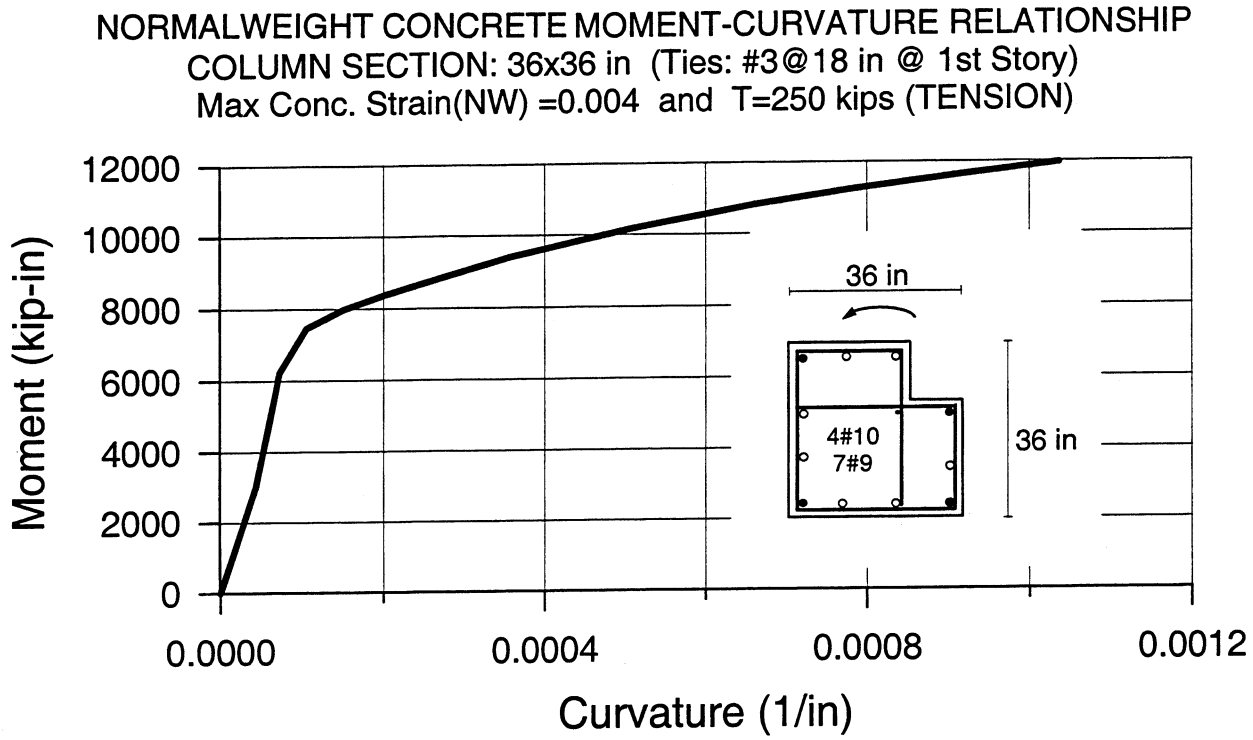

Figure 4.41 Moment-curvature relationship for corner columns at 1st story under tensile force.

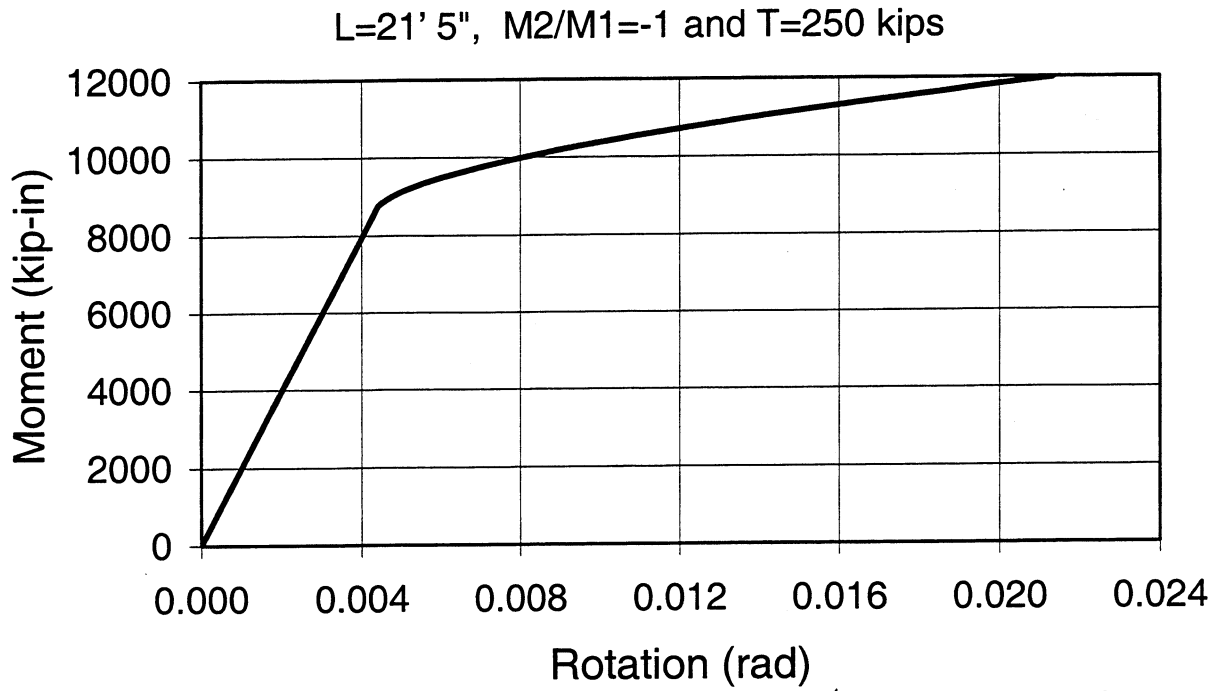

Figure 4.42 Moment-rotation relationship for corner columns at 1st story under tensile force.

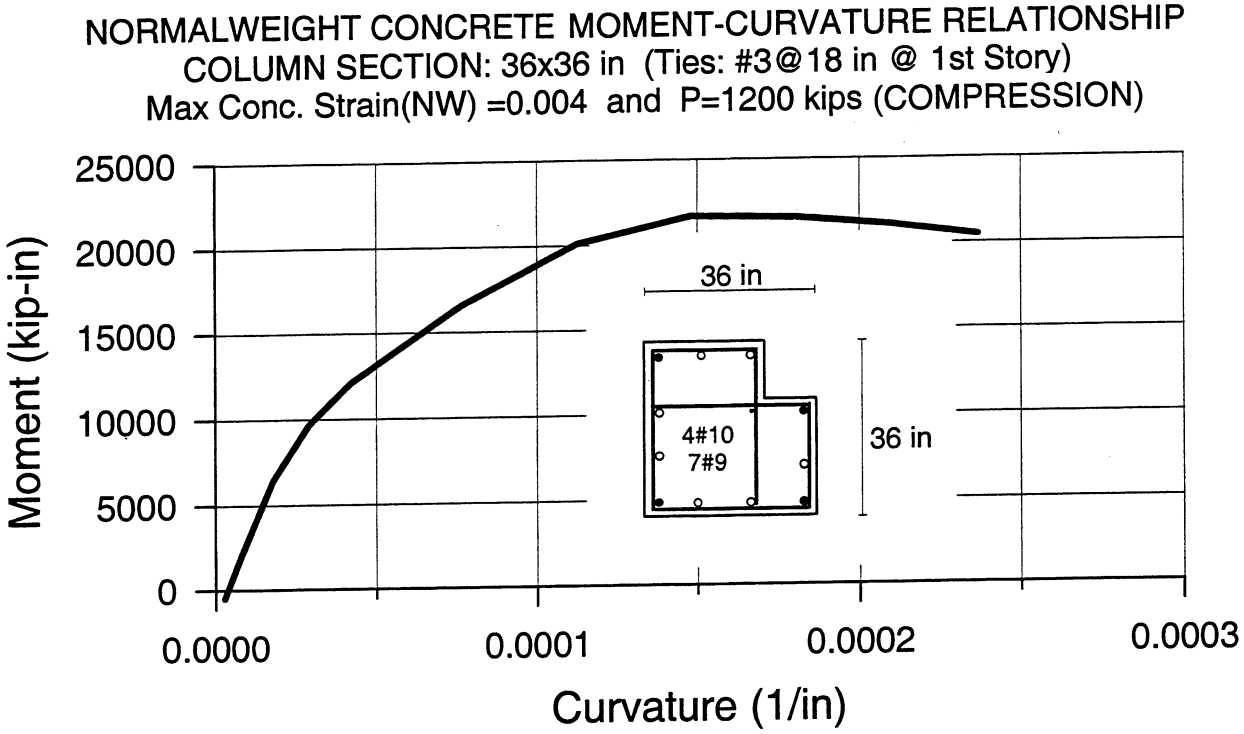

Figure 4.43 Moment-curvature relationship for corner columns at 1st story under compressive force.

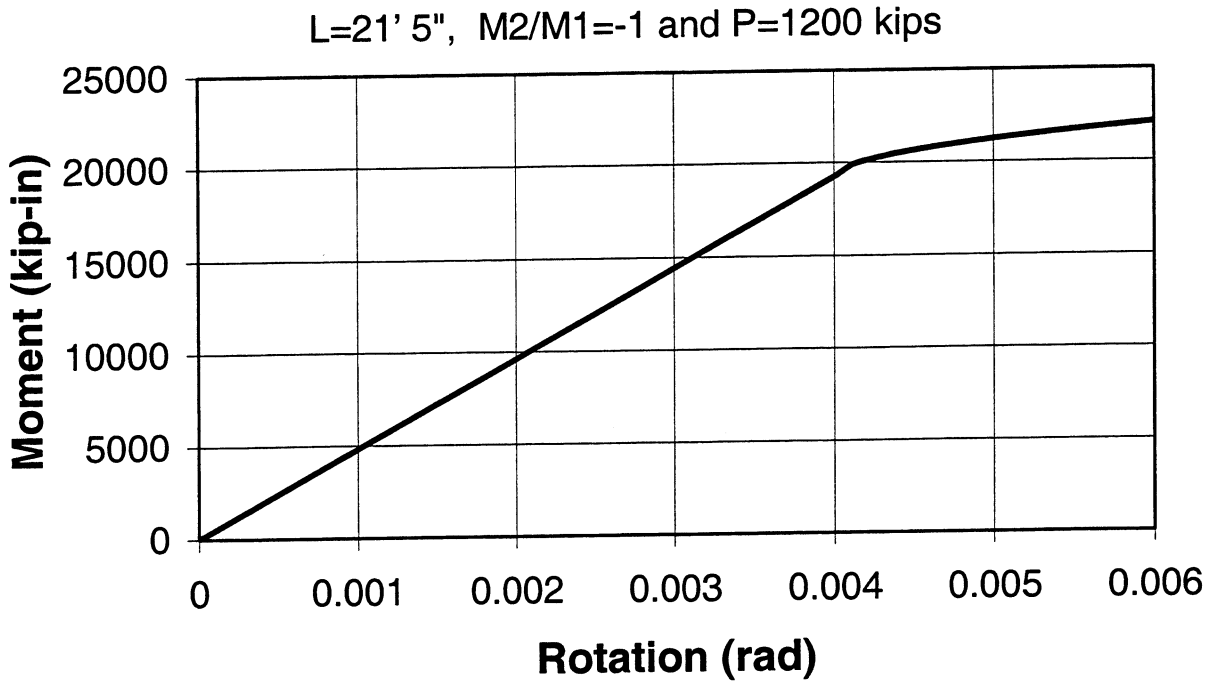

Figure 4.44 Moment-rotation relationship for corner columns at 1st story under compressive force.

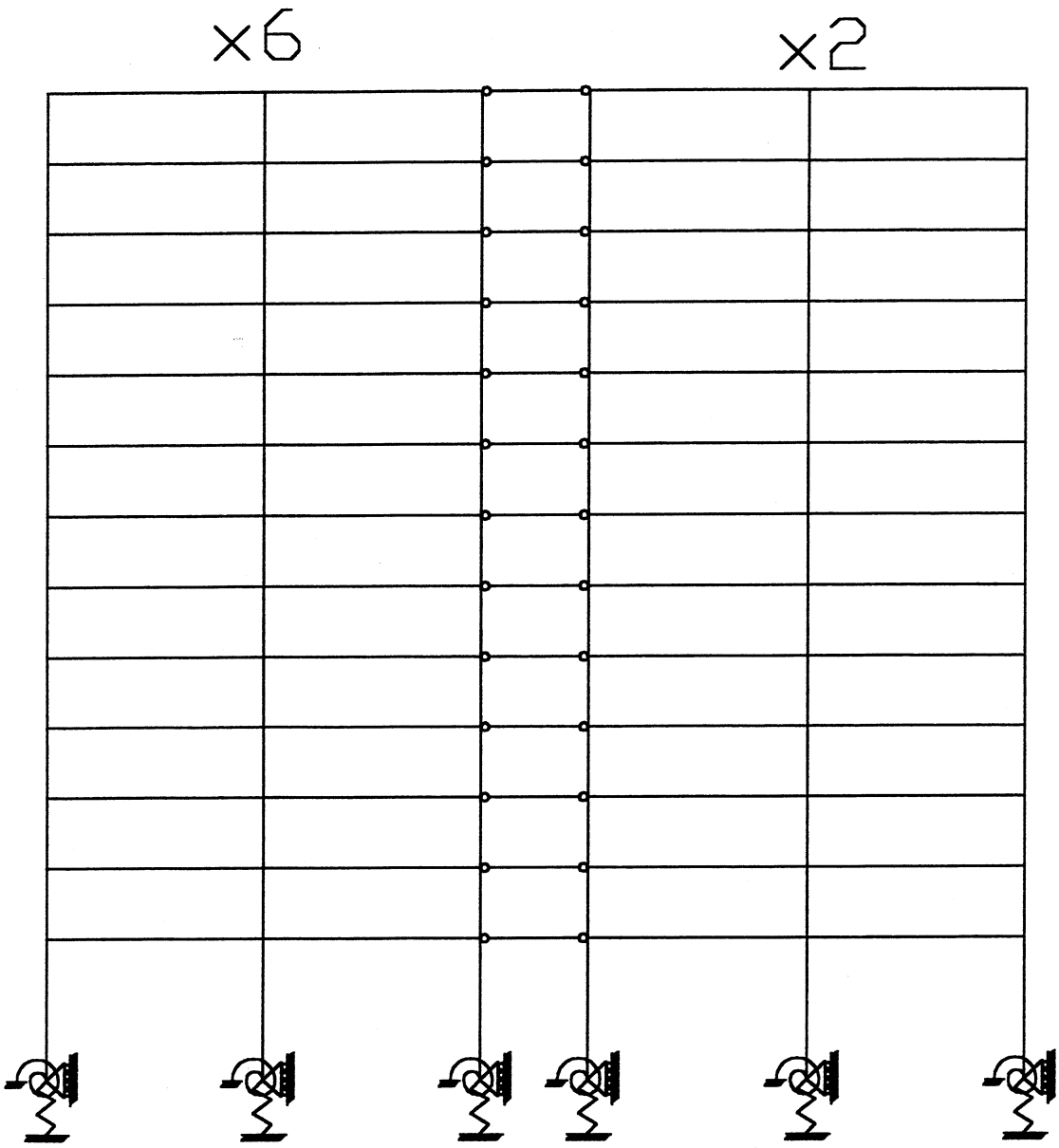

Figure 4.45 The model of the building in the transverse direction.

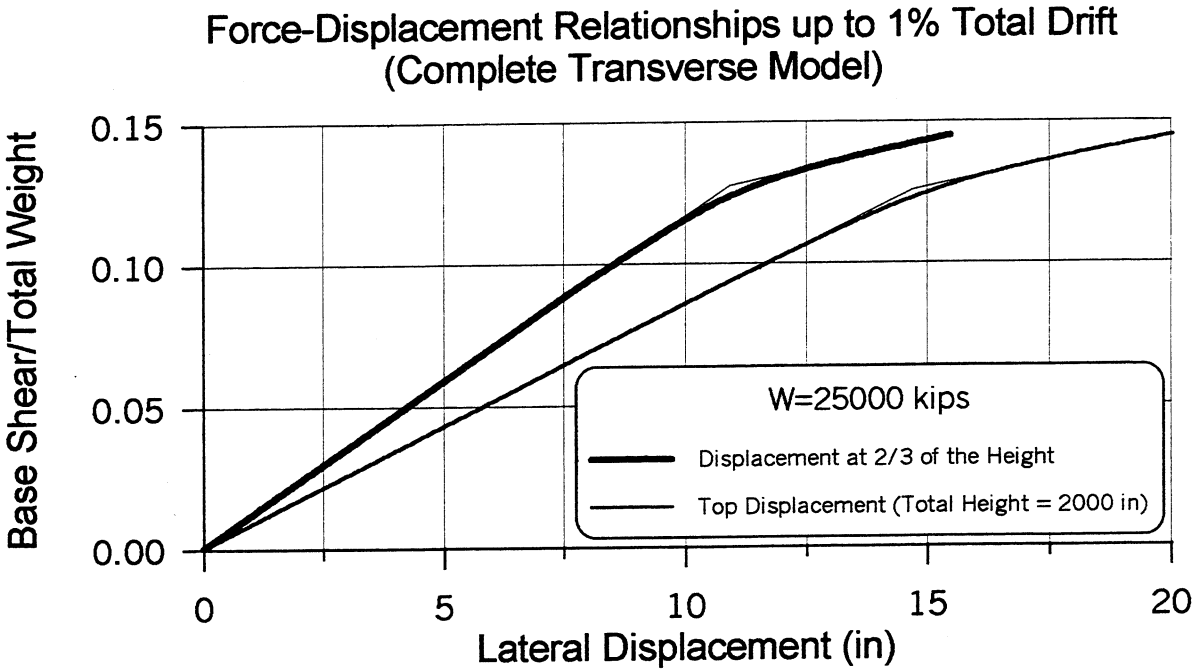

Figure 4.46 Total lateral load-displacement relationships.

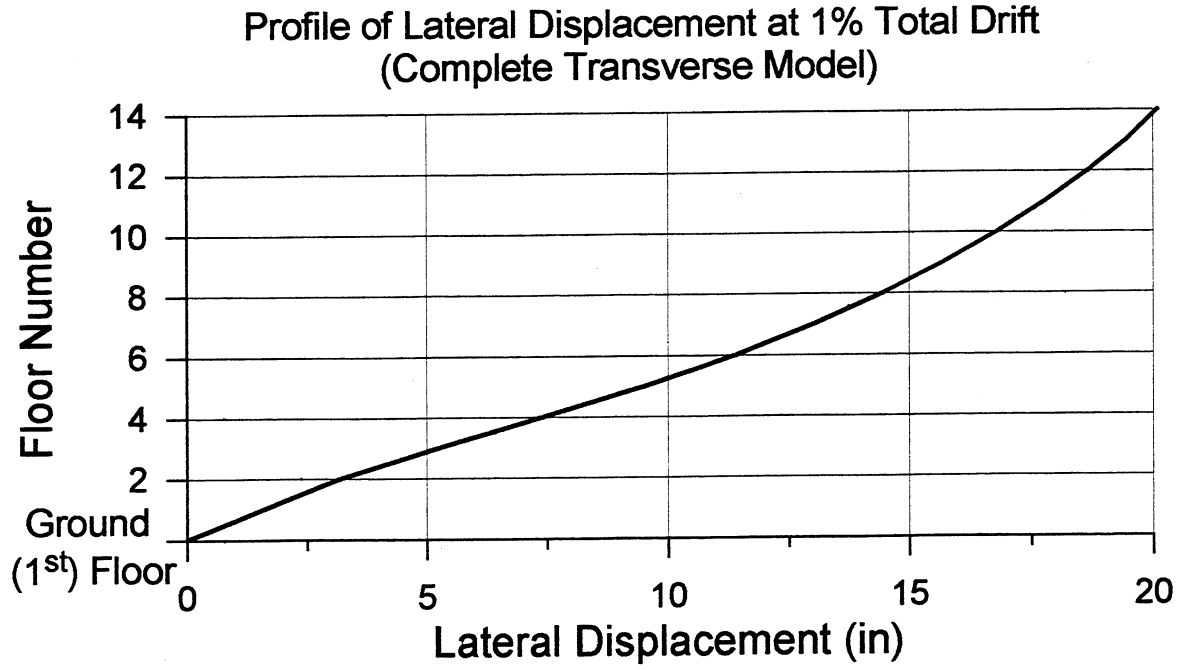

Figure 4.47 Profile of the lateral displacement along the height of the building.

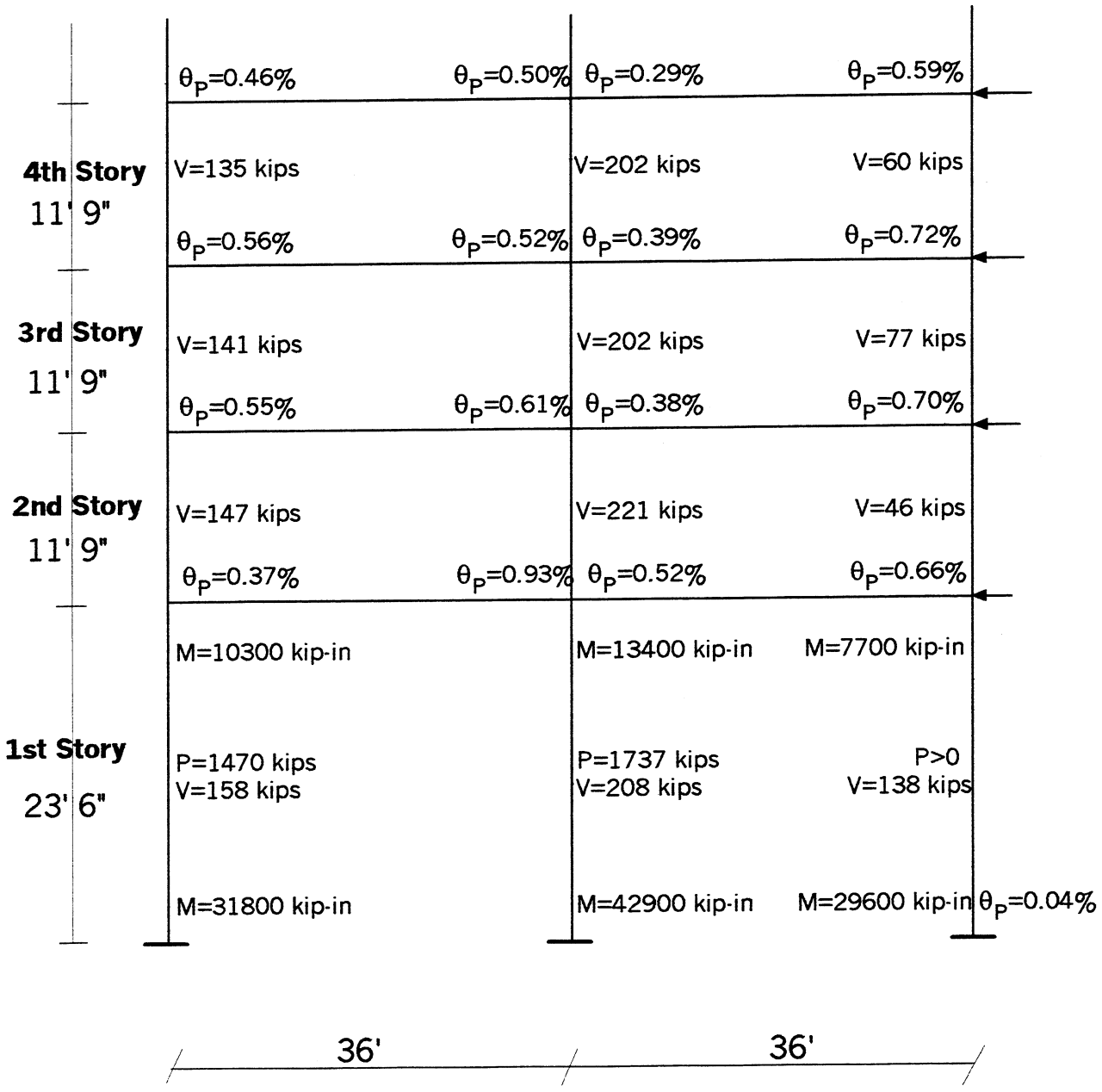

Figure 4.48 Plastic rotations and some of the internal forces of an interior frame at 1% total drift. (The model below the first story columns is not shown)

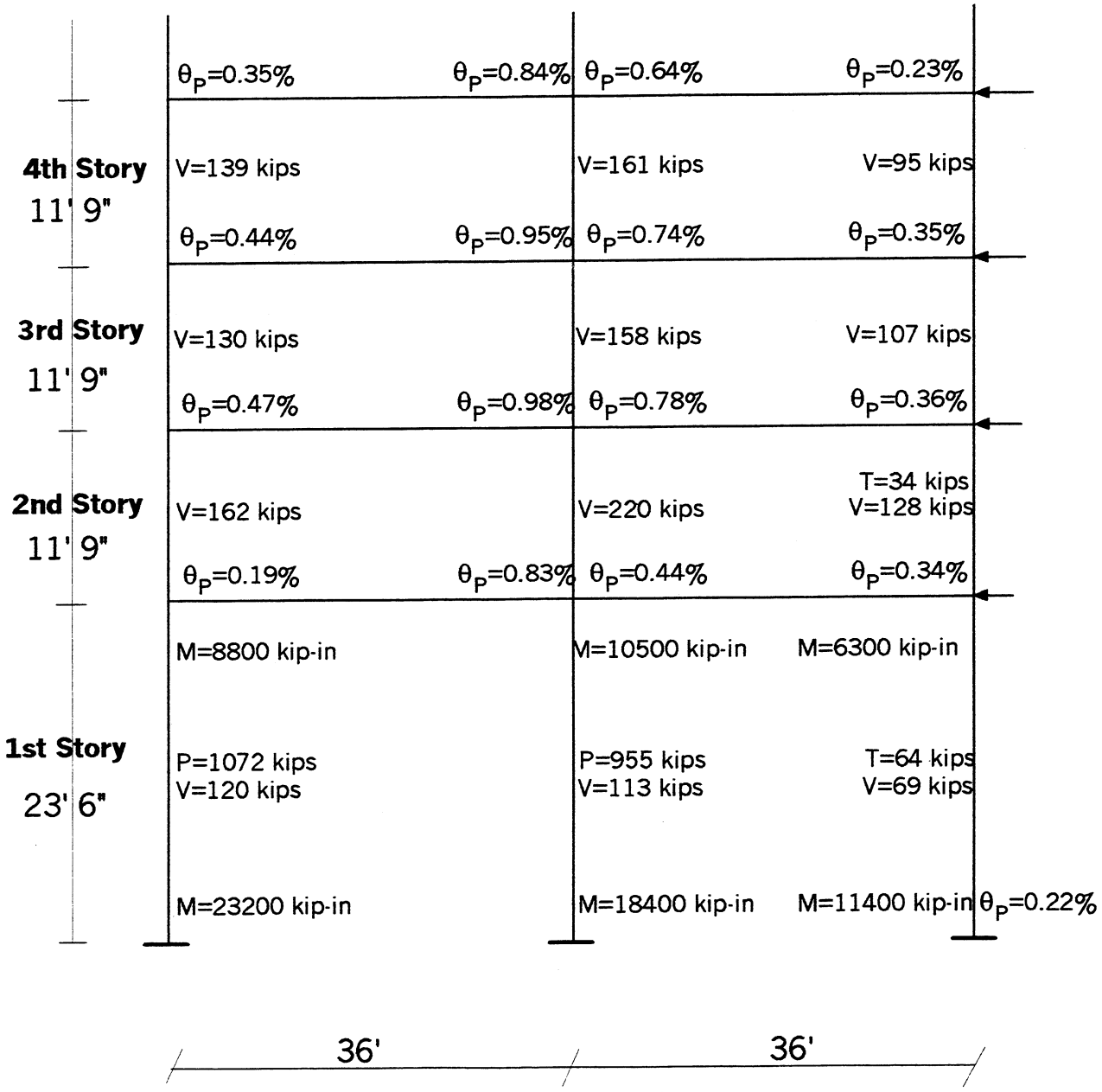

Figure 4.49 Plastic rotations and some of the internal forces of an exterior frame at 1% total drift. (The model below the first story columns is not shown.)

5 Revised Model of Building Structure in Transverse Direction

To have a more realistic model of the building and also to introduce middle nodes at the columns in order to resolve the convergence problem during the numerical solution, the simplified model of the building developed in chapter four has been modified. In the new model, the bond slip of beam reinforcement in the joints is modeled explicitly using a zero length bilinear rotational element, as shown below.

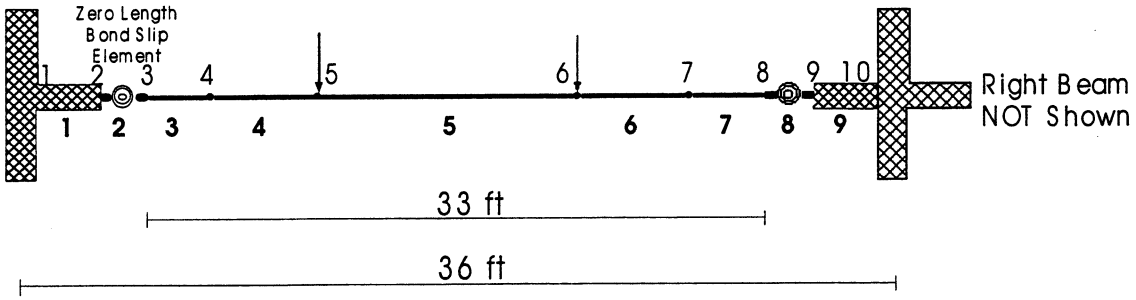

In addition to the end rigid zones, each beam is modeled by 5 segments. Using Drain-2DX, if a column is modeled as one element, in some cases, particularly when the column is under tensile axial force, the program cannot converge. To avoid this problem in the new model, all the columns have middle nodes.

As discussed in chapter two, the apparent period of the building in the transverse direction was about 3.2 sec, and the analyses of the response of the structural model having this period resulted in an estimated response that agreed very well with the recorded response of the

building during the 1995 Northridge earthquake. Therefore, in spite of the fact that the results of a frequency analysis might suggest a slightly different period, the above apparent period of 3.2 sec is used in this new study. It should be noted that the underlying assumptions in a frequency analysis are that the input and the output motions are stationary (i.e., their probabilistic characteristics remain constant over time) which are not exactly correct. While the model with a fixed base has a fundamental period T = 2.5 sec, including basement flexibility increases the T to 2.6 sec. By adjusting the axial stiffness of the added elements to consider the possible effects of the foundation rotation, the period was further increased to 3.2 sec, which is the one that was considered to be the most reliable.

6 Behavior of As-Built Building (Foundation and Basement Flexibility Included)

Using the model described in the previous chapter, the behavior of the as-built structure in a pushover analysis and also under two pulse-type recorded ground motions is studied. Since with the available model of the structure, it is not possible to assign negative stiffness to the beam-column elements, it should be borne in mind that the response of the building estimated in a pushover analysis and under the recorded ground motions is found based on the assumption that all the elements can develop forces having fixed strain-hardening ratios with no limit, which is not quite true. Therefore, the results of the analyses need to be checked against different possible ductile or brittle modes of failure that could limit the displacement capacity of the structure. Limiting the displacement capacity of the structure by ductile modes of failure could be checked by comparing the total rotation demand and capacity. Based on the existence of different weaknesses in the structure, undesirable modes of failure might be the consequence of (1) inadequate transverse reinforcement along the height of the columns; (2) no transverse reinforcement at the beam-column joints; (3) lack of adequate amount and detailing of the longitudinal and transverse reinforcement along the girders; (4) lack of adequate anchorage of the beam bottom reinforcement at the joints; and (5) lack of adequate lap splicing of the longitudinal reinforcement.

6.1 PUSHOVER ANALYSIS UNDER INVERTED TRIANGULARLY DISTRIBUTED LATERAL LOAD

Accounting for P-Δ effect, with constant incremental load of 10 kips, at a roof displacement of 53.1 in., the structure becomes analytically unstable. The displacement, interstory drift index, and the story shear force envelopes are given in Figure 6.1. The maximum interstory drift of 4.3% occurs at the second and third stories, while the global drift index is about 2.7%. Note that only about 0.4% of the drift is caused by the foundation rotation. The maximum base shear is about 14% of the weight of the building.

Figure 6.2 shows the base shear versus roof displacement and its bilinear idealization with a Δ_y=18.5 in. and V_y=0.127W leading to a global displacement ductility of about 2.9. Note that W is the total weight of the building above the ground level. The maximum total plastic rotation (including the beam plastic rotation and rotation as a result of bond slip) is about 4% and occurs at the interior joints of the second floor beams of the interior frames, under positive bending moment (i.e., tension in the bottom reinforcement). Since the beam yield rotation at those locations is about 0.31%, the maximum rotation ductility is about 13.9, which is about 4.8 times the global displacement ductility (μ=2.9). Note that at this point, after the pullout of the bottom bars with 6-in. embedment length, the remaining bottom reinforcement is even less than the minimum flexural reinforcement, therefore, a significant concentration of plastic rotation occurred. The same beam ends under negative bending moments undergo a maximum total plastic rotation of 3.2% and a rotation ductility of about 5.0 with a yield rotation of about 0.81%.

As discussed above, whether such plastic rotations can develop should be verified. Although small amount of tensile (bottom) and large amount of compressive (top) reinforcement at the interior joints of the second floor beams of the interior frames, under positive bending moment result in large curvature capacity (see Figure 4.17) since after pullout of tensile reinforcement with short embedment length the beam sections further away from the column face are flexurally stronger than the beam end section, the plastic hinge length and consequently the rotation capacity of the beams are not large (see Figure 4.27). As shown in the figure, the plastic rotation capacity of the beams is about 1.8%. As shown in Figure 4.25 the plastic rotation capacity of the beams discussed above under negative bending moments is about 2.1%. Therefore the plastic rotation capacity is less than that of demand. In other words, the maximum roof displacement capacity of the structure is less than the 53.1 in., shown in Figures 6.1 and 6.2.

As far as ductile modes of failure are concerned, the plastic rotation demands of about 2.6% at the bottom of the first-story columns are far beyond the plastic rotation capacity of about 0.1%.

Possible nonductile modes of failure could also limit the displacement capacity of the structure below the value found in the pushover analysis. This possibility is discussed in detail in chapter four. For instance, because of the relatively small maximum plastic rotation capacities of the columns at the base of the first story, when these capacities are reached, the flexural capacities of the columns will drop and as a result of excessive plastic deformation, the shear strength of the columns with very little shear reinforcement decreases, particularly on the side of the structure where the overturning moment produces tensile force in the columns, which can lead to a brittle failure of the columns. Therefore, the displacement capacity of the structure is again less than the value found in pushover analysis.

6.2 RESPONSE OF STRUCTURE UNDER PULSE-TYPE GROUND MOTIONS

Analyzing the available recorded earthquake ground motions (EQGMs) at near-fault stations in the direction normal to the fault, two records that have the largest displacement response spectra values at periods near the periods of the structure before and after retrofit were selected for this study. Figure 6.3 shows the time histories of the ground motion recorded at Los Gatos station during the 1989 Loma Prieta earthquake. Figure 6.4 shows the yield coefficient and displacement spectra of this EQGM for ductility values of 1, 2, 3, 4, and 6. Figures 6.5 and 6.6 show similar plots for the recorded ground motion at the Takatori station during the 1995 Kobe earthquake.

6.2.1 1989 Loma Prieta Earthquake Recorded at Los Gatos Station

The displacement, interstory drift index, and the story shear force envelops under the Los Gatos ground motion are given in Figure 6.7. The maximum roof displacement is about 69 in. From the results of the pushover analysis (Figure 6.2) the yield displacement is about 18.5 in., therefore, global displacement ductility is about 3.7. The maximum interstory drift of 5.4% occurs at the third and fourth stories, while the global drift index is about 3.5%. Based on the results of the nonlinear analysis, only about 0.5% of the drift is caused by the foundation rotation. The time history of the roof displacement is shown in Figure 6.8. The maximum base shear of about 20% of the weight of the building occurs at t=9.68 sec, i.e., after the maximum roof displacement

which occurred at about 8.5 sec, when the structure is moving back toward its original position. At this point, while the roof displacement is only about 20 in., the base shear is about 46% higher than that under pushover analysis (at a roof displacement of about 53 in.). Below, an attempt is made to clarify the observed increased base shear.

Comparing the results in terms of base shear force from a pushover analysis and a nonlinear dynamic analysis, the following four factors must be considered. (1) The base shear under dynamic analysis is the summation of the first-story column shear forces and the base shear forces caused by part of viscous damping forces (the portion of the viscous force that is proportional to the structural stiffness). Note that the mass proportional damping forces are included in the column shear forces. At t=9.68 sec, where the maximum base shear occurs, the stiffness proportional damping shear force at the base is about 1620 kips which is about 32% of the total base shear and 47% of the maximum base shear from pushover analysis. (2) In the pushover analysis a fixed distribution of the lateral load is considered, and any deviation from the assumed force distribution affects the base shear force. (3) The P-Δ effect on the base shear might be different in static and dynamic analyses. For instance, at the time the structure undergoes the maximum base shear, which is after a large previous maximum displacement in the negative direction, while the structure is still deformed in that direction, the lateral loads are in the positive direction. In other words, the P-Δ effect in this situation makes the structure stiffer, while in a pushover analysis, the P-Δ effect always makes the structure more flexible and results in smaller base shear for the same level of lateral displacement. (4) Although the maximum base shear occurs at a maximum roof displacement of about -20 in. (t=9.68 sec) it should be considered that first a roof displacement of about -69 in. occurred (see Figure 6.8). Then, during unloading, the roof of the structure moved about 69-20=49 in. toward the original position and the maximum base shear occurred. Therefore the effective lateral displacement (i.e., the displacement toward the original position after the peak displacement in the negative direction was reached, or the incremental displacement after unloading) is really about 49 in. and not -20 in.

Figure 6.4 shows the yield coefficient and displacement spectra of the EQGM recorded at Los Gatos station during the 1989 Loma Prieta earthquake. Since the global displacement ductility of the response of the structural model is about 3.7, the displacement spectra suggest for a T=3.2 sec a maximum displacement of about 80 in., which is even larger than the building roof displacement of 69 in. (the displacement at about 2/3 of the height of the building that could be

representative of an equivalent single-degree-of-freedom system is equal to 60 in.). The yield coefficient spectra suggest a yield coefficient, C_y, of about 0.21. It should be noted that the base shear found from response spectra, C_y W, includes only the maximum hysteretic force (the one produced by the pseudo-acceleration). On the other hand, the story and base shear forces given by the envelope from nonlinear analysis are the maximum of the summation of the hysteretic and viscous forces. However, the spectral response suggests a base shear of 0.21W, which is larger than 0.20W found from the inelastic analysis of the building. It should also be noted that the single-degree-of-freedom system that is considered to develop the spectra does not have any strain hardening and the P-Δ effect is not included either. Thus comparing the base shear obtained from response spectra with that obtained from the nonlinear response of the structure which includes the P-Δ effect, while neglecting the strain hardening reduces the base shear, neglecting the P-Δ effect results in a larger base shear.

As discussed in chapter four, since according to the computer program used in modeling the structure it is not possible to assign negative stiffness to the beam-column elements, the response of the building to the recorded ground motion is computed based on the assumption that all the elements can develop resisting forces having fixed strain hardening with no limit in their maximum values, which is not true. For instance, the maximum first-story column plastic rotation demand is about 4%, which is far beyond the plastic rotation capacity of about 0.1% as shown in Figures 4.33 and 4.35. Furthermore, the large rotation ductility demand at the bottom of first-story columns results in a significant reduction in the shear strength of the columns that have very little transverse reinforcement. Adding the fact that columns could be under a small axial compression force or in the case of the corner columns even under tension, the column shear strength reduces even further. As far as rotational capacity of the beams are concerned, the demand is larger than capacity as well. Undesirable failure modes that can limit the displacement capacity of the structure are discussed in chapter four.

6.2.2 1995 Kobe Earthquake Recorded at Takatori Station

The displacement, interstory drift index, and the story shear force envelopes under the Takatori ground motion are given in Figure 6.9. The maximum roof displacement is about 32 in. From the results of the pushover analysis (Figure 6.2) the yield displacement is about 18.5 in., therefore, the global displacement ductility is about 1.7. The maximum interstory drift of 2.8% occurs at

the 8th, 9th and 10th stories, while the global drift index is about 1.6%. Note that only about 0.5% of the drift is caused by the foundation rotation. It should be noted that unlike the response of the structure to the Los Gatos ground motion, the larger interstory drift index, IDI, occurs at the stories close to the roof of the building, which indicates that the variation of the lateral displacement along the height of the building is very sensitive to the type of the severe pulse-type EQGMs. Thus further study is needed to investigate the effects of the type of pulse ground motion on the lateral displacement profile of shear type buildings. The maximum base shear is about 18% of the weight of the building. The time history of the roof displacement is shown in Figure 6.10.

Figure 6.6 shows the yield coefficient and displacement spectra during the 1995 Kobe Earthquake recorded at Takatori station. Since the global displacement ductility of the response of the structural model is about 1.7, at a T=3.2 sec, the displacement spectra suggest a maximum displacement of about 32 in. which equals the building roof displacement (the displacement at about 2/3 of the height of the building, which could be representative of an equivalent single-degree-of-freedom system, is smaller). The yield coefficient spectra gives a yield coefficient, C_y, of about 0.20, which suggests a base shear larger than 0.18W that was found in the nonlinear analysis of the building model.

6.3 CONCLUDING REMARKS

In the nonlinear pushover and dynamic analyses of the structure conducted in this chapter, it was assumed that neither the plastic rotation capacities nor the undesirable modes of failure limit the lateral displacement capacity of the structure. Obviously because of (1) inadequate transverse reinforcement along the height of the columns; (2) no transverse reinforcement at the beam-column joints; (3) lack of adequate amount and detailing of the longitudinal and transverse reinforcement along the girders; (4) lack of adequate anchorage of the beam bottom reinforcement at the joints; and (5) lack of adequate lap splicing of the longitudinal reinforcement, this assumption is not correct and all the limiting factors need to be checked.

The results of a pushover analysis show that at a top displacement of about 53 in. which corresponds to a global ductility of about 2.9 and an average interstory drift of about 2.7%, the maximum story drift of 4.3% occurs at the second and third stories. This results in a maximum beam rotational ductility of 13.9 that occurs under positive bending moments (tension at the bottom). In other words, unlike the assumption that the beam rotation ductility is equal the global

ductility, as is made in the 1997 FEMA-273, the maximum beam rotation ductility is about 4.8 times the global ductility. This is caused mainly because (1) the maximum interstory drift is larger than the average drift; (2) the plastic rotation at locations with little amount of tensile reinforcement is concentrated; and (3) the pullout of beam bottom reinforcement from the joint, and the resultant distribution of flexural capacity limit the extension of plastic region into the beams.

The maximum interstory drift under Los Gatos ground motion is about 5.4%, which is excessive. Therefore, because of the flexibility of the structure and the weaknesses discussed above, the structure needs to be retrofitted.

The lateral displacements predicted by spectra displacement overestimate the results of nonlinear analyses. This will be discussed in more detail in the following chapters.

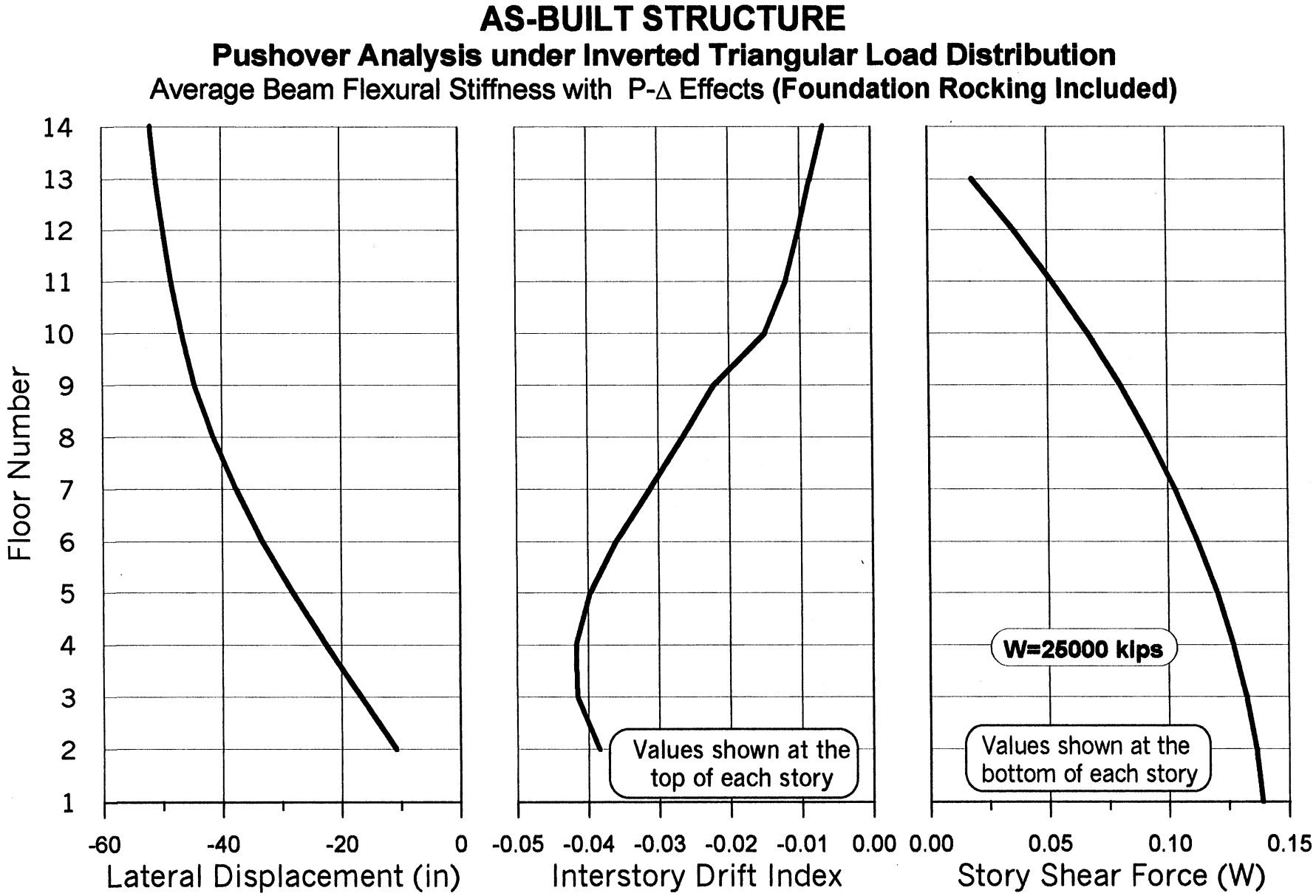

Figure 6.1 Lateral displacement, interstory drift index, and story shear force envelopes.

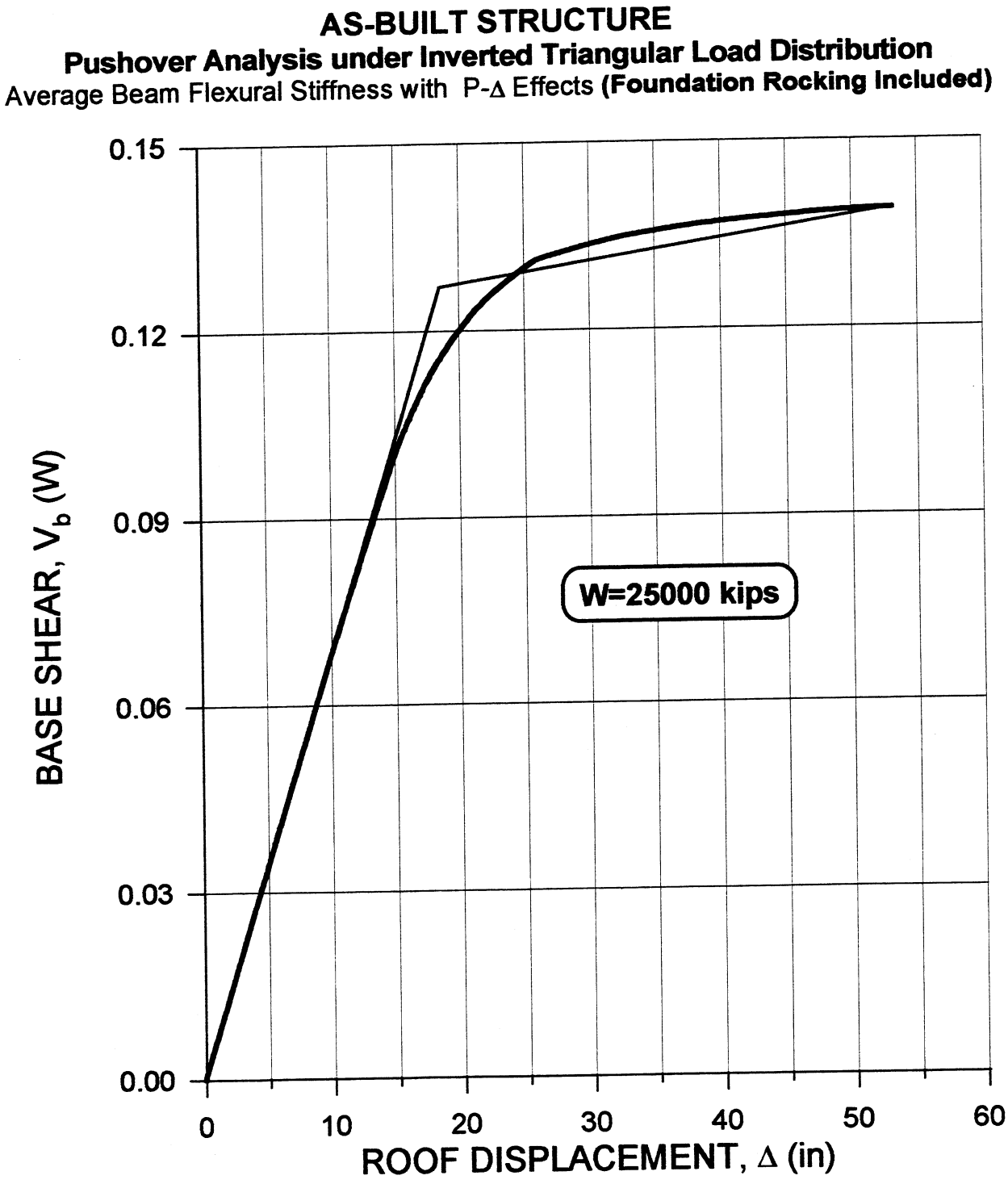

Figure 6.2 Base shear versus roof displacement and its bilinear idealization with Δ_y=18.5 in, V_y=0.127W and μ_Δ=2.9.

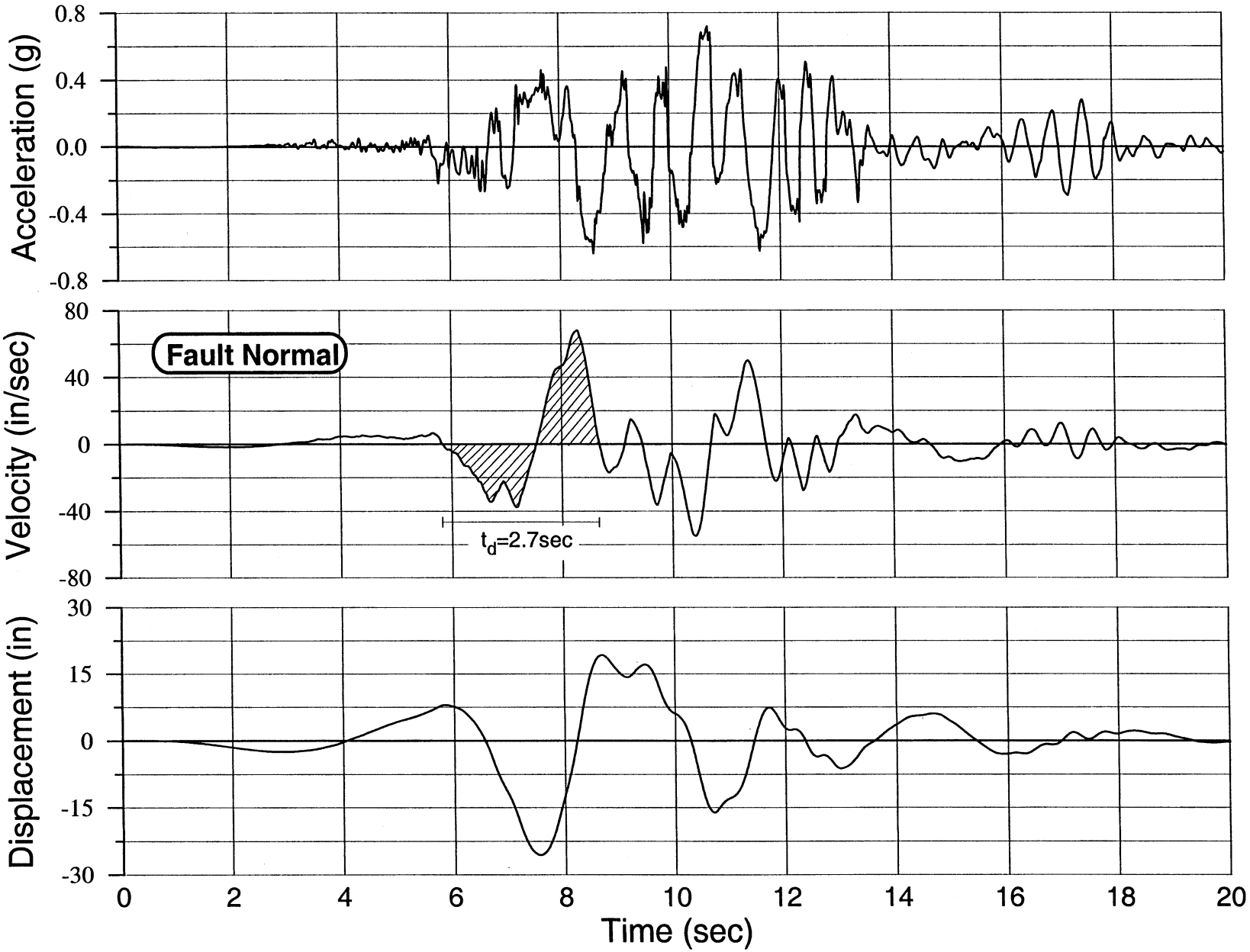

Figure 6.3 Ground acceleration, velocity, and displacement at Los Gatos station during 1989 Loma Prieta earthquake.

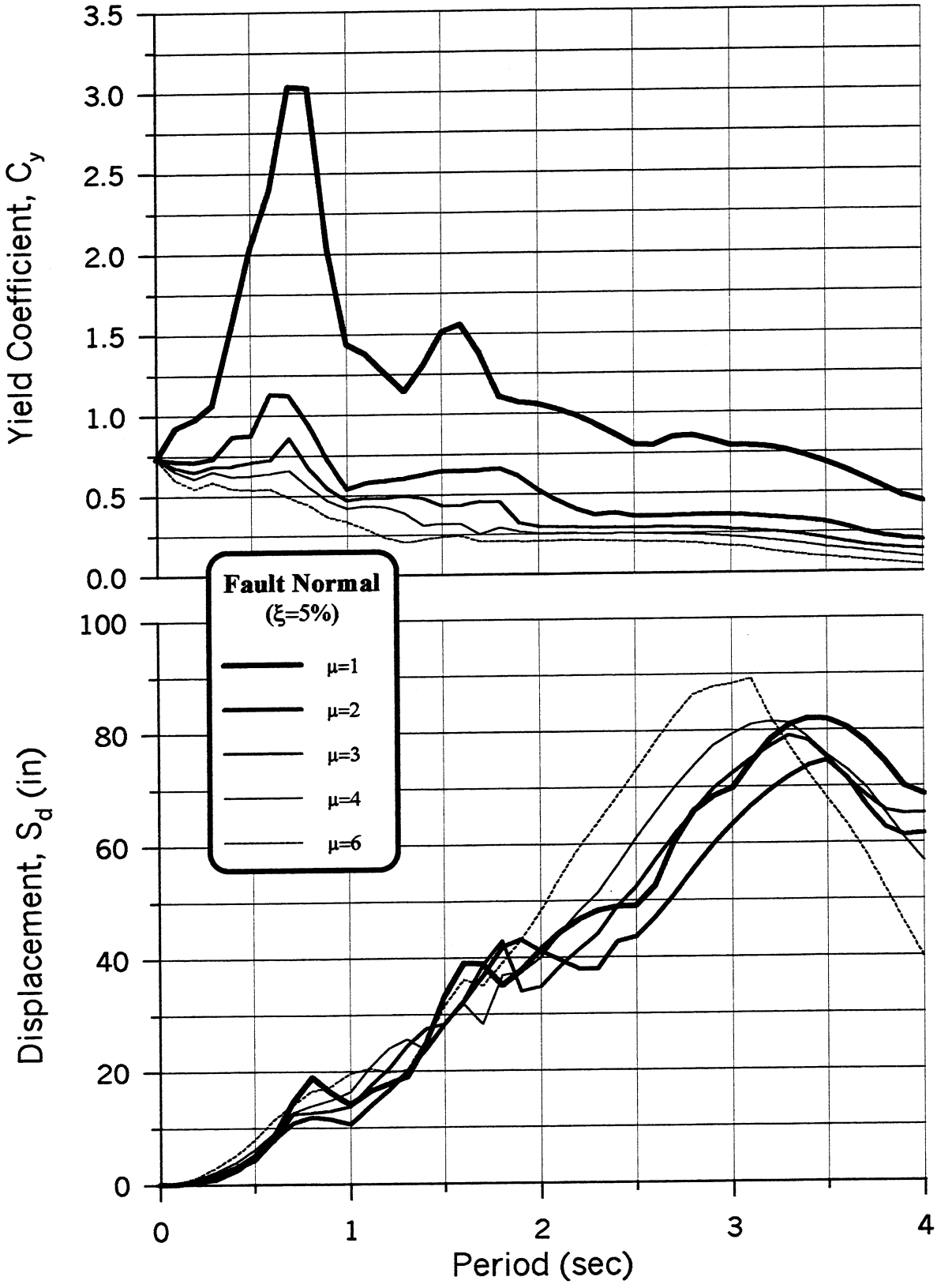

Figure 6.4 Yield coefficient and displacement spectra for the recorded ground motion at Los Gatos station during 1989 Loma Prieta earthquake.

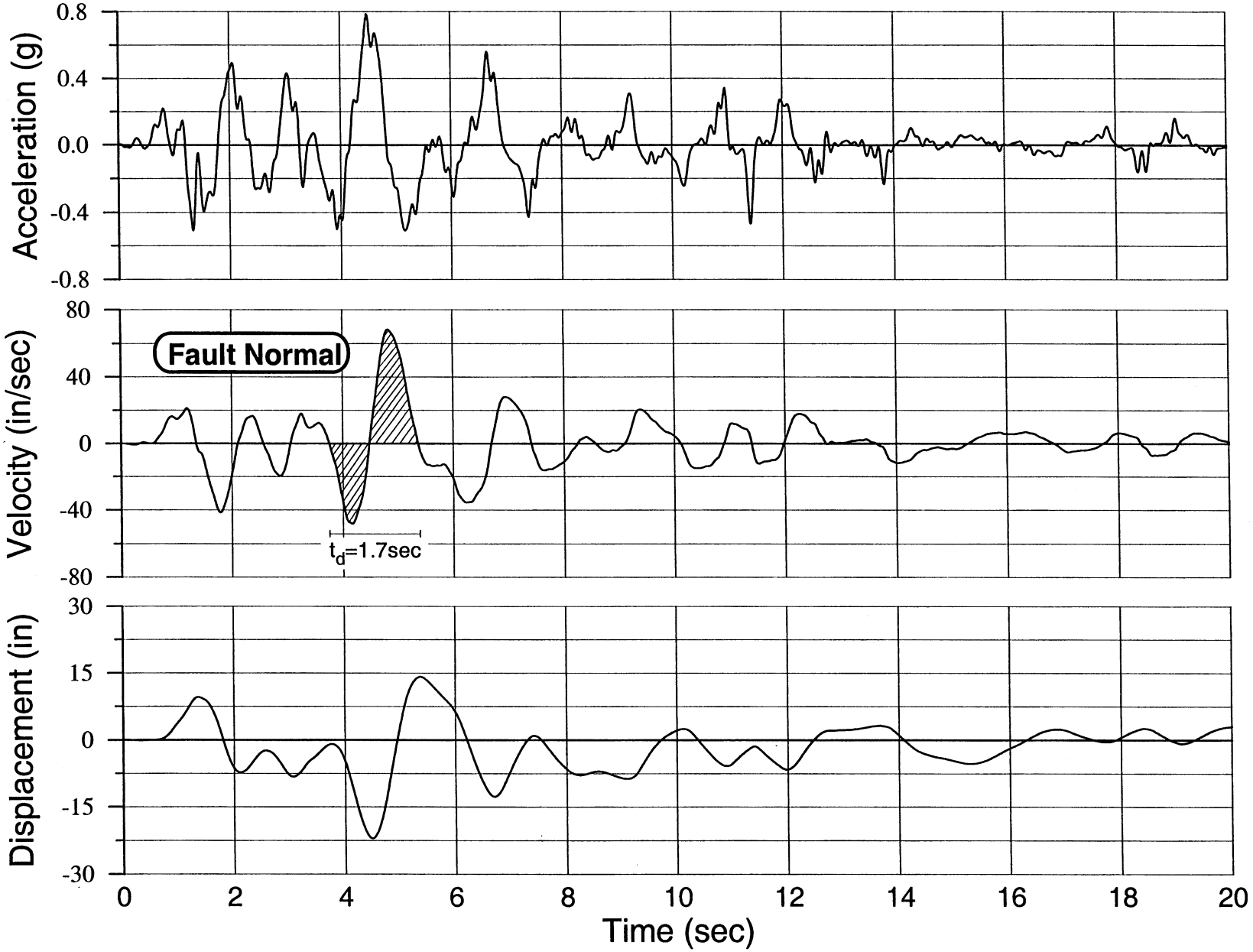

Figure 6.5 Ground acceleration, velocity, and displacement at Takatori station during 1995 Kobe earthquake.

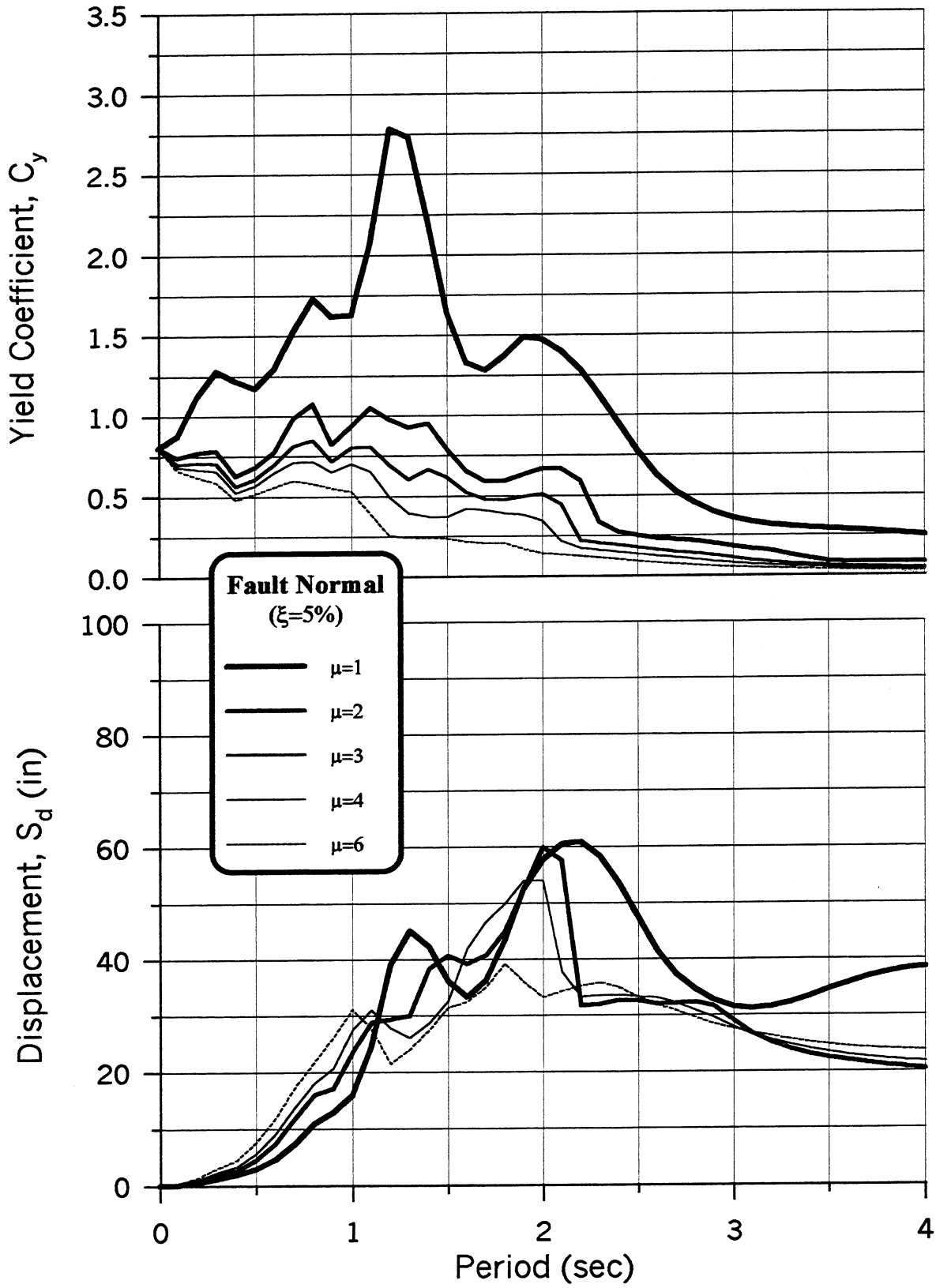

Figure 6.6 Yield coefficient and displacement spectra for the recorded ground motion at Takatori station during 1995 Kobe earthquake.

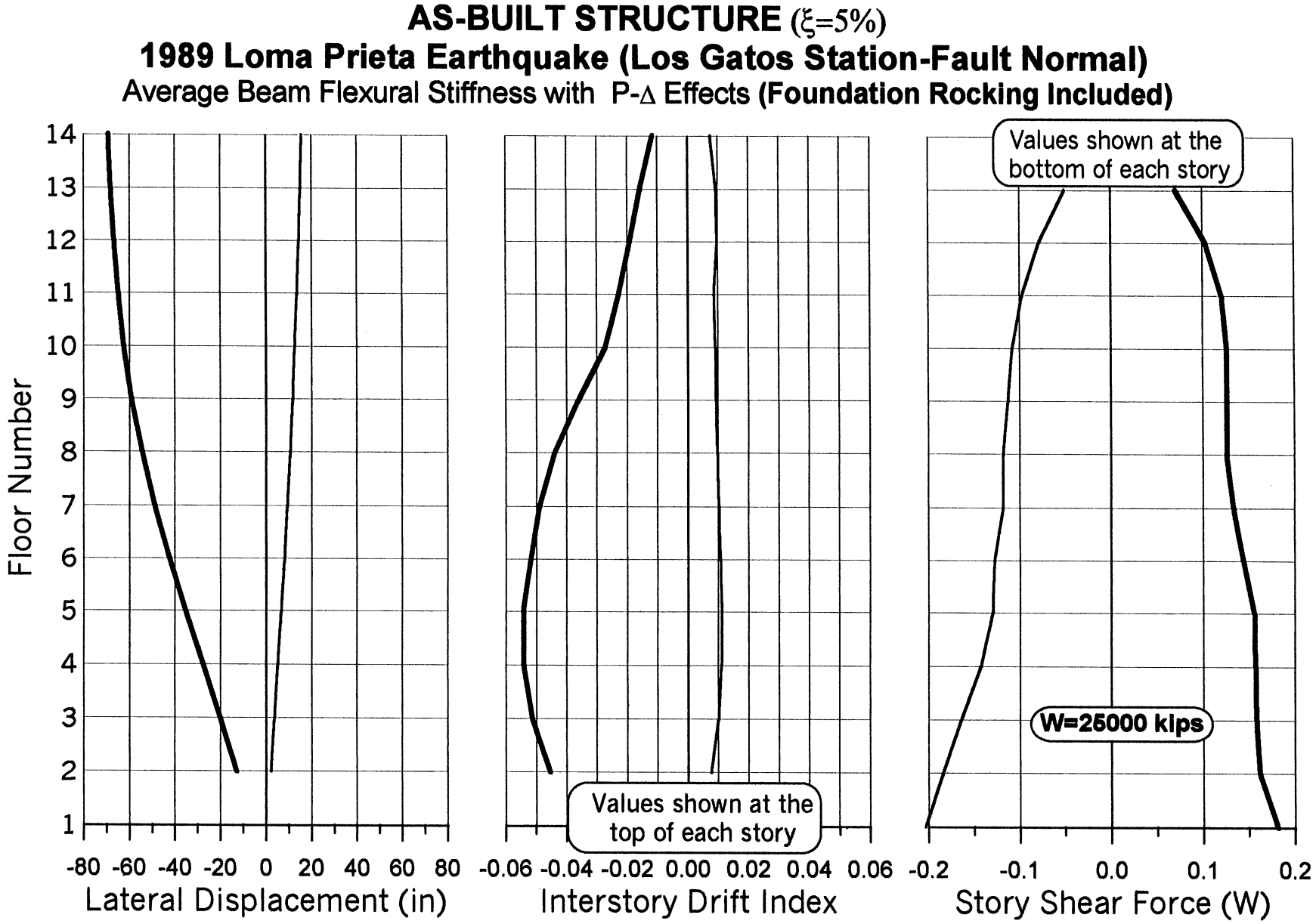

Figure 6.7 Lateral displacement, interstory drift index, and story shear force envelopes.

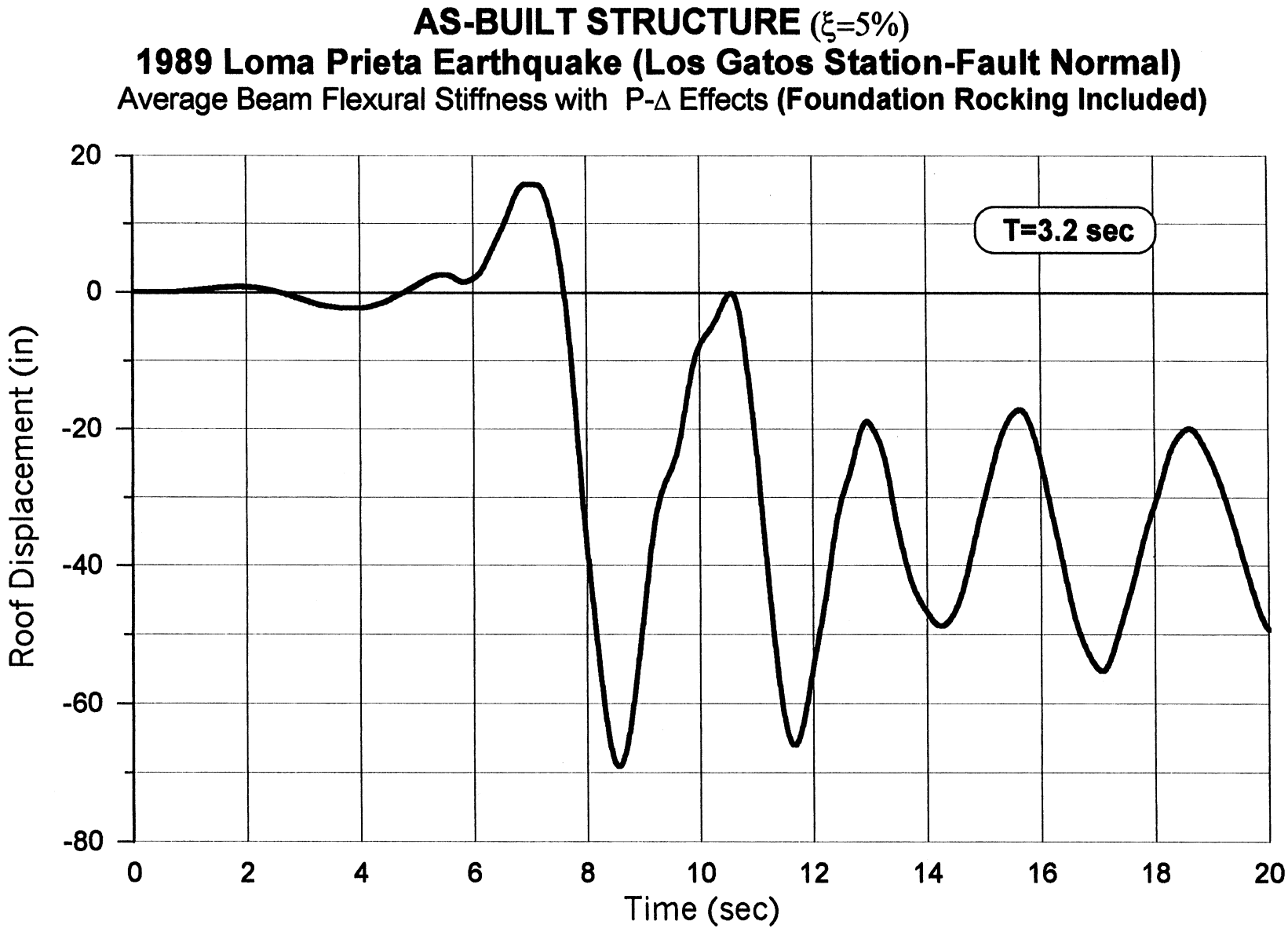

Figure 6.8 Time history of roof displacement.

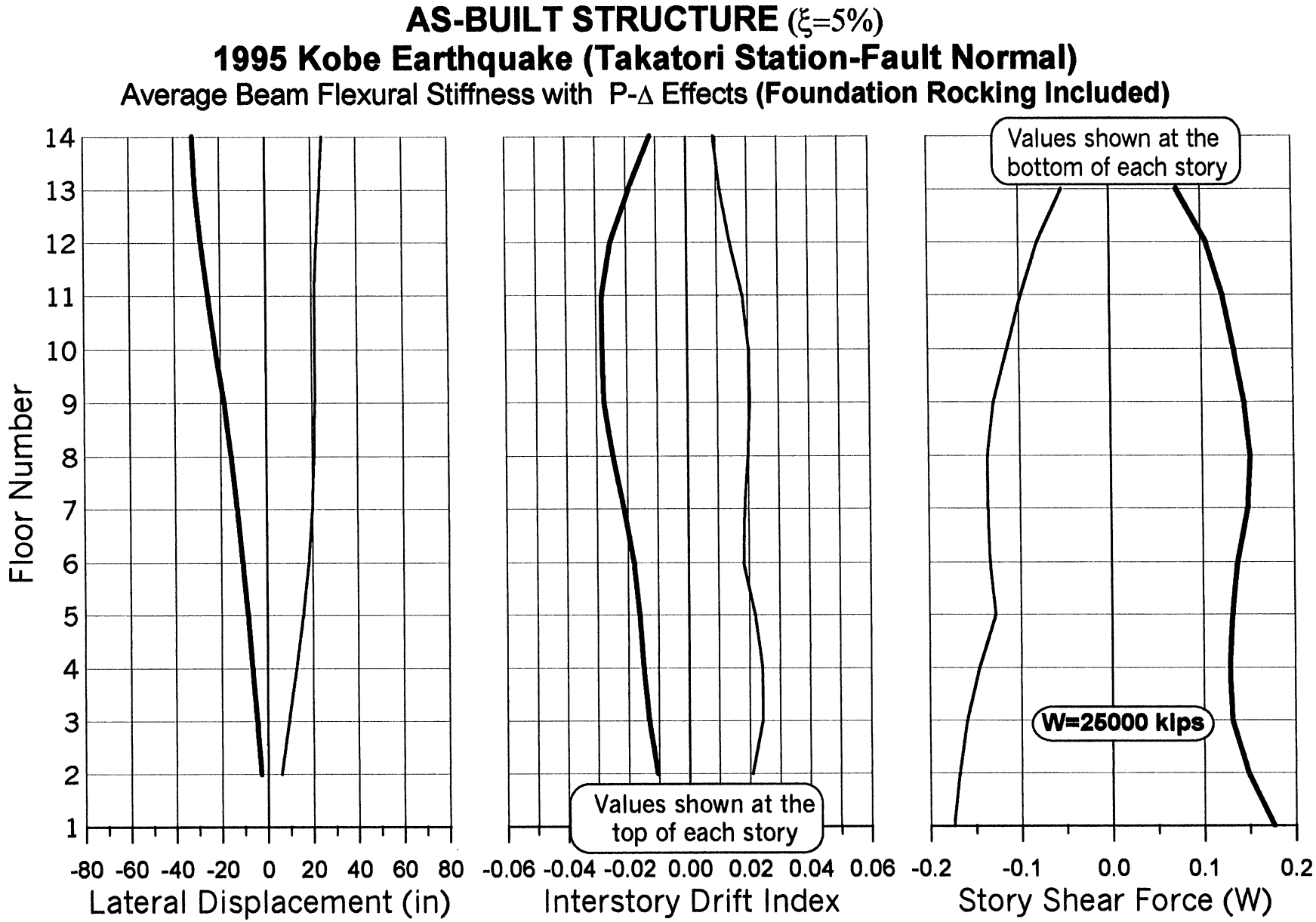

Figure 6.9 Lateral displacement, interstory drift index, and story shear force envelopes.

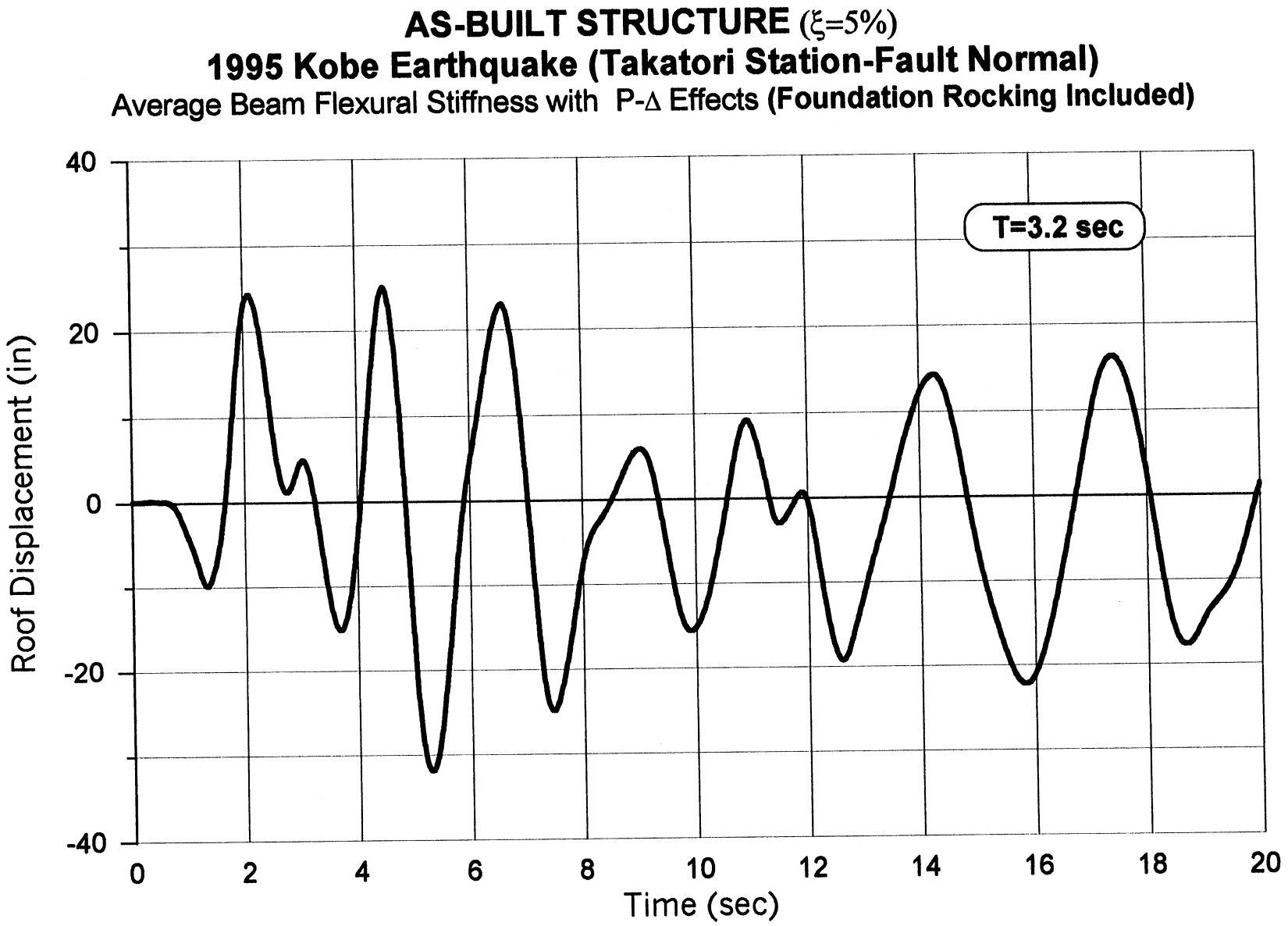

Figure 6.10 Time history of roof displacement.

7 Severe Pulse-Type EQGMs and Effect of Damping on Response of Structures

Since the response of the as-built structure to the severe pulse-type EQGMs is not satisfactory, the possibility of controlling the response of the structure by incorporating additional damping is studied. Although under random types of ground motions and particularly harmonic types, increasing damping can considerably reduce the response of the structure, this might not be the case under pulse-type EQGMs. In this section an attempt is made to study the efficiency of adding damping in controlling the response of structures under pulse-type ground motions. In addition to the two ground motions discussed in section 6-2, four idealized pulse-type ground motions for fault normal and fault parallel are also considered, Figure 7.1.

7.1 CHARACTERISTICS OF NEAR-FAULT RECORDS AND THEIR IDEALIZATION

Although pulse-type ground motions are not only limited to the vicinity of faults and have been observed at sites far from the seismic sources, to idealize these types of ground motions, only near-source records are considered. It is well established that mainly based on the directivity effect of the propagated seismic waves and the expected types on the ground displacement near to the causative faults, the ground velocity may consist of one or two strong pulses for recorded motions parallel and normal to the fault, respectively. Therefore, two idealized fault-normal ground motions and also fault-parallel ground motions are considered in Figure 7.1. Note that the idealized ground motions are such that in the case of fault-normal ground motions, the displacement at the end of motion is equal to zero, while for fault-parallel ground motions there

is a residual displacement at the end of the motion to model the relative movement of the ground on two sides of strike-slip faults.

Studying the wave propagation in shear type structures Iwan (1997) has shown that interstory drift, and as a result, lateral displacement of structures could be calculated using the ground velocity and displacement (the ground velocity has a more important effect, particularly when the damping coefficient is small). Therefore, in idealizing the near-fault records, especial care is given to reasonably modeling the recorded ground velocity and displacement.

Figure 7.1-a shows an idealized fault-normal ground motion with zero displacement at the end and two velocity pulses. The velocity pulses are such that the acceleration time history also starts and ends in zeros. In Figure 7.1-b, another idealized fault-normal ground motions is shown in which the ground velocity is modeled by a simple sine function and as a result, the ground acceleration is not zero neither at the beginning nor at the end. Obviously, it is assumed that for the corresponding real ground motions, there are some slow variations at the beginning and at the end from and to zero that do not have significant dynamic effects on the response of structures and therefore are not modeled. It should be noted that the nonzero accelerations at the beginning and the end correspond to the nonzero slope of the time history of the velocity at those points. Figures 7.1-c and 7.1-d show two idealized fault-parallel ground motions. The peak ground velocity (PGV) of fault-parallel ground motions is not expected to be as high as that of fault-normal ground motions. However, to be able to compare the response of SDOF systems to different types of idealized ground motions, in all the cases the PGV is equal to 1.73 m/s (68 in./s) which is equal to the PGV of the two recorded ground motions considered in this study.

7.2 RESPONSE TO IDEALIZED FAULT-NORMAL GROUND MOTIONS

The displacement response spectra of type a and b fault-normal idealized ground motions for damping coefficients equal to 0.05 and 0.30 and for displacement ductilities from 1.0 to 4.0 are shown in Figures 7.2 and 7.3, respectively. The ratios of the response spectra for the two different damping coefficients are also shown. Note that the horizontal axes are the structural period divided by t_d, where t_d is the total duration of the idealized pulse-type velocity, i.e., t_d=2 sec. It should also be noted that in calculating the response spectra, the free vibration after the ground motion ends is considered. As expected, structures with long period ($T/t_d > 0.75$) and particularly for larger ductilities, the idealized ground motion shown in Figure 7.1-b is somewhat

more demanding than that shown in Figures 7.1-a; however, the ratios of displacement response spectra for the two different damping coefficients in the two cases are fairly similar.

For displacement ductility between one to four and for T/t_d from 0.5 to about 1.2 ($1 < T < 2.4$ sec) increasing the damping coefficient from 0.05 to 0.30 reduces the response spectra by at least 40%. Beyond this range of period, the effect of higher damping is less significant. For instance, as shown in Figure 7.2, for $T/t_d < 0.5$ the effect of higher damping in reducing the response of structures decreases from 50% to zero as T/t_d goes to zero. Therefore, considering the response spectra, one can conclude that, in spite of the fact that the ground motions are of pulse types, depending on the ratio of the period of the structure and the duration of the idealized fault-normal ground motion, increasing the damping could be quite effective in controlling the response of structures.

The yield coefficient C_y (a pseudo-acceleration/g ratio which, if multiplied by the weight, gives the corresponding lateral strength) response spectra of type a and b fault-normal idealized ground motions for damping coefficients equal to 0.05 and 0.30 and for displacement ductilities from 1.0 to 4.0 are shown in Figures 7.4 and 7.5, respectively. Obviously, the ratios of these C_y response spectra for two different damping coefficients are the same as those of the S_d spectra of Figures 7.2 and 7.3, respectively. Note that the peak values of C_y occur at about T/t_d between 0.5 to 0.8, where 0.8 is for $\mu=1$ and $\xi=0.05$ in the case of type b ground motion.

Comparing Figures 7.2 with 7.3 and 7.4 with 7.5, for $T/t_d < 0.25$ and $T/t_d > 0.75$, the response spectra of type b is larger than those of type a, while for $0.25 < T/t_d < 0.75$ it is the other way around. However, apart from the drop in the response spectra at larger values of T/t_d for $\mu=2$, 3, and 4 which is obvious in Figures 7.2 and 7.3 and which will be discussed in section 7-4, for $T/t_d > 0.25$, the response spectra of the two idealized ground motions are not much different, in spite of the considerable difference in the shape of acceleration ground motion. ***This last observation*** will be discussed further in section 7-3. In other words, the sudden initial acceleration at the beginning of type b idealized ground motion only affects very short-period structures differently from the way type a does.

For the as-built structure with a period of about 3.2 sec, the roof displacement under the Los Gatos ground motion is about 69 in ($\mu=3.7$). The strong ground velocity pulse of the Los Gatos ground motion has a fault-normal pulse-type ground velocity that lasts about 2.7 sec, Figure 6.3. Assuming that the response of SDOF systems to the idealized fault-normal ground motions could predict the behavior of the MDOF structure under the Los Gatos ground motion,

for T=3.2 sec (T/t_d=3.2/2.7=1.2) and μ=3.7, Figure 7.2 shows that increasing damping from 0.05 to 0.30 could reduce the lateral displacement by about 40 to 50%. In using the SDOFS response spectra, it should be noted that by increasing damping, the displacement ductility reduces by the same factor that the lateral displacement drops. For example, assuming that the 69-in. roof displacement reduces by about 45% when the damping coefficient is increased to 0.30, the ductility will also be reduced to about 3.7x0.55=2.0. It should also be noted that it is assumed that the effective damping coefficient of the whole soil-structure model is increased from 0.05 to 0.30.

The roof displacement under the Takatori ground motion is about 32 in (μ=1.7). The strong ground velocity pulse of the recorded motion has a fault-normal pulse-type ground velocity that lasts about 1.7 sec, Figure 6.5. At T=3.2 sec (T/t_d=3.2/1.7=1.9) and μ=1.7, increasing damping from 0.05 to 0.30 could reduce the lateral displacement by about 20 to 25%, Figure 7.2. In other words, comparing the Los Gatos and Takatori ground motions, for a structure with a period of about 3.2 sec, since the T/t_d for the Takatori ground motion (=1.9) is significantly larger than the value equal to 1.2 for the Los Gatos ground motion, it is expected that increasing damping will be less effective for the Takatori ground motion.

7.3 EFFECT OF DURATION OF IDEALIZED GROUND MOTIONS ON RESPONSE OF STRUCTURES

When considering the idealized ground motion shown in Figure 7.1, one question that arises is how the response of structures would change if the duration of the idealized ground motion is changed. To answer this question two different approaches are used below.

7.3.1 Linear Wave Propagation in Uniform Shear Beam Element

Iwan (1997) has studied the linear wave propagation in uniform shear beam elements. The following equation (which differs somewhat from the one given in the above reference) gives the derivative of the lateral displacement with respect to the height (drift) as a function of ground velocity, $\dot{u}_g$, ground displacement, u_g, and damping coefficient, ξ, at a height of h=βH and at time t.

$$\frac{\partial u}{\partial y}(h,t)=\frac{T}{4H}\left\{e^{-\pi\beta\xi/2}\left[\dot{u}_g(t-\beta T/4)+\frac{2\pi\xi}{T}u_g(t-\beta T/4)\right]\right\}$$
$$+\sum_{n=1}^{N\le 2tT-\beta/2}(-1)^n e^{-(n+\beta/2)\pi\xi}\left[\dot{u}_g(t-nT/2-\beta T/4)+\frac{2\pi\xi}{T}u_g(t-nT/2-\beta T/4)\right] \quad (7\text{-}1)$$
$$\left\{+\sum_{n=1}^{N\le 2tT+\beta/2}(-1)^n e^{-(n-\beta/2)\pi\xi}\left[\dot{u}_g(t-nT/2+\beta T/4)+\frac{2\pi\xi}{T}u_g(t-nT/2+\beta T/4)\right]\right\}$$

Now assume that the amplitude and the duration of the ground velocity are scaled by $1/\gamma$ and γ, respectively, which means that $(t_d)_{new}=\gamma t_d$, and $(\dot{u}_g(\gamma t))_{new}=\dot{u}_g(t)/\gamma$ and as a result $\dot{u}_g(t)t_d=(\dot{u}_g(\gamma t))_{new}(\gamma t_d)$. In this case only the duration of the ground displacement is changed and its amplitude remains the same, i.e. $(u_g(\gamma t))_{new}=u_g(t)$. Although the ground acceleration is not used in the above equation, it could be worth mentioning that $(\ddot{u}_g(\gamma t))_{new}=\ddot{u}_g(t)/\gamma^2$. To find the drift under this new ground motion, for a structure with a period equal to γ T (note that T/t_d is unchanged) one can multiply and divide the right-hand side of Equation 7-1 by γ as shown below.

$$\frac{\partial u}{\partial y}(h,t)=\frac{\gamma T}{4H}\left\{e^{-\pi\beta\xi/2}\left[\dot{u}_g(t-\beta T/4)/\gamma+\frac{2\pi\xi}{\gamma T}u_g(t-\beta T/4)\right]\right\}$$
$$+\sum_{n=1}^{N\le 2tT-\beta/2}(-1)^n e^{-(n+\beta/2)\pi\xi}\left[\dot{u}_g(t-nT/2-\beta T/4)/\gamma+\frac{2\pi\xi}{\gamma T}u_g(t-nT/2-\beta T/4)\right] \quad (7\text{-}2)$$
$$\left\{+\sum_{n=1}^{N\le 2tT+\beta/2}(-1)^n e^{-(n-\beta/2)\pi\xi}\left[\dot{u}_g(t-nT/2+\beta T/4)/\gamma+\frac{2\pi\xi}{\gamma T}u_g(t-nT/2+\beta T/4)\right]\right\}$$

Knowing the relation between the original and new ground velocity and displacement, the right-hand side of this equation (7-2) is nothing but the drift of a structure with a period equal to γT at time of γt, under new ground motion. In other words, the drift and as a result the displacement of a structure with a period of T at time t under the original ground motion is the same as those for a structure with a period of γT at time γt under the new ground motion. Therefore, since T/t_d is unchanged, as far as $\dot{u}_g(t)t_d=(\dot{u}_g(\gamma t))_{new}(\gamma t_d)$, the spectral displacement as a function of T/t_d is the same for different ground motions. The above discussion

and results given in Figures 7.2 to 7.5 justify the observation made in section 7-2 when the results given in these figures were compared.

7.3.2 Nonlinear Dynamic Analysis of SDOF Systems

Assuming linear variation of acceleration over each time step of solving the differential equation of motion, the incremental equation of motion for a SDOF system can be written as below:

$$\left[\frac{k(t)}{m}+\frac{6}{\Delta t^2}+\frac{3\ c(t)}{\Delta t\ m}\right]\Delta u=-\Delta\ddot{u}_g(t)+\left[\frac{6}{\Delta t}\dot{u}(t)+3\ddot{u}(t)\right]+\frac{c(t)}{m}\left[3\dot{u}(t)+\frac{\Delta t}{2}\ddot{u}(t)\right] \qquad (7\text{-}3)$$

where k(t), c(t), and m are the stiffness, damping, and mass of the SDOF system, respectively. u_g and u are the ground displacement and relative structural displacement, respectively. Dividing both sides of the above equation by γ^2 results in the following equation,

$$\left[\frac{k(t)}{\gamma^2 m}+\frac{6}{\gamma^2\Delta t^2}+\frac{3\ c(t)}{\gamma\Delta t\ \gamma m}\right]\Delta u=-\frac{\Delta\ddot{u}_g(t)}{\gamma^2}+\left[\frac{6}{\gamma\Delta t}\frac{\dot{u}(t)}{\gamma}+\frac{3\ddot{u}(t)}{\gamma^2}\right]+\frac{c(t)}{\gamma m}\left[\frac{3\dot{u}(t)}{\gamma}+\frac{\gamma\Delta t\,\ddot{u}(t)}{2\ \gamma^2}\right] \qquad (7\text{-}4)$$

Based on the fact that for linear structures, $c=2m\omega\xi$, one can conclude that $c(t)=2m\sqrt{\frac{k(t)}{m}}\,\xi$. Therefore, Equation 7-4 could be considered as the incremental equation of motion for a structure with $\left(\sqrt{\frac{k(t)}{m}}\right)_{new}=\frac{1}{\gamma}\sqrt{\frac{k(t)}{m}}$ (in a more specific case this could be interpreted as ($T_{new}=\gamma T$) under $\left(\ddot{u}_g(\gamma t)\right)_{new}=\ddot{u}_g(t)/\gamma^2$, solved at time steps equal to $\gamma\,\Delta t$. The response in this case will be such that $\left(u(\gamma t)\right)_{new}=u(t)$, $\left(\dot{u}(\gamma t)\right)_{new}=\dot{u}(t)/\gamma$, and $\left(\ddot{u}(\gamma t)\right)_{new}=\ddot{u}(t)/\gamma^2$. In other words, if the ground acceleration is scaled such that $\left(\ddot{u}_g(\gamma t)\right)_{new}=\ddot{u}_g(t)/\gamma^2$, the displacement spectra versus T/t_d is unchanged. Obviously, acceleration spectra versus T/td is scaled by $1/\gamma^2$.

7.3.3 Normalized Response Spectra of Idealized Ground Motions

Based on the above discussion, the normalized displacement and yield coefficient spectra for pulse-type a (shown in Figure 7.1) are given in Figures 7.6 and 7.7.

7.4 RESPONSE SPECTRA AS FUNCTION OF CYCLIC DUCTILITY

In all the cases discussed so far, the monotonic ductilities, which is defined as $\mu = |\Delta|_{max} / \Delta_y$, are used to calculate the constant monotonic ductility spectra. As discussed above, there are some drops in the response spectra of larger period structures, Figures 7.2, 7.3, and 7.6. This mainly occurs because (1) there are only two velocity pulses; and (2) depending on the values of the peak displacements in two directions of motion, for large period structures, there might be yielding in one or both directions. By increasing the period of structures, when yielding starts to occur in two directions, for a particular target ductility, the absolute maximum displacement (and yield coefficient) start to drop. To remove this misleading change in the response spectra, using cyclic ductility defined as $\mu_{cyc} = |\Delta_{cyc}|_{max} / \Delta_y$ where $|\Delta_{cyc}|_{max}$ is the maximum displacement measured from previous zero force crossing, the response spectra are calculated for constant cyclic ductility. Figures 7.8 and 7.9 show the constant cyclic ductility response spectra for type a idealized ground motion, as shown in Figure 7.1-a. As can be seen, the response spectra do not have such a drop in their values. Although the constant monotonic ductility response spectra are used throughout this report, depending on the way the displacement capacity is defined, one needs to bare in mind that the maximum displacement demand may need to be modified, based on what was just discussed.

7.5 RESPONSE TO LOS GATOS AND TAKATORI GROUND MOTIONS

The displacement response spectra of the Los Gatos ground motion are shown in Figure 7.10. To be able to compare the responses to the Los Gatos ground motion with those of idealized motions, in Figure 7.11, the displacement response spectra is also shown against T/t_d, where t_d is assumed to be 2.7 sec (see Figure 6.3). Comparing Figures 7.2 and 7.3 with Figure 7.11, the ratios of the responses with 30% and 5% damping in two cases have almost the same shape. To compare the displacement response spectra, since both the idealized ground motion and the Los Gatos ground motion have the same peak ground velocities, PGV, while the duration of the main

pulses of the Los Gatos ground motion is 2.7/2 times larger than the duration of idealized fault-normal ground motion, the displacement response spectra of the idealized ground motion needs to be multiplied by 2.7/2 to be compared with those of the Los Gatos ground motion. Figure 7.12 shows the scaled displacement response spectra of the idealized fault-normal ground motion type (b) to be compared with the Los Gatos displacement spectra shown in Figure 7.11. As can be seen, for T/t_d less than about 0.4 (T less than about 1.0 sec) the response to the Los Gatos ground motion is larger than that of the idealized fault-normal ground motion type (b) which could be explained by higher frequency motions that exist in the Los Gatos ground motion in addition to its main pulses (see Figure 6.3).

The yield coefficient, C_y, response spectra for damping coefficients equal to 0.05 and 0.30 and for displacement ductilities from 1.0 to 4.0 are shown in Figures 7.13 and 7.14. To compare the yield coefficient response spectra, since both the idealized ground motion and the Los Gatos ground motion have the same pick ground velocities, PGV, the yield coefficient response spectra of the idealized ground motion needs to be multiplied by 2.0/2.7 to be compared with those of Los Gatos ground motion. Figure 7.15 shows the scaled yield coefficient response spectra of the idealized fault-normal ground motion to be compared with the Los Gatos yield coefficient spectra shown in Figure 7.14. As discussed before, for T/t_d less than about 0.4 (T less than about 1.0 sec) the response to the Los Gatos ground motion is larger than that of the idealized fault-normal ground motion, which could be explained by higher frequency motions existing in the Los Gatos ground motion in addition to its main pulses (see Figure 6.3). Unlike the Los Gatos ground motion, the two velocity pulses of the idealized ground motion have the same peak value. Therefore, for longer period structures, generally speaking, the response spectra of the idealized ground motion is larger than those of the Los Gatos ground motion.

The displacement response spectra of the Takatori ground motion are shown in Figure 7.16 and 7.17. Note that in Figure 7.17, t_d=1.7 sec. Comparing Figures 7-2 and 7-3 with Figure 7.17, the ratios of the responses with 30% and 5% damping in two cases have almost the same form. To compare the displacement response spectra, since both the idealized ground motion and the Takatori ground motion have the same peak ground velocities, PGV, while the duration of the main pulses of the Takatori ground motion is 1.7/2 times shorter than the duration of idealized fault-normal ground motion, the displacement response spectra of the idealized ground motion needs to be multiplied by 1.7/2 to be compared with those of the Takatori ground motion. Figure 7.18 shows the scaled displacement response spectra of the idealized fault-normal ground

motion to be compared with the Takatori displacement spectra shown in Figure 7.17. As can be seen, for T/t_d less than about 1.2 the response spectra for the idealized and recorded ground motion follow almost the same pattern.

The yield coefficient, C_y, response spectra for damping coefficients equal to 0.05 and 0.30 and for displacement ductilities from 1.0 to 4.0 are shown in Figures 7.19 and 7.20. To compare the yield coefficient response spectra, the yield coefficient response spectra of the idealized ground motion needs to be multiplied by 2/1.7 to be compared with those of the Takatori ground motion. Figure 7.21 shows the scaled yielding coefficient response spectra of the idealized fault-normal ground motion.

7.6 RESPONSE TO IDEALIZED FAULT-PARALLEL GROUND MOTIONS

To study the effects of damping under fault-parallel types of ground motions, two types of idealized ground motions, shown in Figures 7.1-c and 7.1-d are studied. The displacement response spectra of type c and d fault-parallel idealized ground motions for damping coefficients equal to 0.05 and 0.30 and for displacement ductilities from 1.0 to 4.0 are shown in Figures 7.22 and 7.23, respectively. The ratios of the response spectra for two different damping coefficients are also shown. Note that the horizontal axes are the structural period divided by twice the duration t_d of the single velocity pulse ($T/2t_d$). As expected, the idealized ground motion shown in Figure 7.1-d is somewhat more demanding than that shown in Figures 7.1-c; however, the ratios of displacement response spectra in two cases are fairly similar. As expected, for fault-parallel ground motions with only one velocity pulse, increasing damping is not as effective as for fault-normal ground motions. Figures 7.24 and 7.25 show the normalized displacement response spectra.

The yield coefficient response spectra of type c and d fault-parallel idealized ground motions for damping coefficients equal to 0.05 and 0.30 and for displacement ductilities from 1.0 to 4.0 are shown in Figures 7.26 and 7.27, respectively. Obviously, the ratios of the response spectra for two different damping coefficients are the same as those for displacement spectra. Note that the peak values of C_y occur at about $T/2t_d$ between 0.3 to 0.4, which corresponds to structures with periods less than the duration of the severe pulse. Figures 7.28 and 7.29 show the normalized yield coefficient response spectra.

Comparing Figures 7.6 and 7.7 with 7.24 and 7.25, respectively, the response spectra of the idealized fault-normal ground motions with $T/t_d > 0.5$ are larger than those of fault-parallel

ground motions with $T/2t_d > 0.5$. In fact for T/t_d greater than 0.75~1.0, the response spectra of fault-normal ground motion are more than twice those of fault-parallel ground motion with $T/2t_d$ greater than 0.75~1.0. Comparing Figures 7.8 and 7.9 with 7.26 and 7.27, respectively, for $0.25 < T/t_d < 0.5$ and for $\mu < 3$; however, the response spectra of fault-parallel ground motion are larger than those of the fault-normal ground motions.

7.7 CONCLUDING REMARKS

Studying the response spectra of idealized and recorded severe fault-normal pulse-type ground motions, it is shown that if the period of a structure is not far from the duration of the severe pulses (say $0.5 < T/t_d < 1.2$), increasing damping could considerably reduce the response of the structure. For shorter period structures, this effect diminishes as the period of the structures becomes smaller, and for longer period structures the effect of higher damping on controlling the response of structures reduces as well. This period-dependence effect of higher damping on reducing the response of structures could be used as a guide to select more critical pulse-type and perhaps random types of ground motions for structures retrofitted with added damping. This could be done mainly by checking the response of a structure under pulse-type ground motions with t_d away from the period of structure.

As expected, for idealized fault-parallel ground motions with only one velocity pulse, the efficiency of added damping in controlling the response of structures decreases; however, generally speaking, such ground motions are less damaging than fault-normal ground motions.

The normalized response spectra defined in this chapter could be used as a guide to select more damaging pulse-type, and perhaps random type, ground motions, for a particular structure. The ground motions having more number of pulses with larger PGV $\times$ t_d and T/t_d result in larger displacement demand on structures. Note that for T/t_d larger than about one, there is not much increase in displacement demand. As far as the base shear is concerned, ground motions having more number of pulses with larger PGV/t_d and T/t_d closer to ½ to ¾ are more damaging.

The idealized response spectra could be used to find the most critical ground motion for a structure under study. Generally speaking, the larger the PGV and t_d, the larger the lateral displacement. However, care should be given to the value of T/t_d, and the fact that not always a larger value of t_d would result in a larger lateral displacement. As far as the base shear is concerned, from the ordinate of the yield coefficient spectra, the larger the PGV and the smaller

the t_d, the larger the base shear. As mentioned for the displacement spectra, in this case the value of T/t_d also needs to be considered for choosing the critical ground motion.

Structures with a displacement ductility up to 3 and a normalized period, T/t_d, less than about ¾, will require a C_y of at least equal to the peak ground acceleration divided by g. This value that could be quite significant, indicates that, unlike what is suggested by the requirements of the UBC-97, as far as pulse-type ground motions are concerned, short-period structures may be more critical structures than long-period structures.

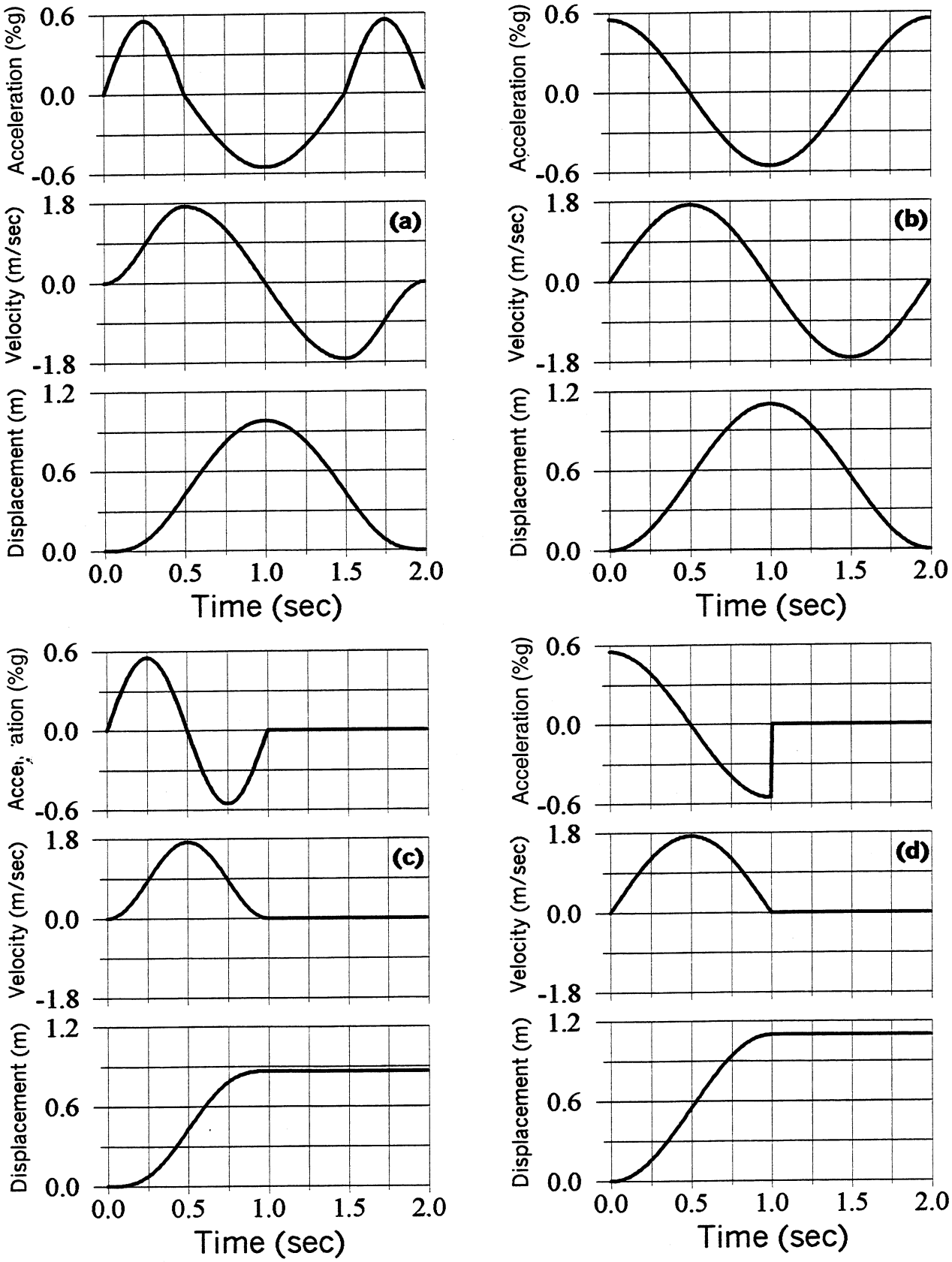

Figure 7.1 Idealized pulse-type EQGMs; (a) and (b) fault normal and (c) and (d) fault parallel.

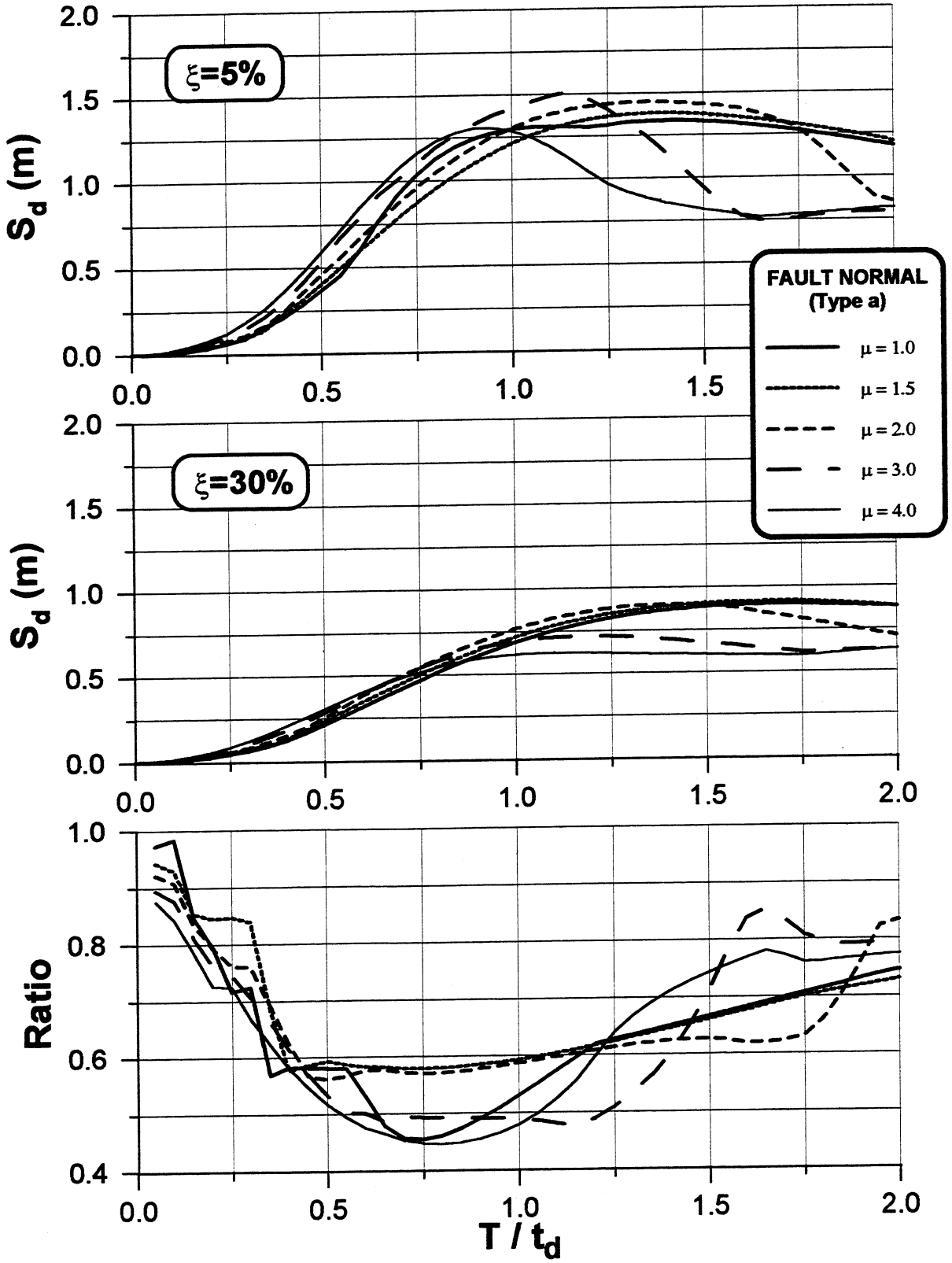

Figure 7.2 Displacement response spectra for idealized fault normal EQGM (type a).

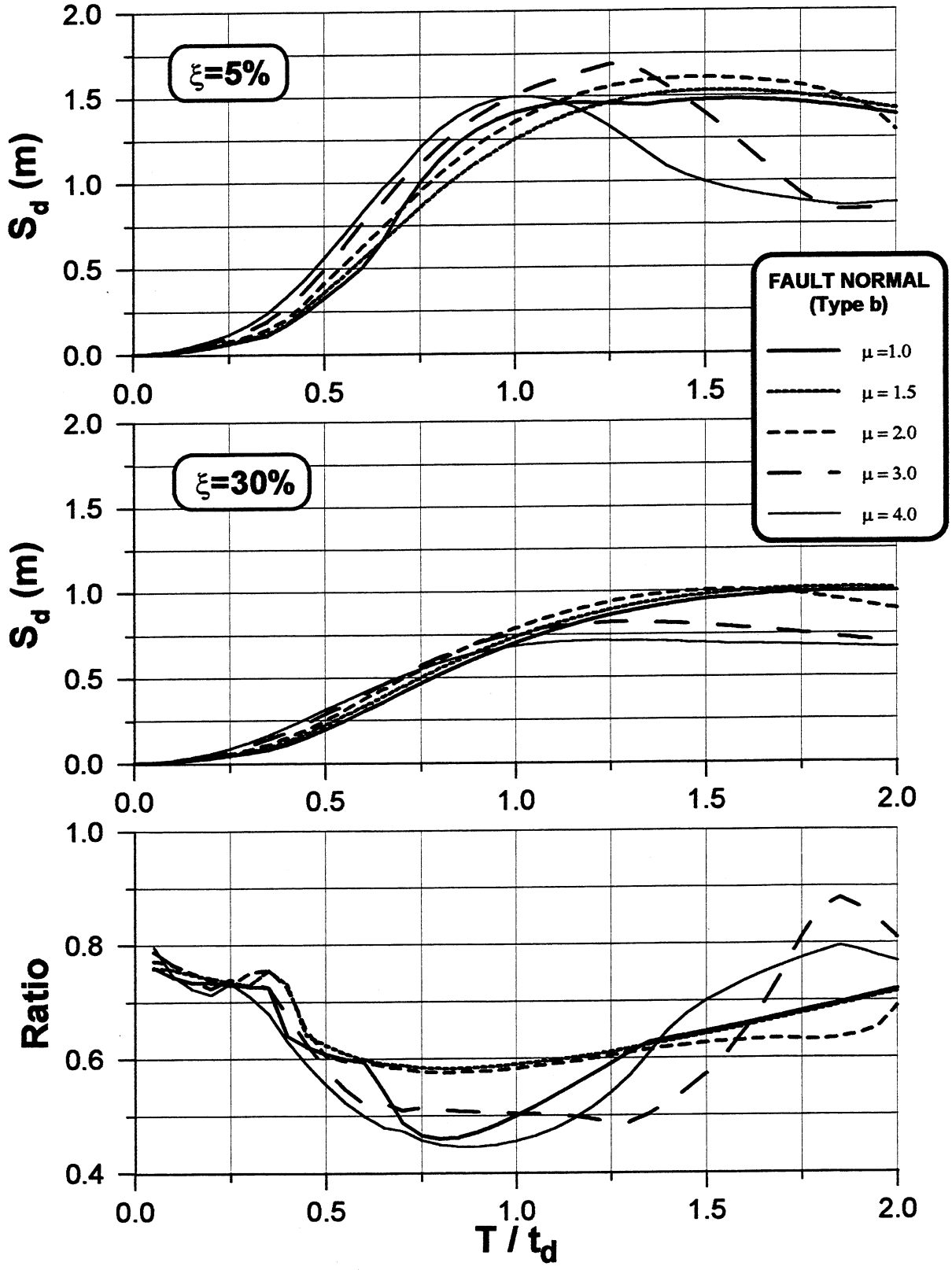

Figure 7.3 Displacement response spectra for idealized fault normal EQGM (type b).

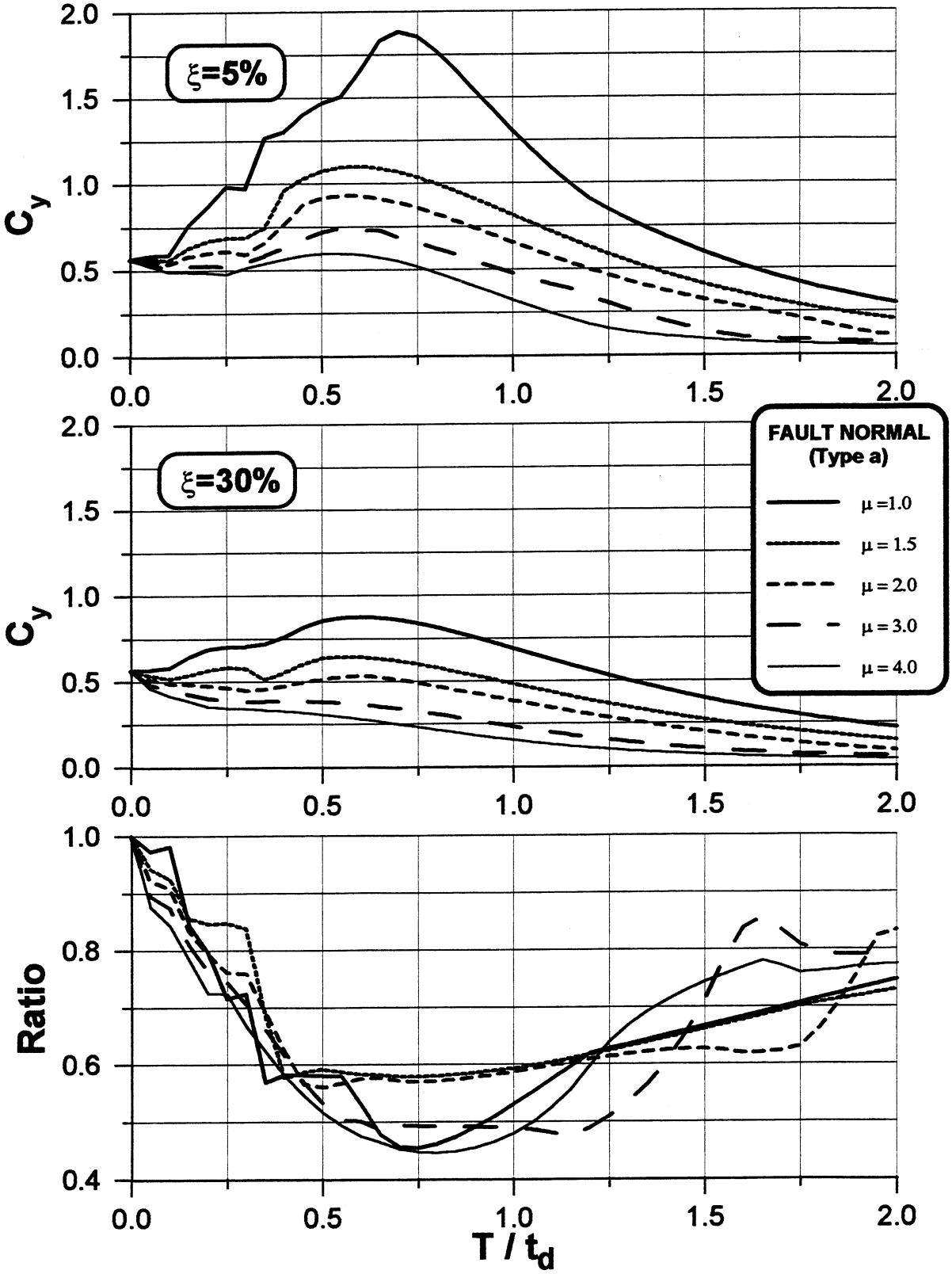

Figure 7.4 Yield coefficient response spectra for idealized fault normal EQGM (type a).

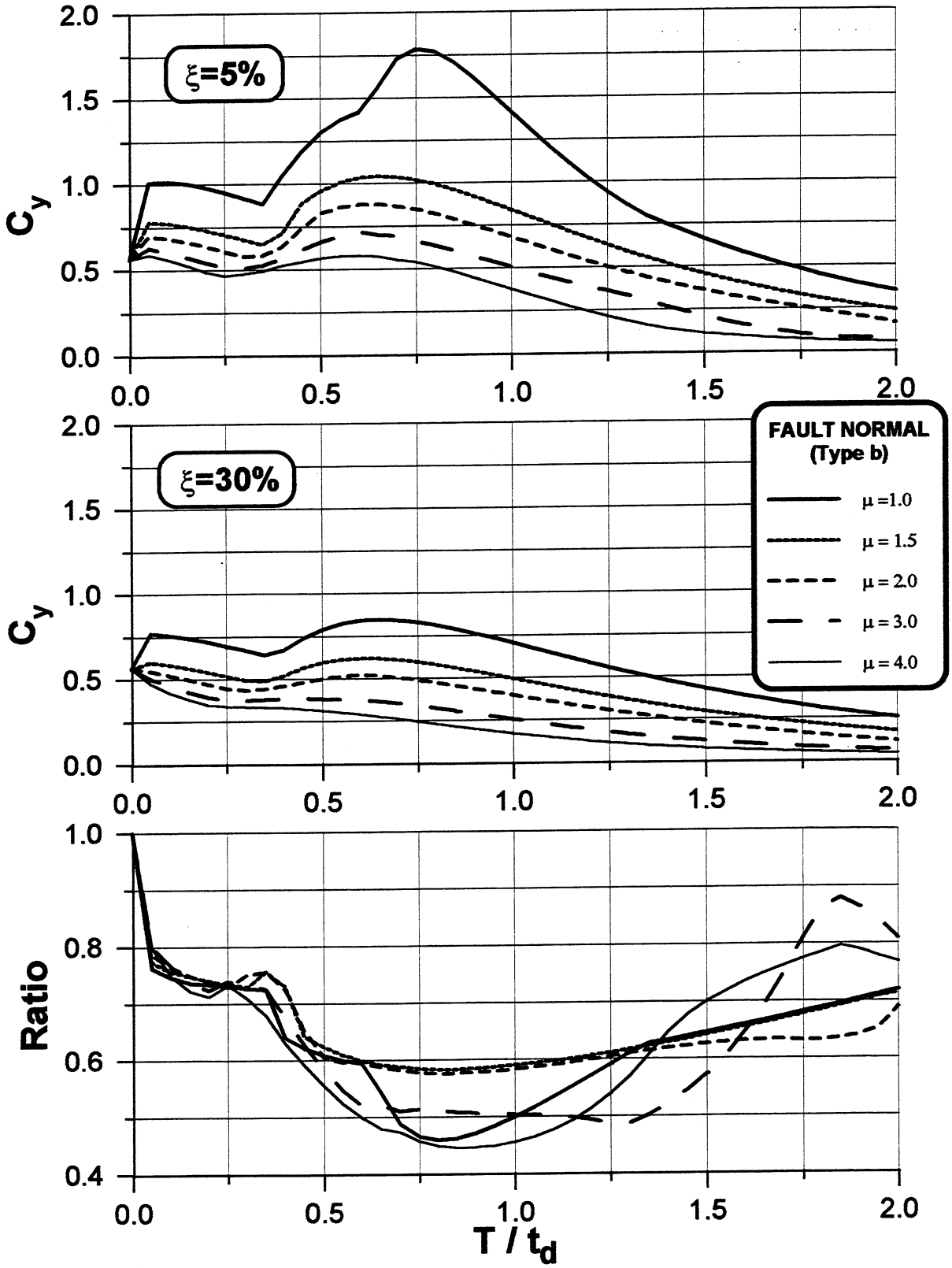

Figure 7.5 Yield coefficient response spectra for idealized fault normal EQGM (type b).

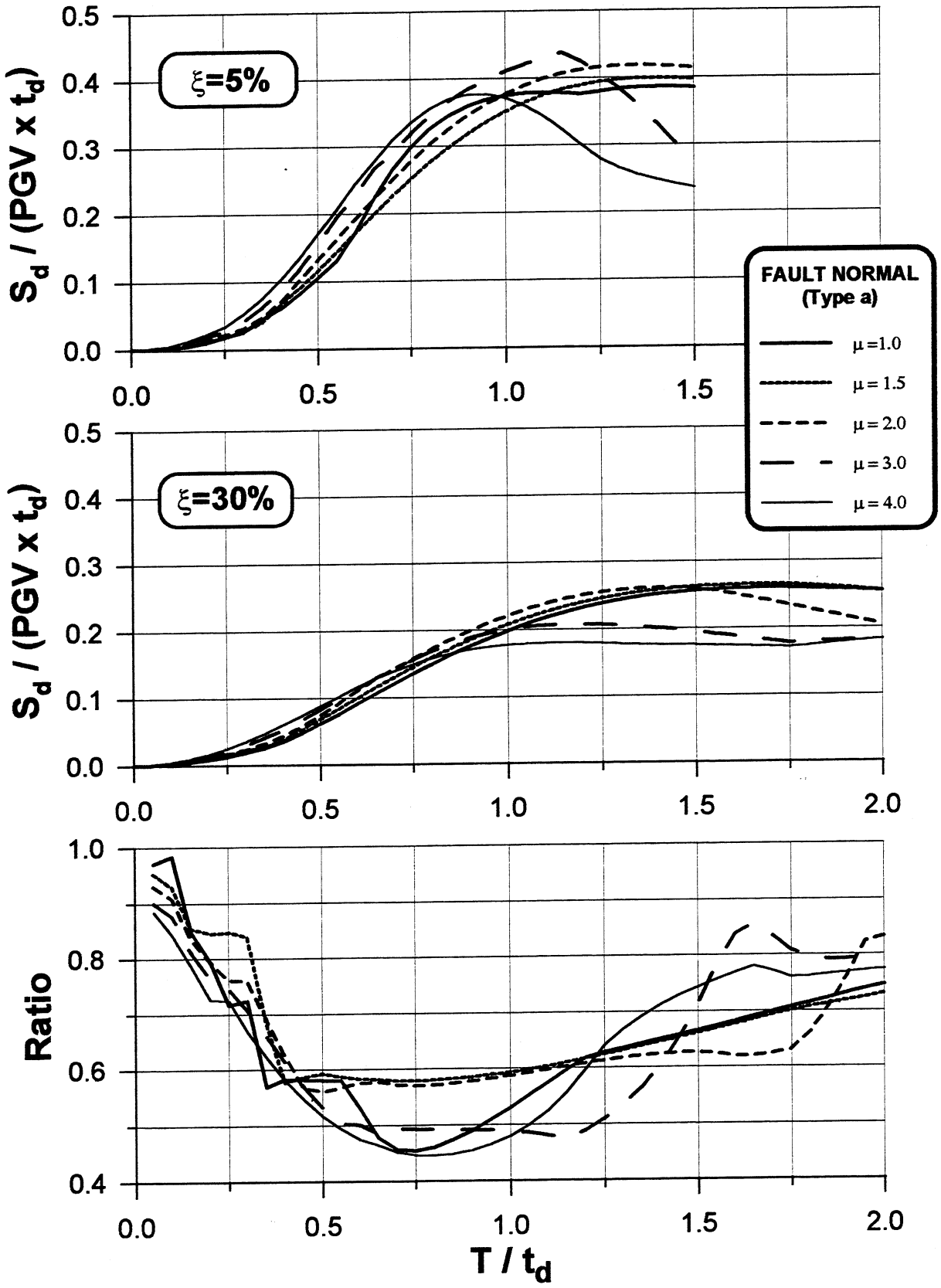

Figure 7.6 Normalized displacement response spectra for idealized fault normal EQGM (type a).

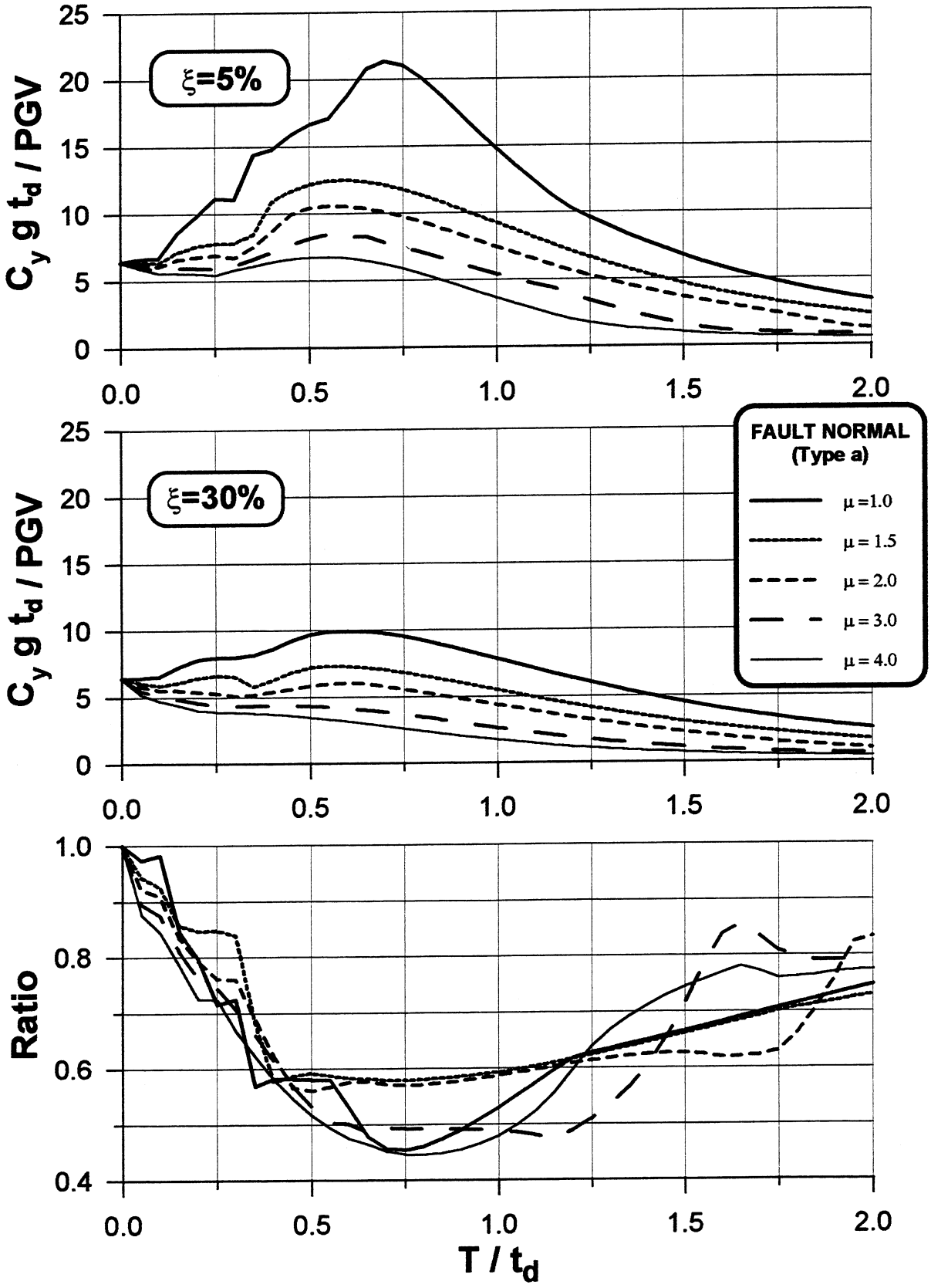

Figure 7.7 Normalized yield coefficient response spectra for idealized fault normal EQGM (type a).

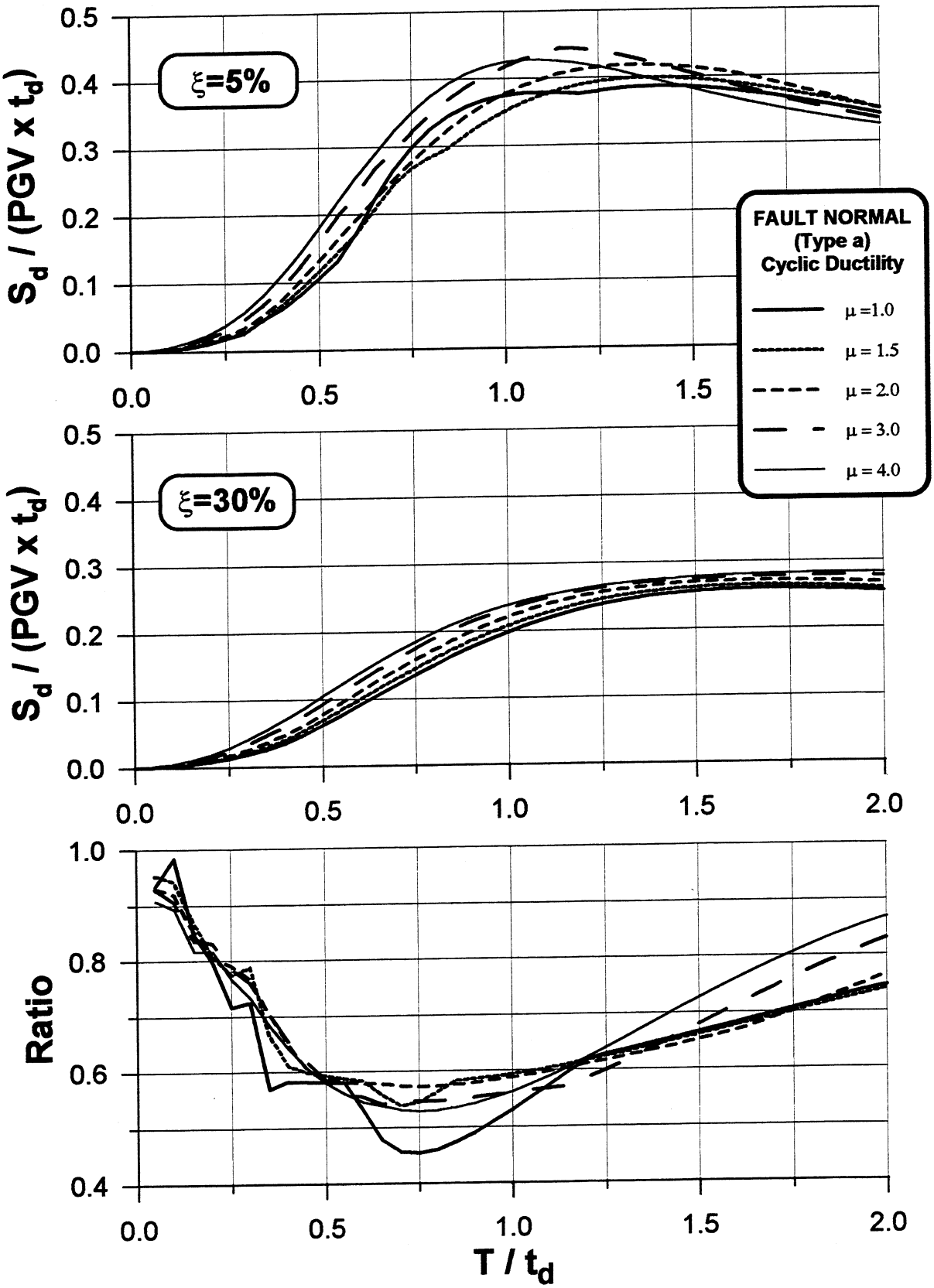

Figure 7.8 Normalized displacement response spectra for idealized fault normal EQGM using cyclic ductility (type a).

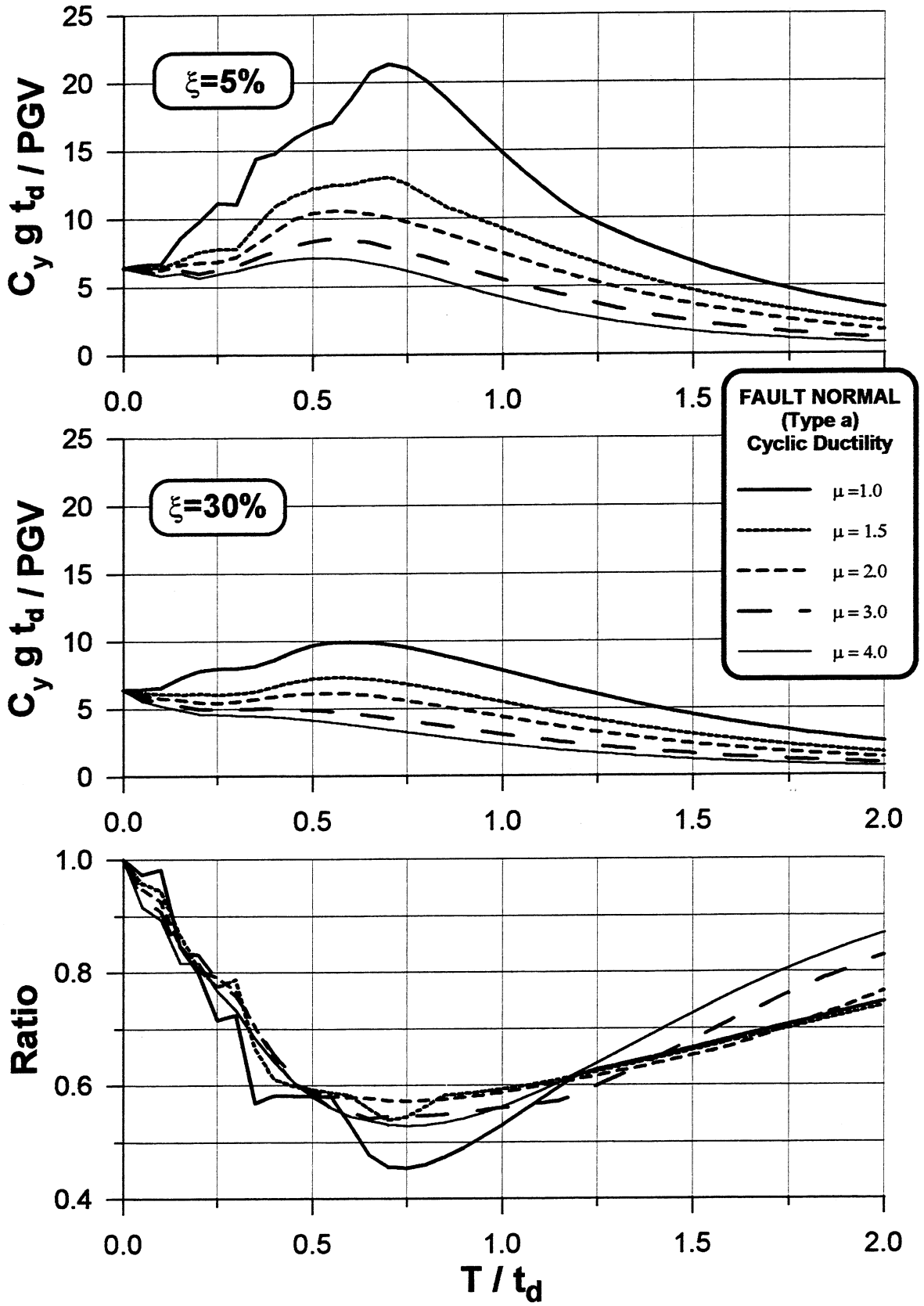

Figure 7.9 Normalized yield coefficient response spectra for idealized fault normal EQGM using cyclic ductility (type a).

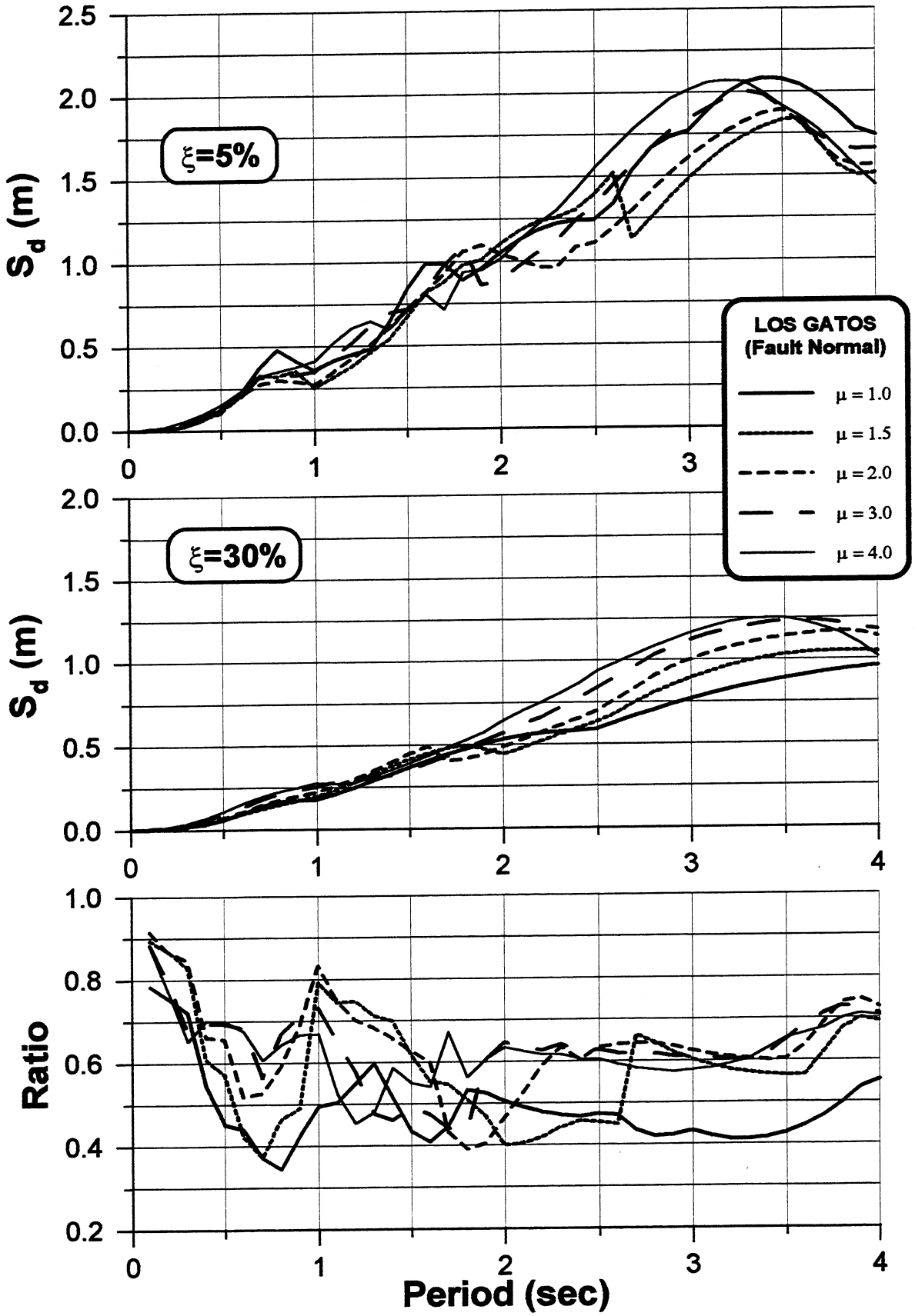

Figure 7.10 Displacement response spectra for fault-normal Los Gatos EQGM recorded during 1989 Loma Prieta earthquake.

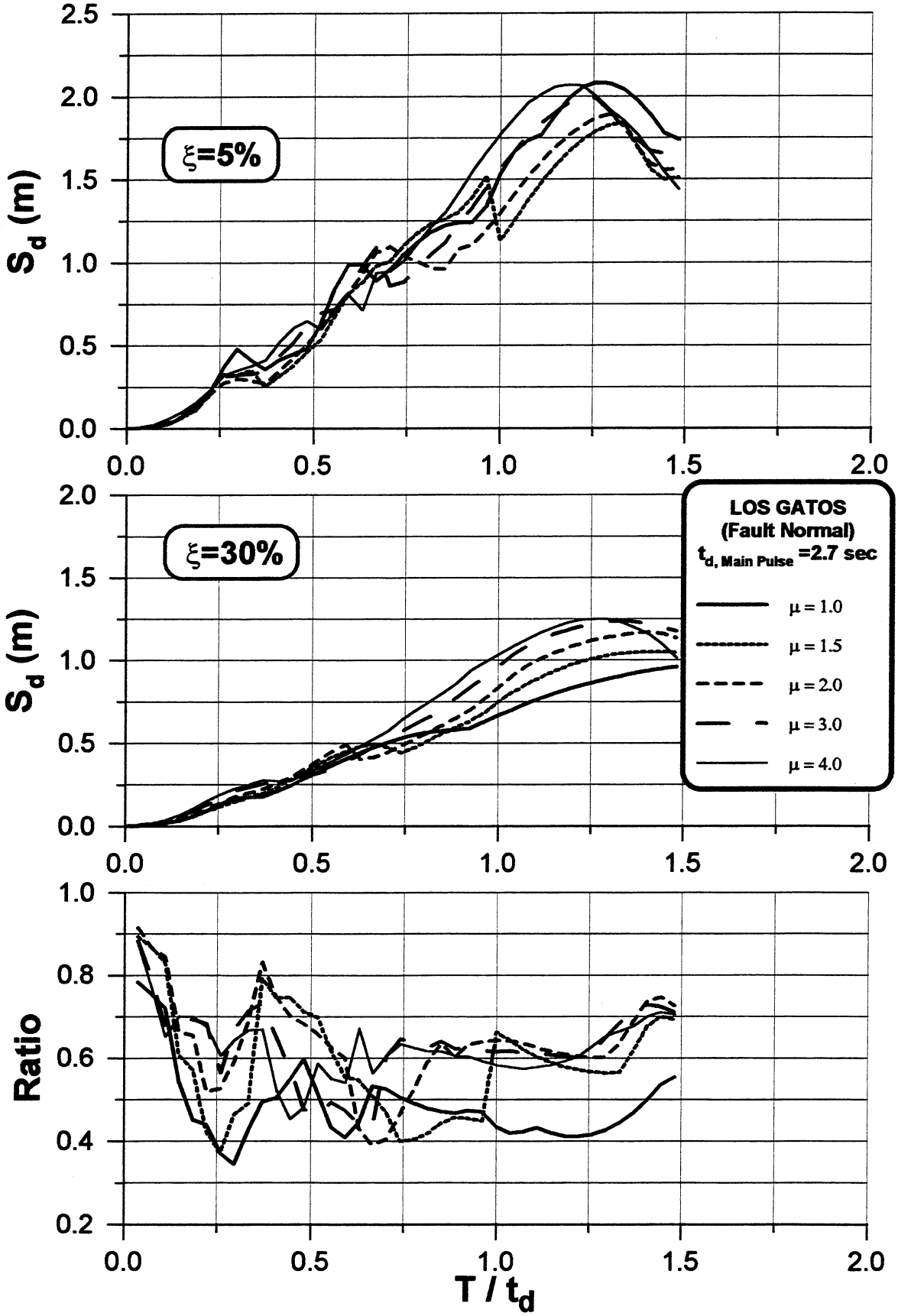

Figure 7.11 Displacement response spectra for fault-normal Los Gatos EQGM recorded during 1989 Loma Prieta earthquake.

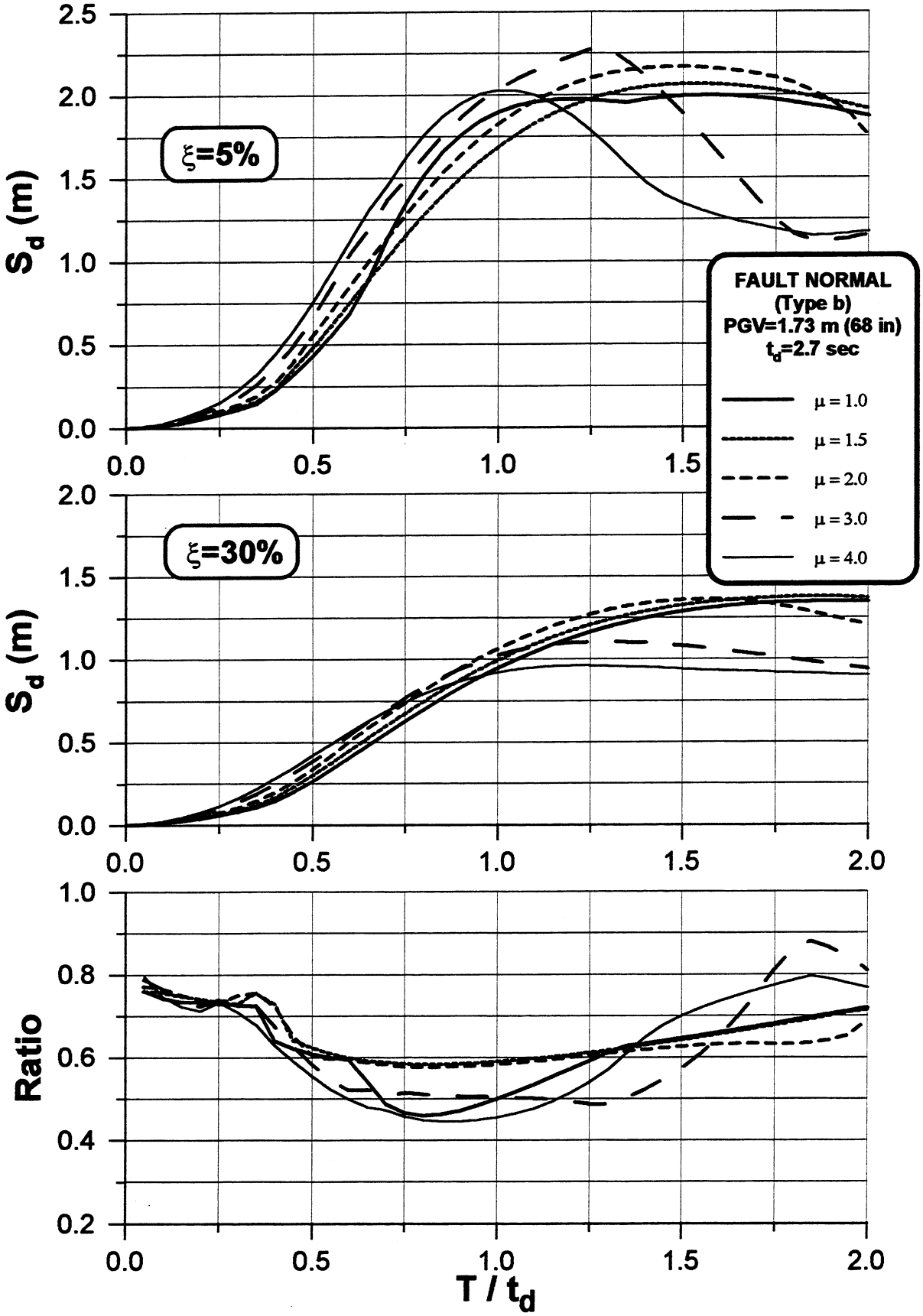

Figure 7.12 Displacement response spectra for idealized fault normal EQGM (type b).

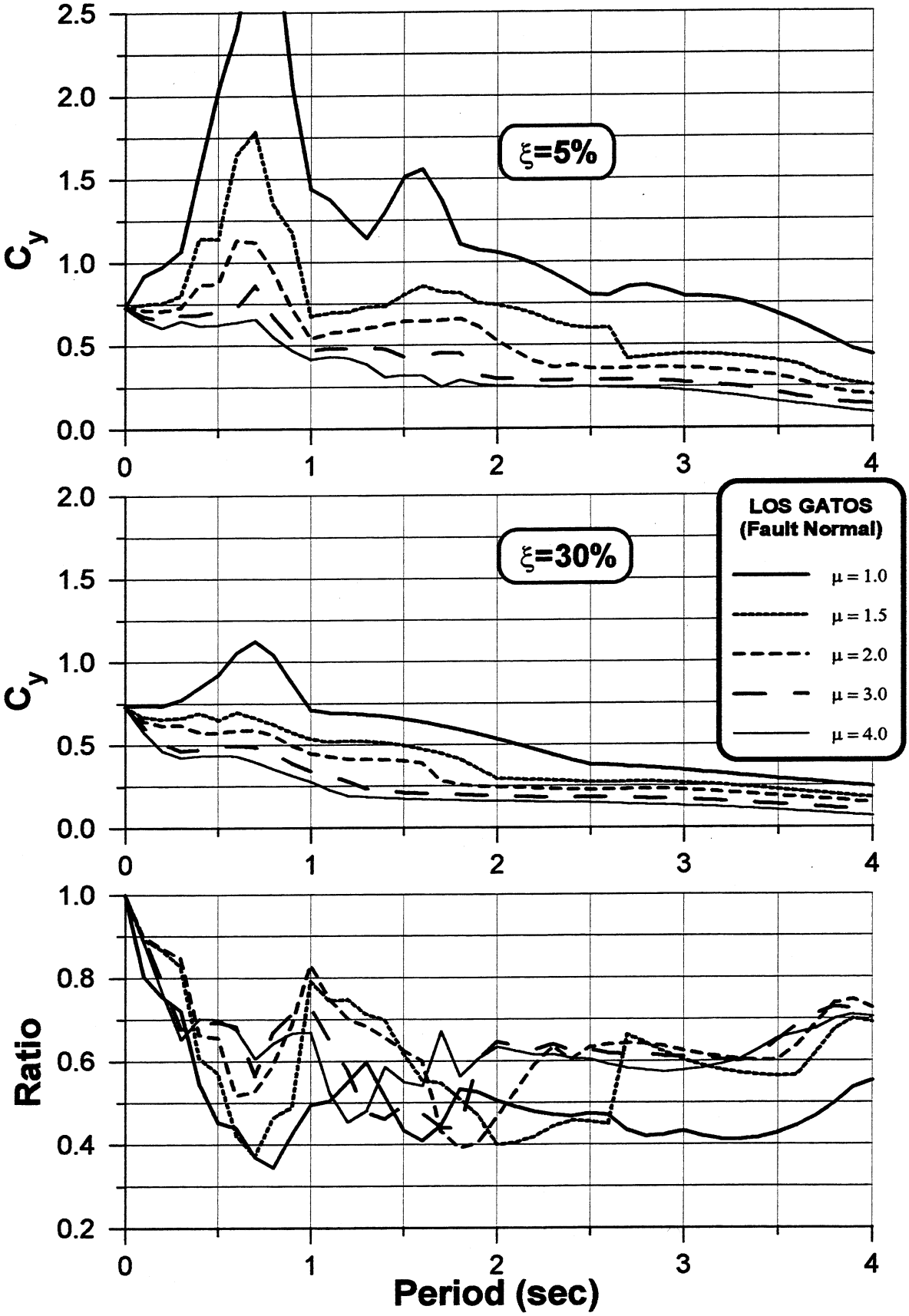

Figure 7.13 Yield coefficient response spectra for fault-normal Los Gatos EQGM recorded during 1989 Loma Prieta earthquake.

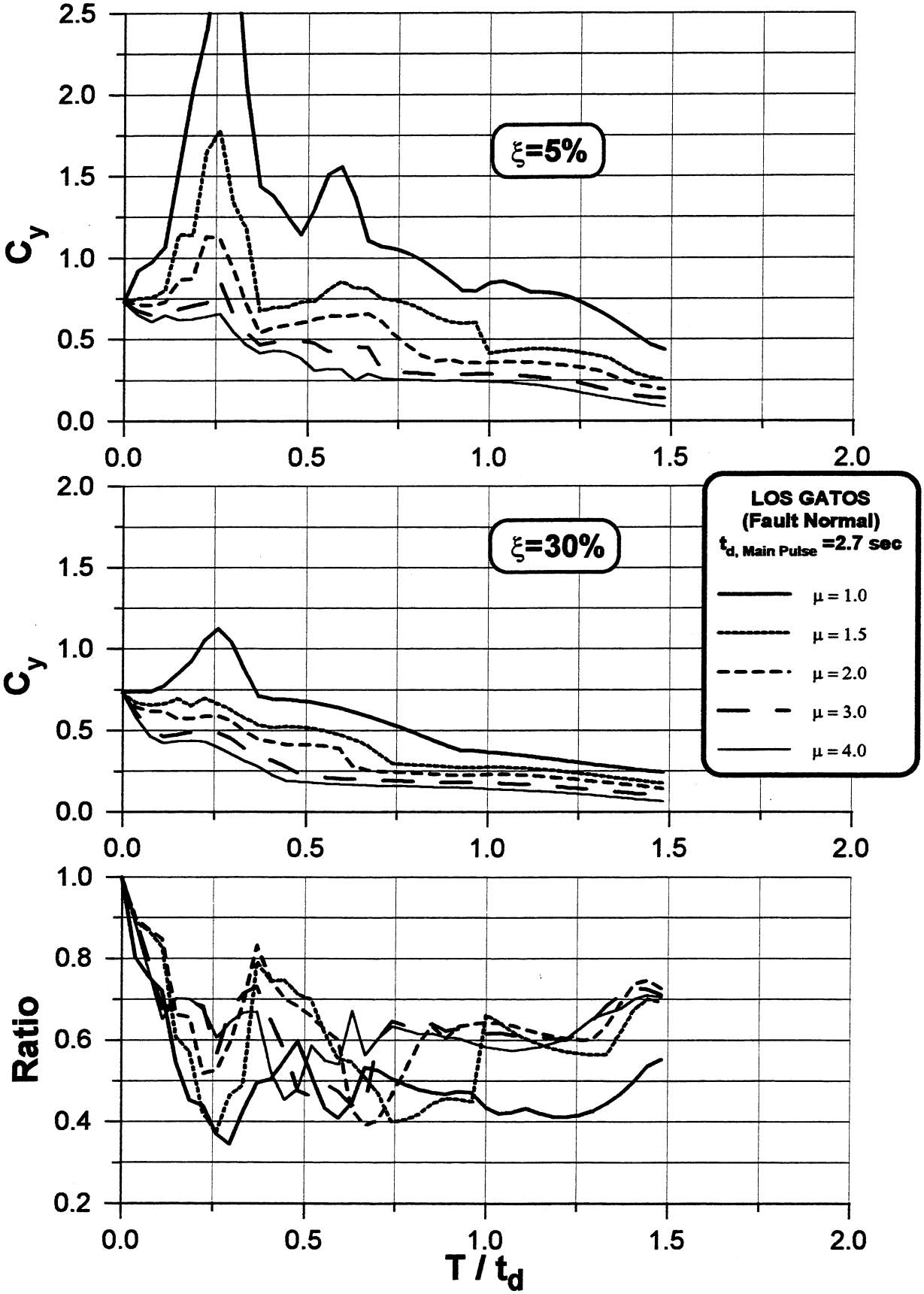

Figure 7.14 Yield coefficient response spectra for fault-normal Los Gatos EQGM recorded during 1989 Loma Prieta earthquake.

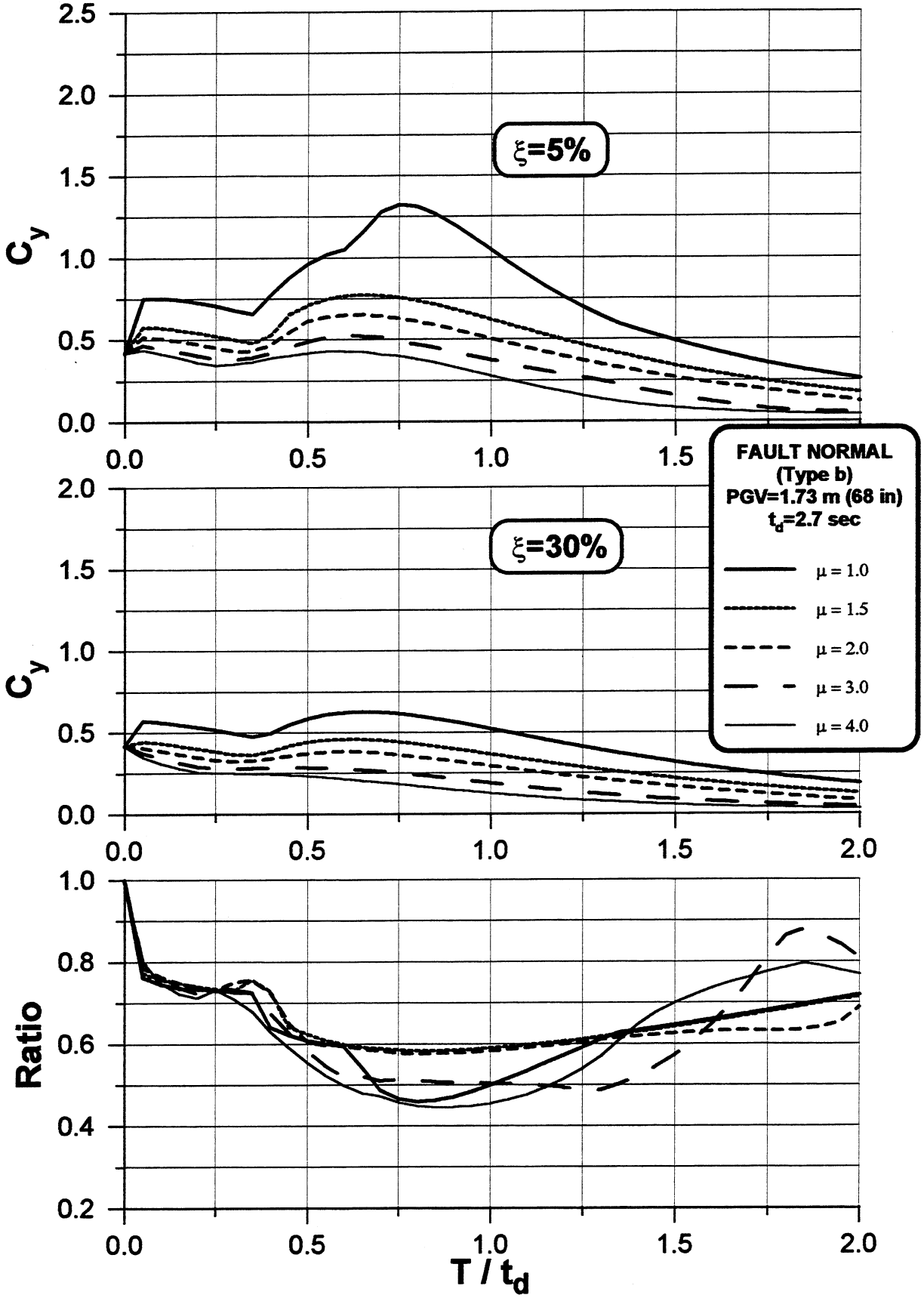

Figure 7.15 Yield coefficient response spectra for idealized fault normal EQGM (type b).

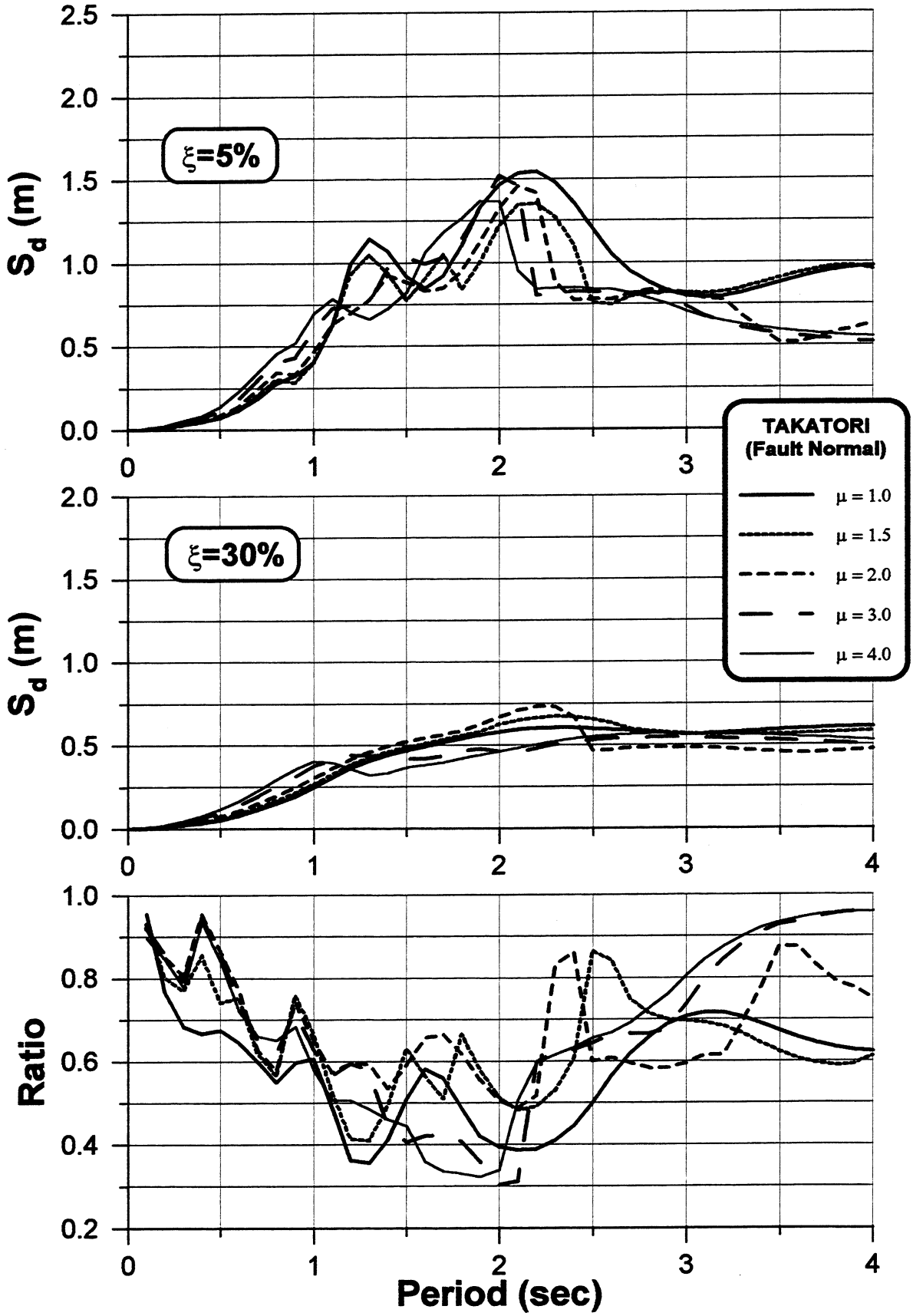

Figure 7.16 Displacement response spectra for fault-normal Takatori EQGM recorded during 1995 Kobe earthquake.

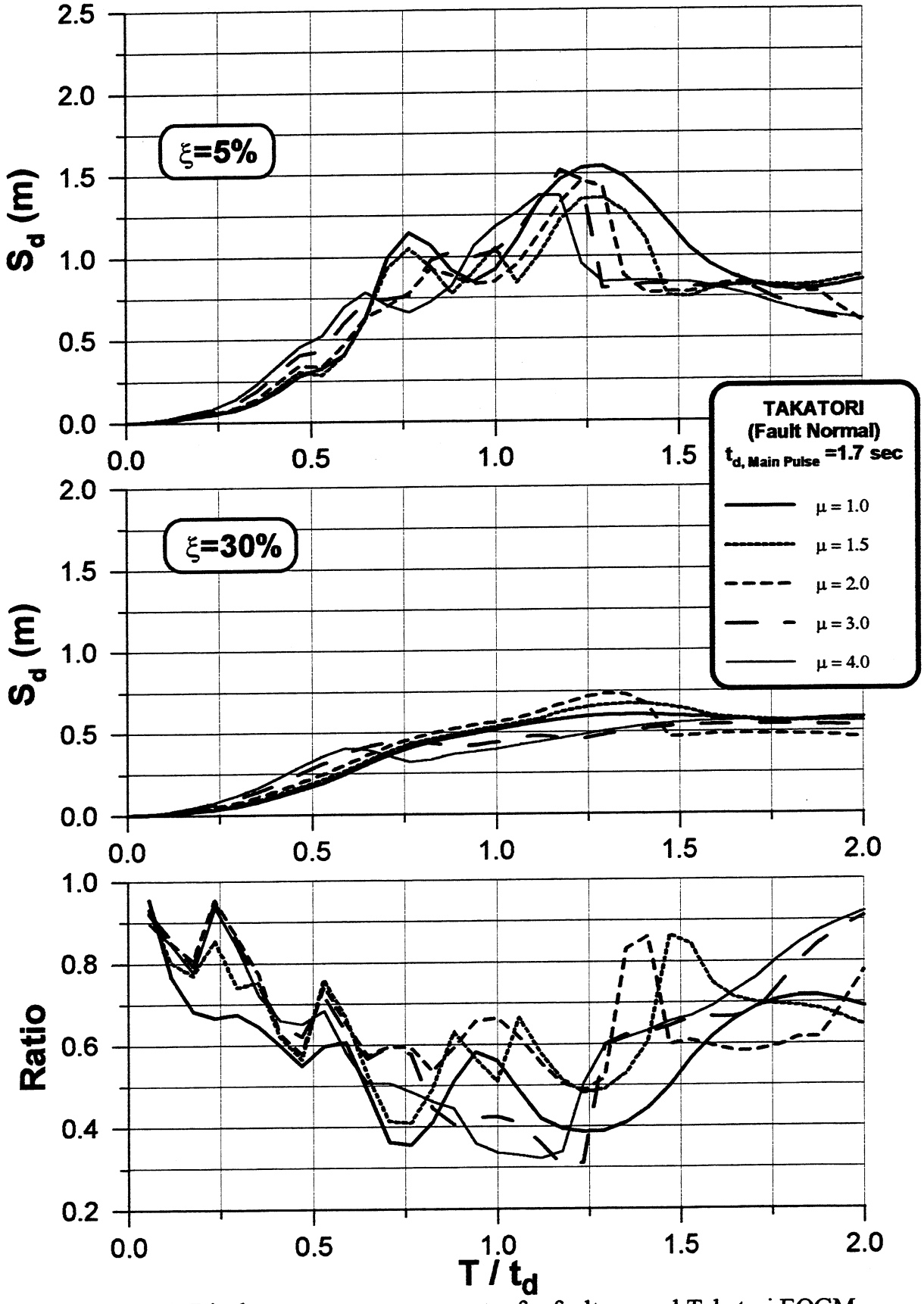

Figure 7.17 Displacement response spectra for fault-normal Takatori EQGM recorded during 1995 Kobe earthquake.

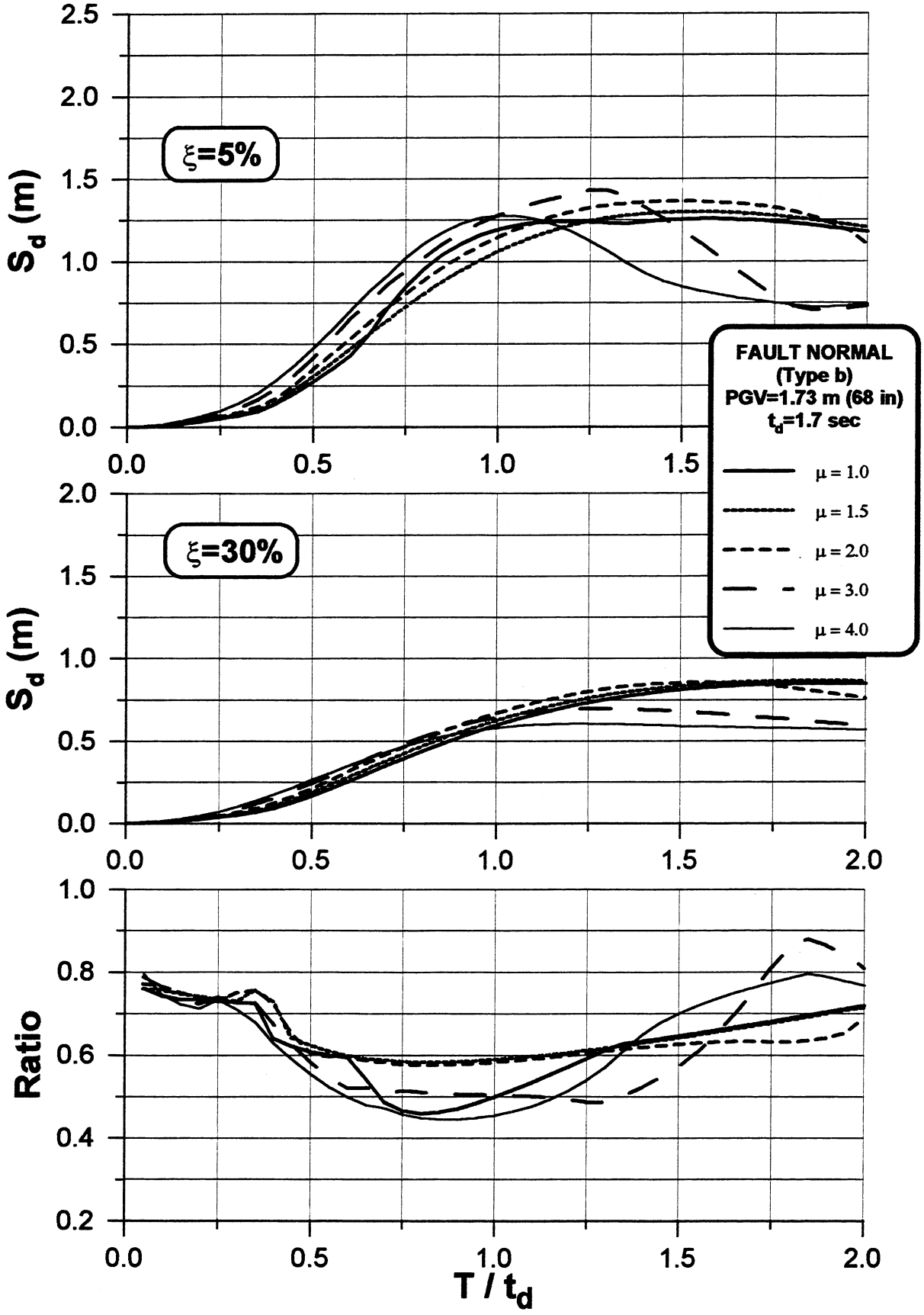

Figure 7.18 Displacement response spectra for idealized fault normal EQGM (type b).

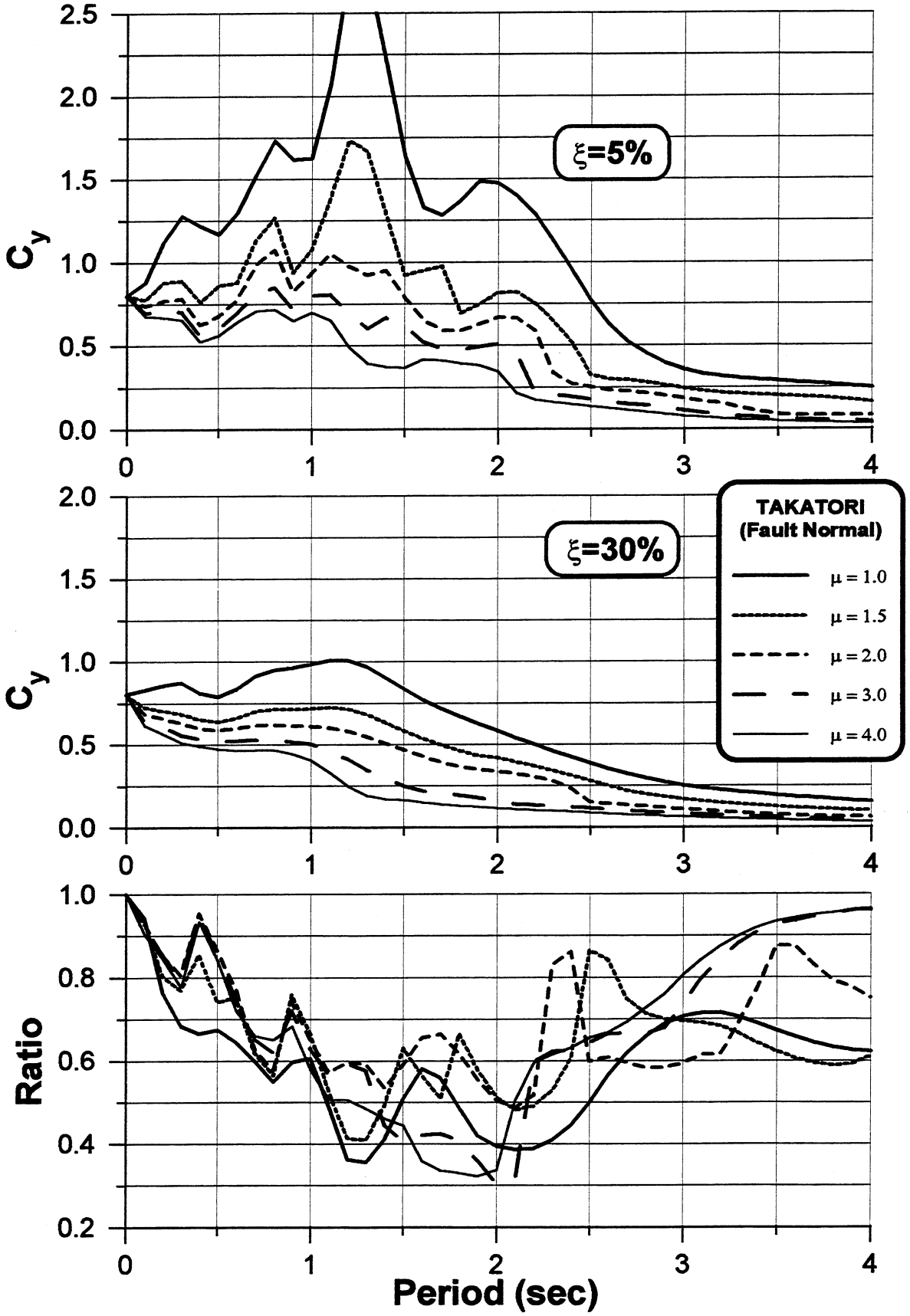

Figure 7.19 Yield coefficient response spectra for fault-normal Takatori EQGM recorded during 1995 Kobe earthquake.

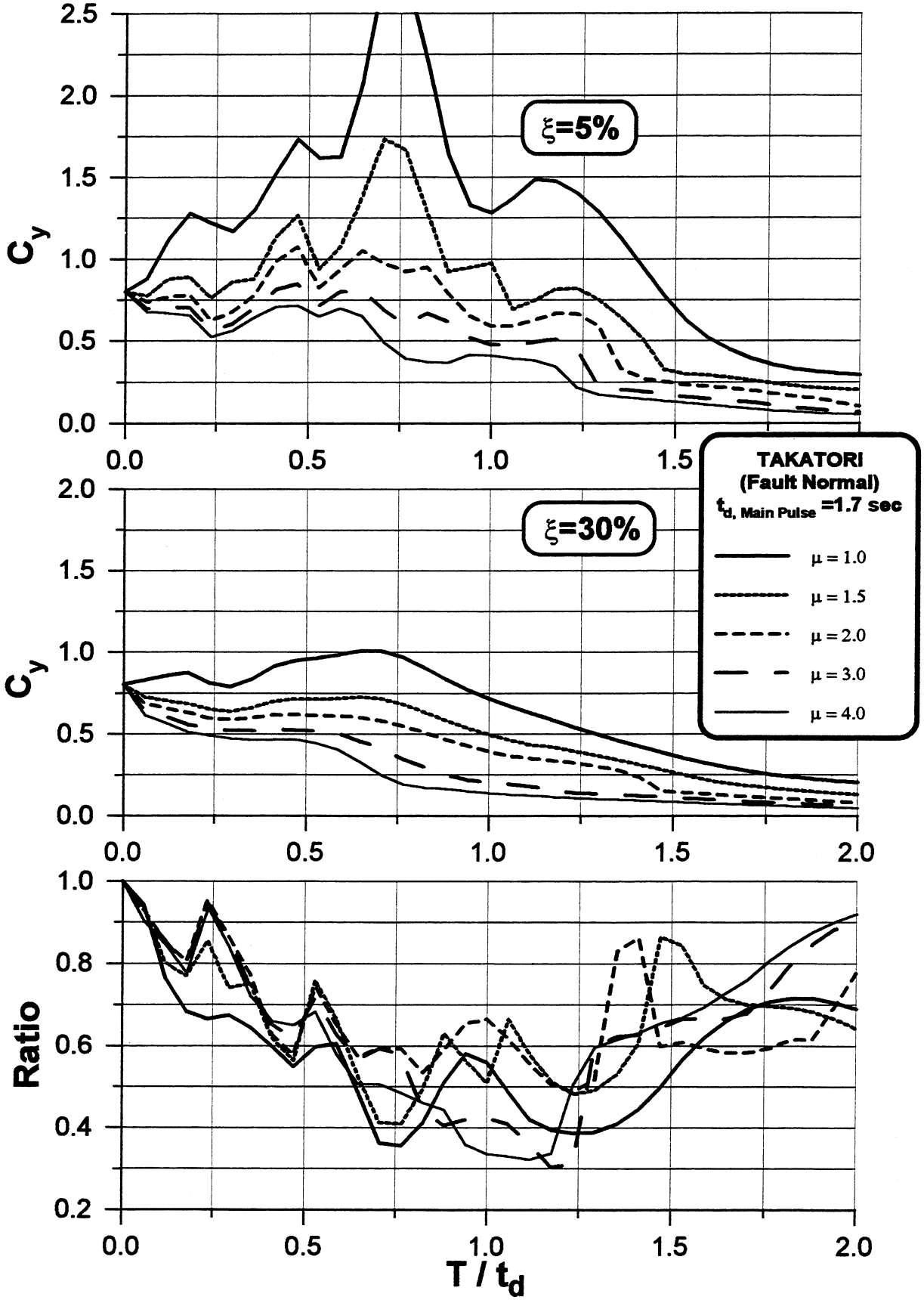

Figure 7.20 Yield coefficient response spectra for fault-normal Takatori EQGM recorded during 1995 Kobe earthquake.

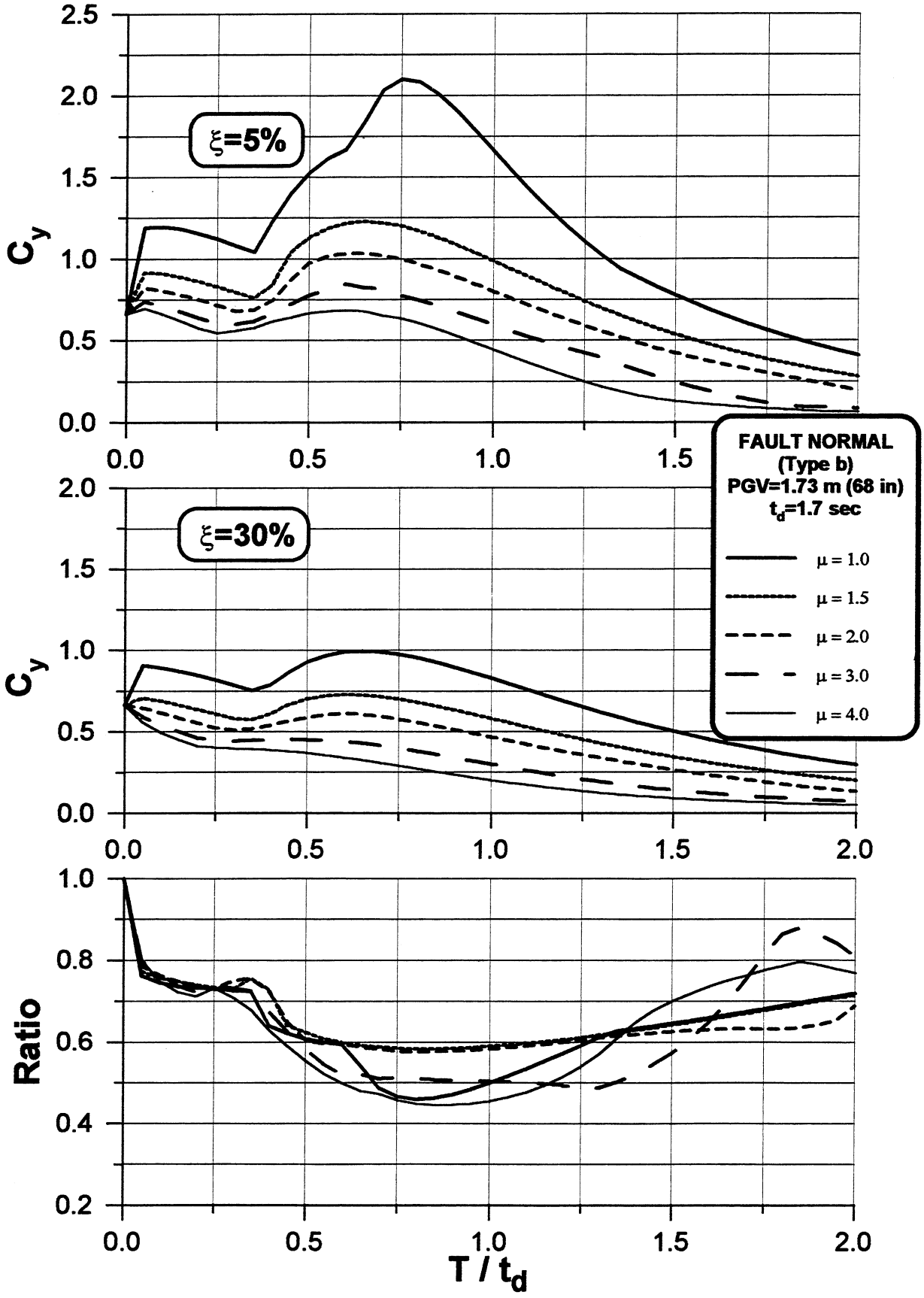

Figure 7.21 Yield coefficient response spectra for idealized fault normal EQGM (type b).

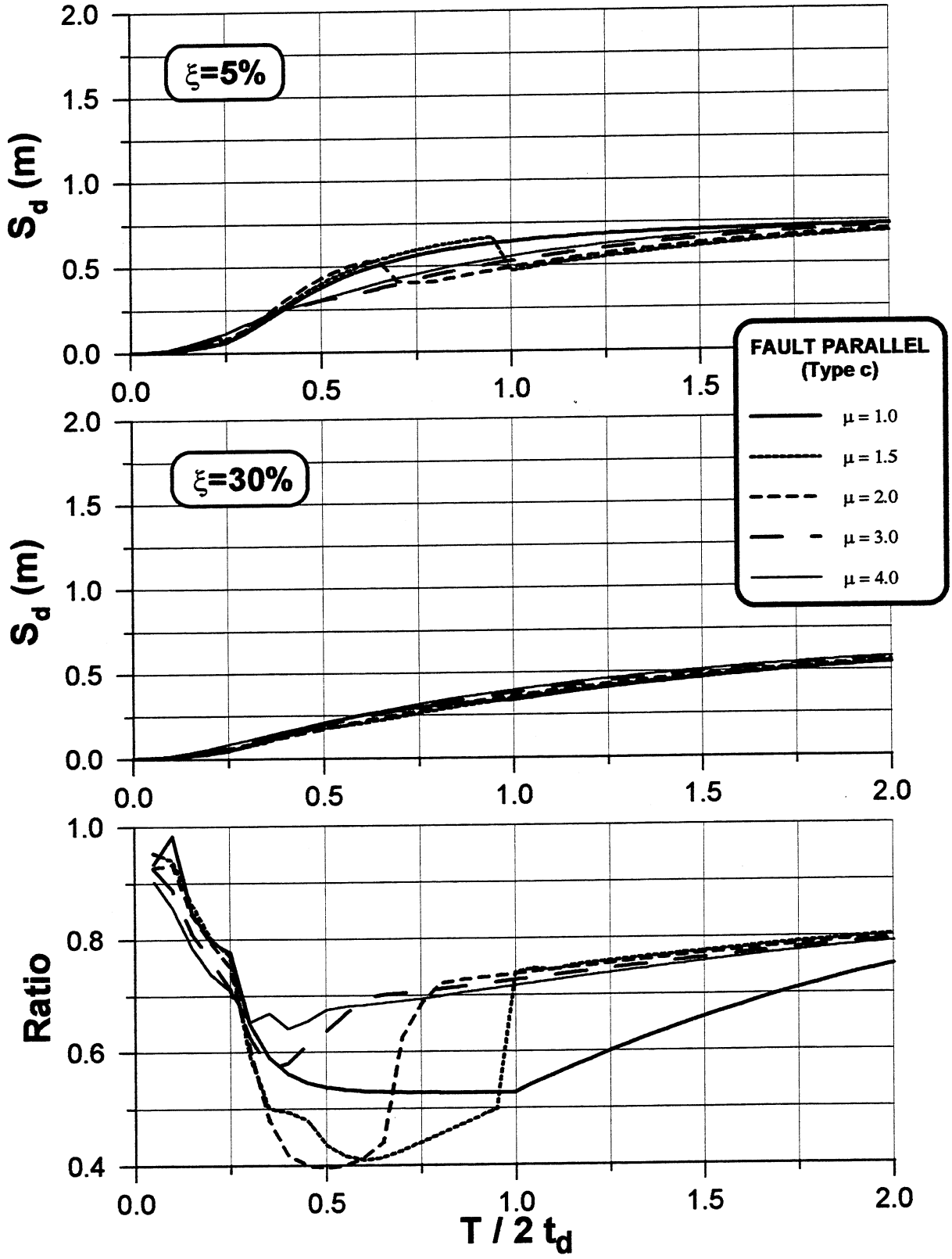

Figure 7.22 Displacement response spectra for idealized fault parallel EQGM (type c).

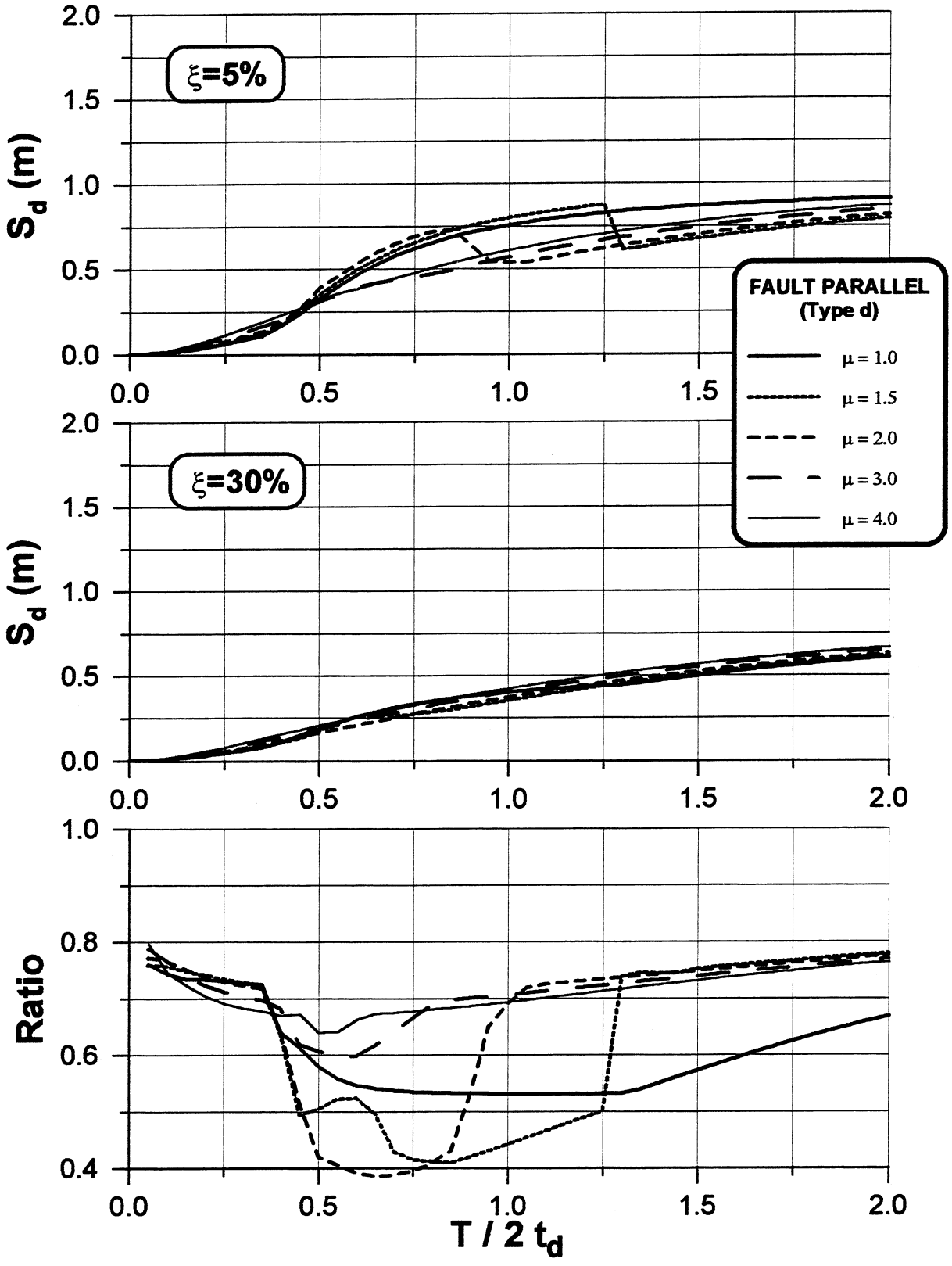

Figure 7.23 Displacement response spectra for idealized fault parallel EQGM (type d).

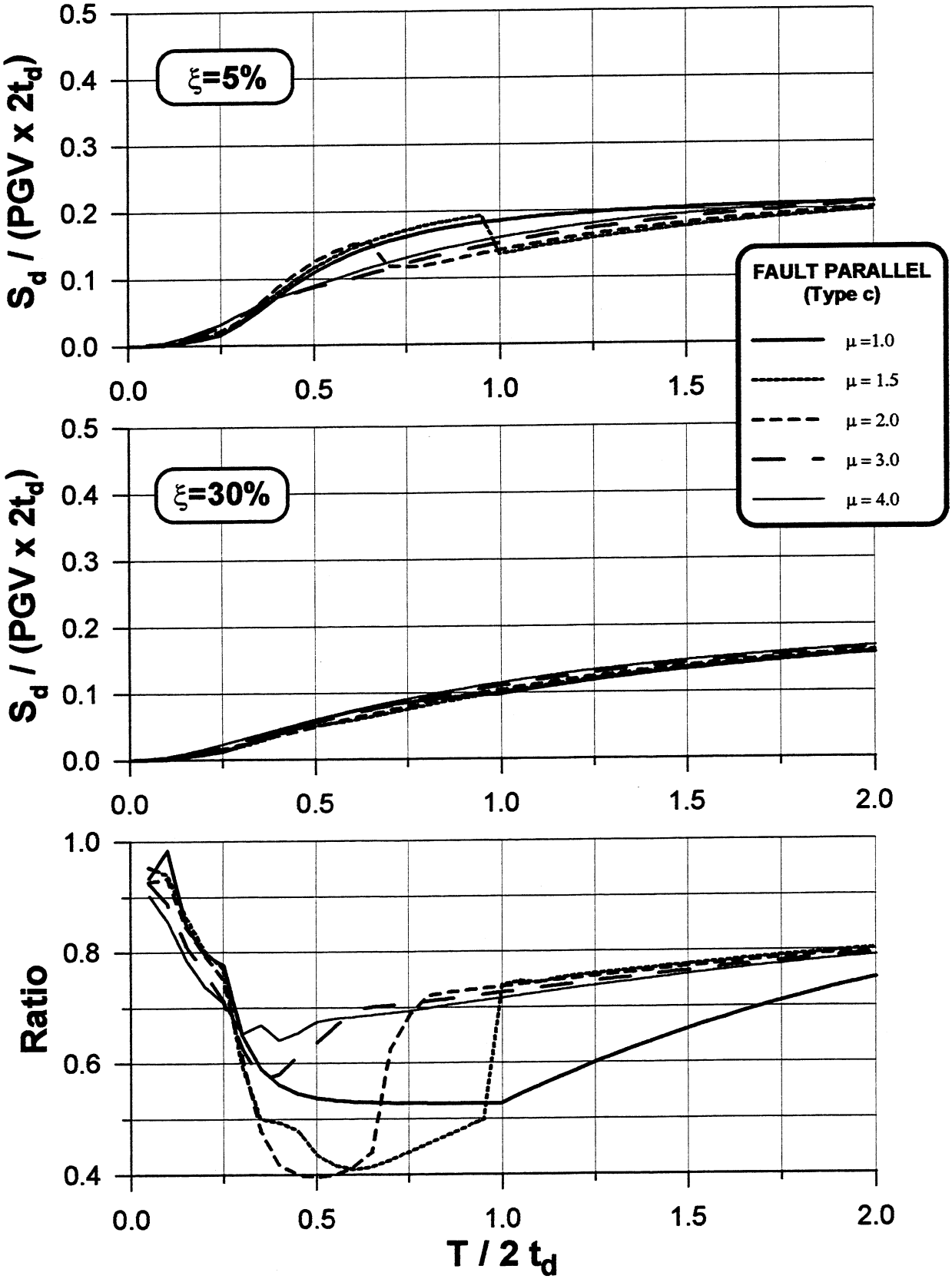

Figure 7.24 Normalized displacement response spectra for idealized fault parallel EQGM (type c).

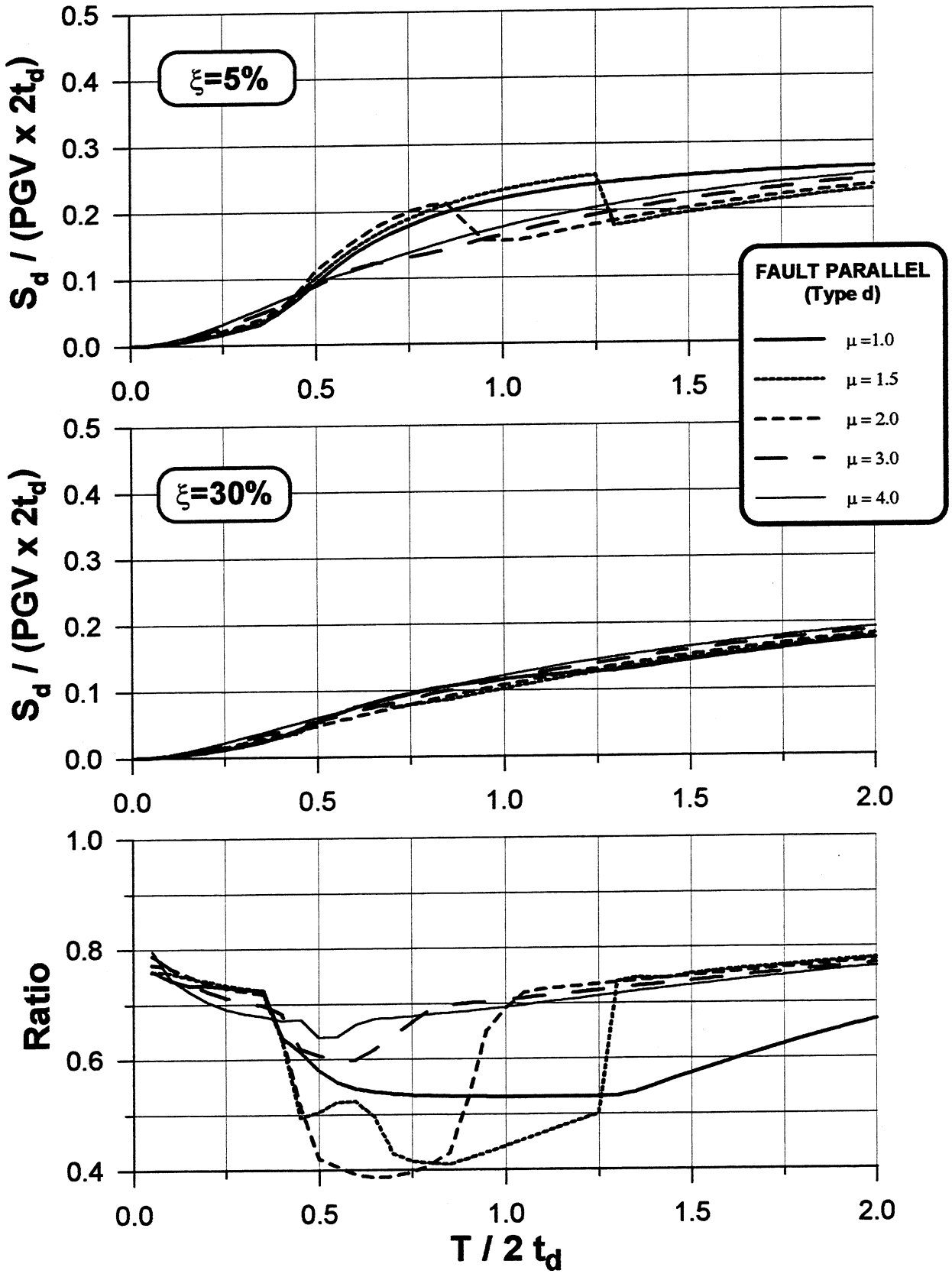

Figure 7.25 Normalized displacement response spectra for idealized fault parallel EQGM (type d).

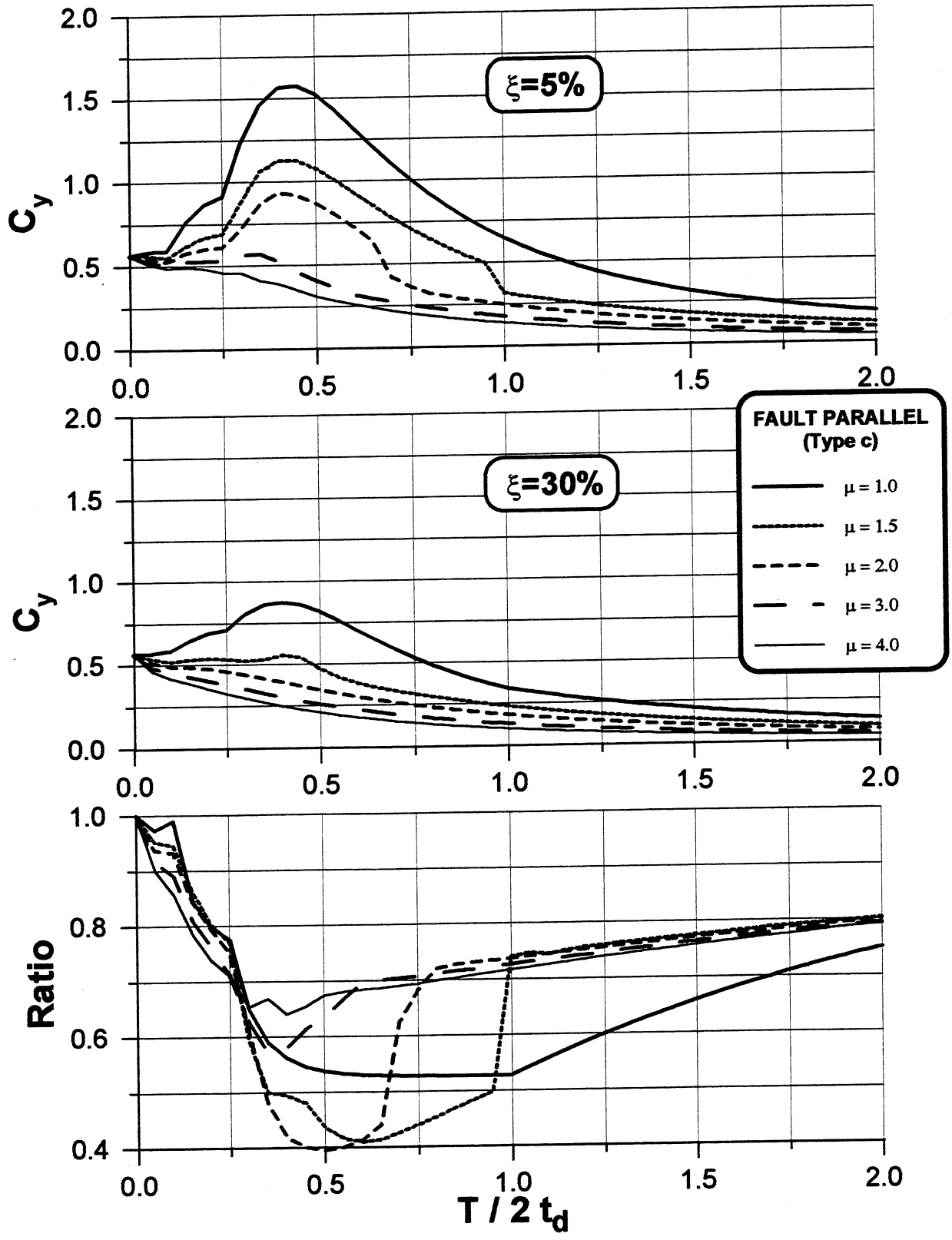

Figure 7.26 Yield coefficient response spectra for idealized fault parallel EQGM (type c).

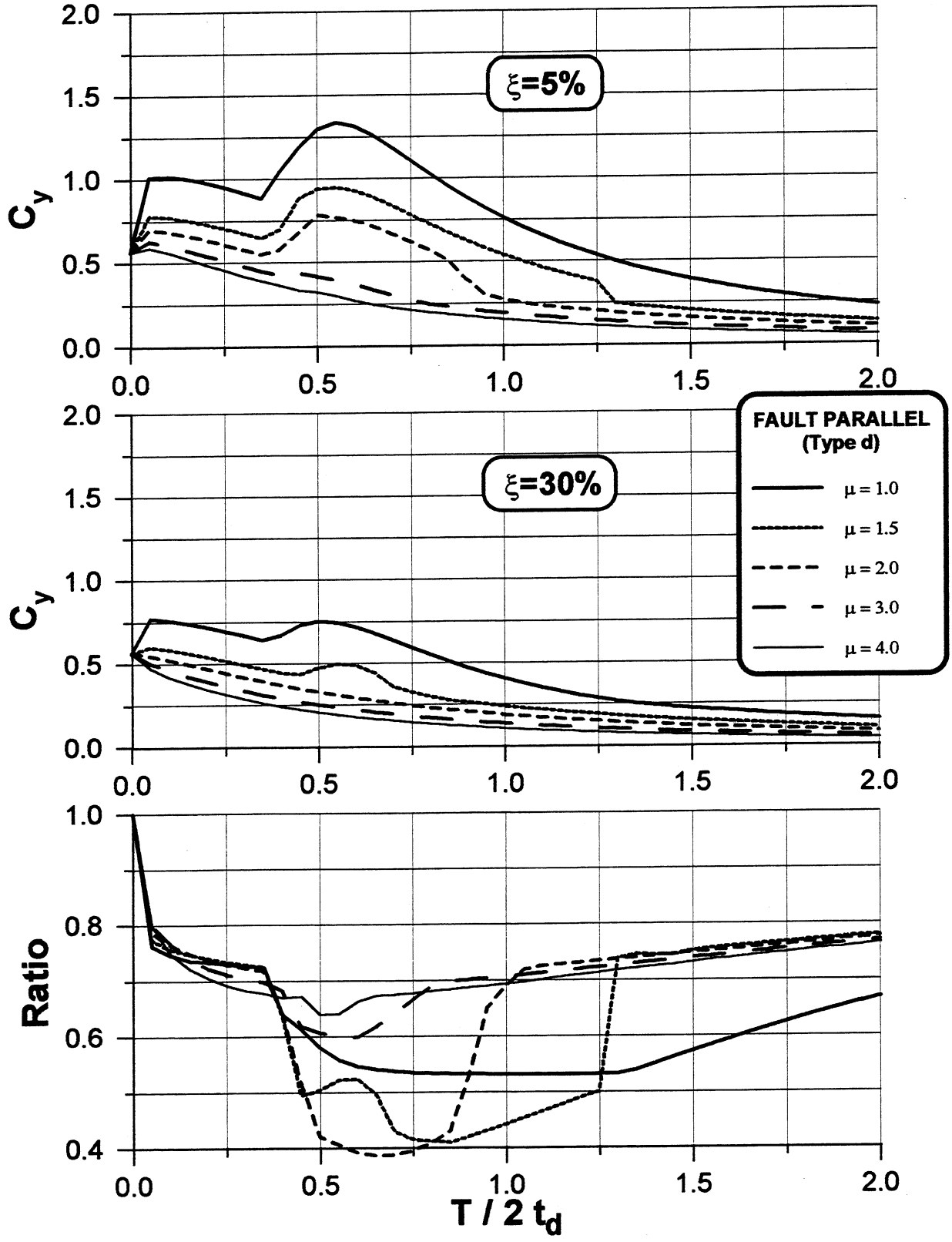

Figure 7.27 Yield coefficient response spectra for idealized fault parallel EQGM (type d).

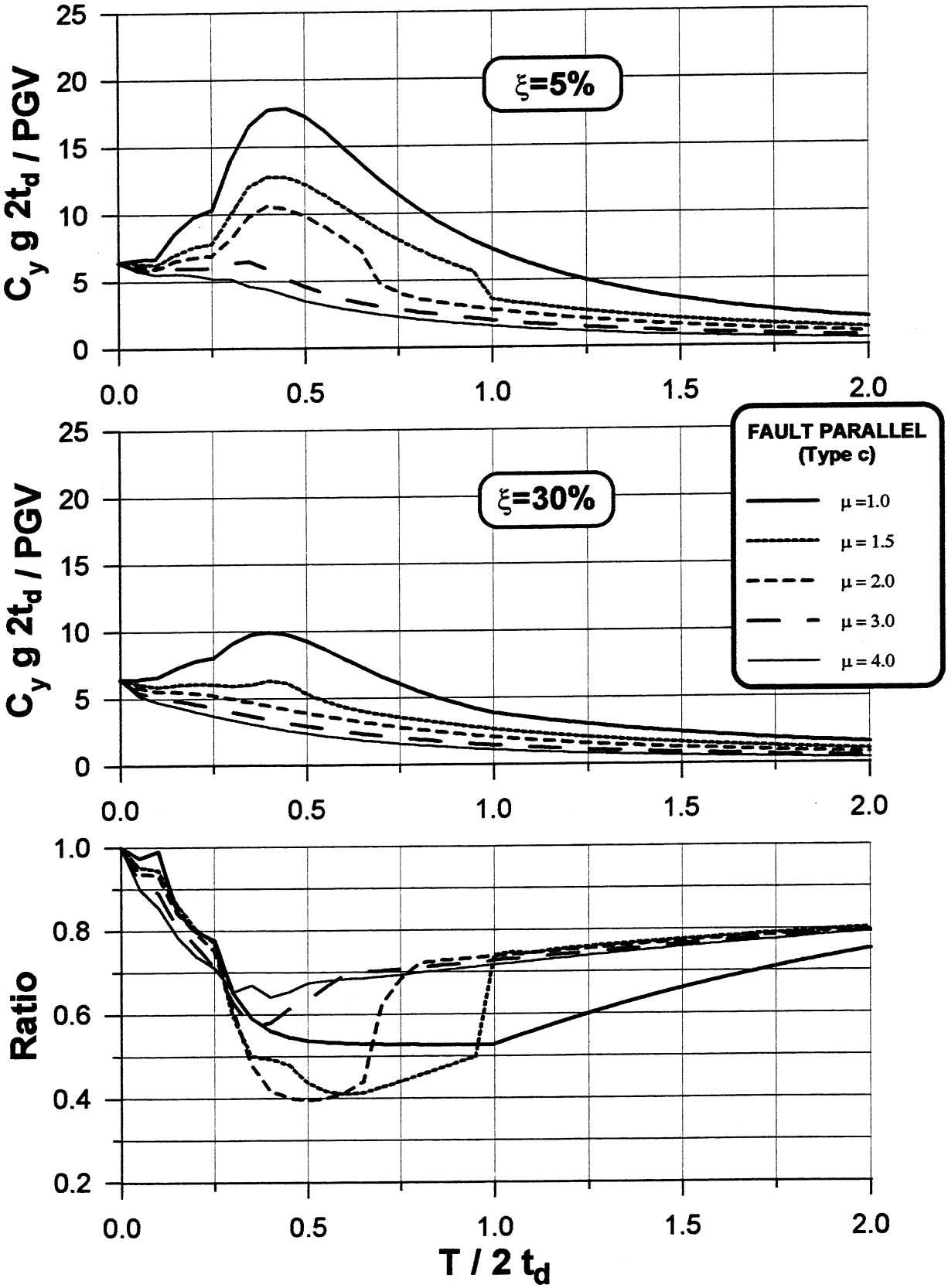

Figure 7.28 Normalized yield coefficient response spectra for idealized fault parallel EQGM (type c).

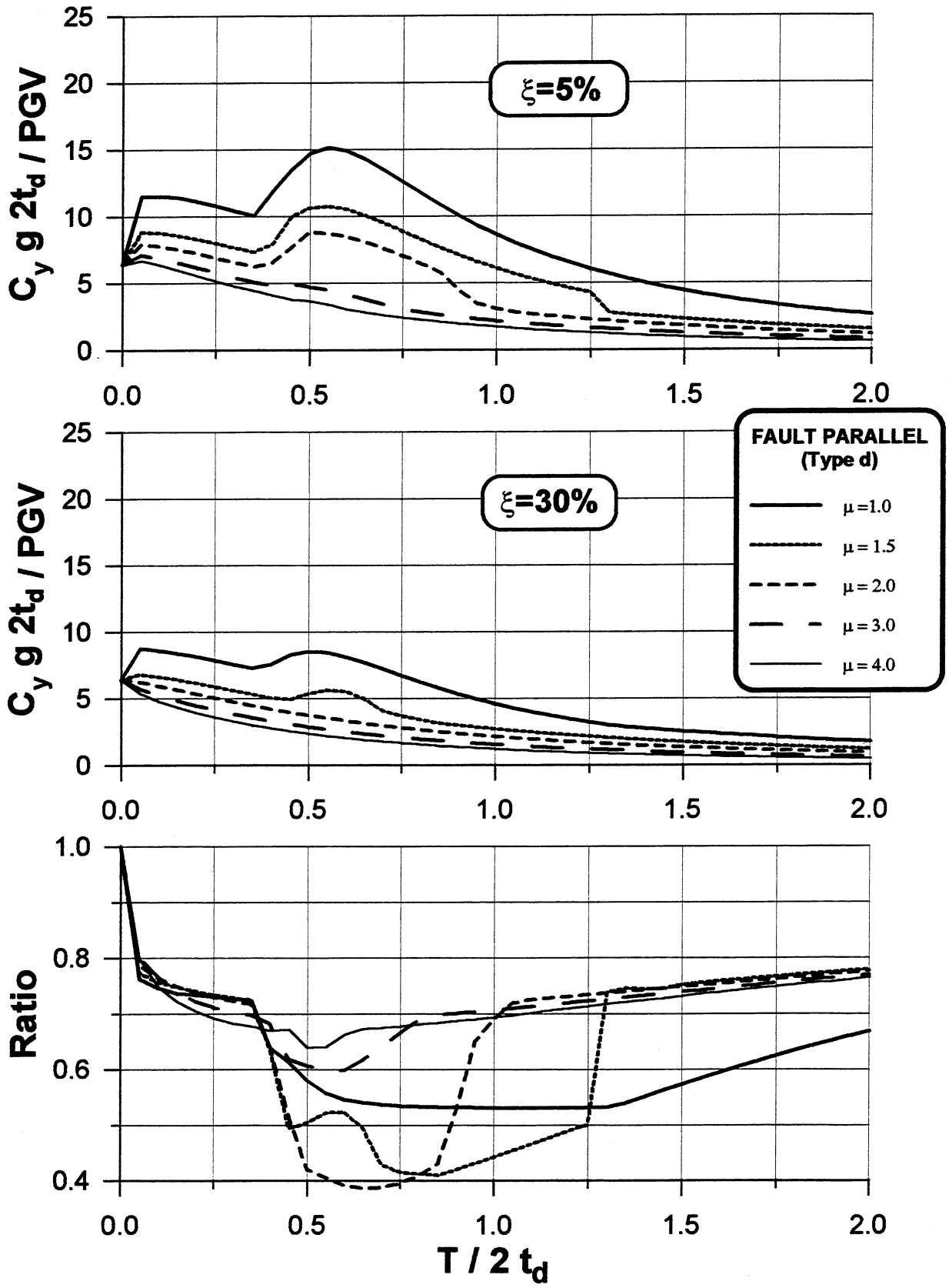

Figure 7.29 Normalized yield coefficient response spectra for idealized fault parallel EQGM (type d).

8 Behavior of As-Built Building with Added Damping (Foundation and Basement Flexibility Included)

As discussed in chapter seven, even under pulse-type ground motions, adding damping to the structure could significantly reduce the response of the structure. To study the possibility of retrofitting the building with added damping, the response of the as-built structure-foundation model with 30% viscous damping in the first two modes of the model has been studied under the two near-field recorded ground motions that have been considered in chapters six and seven.

8.1 1989 LOMA PRIETA EARTHQUAKE GROUND MOTIONS RECORDED AT LOS GATOS STATION

The displacement, interstory drift index, and the story shear force envelopes obtained under the Los Gatos fault-normal ground motion are given in Figure 8.1. The time history of the roof displacement is shown in Figure 8.2. Comparing the results given in these figures with those shown in Figures 6.7 and 7.8, it becomes clear that by increasing the damping coefficient from 0.05 to 0.30, the maximum roof displacement and the maximum IDI dropped by about 40%. It should be noted that based on the response spectra of the idealized fault-normal ground motions, a 40% to 50% reduction was expected. Excluding the drift caused by the foundation rocking, the maximum IDI is equal to 2.7%, which is still larger than the usually acceptable value of 2%. Since the given base shear includes not only shear forces at the first-story columns, but also the shear due to the damping forces, the use of a larger damping coefficient has increased the maximum base shear by about 15%, i.e., from 0.20W to 0.23W.

For a damping coefficient equal to 0.30 and μ=2.3 (roof displacement of 43 in.) at T=3.2 sec (T/t_d=3.2/2.7=1.2), the idealized fault-normal ground motions shown in Figures 7.1-a and 7.1-b predict a maximum displacement of about 42 in. and 47 in., respectively (see Figures 7.6 and 7.12). The response spectra of the Los Gatos ground motion suggest a maximum displacement of about 44 in., Figure 7.10. The maximum lateral displacement of the as-built structure at 2/3 of its height under the Los Gatos ground motion is about 35 in. Therefore, the response spectra of the idealized and Los Gatos ground motions overestimate the structural displacement.

8.2 1995 KOBE EARTHQUAKE GROUND MOTIONS RECORDED AT TAKATORI STATION

The displacement, interstory drift index, and the story shear force envelopes under the Takatori fault-normal ground motion are given in Figure 8.3. Unlike the response under the Los Gatos ground motion, by increasing the damping coefficient from 0.05 to 0.30, the maximum roof displacement dropped only by about 7%. However, the maximum IDI is reduced by about 32% and moved further down. It should be noted that based on the response spectra of the idealized fault-normal ground motions a 20% to 25% reduction in lateral displacement was expected. The time history of the roof displacement is shown in Figure 8.4. Comparing Figures 6.10 and 8.4, the roof displacement responses for the two different levels of damping (5% and 30%) are almost the same from t=4 to 8 sec. It might be worth mentioning that in spite of the fact that the period of the structure is about 3.2 sec, the apparent period of the response from 4 to 8 sec, is about 2.0 sec, which is close to the period of the ground velocity as expected according to the discussion presented in chapter seven. The apparent period is about 3.0 sec from 12 to 18 sec over which there is a significant reduction in the displacement by increasing the damping coefficient. The maximum base shear is increased by 7%.

For a damping coefficient equal to 0.30 and μ=1.6, at T=3.2 sec (T/t_d=3.2/1.7=1.9), the idealized fault-normal ground motions shown in Figures 7.1-(a) and 7.1-(b) predict a maximum displacement of about 28 in. and 33 in., respectively (see Figures 7.3 and 7.18). The maximum lateral displacement of the as-built structure at 2/3 of the height under the Takatori ground motion is only about 20 in (Figure 8.3). Again it can be seen the structural displacement is overestimated by the response spectra.

8.3 DISCUSSION AND SUMMARY

Although increasing damping decreased the lateral displacements and drifts, particularly under the Los Gatos ground motion, the story drift still is not within acceptable limits. For the Los Gatos ground motion, the reduction in the lateral displacement of the structure as a result of using higher damping was fairly well predicted by the response spectra of the fault-normal idealized ground motions. For the Takatori ground motion the predicted reduction due to increase in damping was smaller than those of obtained using the response spectra of idealized fault-normal ground motions; however, the reduction in the drift was larger.

The response spectra of the recorded ground motions as well as those of idealized fault-normal ground motions overestimate the lateral displacement of the structure at 2/3 of the height. The main reason for the overestimation probably is the fact that under a particular ground motion and an assumed damping coefficient, for a given target ductility there is no unique maximum lateral displacement of the SDOF system and the response spectra considers the largest displacement corresponding to the given ductility. In other words, for a particular ground motion, although for given T, ξ, and C_y, the maximum displacement is unique, this is not the case for given T, ξ, and μ. For particular values of T, ξ, and μ, under given ground motion, a different set of C_y and S_d can be found, and among all these sets, the response spectra show the largest set. Therefore, the maximum displacement response of a SDOF system with a given lateral yield strength to a particular ground motion is less than or equal the value given by the corresponding displacement spectra.

Another reason for the overestimation of the response of the as-built structure by the response spectra could be the argument that can be made for elastic building structures. For MDOF elastic building structures, accepting that the lateral displacement at the top portion of the structures is mainly caused by the first mode of vibration, the modal participation factor of the first mode may result in smaller lateral displacement compared to that of a SDOF system with the same period. The lateral displacement at 2/3 of the height of a stick model of an elastic building structure could be approximately calculated as below,

$$\Delta_{2/3H} \approx (\Delta_{2/3H})_{1st\,Mode} = \frac{\boldsymbol{\Phi}_1^T \mathbf{m}\,\mathbf{1}}{\boldsymbol{\Phi}_1^T \mathbf{m} \boldsymbol{\Phi}_1} \phi_{1,2/3H}\ S_{d_1} \tag{8-1}$$

where $\phi_{1,2/3H}$ is the value of the lateral displacement at 2/3 of the height in the first mode of vibration. For the as-built structure the above equation results in $\Delta_{2/3H} \approx S_{d_1}$, which suggests that the displacement at 2/3 of the height should be the same as the value predicted by the response spectra, if the structure remained elastic. The maximum lateral displacement of the as-built structure at 2/3 of its height (assuming that there is no limit on its elastic response and therefore in its elastic strength) under Los Gatos and Takatori ground motions are 75.3 in. and 30.5 in., respectively, and the corresponding response spectra predict values of 76.7 in. and 30.5 in., respectively, which are in good agreement. However the above argument is not quite applicable to inelastic structures.

There are other differences between the results from the displacement response spectra of SDOF systems and what can be obtained in the inelastic analyses carried out in this study. No matter what the displacement ductility is, the structural model has an elastic foundation at the bottom. In the inelastic analyses, the P-Δ effect that makes the structure more flexible is considered, while this effect is not considered in the case for SDOF response spectra. On the other hand, the MDOF model of the as-built structure considers strain hardening while the SDOF model used to calculate the response spectra is based on elastic-perfectly-plastic force deformation relationships.

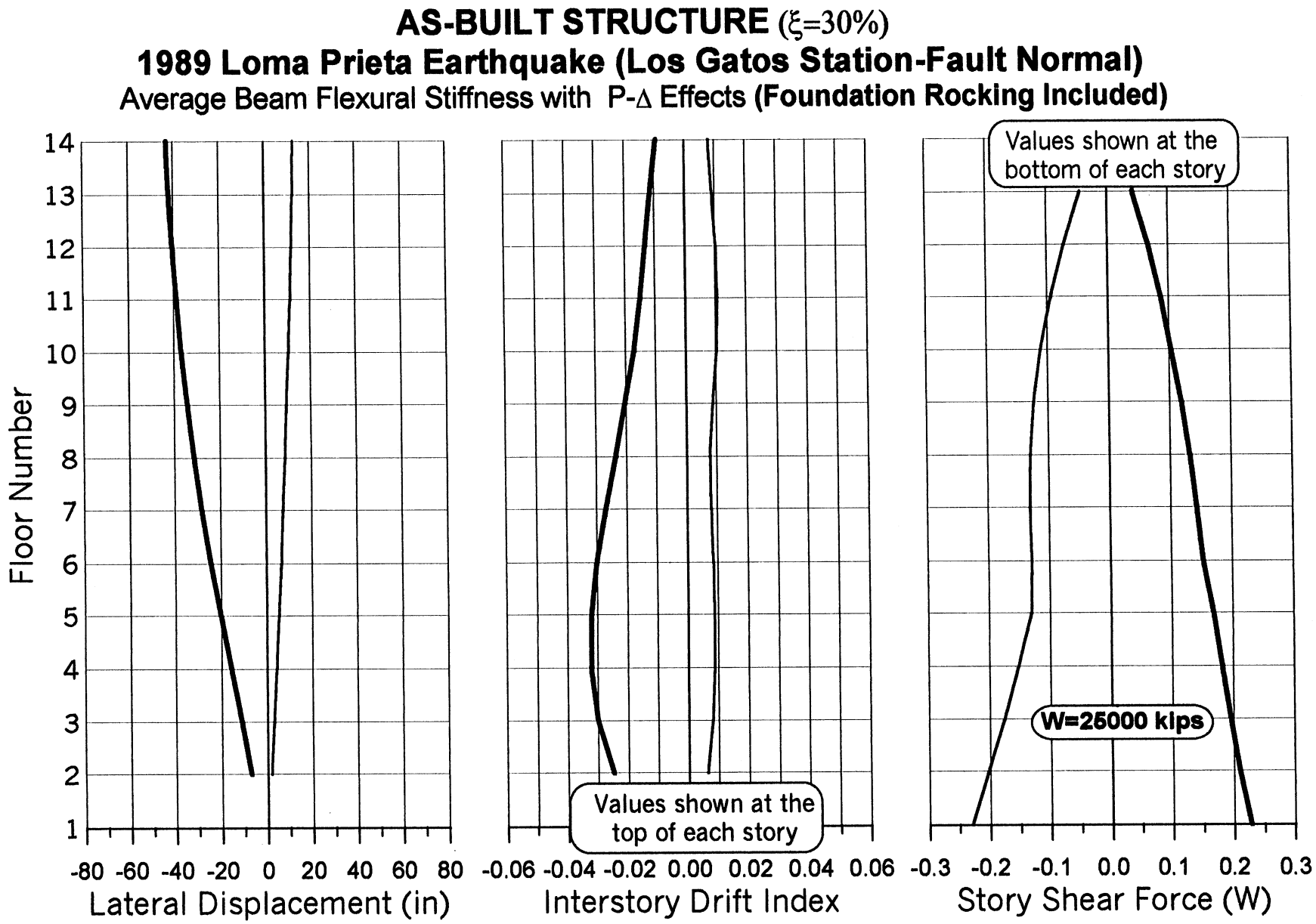

Figure 8.1 Lateral displacement, interstory drift index, and story shear force envelopes.

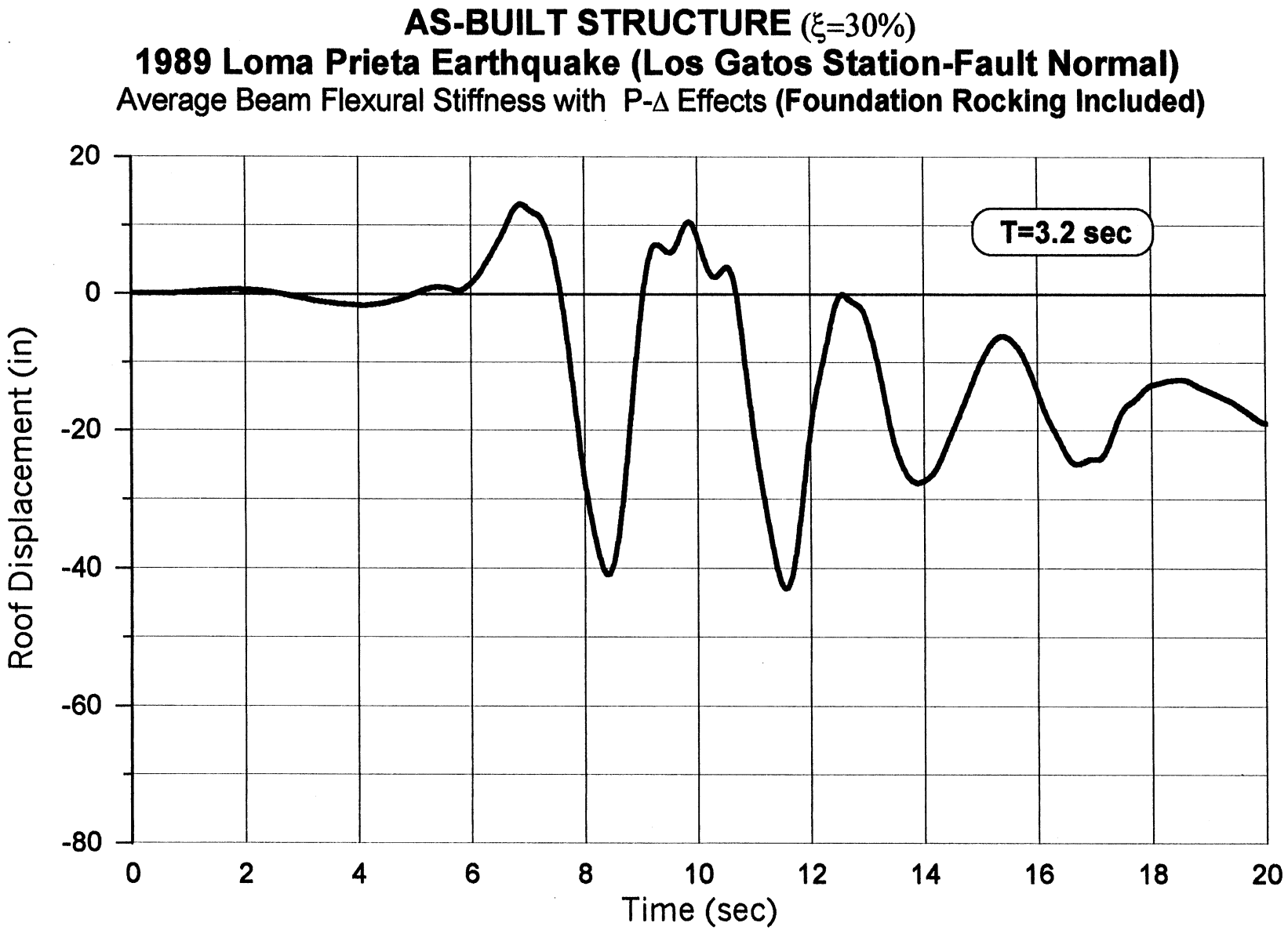

Figure 8.2 Time history of roof displacement.

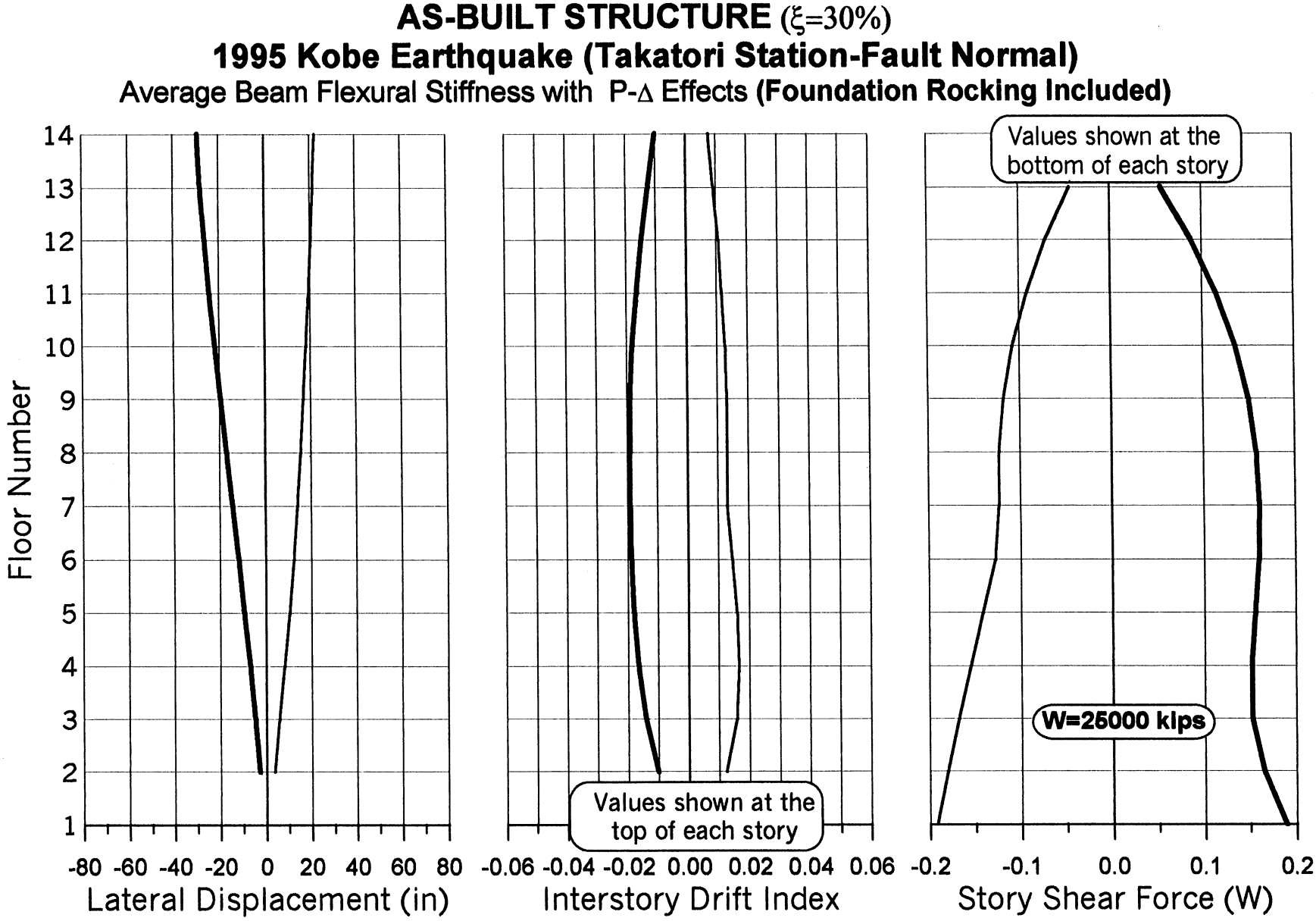

Figure 8.3 Lateral displacement, interstory drift index, and story shear force envelopes.

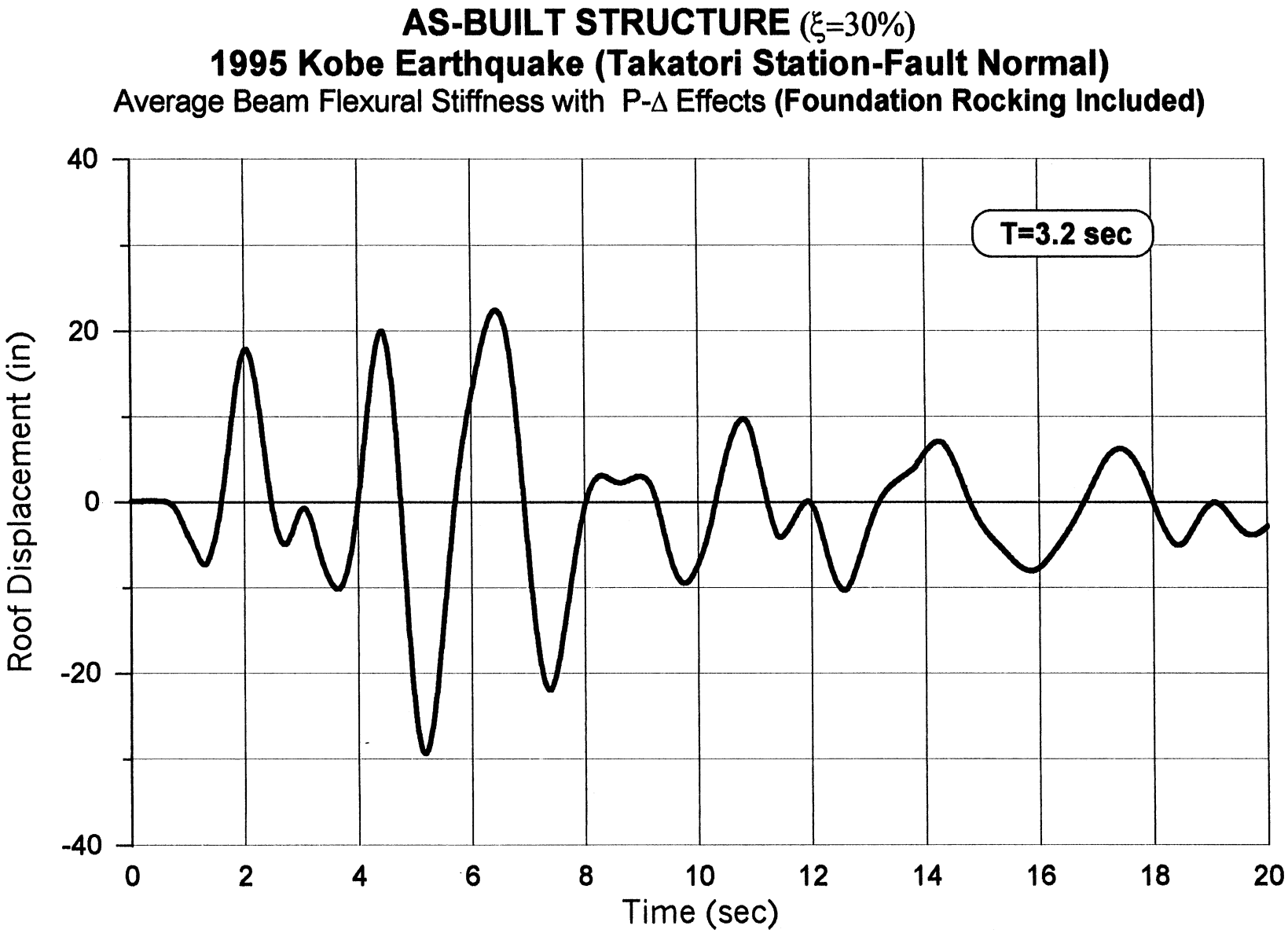

Figure 8.4 Time history of roof displacement.

9 Behavior of As-Built Building (Fixed Base)

If the effects of foundation rotation are not included in the analyses, the first period of the fixed-base structural model in the transverse direction is about 2.6 sec. The analyses of the response of this fixed-base model of the as-built building follows.

9.1 PUSHOVER ANALYSIS UNDER INVERTED TRIANGULARLY DISTRIBUTED LATERAL LOAD

Accounting for P-Δ effect and using a constant total lateral incremental load of 10 kips, at a roof displacement of 44.5 in, the structure becomes analytically unstable, i.e., the solution does not converge for a new 10K incremental of the load. The displacement, interstory drift index, and the story shear force envelopes are given in Figure 9.1. The maximum interstory drift of 3.8% occurs at the second and third stories, while the global drift index is about 2.2%. The maximum base shear is about 14% of the weight of the building. The difference between the results of this analysis and those of the structure with basement and foundation flexibility is mainly caused by the maximum foundation rotation of about 0.4%. Excluding the basement flexural flexibility has altered the maximum IDI slightly.

Figure 9.2 shows the base shear versus roof displacement. The global displacement ductility is about 3.5. The bilinear yield displacement is about 12.7 in. The maximum total plastic rotation (including the beam end plastic rotation and rotation as a result of bond slip) is about 4% and occurs at the interior joints of the second floor beams of the interior frames, under positive bending moment (i.e. tension at the bottom reinforcement). Since the yield rotation for those ends of the second floor beams is about 0.31%, the maximum rotation ductility is about 13.9, which is about 4.0 times the global displacement ductility. The same beam ends under

negative bending moments undergo a rotation ductility of about 5.2 with a yield rotation of about 0.81%. Therefore assuming that the global displacement ductility and beam rotation ductility are equal, as made in the 1997 FEMA-273, could be far off.

9.2 RESPONSE OF BUILDING UNDER PULSE-TYPE GROUND MOTIONS

9.2.1 Response of Structure with 5% Damping

9.2.1.1 1989 Loma Prieta earthquake ground motion recorded at Los Gatos station

The displacement, interstory drift index, and the story shear force envelopes under the Los Gatos ground motion are given in Figure 9.3. The maximum roof displacement is about 72in. From Figure 9.2, it can be assumed that the yield displacement is about 12.7 in., therefore, the global displacement ductility is about 5.8. The maximum interstory drift of 6.1% occurs at the third and fourth stories, while the global drift index is about 3.6%. Note that compared to the structure with flexible basement and foundation rocking (Figure 6.7) both the maximum roof displacement and the maximum IDI are increased. The time history of the roof displacement is shown in Figure 9.4. The maximum base shear of about 19% of the weight of the building occurs at t=9.69 sec.

Figure 6.4 shows the yield coefficient and displacement spectra during the 1989 Loma Prieta Earthquake ground motion recorded at Los Gatos station. Since the global displacement ductility of the response of the structural model is about 5.8, the displacement spectra suggest a maximum displacement of about 79 in., which is even larger than the building roof displacement of 72 in. (the displacement at about 2/3 of the height of the building that could be representative of an equivalent single-degree-of-freedom system is 67 in.). In other words, the response spectra overestimate the lateral displacement of the structure. The yield coefficient spectra suggest a yield coefficient, C_y, of about 0.20. In spite of the fact that C_y does include the damping force, it suggests a larger base shear compared to the base shear found from the inelastic analysis of the building which was about 0.19W. It should be noted that the single-degree-of-freedom system that is considered in the development of the spectra does not include any strain hardening and that the P-Δ effect is not included either.

9.2.1.2 1995 Kobe earthquake ground motion recorded at Takatori station

The displacement, interstory drift index, and the story shear force envelopes under the Takatori ground motion are given in Figure 9.5. The maximum roof displacement is about 31 in. From Figure 9.2, it can be assumed that the yield displacement is about 12.7 in., therefore, the global displacement ductility is about 2.5. The maximum interstory drift of 2.6% occurs at the 8th and 9th stories, while the global drift index is about 1.6%. It should be noted that unlike the response of the structure to the Los Gatos ground motion, the larger interstory drift index, IDI, occurs at the stories close to the roof of the building. The maximum base shear is about 18% of the weight of the building. The time history of the roof displacement is shown in Figure 9.6.

Figure 6.6 shows the yield coefficient and displacement spectra due to the EQGM recorded at Takatori station during the 1995 Kobe Earthquake. Since the global displacement ductility of the response of the structural model is about 2.5, the displacement spectra suggest a maximum displacement of about 31 in., which is almost equal to the building roof displacement; however, the displacement at about 2/3 of the height of the building that could be representative of an equivalent single-degree-of-freedom system is only about 20 in. Therefore, the response spectra overestimate the lateral displacement of the structure. The yield coefficient spectra gives a yield coefficient, C_y, of about 0.21, which suggests a base shear larger than 0.18W, found in the nonlinear analysis of the structure model.

9.2.2 Response of Structure with 30% Damping

To study the possibility of retrofitting the building with added damping, using classical Rayleigh damping, the response of the structural model with 30% viscous damping in the first two modes of the structure has been estimated under the two recorded ground motions discussed above. The damping in modes 3 and 4 is about 50%.

9.2.2.1 1989 Loma Prieta earthquake ground motion recorded at Los Gatos station

The displacement, interstory drift index, and the story shear force envelopes under the Los Gatos fault-normal ground motion are given in Figure 9.7. The time history of the roof displacement is shown in Figure 9.8. Comparing these results with those obtained when 5% damping was

considered (Figure 9.3) it can be seen that by increasing the damping coefficient from 0.05 to 0.30, the maximum roof displacement and the maximum IDI dropped by about 50%. Using the response spectra of the idealized fault-normal ground motions for μ=5.8 and ξ=5% (a roof displacement of 72 in., see Figure 9.3) at T/t_d=2.6/2.7=0.95 (t_d for the significant velocity pulse of the Los Gatos ground motion is about 2.7 sec) from Figures 7.4 and 7.5 a reduction of about 50% was expected when ξ=30% is used. The maximum IDI is equal to 3.1%, which is still larger than 2%. Since the base shear includes the damping forces in addition to the static forces, the use of a larger damping coefficient (6 times) has increased the maximum base shear by about 16%.

9.2.2.2 1995 Kobe earthquake ground motion recorded at Takatori station

The displacement, interstory drift index, and the story shear force envelopes under the Takatori ground motion are given in Figure 9.9. Unlike the response under the Los Gatos ground motion, by increasing the damping coefficient from 0.05 to 0.30, the maximum roof displacement dropped only by about 15% (compare results from Figures 9.5 and 9.9). However, the maximum IDI is reduced by about 28% and occurred at stories that are lower than those with the 5% damped structure. Using the response spectra of the idealized fault-normal ground motions for μ=2.4 (a roof displacement of 31 in) at T/t_d=2.6/1.7=1.5 (t_d for the significant velocity pulse of the Takatori ground motion is about 1.7 sec), a reduction of about 32% was expected. The time history of the roof displacement is shown in Figure 9.10. Comparing Figures 9.6 and 9.10, the roof displacement time history for two different levels of damping is almost the same from t=5 to 8 sec. It might be worth mentioning that in spite of the fact that the period of the structure is about 2.6 sec, the apparent period of the response from 4 to 8 sec is about 2.0 sec, while the apparent period is about 2.9 sec from 13 to 19 sec over which there is a significant reduction in the displacement by increasing the damping coefficient. By increasing the damping coefficient, the maximum base shear, which includes the damping forces, is increased by about 30%.

9.3 SUMMARY

Some of the results of the analyses carried out are summarized in Tables 9.1. In the table, T, is the period of the structure, and Δ_y and μ are the yield displacement and displacement ductility, respectively, in a bilinear idealization of the base shear versus the roof displacement. Δ_{roof} and $\Delta_{2/3H}$ are the maximum displacement at the roof level and at 2/3 of the height, respectively. IDI_{ave}

is equal to Δ_{roof}/H, where H is the total height of the building from the ground. The maximum interstory drift, IDI_{max}, minus the maximum foundation rotation, $max\theta_{found}$, is defined as the maximum tangential interstory drift, IDI_{tang}. The ratio of maximum interstory drift over average interstory drift is defined as IDI_{ratio}. The maximum base shear, V_{base}, is given in terms of percentage of the total weight, W, of the building.

It can be seen in Table 9.1 that under the Los Gatos ground motion, IDI_{tang} is about 4.9%. If the base was fixed, this value would even increase further to 6.1% (for fixed-base structure, $IDI_{tang} = IDI_{max}$). Obviously, neither of these IDIs are acceptable. In spite of the fact that the ground motions are of pulse-types, by increasing the damping from 5% to 30%, IDI_{tang} for rocking foundation and fixed-base structure reduce to about 2.7% and 3.1%, respectively, which are reduced by a factor of about 2, but still larger than 2%. Such large IDIs are associated with large plastic rotation demands in beams and first-story columns, which are beyond their rotation capacities. Also other undesirable modes of failure (as discussed in chapter four) can lead to global, story or local failure of the structure.

In spite of smaller lateral displacement obtained by increasing the damping, the resulting base shear is increased to 0.23W (an increase of about 15%). This is due to the fact that by increasing the damping coefficient, particularly for yielding structures, the maximum base shear does not occur at the maximum lateral displacement where the velocity and therefore the damping forces are zero. In other words, after considerable yielding of the structure, the contribution of the stiffness of the structure to increase the base shear is less significant, while the effect of damping force might even increase, because of a higher velocity after the structures yields. Therefore the summation of the base shear caused by the structural stiffness and damping before the structure reaches the maximum lateral displacement could become higher than the base shear at the maximum displacement.

As expected from the response spectra of the two records, the response of the structure with a period of about 3.2 sec to the Takatori ground motion is less significant (severe) than that due to Los Gatos. Assuming that displacement response spectra is comparable to the displacement of the structure at 2/3 of the height, from Table 9.1, one can conclude that the displacement response spectra for the as-built structure has always overestimated the response of the structure, up to 50% (for an explanation, see section 8.3). This overestimation is more significant for the Takatori ground motion. Although the spectral base shear forces are fairly close to the results of nonlinear analyses, one has to bear in mind that the spectral responses do

not include the viscous damping forces nor do they include the P-Δ effects, and while the first one results in smaller base shear demand, the second one increases the base shear force demand.

As far as the IDI is concerned, one can observe that IDI_{max} varies from 1.3 to 1.8 times IDI_{ave}, which suggests that using IDI_{ave} instead of IDI_{max}, as is suggested by FEMA-273, is unconservative for this building.

Table 9.1 Summary of the results for the as-built structure (W≈25000 kips & H≈2000 inches).

Type of Supports	Response Parameters	Pushover Analysis[1]	Los Gatos Ground Motion (1989 Loma Prieta Earthquake)			Takatori Ground Motion (1995 Kobe Earthquake)		
			Spectral Response[2] (ξ =5%)	Dynamic Analysis[1] (ξ =5%)	Dynamic Analysis[1] (ξ =30%)	Spectral Response[2] (ξ =5%)	Dynamic Analysis[1] (ξ =5%)	Dynamic Analysis[1] (ξ =30%)
Basement & Foundation Flexibility Included (T=3.2 sec) (Δ_y≈18.5in)	Δ_{top} (in)	53 (μ=2.9)		69 (μ=3.7)	43		32 (μ=1.7)	30
	$\Delta_{2/3H}$ (in)	47	80	60	35	32	21	20
	IDI_{ave}	2.7%		3.5%	2.2%		1.6%	1.5%
	IDI_{max}	4.3%		5.4%	3.2%		2.8%	1.9%
	IDI_{ratio}	1.6		1.5	1.5		1.8	1.3
	$max\theta_{found}$	0.4%		0.5%	0.5%		0.5%	0.5%
	IDI_{tang}	3.9%		4.9%	2.7%		2.3%	1.4%
	V_{base} (W%)	14%	21%[3]	20%[4]	23%[4]	20%[3]	18%[4]	19%[4]
Fixed-Base (T=2.6 sec) (Δ_y≈12.7in)	Δ_{top} (in)	45 (μ=3.5)		72 (μ=5.8)	35		31 (μ=2.4)	26
	$\Delta_{2/3H}$ (in)	41	79	67	31	31	20	20
	IDI_{ave}	2.3%		3.6%	1.7%		1.6%	1.3%
	IDI_{max}	3.8%		6.1%	3.1%		2.6%	1.9%
	IDI_{ratio}	1.7		1.7	1.8		1.6	1.5
	V_{base} (W%)	14%	20%[3]	19%[4]	23%[4]	20%[3]	18%[4]	20%[4]

(1) P-Δ effects are included.
(2) Single Degree of Freedom system is elastic-perfectly plastic and P-Δ effect is not included (response for corresponding ductility).
(3) Viscous damping forces not included.
(4) Viscous damping forces included.

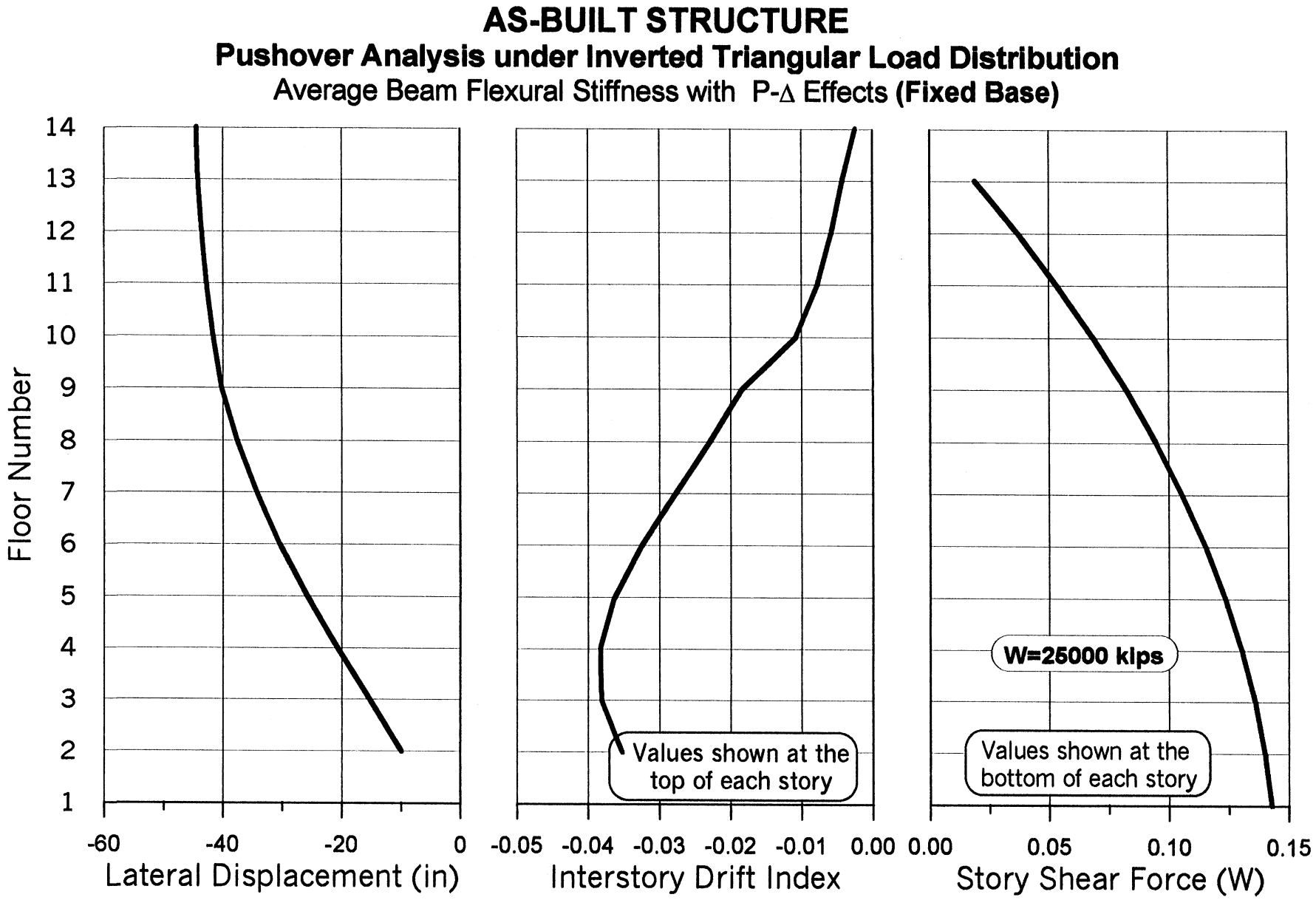

Figure 9.1 Lateral displacement, interstory drift index, and story shear force envelopes.

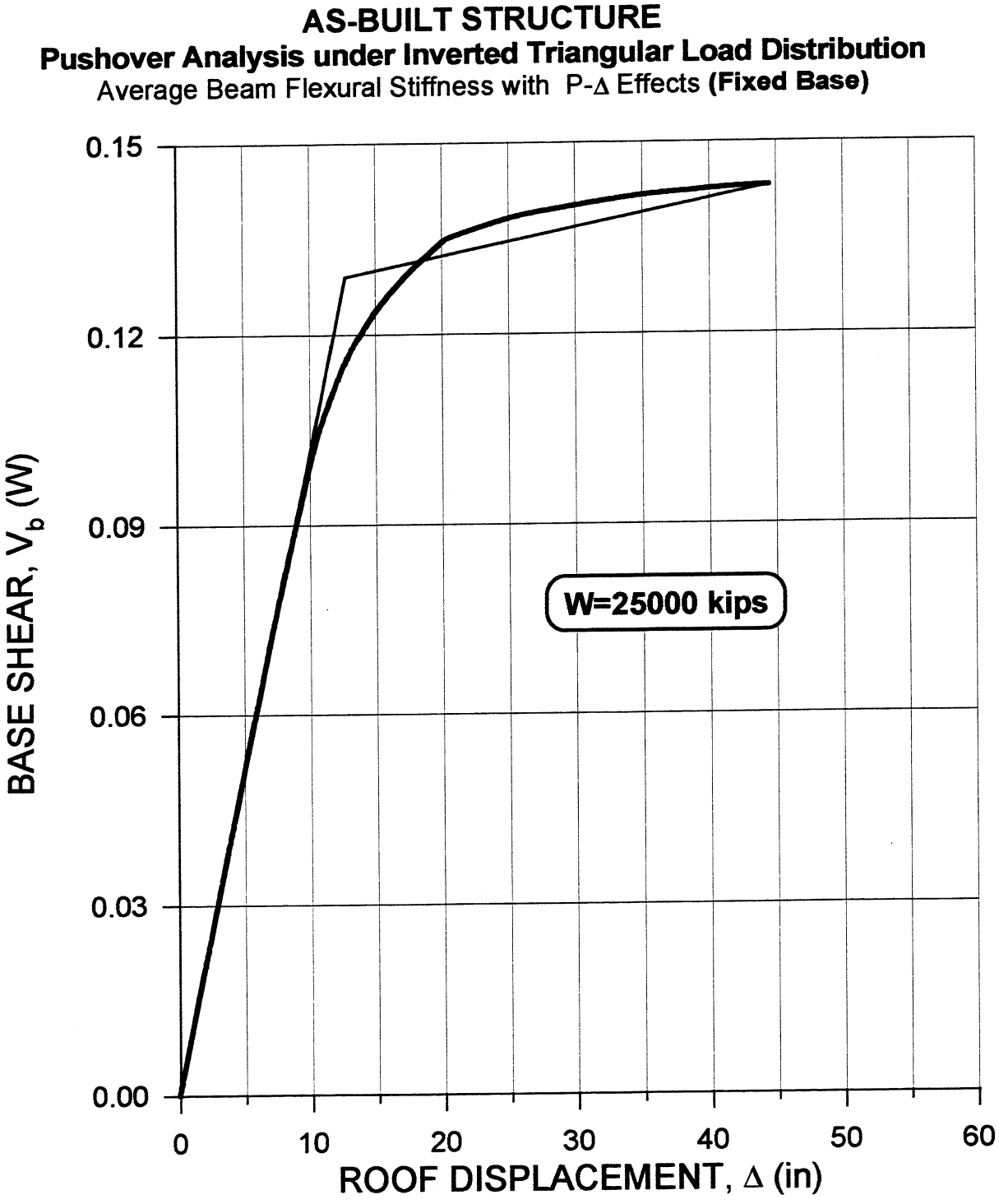

Figure 9.2 Base shear versus roof displacement and its bilinear idealization with Δ_y=12.7 in, V_y=0.129W and μ_Δ=3.5.

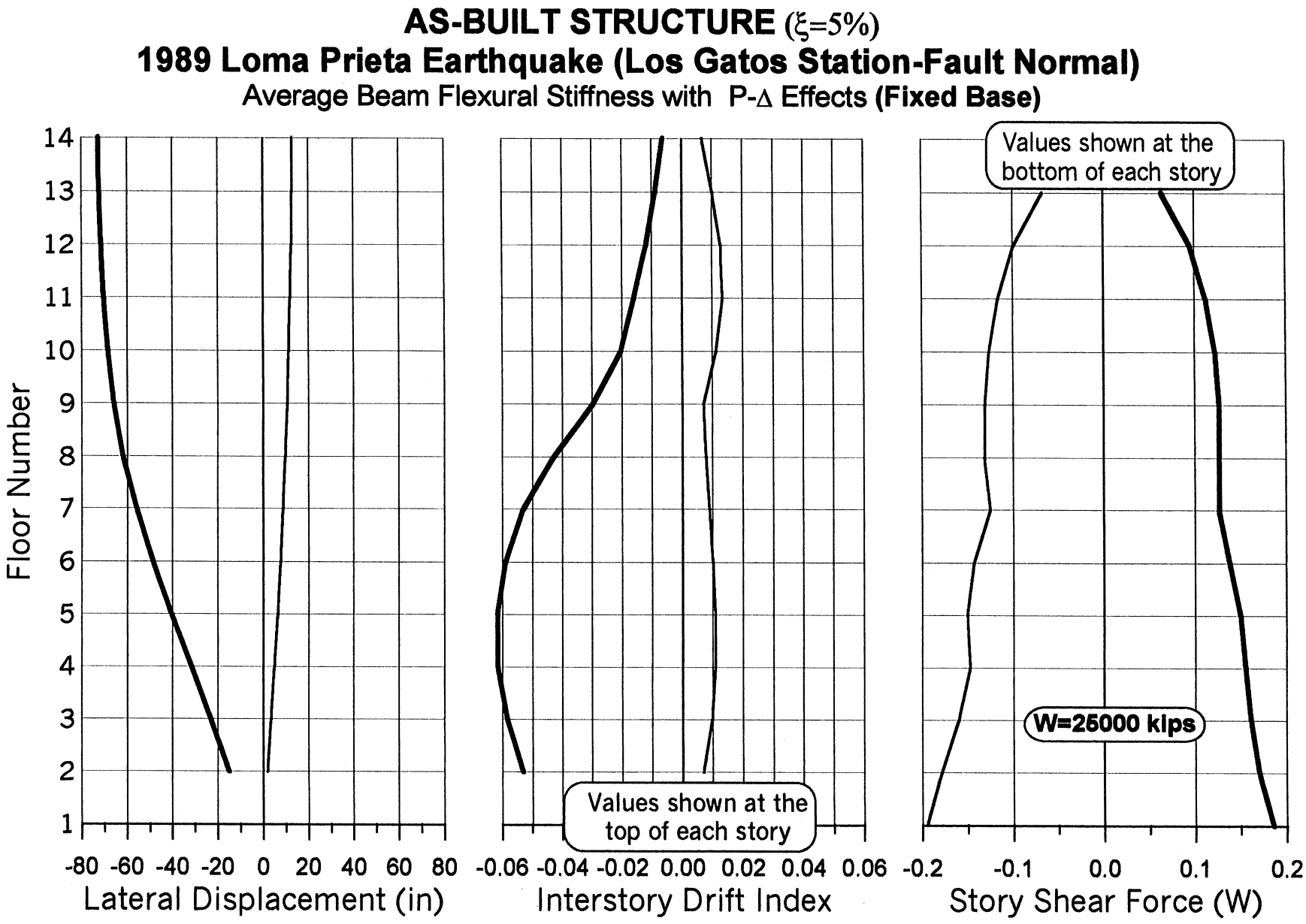

Figure 9.3 Lateral displacement, interstory drift index, and story shear force envelopes.

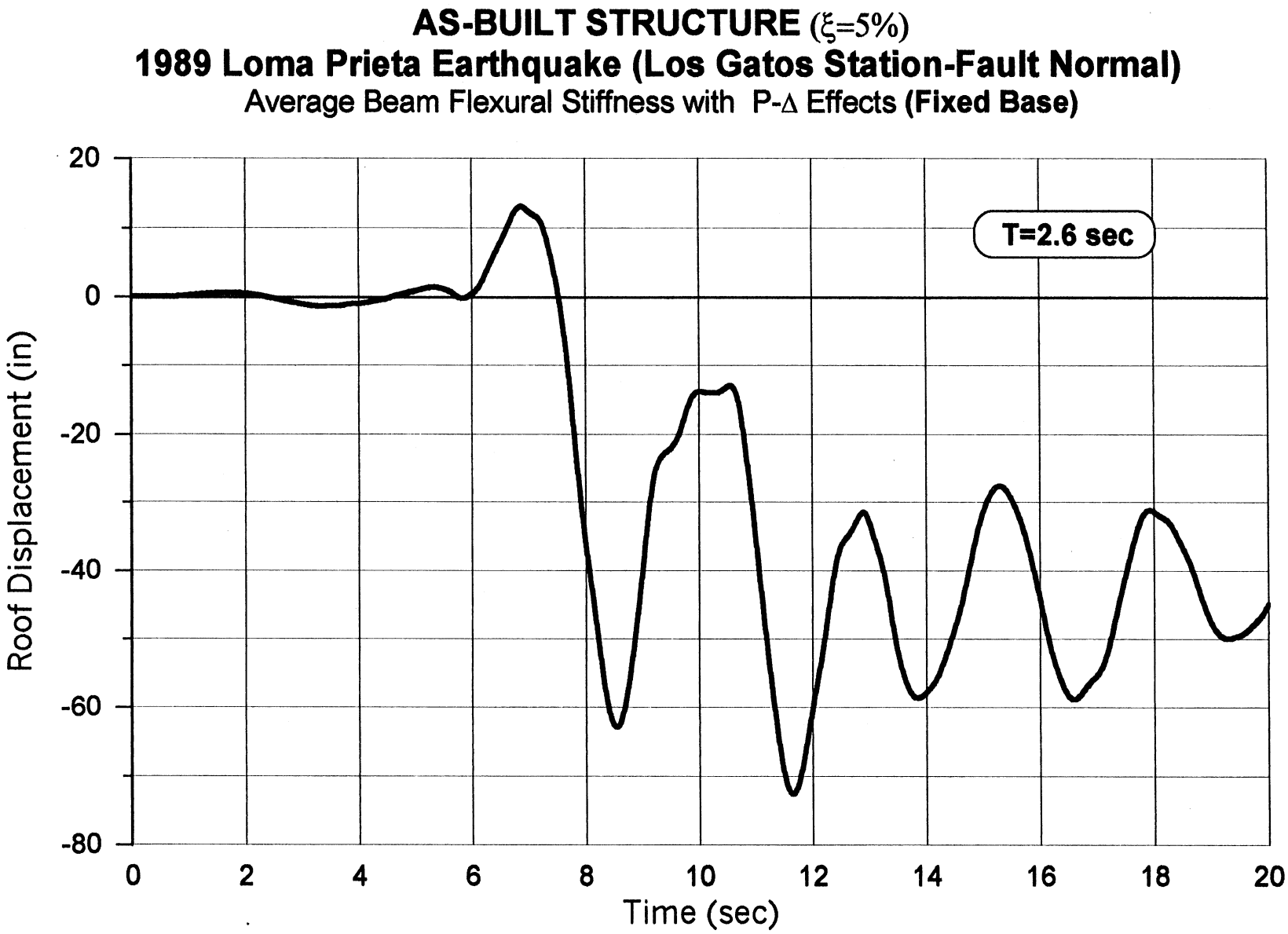

Figure 9.4 Time history of roof displacement.

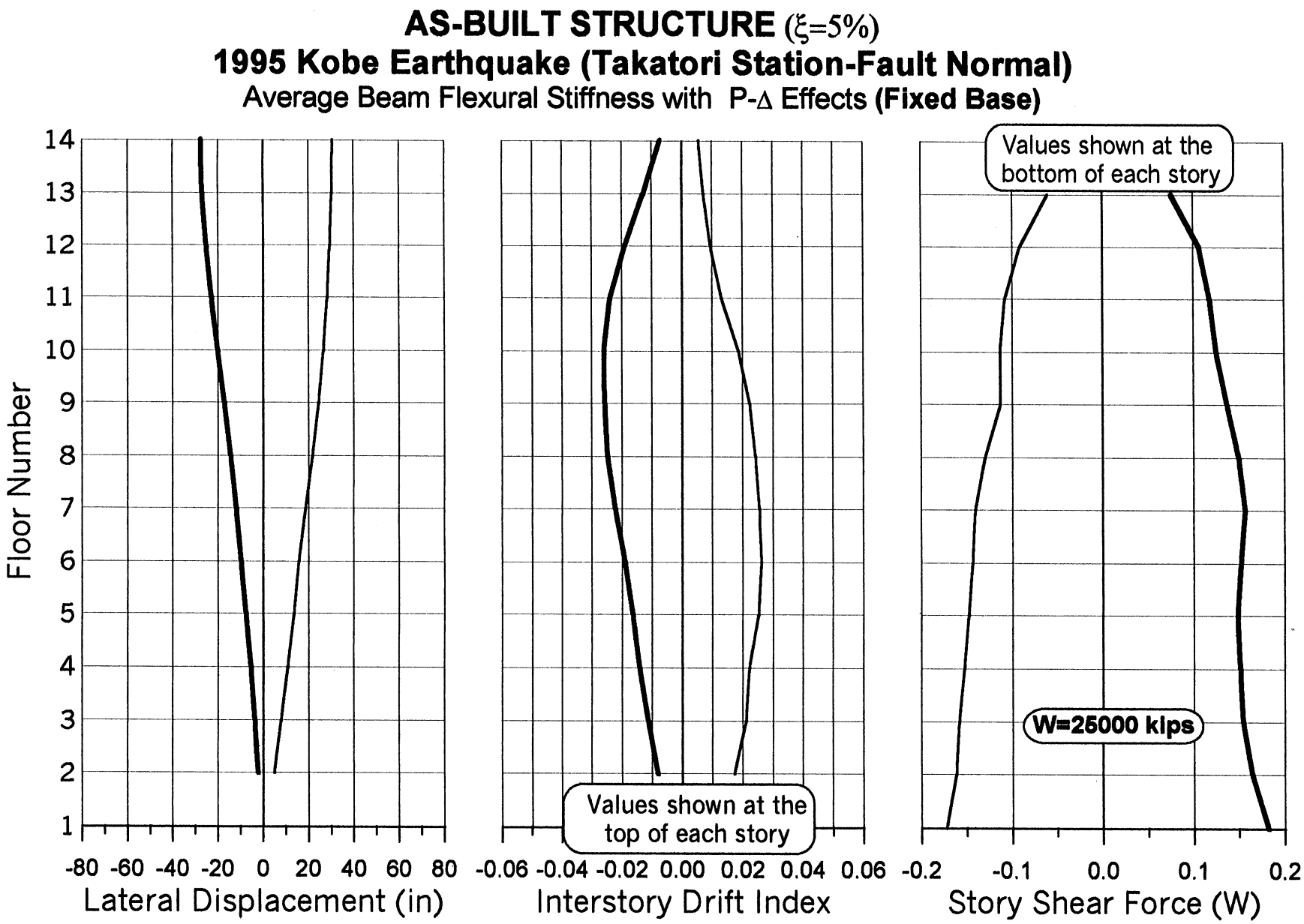

Figure 9.5 Lateral displacement, interstory drift index, and story shear force envelopes.

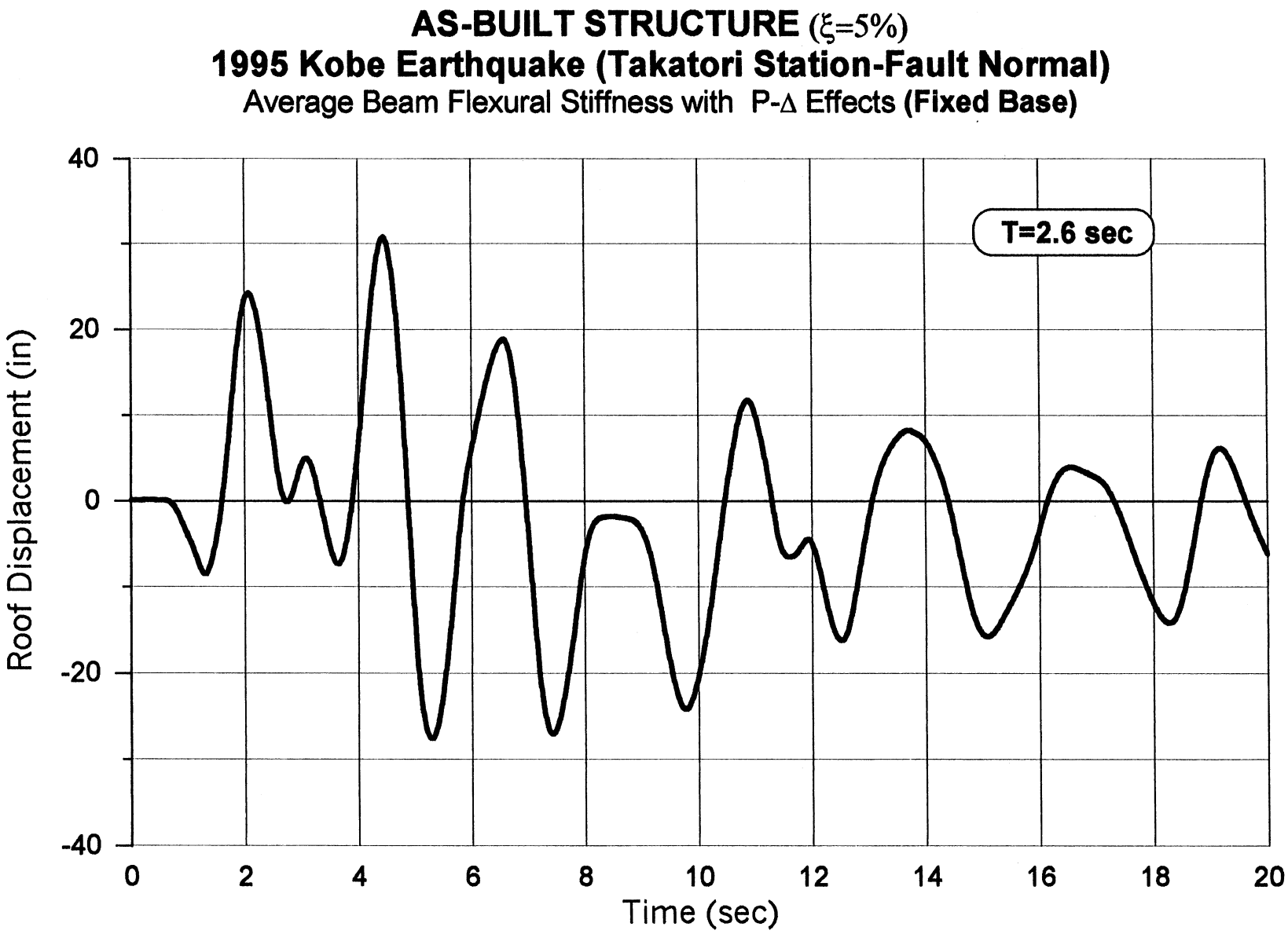

Figure 9.6 Time history of roof displacement.

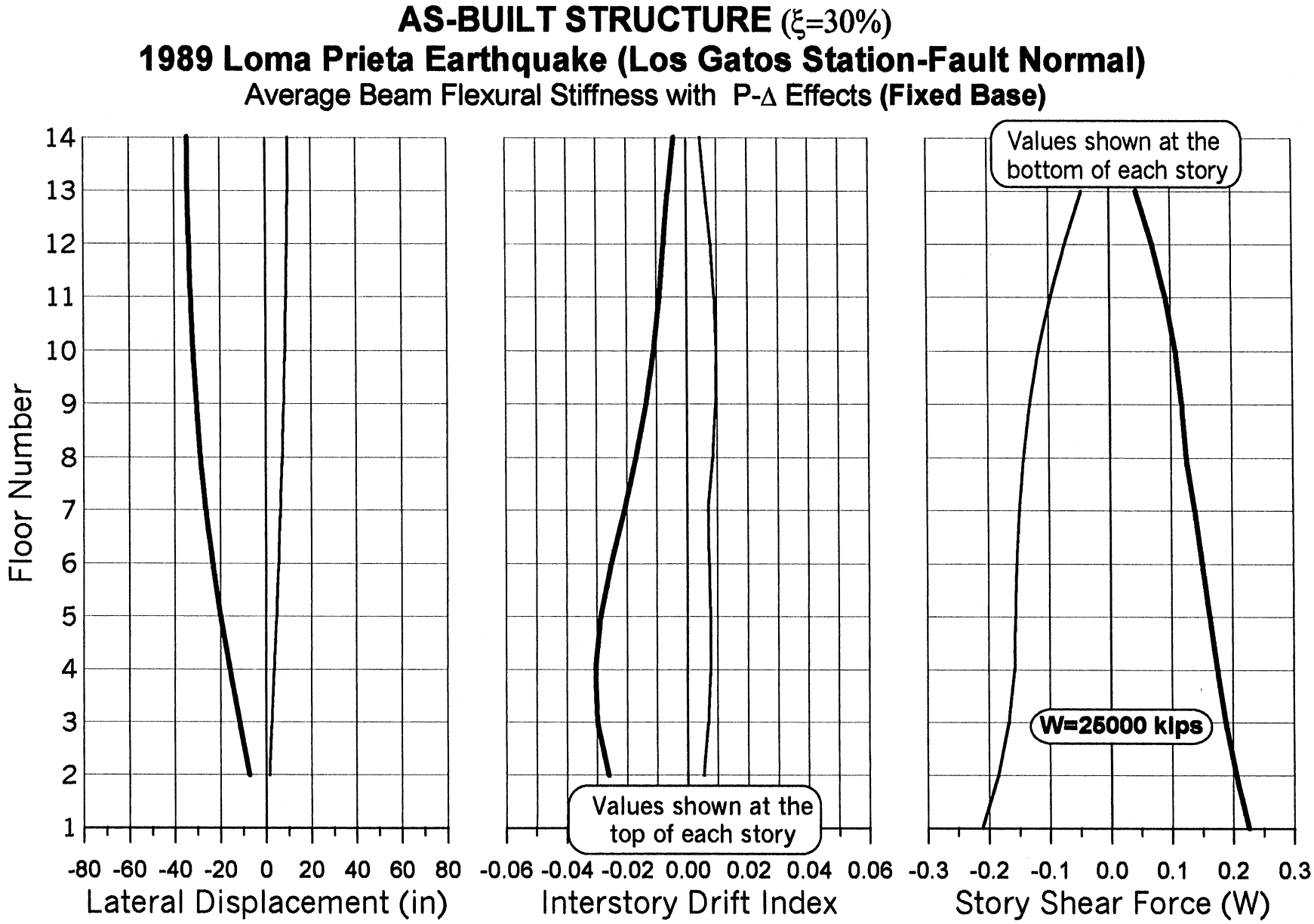

Figure 9.7 Lateral displacement, interstory drift index, and story shear force envelopes.

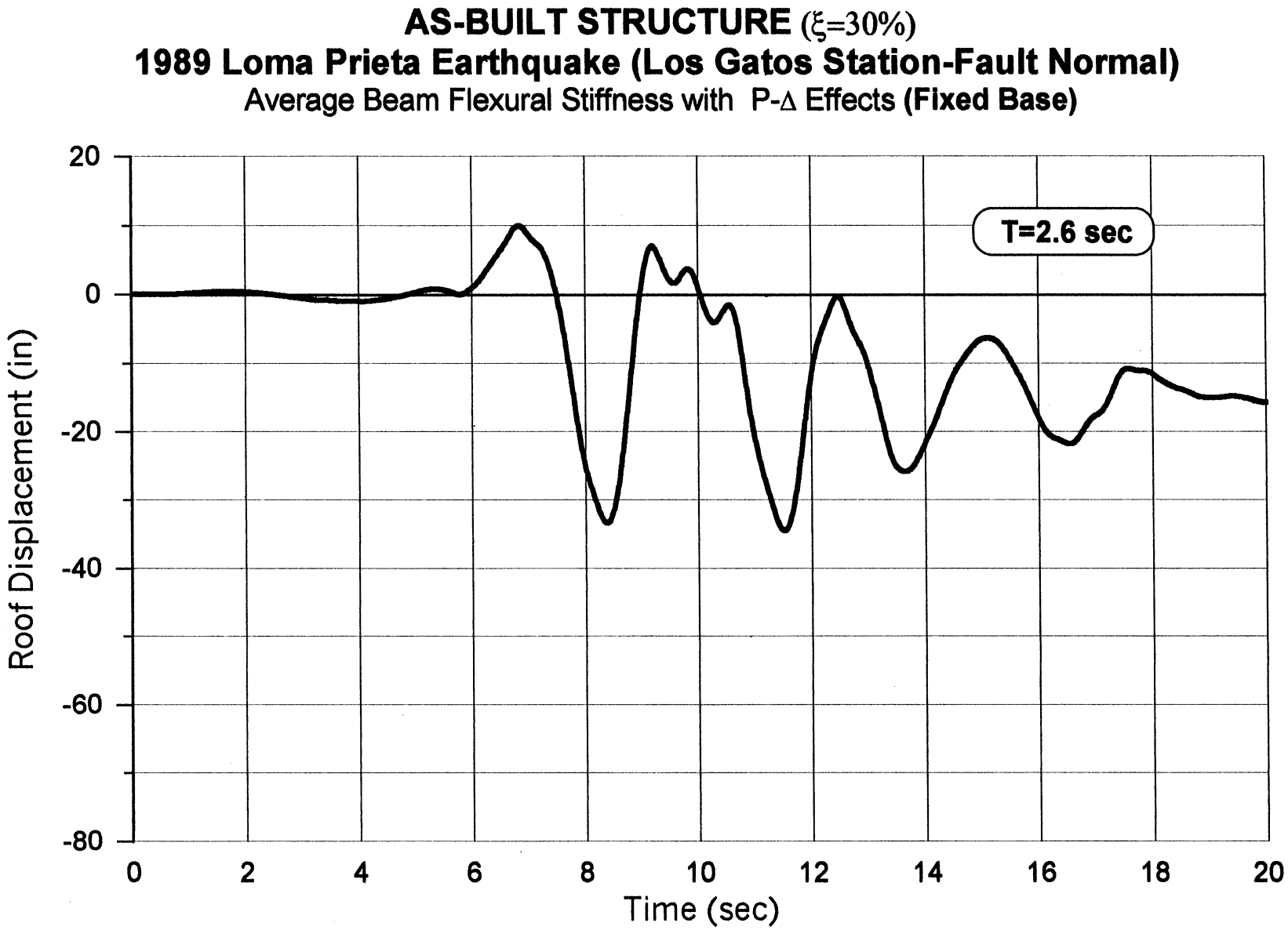

Figure 9.8 Time history of roof displacement.

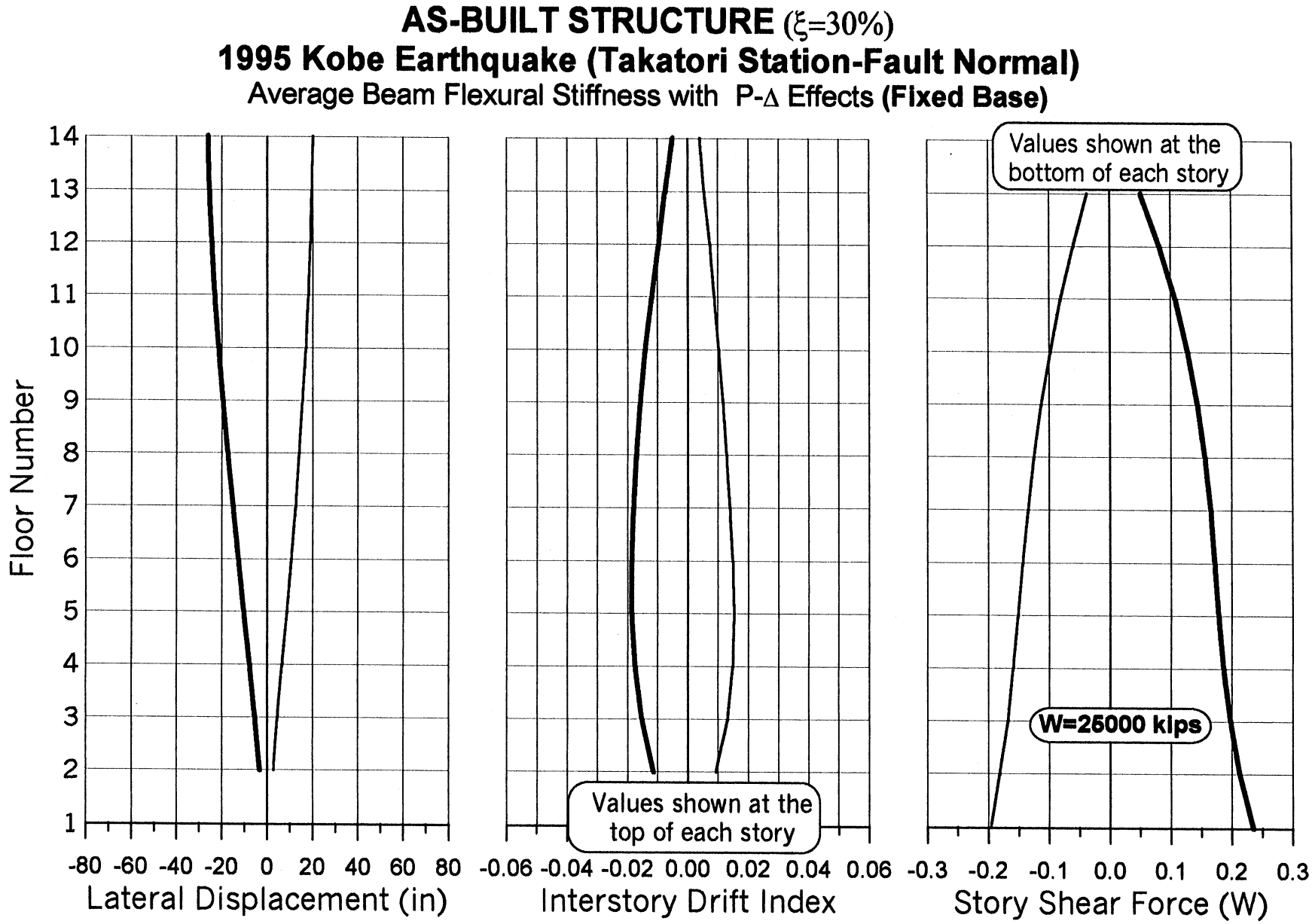

Figure 9.9 Lateral displacement, interstory drift index, and story shear force envelopes.

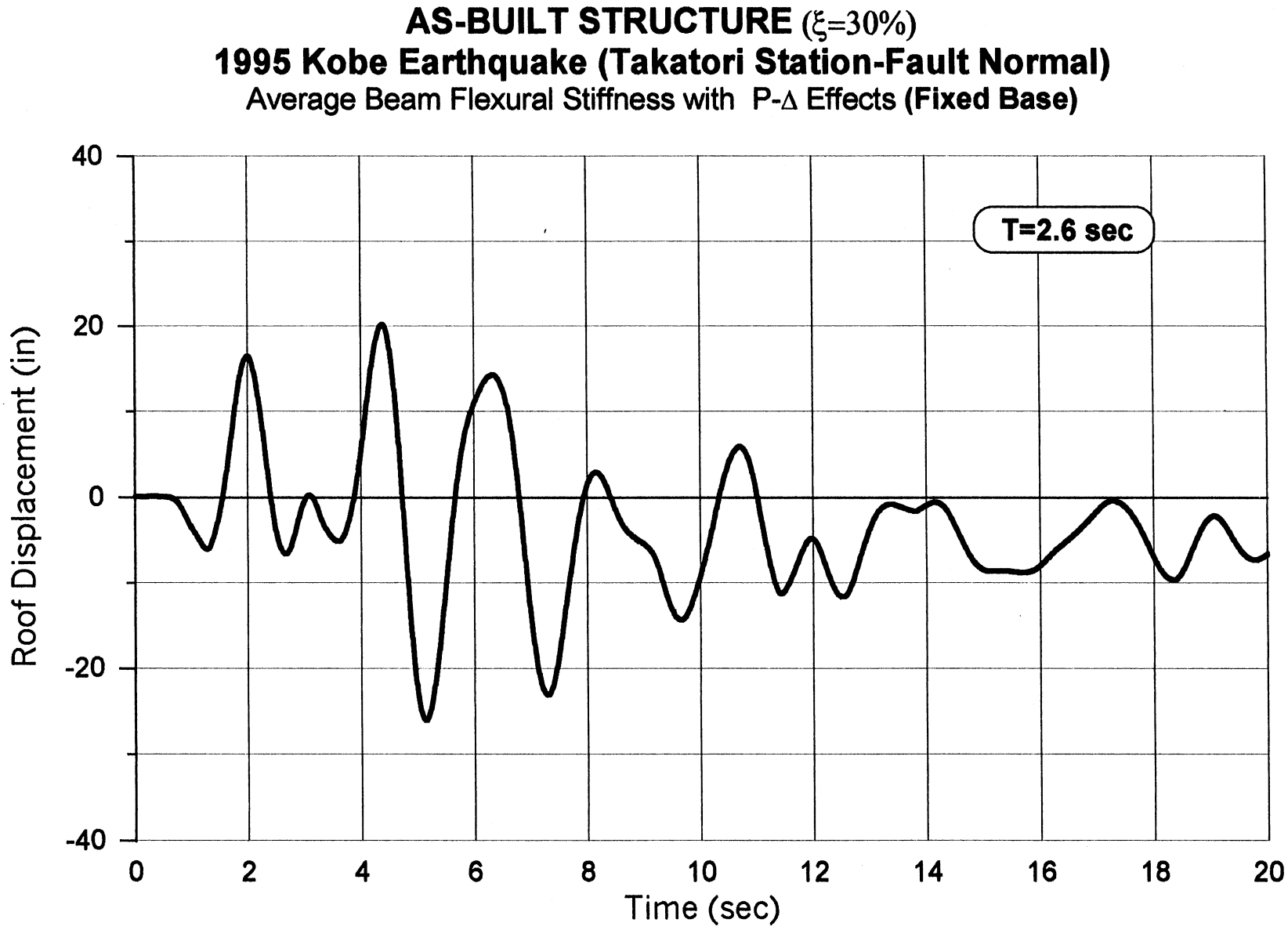

Figure 9.10 Time history of roof displacement.

10 Response of Retrofitted Building with Joint Steel Jacketing and Beam and Column Enhancement Plates

10.1 INTRODUCTORY REMARKS, SELECTION OF STRATEGY, AND GENERAL INFORMATION (CONVENTIONAL APPROACH OF INCREASING STIFFNESS, STRENGTH, AND DUCTILITY CAPACITIES)

A review of the design and the as-built drawings made it clear that the as-built structural system has several weaknesses being the main ones following: (1) inadequate transverse reinforcement along the height of the columns; (2) no adequate shear and confining transverse reinforcement at the girder-column joints; (3) lack of adequate amount and detailing of the longitudinal and transverse reinforcement along the girders; (4) lack of adequate anchorage of the girder bottom reinforcement at the joints; and (5) lack of adequate lap splicing of the longitudinal reinforcement.

The results from linear and nonlinear static (pushover) and dynamic (modal and time history) analyses of the as-built structure, discussed in chapters four through nine, show that the lateral stiffness of the structural system and the shear and flexural strength of most of the members are very low, particularly in the transverse direction (T_1=3.2 sec), and that due to the above weaknesses, the strength and deformation capacities are not adequate to restrict the effects of severe pulse-type EQGMs that could occur at the site of the building. Thus the building needs to be seismically upgraded to survive such types of EQGMs. The demanded deformation capacity (floor displacement, interstory drift index, IDI, and plastic rotations, θ_p) not only exceed the supplied capacities, but also are so large that could result in significant damage to nonstructural components, equipment and contents of the building, and thus are not acceptable.

Thus conventional (or traditional) strategies for upgrading the structural system are discussed in this chapter.

The conventional strategies for upgrading are based on increasing the stiffness or strength or ductility (or any combination of two or three of them). Among different techniques that have been used to achieve such strategies [being the most commonly used the addition of shear walls or braces (particularly steel braces) or steel jacketing of members], the most promising one appears to be the use of steel jacketing. Because of the above detected weaknesses, it becomes clear that it will be necessary not only to jacket the girder-column joints but also to enhance the toughness of the columns and beams. Thus it was decided to jacket also the columns and to encase the girders and a portion of their adjacent slabs.

After several preliminary attempts, it was decided to use ½-in.-thick enhancement plates for the beams at the second floor. To have a gradual variation of stiffness and strength over the height of the building, for the 3rd to 5th, 6th to 8th, 9th to 11th, and 12th to 14th floors, 7/16-in., 3/8-in., 1/4-in., and 3/16-in.-thick plates were used, respectively. The stress-strain relationships for reinforcing bars and for steel plates are shown in Figure 10.1. Assuming a certain spacing of support of the steel plates and its thickness, a maximum compressive strain of 0.02 is assumed to control the buckling of steel plates as well as the encased concrete compressive strain; the moment-curvature relationships for the retrofitted beam sections under negative bending moments are provided in Figures 10.2-10-6. As shown in Figures 10.7-10.11, for the sections under positive bending moments, a maximum compressive strain of about 0.005 to 0.007 results in almost the same level of maximum curvature (except for the second floor beams) as under negative bending moments with maximum compressive strain of 0.02. As discussed in section 4-2, the moment-rotation relationships for different beam segments are calculated. The results for the second and third floor beams are given in Figures 10.12-10.15.

Below, attempts are made to determine if beam rotation capacities are enough for the structure to resist successfully the effects of the two critical ground motions. The summation of the beam end yield moments of the retrofitted structure is almost 5 times that of the as-built structure (measured as and average at the third to fifth floors). Therefore, assuming that the retrofitted structure will have a beam mechanism, the yield strength of the structure should increase by the same ratio of about 5. Also, in an average sense, the beam flexural stiffness is increased by about five times. Therefore, assuming that for the retrofitted structure the beam flexibility is more important than column flexibility, the structure is almost five times stronger

and also five times stiffer (excluding the flexibility below the first-story columns). Therefore, in a pushover analysis under inverted triangularly lateral load distribution, the roof displacement at the first significant (idealized) yielding of the fixed-base structure remains almost the same as that of the as-built structure, which is about 12 in. Since for the as-built structure, the contribution of the foundation rotation in roof displacement at this yielding level in a pushover analysis is about 7 in., for a structure five times stronger, this contribution will be about 35 in. (it is assumed that the foundation is not modified and remains elastic). Regarding the period of the structure, the period of the as-built structure, is about 3.2 sec, of which 0.6 sec comes from the flexibility of the first-story column supports. By making the structure stiffer, the period of the fixed-base structure would be about $(3.2 - 0.6 \text{ sec}/\sqrt{5}) \approx 1.16 \text{ sec}$. Considering the fact that for the stiffer structure, the contribution of the foundation and basement flexibility would be larger than 0.6 sec, one can assume that the period of the retrofitted structure would be about 2 sec. Comparing Figures 6.4 and 6.6, at a period of about 2 sec, the Takatori record gives a spectral displacement of about 50 to 60 in. for a period of about 2 sec,, which is larger than that of the Los Gatos record. Since the yield displacement of the structure is about 35+12=47 in., the global ductility of the structure is less than about 1.3, and as a result a maximum displacement of about 55 in. should be reasonable. Assuming that this displacement occurs at the 2/3 of the height of the structure, the corresponding average plastic IDI is about (55-47)/[(2/3)*2000] = 0.006 radian. Note that (55-47) in./(2/3) = 12 in. is the plastic displacement. Looking at Figures 10.12-10.15, the beam plastic rotation capacity is more than 0.006; therefore, if the maximum IDI is not significantly larger than the average IDI for the bottom 2/3 of the height of the structure, the rotation capacity seems to be enough.

For all the columns, ½-in.-thick enhancement plates are used. The moment-axial load interaction diagrams for the second story columns of interior frames with and without strength reduction factor Φ are shown in Figures 10.16 and 10.17.

Note that in the structural model of the retrofitted building, it is assumed that there is no bond slip at the joints.

10.2 STRUCTURE WITH FOUNDATION AND BASEMENT FLEXIBILITY

10.2.1 Pushover Analysis under Inverted Triangularly Distributed Lateral Load

Accounting for P-Δ effect, at a roof displacement of 100 in., the displacement, interstory drift index, and the story shear force envelopes are given in Figure 10.18. A maximum interstory drift of 12.3% occurs at the first story as a consequence of the envelopment of a story mechanism at this first story. The first-story column plastic hinge rotation varies from 6.9% to 11.4%. To see if the same story mechanism could form under the recorded ground motions, the displacement, interstory drift index, and the story shear force envelopes under the Los Gatos are calculated and shown in Figure 10.19. Although the maximum displacement at the roof is only about 43 in., the same story mechanism is developed. To avoid a weak-column strong-beam system, the first-story column ½-in.-thick plates are replaced by 1-in.-thick plates. The moment-axial load interaction diagrams for the first-story columns of interior frames with 1-in. enhancement plates are shown in Figures 10.20 and 10.21.

Using 1-in.-thick enhancement plates for the first-story columns, at a roof displacement of 100 in., the displacement, interstory drift index, and the story shear force envelopes obtained from a pushover analysis are shown in Figure 10.22. As can be seen from the IDI, the story mechanism seems to be avoided. The maximum interstory drift of 7% occurs at the third and fourth stories, while the global drift index is about 5%, of which 2% comes from the foundation rotation. The maximum base shear (17900 kips) is about 64% of the weight of the building, (W=28000 kips).

It should be noted that for a lateral roof displacement of about 50 in., compared to the as-built structure, the base shear (and almost proportionally the overturning moment) is increased by a factor of about 4.0. In other words, the pile foundation undergoes forces about 4.3 times the forces corresponding to the as-built structure. As discussed in chapter four, at least 0.6 sec of the 3.2 sec period of the as-built structure comes from the foundation rocking, and probably the damage observed in the basement shear walls during the Northridge earthquake was due to the shear forces transferred to the shear walls as a result of the rocking behavior. Now, having much larger forces transferred to the foundation, retrofitting of the foundation needs to be studied, which is beyond the scope of this report.

Figure 10.23 shows the base shear versus roof displacement. The global displacement ductility is about 2.3. The bilinear yield equivalent displacement is about 44 in. The maximum

beam plastic rotation is about 3.3% and occurs at the fourth floor beams of the interior frames, under negative bending moment. The maximum plastic rotations at the bottom of the first-story columns varies from 2.9% to 3.6%. It should be noted that the interior (center) columns of exterior frames develop plastic hinges at stories above the first story as well with large plastic rotations (4.3% at the second story), which suggests that these columns need to be made even stronger.

10.2.2 Response of Building under Pulse-Type Ground Motions

10.2.2.1 Response of structure with 5% damping

10-2-2-1-A 1989 Loma Prieta earthquake ground motion recorded at Los Gatos station. The period of the structure is about 2.3 sec. The displacement, interstory drift index, and the story shear force envelops under the Los Gatos ground motion are given in Figure 10.24. The maximum roof displacement is about 61 in. From Figure 10.23, the yield displacement is about 44 in., therefore, the global displacement ductility is about 1.4. The maximum interstory drift of 3.8% occurs at the fourth and fifth stories, while the global drift index is about 3.1%. Note that about 1.9% of the drift is caused by the foundation rotation; therefore, the maximum tangential IDI is about 1.9%, which could be acceptable. The maximum beam plastic rotation is about 1.1% and occurs at the 5th floor of the interior frames, which is smaller than the plastic rotation capacity of the beam as shown in Figure 10.15. The maximum column plastic rotation, which occurs at the base of the first-story columns, is about 1.4%. For interior frames, the column plastic hinges above the first story occurs only at the bottom of the second story, with a maximum of 0.5%. However, plastic hinges at many stories above the first story are developed at the center columns of the exterior frames. The maximum base shear is about 58% of the weight of the building. The time history of the roof displacement is shown in Figure 10.25.

Figure 6.4 shows the yield coefficient and displacement spectra during the 1989 Loma Prieta earthquake recorded at Los Gatos station. Since the global displacement ductility of the response of the structural model is about 1.4, at a period of 2.3 sec, the displacement spectra suggest a maximum displacement of about 50 in., which is larger than the maximum displacement of 44 in. at the 2/3 of the height of the building; see Figures 10.24 (to be representative of an equivalent single-degree-of-freedom system). The yield coefficient spectra suggest a yield coefficient, C_y, of about 0.66. In spite of the fact that C_y does include the

damping force, it suggests a larger base shear compared to the base shear found from the inelastic analysis of the building, which is about 0.58W. It should be noted that the single-degree-of-freedom system that is considered in the development of the spectra does not have any strain hardening and that the P-Δ effect is not included either.

10-2-2-1-B 1995 Kobe earthquake ground motions recorded at Takatori station. The displacement, interstory drift index, and the story shear force envelopes under the Takatori ground motion are given in Figure 10.26. The maximum roof displacement is about 60 in. Assuming a yield displacement of 44 in. (see Figure 10.23) the global displacement ductility is about 1.4. The maximum interstory drift of 3.7% occurs at the 5^{th} and 6^{th} stories, while the global drift index is about 3.1%. Note that about 1.8% of the drift is caused by the foundation rotation; therefore, the maximum tangential IDI is about 1.9%, which could be acceptable. The values of the plastic hinge rotations are fairly similar to those under the Los Gatos recorded ground motion. The maximum base shear is about 58% of the weight of the building. The time history of the roof displacement is shown in Figure 10.27.

Figure 6.6 shows the yield coefficient and displacement spectra during the 1995 Kobe earthquake recorded at Takatori station. The global displacement ductility of the response of the structural model is about 1.4. At a period of about 2.3 sec, the displacement spectra for ductility equal 2 shows a sudden drop. Interpolating the spectral value at T=2.3 sec between curves for ductilities equal to 1.0 and 2.0 suggests a maximum displacement of about 55 in., which is larger than the maximum displacement of about 43 in. at the 2/3 of the height of the building (to be representative of an equivalent single-degree-of-freedom system). It should be noted that, between T=2.3 sec and 2.4 sec, as a result of yielding of the SDOF system prior to the excursion corresponding to maximum displacement, there is a sudden drop in spectral values. The yield coefficient spectra suggest a yield coefficient, Cy, of about 0.8, which suggests a larger base shear compared to the base shear found from the inelastic analysis of the building which is about 0.58W.

10.2.2.2 Response of structure with 30% damping

10-2-2-2-A 1989 Loma Prieta earthquake ground motions recorded at Los Gatos station. The displacement, interstory drift index, and the story shear force envelopes under the Los Gatos ground motion are given in Figure 10.28. The time history of the roof displacement is shown in

Figure 10.29. The maximum roof displacement is about 31 in., which is less than the yield displacement. By increasing the damping coefficient from 0.05 to 0.30, the maximum roof displacement and the maximum IDI dropped by about 50%. Excluding a 1% drift caused by the foundation rocking, the maximum IDI is only about 0.7%. The maximum base shear is also dropped by about 40%, to a value of about 0.35W.

10-2-2-2-B 1995 Kobe earthquake recorded at Takatori station. The displacement, interstory drift index, and the story shear force envelopes under the Takatori ground motion are given in Figure 10.30. The time history of the roof displacement is shown in Figure 10.31. The maximum roof displacement is about 33 in., which is less than the yield displacement. By increasing the damping coefficient from 0.05 to 0.30, the maximum roof displacement and the maximum IDI dropped by about 45%. Excluding a 1% drift caused by the foundation rocking, the maximum IDI is only about 0.8%. The maximum base shear is also dropped by about 40%.

10.2.2.3 Response of structure with thicker enhancement plates for first 3 story columns with 5% damping under Los Gatos ground motion

To minimize the formation of column plastic hinges in the stories above the first story, 1-in.-thick enhancement plates are used for the first three story columns. Figure 10.32 shows the displacement, interstory drift index, and the story shear force envelopes under the Los Gatos ground motions, which is very similar to Figure 10.24 (i.e., when 1-in. plates are used only for the first-story columns). For interior frames, there is no column plastic hinges formed above except at the base of the first story columns. However, still the center columns of the exterior frames (i.e., the frames at the end of the building) undergo a maximum plastic rotation of about 0.5% above the first three stories.

10.3 STRUCTURE WITH FIXED-BASE SUPPORTS

The first period of the fixed-base structural model in the transverse direction is about 1.3 sec.

10.3.1 Pushover Analysis under Inverted Triangularly Distributed Lateral Load

Including the P-Δ effect, at a roof displacement of 100 in., the displacement, interstory drift index, and the story shear force envelopes are given in Figure 10.33. The maximum interstory drift of 7.6% occurs at the fourth stories, while the global drift index is about 5%. The maximum

base shear is about 71% of the weight of the building. Figure 10.34 shows the base shear versus roof displacement. The global displacement ductility is about 6.7. The yield displacement for the bilinear idealization is about 15 in. The maximum beam plastic rotation is about 5% and occurs at the fourth floor beams of the interior frames. Except for the interior columns of the exterior frames, there is no development of plastic hinges in the columns above the first story. The maximum first-story column base plastic rotation is about 6.4%.

10.3.2 Response of Building under Pulse-Type Ground Motions

10.3.2.1 Response of structure with 5% damping

10-3-2-1-A 1989 Loma Prieta earthquake ground motions recorded at Los Gatos station. The displacement, interstory drift index, and the story shear force envelops under the Los Gatos ground motion are given in Figure 10.35. The maximum roof displacement is about 23 in. Assuming a yield displacement of 15 in., the global displacement ductility is about 1.5. The maximum interstory drift of 1.7% occurs at the fourth and fifth stories, while the global drift index is about 1.2%. Note that in the case of structure with the flexibility at the base, the maximum roof displacement and maximum IDI, excluding the effects of foundation rotation, are about 24 in. and 1.9%, respectively which are close to the values found here.

The time history of the roof displacement is shown in Figure 10.36. The maximum base shear is about 60% of the weight of the building. For the structure with base flexibility, this value was about 0.58 W.

Figure 6.4 shows the yield coefficient and displacement spectra during the 1989 Loma Prieta Earthquake recorded at Los Gatos station. Since the global displacement ductility of the response of the structural model is about 1.5, the displacement spectra suggest a maximum displacement of about 22 in., which is bit larger than the 19-in. building maximum displacement at 2/3 of the height. The yield coefficient spectra suggest a yield coefficient, C_y, of about 0.88. In spite of the fact that C_y does include the damping force, it suggests a larger base shear compared to the base shear found from the inelastic analysis of the building which was about 0.60W. It should be noted that the single-degree-of-freedom system that is considered in the development of the spectra does not have any strain hardening and that the P-Δ effect is not included either.

10-3-2-1-B 1995 Kobe earthquake recorded at Takatori station. The displacement, interstory drift index, and the story shear force envelopes under the Takatori ground motion are given in Figure 10.37. The maximum roof displacement is about 37 in. Based on the results shown in Figure 10.34, the yield displacement is about 15 in.; thus, the global displacement ductility is about 2.5. The maximum interstory drift of 2.8% occurs at the fifth stories (larger than 2%), while the global drift index is about 1.9%. The response of the structure to the Los Gatos ground motions for the fixed-base structure was very close to the results for the structure with base flexibility, if the effects of foundation rocking were excluded. On the other hand, under the Takatori recorded ground motion, that is not the case. For instance, in the case of structure with the flexibility at the base, the maximum roof displacement and maximum IDI, excluding the effects of foundation rotation, are about 24 in. and 1.9%, respectively, which are about 2/3 of the values found for the fixed-base structure.

The time history of the roof displacement is shown in Figure 10.38. The maximum base shear is about 66% of the weight of the building. For the structure with base flexibility, this value was about 0.58 W.

Figure 6.6 shows the yield coefficient and displacement spectra for the EQGMs recorded at Takatori station during the 1995 Kobe Earthquake. Since the global displacement ductility of the response of the structural model is about 2.5, the displacement spectra suggest a maximum displacement of about 30 in., which is very close to the 31 in. building maximum displacement at 2/3 of the height. The yield coefficient spectra suggest a yield coefficient, C_y, of about 0.80, which suggests a base shear larger than the base shear found from the inelastic analysis of the building, which was about 0.66W.

10.3.2.2 Response of structure with 30% damping

10-3-2-2-A 1989 Loma Prieta earthquake ground motions recorded at Los Gatos station. The displacement, interstory drift index, and the story shear force envelopes under the Los Gatos ground motion are given in Figure 10.39. The time history of the roof displacement is shown in Figure 10.40. By increasing the damping coefficient from 0.05 to 0.30, the maximum roof displacement and the maximum IDI dropped by about 35% and 40%, respectively. The IDI_{max} is equal to 1.0%, which occurs at the fourth and fifth stories. There is also a small reduction of about 5% in the base shear.

10-3-2-2-B 1995 Kobe earthquake ground motions recorded at Takatori station. The displacement, interstory drift index, and the story shear force envelopes under the Takatori ground motion are given in Figure 10.41. The time history of the roof displacement is shown in Figure 10.42. By increasing the damping coefficient from 0.05 to 0.30, the maximum roof displacement and the maximum IDI dropped by about 45% and 50%, respectively, but there is a small increase of about 8% in the base shear.

10.4 SUMMARY

Some of the results of the analyses carried out on the retrofitted structure jacketing and encasing of different structural components with enhancement steel plates are summarized in Tables 10.1. For a definition of the parameters see Section 9-3. By adding enhancement steel plates, the maximum IDI_{tang} for the structure with rocking foundation is reduced to 1.9% (see Table 10.1) which could be acceptable. However, for the fixed-base structure $IDI_{max} = IDI_{tang}$ is about 2.8%. Furthermore, the maximum base shear forces for the retrofitted structures with foundation rocking is about 0.58W, which is too large a value to be carried by an already flexible pile foundation that is designed against much smaller forces. Analyzing the degree of improvement in the performance (response) of the building through nonlinear static (pushover) and dynamic (time-history) analyses, it is concluded that this conventional strategy will not lead to an efficient economical solution.

For the retrofitted structures with foundation rocking, increasing the damping coefficient from 0.05 to 0.30 could reduce the base shear to about 0.35W (see Figure 10.28). Unlike for the structure with foundation rocking, if the base were fixed, increasing damping could result in larger base shear forces.

It was also observed that the displacement response spectra determined from the use of the SDOF overestimate the structural displacements and the base shear forces. In some cases this overestimation could have been explained by sudden reduction of the response spectra for a bit larger structural period. For a more detailed discussion of the comparison of the results obtained from the response of SDOF systems and the MDOF structure, see Section 8-3. Although the spectral base shear forces are fairly close to the results of nonlinear analyses, one has to bear in mind that the spectral responses presented in this report do not include the viscous damping forces nor do they include the P-Δ effects, and while the first one results in smaller base shear, the second one increases the base shear forces.

As far as the IDI is concerned, one can observe that IDI_{max} varies from 1.1 to 1.5 times IDI_{ave}, which again suggests that using IDI_{ave} instead of IDI_{max}, as is done in some seismic provisions and/or guidelines, is not conservative.

Table 10.1 Summary of the results for the retrofitted structure (W≈28000 kips & H≈2000 inches).

Type of Supports	Response Parameters	Pushover Analysis[1]	Los Gatos Ground Motion (1989 Loma Prieta Earthquake)			Takatori Ground Motion (1995 Kobe Earthquake)		
			Spectral Response[2] (ξ =5%)	Dynamic Analysis[1] (ξ =5%)	Dynamic Analysis[1] (ξ =30%)	Spectral Response[2] (ξ =5%)	Dynamic Analysis[1] (ξ =5%)	Dynamic Analysis[1] (ξ =30%)
Basement & Foundation Flexibility Included (T=2.3 sec) (Δ_y≈44 in)	Δ_{top} (in)	100(μ=2.3)		61 (μ=1.4)	31		60 (μ=1.4)	33
	$\Delta_{2/3H}$ (in)	78	50	44	21	55	43	22
	IDI_{ave}	5.0%		3.1%	1.6%		3.1%	1.7%
	IDI_{max}	7.0%		3.8%	1.7%		3.7%	1.8%
	IDI_{ratio}	1.4		1.2	1.1		1.2	1.1
	$max\theta_{found}$	2.0%		1.9%	1.0%		1.8%	1.0%
	IDI_{tang}	5.0%		1.9%	0.7%		1.9%	0.8%
	V_{base} (W%)	64%	66%[3]	58%[4]	35%[4]	68%[3]	58%[4]	35%[4]
Fixed-Base (T=1.3 sec) (Δ_y≈15 in)	Δ_{top} (in)	100(μ=6.7)		23 (μ=1.5)	15		37 (μ=2.5)	21
	$\Delta_{2/3H}$ (in)	89	18	19	10	31	32	16
	IDI_{ave}	5.0%		1.2%	0.75%		1.9%	1.1%
	IDI_{max}	7.6%		1.7%	1.0%		2.8%	1.5%
	IDI_{ratio}	1.5		1.4	1.3		1.5	1.4
	V_{base} (W%)	71%	73%[3]	60%[4]	56%[4]	76%[3]	66%[4]	71%[4]

(1) P-Δ effects are included.
(2) Single Degree of Freedom system is elastic-perfectly plastic and P-Δ effect is not included (response for corresponding ductility).
(3) Viscous damping forces not included.
(4) Viscous damping forces included.

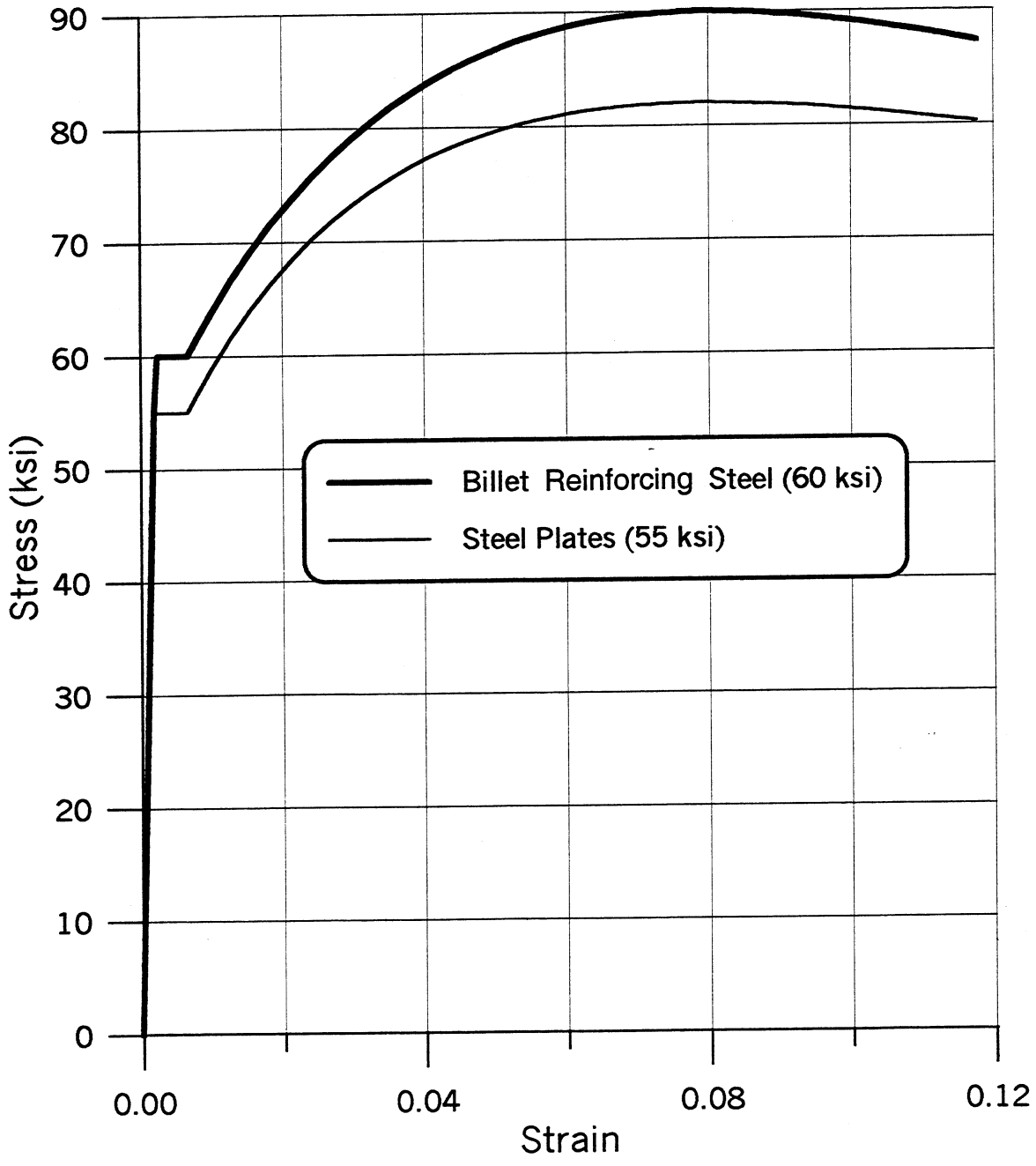

Figure 10.1 Steel stress-strain relationships.

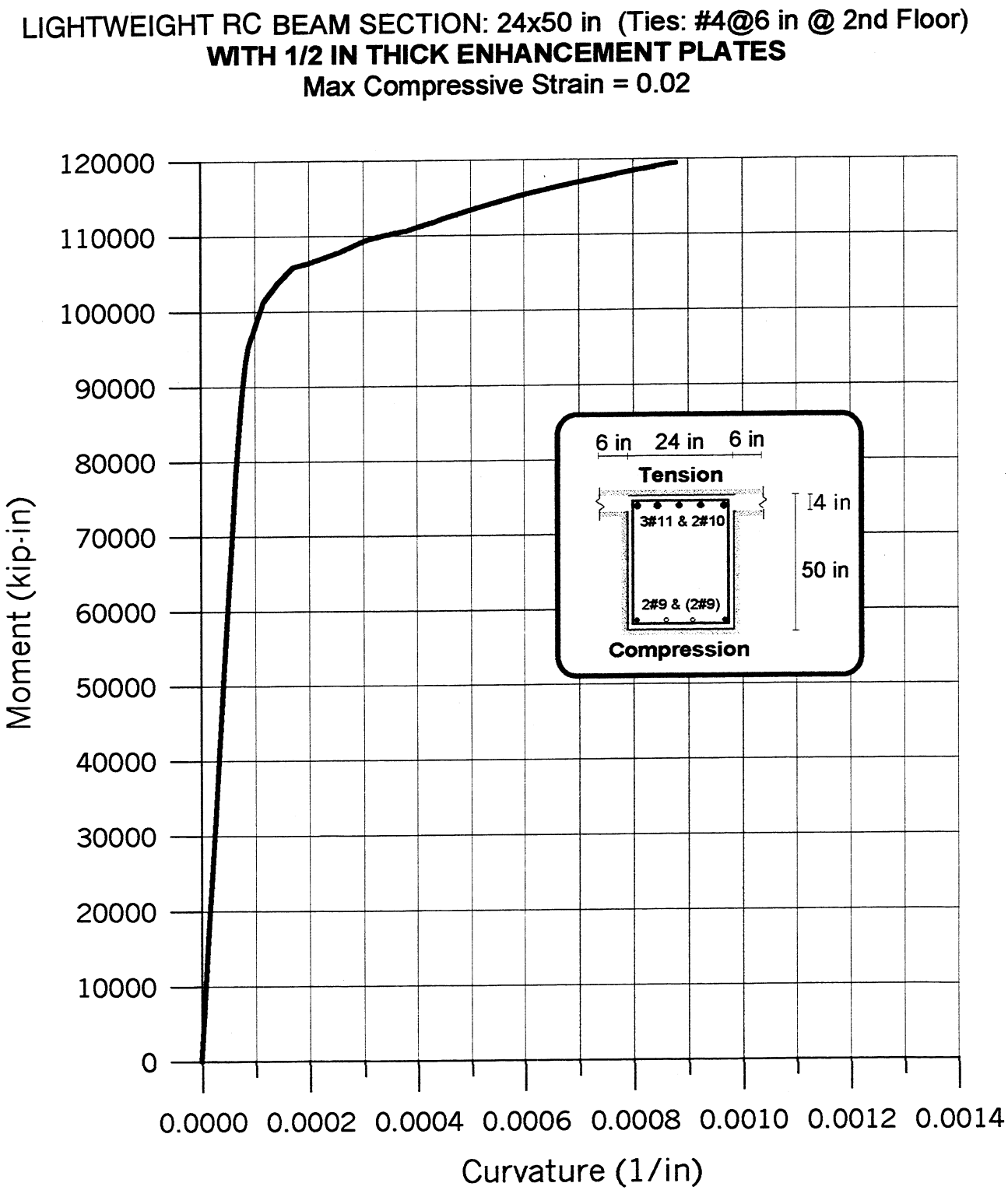

Figure 10.2 Moment-curvature relationship for retrofitted beams at second floor.

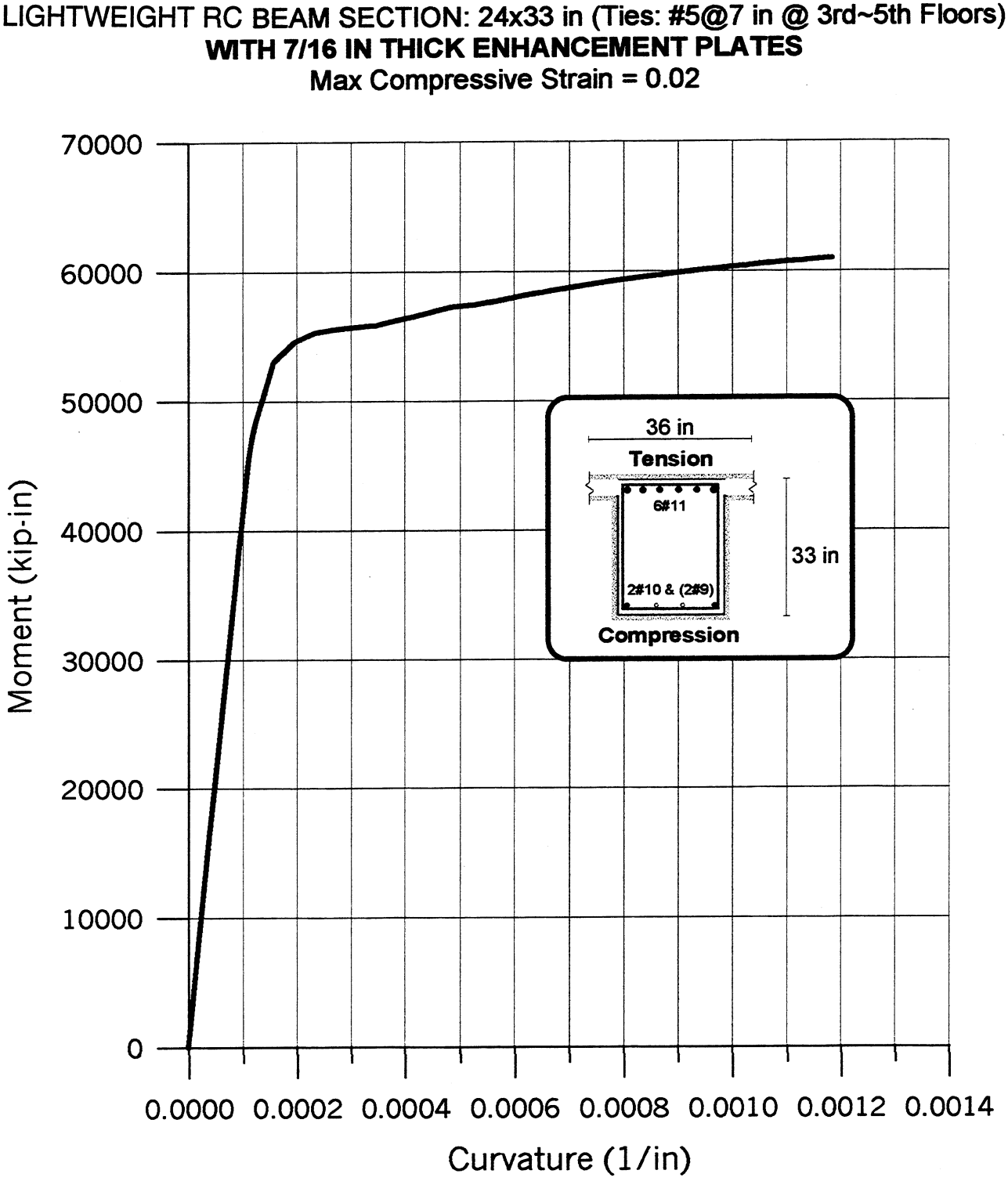

Figure 10.3 Moment-curvature relationship for retrofitted beams at 3rd to 5th floors.

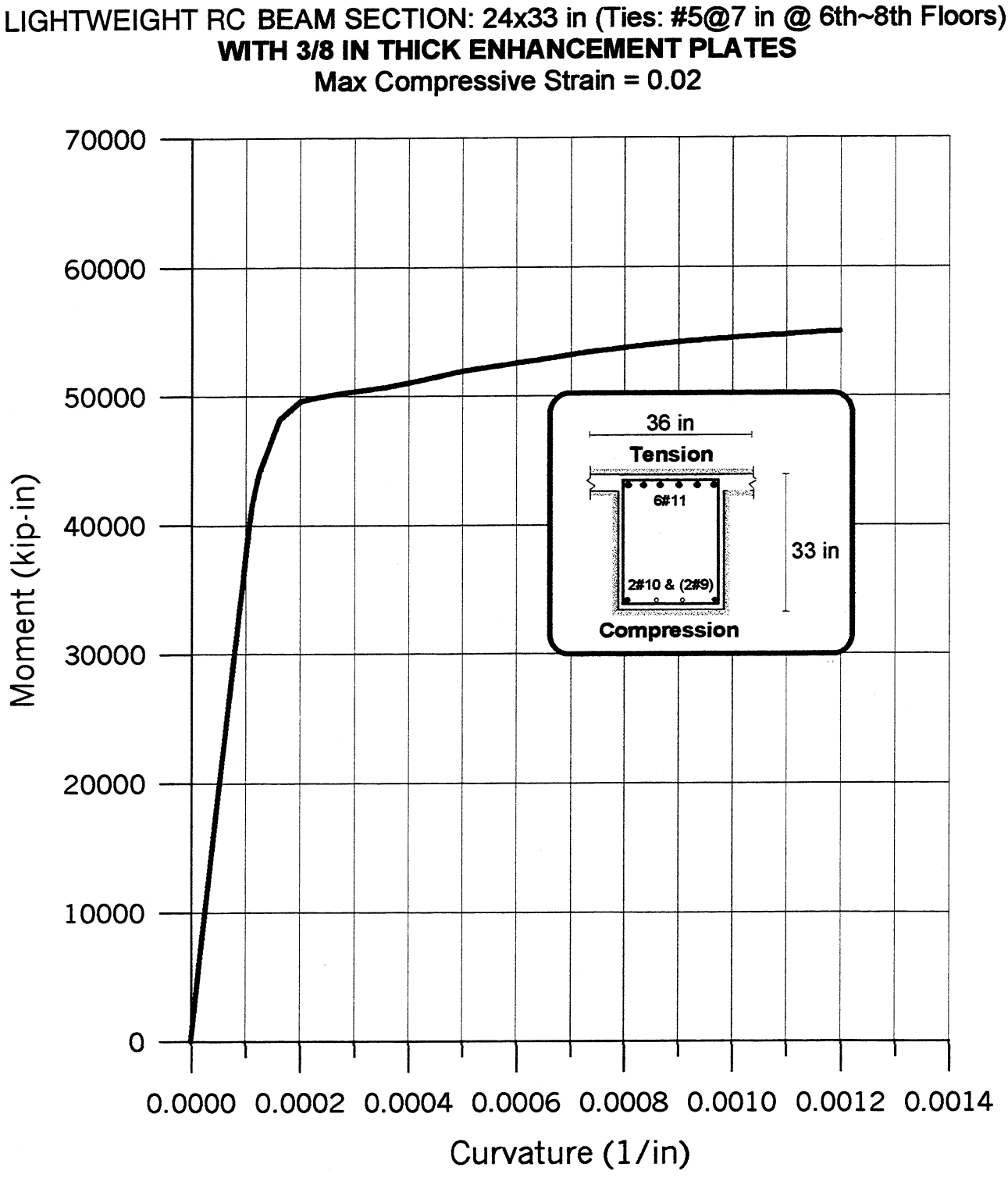

Figure 10.4 Moment-curvature relationship for retrofitted beams at 6th to 8th floors.

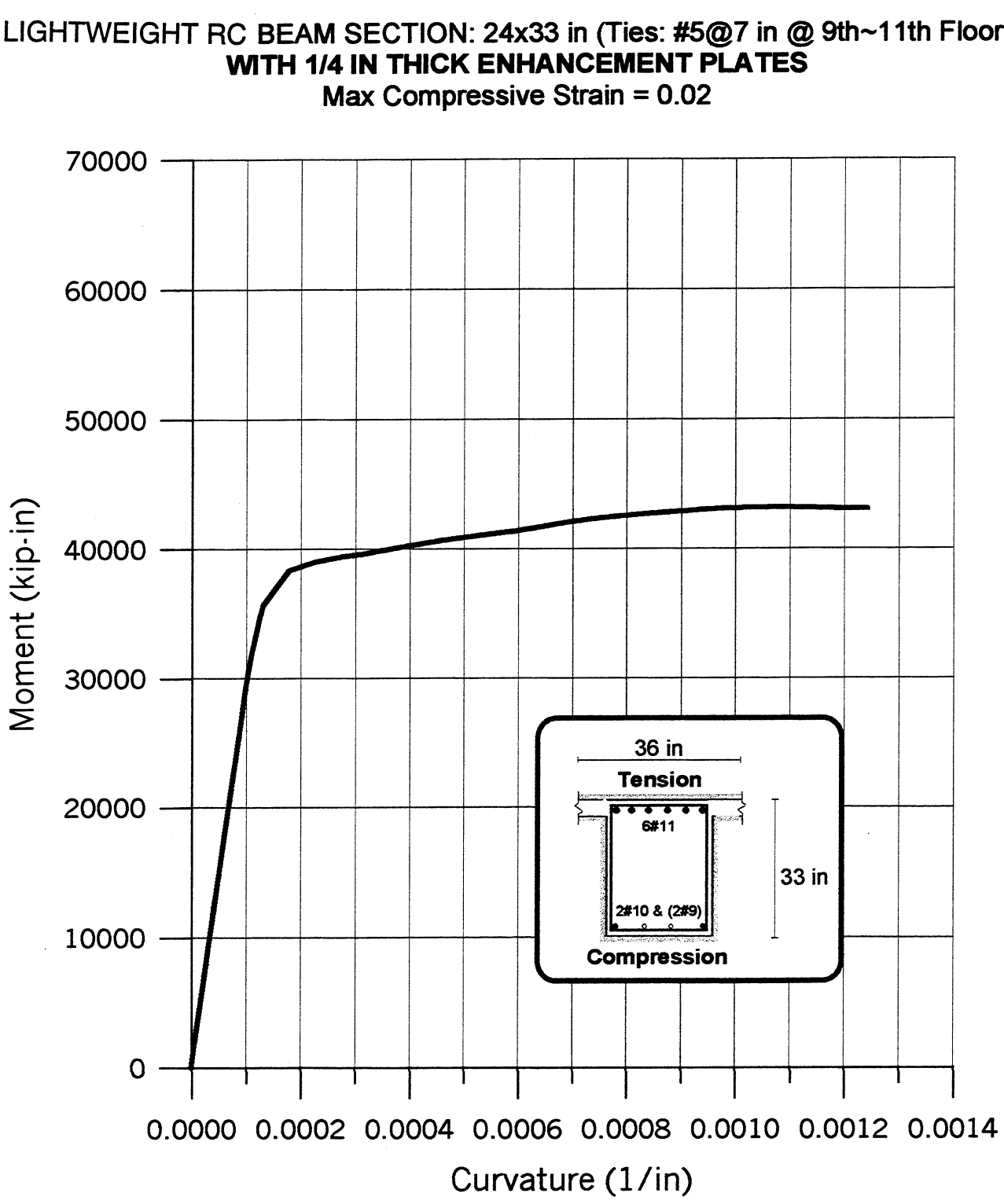

Figure 10.5 Moment-curvature relationship for retrofitted beams at 9th to11th floors.

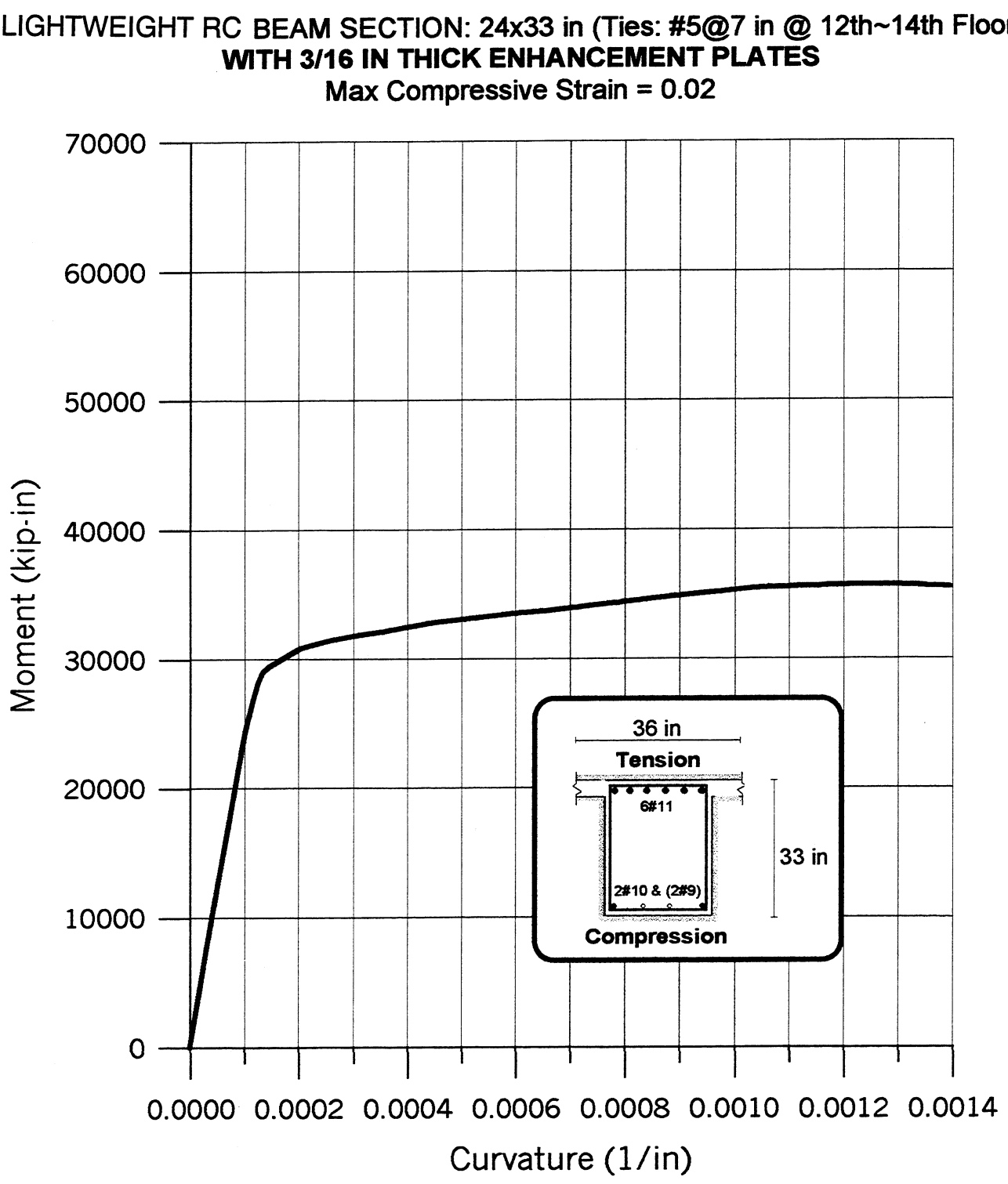

Figure 10.6 Moment-curvature relationship for retrofitted beams at 12th to14th floors.

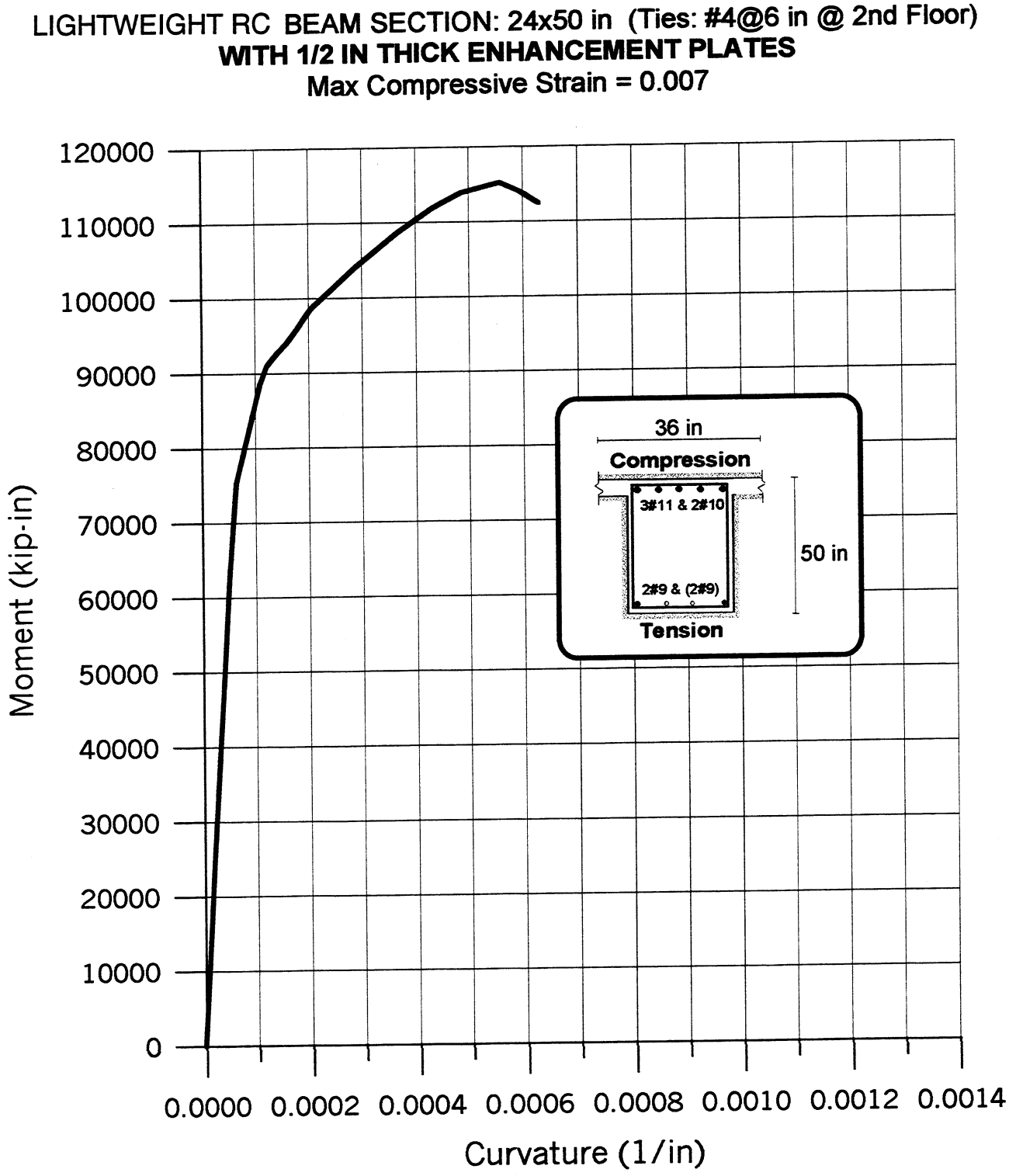

Figure 10.7 Moment-curvature relationship for retrofitted beams at second floor.

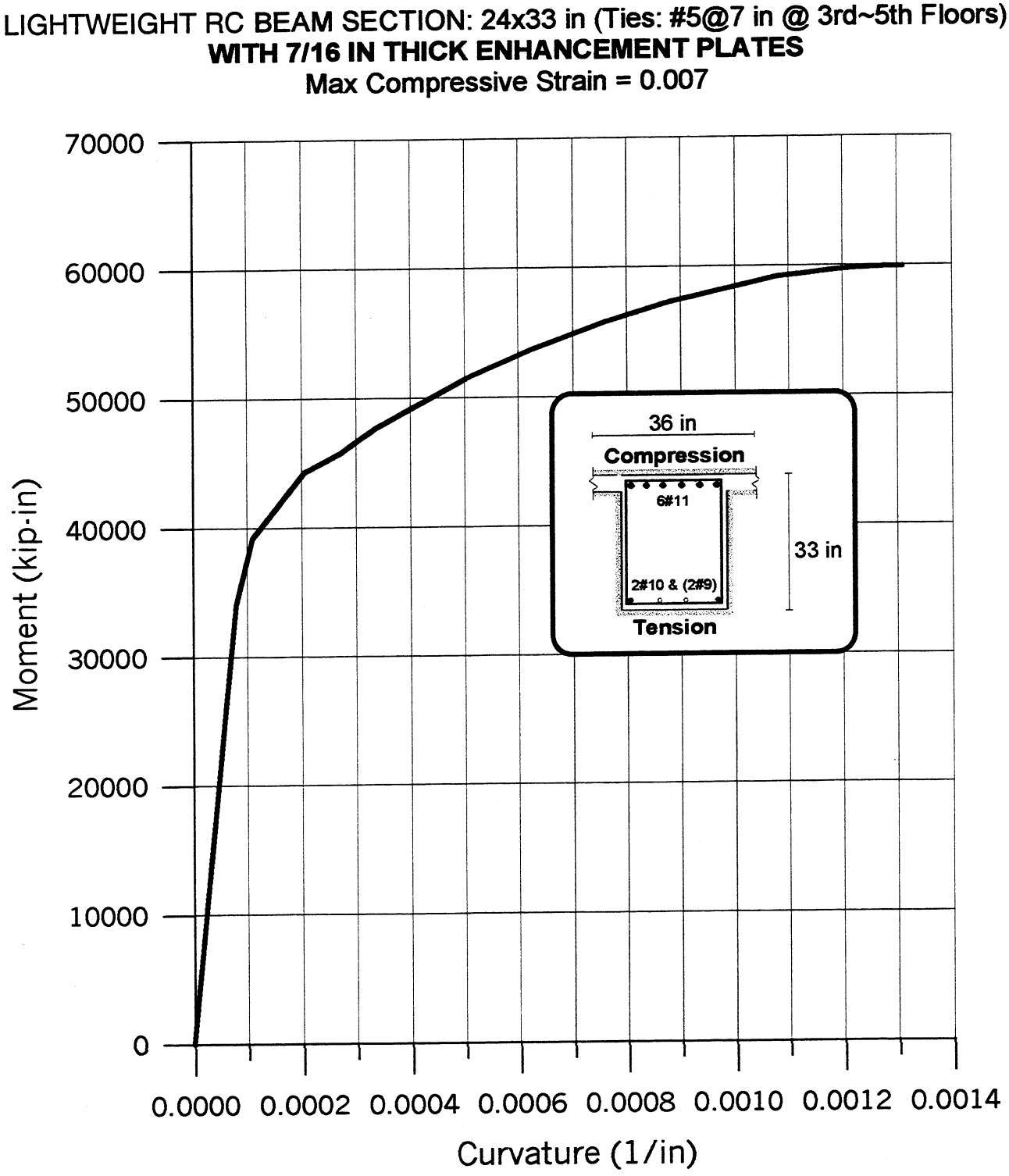

Figure 10.8 Moment-curvature relationship for retrofitted beams at 3rd to 5th floors.

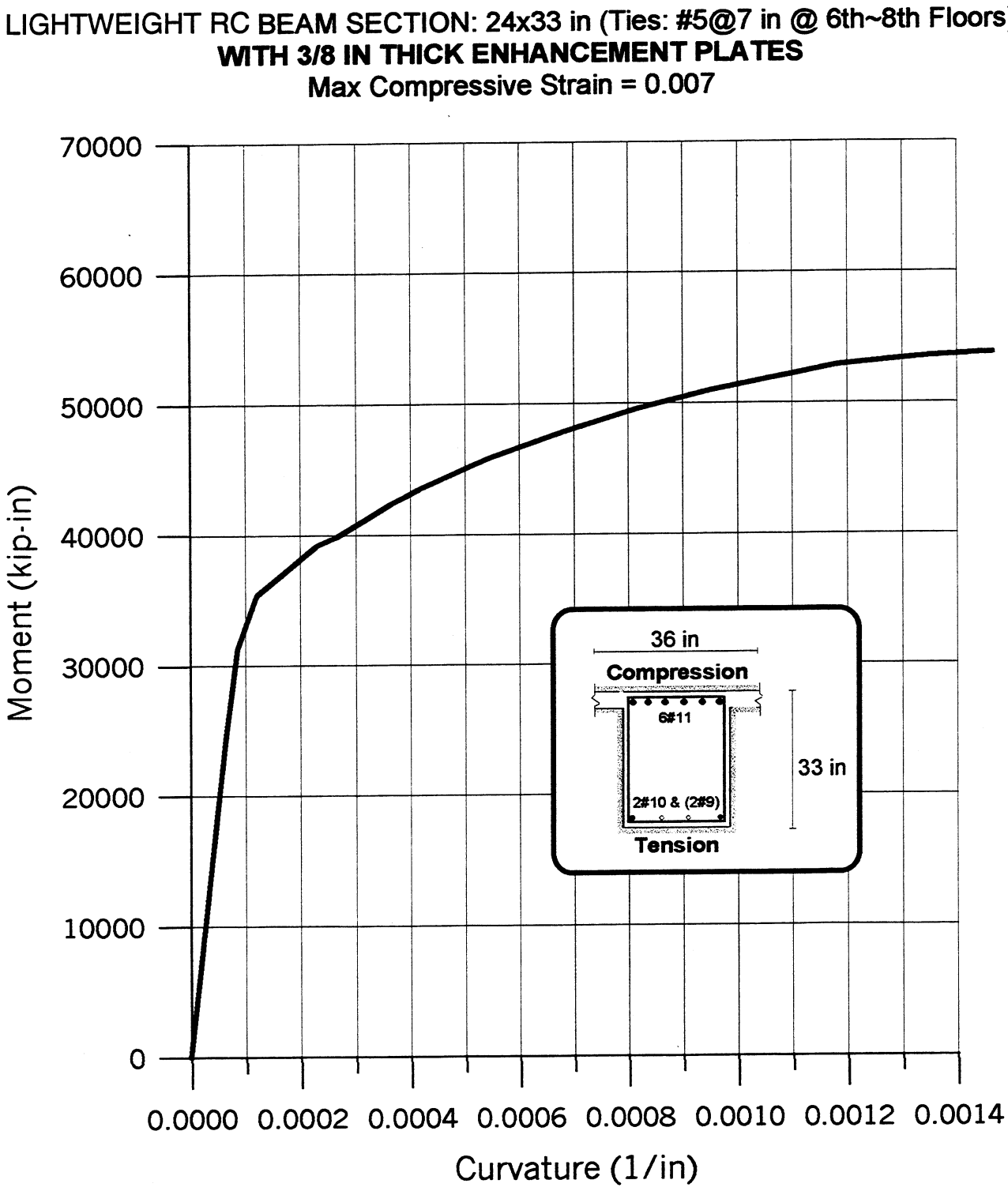

Figure 10.9 Moment-curvature relationship for retrofitted beams at 6th to 8th floors.

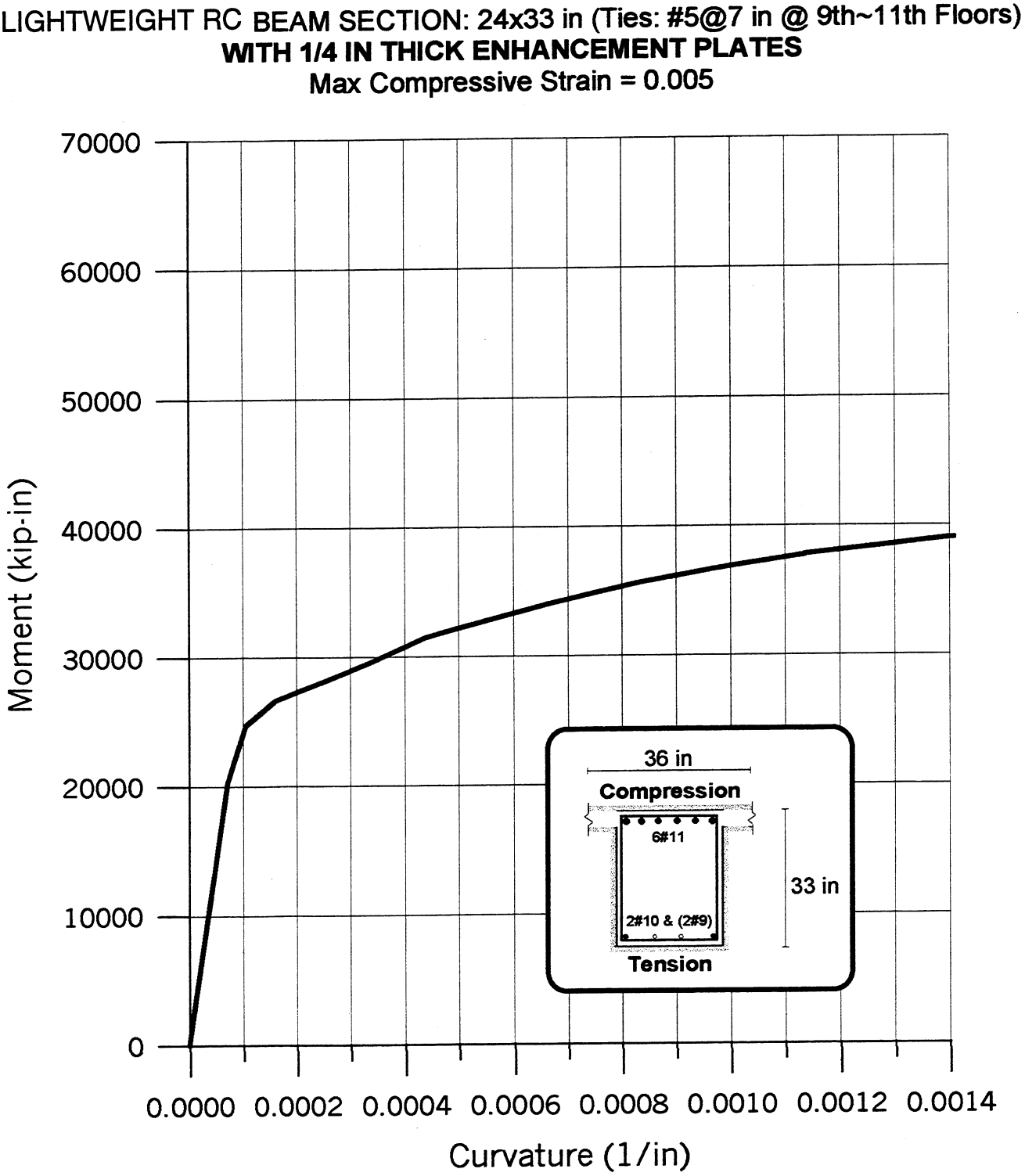

Figure 10.10 Moment-curvature relationship for retrofitted beams at 9th to11th floors.

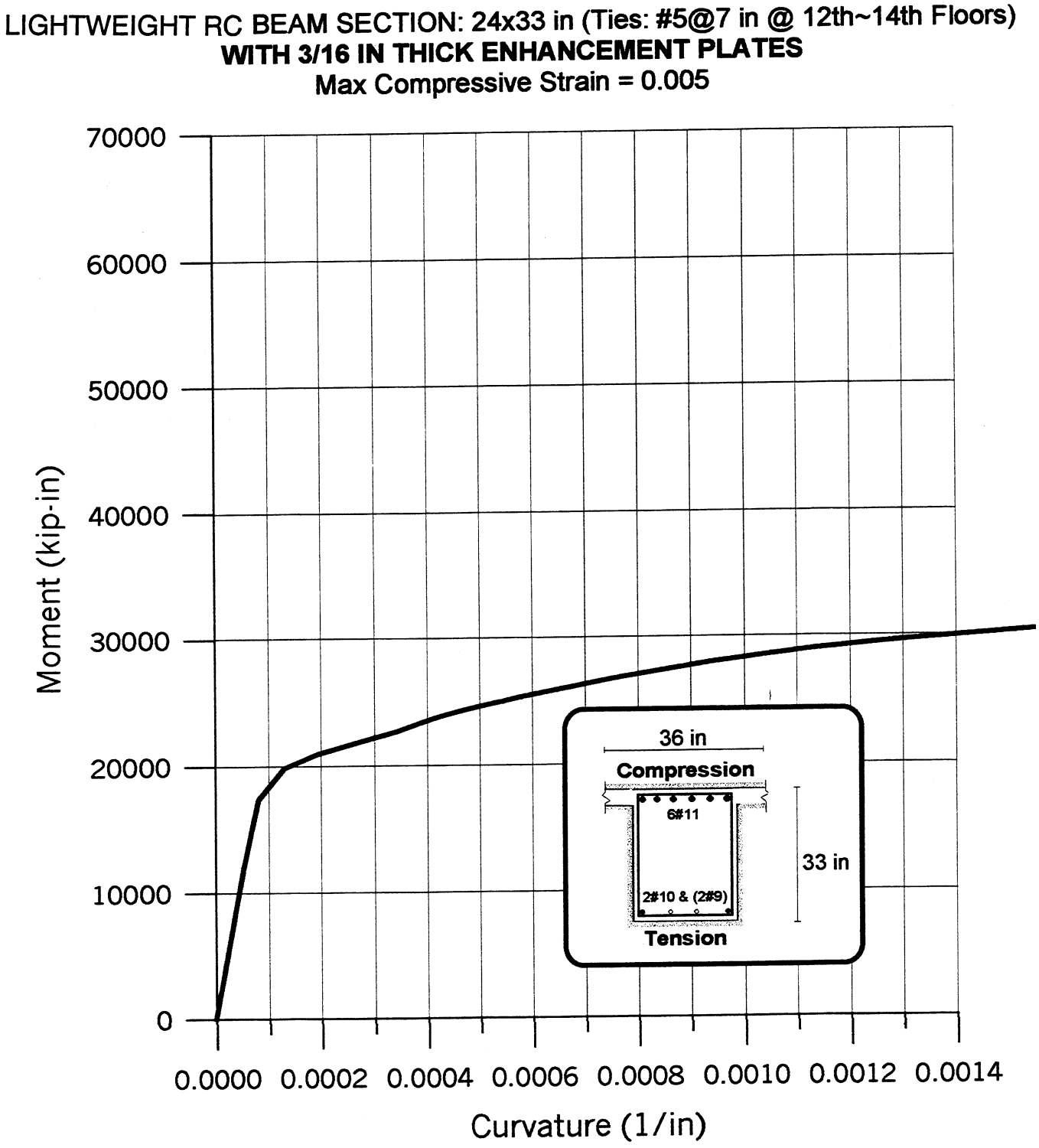

Figure 10.11 Moment-curvature relationship for retrofitted beams at 12th to14th floors.

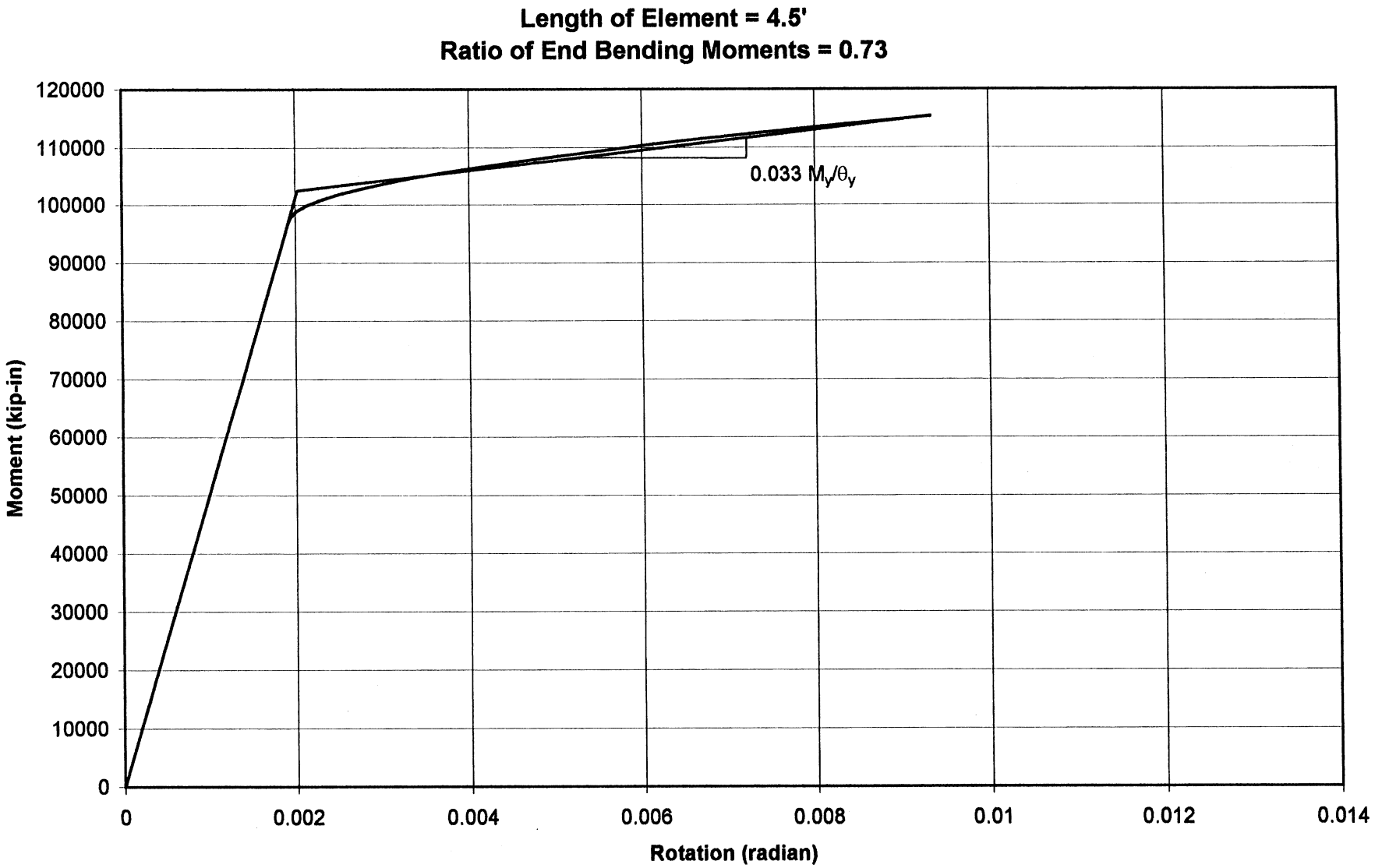

Figure 10.12 Moment-rotation relationship under positive bending moment for the end segment of the second floor interior beam.

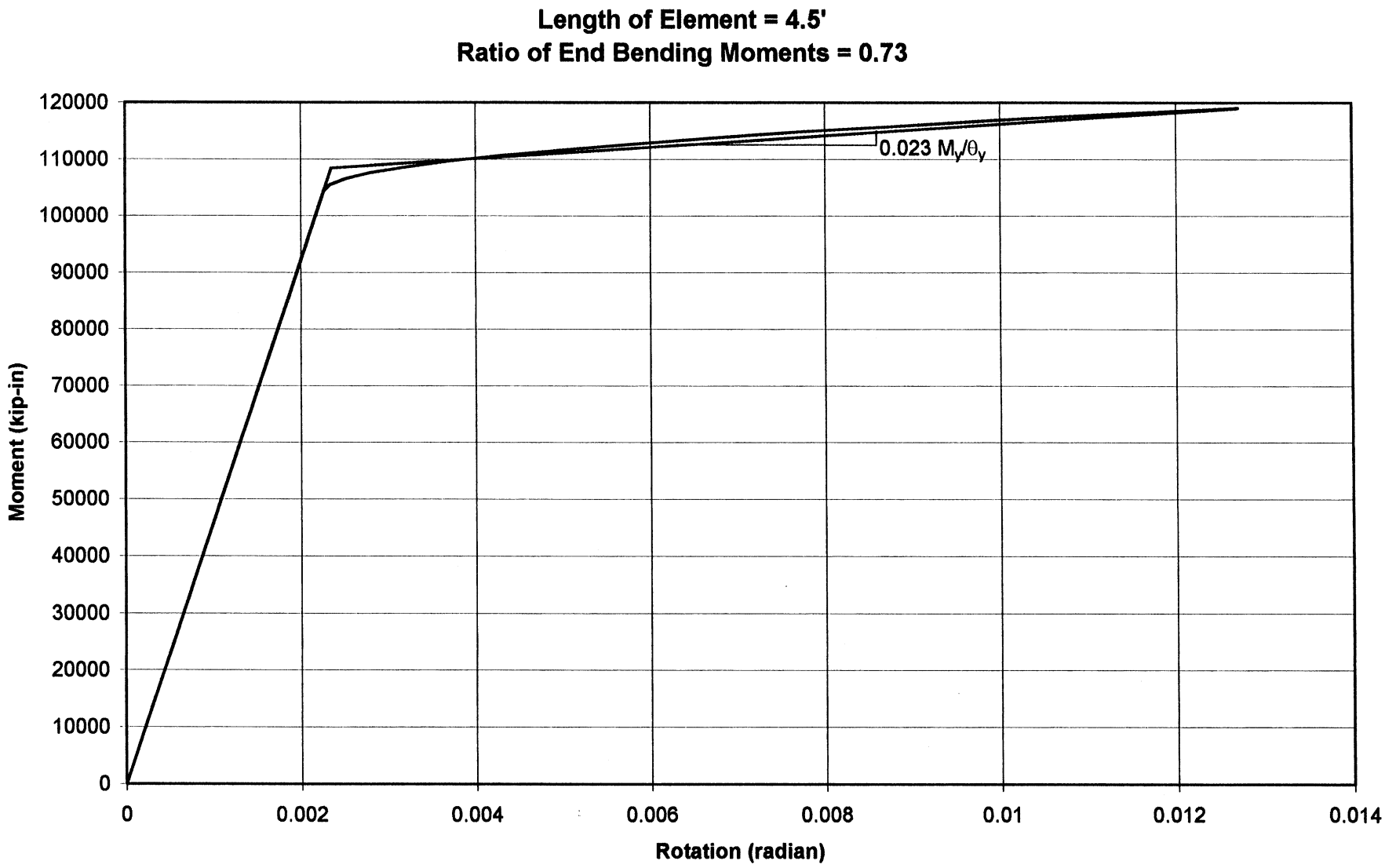

Figure 10.13 Moment-rotation relationship under negative bending moment for the end segment of the second floor interior beam.

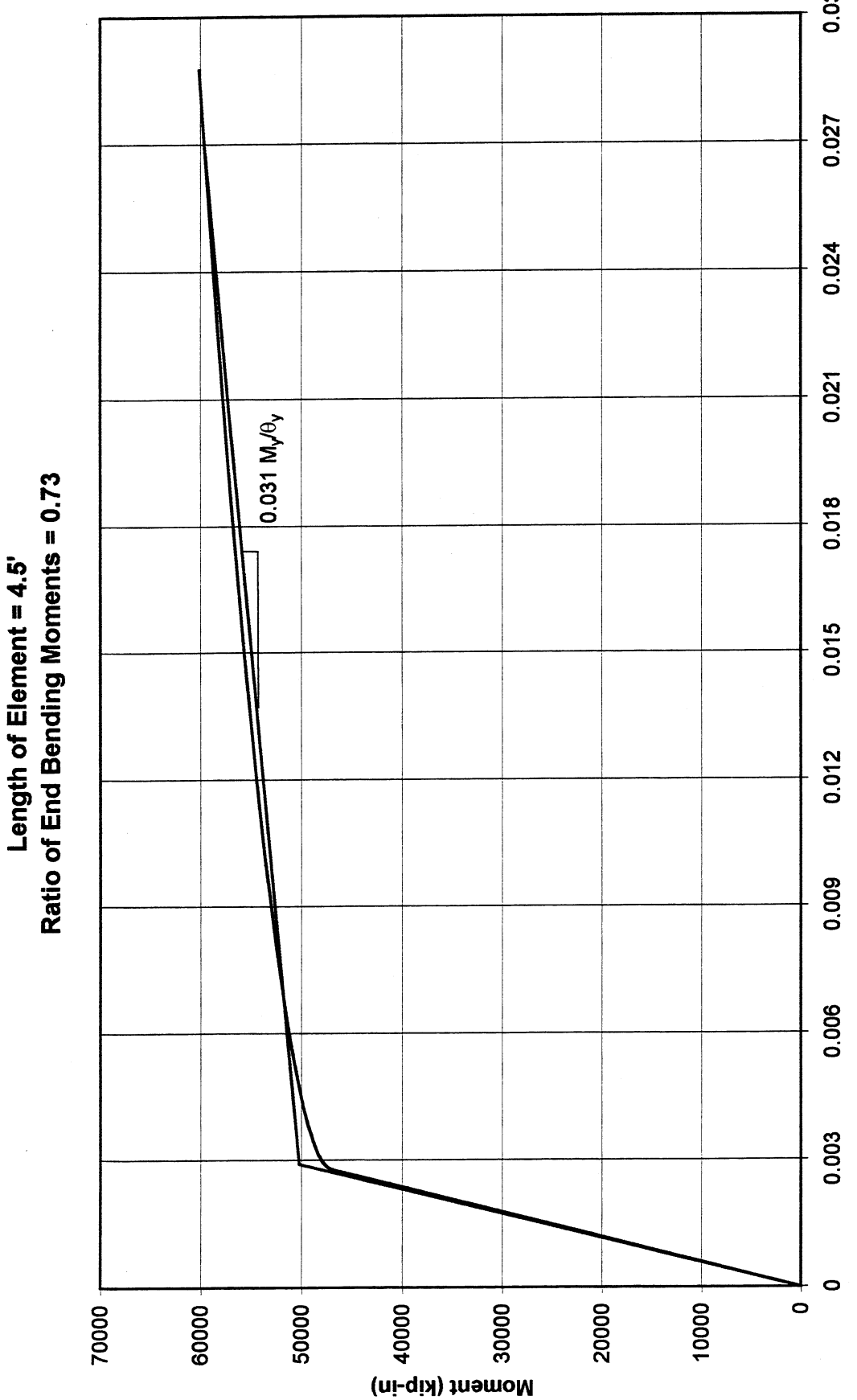

Figure 10.14 Moment-rotation relationship under positive bending moment for the end segment of the third floor interior beam.

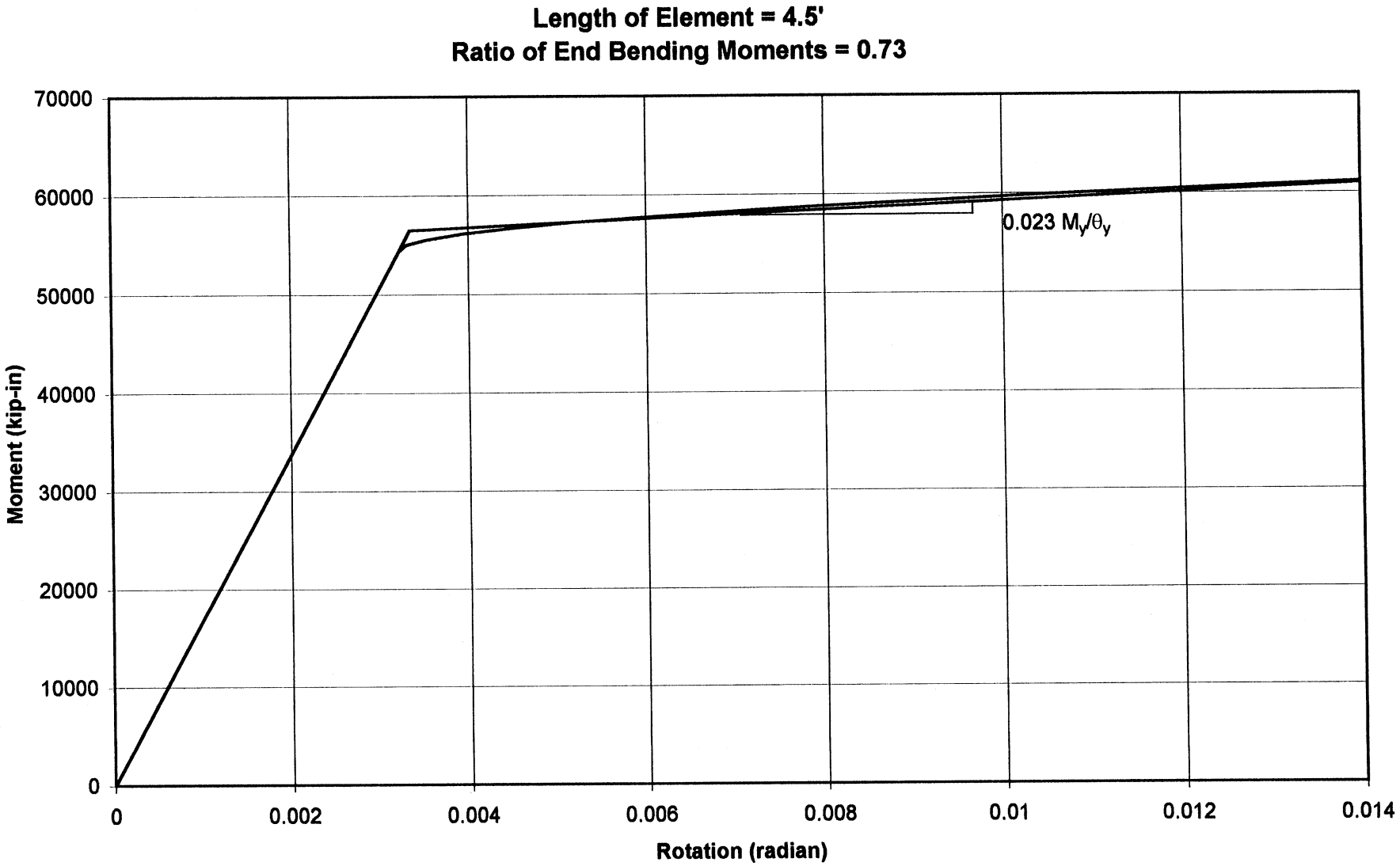

Figure 10.15 Moment-rotation relationship under negative bending moment for the end segment of the third floor interior beam.

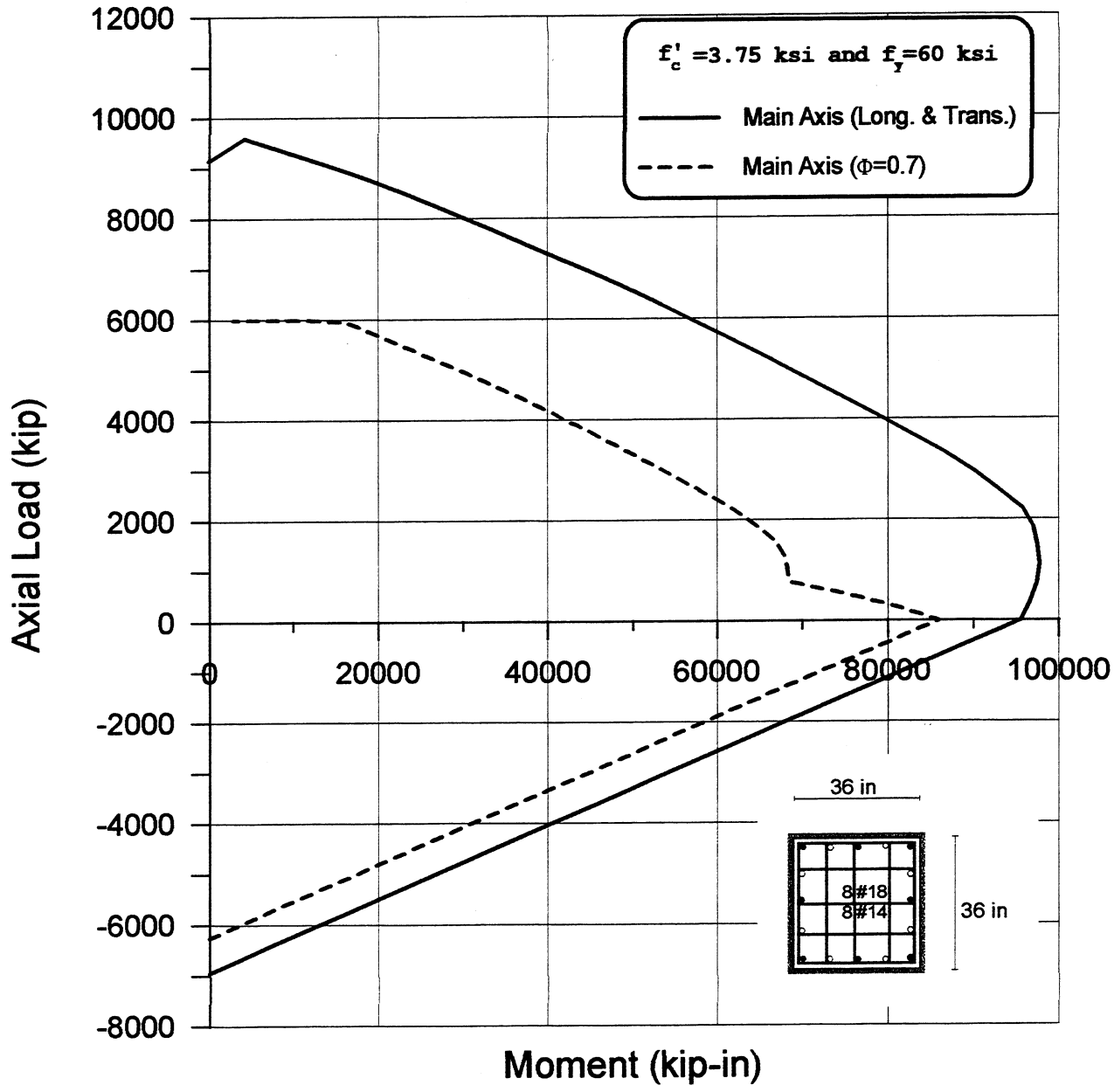

Figure 10.16 Moment-axial load interaction diagram for retrofitted column (2A-F) in 2nd story.

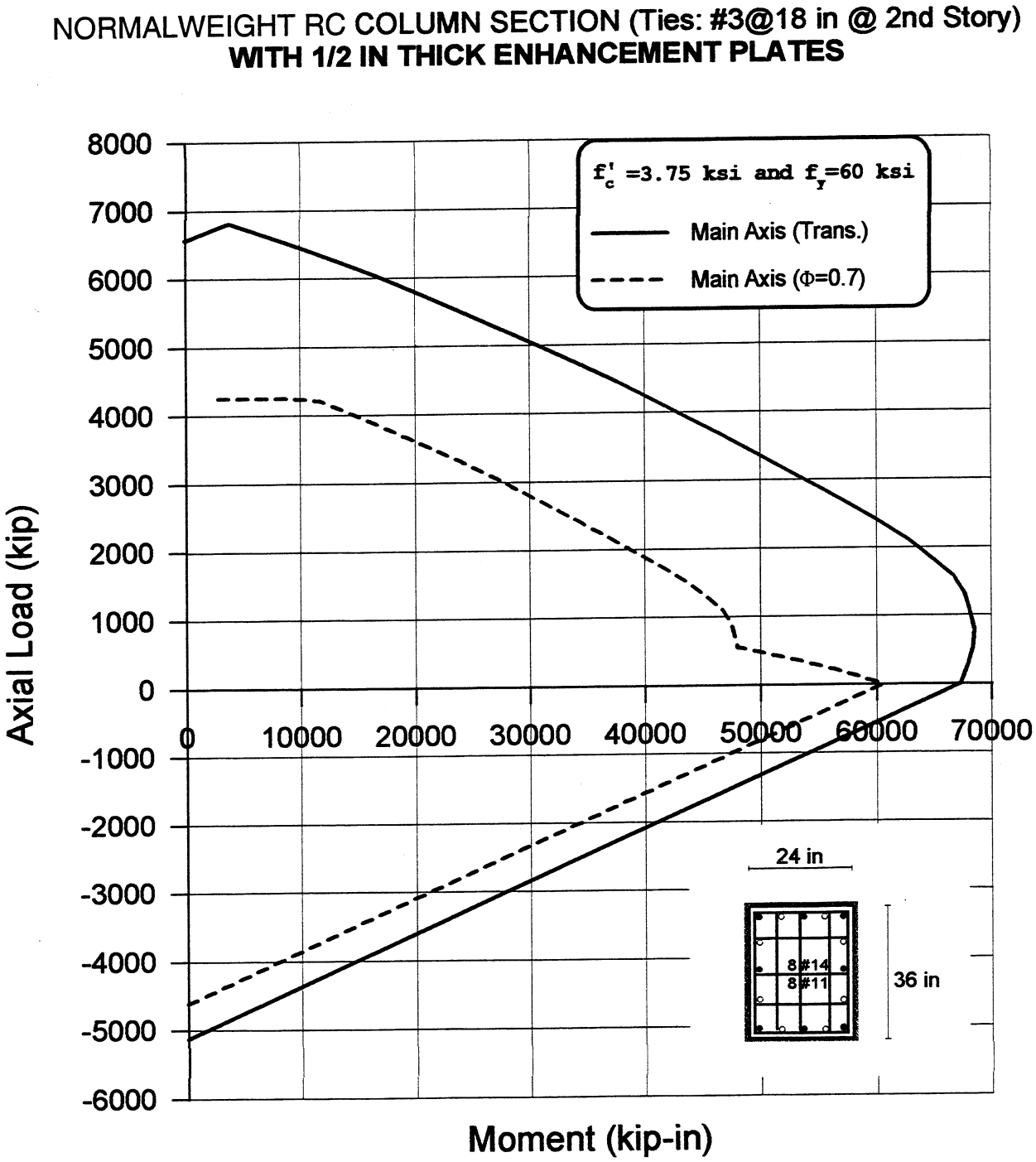

Figure 10.17 Moment-axial load interaction diagram for retrofitted column (1A-F) in 2nd story.

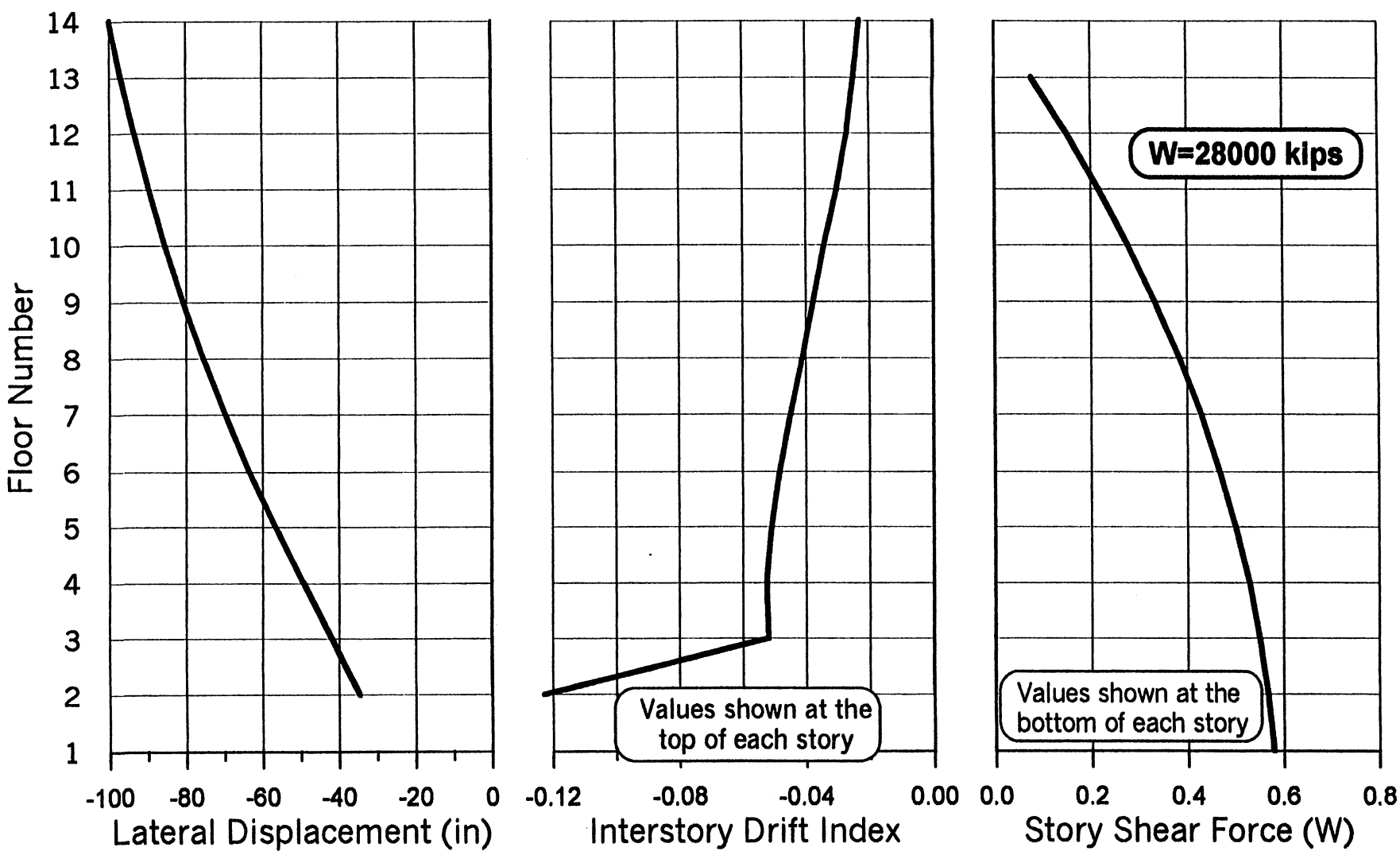

Figure 10.18 Lateral displacement, interstory drift index, and story shear force envelopes.

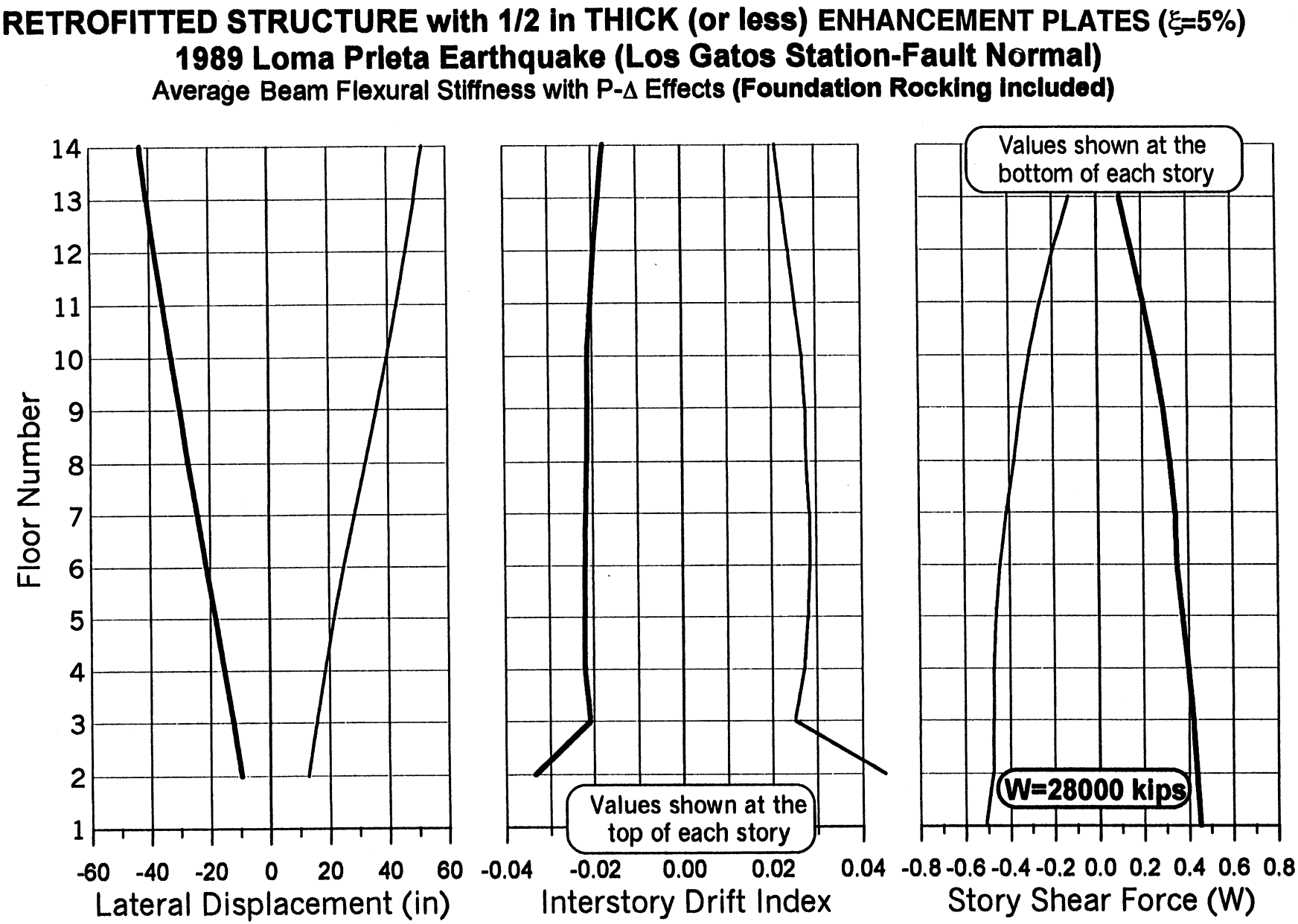

Figure 10.19 Lateral displacement, interstory drift index, and story shear force envelopes.

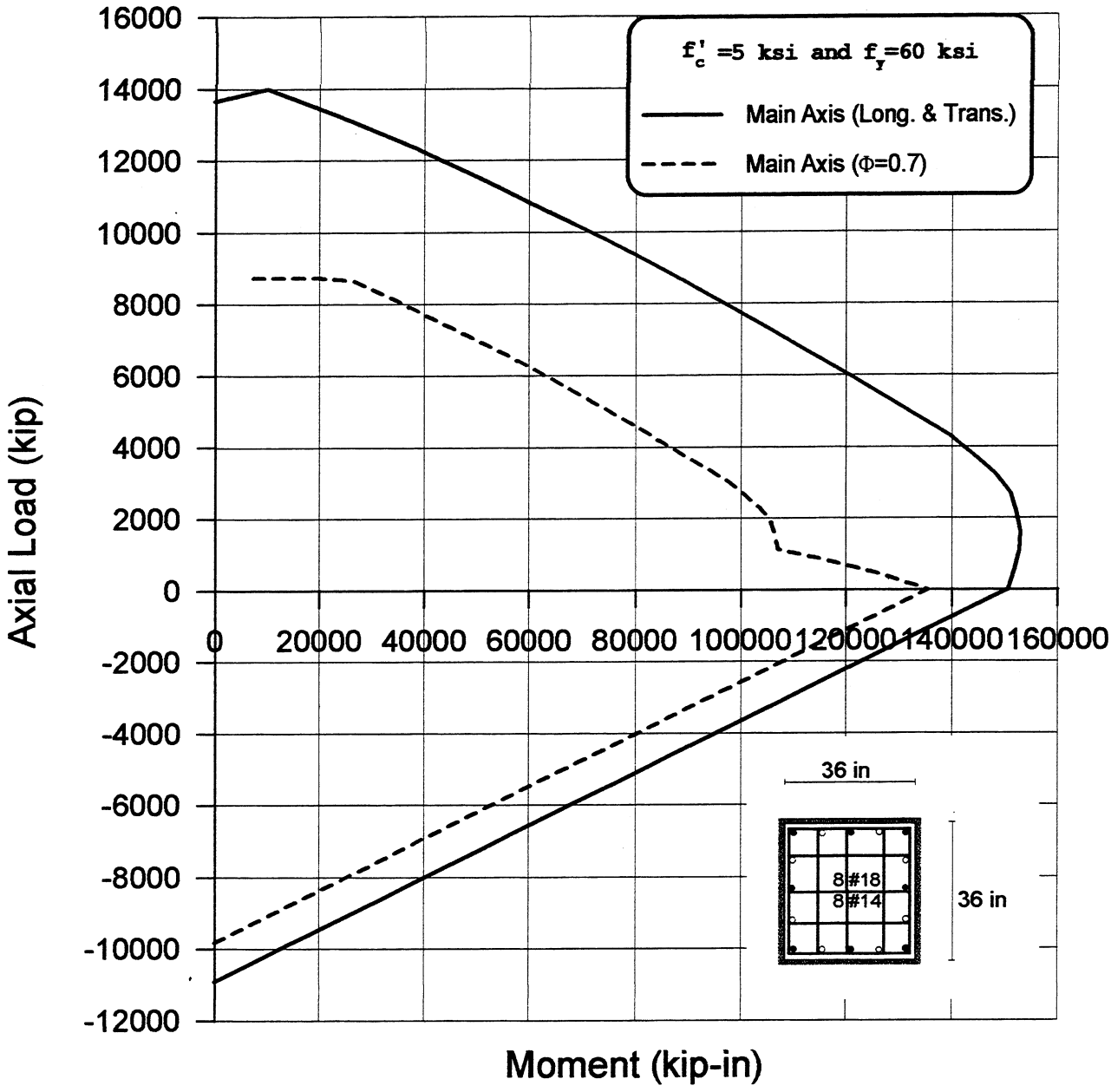

Figure 10.20 Moment-axial load interaction diagram for retrofitted column (2A-F) in 1st story.

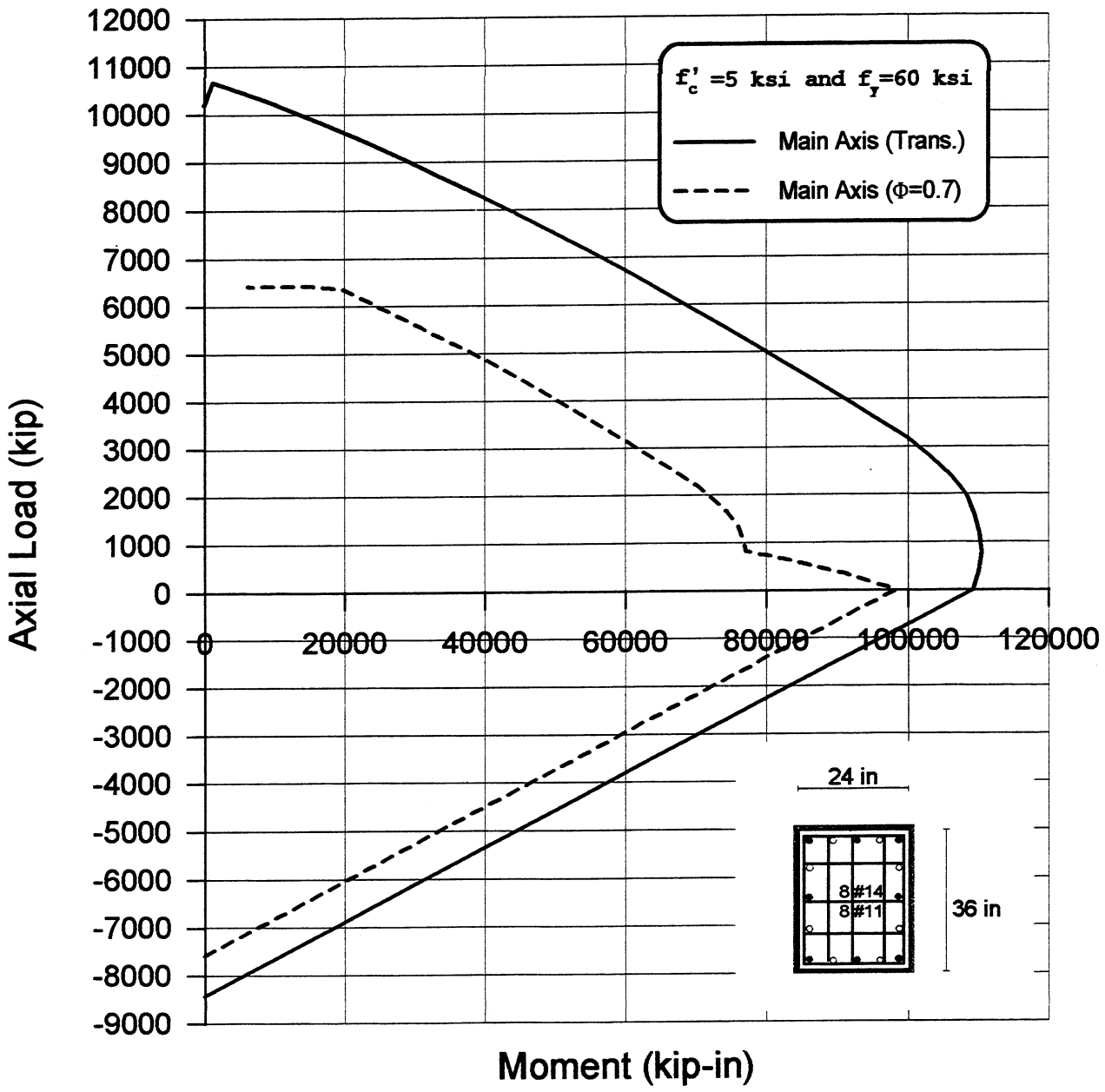

Figure 10.21 Moment-axial load interaction diagram for retrofitted column (1A-F) in 1st story.

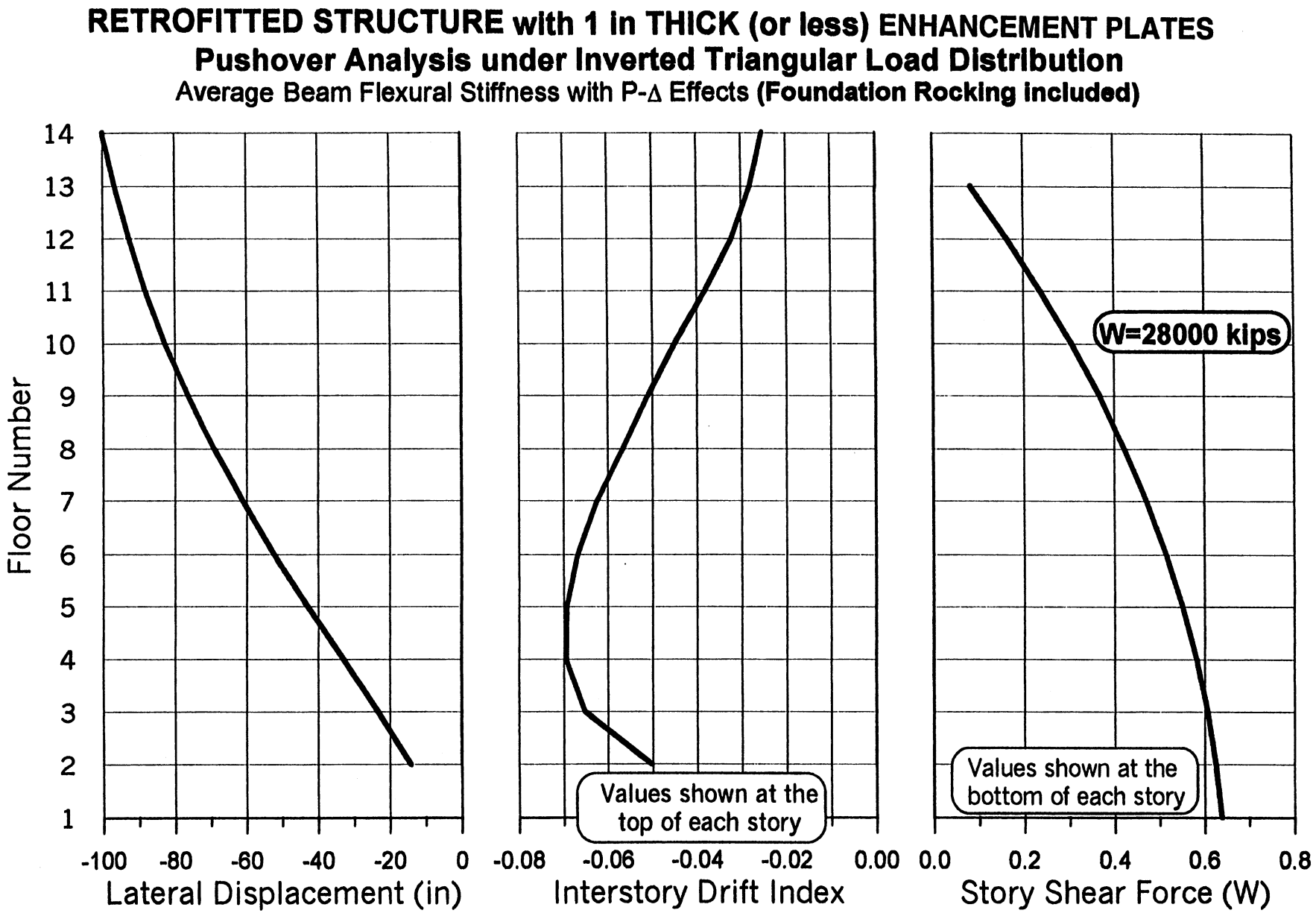

Figure 10.22 Lateral displacement, interstory drift index, and story shear force envelopes.

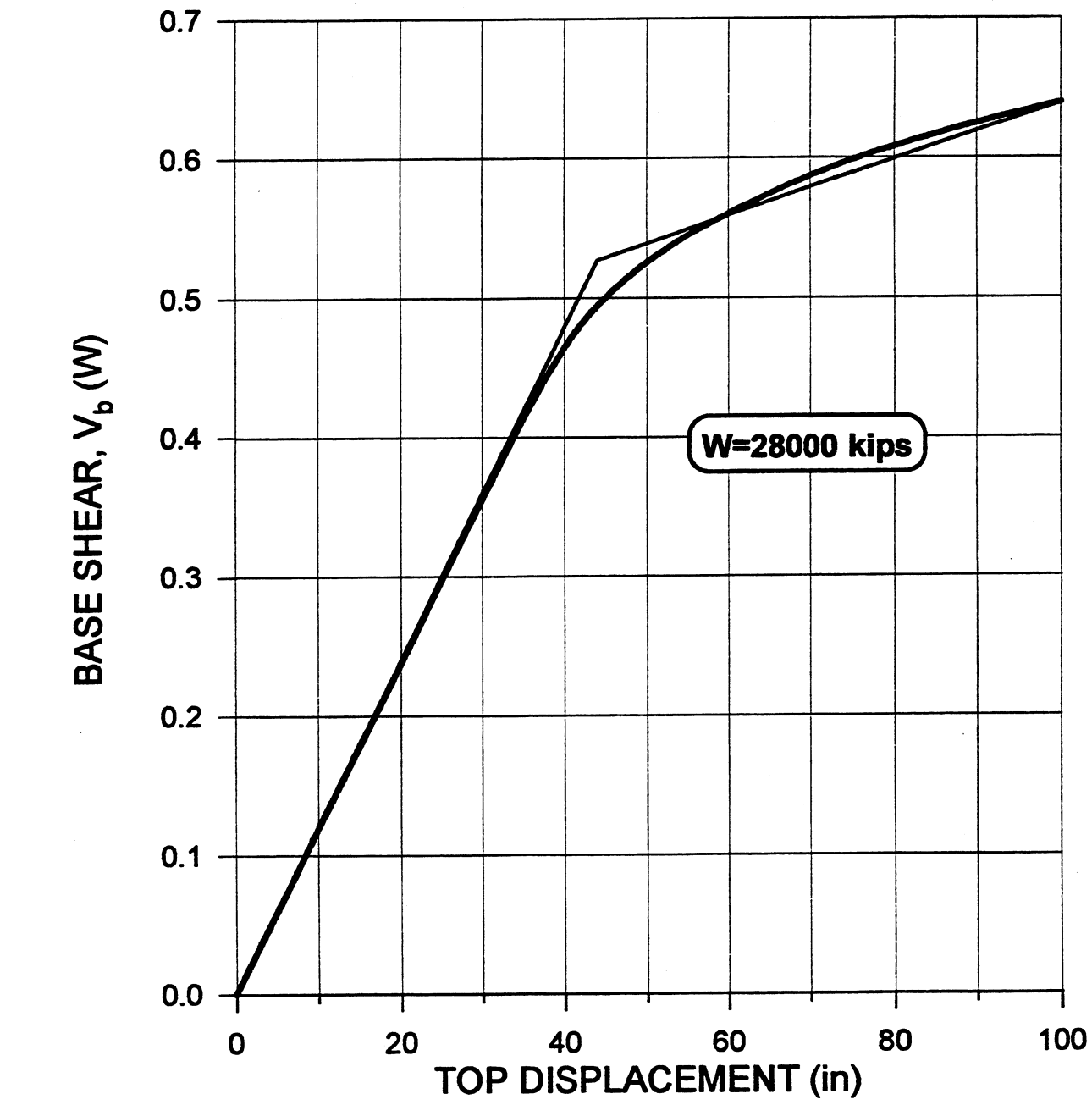

Figure 10.23 Base shear versus roof displacement and its bilinear idealization with Δ_y=44 in, V_y=0.53W and μ_Δ=2.3.

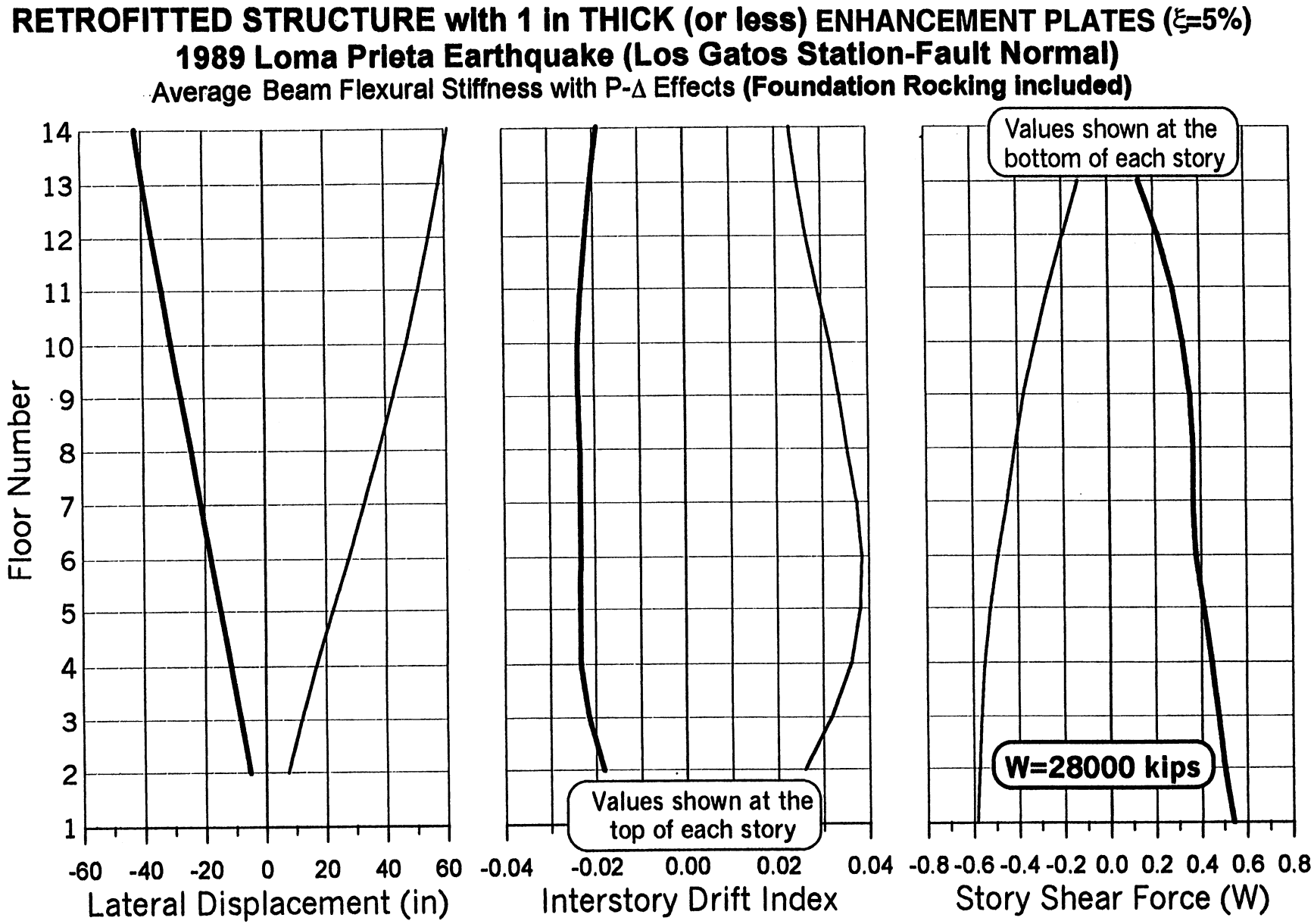

Figure 10.24 Lateral displacement, interstory drift index, and story shear force envelopes.

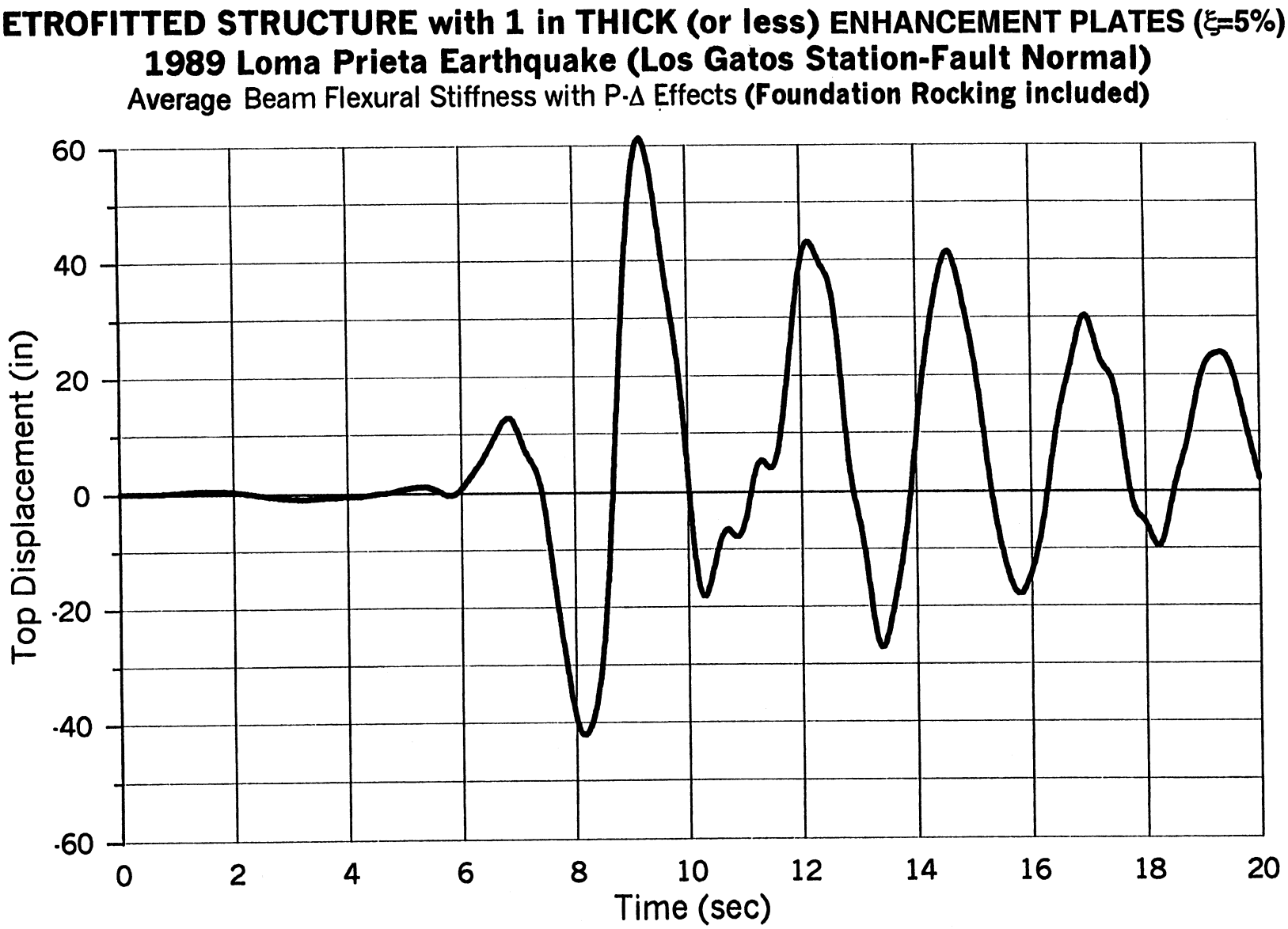

Figure 10.25 Time history of roof displacement.

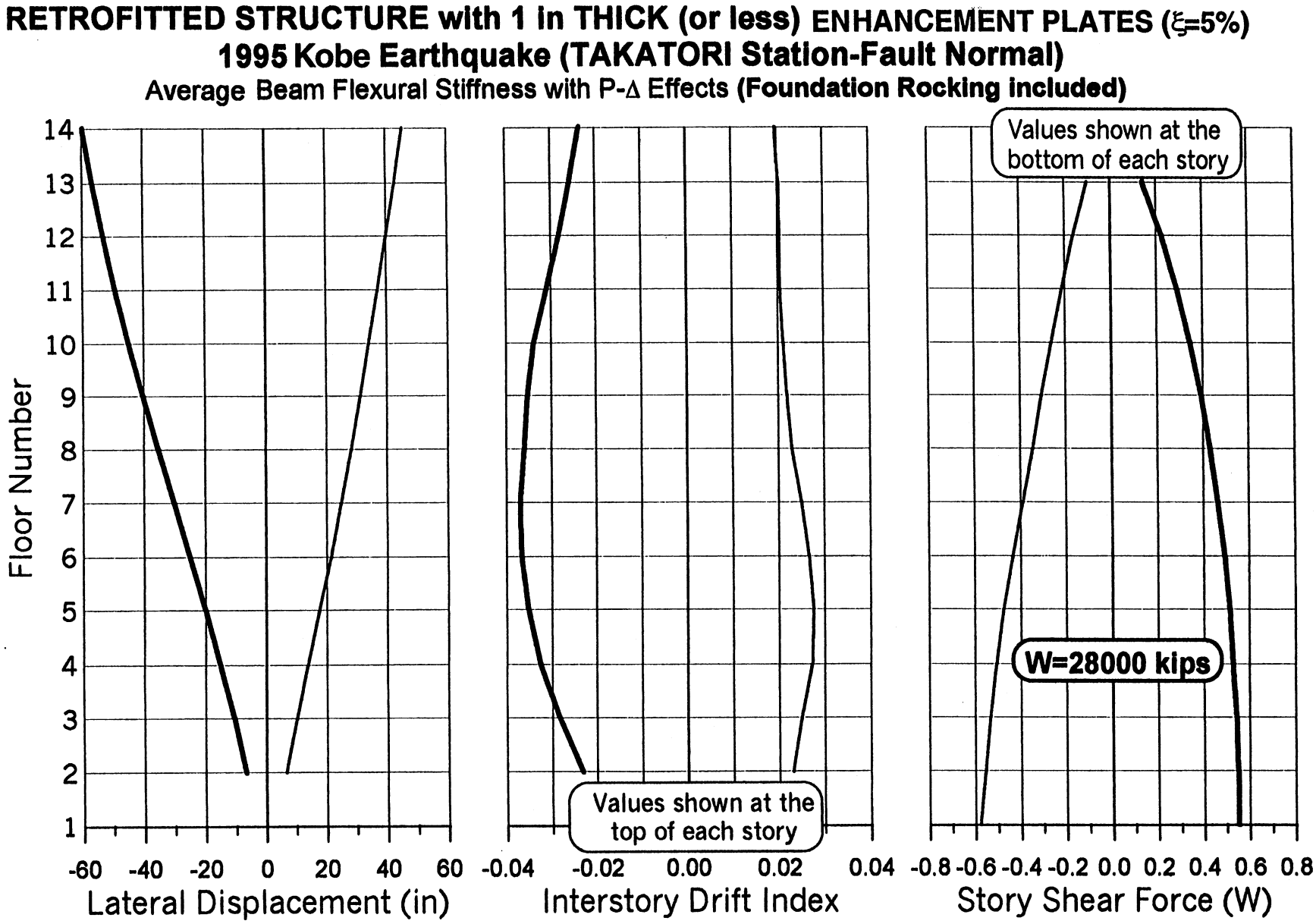

Figure 10.26 Lateral displacement, interstory drift index, and story shear force envelopes.

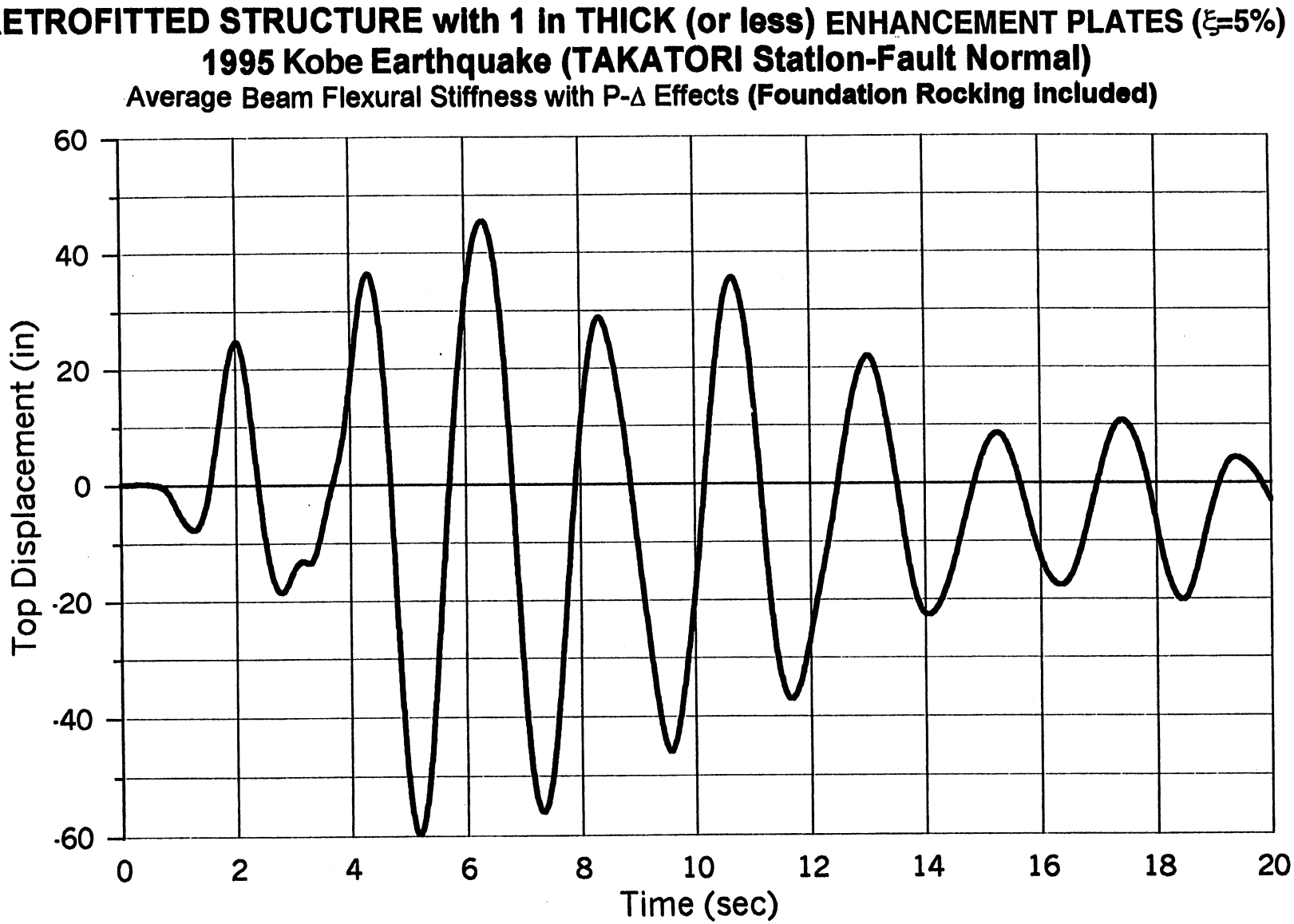

Figure 10.27 Time history of roof displacement.

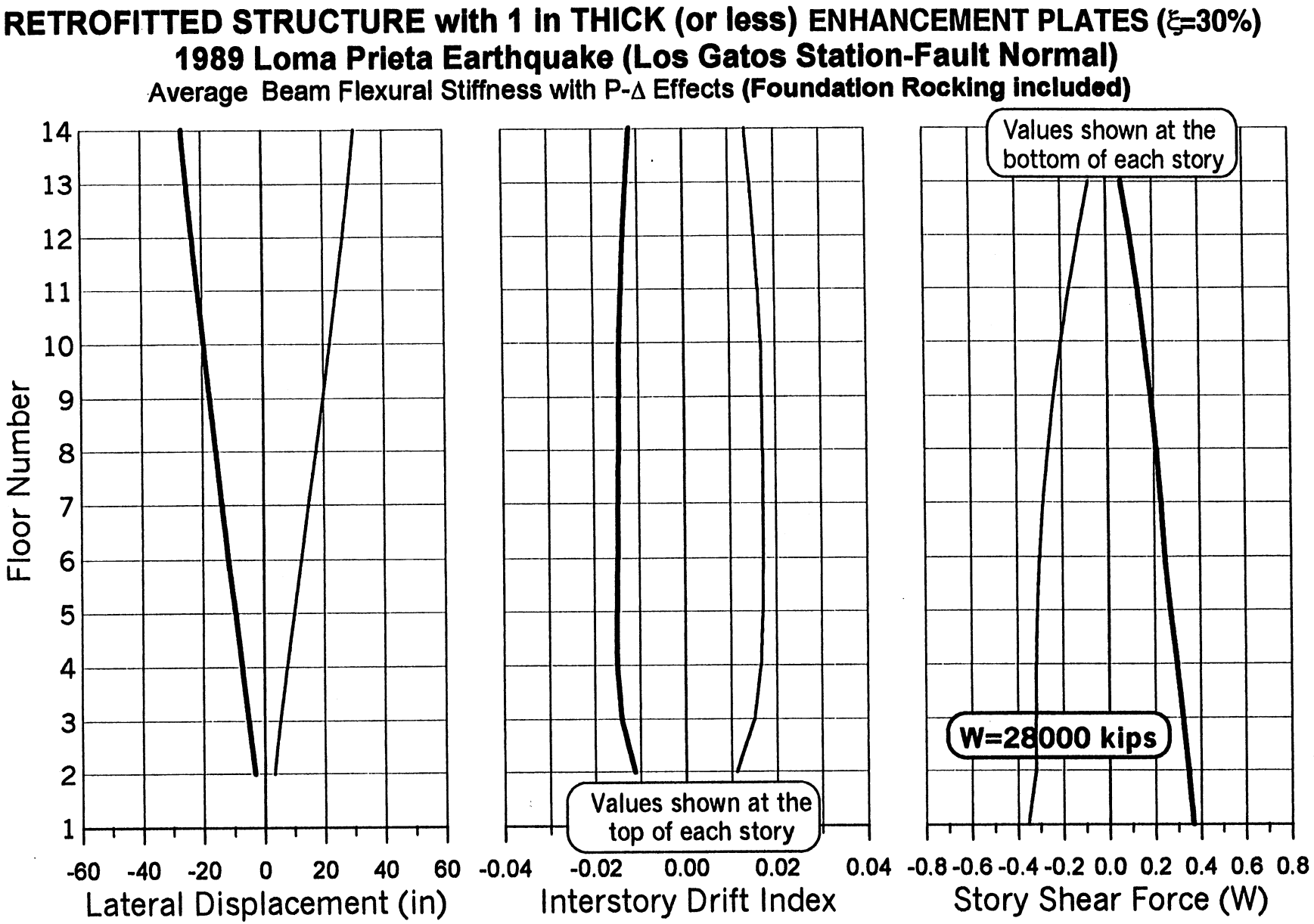

Figure 10.28 Lateral displacement, interstory drift index, and story shear force envelopes.

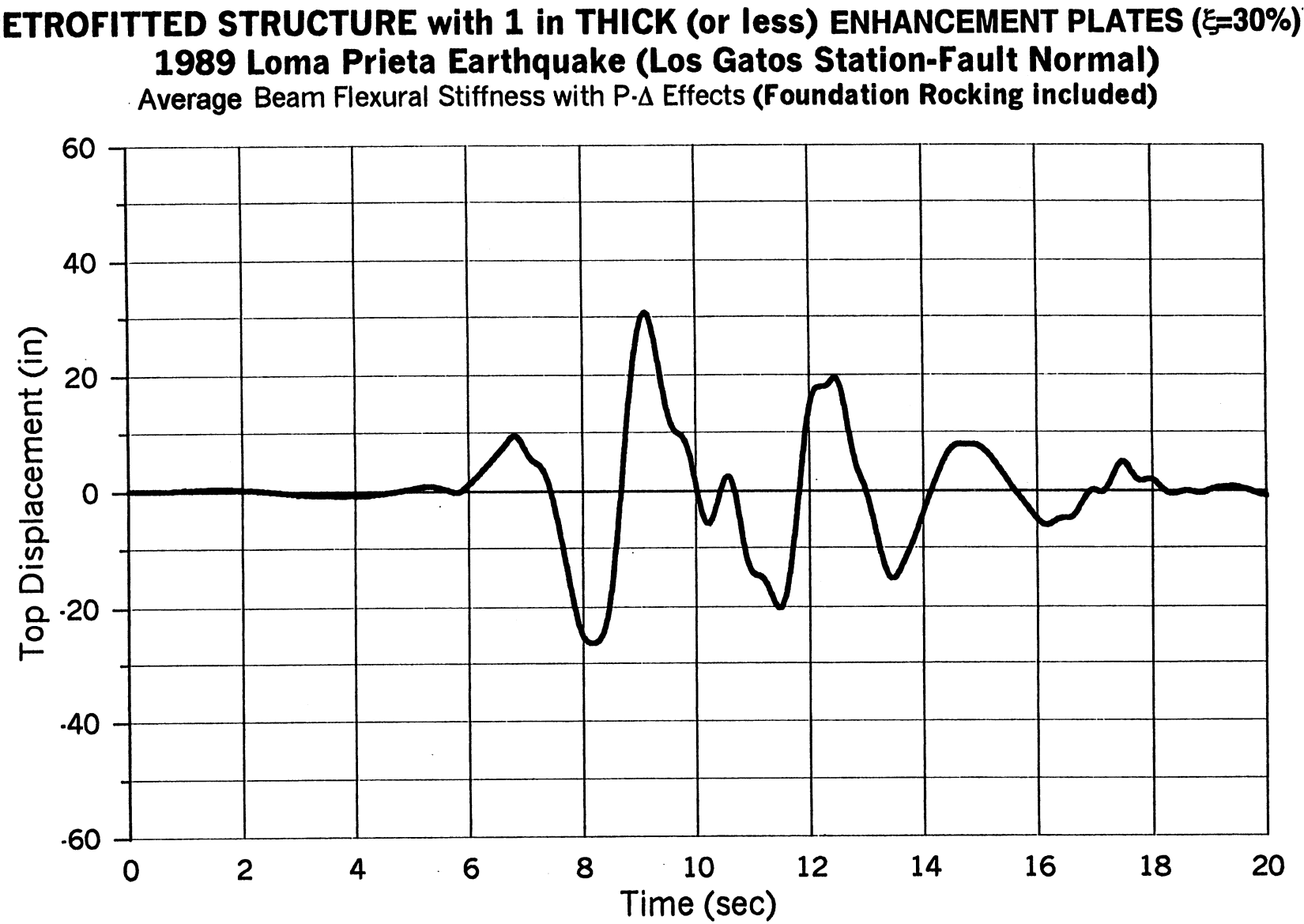

Figure 10.29 Time history of roof displacement.

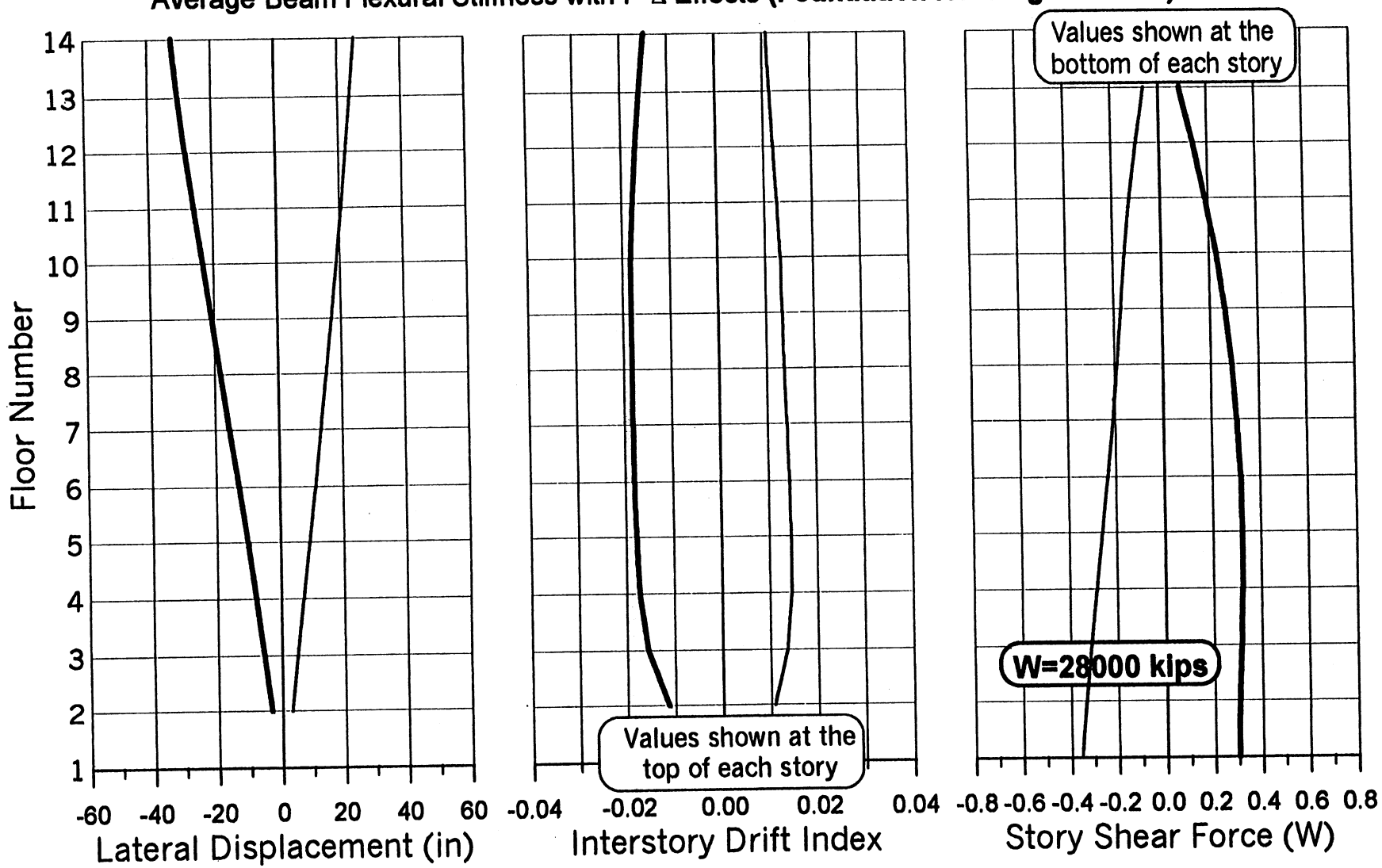

Figure 10.30 Lateral displacement, interstory drift index, and story shear force envelopes.

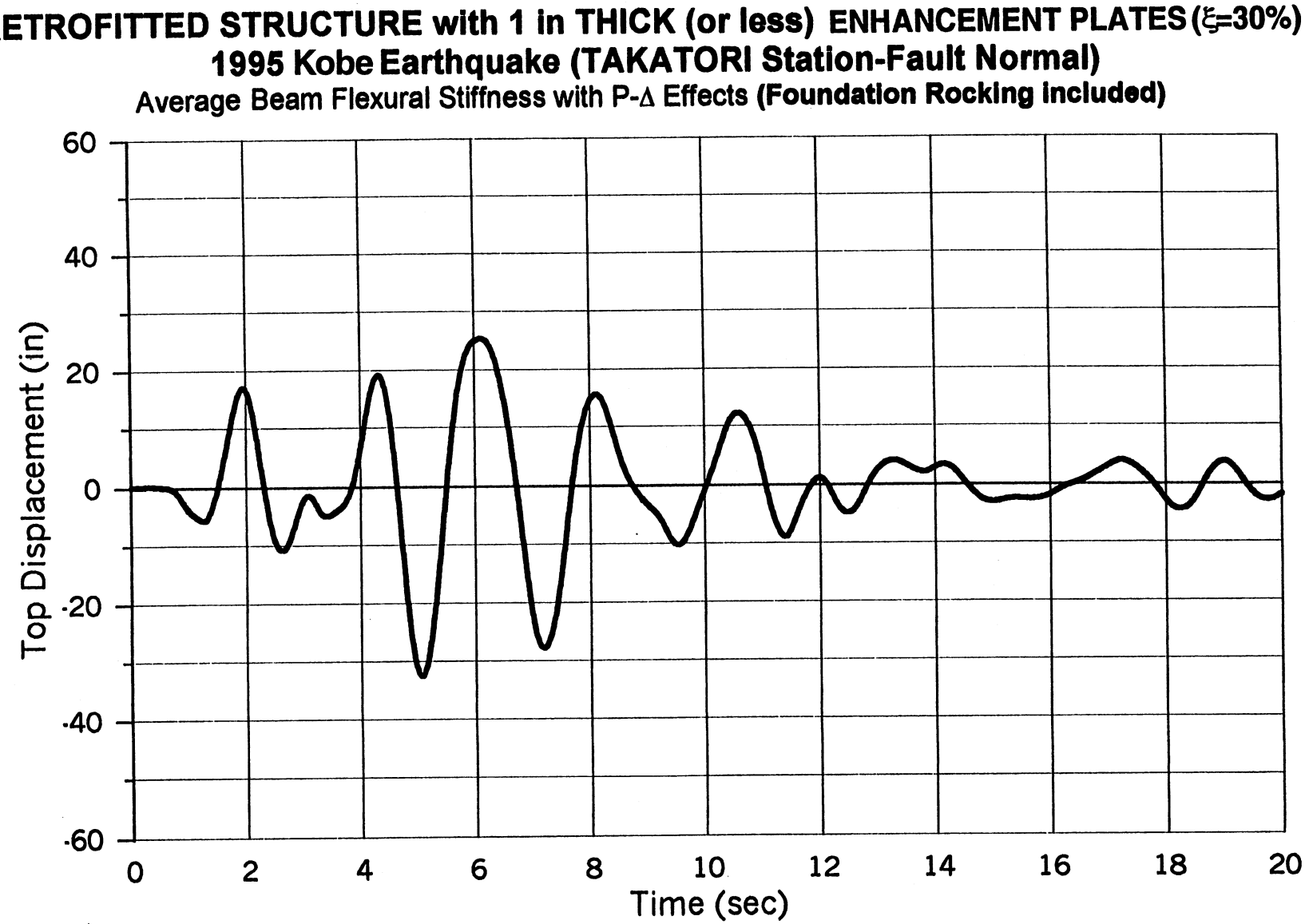

Figure 10.31 Time history of roof displacement.

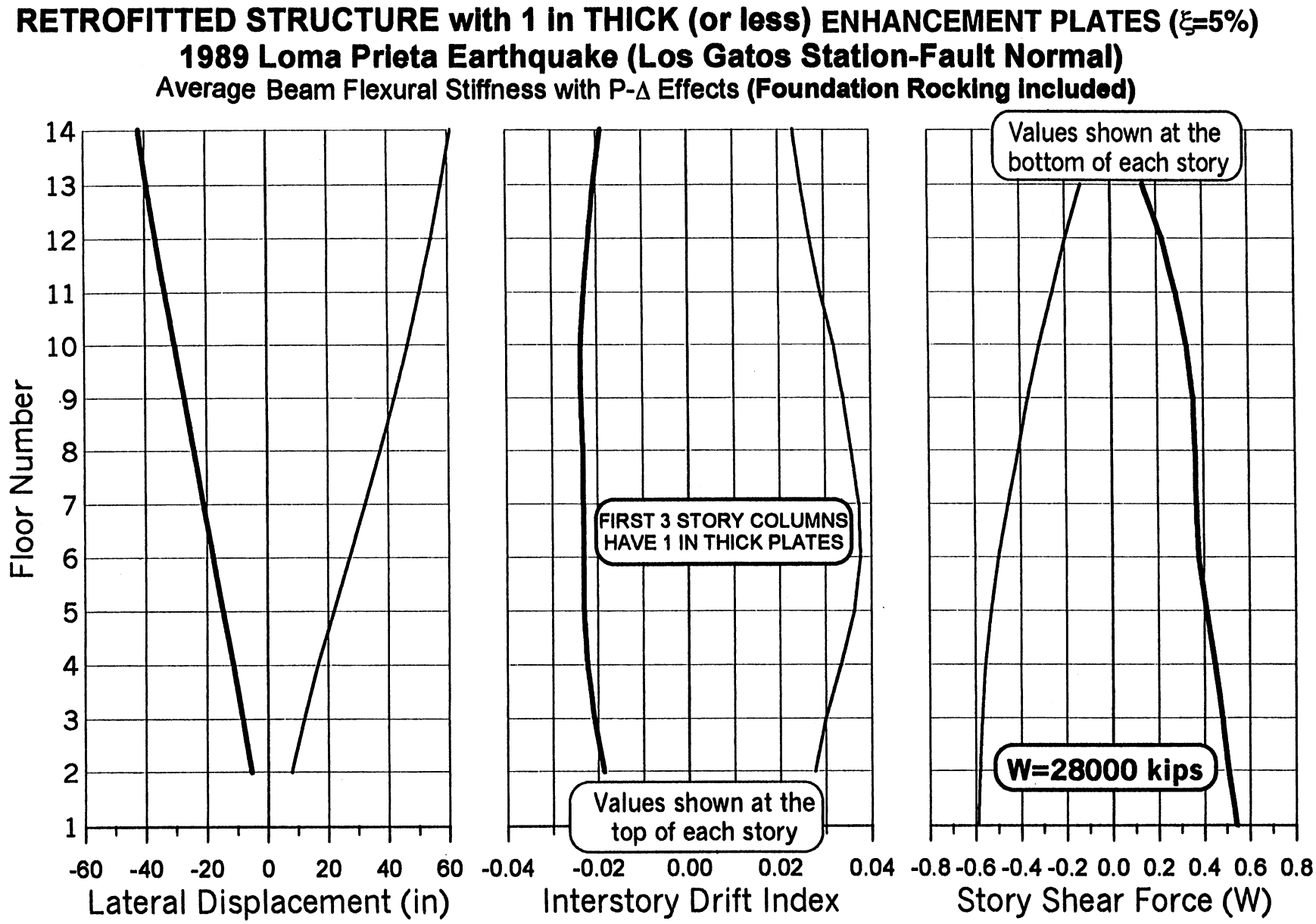

Figure 10.32 Lateral displacement, interstory drift index, and story shear force envelopes.

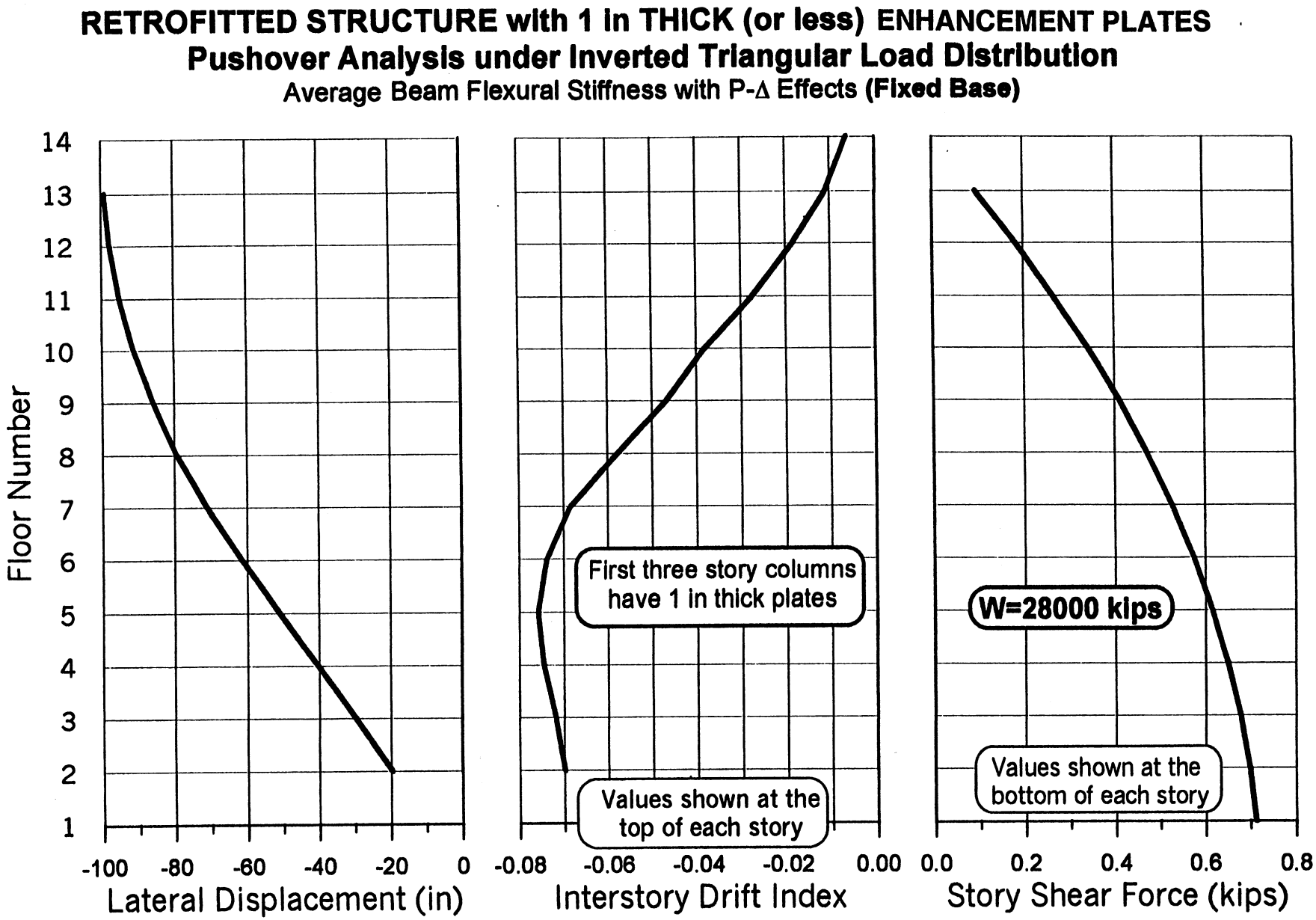

Figure 10.33 Lateral displacement, interstory drift index, and story shear force envelopes.

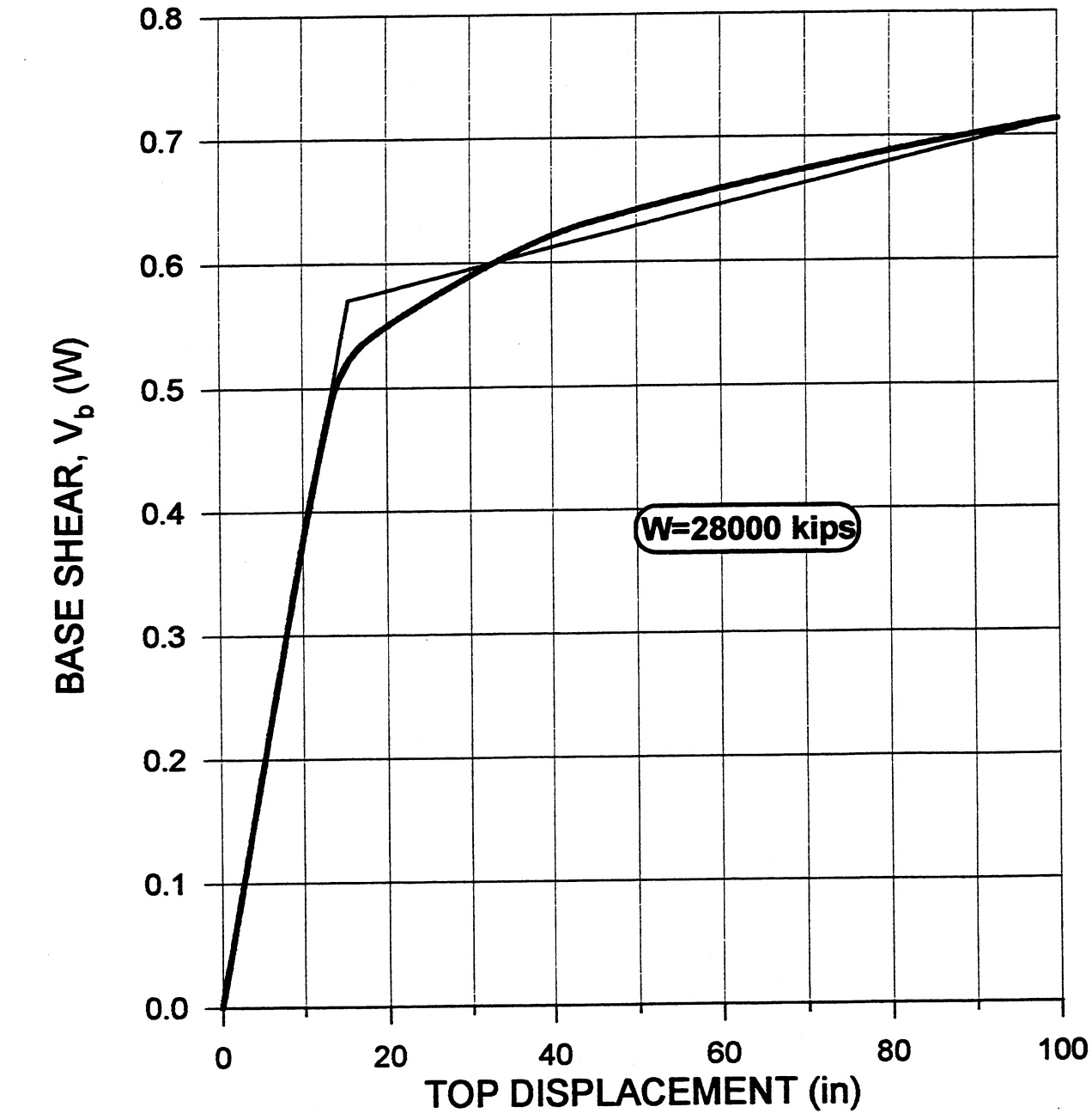

Figure 10.34 Base shear versus roof displacement and its bilinear idealization with Δ_y=15 in, V_y=0.57W and μ_Δ=6.7.

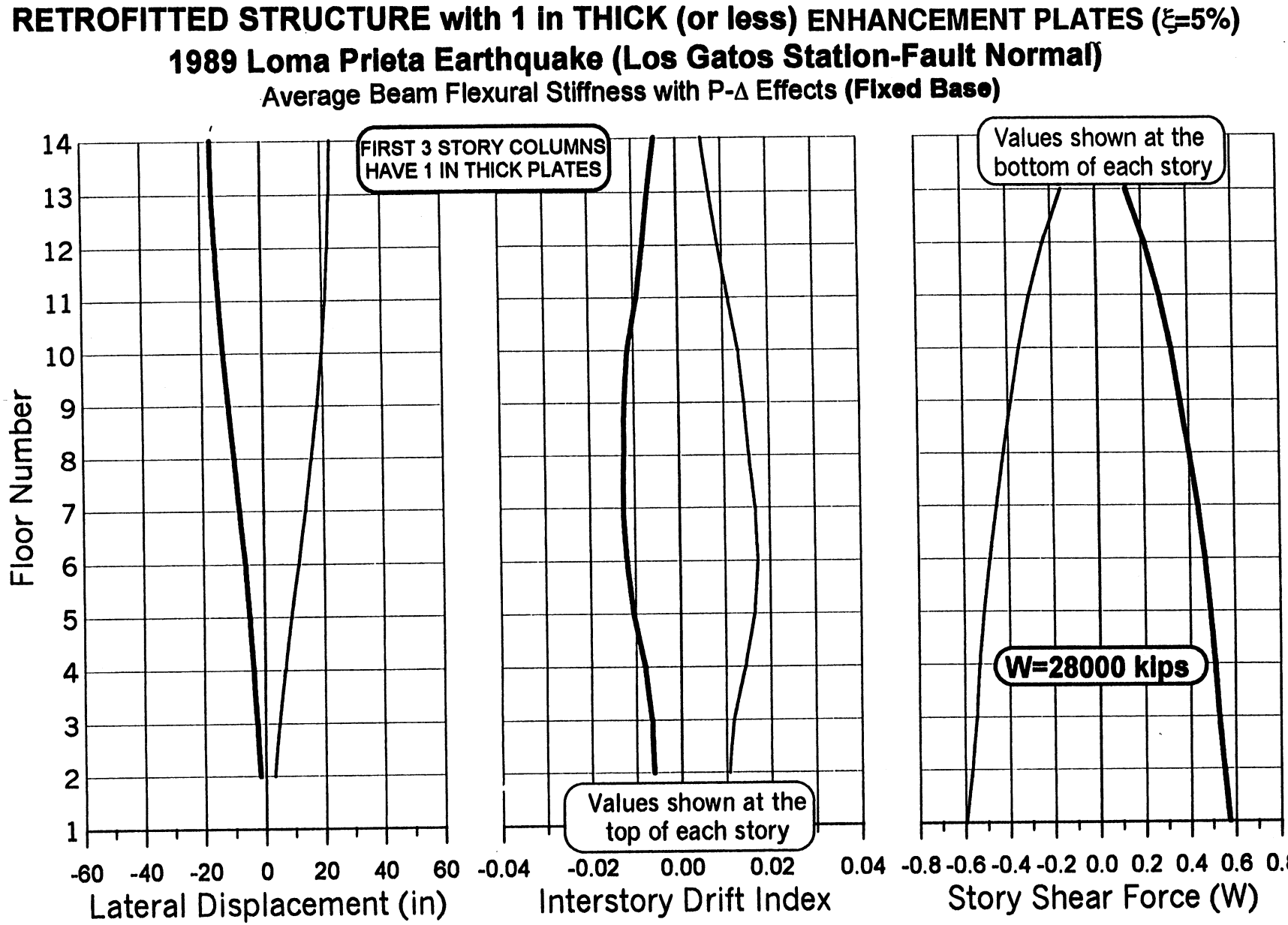

Figure 10.35 Lateral displacement, interstory drift index, and story shear force envelopes.

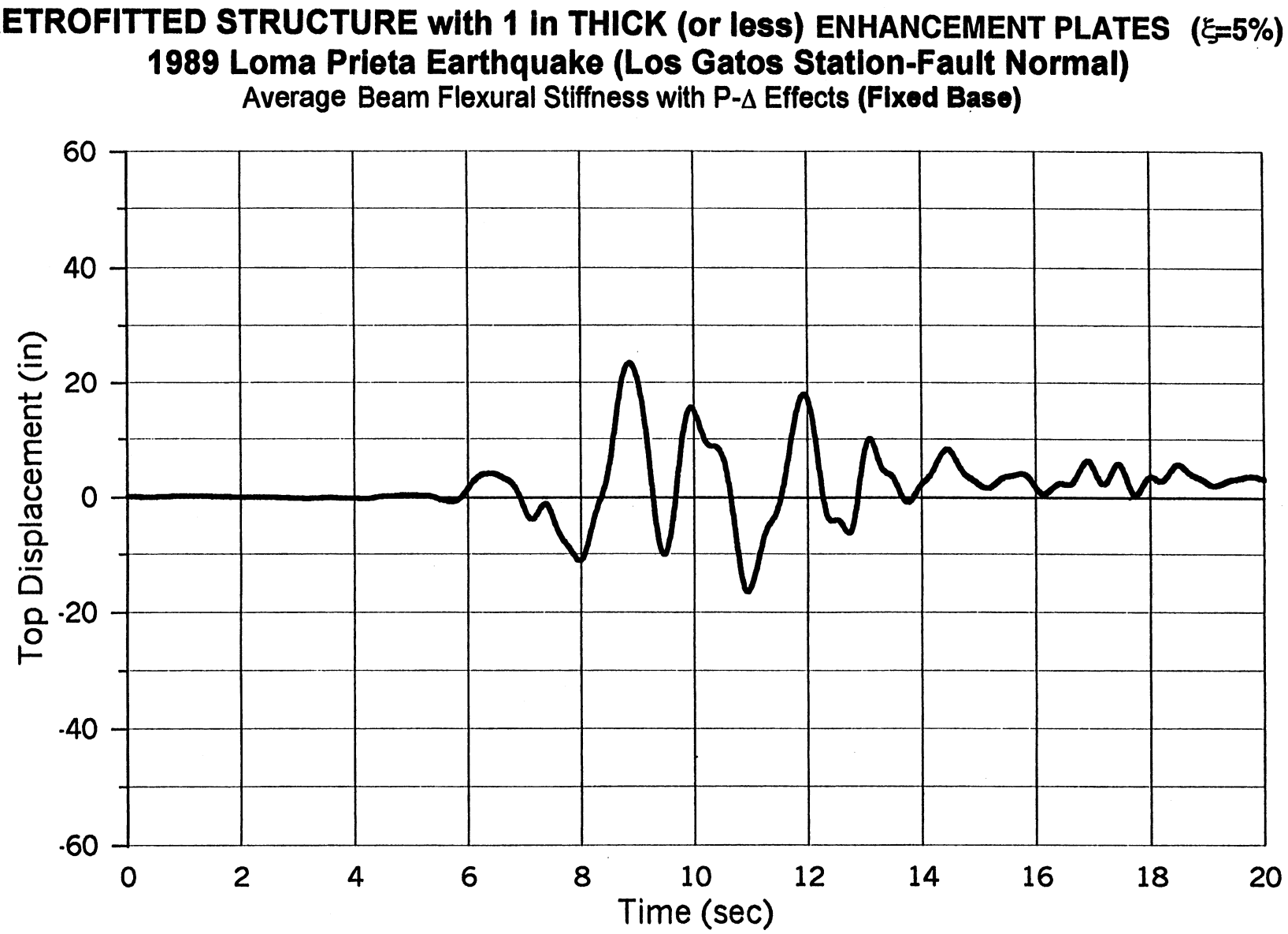

Figure 10.36 Time history of roof displacement.

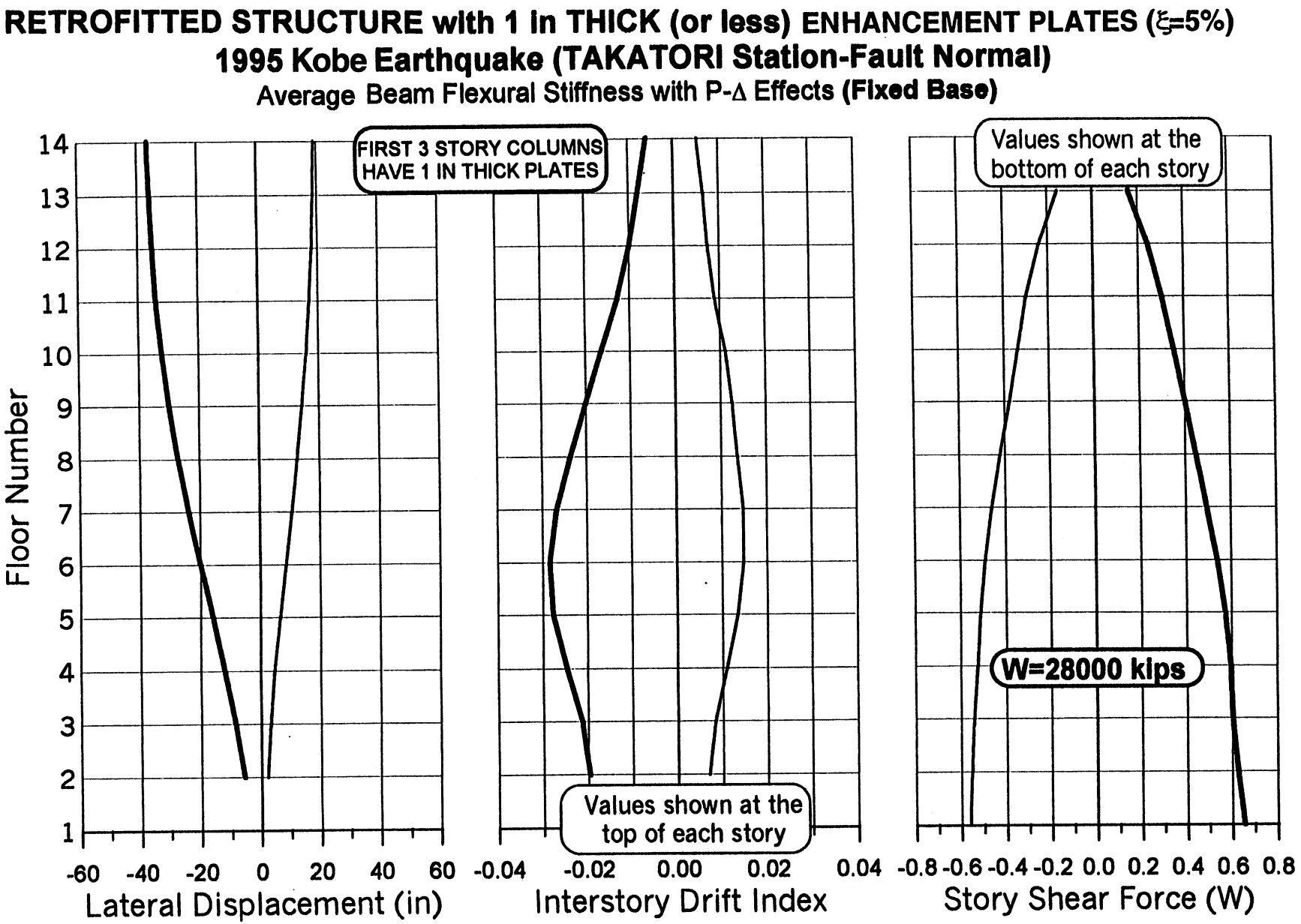

Figure 10.37 Lateral displacement, interstory drift index, and story shear force envelopes.

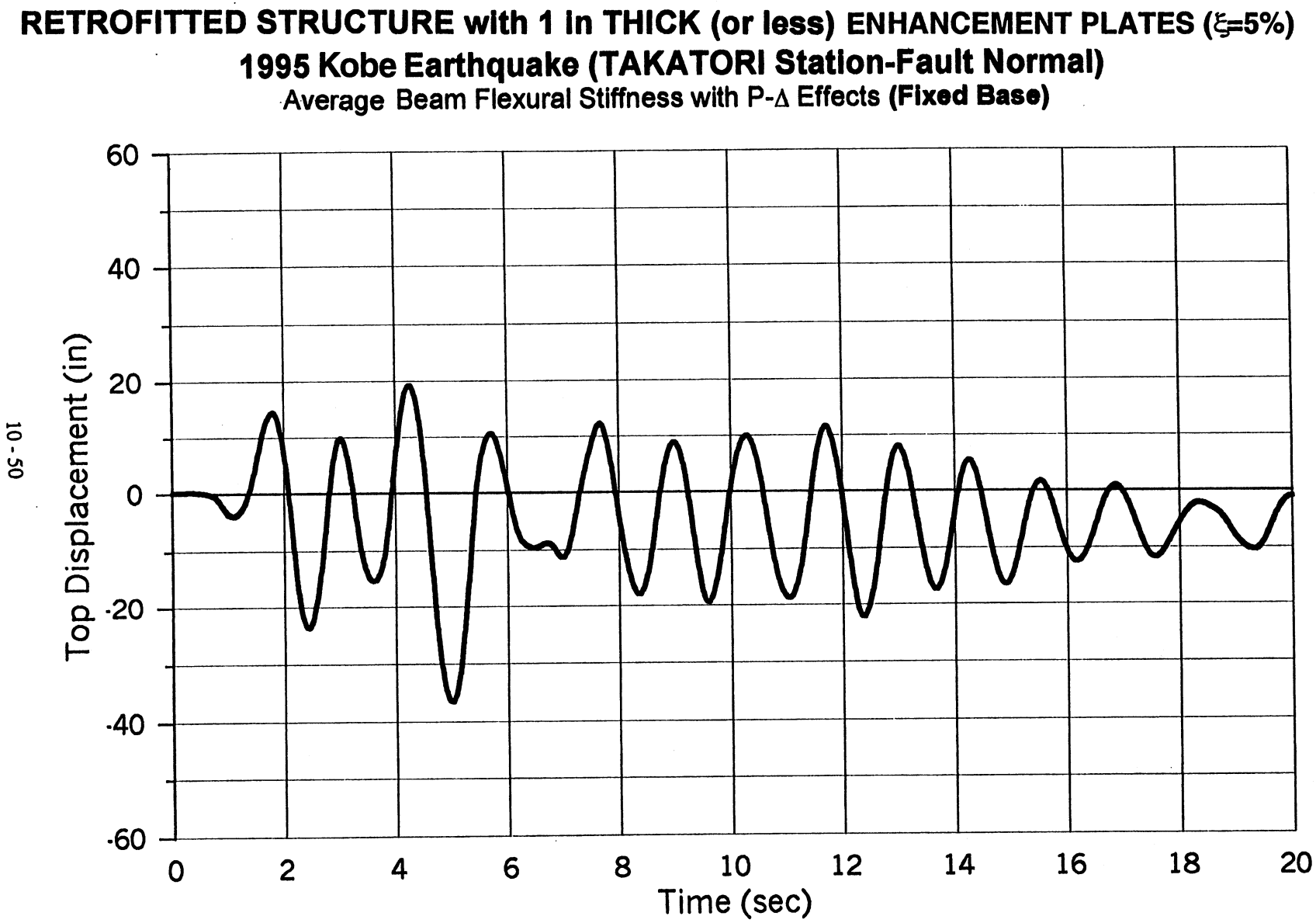

Figure 10.38 Time history of roof displacement.

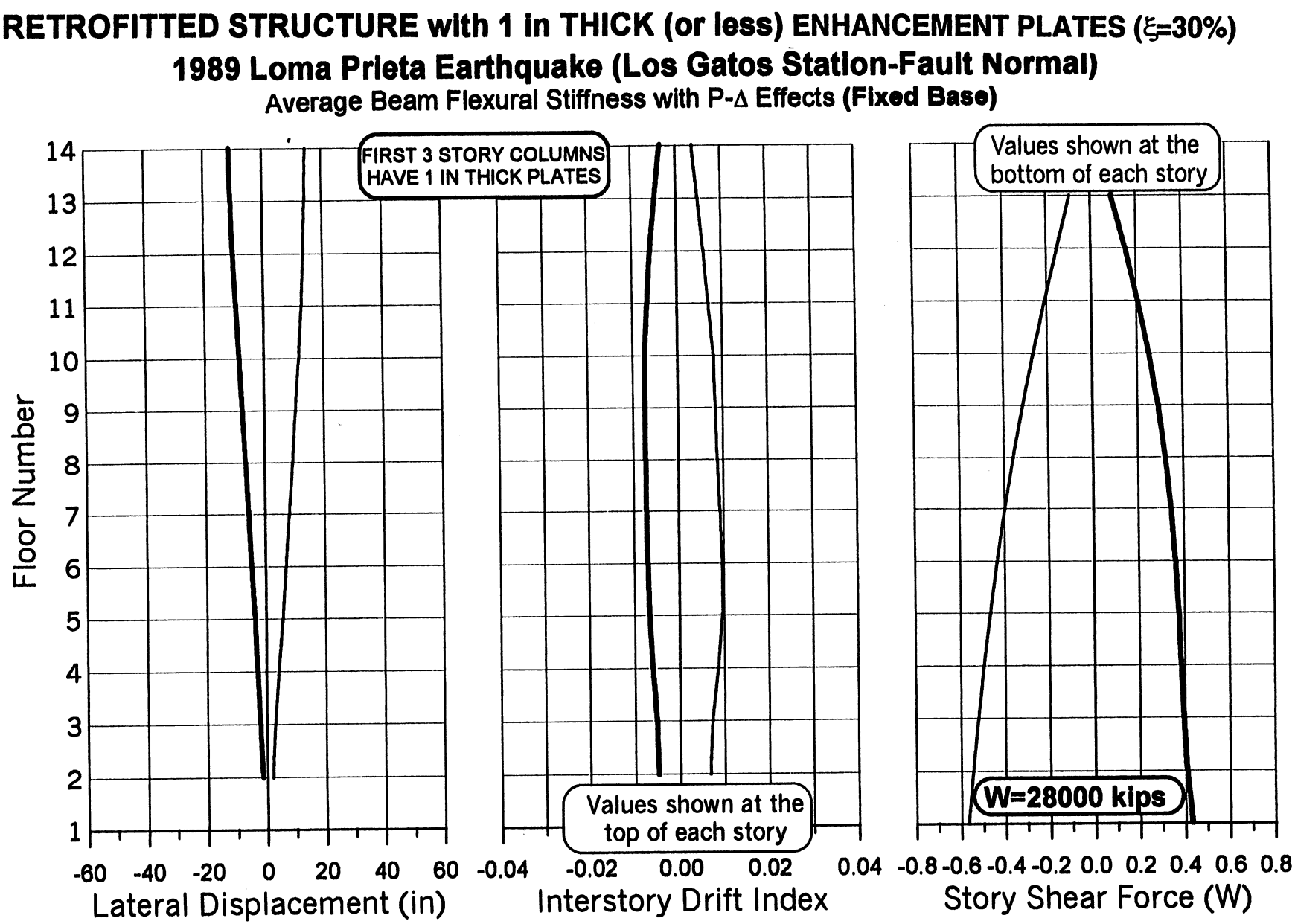

Figure 10.39 Lateral displacement, interstory drift index, and story shear force envelopes.

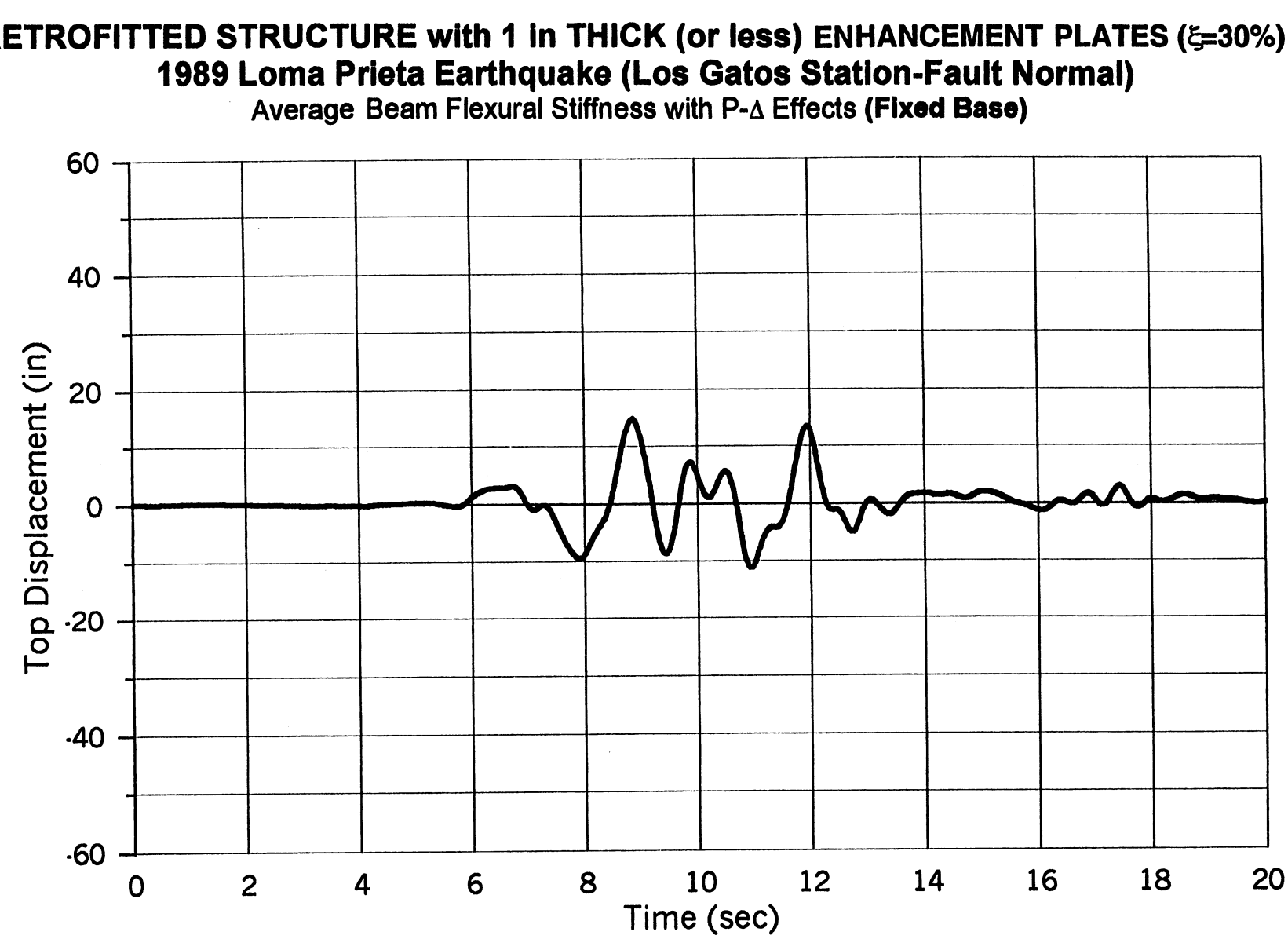

Figure 10.40 Time history of roof displacement.

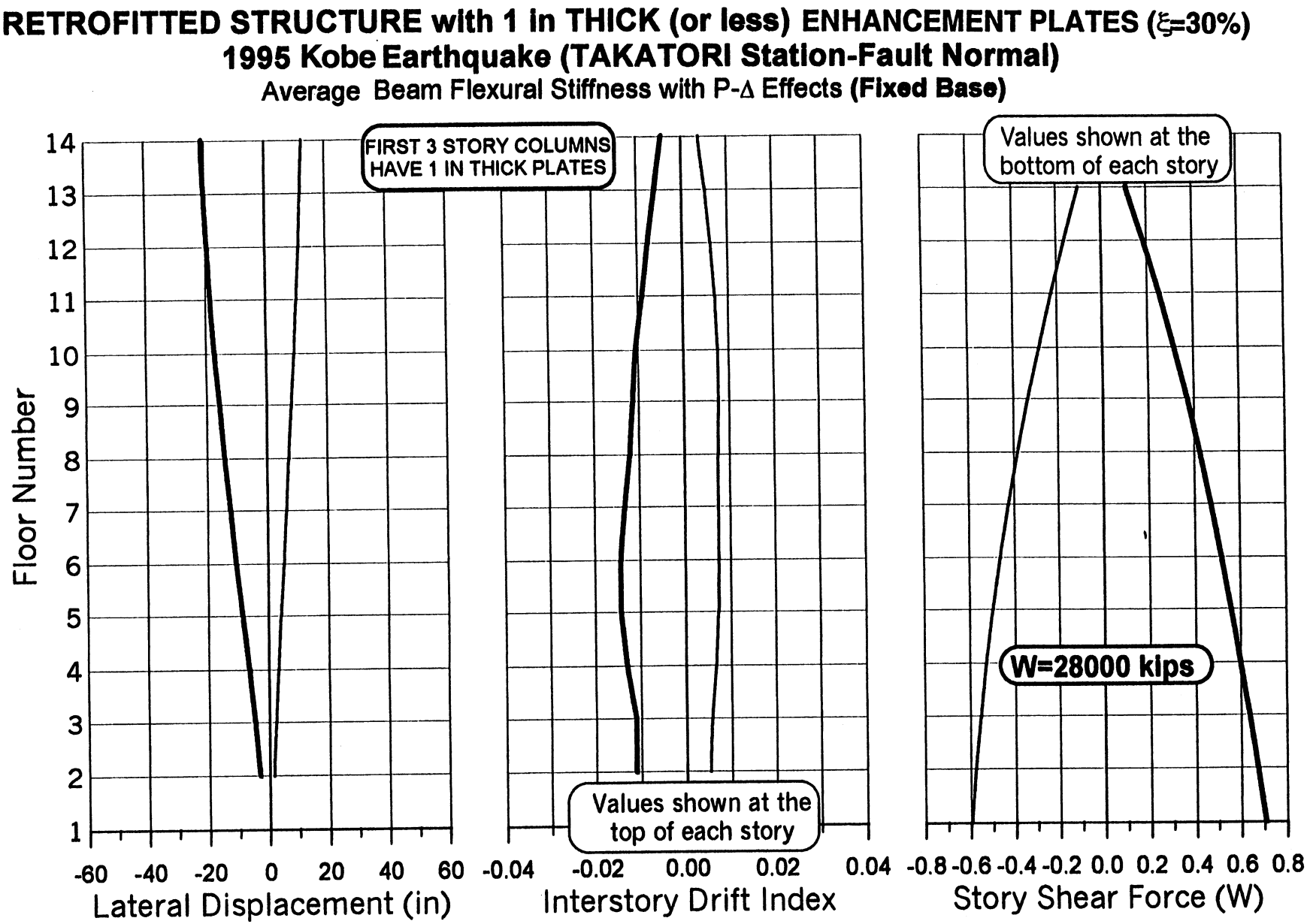

Figure 10.41 Lateral displacement, interstory drift index, and story shear force envelopes.

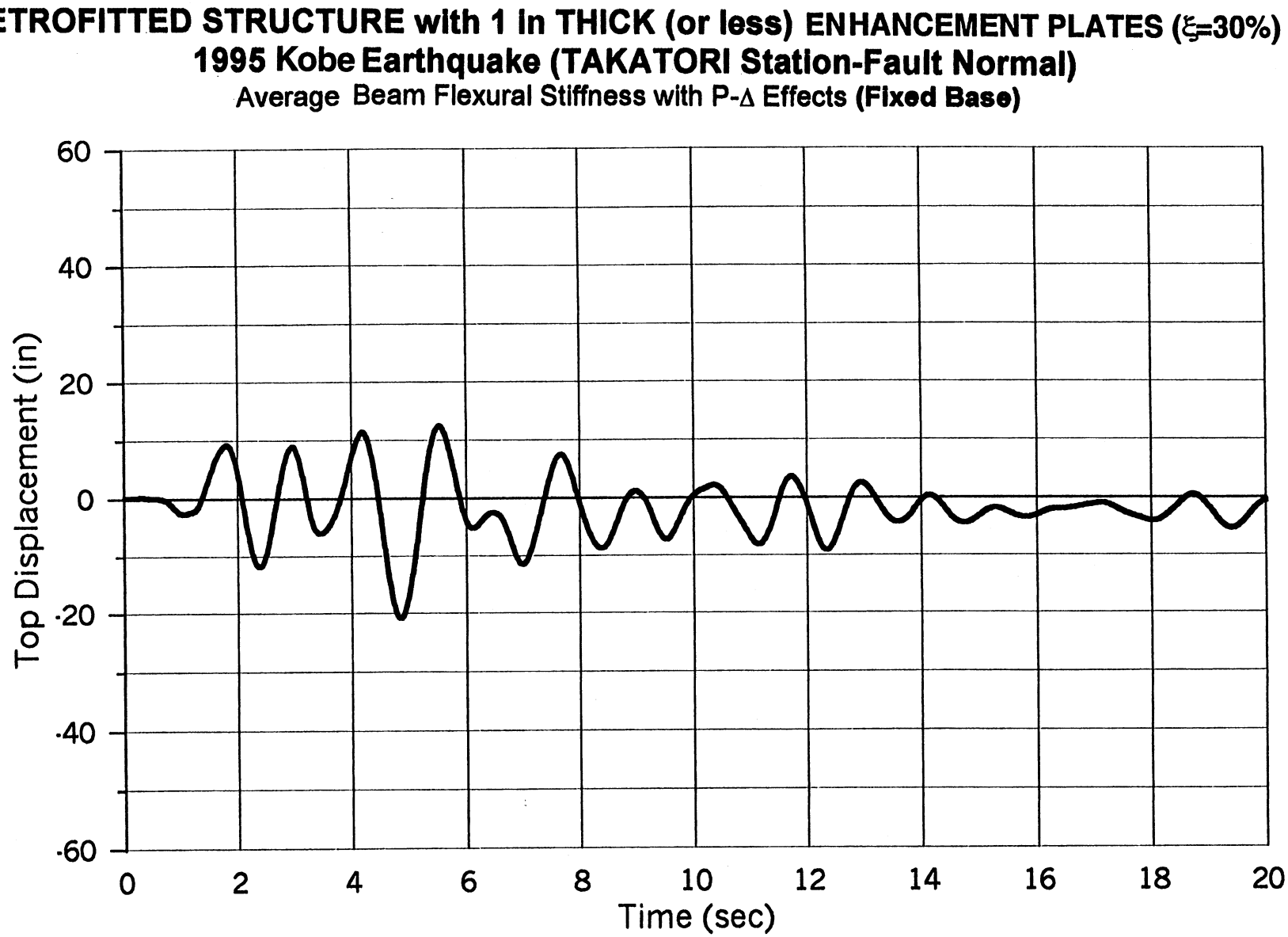

Figure 10.42 Time history of roof displacement.

11 Seismic Upgrading of Existing Building with Thinnest Practical Steel Plates and Use of Innovative Approach for Decreasing Demands

11.1 INTRODUCTORY REMARKS AND SELECTION OF INNOVATIVE STRATEGY

As discussed in the previous chapter, after trying stiffening, strengthening, and toughening the structural members with different thickness of steel plates and analyzing the degree of improvement in the performance (response) of the building through nonlinear static (pushover) and dynamic (time-history) analyses, it was concluded that this conventional strategy of just increasing the capacity of the structure will not lead to an efficient economical solution. Thus the use of an innovative strategy based on attempting to decrease (control) the demands was tried out rather than just trying to increase the supplied strength and stiffness because it lead to increase in the demands.

To minimize the observed weaknesses (see chapter six) it was considered necessary first to use the strategy of steel jacketing and encasing the structural members with steel plates but using the minimum practical steel plate thickness and then to decrease the demands (damage) by an innovative procedure. After a review of all available innovative strategies and techniques for controlling the demands (damage), it was concluded that one of the best strategies would be to increase the energy dissipation through the use of additional damping.

According to the above strategies, all the beams were encased with 1/8-in.-thick enhancement steel plates. Assuming that the thin 1/8-in.-thick steel plates are connected to the concrete to avoid its early buckling, a maximum compressive strain of 0.02 is assumed to control

the buckling of steel plates as well as the concrete crushing, the moment-curvature relationships for the retrofitted beam sections under negative bending moments are provided in Figures 11.1 and 11.2. For sections under positive bending moments, a maximum compressive strain of about 0.004 to 0.005, results in almost the same level of maximum curvature as under negative bending moments with maximum compressive strain of 0.02. These results are given Figures 11.3 and 11.4. Then, as discussed in section 4.2, the moment-rotation relationships for different beam segments are calculated. Note that the ratio between the yield positive to negative bending moment which was as low as 0.3 is now more than 0.6. This ratio for the maximum bending moments is even larger.

For all the columns, 1/8-in.-thick enhancement plates are used. The moment-axial load interaction diagrams and also the moment-curvature relationships for the first-story columns of interior frames are shown in Figures 11.5 and 11.8.

11.2 STRUCTURE WITH FOUNDATION AND BASEMENT FLEXIBILITY

11.2.1 Pushover Analysis under Inverted Triangularly Distributed Lateral Load

With constant incremental load of 10 kips, at a roof displacement of 61.4 in., the structure becomes analytically unstable. The displacement, interstory drift index, and the story shear force envelopes are given in Figure 11.9. The force-roof displacement relationship is given in Figure 11.10. At the point the structure becomes analytically unstable, it is on the verge of forming a story mechanism at the first story. A maximum interstory drift of 5.2% occurs at the first story, while the global drift index is about 3.1%. To avoid a weak-column strong-beam system, the first story column plates are replaced by ¼-in. steel plates. Since the corner columns are also very weak, ¼-in. steel plates are used for the corner columns at all the stories.

Using ¼-in.-thick enhancement plates for the first-story columns, at a roof displacement of 100 in., without having an analytically unstable structure, the displacement, interstory drift index, and the story shear force envelopes are calculated and shown in Figure 11.11. The maximum interstory drift of 8.7% occurs at the first story, while the global drift index is about 5% of which about 1% comes from the foundation rotation. The maximum base shear is about 30% of the weight of the building (W=26000 kips). Figure 11.12 shows the base shear versus roof displacement as well as its idealization by a bilinear relationship. In this idealization, the yield displacement is about 29 in. and therefore the global displacement ductility is about 3.4.

11.2.2 Response of Building under Pulse-Type Ground Motions

11.2.2.1 Response of structure with 5% damping

11-2-2-1-A 1989 Loma Prieta earthquake recorded at Los Gatos station. The period of the structure is about 2.6 sec. The displacement, interstory drift index, and the story shear force envelopes under the Los Gatos ground motion are given in Figure 11.13. The maximum roof displacement is about 52 in. As from Figure 11.12, the yield displacement is about 29 in., therefore, the global displacement ductility is about 1.8. The maximum interstory drift of about 4.0% occurs at the first three stories, while the global drift index is about 2.6%. It should be noted that about 0.7% of the drift is caused by the foundation rotation; therefore, the maximum tangential IDI is about 3.3%, which is not acceptable. The maximum base shear is about 34% of the weight of the building, which is larger than the value attained from pushover analysis (30%W), in spite of the fact that this value was obtained for a 100-in. displacement of the roof which is almost two times the maximum displacement obtained under the Los Gatos record.

Figure 6.4 shows the yield coefficient and displacement spectra due to the EQGM recorded at Los Gatos station during the 1989 Loma Prieta earthquake. Since the global displacement ductility of the response of the structural model is about 1.8, the displacement spectra suggest a maximum displacement of about 59 in. This is a directly calculated value. Interpolation using Figure 6.4 leads to a value of about 50 in. These values are larger than the maximum displacement at 2/3 of the height of the building (to be representative of an equivalent single degree of freedom system). The yield coefficient spectra suggest a yield coefficient, C_y, of about 0.50 rather than the time history maximum base shear of 0.34W, i.e. $(C_y)_{max}$ =0.34. In spite of the fact that C_y does include the damping force and the single-degree-of-freedom system that is considered in the development of the spectra does not have any strain hardening, it suggests a larger base shear compared to the base shear found from the inelastic analysis of the building which is about 0.34W. It should be noted that inclusion of P-Δ effects in the analysis of the building results in more flexible structure which to some extent will result in smaller base shear forces.

11-2-2-1-B 1995 Kobe earthquake ground motions recorded at Takatori station. The displacement, interstory drift index, and the story shear force envelopes under the Takatori ground motion are given in Figure 11.14. The maximum roof displacement is about 38 in. From

Figure 11.12, the yield displacement is about 29 in., therefore, the global displacement ductility is about 1.3. The maximum interstory drift of 2.7% occurs at the sixth and seventh stories, while the global drift index is about 1.9%. Note that about 0.7% of the drift is caused by the foundation rotation, therefore, the maximum tangential IDI is about 2.0%, which is within the acceptable range. The maximum base shear is about 30% of the weight of the building.

Figure 6.6 shows the yield coefficient and displacement spectra due to the EQGM recorded at Takatori station during the 1995 Kobe Earthquake. The global displacement ductility of the response of the structural model is about 1.3. At a period of about 2.6 sec, the displacement spectra for ductility equal 1.3 suggest a maximum displacement of about 31 in., which is close to the maximum displacement of about 32 in. at the 2/3 of the height of the building (to be representative of an equivalent single-degree-of-freedom system). The yield coefficient spectra suggest a yield coefficient, C_y, of about 0.33 which results in a base shear that is also close to the base shear found from the inelastic analysis of the building which is about 0.30W.

11.2.2.2 Response of structure with 30% damping

The behavior of the structure using the same enhancement plates discussed above with additional viscoelastic or viscous damping is discussed in this section.

11-2-2-2-A 1989 Loma Prieta earthquake ground motions recorded at Los Gatos station. The displacement, interstory drift index, and the story shear force envelopes under the Los Gatos ground motion are given in Figure 11.15. The maximum roof displacement is about 31 in., which is close to the idealized yield displacement. By increasing the damping coefficient, ξ, from 0.05 to 0.30, the maximum roof displacement and the maximum IDI dropped by about 40% and 48%, respectively. Excluding a 0.7% drift caused by the foundation rocking, the maximum tangential IDI is only about 1.4% which is well within the acceptable range. By increasing damping coefficient, the base shear is not changed and still is equal to about 34% of the weight of the building.

11-2-2-2-B 1995 Kobe earthquake ground motions recorded at Takatori station. The displacement, interstory drift index, and the story shear force envelopes under the Takatori ground motion are given in Figure 11.16. The maximum roof displacement is about 31 in., which

is close to the yield displacement. By increasing the damping coefficient from 0.05 to 0.30, the maximum roof displacement and the IDI_{max} dropped by about 25%. Excluding a 0.7% drift caused by the foundation rocking, the maximum IDI_{tang} is only about 1.3%. There is a small reduction in base shear, from 0.30W to 0.29W.

11.3 SUMMARY

Some of the results of the analyses carried out are summarized in Table 11.1. Nonlinear analysis of the response of the lightly steel jacketed and encased structure with different amount of total ξ_{eff} indicated that with a $\xi_{eff} \equiv 30\%$ it was possible to adequately control the response to the most critical pulse-type EQGMs. By adding minimum enhancement plates having minimum practical thickness, along with viscoelastic or viscous dampers ($\xi_{eff} \equiv 30\%$), the IDI_{tang} for the structure with rocking foundation is reduced to 1.4% and 1.3% under the Los Gatos and Takatori ground motions, respectively (see Table 11.1). Furthermore, the base shear for the retrofitted structures with foundation rocking is now limited to only 34% of the weight of the building.

If the dampers were not added, the IDI_{tang} for the structure with rocking foundation would be about 3.3% and 2.0% under the Los Gatos and Takatori ground motions, respectively, which is not acceptable.

Although response spectra of the Los Gatos ground motion overestimates the time-history response of the structure, the time-history response of the structure to the Takatori ground motion is fairly well predicted by the response spectra.

Table 11.1 Lightly Retrofitted Structure (W≈26000 kips & H≈2000 inches)

Type of Supports	Response Parameters	Pushover Analysis[1]	Los Gatos Ground Motion (1989 Loma Prieta Earthquake)			Takatori Ground Motion (1995 Kobe Earthquake)		
			Spectral Response[2] (ξ =5%)	Dynamic Analysis[1] (ξ =5%)	Dynamic Analysis[1] (ξ =30%)	Spectral Response[2] (ξ =5%)	Dynamic Analysis[1] (ξ =5%)	Dynamic Analysis[1] (ξ =30%)
Basement & Foundation Flexibility Included (T=2.6 sec) (Δ_y≈29 in)	Δ_{top} (in)	100(μ=3.4)		52 (μ=1.8)	31		38 (μ=1.3)	31
	$\Delta_{2/3H}$ (in)	92	59	44	25	31	32	22
	IDI_{ave}	5.0%		2.6%	1.6%		1.9%	1.6%
	IDI_{max}	8.7%		4.0%	2.1%		2.7%	2.0%
	IDI(ratio)	1.7		1.5	1.3		1.4	1.3
	$max\theta_{found}$	1.0%		0.7%	0.7%		0.7%	0.7%
	IDI_{tang}	7.7%		3.3%	1.4%		2.0%	1.3%
	V_{base} (W%)	30%	50%[3]	34%[4]	34%[4]	33%[3]	30%[4]	29%[4]

(1) P-Δ effects are included.
(2) Single Degree of Freedom system is elastic-perfectly plastic and P-Δ effect is not included (response for corresponding ductility).
(3) Viscous damping forces not included.
(4) Viscous damping forces included.

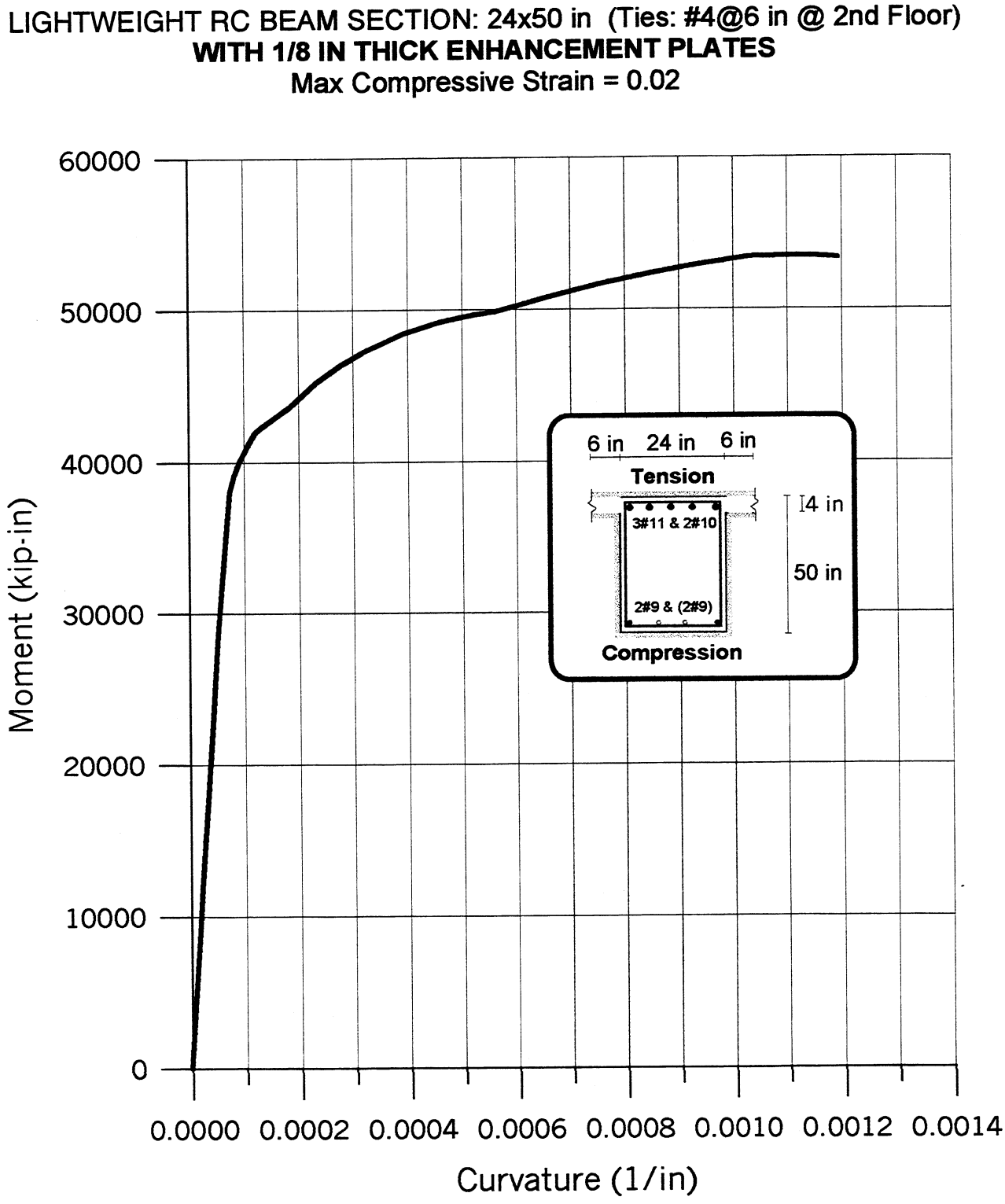

Figure 11.1 Moment-curvature relationship for retrofitted beams at second floor.

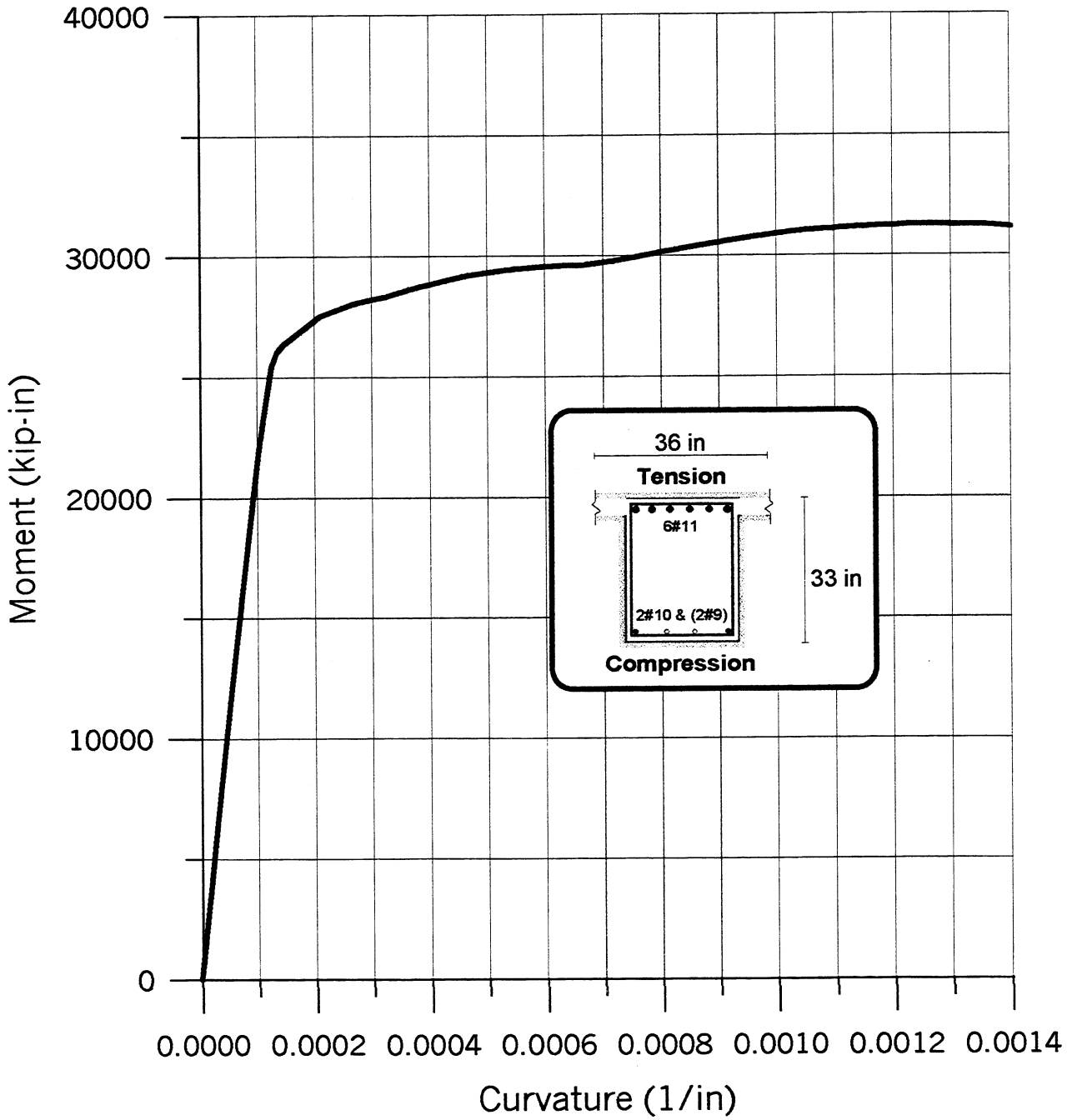

Figure 11.2 Moment-curvature relationship for retrofitted beams at 3rd to 5th floors.

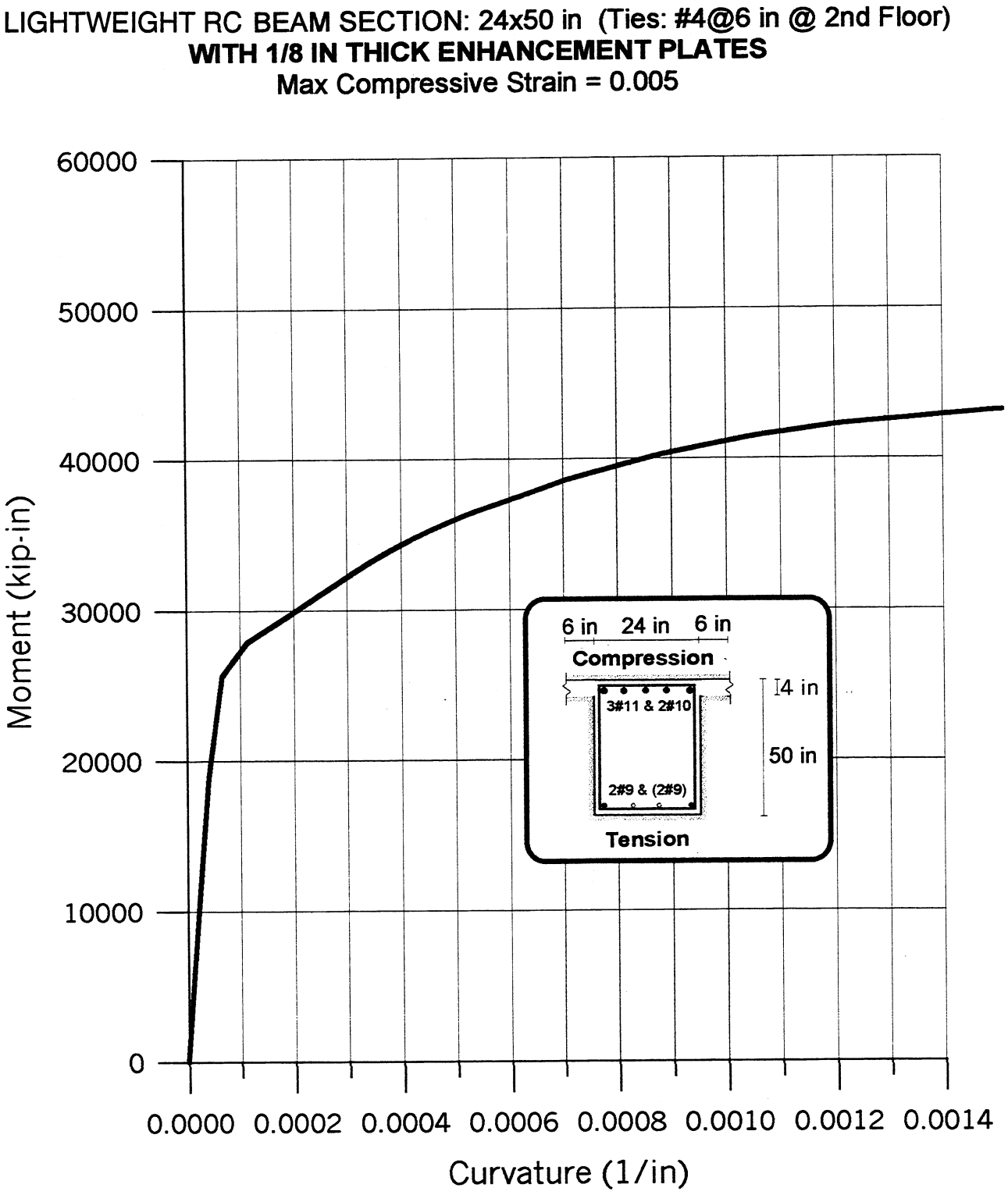

Figure 11.3 Moment-curvature relationship for retrofitted beams at second floor.

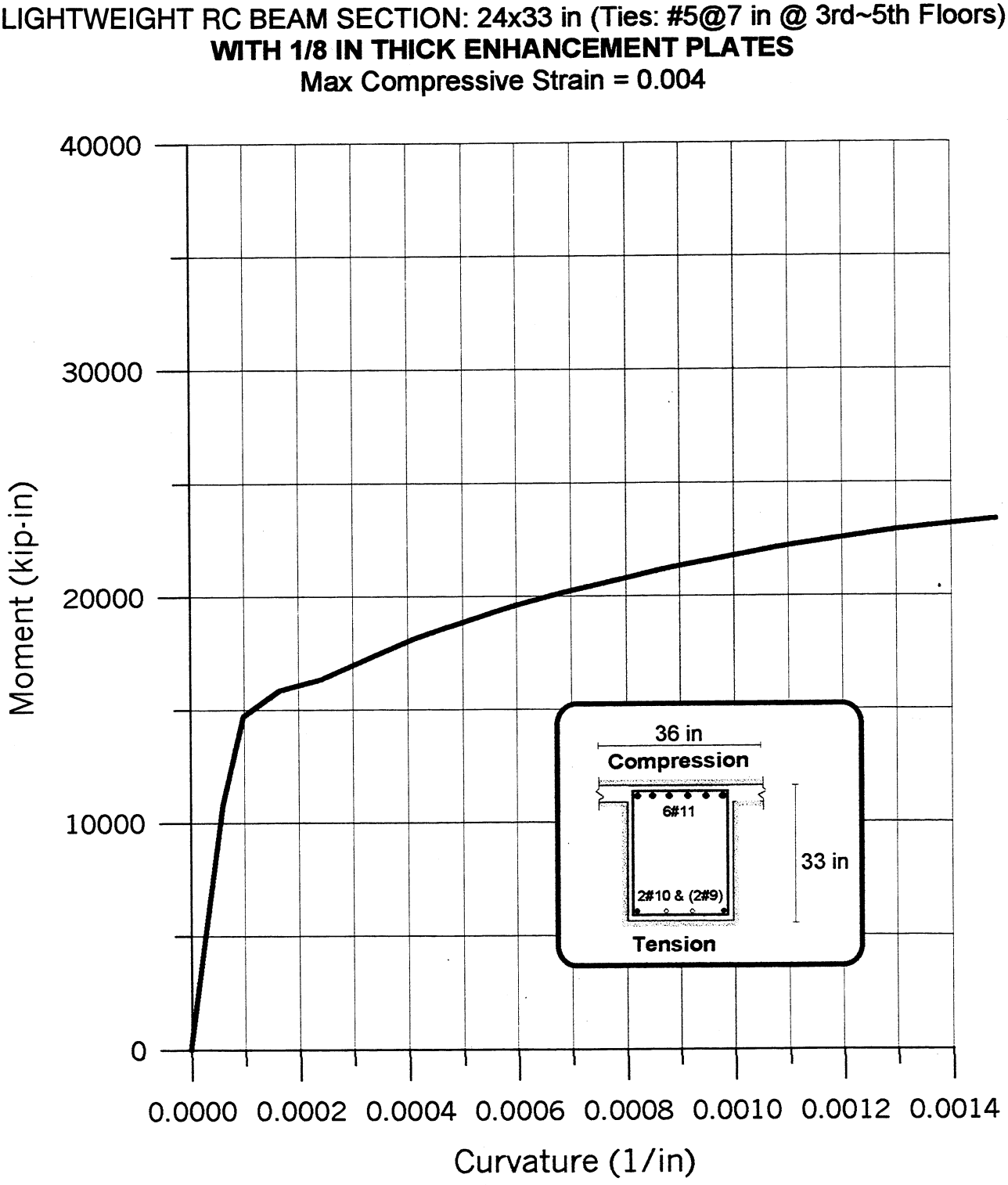

Figure 11.4 Moment-curvature relationship for retrofitted beams at 3rd to 5th floors.

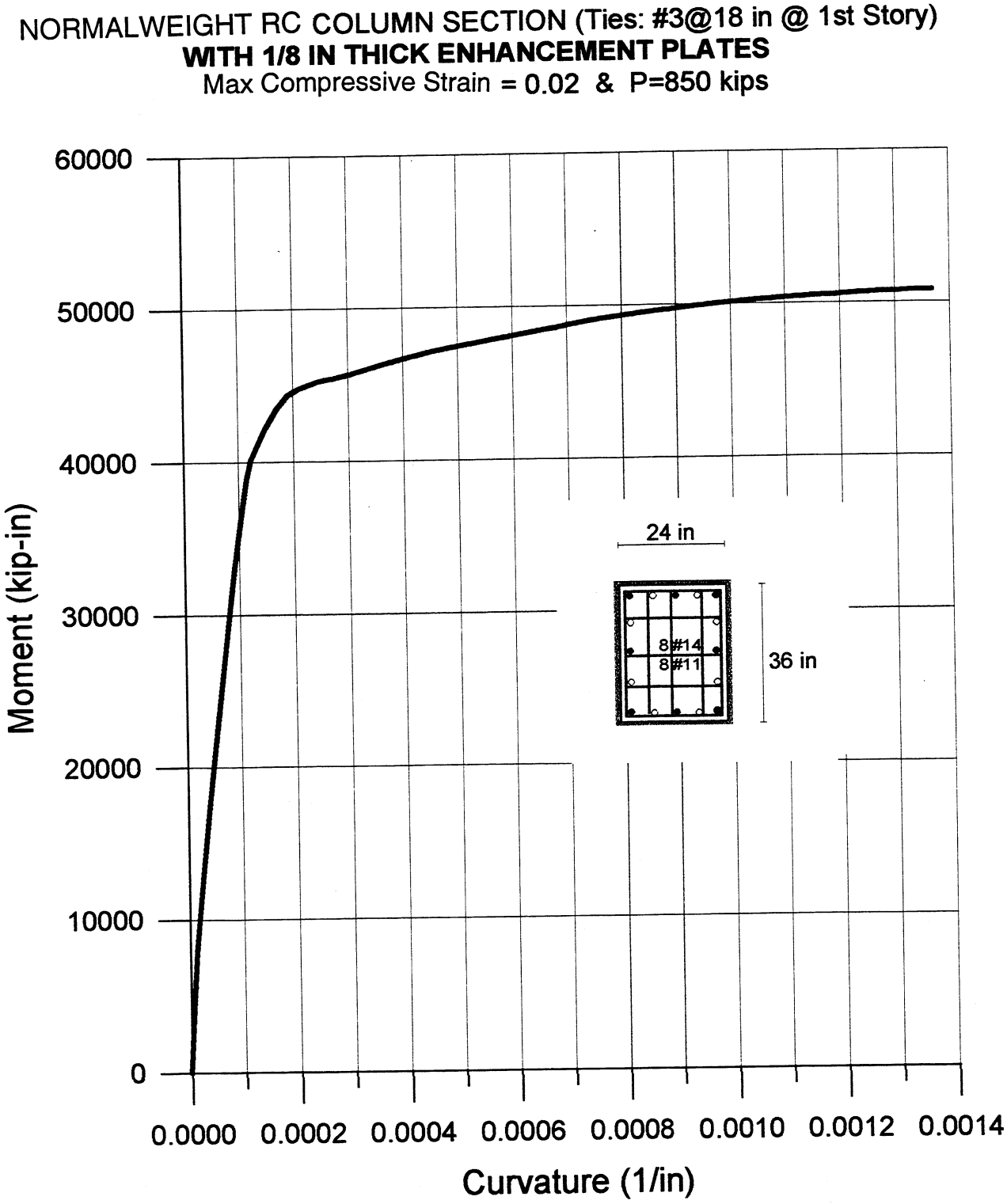

Figure 11.5 Moment-curvature relationship for retrofitted column (1A-F) in first story.

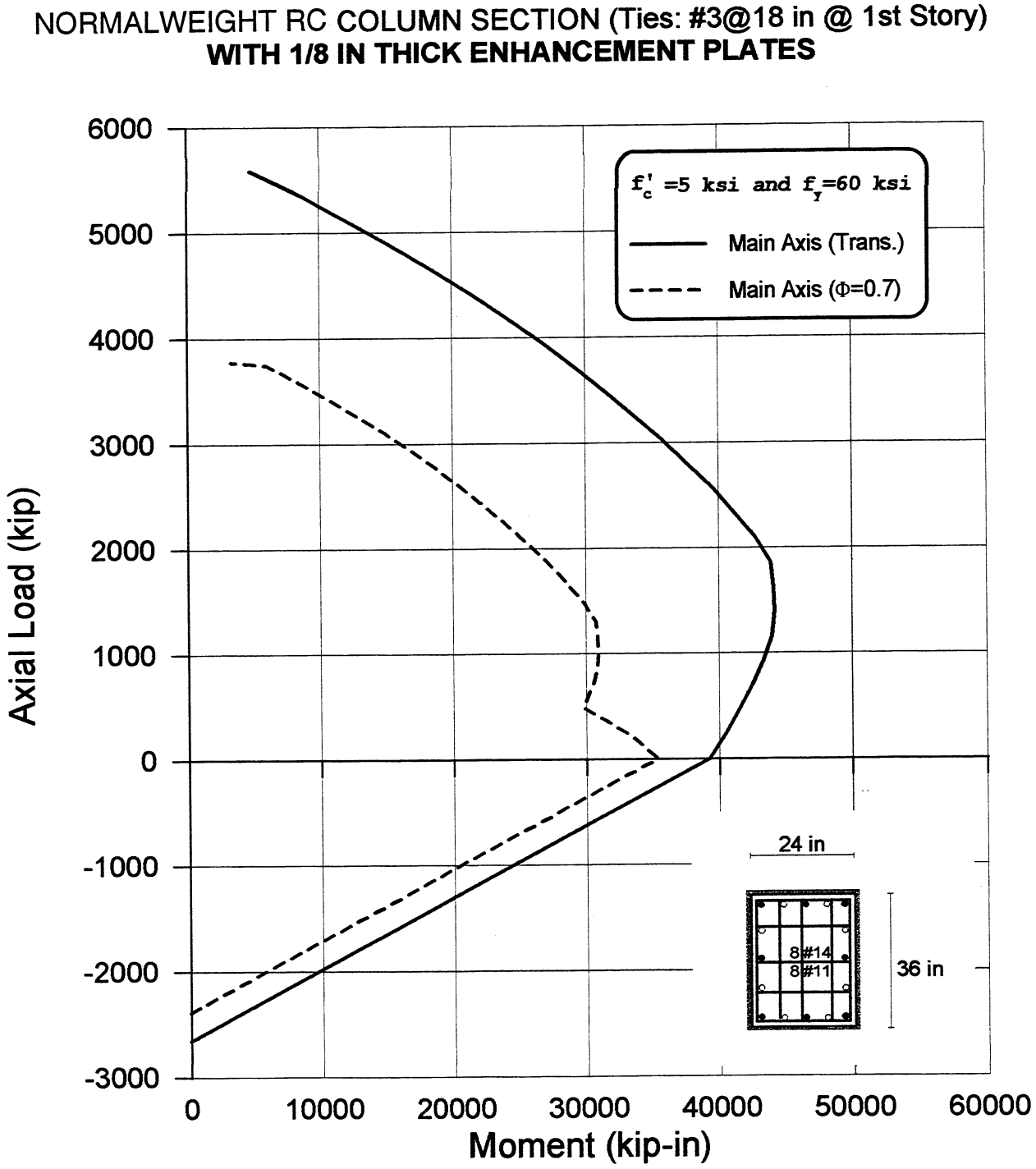

Figure 11.6 Moment-axial load interaction diagram for retrofitted column (1A-F) in 1st story.

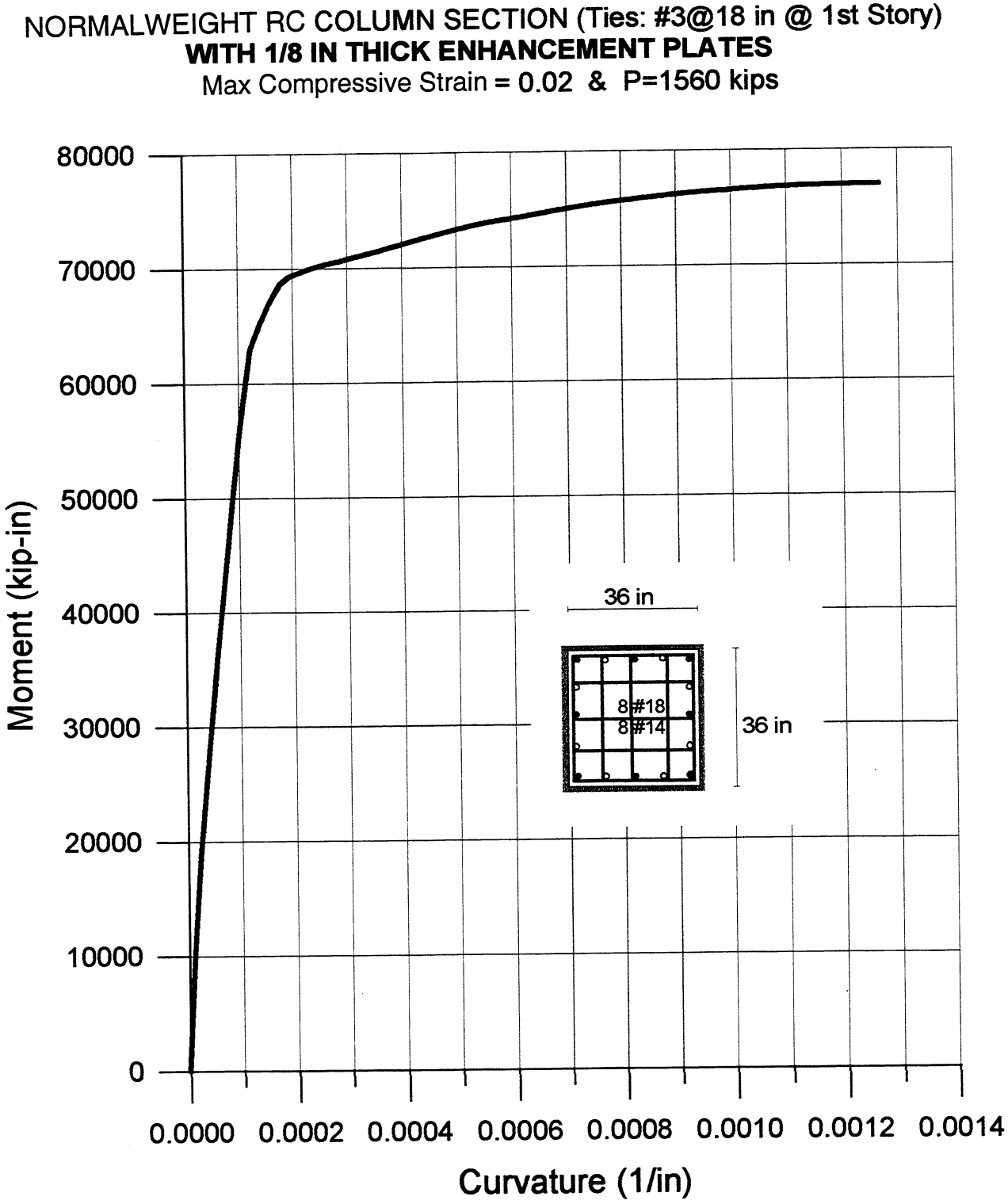

Figure 11.7 Moment-curvature relationship for retrofitted column (2A-F) in first story.

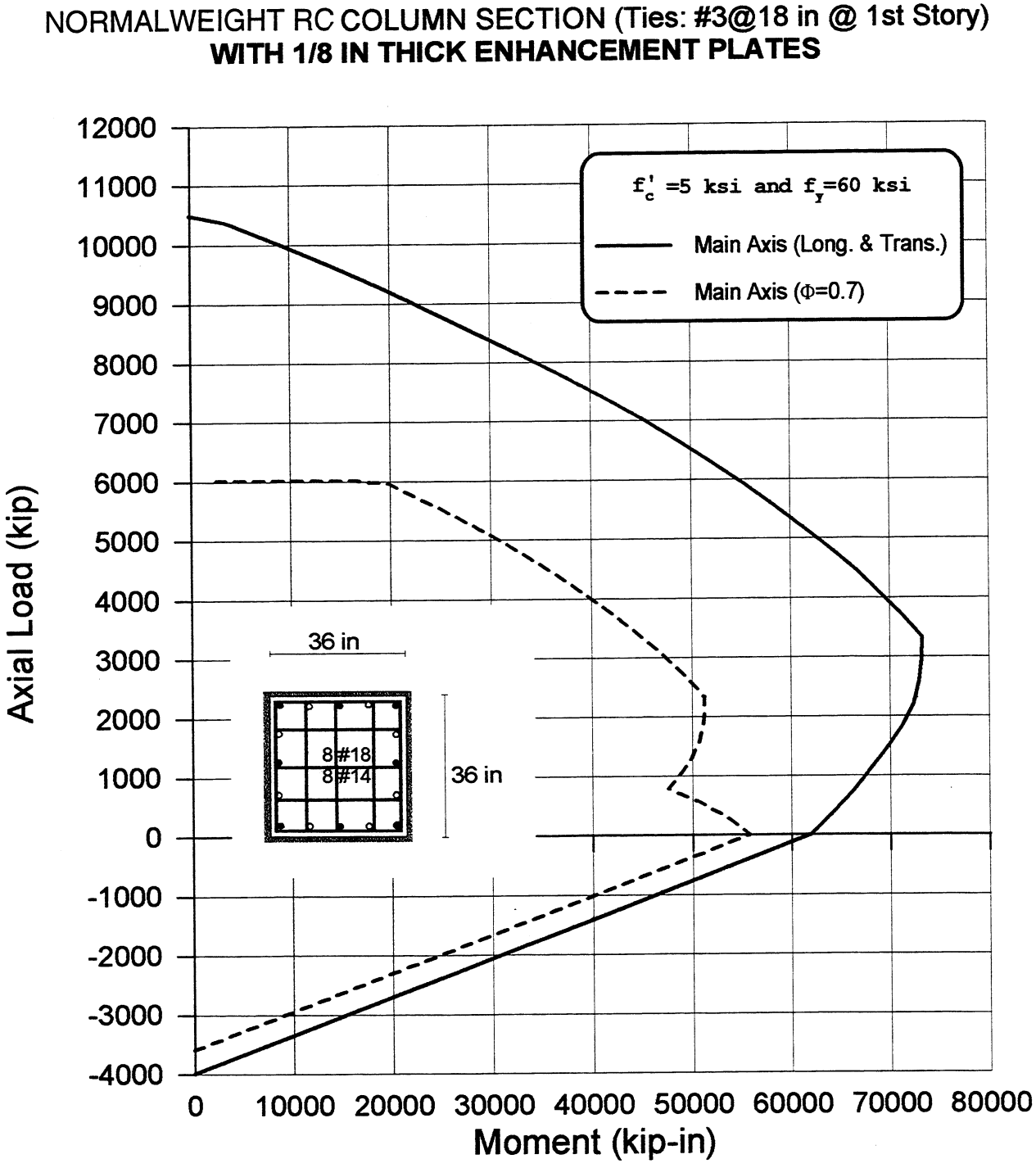

Figure 11.8 Moment-axial load interaction diagram for retrofitted column (2A-F) in first story.

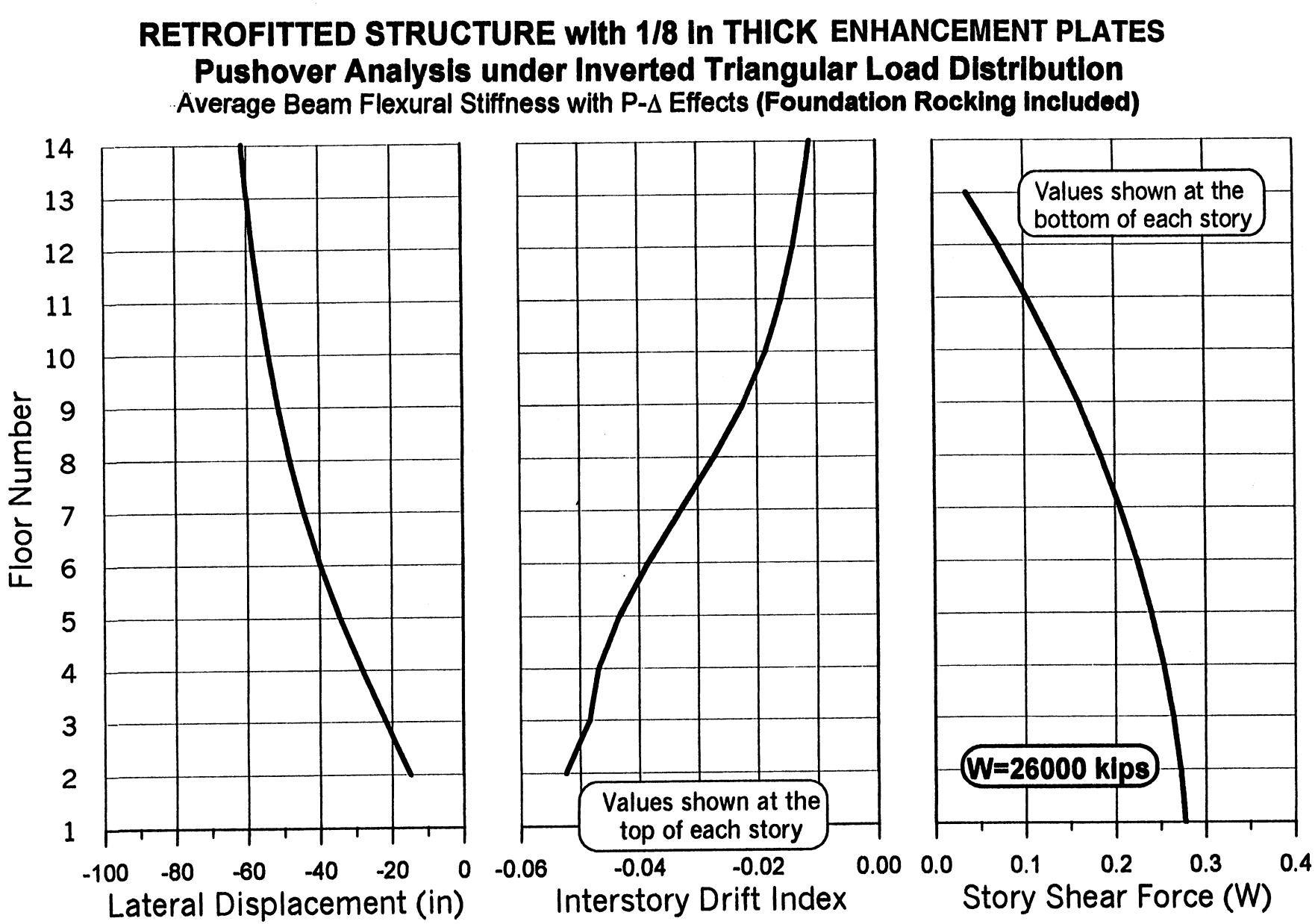

Figure 11.9 Lateral displacement, interstory drift index, and story shear force envelopes.

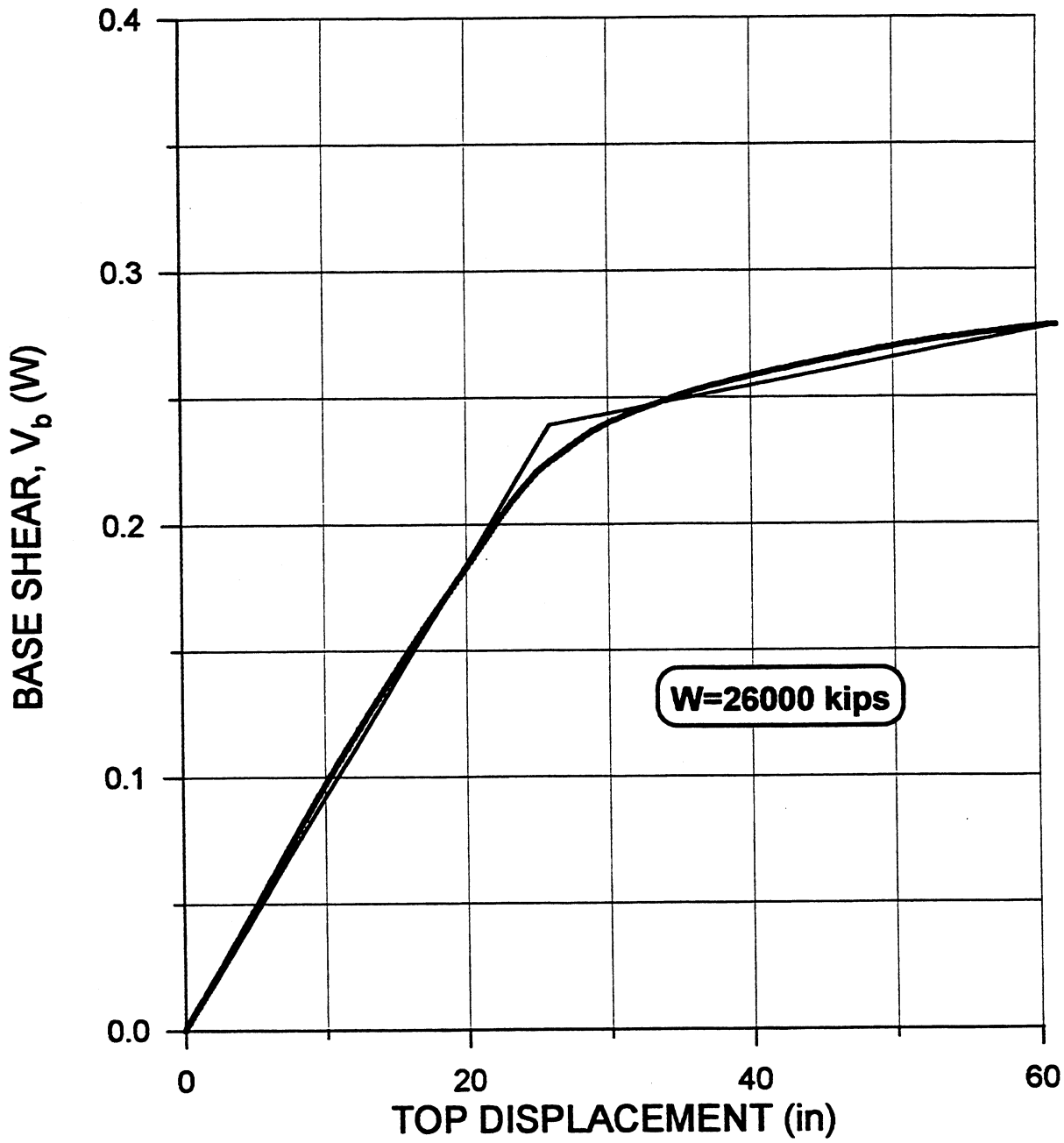

Figure 11.10 Base shear versus roof displacement and its bilinear idealization with Δ_y=25 in, V_y=0.24W and μ_Δ=2.4.

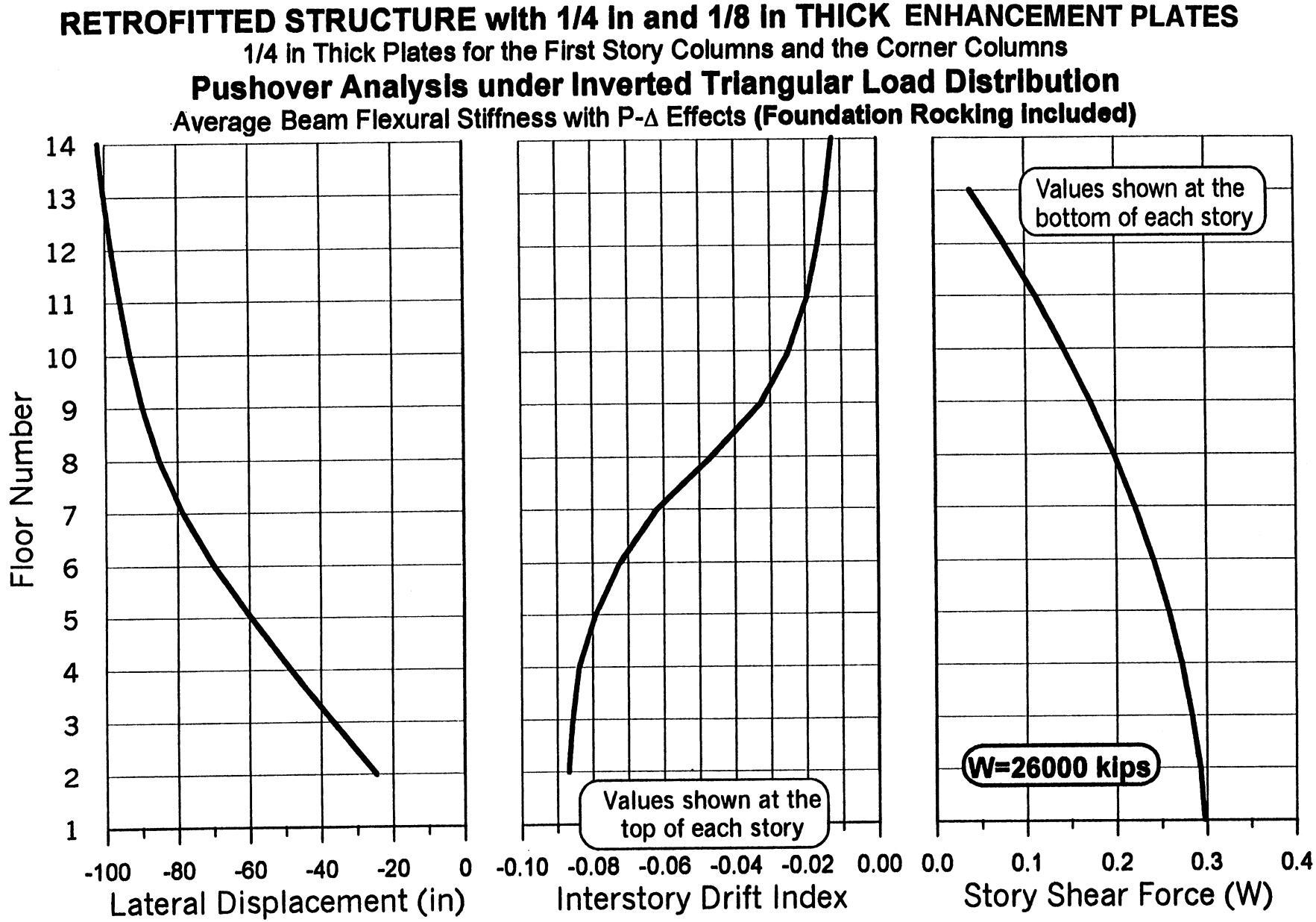

Figure 11.11 Lateral displacement, interstory drift index, and story shear force envelopes.

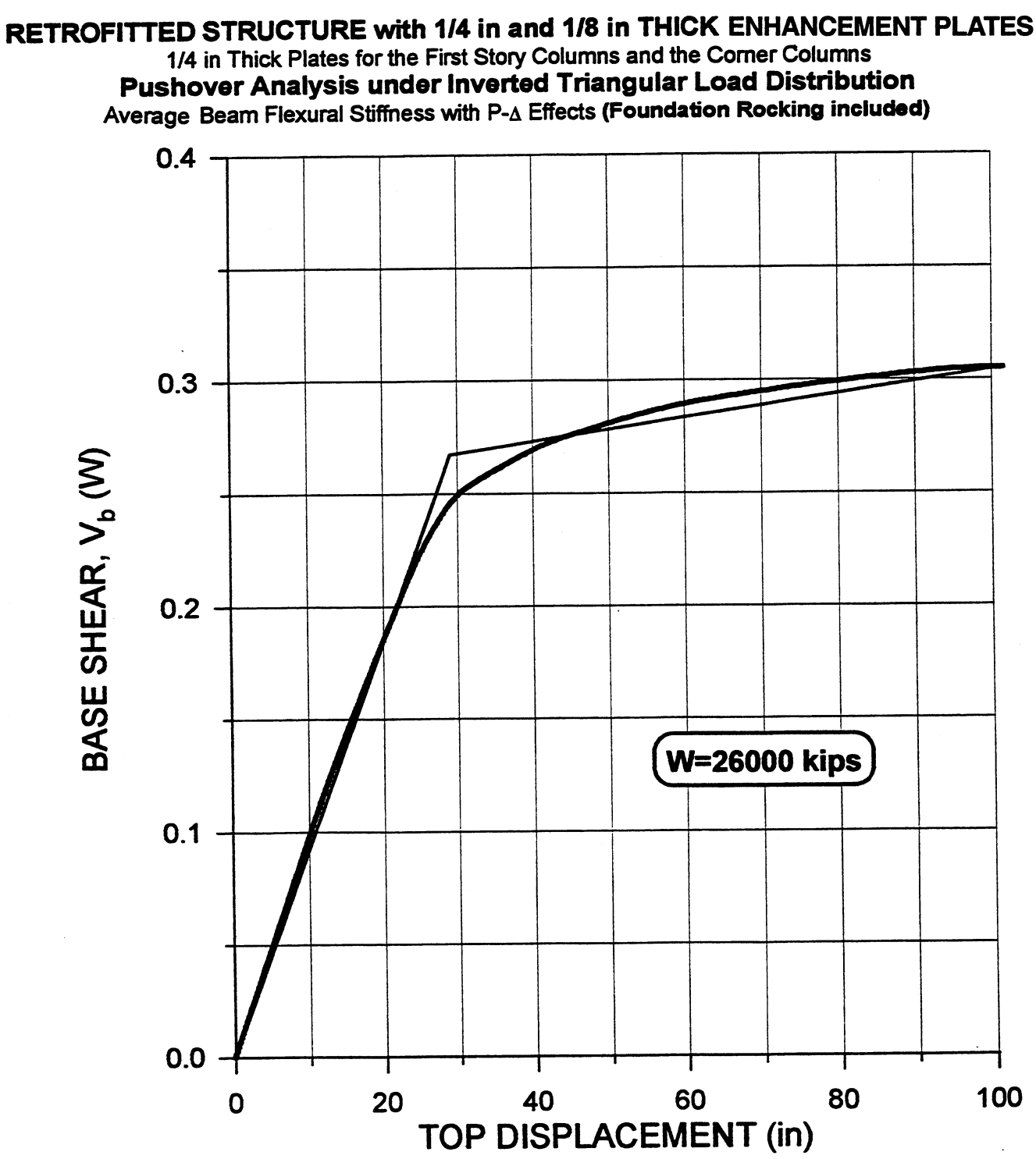

Figure 11.12 Base shear versus roof displacement and its bilinear idealization with Δ_y=29 in, V_y=0.27W and μ_Δ=3.5.

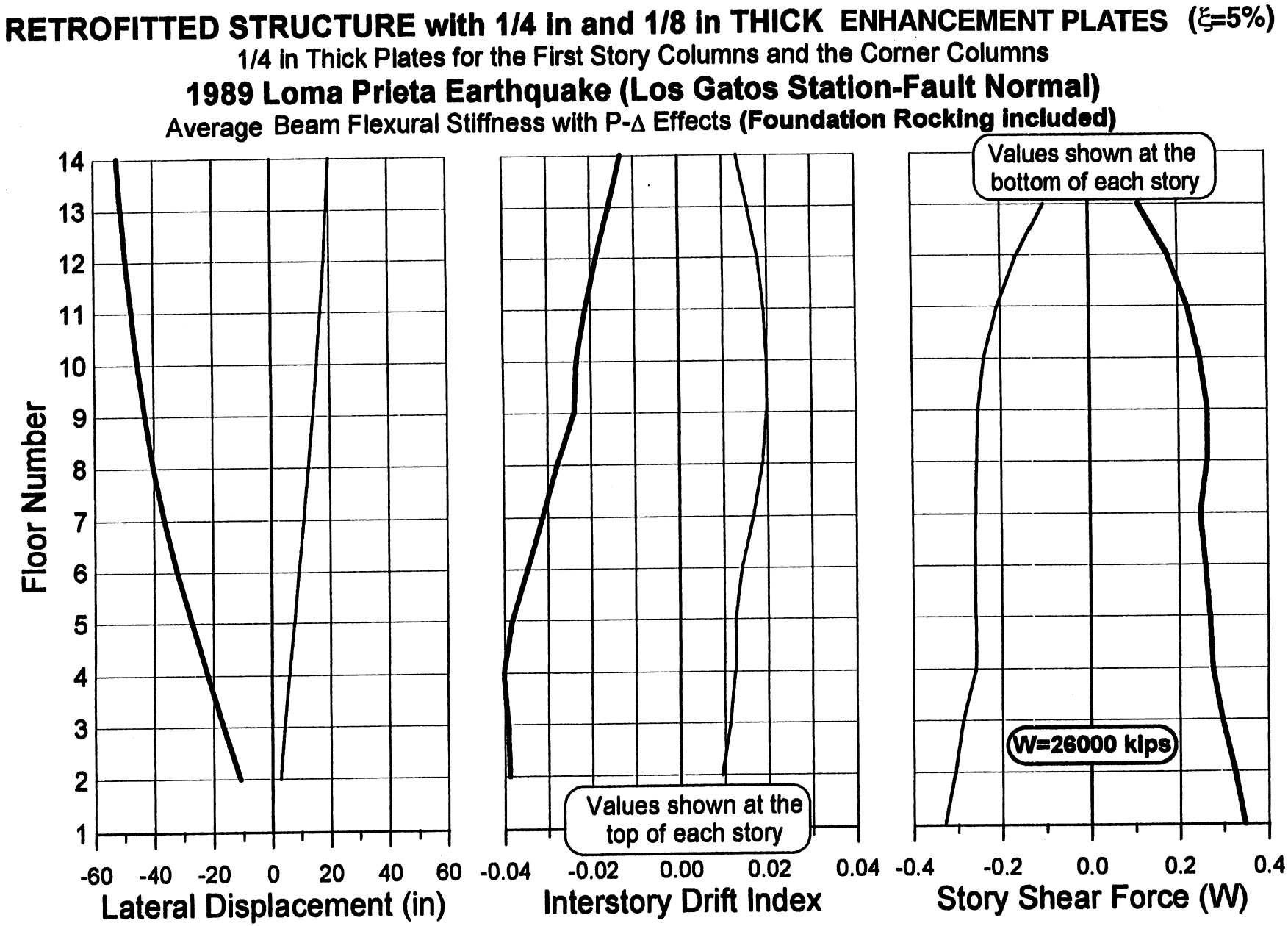

Figure 11.13 Lateral displacement, interstory drift index, and story shear force envelopes.

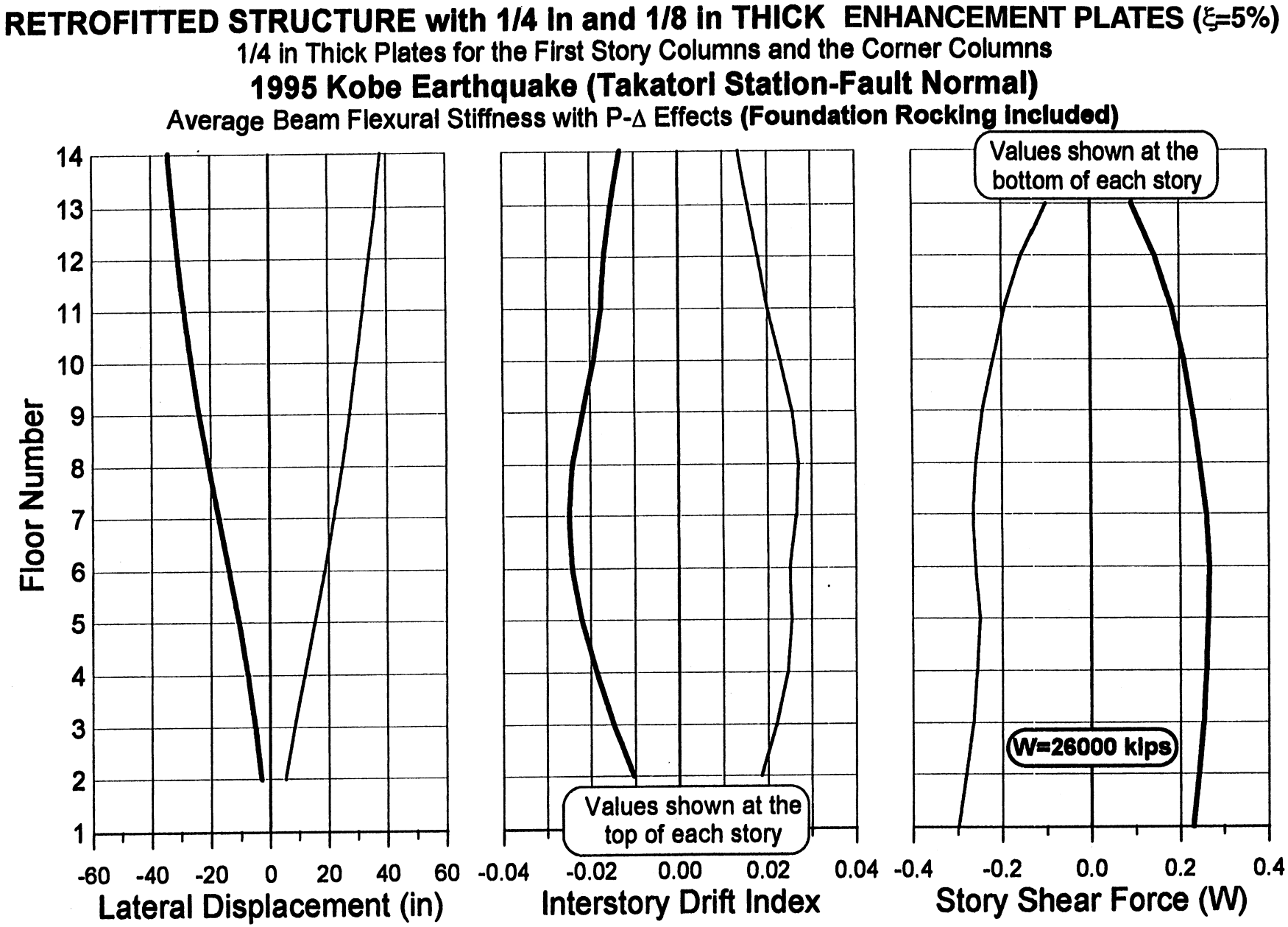

Figure 11.14 Lateral displacement, interstory drift index, and story shear force envelopes.

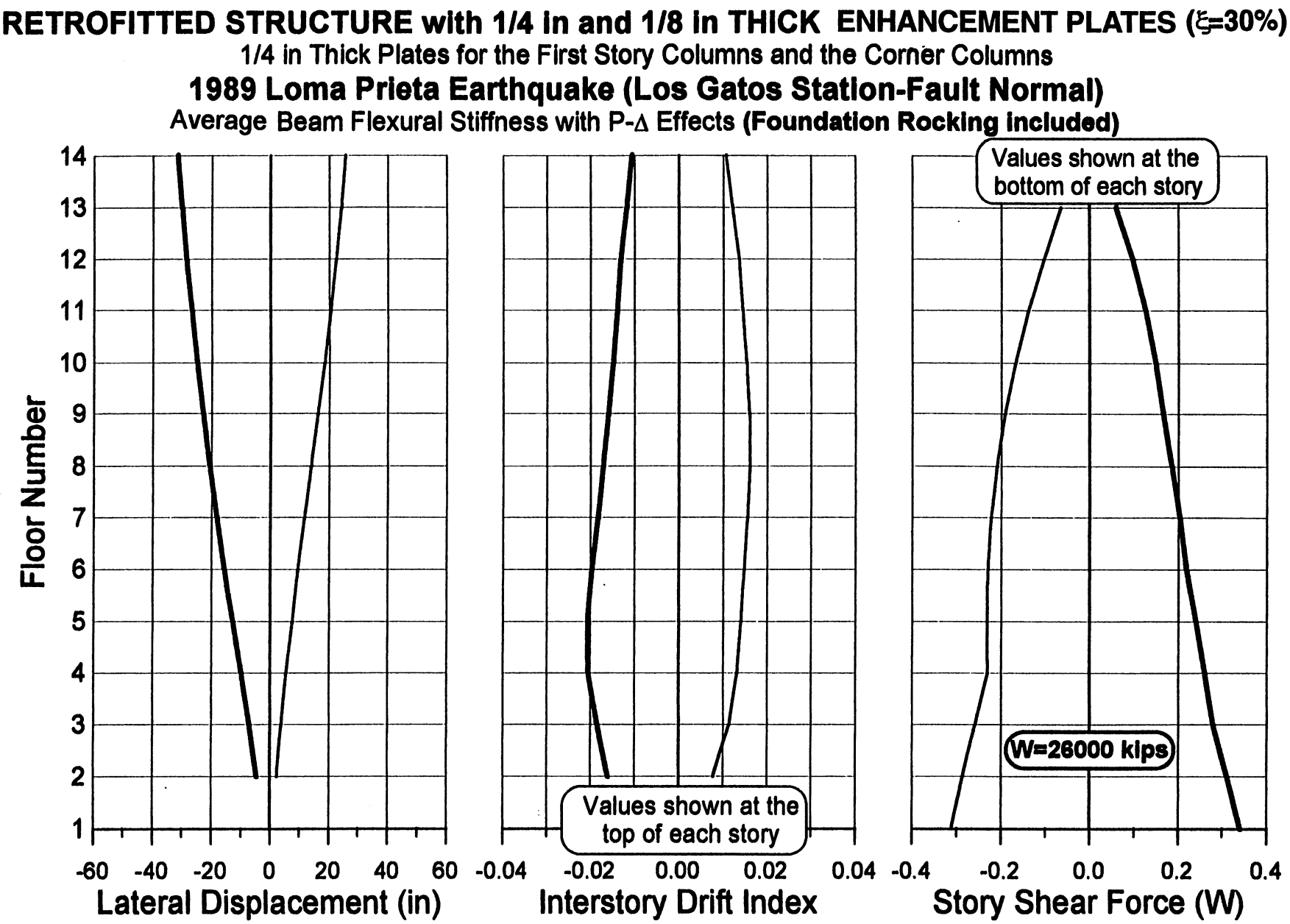

Figure 11.15 Lateral displacement, interstory drift index, and story shear force envelopes.

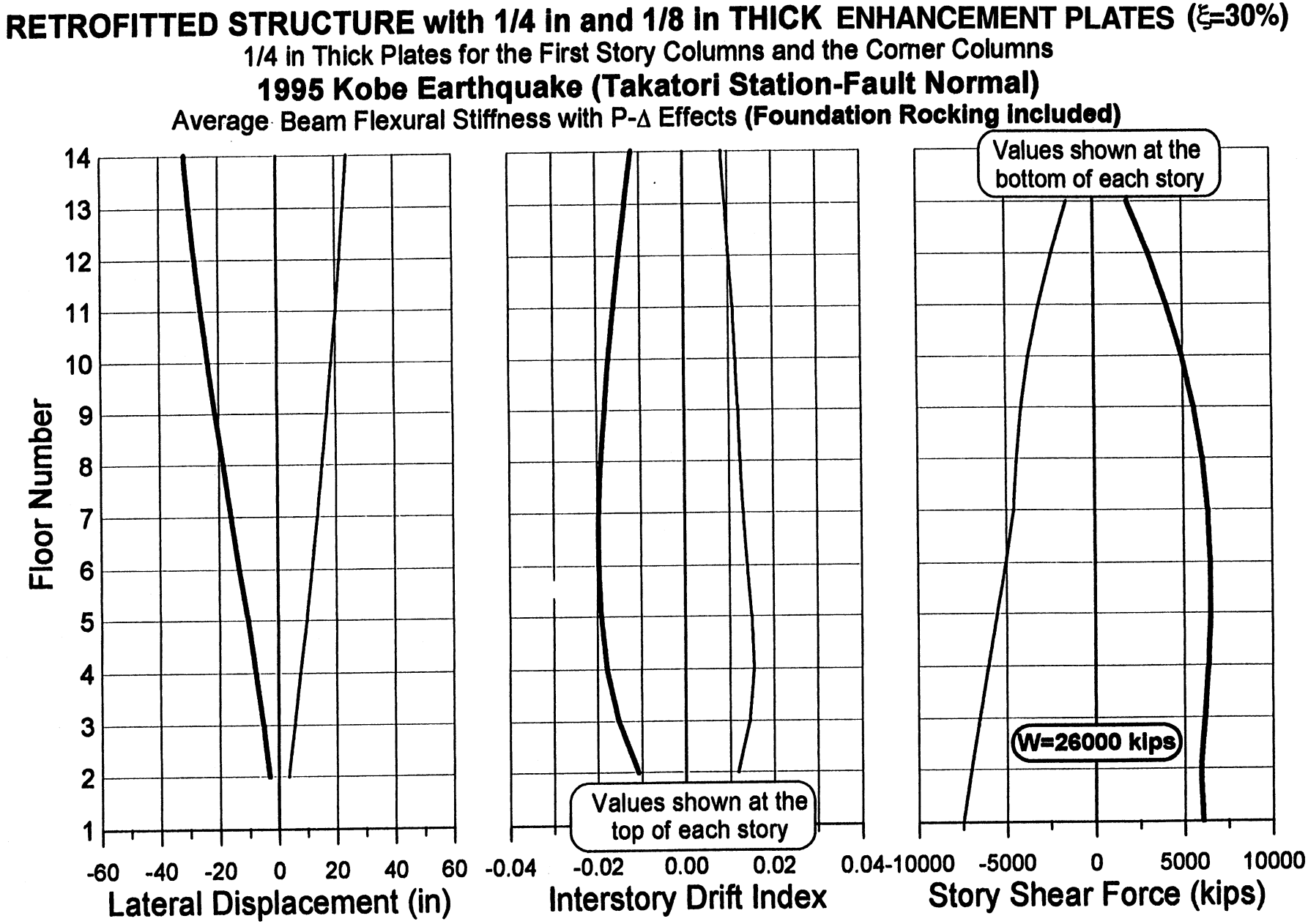

Figure 11.16 Lateral displacement, interstory drift index, and story shear force envelopes.

12 Summary, Conclusions, and Recommendations

12.1 SUMMARY

A review of the design and the as-built drawings made it clear that the structural system has several weaknesses being the main ones following: (1) inadequate transverse reinforcement along the height of the columns; (2) no transverse reinforcement at the girder-column joints; (3) lack of adequate amount and detailing of the longitudinal and transverse reinforcement along the girders; (4) lack of adequate anchorage of the girder bottom reinforcement at the joints; and (5) lack of adequate lap splicing of the longitudinal reinforcement.

In addition to the above weaknesses, results from linear and nonlinear static (pushover) and dynamic (modal and time history) analyses show that the lateral stiffness of the structural system is very low, particularly in the transverse direction (T_1=3.2 sec) and that several members have yielding strength that is not adequate. Therefore, the supplied strength and deformation capacities are not adequate to control, within acceptable limits, its response to severe pulse-type EQGMs that could occur at the site of the building. In other words, the deformation demands (floor displacement, interstory drift index, IDI, and plastic rotations, θ_p) not only exceed the supplied capacities, but also are so large to be unacceptable. Thus, the building needs to be seismically upgraded to survive such types of EQGMs and conventional (or traditional) and innovative strategies for upgrading the structural system were attempted.

The conventional strategies for upgrading are based on increasing the stiffness, strength, and ductility (or any combination of one, two or three of them). Among different techniques that have been used to achieve such strategies the most promising one for the building under study

appears to be steel jacketing of the structural elements. Because of the above detected weaknesses, not only the beam-column joints need to be jacketed, but also it is necessary to enhance the toughness of the columns and beams. Thus it is decided to jacket the columns and to encase the girders and a portion of their adjacent slabs as well.

12.2 CONCLUSIONS

After trying different thicknesses of steel plates and analyzing the degree of improvement in the performance (response) of the building through nonlinear static (pushover) and dynamic (time-history) analyses, it is concluded that this conventional strategy will not lead to an efficient economical solution. Thus the use of an innovative strategy is attempted to decrease (control) the demands rather than just trying to increase the strength and stiffness which led to increase in the demands.

Because of the observed weaknesses of the existing structure, it was clear that no matter what strategy was used, it was necessary to avoid the pullout of the beam reinforcing bars and to increase the toughness (particularly through the increase of the plastic deformation capacity) at the critical regions. Thus it was decided to remove these weaknesses by implementing the above steel jacketing and encasing strategy but by using the minimum practical steel plate thickness.

Initially it appeared that for the safety performance level, increasing damping would not be quite sufficient because the critical EQGMs for such a performance level are the severe pulse-type EQGMs. According to the literature available for pulse-type of EQGMs, adding damping would not help very much. However, due to the fact that the recorded severe pulses do not consist of only one severe acceleration pulse, but at least three successive pulses leading to the development of two severe (high-intensity and long-duration) velocity pulses, it was decided to try this possible solution.

Considering the two near-field recorded fault-normal ground motions and also two idealized fault-normal ground motions, all having the same PGV=68 in./sec (173 cm/sec), it is shown that even under pulse-type ground motions, increasing the damping could considerably reduce the response of structures. The results for recorded and idealized fault-normal ground motions are summarized in Tables 12.1 and 12.2.

The results of nonlinear dynamic analysis show that under the Los Gatos ground motion, increasing damping from 0.05 to 0.30 reduces the response by at least 40% and generally

speaking, this reduction can be predicted fairly reasonably, by looking at the response spectra of the records or of the idealized ground motions. Also since the lateral displacement of structures at the peaks are mainly controlled by the first mode of vibration, which has its own modal participation mass ratio (say about 0.85 for frame structures) the SDOFS response spectra overestimate the response of MDOF structures.

After a review of all available innovative strategies and considering the above conclusions, it appeared that one of the best strategies to decrease the demands would be to use additional damping (ξ_{eff}). Nonlinear analysis of the response of the light steel-jacketed and encased structure with different amount of total ξ_{eff} indicated that with a $\xi_{eff} = 30\%$ it was possible to adequately control the response of the upgraded structure to the most critical pulse-type EQGMs.

12.3 RECOMMENDATIONS

The results of the studies conducted, presented, and discussed in this report indicate that for existing nonductile RC moment frame buildings located in sites near active faults (the rupture of which can originate severe pulse-type EQGMs) and for which buildings the value of the fundamental period T is close to the value of the duration of the severe pulses t_d (say in the range of $0.5 \leq T/t_d \leq 1.2$), the addition of supplementary damping (i.e., increase of the ξ_{eff}) appears to be a promising seismic upgrading strategy. Therefore, what is now needed, and thus highly recommended, is to carry out an investigation on how this strategy of increasing the ξ_{eff} up to 30% can be attained efficiently (technically and economically) in the field, i.e., in the practice, through the use of a number of real dampers. This investigation should address the following issues: (1) How many dampers are needed? (2) Where should they be located? (3) How will these dampers be supported, i.e., what kind of secondary structure is needed and how will this structure be interconnected with the dampers and the primary existing structure? (4) How are the dynamic characteristics of the primary structure modified by the addition of the secondary structure and the dampers? (5) What is the response of the total seismically upgraded structure to the critical EQGMs that can be expected in the future?

Based on the results obtained in the above recommended investigation, attempts should be made to formulate a step-by-step simple but reliable and practical approach that can be codified and used in practice for the seismic assessment of the vulnerability of existing

nonductile RC moment frame buildings and for their upgrading using the strategy and techniques discussed in this report.

Table 12.1 Los Gatos Ground Motion (t_d=2.7 sec)

Structure	Basement & Foundation Condition	T -sec (T/t_d)	Damping Ratio = 0.05					Damping Ratio = 0.30					Ratio				
			Nonlinear		Displ. Spectra			Nonlinear		Displ. Spectra			Nonlinear		Displ. Spectra		
			IDI_m	$\Delta_{2/3}$ (μ)	GM	a^1	b^2	IDI_m	$\Delta_{2/3}$ (μ)	GM	a^1	b^2	IDI_m	$\Delta_{2/3}$	GM	a^1	b^2
As-Built Building	Flexible	**3.2 (1.2)**	5.4%	60 (3.7)	80	64	77	3.2%	35 (2.3)	44	42	47	0.59	0.58	0.55	0.66	0.61
	Fixed	**2.6 (.96)**	6.1%	67 (5.8)	79	50	63	3.1%	31 (2.8)	33	38	41	0.51	0.46	0.42	0.76	0.64
Heavily Retrofitted	Flexible	**2.3 (.85)**	3.8%	44 (1.4)	50	57	58	1.7%	21 (0.7)	24	30	32	0.45	0.48	0.48	0.52	0.56
	Fixed	**1.3 (.48)**	1.7%	19 (1.5)	18	18	18	1.0%	10 (1.0)	12	11	11	0.59	0.53	0.67	0.62	0.62
Lightly Ret	Flexible	**2.6 (.96)**	4.0%	44 (1.8)	59	66	68	2.1%	25 (1.1)	26	38	38	0.53	0.57	0.44	0.57	0.56

(1) Model (a) Fault Normal Idealization , Figure 7.1.
(2) Model (b) Fault Normal Idealization , Figure 7.1.
All the displacements are in inches.

Table 12.2 Takatori Ground Motion (t_d=1.7 sec)

Structure	Basement & Foundation Condition	T -sec (T/t_d)	Damping Ratio = 0.05					Damping Ratio = 0.30					Ratio				
			Nonlinear		Displ. Spectra			Nonlinear		Displ. Spectra			Nonlinear		Displ. Spectra		
			IDI_m	$\Delta_{2/3}$ (μ)	GM	a^1	b^2	IDI_m	$\Delta_{2/3}$ (μ)	GM	a^1	b^2	IDI_m	$\Delta_{2/3}$	GM	a^1	b^2
As-Built Building	Flexible	**3.2 (1.9)**	2.8%	21 (1.7)	32	34	47	1.9%	20 (1.6)	22	27	33	0.68	0.95	0.69	0.80	0.71
	Fixed	**2.6 (1.5)**	2.6%	20 (2.4)	31	38	51	1.9%	20 (2.1)	19	30	33	0.73	1.00	0.61	0.78	0.65
Heavily Retrofitted	Flexible	**2.3 (1.4)**	3.7%	43 (1.4)	55	46	50	1.8%	22 (0.8)	24	29	31	0.49	0.51	0.44	0.63	0.61
	Fixed	**1.3 (.75)**	2.8%	32 (2.5)	31	34	34	1.5%	16 (1.4)	16	16	16	0.54	0.50	0.52	0.48	0.48
Lightly Ret	Flexible	**2.6 (1.5)**	2.7%	32 (1.3)	31	45	50	2.0%	22 (1.1)	24	30	31	0.74	0.69	0.77	0.66	0.63

(1) Model (a) Fault Normal Idealization , Figure 7.1.
(2) Model (b) Fault Normal Idealization , Figure 7.1.
All the displacements are in inches.

References

ACI-318-95. 1995. *Building code requirements for structural concrete.* Farmington Hills, Mich: American Concrete Institute.

ATC-13. 1985. *Earthquake damage evaluation data for California.* Applied Technology Council. Redwood City, Calif.

Blume, J. *San Fernando, 1973, California, earthquake of February 9, 1971.* Vol. I-B. Washington, D.C.: U.S. Department of Commerce.

FEMA-273. 1997. *NEHRP guidelines for the seismic rehabilitation of buildings.* Washington, D.C.: Building Seismic Safety Council.

Iwan, W. D. 1997. Drift spectrum: measure of demand for earthquake ground motions. *J. of Structural Engineering* 123 (4): 397–404.

Large, G. E., and T. Y. Chen. 1968. *Reinforced concrete design,* 3rd ed. New York: The Ronald Press.

Naeim, Farzad. 1997. *Performance of extensively instrumented buildings during the January 17, 1994 Northridge earthquake.* Los Angeles: John A. Martin & Associates, Inc.

Newmark, N. M., and W. J. Hall. 1982. *Earthquake spectra and design.* Oakland, Calif.: Earthquake Engineering Research Institute.

Oesterle, R.G. 1986. *Inelastic analysis for in-plane strength of RC structural walls.* Ph.D. Dissertation. Evanston, Ill.: Northwestern University,

Sasani, M. 1997. Discussion of evaluation of UBC-94 provisions for seismic design of RC structural walls. *Earthquake Spectra* 13(1).

Scott, B. D., R. Park, M. J. N. Priestley. 1982. Stress-strain behavior of concrete confined by overlapping hoops at low and high strain rates. *ACI J.* (January – February).